Applied Hydraulic Transients

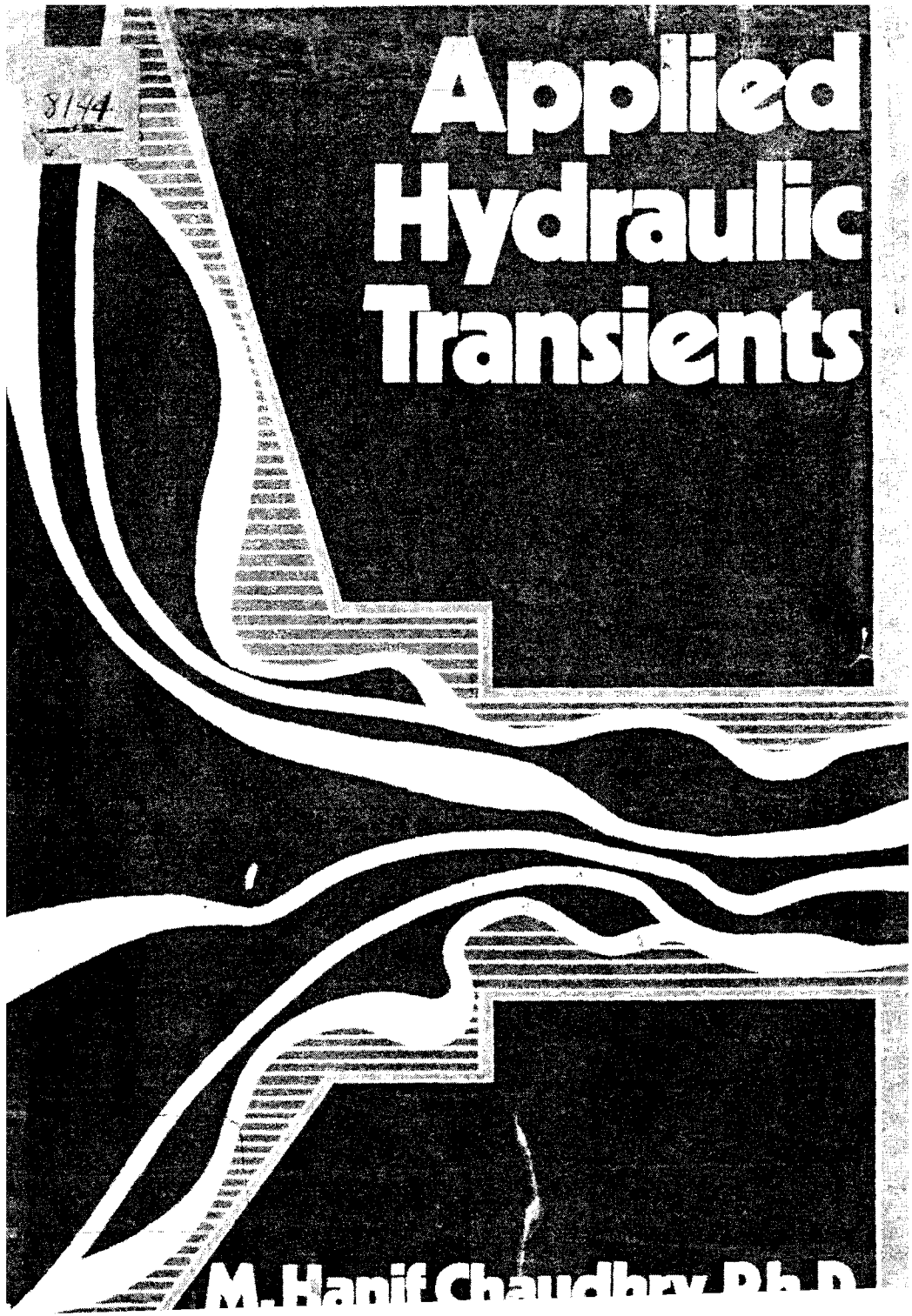

M. Hanif Chaudhry, Ph.D.

APPLIED HYDRAULIC TRANSIENTS

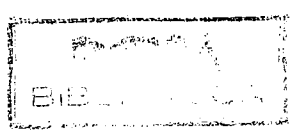

APPLIED HYDRAULIC TRANSIENTS

by

M. Hanif Chaudhry, Ph.D.

British Columbia Hydro and Power Authority
Vancouver, British Columbia, Canada

VNR VAN NOSTRAND REINHOLD COMPANY
NEW YORK CINCINNATI ATLANTA DALLAS SAN FRANCISCO
LONDON TORONTO MELBOURNE

Van Nostrand Reinhold Company Regional Offices:
New York Cincinnati Atlanta Dallas San Francisco

Van Nostrand Reinhold Company International Offices:
London Toronto Melbourne

Library of Congress Catalog Card Number: 78-4087
ISBN: 0-442-21517-7

Manufactured in the United States of America

Published by Van Nostrand Reinhold Company
135 West 50th Street, New York, NY 10020

Published simultaneously in Canada by Van Nostrand Reinhold Ltd.

15 14 13 12 11 10 9 8 7 6 5 4 3 2 1

Library of Congress Cataloging in Publication Data

Chaudhry, M. Hanif.
Applied hydraulic transients.

Includes index.
1. Hydraulic transients. I. Title.
TC163.C43 620.1'064 78-4087
ISBN 0-442-21517-7

PREFACE

In the last decade, the use of digital computers for analyzing hydraulic transients has increased by leaps and bounds, and the graphical and arithmetical methods for such analyses have been replaced by sophisticated numerical techniques. Not only has this change reduced the amount of laborious computations, but it has resulted in more precise results and has made the analysis of complex systems possible. *Applied Hydraulic Transients* provides a comprehensive and systematic discussion of hydraulic transients and presents various methods of analyses suitable for digital computer solution. The book is suitable as a reference for practicing engineers and researchers and as a textbook for senior-level undergraduate and graduate students. The field of application of the book is very broad and diverse and covers areas such as hydroelectric projects, pumped-storage schemes, water-supply systems, nuclear power plants, oil pipelines, and industrial piping systems.

Each chapter of the book is developed in a systematic manner from first principles. A very strong emphasis is given to the practical applications, and advanced mathematics and unnecessary theoretical details have been avoided as much as possible. However, wherever inclusion of such details was considered necessary from the point of view of researchers, they are presented in such a manner that a practicing engineer can skip them without losing continuity of the text. Several case studies, problems of applied nature, and design criteria are included, which will be helpful to design engineers and will introduce students to the design of real-life projects. Solved examples are given for illustration purposes, extensive lists of up-to-date references are included at the end of each chapter for further study, and sample computer programs and flowcharts are presented to familiarize the reader with digital computer applications. Approximate methods and design charts are appended to the text for quick computations during the preliminary design stages.

Because of the diverse nature of application, the various chapters have been

written so that they can be read individually. Sometimes, however, other parts of the book had to be referred to in order to avoid duplication. This has been done in such a manner that only the section referred to may be read and not the whole chapter. This mode of presentation will allow practicing engineers to read only those parts of the book that are of their immediate interest, and will allow teachers to select the chapters most relevant to their courses.

SI (*Système Internationale*) units are used throughout the book. However, wherever empirical constants are involved or numerical constants are introduced in the derivations, their corresponding values in the English units are given in the footnotes. With these footnotes and the conversion table of Appendix F, any reader preferring to use the English units may do so without much difficulty.

The sequence of presentation is as follows: In Chapter 1, commonly used terms are defined, a brief history of hydraulic transients is presented, and fundamental concepts are introduced. The dynamic and continuity equations for a one-dimensional flow in closed conduits are derived in Chapter 2, and various numerical methods available for their solution are discussed. The details of the method of characteristics are presented in Chapter 3. The next four chapters are problem-oriented and discuss transients in pumping systems (Chapter 4), in hydroelectric power plants (Chapter 5), in nuclear power plants (Chapter 6), and in oil pipelines (Chapter 7). The analysis of transients in homogeneous, two-phase flows is also presented in Chapter 6. Resonance in pressurized piping systems is discussed in Chapter 8, and the details of the transfer matrix method are outlined. Transient cavitation and liquid column separation are discussed in Chapter 9, and various methods for eliminating or alleviating undesirable transients are presented in Chapter 10. The analysis of surge tanks using a lumped-system approach is presented in Chapter 11. In Chapter 12, transients in open channels are discussed, and the details of explicit and implicit finite-difference methods are outlined. A number of design charts and sample computer programs are presented in Appendixes A through D.

The book presents in a systematic manner a collection of my own contributions, some of which have not previously been published, as well as material drawn from various sources. Every attempt has been made to identify the source of material; any oversight in this regard is strictly unintentional.

M. H. Chaudhry, Ph.D.
Vancouver, B.C.
Canada

ACKNOWLEDGMENTS

I would like to express my gratitude to Professors V. L. Streeter, E. B. Wylie, C. S. Martin and G. Evangelisti, and to J. Parmakian. Their excellent publications were a source of inspiration during the preparation of this book. My former teacher and research supervisor, Dr. E. Ruus, Professor of Civil Engineering, reviewed the entire manuscript and offered many useful suggestions for its improvement; in addition, I am thankful to him and to the Department of Civil Engineering, University of British Columbia (UBC), Vancouver, Canada, for giving me the opportunity and privilege to participate in giving lectures, based on parts of this book, to the graduate students.

Thanks are extended to my employer, British Columbia Hydro and Power Authority (BCHPA), for granting me permission to include the results of tests conducted on a number of their power plants and a number of design studies for their projects. These studies were undertaken under the technical and administrative supervision of F. J. Patterson, Manager, Hydroelectric Design Division. J. W. Forster, Assistant Manager, Hydroelectric Design Division, and I. C. Dirom, Manager, Development Department, provided encouragement throughout the preparation of the book, and each reviewed several chapters. Dr. P. W. W. Bell, Supervisor, Hydraulic Section, reviewed eight chapters and did the hydraulic transient studies summarized in "Design" on page 324. Professor Emeritus E. S. Pretious and F. El-Fitiany, a Ph.D. candidate, both of UBC and D. E. Cass, Engineer, BCHPA, reviewed several chapters. Their comments and suggestions for improving the presentation are appreciated. R. E. Johnson, Senior Engineer, was in charge of instrumentation for the prototype tests presented in Sections 3.8, 5.8, and 10.7 and devised the gauges for measuring water levels during the tests of Section 12.11; D. E. Cass assisted in the studies reported in Sections 4.9 and 4.10; R. M. Rockwell, Supervisor, System Standards Section and J. H. Gurney, Engineer, prepared Figs. 5.8 and 5.18; W. S. McIlquham and G. Arczynski, Senior Engineers, prepared turbine characteristics

for the studies of Sections 5.5, 5.8, and 10.7; G. Vandenburg, Senior Engineer, prepared Fig. 10.5; Dr. E. A. Portfors, Head, Hydraulic Division, Klohn Leonoff Consultants Ltd., for several discussions during studies of Sections 3.8, 5.8, and 10.7; K. H. Kao, C. J. Gibbs, and W. A. Johnson, Engineers, did the programming for the case study of Section 12.15; F. E. Parkinson, Vice-President, and S. Alam, Senior Engineer, Lasalle Hydraulic Laboratory, conducted the hydraulic model studies of Section 12.15; and Engineers L. S. Howard, D. E. Cass, and J. H. Gurney assisted in the proofreading.

I am thankful to Westinghouse Electric Corporation for granting permission to include material from their reports in Section 6.8 and to J. M. Geets, Manager, BOP Systems Design, Westinghouse, who enthusiastically furnished a number of relevant reports; to C. F. Whitehead, Vice-President, Engineering, Ebasco Services Inc., New York, for providing photographs for Section 1.7 and to Ebasco for granting permission to include these photographs in the book; and to Dr. W. T. Hancox, Head, Thermalhydraulics Research Branch, Atomic Energy of Canada; to Professor F. W. Wood, Queen's University, Kingston, Ontario, and Glenfield & Kennedy Ltd., Scotland, for granting permission to include material from their publications. I am grateful to the Department of Water Resources, State of California, and to the following members of the department: D. L. Smith, Senior Mechanical Engineer. M. L. Chauhan, Associate Mechanical Engineer, and L. O. Well, Assistant Mechanical Engineer, for providing the test data of Section 4.9.

Thanks are also due to the American Society of Civil Engineers, American Society of Mechanical Engineers, International Association for Hydraulic Research, British Hydromechanic Research Association, the Water Power and Dam Construction, and the L'Energia Elettrica for allowing inclusion of material from their copyrighted publications.

I would like to extend my thanks to F. Ching and D. Reid for typing the manuscript and to L. Myles and P. Wong for preparing the figures and illustrations. My wife, Shamim, helped in numerous ways in completing the manuscript. I am thankful to her and to our son, Asif, for many hours that should have been spent with them but were required in the preparation of this book.

M. H. Chaudhry

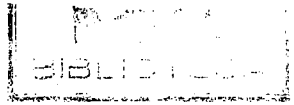

CONTENTS

APPLIED HYDRAULIC TRANSIENTS

CHAPTER 1

INTRODUCTION

In this chapter, a number of commonly used terms are defined, and a brief history of the development of the knowledge of hydraulic transients is presented. The basic waterhammer equations for the change in pressure caused by an instantaneous change in flow velocity are then derived. A description of the propagation and reflection of waves produced by closing a valve at the downstream end of a single pipeline is presented. This is followed by a discussion of the classification and causes of hydraulic transients.

1.1 DEFINITIONS

Terms commonly used are defined in this section; less common terms are defined in the text wherever they appear for the first time.

Steady and Unsteady Flow. If the flow conditions, such as pressure, velocity, and discharge, at a point do not change with time, then the flow is said to be *steady*. If the conditions change with time, the flow is termed *unsteady*. Strictly speaking, turbulent flows are always unsteady since the conditions at a point are changing continuously. However, by considering temporal mean values over a short period, these flows are considered as steady if the temporal mean conditions do not change with time. When referring to the steady or unsteady turbulent flows herein, we will use the temporal mean conditions.

Transient-State or Transient Flow. The intermediate-stage flow, when the flow conditions are changed from one steady-state condition to another steady state, is called *transient-state flow or transient flow*.

Uniform and Nonuniform Flow. If the velocity is constant with respect to distance at any given time, the flow is called *uniform flow*, whereas if the velocity varies with distance, the flow is called *nonuniform*.

Steady-Oscillatory or Periodic Flow. If the flow conditions are varying with time and if they repeat after a fixed time interval, the flow is called *steady-*

oscillatory flow and the time interval at which conditions are repeating is referred to as the *period*. If T is the period in seconds, then the frequency of oscillations, f, in cycles/s and in rad/s is $1/T$ and $2\pi/T$, respectively. Frequency expressed in rad/s is called *circular frequency* and is usually designated by ω.

Column Separation. If the pressure in a closed conduit drops below the vapor pressure of a liquid, then cavities are formed in the liquid and the liquid column may separate.

Waterhammer. In the past, terms such as *waterhammer*, *oilhammer*, and *steamhammer* referred to the pressure fluctuations caused by a flow change depending upon the fluid involved. Nowadays, however, the term *hydraulic transient* is used more frequently.

The following discussion will be helpful in clarifying the preceding definitions. Let us assume that the downstream valve of the pipeline (see Fig. 1.1a) is fully open, the water is flowing with velocity V_o, and at time, $t = t_o$, the valve is suddenly closed. As a result of the valve closure, the flow through the valve is instantly reduced to zero, and because of the conversion of the kinetic energy into elastic energy, pressure rises at the valve, and a pressure wave travels in the upstream direction. This wave is reflected from the reservoir and travels back and forth between the valve and the reservoir. Due to friction losses, this wave is dissipated as it travels in the pipeline, and finally—let us say, at time t_1—the pressure in the entire pipeline becomes equal to the reservoir head, and flow is completely stopped.

Based upon the definitions given previously, the flow is steady when the conditions are constant with respect to time (i.e., for $t < t_o$ and $t > t_1$); and the intermediate flow (i.e., $t_o \leqslant t \leqslant t_1$) when the conditions are changing from the initial steady state to the final steady state is transient flow.

Now let us consider another situation. Let the valve be opened and closed periodically at a frequency, ω_f. After a number of cycles, the flow conditions in the pipeline will become periodic too, having frequency ω_f. This flow is called *steady-oscillatory flow*.

1.2 HISTORICAL BACKGROUND*

The study of hydraulic transients began with the investigation of the propagation of sound waves in air, the propagation of waves in shallow water, and the flow of blood in arteries. However, none of these problems could be solved rigorously until the development of the theories of elasticity and calculus, and

*Most of the material presented in Section 1.2 is based on Ref. 1; readers interested in the history of hydraulics should see Ref. 2.

the solution of partial differential equations. Newton presented, in his *Principia*,[3] the results of his investigations on the propagation of sound waves in air and on the propagation of water waves in canals. Both Newton and Lagrange obtained theoretically the velocity of sound in air as 298.4 m/s as compared to their experimental value of 348 m/s. Lagrange erroneously attributed this difference to experimental error, whereas Newton explained that the theoretical velocity was incorrect and that this discrepancy was due to spacing of the solid particles of air and the presence of vapors in air. By comparing the oscillations of a liquid in a U-tube to that of a pendulum, Newton derived an incorrect expression for the celerity of water waves in a canal as $\pi\sqrt{L/g}$, where L = the wavelength and g = acceleration due to gravity.

Euler[4] developed a detailed theory of the propagation of elastic waves and derived the following partial differential equation for wave propagation:

$$\frac{\partial^2 y}{\partial t^2} = a^2 \frac{\partial^2 y}{\partial x^2} \tag{1.1a}$$

in which $a^2 = gh$; x = the equilibrium position of a particle; y = the particle displacement; and h = height of the air column. He also developed a general solution of this equation as

$$y = F(x + at) + f(x - at) \tag{1.1b}$$

in which F and f = the travelling waves. Euler also tried, but failed, to obtain a solution for the flow of blood through arteries.[5]

Lagrange analyzed[6] the flow of compressible and incompressible fluids. For this purpose, he developed the concept of *velocity potential*. He also derived a correct expression for the celerity of waves in a canal as $c = \sqrt{gd}$, in which d = canal depth. In 1789, Monge developed a graphical method for integrating the partial differential equations[7] and introduced the term *method of characteristics*. About 1808, Laplace[8] pointed out the reasons for the difference between the theoretical and measured values of the velocity of sound in air. He explained that the relationships derived by Newton and Lagrange were based on Boyle's law and that this law was not valid under varying pressures since the air temperature did not remain constant. He reasoned that the theoretical velocity would increase by about 20 percent if the adiabatic conditions were used instead of the isothermal conditions.

Young[9] investigated the flow of bloodstreams, friction losses, bend losses, and the propagation of pressure waves in pipes. Helmholtz appears to be the first to point out that the velocity of pressure waves in water contained in a pipe was less than that in unconfined water. He correctly attributed this difference to the elasticity of pipe walls. In 1869, Riemann[10] developed and applied a three-dimensional equation of motion and its simplified one-dimensional form to such

fields as vibrating rods and sound waves. Weber[11] studied the flow of an incompressible fluid in an elastic pipe and conducted experiments to determine the velocity of pressure waves. He also developed the dynamic and continuity equations that are the bases of our studies. Marey[12] conducted extensive series of tests to determine the velocity of pressure waves in water and in mercury and concluded that the wave velocity was:

1. independent of the amplitude of the pressure waves
2. three times greater in mercury than in water
3. proportional to the elasticity of the tube.

Resal[13] developed the continuity and dynamic equations and a second-order wave equation. He used Marey's experimental results to verify his analytical studies. In 1877, Lord Rayleigh published his book on the theory of sound,[14] which summarized the earlier studies and his own research.

Korteweg[15] was the first to determine the wave velocity considering the elasticity of both the pipe wall and the fluid; earlier investigators had considered only one of the two at a time.

Although Wood[1] lists Michaud[16] as the first to deal with the problem of waterhammer, recent investigations by Anderson[17] have shown that actually Menabrea[18] was the first to study this problem. Michaud[16] studied the problem of waterhammer, and the design and use of air chambers and safety valves. Gromeka included the friction losses[19] in the analysis of waterhammer for the first time. He assumed, however, that the liquid was incompressible and that the friction losses were directly proportional to the flow velocity.

Weston[20] and Carpenter,[21] both American engineers, conducted a number of experiments to develop a theoretical relationship between the velocity reduction in a pipe and the corresponding pressure rise. However, neither one succeeded because their pipelines were short. Frizell[22] presented an analysis of waterhammer based on studies undertaken while acting as a consulting engineer for the Ogden hydroelectric development in Utah. This power plant had a 9449-m-long penstock. Frizell developed expressions for the velocity of waterhammer waves and for the pressure rise due to instantaneous reduction of the flow. He stated that the wave velocity would be the same as that of sound in unconfined water if the modulus of elasticity of the pipe walls was infinite. He also discussed the effects of branch lines, wave reflections, and successive waves on speed regulation. Unfortunately, Frizell's work has not been appreciated as much as that of his contemporaries, Joukowski and Allievi.

In 1897, Joukowski conducted extensive experiments in Moscow on pipes with the following dimensions (expressed in length and diameter, respectively): 7620 m, 50 mm; 305 m, 101.5 mm; and 305 m, 152.5 mm. Based on his experimental and theoretical studies, he published his classic report[23] on the

basic theory of waterhammer. He developed a formula for the wave velocity, taking into consideration the elasticity of both the water and the pipe walls. He also developed the relationship between the velocity reduction and the resulting pressure rise by using two methods: the conservation of energy and the continuity condition. He discussed the propagation of a pressure wave along the pipe and the reflection of the pressure waves from the open end of a branch. He studied the effects of air chambers, surge tanks, and spring safety valves on waterhammer pressures. He also investigated the effects of the variation of closing rates of a valve and found that the pressure rise was a maximum for closing times, $T \leqslant 2L/a$, in which L = length of the pipeline and a = wave velocity.

Allievi developed the general theory of waterhammer from first principles and published it in 1902.[24] The dynamic equation that he derived was more accurate than that of Korteweg. He showed that the term $V(\partial V/\partial x)$ in the dynamic equation was not important as compared to the other terms and could be dropped. He introduced two dimensionless parameters,

$$\left.\begin{aligned} \rho &= \frac{aV_o}{2gH_o} \\ \theta &= \frac{aT_c}{2L} \end{aligned}\right\} \tag{1.2}$$

in which a = waterhammer wave velocity; V_o = steady-state velocity; L = length of the pipeline; T_c = valve-closure time; ρ = one-half of the ratio of the kinetic energy of the fluid to the potential energy stored in the fluid and the pipe walls at pressure head H_o; and θ = the valve-closure characteristics. For the valve-closure time, T_c, Allievi obtained an expression for the pressure rise at the valve and presented charts for the pressure rise and drop caused by a uniformly closing or opening valve. Braun[25,26] presented equations similar to those presented by Allievi in his second publication.[27] In a later publication, Braun[28] claimed priority over Allievi, and it appears that the so-called Allievi's constant, ρ, was actually introduced by Braun. However, Allievi is still considered to be the originator of the basic waterhammer theory. Allievi[27] also studied the rhythmic movement of a valve and proved that the pressure cannot exceed twice the static head.*

Joukowski's and Allievi's theories were mainly used in the first two decades of the 20th century. Camichel et al.[30] demonstrated that doubling of pressure head is not possible unless $H_o > aV_o/g$. Constantinescu[31] described a mechanism to transmit mechanical energy by using the waterhammer waves. In World

*For details of Allievi's work, interested readers should consult Refs. 24, 27, and 29.

War I, British fighter planes were equipped with the Constantinescu gear for firing the machine guns. Based on Joukowski's theory, Gibson[32] presented a paper that included, for the first time, nonlinear friction losses in the analysis. He also invented an apparatus[33] to measure the turbine discharge using the pressure-time history following a load rejection.

Strowger and Kerr presented[34] a step-by-step computational procedure to determine the speed changes of a hydraulic turbine caused by load changes. Waterhammer pressures, changes in the turbine efficiency at various gate openings, and the uniform and nonuniform gate movements were considered in the analysis.

In his discussion of Strowger and Kerr's analysis, Wood[35] introduced the graphical method for waterhammer analysis. Löwy[36] independently developed and presented an identical graphical method in 1928. He also studied resonance caused by periodic valve movements and pressure drop due to gradual opening of valves and gates. He considered the friction losses in his analysis by including the friction terms in the basic partial differential equations. Schnyder[37] included complete pump characteristics in his analysis of waterhammer in pipelines connected to centrifugal pumps. Bergeron[38] extended the graphical method to determine the conditions at the intermediate sections of a pipeline, and Schnyder[39] was the first to include the friction losses in the graphical analysis. At a symposium[40] sponsored jointly by the American Society of Civil Engineers and the American Society of Mechanical Engineers in 1933 in Chicago, several papers were presented on the analysis of waterhammer in penstocks and in discharge pipelines.

Angus[41] outlined basic theory and some applications of the graphical method including "lumped" friction losses, and Bergeron[42] presented a paper describing the theory of plane elastic waves in various media. Another symposium[43] on waterhammer was held in 1937 at the annual meeting of the American Society of Mechanical Engineers. At this symposium, papers were presented on the analysis of air chambers and valves, on the inclusion of complete pump characteristics, and on the comparison of the computed and measured results. By linearizing the friction term, Wood[44] used Heaviside's Operational Calculus, and later Rich[45] used Laplace transforms for the analysis of waterhammer in pipelines. Angus[46] presented in 1938 the analysis of compound and branching pipelines and water-column separation. Other papers on water-column separation were published by Lupton,[47] Richard,[48] and Duc.[49]

From 1940 to 1960, in addition to books by Rich,[50] Jaeger,[51] and Parmakian,[52] numerous papers were published on the analysis of waterhammer. Because of their large number, they are not listed herein. Instead, important contributions are discussed and listed in the following chapters.

Ruus[53a,53b] was the first to present procedures for determining a valve-closure sequence, called *optimum valve closure*, so that the maximum pressure remained within the prescribed limits. Later on, Cabelka and Franc,[54] and Streeter[55] independently developed the concept and the latter extended and computerized it for complex piping systems.

Gray[56] introduced the method of characteristics for a computer-oriented waterhammer analysis. Lai[57] used it in his doctoral dissertation, and his joint paper with Streeter[58] was the pioneer publication that made this method and the use of computers for the analysis of transients popular. Later on, Streeter published numerous papers on the method of characteristics as well as a text[59] on hydraulic transients. These and important contributions of others are listed in Chapter 3.

On the theory of surge tanks, early European contributions were made by Léauté,[60] Rateau,[61] Prášil,[62] and Vogt.[63] Calame and Gaden,[64] and Frank and Schüller[65] summarized the earlier investigations and their own research. Thoma[66] was the first to show that the surge tank of a governed hydraulic turbine would be stable only if the cross-sectional area of the surge tank were more than a certain minimum value, now commonly known as the *Thoma area*. Johnson[67] invented the differential surge tank to develop accelerating or decelerating heads rapidly. Other contributors to the theory of surge tanks are Escande,[68] Jaeger,[51,70] Gardel,[69] Binnie,[71] Evangelisti,[72] Paynter,[73,74] and Marris.[75]

1.3 PRESSURE CHANGES CAUSED BY AN INSTANTANEOUS VELOCITY CHANGE

Let us consider the piping system of Fig. 1.1, in which a fluid is flowing with velocity V_o, and the initial pressure upstream of the valve is p_o. If the valve setting is changed instantaneously at time $t = 0$, the velocity changes to $V_o + \Delta V$, the pressure at the valve becomes $p_o + \Delta p$, the fluid density ρ_o is changed to $\rho_o + \Delta\rho$, and a pressure wave of magnitude Δp travels in the upstream direction. Let us designate the velocity of propagation of the pressure wave (commonly called *waterhammer wave velocity*) by a, and, to simplify the derivation, let us assume that the pipe is rigid, i.e., its diameter does not change due to pressure changes.

The unsteady flow situation of Fig. 1.1*a* is converted into a steady condition by superimposing, on the control volume, velocity a in the downstream direction. This is equivalent to assuming that an observer is traveling in the upstream direction with velocity a. To this observer, the moving wave front appears stationary (Fig. 1.1*b*), and the inflow and outflow velocities from the control volume are $(V_o + a)$ and $(V_o + \Delta V + a)$, respectively.

Let us consider distance, x, and velocity, V, as positive in the downstream

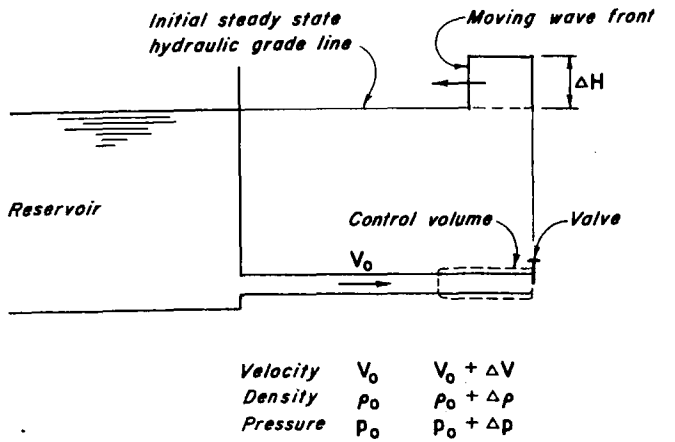

(a) Unsteady flow

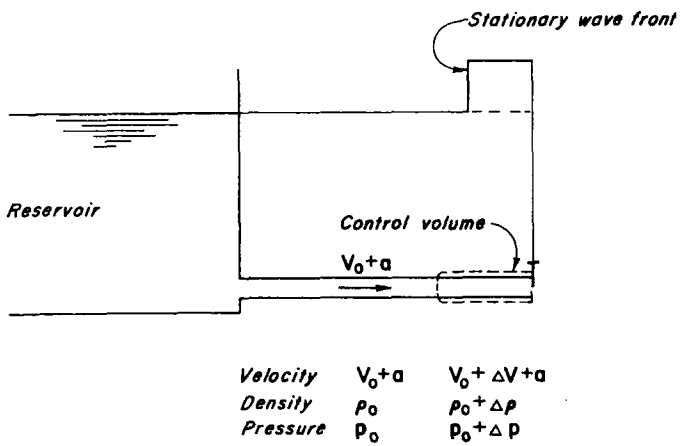

(b) Unsteady flow converted to steady flow by superimposing velocity a

Figure 1.1. Pressure rise in a pipeline due to instantaneous reduction of velocity ($\Delta p = \rho g \Delta H$).

direction. Then the rate of change of momentum in the positive x-direction

$$= \rho_o (V_o + a) A \, [(V_o + \Delta V + a) - (V_o + a)]$$

$$= \rho_o (V_o + a) A \, \Delta V \tag{1.3}$$

Neglecting friction, the resultant force, F, acting on the fluid in the control volume in the positive x-direction, is $p_o A - (p_o + \Delta p)A$, i.e.,

$$F = -\Delta p \, A \tag{1.4}$$

According to Newton's second law of motion, the time rate of change of momentum is equal to the net force. Hence, it follows from Eqs. 1.3 and 1.4 that

$$\Delta p = -\rho_o (V_o + a) \Delta V \tag{1.5}$$

We will see in Chapter 2 that in most of the transient conditions in metal or concrete pipes or in the rock tunnels, a (approximately 1000 m/s) is much greater than V_o (<10 m/s). Hence, V_o in Eq. 1.5 may be neglected. Also, since

$$p = \rho g H, \tag{1.6}$$

in which H is the piezometric head, Eq. 1.5 may be written as

$$\Delta p = -\rho_o a \, \Delta V \tag{1.7}$$

or

$$\Delta H = -\frac{a}{g} \Delta V \tag{1.8}$$

The negative sign on the right hand side of Eq. 1.8 indicates that the pressure increases (i.e., ΔH is positive) for a reduction in velocity (i.e., for negative ΔV) and vice versa. Also note that Eq. 1.8 was derived for the case of velocity changes occurring at the downstream end of a pipe and for the wave front moving in the upstream direction. Proceeding similarly, it can be proved that, if the velocity was changed at the upstream end and the wave was moving in the downstream direction, then

$$\Delta H = \frac{a}{g} \Delta V \tag{1.9}$$

Note that there is no negative sign on the right-hand side of Eq. 1.9. This shows that in this case, the pressure increases for an increase in velocity and the pressure decreases with a decrease in velocity.

It was assumed previously that the fluid density changes to $\rho_o + \Delta\rho$ as a result of the change in pressure. For the control volume of Fig. 1.1b,

$$\text{Rate of mass inflow} = \rho_o A (V_o + a) \tag{1.10}$$

$$\text{Rate of mass outflow} = (\rho_o + \Delta\rho)A(V_o + \Delta V + a) \tag{1.11}$$

The increase in the mass of control volume due to density change is small and may be neglected. Therefore, the rate of mass inflow is equal to the rate of mass outflow. Hence,

$$\rho_o A(V_o + a) = (\rho_o + \Delta\rho)A(V_o + \Delta V + a) \tag{1.12}$$

which upon simplification becomes

$$\Delta V = -\frac{\Delta\rho}{\rho_o}(V_o + \Delta V + a). \tag{1.13}$$

Since $(V_o + \Delta V) \ll a$, Eq. 1.13 may be written as

$$\Delta V = -\frac{\Delta\rho}{\rho_o} a \tag{1.14}$$

The bulk modulus of elasticity, K, of a fluid is defined[76] as

$$K = \frac{\Delta p}{\Delta\rho/\rho_o} \tag{1.15}$$

It follows from Eqs. 1.14 and 1.15 that

$$a = -K\frac{\Delta V}{\Delta p} \tag{1.16}$$

On the basis of Eq. 1.7, Eq. 1.16 becomes

$$a = \frac{K}{a\rho_o} \tag{1.17}$$

which may be written as

$$a = \sqrt{\frac{K}{\rho_o}} \tag{1.18}$$

Note that the expression of Eq. 1.18 is the velocity of waterhammer waves in a compressible fluid confined in a *rigid* pipe. In the next chapter, we will discuss how this expression is modified if the pipe walls are elastic.

Example 1.1

Compute the velocity of pressure waves in a 0.5-m-diameter pipe conveying oil from a reservoir to a valve. Determine the pressure rise if a steady flow of 0.4 m^3/s is instantaneously stopped at the downstream end by closing the valve.

Assume that the pipe is rigid; the density of the oil, $\rho = 900$ kg/m^3; and the bulk modulus of elasticity of the oil, $K = 1.5$ GPa.

Solution:

$$A = \frac{\pi}{4}(0.5)^2 = 0.196 \text{ m}^2$$

$$V_o = Q_o/A = 0.4/0.196 = 2.04 \text{ m/s}$$

$$a = \sqrt{\frac{K}{\rho}} \qquad \text{(Eq. 1.18)}$$

$$= \sqrt{\frac{1.5 \times 10^9}{900}} = 1291 \text{ m/s}$$

As the flow is completely stopped, $\Delta V = 0 - 2.04 = -2.04$ m/s; therefore,

$$\Delta H = -\frac{a}{g}\Delta V$$

$$= -\frac{1291}{9.81}(-2.04) = 268.5 \text{ m}$$

Since the sign of ΔH is positive, it is a pressure rise.

1.4 WAVE PROPAGATION AND REFLECTIONS IN A SINGLE PIPELINE

Let us consider the piping system shown in Fig. 1.2, in which flow conditions are steady and at time $t = 0$, the valve is instantaneously closed. If the system is assumed frictionless, then the initial steady-state pressure head along the length of the pipeline is H_o. Let the distance x and the velocity V be positive in the downstream direction.

The sequence of events following the valve closure can be divided into four parts (Fig. 1.2) as follows:

1. $0 < t \leq L/a$ *(Fig. 1.2a and b)*

   As soon as the valve is closed, the flow velocity at the valve is reduced to zero, which causes a pressure rise of $\Delta H = +(a/g)V_o$. Because of this pressure rise, the pipe expands (in Fig. 1.2, the initial steady-state pipe diameter is shown by dotted lines), the fluid is compressed thus increasing the fluid density, and a positive pressure wave propagates toward the reservoir. Behind this wave, the flow velocity is zero, and all the kinetic energy has been converted into elastic energy. If a is the velocity of the waterhammer waves

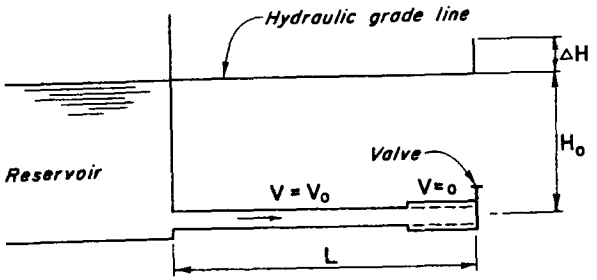

(a) Conditions at $t + \epsilon$

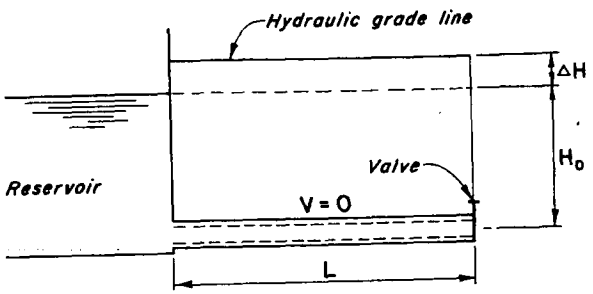

(b) Conditions at $t = \frac{L}{a}$

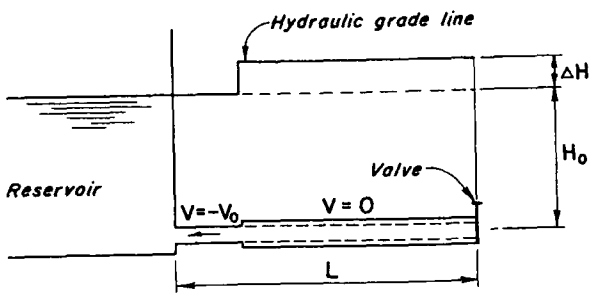

(c) Conditions at $t = \frac{L}{a} + \epsilon$

Figure 1.2. Propagation of pressure waves caused by instantaneous closure of valve.

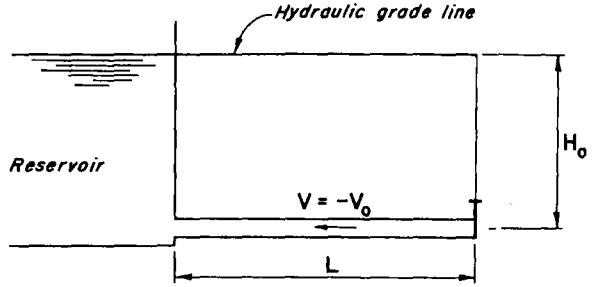

(d) Conditions at $t = \frac{2L}{a}$

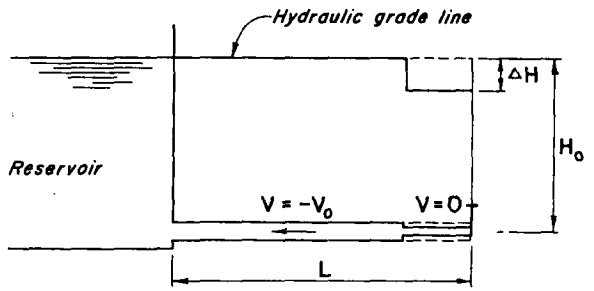

(e) Conditions at $t = \frac{2L}{a} + \epsilon$

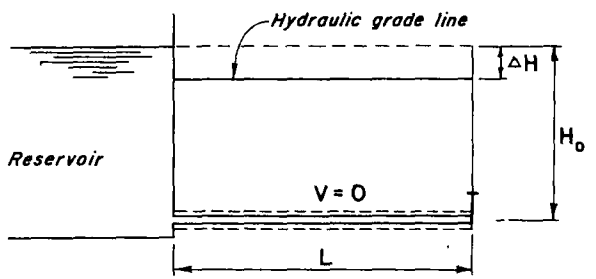

(f) Conditions at $t = \frac{3L}{a}$

Figure 1.2. (*Continued*)

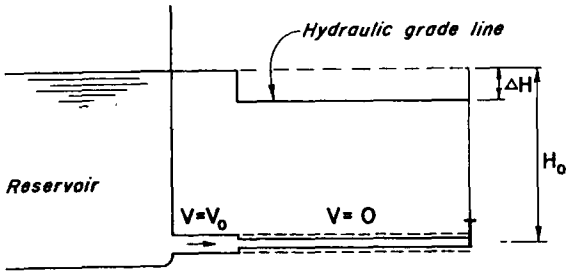

(g) Conditions at $t = \frac{3L}{a} + \epsilon$

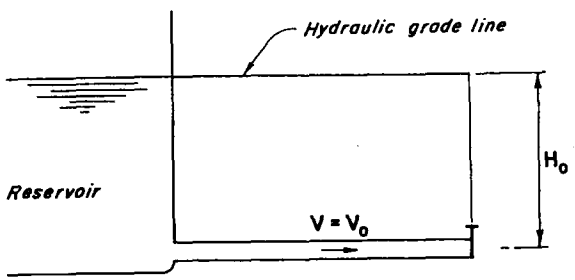

(h) Conditions at $t = \frac{4L}{a}$

Figure 1.2. (*Continued*)

and L is the length of the pipeline, then at time $t = L/a$, along the entire length of the pipeline, the pipe is expanded, the flow velocity is zero, and the pressure head is $H_o + \Delta H$.

2. $L/a < t \leqslant 2L/a$ *(Fig. 1.2c and d)*

As the reservoir level is constant, the conditions are unstable at the reservoir end when the wave reaches there because the pressure on a section on the reservoir side is H_o while the pressure on an adjacent section in the pipe is $H_o + \Delta H$. Because of this pressure differential, the fluid starts to flow from the pipeline into the reservoir with velocity $-V_o$. Thus, the velocity is changed from 0 to $-V_o$, which causes the pressure to drop from $H_o + \Delta H$ to

H_o. In other words, a negative wave travels toward the valve such that the pressure behind the wave (i.e., on the upstream side) is H_o and the fluid velocity is $-V_o$. At $t = 2L/a$, the pressure head in the entire pipeline is H_o, and the fluid velocity is $-V_o$.

3. $2L/a < t \leqslant 3L/a$ *(Fig. 1.2e and f)*

Since the valve is completely closed, a negative velocity cannot be maintained at the valve. Therefore, the velocity is instantaneously changed from $-V_o$ to 0. Because of this, the pressure is reduced to $H_o - \Delta H$, and a negative wave propagates in the upstream direction. Behind this wave, the pressure is $H_o - \Delta H$, and the fluid velocity is zero. At time $t = 3L/a$, the pressure head in the entire pipeline is $H_o - \Delta H$, and the fluid velocity is zero.

4. $3L/a < t \leqslant 4L/a$ *(Fig. 1.2g and h)*

As soon as this negative wave reaches the reservoir, an unbalanced condition is created again at the upstream end. Now the pressure is higher on the reservoir side than in the pipeline. Therefore, the fluid starts to flow towards the valve with velocity V_o, and the pressure head is restored to H_o. At time $t = 4L/a$, the pressure head in the entire pipeline is H_o, and the flow velocity is V_o. Thus, the conditions in the pipeline are the same as during the initial steady-state conditions.

As the valve is completely closed, the preceding sequence of events starts again at $t = 4L/a$. Figure 1.2 illustrates the sequence of events along the pipeline, while Fig. 1.3 shows the pressure variation at the valve end with time. As we assumed the system is frictionless, this process continues and the conditions are repeated at an interval of $4L/a$. This interval after which conditions are repeated is termed the *theoretical period* of the pipeline. In real physical systems, however, pressure waves are dissipated due to friction

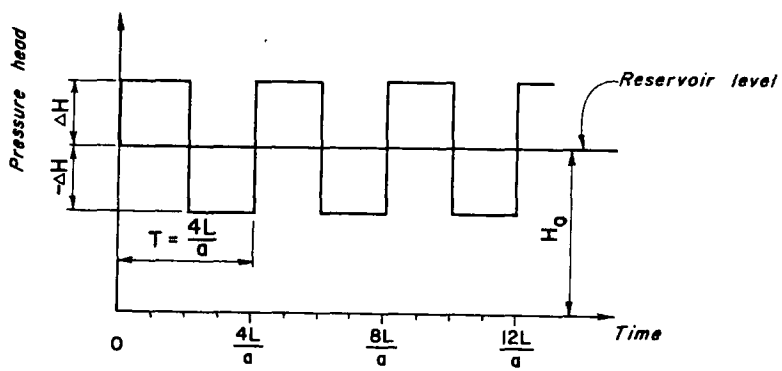

Figure 1.3. Pressure variation at valve; friction losses neglected.

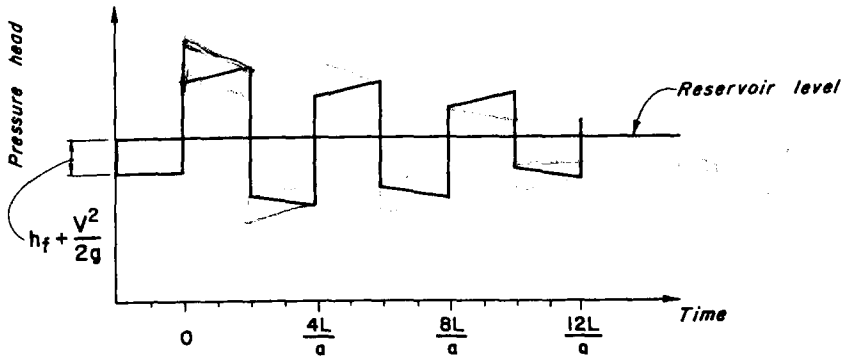

Figure 1.4. Pressure variation at valve; friction losses considered.

losses as the waves propagate in the pipeline, and the fluid becomes stationary after a short time.

If the friction losses are taken into consideration, then the pressure variation at the valve with time will be as shown in Fig. 1.4.

1.5 CLASSIFICATION OF HYDRAULIC TRANSIENTS

Depending upon the conduit in which the transient conditions are occurring, transients may be classified into three categories:

1. transients in closed conduits
2. transients in open channels
3. combined free-surface-pressurized transient flow.

The analysis of transients in closed conduits may be further subdivided into two types: distributed systems and lumped systems. In the former case, the fluid is considered compressible, and the transient phenomenon occurs in the form of traveling waves. Examples in which such transients occur are water-supply pipes, power plant conduits, and gas-transmission lines. In the analysis of lumped systems, any change in the flow conditions is assumed to take place instantaneously throughout the fluid, i.e., the fluid is considered as a solid body. Example of such a system is the slow oscillations of water level in a surge tank following a load change on the turbine.

Mathematically, the transients in the distributed systems are represented by partial differential equations, whereas the transients in the lumped systems are described by ordinary differential equations. If $\omega L/a$ is much less than 1, then

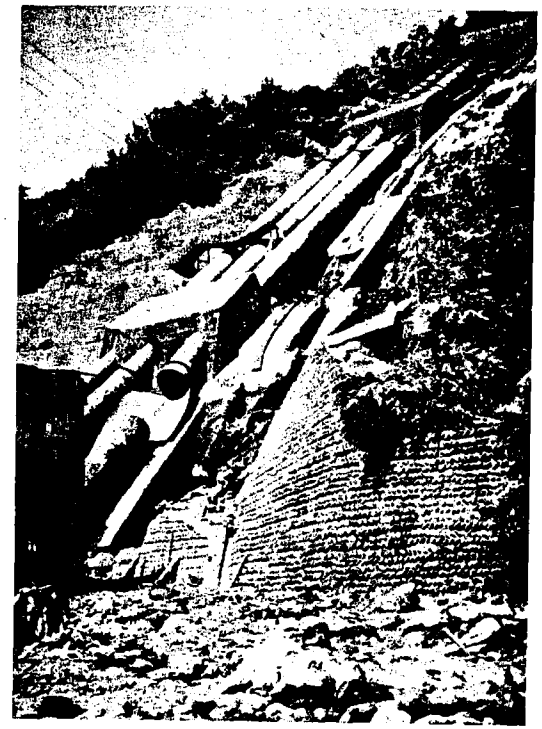

Figure 1.5. View of burst penstock of Oigawa Power Station, Japan, due to excessive transient pressures caused by operating errors and malfunctioning of equipment. (After Bonin[80] Courtesy of Ebasco Services Inc., New York.)

the system may be analyzed as a lumped system[77]; otherwise, the system must be analyzed as a distributed system. In the preceding expression, ω = frequency, L = length of the pipeline, and a = wave velocity.

Transients in open channels may be divided into two types depending upon the rate at which they occur: (1) gradually varied flow, such as flood waves in rivers, and (2) rapidly varied flow, such as surges in power canals. If the wave front in the rapidly varied flow is steep, it is referred to as a *bore*.

Sometimes a free-flow becomes pressurized due to priming of the conduits during the transient-state conditions. Such flows are called combined free-surface-pressurized flows. Examples of such flows are flow in sewers following a rainstorm, and flow in the tailrace tunnel of a hydroelectric power plant following rapid acceptance of load on turbines.

Figure 1.5. (*Continued*)

1.6 CAUSES OF TRANSIENTS

As defined previously, the intermediate-stage flow, when the conditions are changed from one steady state to another, is termed *transient-state flow*. In other words, the transient conditions are initiated whenever the steady-state conditions are disturbed. Such a disturbance may be caused by changes, planned or accidental, in the settings of the control equipment of a man-made system and by changes in the inflow or outflow of a natural system.

Common examples of the causes of transients in engineering systems are:

1. Opening, closing, or "chattering" of valves in a pipeline
2. Starting or stopping the pumps in a pumping system
3. Starting-up a hydraulic turbine, accepting or rejecting load
4. Vibrations of the vanes of a runner or an impeller, or of the blades of a fan

Figure 1.6. View of collapsed section of penstock of Oigawa Power Station, Japan, caused by vacuum upstream of the burst section. (After Bonin[80] Courtesy of Ebasco Services Inc., New York.)

5. Sudden changes in the inflow or outflow of a canal by opening or closing the control gate
6. Failure or collapse of a dam
7. Sudden increases in the inflow to a river or a sewer due to flash storm runoff.

1.7 SYSTEM DESIGN AND OPERATION

To design a system, the system layout and parameters are first selected, and the system is analyzed for transients caused by various possible operating conditions. If the system response is not acceptable, such as the maximum and minimum pressures are not within the prescribed limits, then either the system layout or

Figure 1.6. (*Continued*)

the parameters are changed, or various control devices are provided and the system is analyzed again. This procedure is repeated until a desired response is obtained. For a particular system, a number of control devices may be suitable, or it may be economical either to modify the operating conditions, if possible, or to change the acceptable response. However, the final aim is always to have an *overall* economical system that yields acceptable response.

The system must be designed for various normal operating conditions expected to occur during its life. And, similarly, it is mandatory that the system be operated strictly according to the operating guidelines. Failure to do so has caused spectacular accidents[78–83] and has resulted in extensive property damage and many times loss of life. Figures 1.5 and 1.6 show the burst and the collapsed sections of the penstock of the Oigawa Power Station[80] caused by operating errors and malfunctioning equipment.

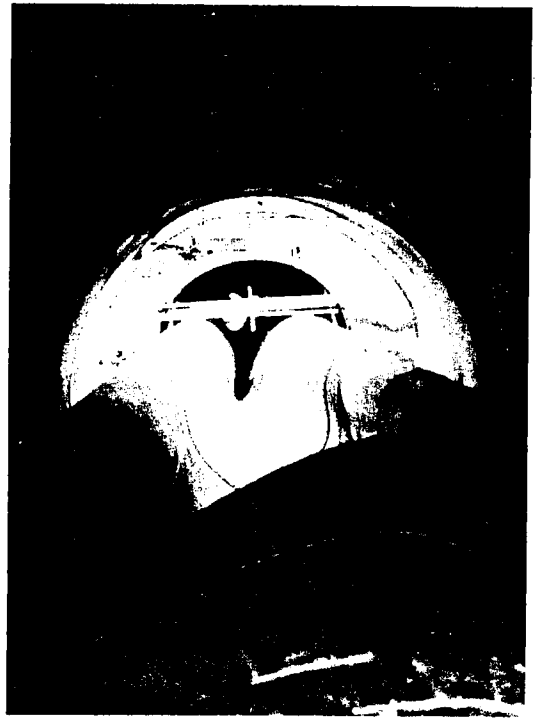

Figure 1.6. (*Continued*)

If the data for a system are not precisely known, then the system should be analyzed for the expected range of various variables.

During the commissioning of a newly built system or after major modifications, the system should be tested for various possible operating conditions. To avoid catastrophes, it is usually advisable to conduct the tests in a progressive manner. For example, if there are four parallel pumping-sets on a pipeline, the tests for power failure should begin with one pumping-set and progressively increase to all four.

1.8 SUMMARY

In this chapter, the most commonly used terms were first defined. A brief historical background of the development of the knowledge of hydraulic

transients was presented, and expressions were derived for the pressure rise or drop due to an instantaneous increase or decrease in the flow velocity. The chapter was concluded by a discussion of the classification and causes of hydraulic transients.

PROBLEMS

1.1 Derive Eq. 1.9 from first principles.

1.2 Derive Eq. 1.8 assuming that the pipe is inclined to the horizontal at an angle θ.

1.3 Compute the wave velocity in a 2-m-diameter pipe conveying seawater. Assume the pipe is rigid.

1.4 What would be the pressure rise if an initial steady discharge of 10 m^3/s was instantaneously stopped at the downstream end of the pipeline of Problem 1.3?

1.5 A valve is suddenly opened at the downstream end of a 1-m-diameter pipeline such that the flow velocity is increased from 2 to 4 m/s. Compute the pressure drop due to the opening of the valve. Assume the liquid is water.

1.6 Prove that if the fluid is incompressible and the pipe walls are assumed rigid, then the pressure rise

$$\Delta H = -\frac{L}{g}\frac{dV}{dt}$$

in which L = length of the pipe and dV/dt = the rate of change of velocity with respect to time. (*Hint:* Apply Newton's second law of motion to the fluid volume.)

1.7 Plot the pressure variation with time at the mid-length of the pipeline shown in Fig. 1.2 following instantaneous closure of the valve. Assume the system is frictionless.

ANSWERS

1.3 1488 m/s

1.4 482.81 m

1.5 301.86 m

REFERENCES

1. Wood, F. M., "History of Waterhammer," *Report No. 65, Department of Civil Engineering*, Queen's University at Kingston, Ontario, Canada, April 1970.

2. Rouse, H. and Ince, S., *History of Hydraulics*, Dover Publications, New York, 1963.
3. Newton, I., *The Principia*, Royal Soc., London, Book 2, Proposition 44–46, 1687.
4. Euler, L., "De la Propagation du Son," *Mémoires de l'Acad. d. Wiss.*, Berlin, 1759.
5. Euler, L., "Principia pro Motu Sanguinis per Arterias Determinando," Opera Postume Tomus Alter, XXXIII, 1775.
6. Lagrange, I. L., *Mecanique Analytique*, Paris, Bertrand's ed., 1788, p. 192.
7. Monge, G., "Graphical Integration," *Ann. des Ing. Sortis des Ecoles de Gand*, 1789.
8. Laplace, P. S., *Celestial Mechanics*, 4 volumes, Bowditch translation.
9. Young, T., "Hydraulic Investigations," *Phil. Trans., Royal Society*, London, 1808, pp. 164–186.
10. Riemann, B., *Partielle Differentialgleichungen*, Braunschweig, 1869.
11. Weber, W., "Theorie der durch Wasser oder andere incompressible Flüssigkeiten in elastischen Rohren fortgepflanzten Wellen," *Berichte über die Verhandlungen der Königlichen Sachsischen Gesselschaft der Wissenschaften zu Leipzig*, Leipzig, Germany, Mathematisch-Physische Klasse, 1866, pp. 353–357.
12. Marey, M., "Mouvement des Ondes Liquides pour Servir a la Théorie du Pouls," Travaux du Laboratoire de M. Marey, 1875.
13. Resal, H., "Note sur les petits mouvements d'un fluide incompressible dans un tuyau élastique," *Journal de Mathematiques Pures et Appliquées*, Paris, France, 3rd Series, vol. 2, 1876, pp. 342–344.
14. Rayleigh, J. W. S., *Theory of Sound*, 1877.
15. Korteweg, D. J., "Ueber die Fortpflanzungsgeschwindingkeit des Schalles in elastischen Rohren," *Annalen der Physik und Chemie*, Wiedemann, ed., New Series, vol. 5, no. 12, 1878, pp. 525–542.
16. Michaud, J., "Coups de bélier dans les conduites. Étude des moyens employés pour en atteneur les effets," *Bulletin de la Société Vaudoise des Ingénieurs et des Architectes*, Lausanne, Switzerland, 4^e année, nos. 3 and 4, Sept. and Dec. 1878, pp. 56–64, 65–77.
17. Anderson, A., "Menabrea's Note on Waterhammer: 1858," *Jour., Hyd. Div., Amer. Soc. Civ. Engrs.*, vol. 102, Jan. 1976, pp. 29–39.
18. Menabrea, L. F., "Note sur les effects de choc de l'eau dans les conduites," *Comptes Rendus Hebdomadaires des Séances de L'Academie des Sciences*, Paris, France, vol. 47, July–Dec. 1858, pp. 221–224.
19. Gromeka, I. S., "Concerning the Propagation Velocity of Waterhammer Waves in Elastic Pipes," Scientific Soc. of Univ. of Kazan, Kazan, U.S.S.R., May 1883.
20. Weston, E. B., "Description of Some Experiments Made on the Providence, R. I., Water Works to Ascertain the Force of Water Ram in Pipes," *Trans. Amer. Soc. of Civil Engrs.*, vol. 14, 1885, p. 238.
21. Carpenter, R. C., "Experiments on Waterhammer," *Trans. Amer. Soc. of Mech. Engrs.*, 1893–1894.
22. Frizell, J. P., "Pressures Resulting from Changes of Velocity of Water in Pipes," *Trans. Amer. Soc. Civil Engrs.*, vol. 39, June 1898, pp. 1–18.
23. Joukowski, N. E., *Mem. Imperial Academy Soc. of St. Petersburg*, vol. 9, no. 5, 1898, 1900 (in Russian, translated by O. Simin, *Proc. Amer. Water Works Assoc.*, vol. 24, 1904, pp. 341–424).
24. Allievi, L., "Teoria generale del moto perturbato dell'acqu anei tubi in pressione," *Ann. Soc. Ing. Arch. italiana*, 1903 (French translation by Allievi, *Revue de Mécanique*, 1904).
25. Braun, E., *Druckschwankungen in Rohrleitungen*, Wittwer, Stuttgart, 1909.
26. Braun, E., *Die Turbine, Organ der turbinentechnischen Gesellschaft*, Berlin, 1910.

27. Allievi, L., "Teoria del colpo d'ariete," *Atti Collegio Ing. Arch.*, 1913 (English translation by E. E. Halmos, "The Theory of Waterhammer," *Trans. Amer. Soc. Mech. Engrs.*, 1929).
28. Braun, E., "Bermerkungen zur Theorie der Druckschwankungen in Rohrleitungen," *Wasserkraft und Wasserwirtschaft*, vol. 29, no. 16, Munich, Germany, 1939, pp. 181–183.
29. Allievi, L., "Air Chambers for Discharge Pipes," *Trans. Amer. Soc. Mech. Engrs.*, vol. 59, Nov. 1937, pp. 651–659.
30. Camichel, C., Eydoux, D., and Gariel, M., "Étude Théorique et Expérimentale des Coups de Bélier," Dunod, Paris, France, 1919.
31. Constantinescu, G., Ann. des Mines de Roumanie, Dec. 1919, Jan. 1920.
32. Gibson, N. R., "Pressures in Penstocks Caused by Gradual Closing of Turbine Gates," *Trans. Amer. Soc. Civil Engrs.*, vol. 83, 1919–1920, pp. 707–775.
33. Gibson, N. R., "The Gibson Method and Apparatus for Measuring the Flow of Water in Closed Conduits," *Trans. Amer. Soc. Mech. Engrs.*, vol. 45, 1923, pp. 343–392.
34. Strowger, E. B. and Kerr, S. L., "Speed Changes of Hydraulic Turbines for Sudden Changes of Load," *Trans. Amer. Soc. Mech. Engrs.*, vol. 48, 1926, pp. 209–262.
35. Wood, F. M., discussion of *Ref. 34*, *Trans. Amer. Soc. Mech. Engrs.*, vol. 48, 1926.
36. Löwy, R., *Druckschwankungen in Druckrohrleitungen*, Springer, 1928.
37. Schnyder, O., "Druckstösse in Pumpensteigleitungen," *Schweizerische Bauzeitung*, vol. 94, Nov.-Dec. 1929, pp. 271–273, 283–286.
38. Bergeron, L., "Variations de regime dans les conduites d'eau," *Comptes Rendus des Travaux de la Soc. Hydrotech. de France*, 1931.
39. Schnyder, O., "Ueber Druckstösse in Rohrleitungen," *Wasserkraft u. Wasserwirtschaft*, vol. 27, Heft 5, 1932, pp. 49–54, 64–70.
40. "Symposium on Waterhammer," *Amer. Soc. of Mech. Engrs. and Amer. Soc. of Civil Engrs.*, Chicago, Illinois, June 1933.
41. Angus, R. W., "Simple Graphical Solutions for Pressure Rise in Pipe and Pump Discharge Lines," *Jour. Engineering Institute of Canada*, Feb. 1935, pp. 72–81.
42. Bergeron, L., "Méthod graphique generale de calcul des propagations d'ondes planes," *Soc. des Ing. Civils de France*, vol. 90, 1937, pp. 407–497.
43. Symposium on Waterhammer, Annual Meeting, *Amer. Soc. of Mech. Engrs.*, Dec. 1937.
44. Wood, F. M., "The Application of Heavisides Operational Calculus to the Solution of Problems in Waterhammer," *Trans. Amer. Soc. of Mech. Engrs.*, vol. 59, Nov. 1937, pp. 707–713.
45. Rich, G., "Waterhammer Analysis by the Laplace-Mellin Transformations," *Trans. Amer. Soc. Mech. Engrs.*, 1944–1945.
46. Angus, R. W., "Waterhammer Pressure in Compound and Branched Pipes," *Proc. Amer. Soc. Civ. Engrs.*, Jan. 1938, pp. 340–401.
47. Lupton, H. R., "Graphical Analysis of Pressure Surges in Pumping Systems," *Jour. Inst. Water Engrs.*, 1953.
48. Richard, R. T., "Water Column Separation in Pump Discharge Lines," *Trans. Amer. Soc. Mech. Engrs.*, 1956.
49. Duc, F., "Water Column Separation," *Sulzer Tech. Review*, vol. 41, 1959.
50. Rich, G. R., *Hydraulic Transients*, 1st Ed., McGraw-Hill Book Co., Inc., New York, 1951 (Dover Reprint).
51. Jaeger, C., *Engineering Fluid Mechanics*, translated from German by Wolf, P. O., Blackie & Son Ltd., London, 1956.

52. Parmakian, J., *Waterhammer Analysis*, Prentice-Hall, Inc., Englewood Cliffs, N.J., 1955 (Dover Reprint, 1963).
53a. Ruus, E., "Bestimmung von Schliessfunctionen welche den kleinsten Wert des maximalen Druckstosses ergeben," thesis presented to the Technical Univ. of Karlsruhe, Germany, in partial fulfillment of the requirements for the degree of Doctor of Engineering, 1957.
53b. Ruus, E., "Optimum Rate of Closure of Hydraulic Turbine Gates," presented at Amer. Soc. Mech. Engrs.–Engineering Inst. of Canada Conference, Denver, Colorado, April 1966.
54. Cabelka, J., and Franc, I., "Closure Characteristics of a Valve with Respect to Waterhammer," *Proc., Eighth Congress, International Assoc. for Hydraulic Research*, Montreal, Canada, Aug. 1959, pp. 6-A-1 to 6-A-23.
55. Streeter, V. L., "Valve Stroking to Control Waterhammer," *Jour., Hyd. Div., Amer. Soc. Civil Engrs.*, vol. 89, March 1963, pp. 39–66.
56. Gray, C. A. M., "The Analysis of the Dissipation of Energy in Waterhammer," *Proc. Amer. Soc. Civ. Engrs.*, Proc. paper 274, vol. 119, 1953, pp. 1176–1194.
57. Lai, C., "A Study of Waterhammer Including Effect of Hydraulic Losses," thesis presented to the University of Michigan, Ann Arbor, Michigan, in partial fulfillment of the requirements for the degree of Doctor of Philosophy, 1962.
58. Streeter, V. L., and Lai, C., "Waterhammer Analysis Including Fluid Friction," *Trans. Amer. Soc. Civ. Engrs.*, vol. 128, 1963, pp. 1491–1524 (see also discussions by Gray, C. A. M., pp. 1530–1533, and by Paynter, H. M., pp. 1533–1538).
59. Streeter, V. L., and Wylie, E. B., *Hydraulic Transients*, McGraw-Hill Book Co., New York, 1967.
60. Léauté, "Mémoires sur les oscillations à longues périodes dans les machines actionnées par des moteurs hydrauliques," *J. Ecole Polytechn.*, Cahier XLVII, Paris, 1880.
61. Rateau, A., *Traité des Turbomachines*, Dunod, Paris, 1900.
62. Prášil, F., "Wasserschlossprobleme," *Schweiz. Bauztg.*, 52, 1908.
63. Vogt, F., *Berechnung und Konstruktion des Wasserschlosses*, Enke, Stuttgart, 1923.
64. Clame, J., and Gaden, D., *Théorie des Chambres d'équilibre*, Paris, 1926.
65. Frank, J., and Schüller, J., *Schwingungen in den Zuleitungs-und Ableitungskanälen von Wasserkraftanlagen*, Springer, Berlin, 1938.
66. Thoma, D., *Zur Theorie des Wasserschlosses bei selbsttätig geregelten Turbinenanlagen*, Oldenbourg, Munich, 1910.
67. Johnson, R. D., "The Differential Surge Tank," *Trans. Amer. Soc. Civ. Engrs.*, vol. 78, 1915, pp. 760–805.
68. Escande, L., "Recherches théoriques et expérimentales sur les oscillations de l'eau dans les chambres d'équilibre," Paris, 1943.
69. Gardel, A., *Chambres d'Equilibre*, Rouge et Cie, Lausanne, Switzerland, 1956.
70. Jaeger, C., "Present Trends in Surge Tank Design," *Proc. Inst. of Mech. Engrs.*, England, vol. 168, 1954, pp. 91–103.
71. Binnie, A. M., "Oscillations in Closed Surge Tanks," *Trans. Amer. Soc. Mech. Engrs.*, vol. 65, 1943.
72. Evangelisti, G., "Pozzi Piezometrici e Stabilità di Regolazione," *Energia Elettrica*, vol. 27, nos. 5 and 6, 1950, vol. 28, no. 6, 1951, vol. 30, no. 3, 1953.
73. Paynter, H. M., "Transient Analysis of Certain Nonlinear Systems in Hydroelectric Plants," thesis presented to Massachusetts Institute of Technology, Massachusetts, in partial fulfillment of the requirements of degree of doctor of philosophy, 1951.

74. Paynter, H. M., "Surge and Water-Hammer Problems," Electrical Analogies and Electronic Computer Symposium, *Trans. Amer. Soc. Civil Engrs.*, vol. 118, 1953, pp. 962–1009.
75. Marris, A. W., "Large Water Level Displacements in the Simple Surge Tank," *Jour. Basic Engineering, Trans. Amer. Soc. of Mech. Engrs.*, vol. 81, 1959, pp. 446–454.
76. Streeter, V. L., *Fluid Mechanics*, 4th Ed., McGraw-Hill Book Co., New York, 1966, p. 15.
77. Chaudhry, M. H., "Resonance in Pressurized Piping Systems," thesis presented to the University of British Columbia, Vancouver, Canada, in partial fulfillment of the requirements for the degree of doctor of philosophy, 1970, p. 24.
78. Rocard, Y., "Les Phenomenes d'Auto-Oscillation dans les Installations Hydrauliques," Hermann, Paris, 1937.
79. Jaeger, C., "Water Hammer Effects in Power Conduits," *Civil Engineering Pub. Works Rev.*, London, vol. 23, nos. 500–503, Feb.–May, 1948.
80. Bonin, C. C., "Water-Hammer Damage to Oigawa Power Station," *Jour. Engineering for Power, Amer. Soc. Mech. Engrs.*, April 1960, pp. 111–119.
81. Jaeger, C., "The Theory of Resonance in Hydropower Systems. Discussion of Incidents Occurring in Pressure Systems," *Jour. Basic Engineering, Amer. Soc. Mech. Engrs.*, vol. 85, Dec. 1963, pp. 631–640.
82. Kerensky, G., Discussion of "The Velocity of Water Hammer Waves," by Pearsall, I. S., *Symposium on Surges in Pipelines, Inst. of Mech. Engrs.*, London, vol. 180, Pt 3E, 1965–1966, p. 25.
83. Pulling, W. T., "Literature Survey of Water Hammer Incidents in Operating Nuclear Power Plants," Report No. WCAP-8799, *Westinghouse Electric Corporation*, Pittsburgh, Pennsylvania, Nov. 1976.

CHAPTER 2

EQUATIONS OF UNSTEADY FLOW THROUGH CLOSED CONDUITS

Unsteady flow through closed conduits is described by the dynamic and continuity equations. In this chapter, the derivation of these equations is presented, and methods available for their solution are discussed.

2.1 ASSUMPTIONS

The following assumptions are made in the derivation of the equations:

1. Flow in the conduit is one-dimensional,[1–3] and the velocity distribution is uniform over the cross section of the conduit.
2. The conduit walls and the fluid are linearly elastic, i.e., stress is proportional to strain.[4] This is true for most conduits such as metal, concrete and wooden pipes, and lined or unlined rock tunnels.
3. Formulas for computing the steady-state friction losses in conduits are valid during the transient state. The validity of this assumption has not as yet been verified. For computing frequency-dependent friction, Zielke[5] has developed a procedure for laminar flows, and Hirose[6] has proposed an empirical procedure for turbulent flows. However, these procedures are too complex and cumbersome for general use, and we will not discuss them further.

2.2 DYNAMIC EQUATION

We will use the following notation: distance, x, discharge, Q, and flow velocity, V, are considered positive in the downstream direction (see Fig. 2.1), and H is the piezometric head at the centerline of the conduit above the specified datum.

Let us consider a horizontal element of fluid having cross-sectional area A and length δx, within a conduit as shown in Fig. 2.1. If the piezometric head and the velocity at distance x are H and V, then their corresponding values at $x + \delta x$ are $H + (\partial H/\partial x)\,\delta x$ and $V + (\partial V/\partial x)\,\delta x$, respectively. In the x-direction, three

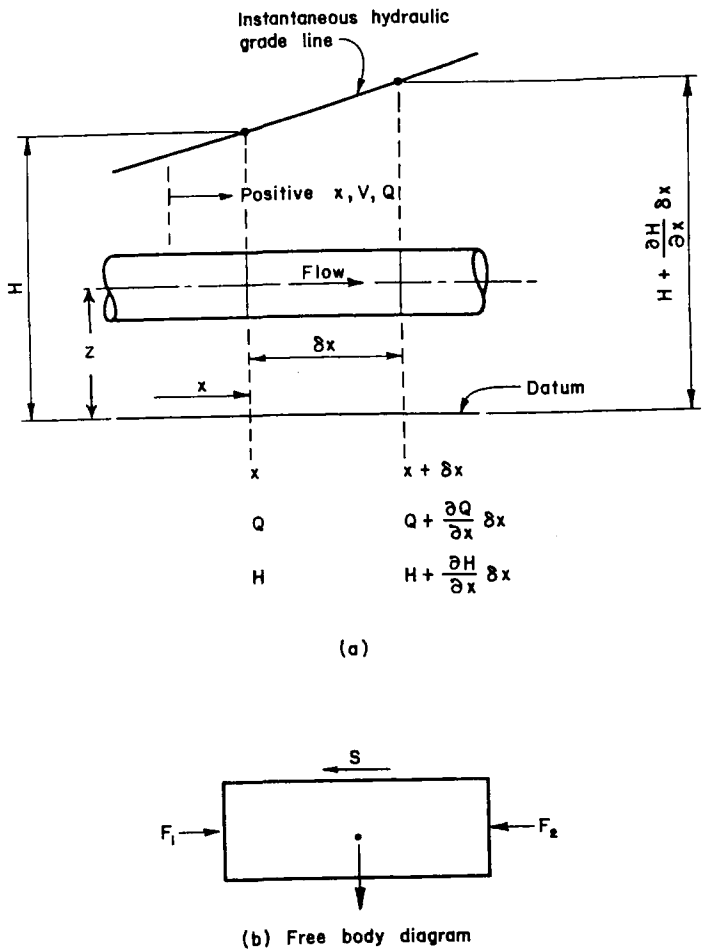

Figure 2.1. Notation for dynamic equation.

forces, F_1, F_2, and S, are acting on the element. F_1 and F_2 are forces due to pressure while S is the shear force due to friction. If γ = specific weight of the fluid, A = cross-sectional area of conduit, and z = height of conduit above datum, then

$$F_1 = \gamma A (H - z) \tag{2.1}$$

$$F_2 = \gamma \left(H - z + \frac{\partial H}{\partial x}\delta x\right) A \tag{2.2}$$

If the Darcy-Weisbach formula[1] is used for computing the friction losses, then the shear force

$$S = \frac{\gamma}{g}\frac{fV^2}{8}\pi D\,\delta x \tag{2.3}$$

in which g = acceleration due to gravity, f = friction factor, and D = diameter of the conduit. The resultant force, F, acting on the element is given by the equation

$$F = F_1 - F_2 - S \tag{2.4}$$

Substitution of the expressions for F_1, F_2, and S from Eqs. 2.1 through 2.3 into Eq. 2.4 yields

$$F = -\gamma A \frac{\partial H}{\partial x}\delta x - \frac{\gamma}{g}\frac{fV^2}{8}\pi D\,\delta x \tag{2.5}$$

According to Newton's second law of motion,

$$\text{Force} = \text{Mass} \times \text{Acceleration}. \tag{2.6}$$

For the fluid element under consideration,

$$\left.\begin{aligned}\text{Mass of the element} &= \frac{\gamma}{g} A\,\delta x \\ \text{Acceleration of the element} &= \frac{dV}{dt}\end{aligned}\right\} \tag{2.7}$$

Substitution of Eqs. 2.5 and 2.7 into Eq. 2.6 and division by $\gamma A\,\delta x$ yield

$$\frac{dV}{dt} = -g\frac{\partial H}{\partial x} - \frac{fV^2}{2D} \tag{2.8}$$

We know from elementary calculus that the total derivative

$$\frac{dV}{dt} = \frac{\partial V}{\partial t} + \frac{\partial V}{\partial x}\frac{dx}{dt} \tag{2.9a}$$

or

$$\frac{dV}{dt} = \frac{\partial V}{\partial t} + V\frac{\partial V}{\partial x} \tag{2.9b}$$

Substituting Eq. 2.9b into Eq. 2.8 and rearranging,

$$\frac{\partial V}{\partial t} + V\frac{\partial V}{\partial x} + g\frac{\partial H}{\partial x} + \frac{fV^2}{2D} = 0 \tag{2.10}$$

In most of the transient problems,[7] the term $V(\partial V/\partial x)$ is significantly smaller than the term $\partial V/\partial t$. Therefore, the former may be neglected. To account for the reverse flow, the expression V^2 in Eq. 2.10 may be written as $V|V|$, in which $|V|$ is the absolute value of V. By writing Eq. 2.10 in terms of discharge, Q, and rearranging, we obtain

$$\frac{\partial Q}{\partial t} + gA\frac{\partial H}{\partial x} + \frac{f}{2DA}Q|Q| = 0 \tag{2.11}$$

In Eqs. 2.3, 2.5, 2.8, 2.10, and 2.11, the Darcy-Weisbach formula has been used for calculating the friction losses. If a general exponential formula had been used for these losses, then the last term of Eq. 2.11 could be written as $kQ|Q|^m/D^b$, with the values of k, m, and b depending upon the formula employed. For example, for the Hazen-Williams formula, $m = 1.85$ and $b = 2.87$, while, as derived above, for the Darcy-Weisbach formula, $m = 1$ and $b = 3$. If correct values of m and b are used,[8] the results are independent of the formula employed, i.e., the Darcy-Weisbach and the Hazen-Williams formulas would give comparable results.

2.3 CONTINUITY EQUATION

Let us consider the control volume shown in Fig. 2.2. The volume of fluid inflow, $\forall_{in}$, and outflow, $\forall_{out}$, during time interval δt are

$$\forall_{in} = V\pi r^2\,\delta t \tag{2.12}$$

$$\forall_{out} = \left(V + \frac{\partial V}{\partial x}\delta x\right)\pi r^2\,\delta t \tag{2.13}$$

in which r = radius of the conduit. The increase in the fluid volume, $\delta\forall_{in}$, during time δt is

$$\delta\forall_{in} = \forall_{in} - \forall_{out} = -\frac{\partial V}{\partial x}\delta x\,\delta t\,\pi r^2 \tag{2.14}$$

The pressure change, δp, during time interval δt is $(\partial p/\partial t)\,\delta t$. This pressure change causes the conduit walls to expand or contract radially and causes the length of the fluid element to decrease or increase due to fluid compressibility (see Fig. 2.2).

Let us first consider the volume change, $\delta\forall_r$, due to the radial expansion or contraction* of the conduit. The radial or hoop stress, σ, in a conduit due to

*To simplify the derivation, we are neglecting the elongation or shortening of the fluid element due to Poisson ratio effects. Any reader interested in the derivation of the continuity equation including these effects should see Ref. 7.

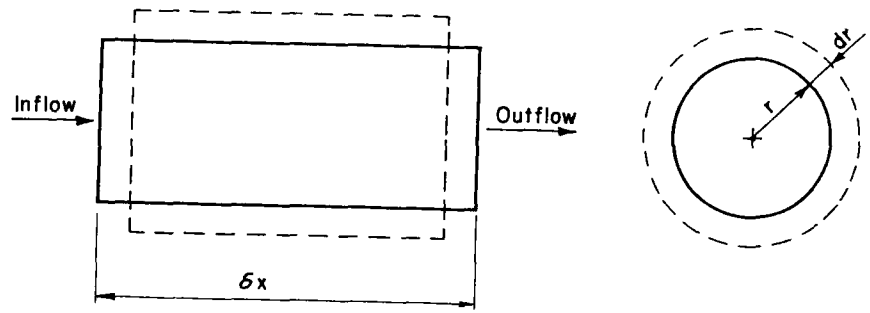

Figure 2.2. Notation for continuity equation.

the pressure p is given by the equation[4]

$$\sigma = \frac{pr}{e} \tag{2.15}$$

in which e = the conduit wall thickness. Hence, the change in hoop stress, $\delta\sigma$, caused by δp may be written as

$$\delta\sigma = \delta p\,\frac{r}{e} = \frac{\partial p}{\partial t}\delta t\,\frac{r}{e} \tag{2.16}$$

Since the radius r has increased to $r + \delta r$, the change in strain

$$\delta\epsilon = \frac{\delta r}{r} \tag{2.17}$$

If the conduit walls are assumed linearly elastic, then

$$E = \frac{\delta\sigma}{\delta\epsilon} \tag{2.18}$$

in which E = Young's modulus of elasticity. Substitution of expressions for $\delta\sigma$ and $\delta\epsilon$ from Eqs. 2.16 and 2.17 into Eq. 2.18 yields

$$E = \frac{(\partial p/\partial t)\,\delta t\,(r/e)}{\delta r/r} \tag{2.19}$$

or

$$\delta r = \frac{\partial p}{\partial t}\frac{r^2}{eE}\delta t \tag{2.20}$$

The change in the volume of the element due to the radial expansion or contraction of the conduit is

$$\delta\forall_r = 2\pi r\,\delta x\,\delta r \tag{2.21}$$

Substituting for δr from Eq. 2.20 yields

$$\delta \mathcal{V}_r = 2\pi \frac{\partial p}{\partial t} \frac{r^3}{eE} \delta t \, \delta x \tag{2.22}$$

Let us now derive an expression for the change in volume, $\delta \mathcal{V}_c$, due to compressibility of the fluid. The initial volume of the fluid element

$$\mathcal{V} = \pi r^2 \, \delta x \tag{2.23}$$

The bulk modulus of elasticity of a fluid, K, is defined[1] as

$$K = \frac{-\delta p}{\delta \mathcal{V}_c / \mathcal{V}} \tag{2.24}$$

By substituting for $\mathcal{V}$ from Eq. 2.23 and noting that $\delta p = (\partial p/\partial t)\, \delta t$, Eq. 2.24 becomes

$$\delta \mathcal{V}_c = \frac{-\partial p}{\partial t} \frac{\delta t}{K} \pi r^2 \, \delta x \tag{2.25}$$

If we assume that the fluid density remains constant, then it follows from the law of conservation of mass that

$$\delta \mathcal{V}_{\text{in}} + \delta \mathcal{V}_c = \delta \mathcal{V}_r. \tag{2.26}$$

Substitution of expressions for $\delta \mathcal{V}_{\text{in}}$, $\delta \mathcal{V}_r$, and $\delta \mathcal{V}_c$ from Eqs. 2.14, 2.22, and 2.25 into the above equation and division by $\pi r^2 \, \delta x \, \delta t$ yield

$$-\frac{\partial V}{\partial x} - \frac{1}{K} \frac{\partial p}{\partial t} = \frac{2r}{eE} \frac{\partial p}{\partial t} \tag{2.27}$$

or

$$\frac{\partial V}{\partial x} + \frac{\partial p}{\partial t} \left(\frac{2r}{eE} + \frac{1}{K} \right) = 0 \tag{2.28}$$

Let us define

$$a^2 = \frac{K}{\rho [1 + (KD/eE)]} \tag{2.29}$$

in which ρ = mass density of the fluid. Noting that $p = \rho g H$, rearranging the terms, and substituting $Q = VA$, Eq. 2.28 becomes

$$\frac{a^2}{gA} \frac{\partial Q}{\partial x} + \frac{\partial H}{\partial t} = 0 \tag{2.30}$$

It will be shown in the next chapter that a is the velocity of waterhammer waves. Expressions for a for various conduits and support conditions are presented in Section 2.6.

2.4 GENERAL REMARKS ON DYNAMIC AND CONTINUITY EQUATIONS

The dynamic equation, Eq. 2.11, and the continuity equation, Eq. 2.30, are a set of first-order partial differential equations. In these equations, there are two independent variables, x and t, and two dependent variables, Q and H. Other variables, A and D, are characteristics of the conduit system and are time-invariant but may be functions of x. Although the wave velocity, a, depends upon the characteristics of the system, laboratory tests have shown that it is significantly reduced[9] by reduction of pressure even when it remains above the vapor pressure. The friction factor f varies with the Reynolds number. However, f is considered constant herein because the effects of such a variation on the transient-state conditions are negligible.

Discussion about the type of Eqs. 2.11 and 2.30 now follows; any reader not interested in the mathematical details may proceed to Section 2.5.

Since the nonlinear terms in Eqs. 2.11 and 2.30 involve only the first power of the derivatives, the equations are called *quasi-linear*. These equations may be further classified as *elliptic*, *parabolic*, or *hyperbolic* as follows:

Equations 2.11 and 2.30 may be written in matrix form as

$$\frac{\partial}{\partial t} \begin{Bmatrix} Q \\ H \end{Bmatrix} = - \left[\mathbf{B}(Q, H) \right] \frac{\partial}{\partial x} \begin{Bmatrix} Q \\ H \end{Bmatrix} - \left[\mathbf{G}(Q, H) \right]$$

in which

$$\mathbf{B} = \begin{bmatrix} 0 & gA \\ \dfrac{a^2}{gA} & 0 \end{bmatrix} \tag{2.31}$$

and

$$\mathbf{G} = \begin{Bmatrix} \dfrac{f Q |Q|}{2DA} \\ 0 \end{Bmatrix} \tag{2.32}$$

The eigenvalues, λ, of matrix $\mathbf{B}$ determine the type of the set of equations. The characteristic equation[10] of matrix $\mathbf{B}$ is

$$\lambda^2 - a^2 = 0 \tag{2.33}$$

Hence,

$$\lambda = \pm a \tag{2.34}$$

Since a is real, both eigenvalues are real and distinct, and hence Eqs. 2.11 and 2.33 form a set of hyperbolic partial differential equations.

2.5 METHODS FOR SOLVING CONTINUITY AND DYNAMIC EQUATIONS

As demonstrated previously, the dynamic and continuity equations are quasi-linear, hyperbolic, partial differential equations. A closed-form solution of these equations is impossible. However, by neglecting or linearizing the nonlinear terms, various graphical[7,11,12] and analytical[13–15] methods have been developed. These methods are approximate and cannot be used to analyze large systems or systems having complex boundary conditions. Although some of these methods have been programmed for analysis on a digital computer,[16,17] they are not presented herein because their programming is difficult. We will discuss techniques that are more suitable for computer analysis, such as the implicit finite-difference method[18] and the method of characteristics.[8,18–24]

In the implicit finite-difference method, the partial derivatives are replaced by finite differences, and the resulting algebraic equations for the whole system are then solved simultaneously. Depending upon the size of the system, this involves a simultaneous solution of a large number of nonlinear equations. The analysis by this method becomes even more complicated in systems having complex boundary conditions, which must be solved by an iterative technique. The method has the advantage that it is unconditionally stable. Therefore, larger time steps can be used, which results in economizing computer time. However, the time step cannot be increased arbitrarily because it results in smoothing the pressure peaks. Details of this method are presented in Section 6.7.

In the method of characteristics, the partial differential equations are first converted into ordinary differential equations, which are then solved by an explicit finite-difference technique. Because each boundary condition and each conduit section are analyzed separately during a time step, this method is particularly suitable for systems with complex boundary conditions. The disadvantage of this method is that small time steps must be used to satisfy the Courant condition[18] for stability. To overcome this, a combination of the implicit finite difference and the method of characteristics[23] may be used. This is discussed in detail in Chapter 3.

2.6 VELOCITY OF WATERHAMMER WAVES

An expression for the velocity of waterhammer waves in a rigid conduit was derived in Section 1.2. However, in addition to the bulk modulus of elasticity,

K, of the fluid, the velocity of waterhammer waves depends upon the elastic properties of the conduit, as well as on the external constraints. Elastic properties include the conduit size, wall thickness, and wall material; the external constraints include the type of supports and the freedom of conduit movement in the longitudinal direction. The bulk modulus of elasticity of a fluid depends upon its temperature, pressure, and the quantity of undissolved gases. Pearsall[25] has shown that the wave velocity changes by about 1 percent per 5°C. The fluid compressibility is increased by the presence of free gases, and it has been found[25] that 1 part of air in 10,000 parts of water by volume reduces the wave velocity by about 50 percent.*

Solids in liquids have similar but less drastic influence, unless they are compressible. Laboratory[9] and prototype tests[25] have shown that the dissolved gases tend to come out of solution when the pressure is reduced, even when it remains above the vapor pressure. This causes a significant reduction in the wave velocity. Therefore, the wave velocity for a positive wave may be higher than that of a negative wave. Further prototype tests are needed to quantify the reduction in the wave velocity due to reduction of pressures.

Halliwell[26] presented the following general expression for the wave velocity:

$$a = \sqrt{\frac{K}{\rho[1 + (K/E)\,\psi]}} \tag{2.35}$$

in which ψ is a nondimensional parameter that depends upon the elastic properties of the conduit; E = Young's modulus of elasticity of the conduit walls; and K and ρ are the bulk modulus of elasticity and density of the fluid, respectively. The moduli of elasticity of commonly used materials for conduit walls and the bulk moduli of elasticity and mass densities of various liquids are listed in Tables 2.1 and 2.2.

Expressions for ψ for various conditions are as follows:

1. *Rigid Conduits*

$$\psi = 0 \tag{2.36}$$

2. *Thick-Walled Elastic Conduits*
   a. Conduit anchored against longitudinal movement throughout its length

$$\psi = 2(1 + \nu)\frac{R_o^2 + R_i^2}{R_o^2 - R_i^2} - \frac{2\nu R_i^2}{R_o^2 - R_i^2} \tag{2.37}$$

in which ν = the Poisson's ratio and R_o and R_i = the external and internal radii of the conduit.

*For a derivation of expressions for the wave velocity in gas-liquid mixtures, see Section 9.5.

Table 2.1. Young's modulus of elasticity and Poisson's ratio for various pipe materials.*

Material	Modulus of Elasticity, E** (GPa)	Poisson's Ratio
Aluminum alloys	68–73	0.33
Asbestos cement, transite	24	
Brass	78–110	0.36
Cast iron	80–170	0.25
Concrete	14–30	0.1–0.15
Copper	107–131	0.34
Glass	46–73	0.24
Lead	4.8–17	0.44
Mild steel	200–212	0.27
Plastics		
ABS	1.7	0.33
Nylon	1.4–2.75	
Perspex	6.0	0.33
Polyethylene	0.8	0.46
Polystyrene	5.0	0.4
PVC rigid	2.4–2.75	
Rocks		
Granite	50	0.28
Limestone	55	0.21
Quartzite	24.0–44.8	
Sandstone	2.75–4.8	0.28
Schist	6.5–18.6	

*Compiled from Refs. 12, 25, and 31.
**To convert E into lb/in.^{2}, multiply the values given in this column by 145.038×10^3.

b. Conduit anchored against longitudinal movement at the upper end

$$\psi = 2\left[\frac{R_o^2 + 1.5R_i^2}{R_o^2 - R_i^2} + \frac{\nu(R_o^2 - 3R_i^2)}{R_o^2 - R_i^2}\right] \tag{2.38}$$

c. Conduit with frequent expansion joints

$$\psi = 2\left(\frac{R_o^2 + R_i^2}{R_o^2 - R_i^2} + \nu\right) \tag{2.39}$$

3. *Thin-Walled Elastic Conduits*

a. Conduit anchored against longitudinal movement throughout its length

$$\psi = \frac{D}{e}(1 - \nu^2) \tag{2.40}$$

in which D = conduit diameter and e = wall thickness.

Table 2.2. Bulk modulus of elasticity and density of common liquids at atmospheric pressure.*

Liquid	Temperature (°C)	Density, ρ† (kg/m^3)	Bulk Modulus of Elasticity, K‡ (GPa)
Benzene	15	880	1.05
Ethyl alcohol	0	790	1.32
Glycerin	15	1,260	4.43
Kerosine	20	804	1.32
Mercury	20	13,570	26.2
Oil	15	900	1.5
Water, fresh	20	999	2.19
Water, sea	15	1,025	2.27

*Compiled from Refs. 12, 25, 32, and 33.
†To determine the specific weight of the liquid, in lb$_f$/ft^3, multiply the values given in this column by 62.427×10^{-3}.
‡To convert K into lb/in.^{2}, multiply the values given in this column by 145.038×10^3.

b. Conduit anchored against longitudinal movement at the upper end

$$\psi = \frac{D}{e}(1.25 - \nu) \tag{2.41}$$

c. Conduit with frequent expansion joints

$$\psi = \frac{D}{e} \tag{2.42}$$

4. *Tunnels Through Solid Rock*

Halliwell[26] has derived long expressions for ψ for lined and unlined rock tunnels. Usually, the rock characteristics cannot be precisely estimated because of nonhomogeneous rock conditions and because of the presence of fissures. Therefore, in our opinion, using Halliwell's expressions for practical applications is unwarranted. Instead, the following expressions based on Parmakian's equations[7] may be used.

a. Unlined tunnel

$$\left.\begin{aligned}\psi &= 1\\ E &= G\end{aligned}\right\} \tag{2.43}$$

in which G = modulus of rigidity of the rock.

b. Steel-lined tunnel

$$\psi = \frac{DE}{GD + Ee} \tag{2.44}$$

in which e = thickness of the steel liner and E = modulus of elasticity of steel.

5. *Reinforced Concrete Pipes*

The reinforced concrete pipe is replaced by an equivalent steel pipe having equivalent thickness[7]

$$e_e = E_r e_c + \frac{A_s}{l_s} \tag{2.45}$$

in which e_c = thickness of the concrete pipe; A_s and l_s are the cross-sectional area and the spacing of steel bars, respectively; and E_r = ratio of the modulus of elasticity of concrete to that of steel. Usually the value of E_r varies from 0.06 to 0.1. However, to allow for any cracks in the concrete pipe, a value of 0.05 is suggested.[7] Having computed e_e, the wave velocity may be determined from Eq. 2.35 using the modulus elasticity of steel.

6. *Wood-Stave Pipes*

The thickness of a uniform steel pipe equivalent to the wood-stave pipe is determined[7] from Eq. 2.45 using $E_r = \frac{1}{60}$, e_c = thickness of wood staves, and A_s and l_s are the cross-sectional area and the spacing of the steel bands, respectively. The wave velocity is then computed from Eq. 2.35.

7. *Polyvinyl Chloride (PVC) and Reinforced Plastic Pipe*

Investigations reported in Ref. 27 show that Eq. 2.35 can be used for computing wave velocity in the polyvinyl chloride (PVC) and reinforced plastic pipes, provided a proper value of the modulus of elasticity for the wall material is used.

8. *Noncircular Conduits*

The following expression for ψ is obtained from the equation for the wave velocity in the *thin-walled rectangular conduits* derived by Jenkner[28] by using the steady-state bending theory and by allowing the corners of the conduit to rotate:

$$\psi = \frac{\beta b^4}{15 e^3 d} \tag{2.46}$$

in which $\beta = 0.5(6 - 5\alpha) + 0.5(d/b)^3[6 - 5(b/d)^2]$, $\alpha = [1 + (d/b)^3]/[1 + (d/b)]$, b = width of the conduit (longer side), and d = depth of the conduit (shorter side).

Thorley and Guymer[29] have included the influence of the shear force on the bending deflection of the thick-walled ($l/e < 20$) rectangular conduits while deriving the equations for the wave velocity. From these equations, the following expression is obtained for a *thick-walled conduit having a square cross section:*

$$\psi = \frac{1}{15}\left(\frac{l}{e}\right)^3 + \frac{l}{e}\left(1 + \frac{E}{2G}\right) \tag{2.47}$$

in which e = wall thickness, $(l - e)$ = inside dimension of the conduit, and G = shear modulus of the wall material.

Based on the equations presented by Thorley and Twyman,[30] the following expression is obtained for ψ for a *thin-walled hexagonal conduit:*

$$\psi = 0.0385\left(\frac{l}{e}\right)^3 \tag{2.48}$$

in which l = mean width of one of the flat sides of the hexagonal section.

2.7 CASE STUDY

The data for the steel penstock of the Kootenay Canal hydroelectric power plant, owned and operated by British Columbia Hydro and Power Authority, are listed in the following table:

Pipe No.	Length (m)	Diameter (m)	Wall Thickness, (mm)	Remarks
1	244.	6.71	19	Expansion coupling at one end
2	36.5	5.55	22	Encased in concrete

For conducting a transient analysis, the waterhammer wave velocity in each section of the penstock was determined as follows. The values of E for steel, G for concrete, and K and ρ for water were taken as 207 GPa, 20.7 GPa, 2.19 GPa, and 999 kg/m^3, respectively.

Pipe No. 1

$$\frac{D}{e} = \frac{6.71}{0.019} = 353$$

As the pipe is anchored at one end,

$$\psi = \frac{D}{e}(1.25 - \nu) \qquad \text{(Eq. 2.41)}$$

$$= 353(1.25 - 0.30)$$

$$= 335.4$$

$$a = \sqrt{\frac{K}{\rho[1 + (K/E)\psi]}} \qquad \text{(Eq. 2.35)}$$

$$\frac{K}{E} = \frac{2.19}{207} = 0.0106$$

$$a = \sqrt{\frac{2.19 \times 10^9}{999(1 + 0.0106 \times 335.4)}}$$

$$= 694 \text{ m/s.}$$

Pipe No. 2

Equations for a steel-lined tunnel may be used to compute the wave velocity in pipe No. 2.

$$\psi = \frac{D E}{G D + E e} \qquad \text{(Eq. 2.44)}$$

$$= \frac{5.55 \times 207 \times 10^9}{20.7 \times 10^9 \times 5.55 + 207 \times 10^9 \times .022}$$

$$= 9.62$$

$$a = \sqrt{\frac{2.19 \times 10^9}{999(1 + 0.0106 \times 9.62)}}$$

$$= 1410 \text{ m/s.}$$

2.8 SUMMARY

In this chapter, the derivation of the dynamic and continuity equations were presented, and the assumptions used in these derivations were discussed. It was demonstrated that these equations are quasi-linear, hyperbolic, partial differential equations, and various methods available for their solution were discussed. Expressions for the velocity of waterhammer waves in the closed conduits were presented.

PROBLEMS

2.1. Derive the dynamic equation considering the conduit is inclined at angle θ to the horizontal.

2.2. Compute the velocity of waterhammer waves in a 3.05-m-diameter steel penstock having a wall thickness of 25 mm if it:

1. is embedded in a concrete dam
2. is anchored at the upstream end
3. has expansion joints throughout its length.

2.3. Determine the velocity of waterhammer waves in a reinforced concrete pipe having 1.25-m diameter, 0.15-m wall thickness, and carrying water. The 20-mm reinforcing bars have a spacing of 0.5 m, and the pipe has expansion joints throughout its length.

2.4. A 0.2-m-diameter copper pipe having a wall thickness of 25 mm is conveying kerosene oil at 20°C from a container to a valve. If the valve is closed instantly, at what velocity would the pressure waves propagate in the pipe? Assume the pipe is anchored at the upper end.

2.5. Figure 5.10 shows the power conduits of an underground hydroelectric power station. Compute the wave velocity in each section of the conduit. Assume modulus of rigidity of rock = 5.24 GPa.

ANSWERS

2.2.
1. 1413 m/s
2. 992 m/s
3. 978 m/s

2.3. 913 m/s

2.4. 1232 m/s

REFERENCES

1. Streeter, V. L., *Fluid Mechanics*, Third Edition, McGraw-Hill Book Co., New York, 1966.
2. Streeter, V. L. (ed.), *Handbook of Fluid Dynamics*, McGraw-Hill Book Co., New York, 1961.
3. Rouse, H. (ed.), *Advanced Mechanics of Fluids*, John Wiley & Sons, Inc., New York, 1959.
4. Timoshenko, S., *Strength of Materials*, Second Edition, Part 2, Van Nostrand Co., Inc., New York, 1941.
5. Zielke, W., "Frequency-Dependent Friction in Transient Pipe Flow," *Jour. Basic Engineering, Amer. Soc. Mech. Engrs.*, March 1968.

6. Hirose, M., "Frequency-Dependent Wall Shear in Transient Fluid Flow Simulation of Unsteady Turbulent Flow," *Master's Thesis*, Massachusetts Institute of Technology, Mass., 1971.
7. Parmakian, J., *Waterhammer Analysis*, Dover Publications, Inc., New York, 1963.
8. Evangelisti, G., "Waterhammer Analysis by the Method of Characteristics," *L'Energia Elettrica*, Nos. 10-12, 1969, pp. 673-692, 759-770, 839-858.
9. Streeter, V. L., "Numerical Methods for Calculation of Transient Flow," *Proc., First International Conference on Pressure Surges*, Canterbury, England, published by British Hydromechanic Research Association, Cranfield, England, Sept. 1972, pp. A1-1-A1-11.
10. Wylie, C. R., *Advanced Engineering Mathematics*, Third Edition, McGraw-Hill Book Co., New York, 1967.
11. Bergeron, L., *Waterhammer in Hydraulics and Wave Surges in Electricity*, John Wiley & Sons, Inc., New York, 1961.
12. Pickford, J., *Analysis of Surge*, Macmillan and Co. Ltd., London, 1969.
13. Allievi, L., "Theory of Waterhammer," translated by E. E. Halmos, Ricardo Garoni, Rome, 1925.
14. Rich, G. R., *Hydraulic Transients*, Dover Publications, Inc., New York, 1963.
15. Wood, F. M., "The Application of Heavisides Operational Calculus to the Solution of Problems in Waterhammer," *Trans. Amer. Soc. Mech. Engrs.*, vol. 59, Nov. 1937, pp. 703-713.
16. Harding, D. A., "A Method of Programming Graphical Surges in Pipelines," *Proc. Institution of Mech. Engrs.*, London, Nov. 2-3, 1965, vol. 180, Part 3E, pp. 83-97.
17. Enever, K. J., "The Use of the Computerized Graphical Method of Surge Analysis with particular Reference to a Water Supply Problem," *Symp. on Pressure Transients*, The City University, London, Nov. 25, 1970.
18. Perkins, F. E., Tedrow, A. C., Eagleson, P. S., and Ippen, A. T., "Hydro-power Plant Transients," Part II and III, Dept. of Civil Engineering, Hydrodynamics Lab., Report No. 71, Massachusetts Institute of Technology, Sept. 1964.
19. Lister, M., "The Numerical Solution of Hyperbolic Partial Differential Equations by the Method of Characteristics," in Ralson, A., and Wilf, H. S. (eds.), *Mathematical Method for Digital Computers*, John Wiley & Sons, Inc., New York, 1960, pp. 165-179.
20. Abbott, M. B., *An Introduction to the Method of Characteristics*, American Elsevier, New York, 1966.
21. Streeter, V. L. and Lai, C., "Waterhammer Analysis Including Fluid Friction," *Jour. Hydraulics Div., Amer. Soc. Civil Engrs.*, vol. 88, No. HY3, May 1962, pp. 79-112.
22. Streeter, V. L. and Wylie, E. B., *Hydraulic Transients*, McGraw-Hill Book Co., New York, 1967, pp. 22-52.
23. Streeter, V. L., "Waterhammer Analysis," *Jour., Hydraulics Div., Amer. Soc. Civil Engrs.*, vol. 95, No. HY6, Nov. 1969, pp. 1959-1971.
24. Evangelisti, G., Boari, M., Guerrini, P., and Rossi, R., "Some Applications of Waterhammer Analysis by the Method of Characteristics," *L'Energia Elettrica*, Nos. 1 and 6, 1973, pp. 1-12, 309-324.
25. Pearsall, I. S., "The Velocity of Waterhammer Waves," *Proc. Symposium on Surges in Pipelines, Inst. of Mech. Engrs.*, England, vol. 180, Part 3E, Nov. 1965, pp. 12-27.
26. Halliwell, A. R., "Velocity of a Waterhammer Wave in an Elastic Pipe," *Jour., Hydraulics Div., Amer. Soc. Civil Engrs.*, vol. 89, No. HY4, July 1963, pp. 1-21.
27. Watters, G. Z., Jeppson, R. W., and Flammer, G. H., "Water Hammer in PVC and Reinforced Plastic Pipe," *Jour., Hyd. Div., Amer. Soc. Civil Engrs.*, vol. 102, July 1976, pp. 831-843. (See also Discussion by Goldberg, D. E., and Stoner, M. A., June 1977.)

28. Jenkner, W. R., "Über die Druckstossgeschwindigkeit in Rohrleitungen mit quadratischen und rechteckigen Querschnitten," *Schweizerische Bauzeitung*, vol. 89, Feb. 1971, pp. 99-103.
29. Thorley, A. R. D. and Guymer, G., "Pressure Surge Propagation in Thick-Walled Conduits of Rectangular Cross Section," *Jour. Fluid Engineering, Amer. Soc. Mech. Engrs.*, vol. 98, Sept. 1976, pp. 455-460.
30. Thorley, A. R. D. and Twyman, J. W. R., "Propagation of Transient Pressure Waves in a Sodium-Cooled Fast Reactor," *Proc. Second Conf. on Pressure Surges*, London, published by British Hydromechanic Research Assoc., 1977.
31. Roark, R. J., *Formulas for Stress and Strain*, 4th ed., McGraw-Hill Book, New York, 1965.
32. *Hydraulic Models*, Manual of Engineering Practice No. 25, Committee of Hyd. Div. on Hyd. Research, Amer. Soc. Civil Engineers, July 1942.
33. Baumeister, T. (ed.), *Standard Handbook for Mechanical Engineers*, 7th ed., McGraw-Hill Book Co., New York, 1967.

ADDITIONAL REFERENCES

Joukowsky, N., "Waterhammer," Translated by O. Simin, *Proc. Amer. Water Works Assoc.*, vol. 24, 1904, pp. 341-424.

Kennison, H. F., "Surge-Wave Velocity–Concrete Pressure Pipe," *Trans. Amer. Soc. Mech. Engrs.*, Aug. 1956, pp. 1323-1328.

Tison, G., "Permanente en niet-permanente stromingen door leidingen in Kunststof," *Thesis* presented to the University of Ghent, Ghent, Belgium, in partial fulfillment of the requirements for the degree of doctor of engineering, 1960.

Mock, F. J., "Modellbehandlung von Druckstossprobleme mit Hilfe von Kunststoffrohren," Mitteilung No. 56, Institut fur Wasserbau and Wasserwirtschaft, Technical University, Berlin 1962.

Rahm, S. L. and Lindvall, G. K. E., "A Laboratory Investigation of Transient Pressure Waves in Pre-Stressed Concrete Pipes," *Proc. 10th International Assoc. for Hydraulic Research*, London, 1963, pp. 47-53.

Swaminathan, K. V., "Waterhammer Wave Velocity in Concrete Tunnels," *Water Power*, March 1965, 117-121.

Thorley, A. R. D., "Pressure Transients in Hydraulics Pipelines," *Amer. Soc. Mech. Engrs.*, Paper No. 68-WA/FE-2, Dec. 1968, 8 pp.

Swaffield, J. A., "The Influence of Bends on Fluid Transients Propagated in Incompressible Pipe Flow," *Proc. Institution of Mech. Engrs.*, vol. 183, Part 1, No. 29, 1968-69, pp. 603-614.

Wood, D. J. and Funk, J. E., "A Boundary-Layer Theory for Transient Viscous Losses in Turbulent Flow," *Jour. Basic Engineering, Trans. Amer. Soc. Mech. Engrs.*, Series D, vol. 92, No. 4, Dec. 1970, pp. 865-873.

Weyler, M. E., Streeter, V. L., and Larsen, P. S., "An Investigation of the Effect of Cavitation Bubble on the Momentum Loss in Transient Pipe Flow," *Jour. Basic Engineering, Amer. Soc. Mech. Engrs.*, March 1971, pp. 1-10.

Safwat, H. H., "Measurements of Transient Flow Velocities for Waterhammer Applications," *Amer. Soc. of Mech. Engrs.*, Paper No. 71-FE-29, May 1971, 8 pp.

Trikha, A. K., "An Efficient Method for Simulating Frequency-Dependent Friction in Transient Liquid Flow," *Jour., Fluid Engineering, Amer. Soc. Mech. Engrs.*, vol. 97, March 1975, pp. 97-105.

CHAPTER 3

METHOD OF CHARACTERISTICS

3.1 INTRODUCTION

In the last chapter, it was demonstrated that the equations describing the transient-state flow in closed conduits are hyperbolic, partial differential equations, and a number of methods available for their solution were discussed. The details of the method of characteristics are presented in this chapter. The equations for simulating a conduit are derived, and the boundary conditions for a number of simple end conditions are developed. The stability and convergence criteria for the stability of the finite-difference scheme are then presented, and a procedure for the analysis of piping systems is outlined. The chapter concludes with the presentation of a case study.

We will endeavor to keep the derivation of the equations free of advanced mathematics. Readers having an elementary knowledge of partial differential equations should be able to follow the development of these equations; those interested in a rigorous treatment should refer to Refs. 1 through 9. In deriving these equations, we will follow the general approach proposed by Lister[11] and later adopted by Streeter and Wylie.[10] A number of innovations presented by Evangelisti[2] will also be outlined.

3.2 CHARACTERISTIC EQUATIONS

To facilitate discussion, let us rewrite the dynamic and continuity equations (Eqs. 2.11 and 2.30) derived in the last chapter as

$$L_1 = \frac{\partial Q}{\partial t} + gA\frac{\partial H}{\partial x} + \frac{f}{2DA}Q|Q| = 0 \tag{3.1}$$

$$L_2 = a^2\frac{\partial Q}{\partial x} + gA\frac{\partial H}{\partial t} = 0 \tag{3.2}$$

Let us consider a linear combination of Eqs. 3.1 and 3.2, i.e.,

$$L = L_1 + \lambda L_2$$

or

$$\left(\frac{\partial Q}{\partial t} + \lambda a^2\frac{\partial Q}{\partial x}\right) + \lambda gA\left(\frac{\partial H}{\partial t} + \frac{1}{\lambda}\frac{\partial H}{\partial x}\right) + \frac{f}{2DA}Q|Q| = 0 \tag{3.3}$$

If $H = H(x, t)$ and $Q = Q(x, t)$ are solutions of Eqs. 3.1 and 3.2, then the total derivatives may be written as

$$\frac{dQ}{dt} = \frac{\partial Q}{\partial t} + \frac{\partial Q}{\partial x}\frac{dx}{dt} \tag{3.4}$$

and

$$\frac{dH}{dt} = \frac{\partial H}{\partial t} + \frac{\partial H}{\partial x}\frac{dx}{dt} \tag{3.5}$$

By defining the unknown multiplier λ as

$$\frac{1}{\lambda} = \frac{dx}{dt} = \lambda a^2 \tag{3.6}$$

or

$$\lambda = \pm\frac{1}{a} \tag{3.7}$$

and by using Eqs. 3.4 and 3.5, Eq. 3.3 can be written as

$$\frac{dQ}{dt} + \frac{gA}{a}\frac{dH}{dt} + \frac{f}{2DA}Q|Q| = 0 \tag{3.8}$$

if

$$\frac{dx}{dt} = a \tag{3.9}$$

and

$$\frac{dQ}{dt} - \frac{gA}{a}\frac{dH}{dt} + \frac{f}{2DA}Q|Q| = 0 \tag{3.10}$$

if

$$\frac{dx}{dt} = -a \tag{3.11}$$

Note that Eq. 3.8 is valid if Eq. 3.9 is satisfied and that Eq. 3.10 is valid if Eq. 3.11 is satisfied. In other words, by imposing the relations given by Eqs. 3.9 and 3.11, we have converted the partial differential equations (Eqs. 3.1 and 3.2) into ordinary differential equations in the independent variable t.

In the x-t plane, Eqs. 3.9 and 3.11 represent two straight lines having slopes $\pm 1/a$. These are called *characteristic lines*. Mathematically, these lines divide the x-t plane into two regions, which may be dominated by two different kinds of solution, i.e., the solution may be discontinuous along these lines.[9] Physically, they represent the path traversed by a disturbance. For example, a disturbance at point A (Fig. 3.1) at time t_o would reach point P after time Δt.

Prior to presenting a procedure for solving Eqs. 3.8 and 3.10, let us first discuss the physical significance of characteristic lines in the x-t plane. To facilitate discussion, let us consider a single pipeline shown in Fig. 3.2. The *compatibility equations* (Eqs. 3.8 and 3.10) are valid along the pipe length (i.e., for $0 < x < L$) and special *boundary conditions* are required at the ends (i.e., at $x = 0$ and at $x = L$) (Fig. 3.3). In the example under consideration, there is a constant-head reservoir at the upper end (at $x = 0$) and a valve at the downstream end (at $x = L$), and the transient conditions are produced by closing the valve. Let us assume that there is steady flow in the pipe at time $t = 0$ when the valve is instantaneously closed. This reduces the flow through the valve to zero and results in a pressure rise at the valve. Because of this pressure rise, a pressure wave travels in the upstream direction. If the path of this wave is plotted on the x-t plane, it will be represented by line BC as shown in Fig. 3.4. It is clear from this figure that the conditions in Region I depend only upon the initial conditions because the upstream boundary conditions did not change, whereas in Region II they depend upon the conditions imposed by the downstream boundary. Thus, the characteristic line BC separates the two types of solutions. If excitations are imposed simultaneously at points A and B, then the region influenced by the initial conditions is as shown in Fig. 3.5; the characteristic line AC separates the regions

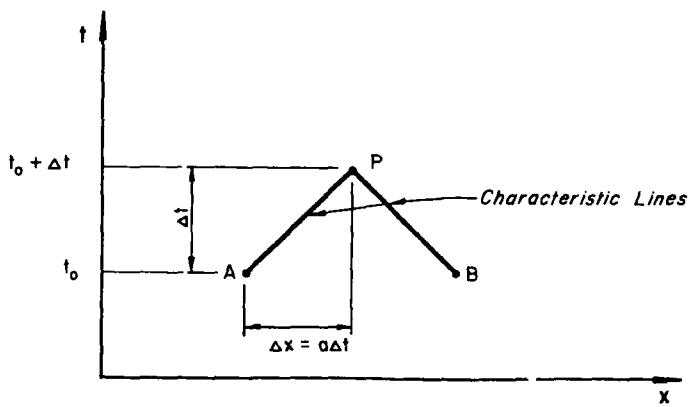

Figure 3.1. Characteristic lines in x-t plane.

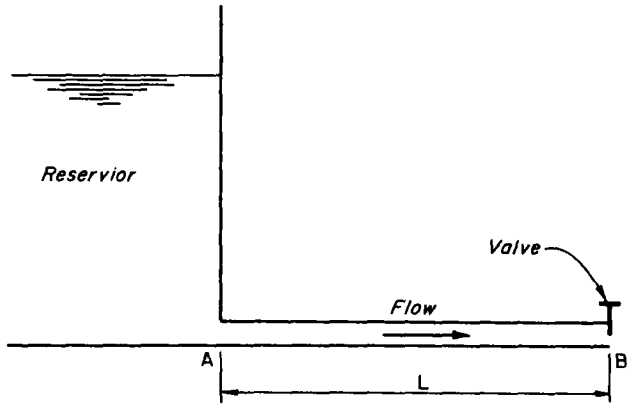

Figure 3.2. Single pipeline.

influenced by the upstream boundary and the initial conditions, and the line BC separates the regions influenced by the downstream boundary and the initial conditions. In other words, the characteristic lines on the x-t plane represent the traveling paths of perturbations initiated at various locations in the system.

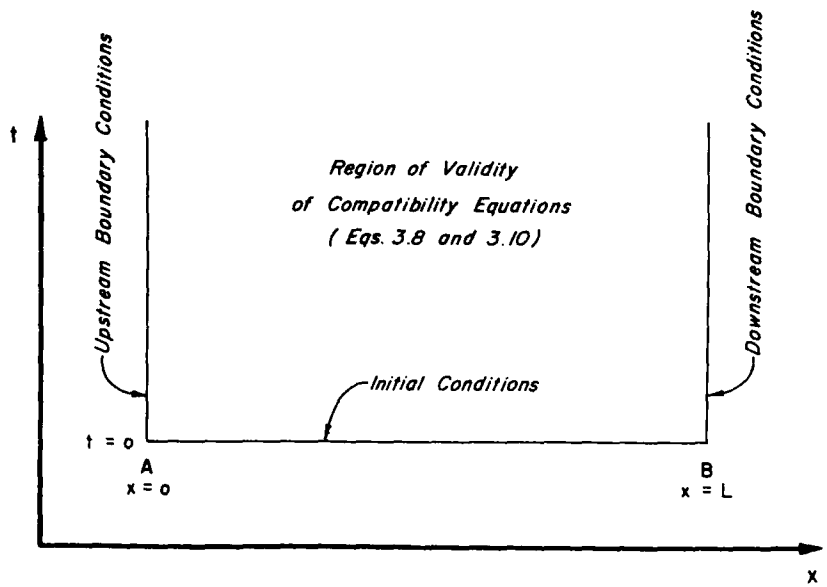

Figure 3.3. Regions of validity for a single pipeline.

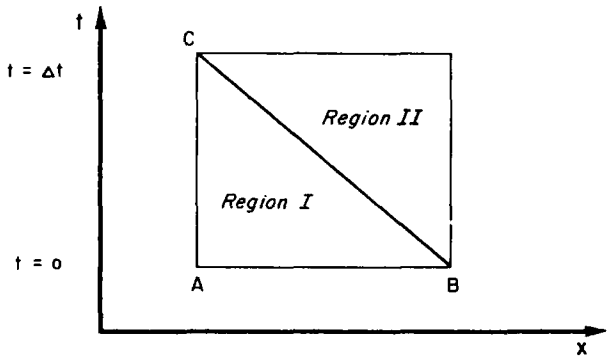

Figure 3.4. Excitation at downstream end.

To solve Eqs. 3.8 through 3.11, a number of finite-difference schemes have been proposed: Streeter and Wylie[10] use a first-order finite-difference technique; Evangelisti[2] suggests a predictor-corrector method; and Lister[11] employs both first- and second-order finite-difference schemes. Because the time intervals used in solving these equations for practical problems are usually small, a first-order technique suggested by Streeter and Wylie is sufficiently accurate and is discussed here. However, if the friction losses are large, then a first-order approximation may yield unstable results. For such cases, a predictor-corrector method or a second-order approximation (see Section 7.4) should be used to avoid instability of the finite-difference scheme.

Referring to Fig. 3.1, let the conditions at time $t = t_o$ be known. These are either initially known (i.e., at $t = 0$, these are initial steady-state conditions) or have been calculated for the previous time step. We want to compute the unknown conditions at $t_o + \Delta t$. Referring to Fig. 3.1, we can write along the positive characteristic line AP,

$$dQ = Q_P - Q_A \tag{3.12}$$

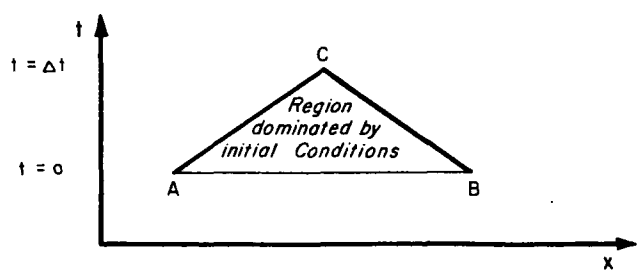

Figure 3.5. Excitation at upstream and downstream ends.

$$dH = H_P - H_A \tag{3.13}$$

Similarly, we can write along the negative characteristic line BP.

$$dQ = Q_P - Q_B \tag{3.14}$$

$$dH = H_P - H_B \tag{3.15}$$

The subscripts in Eqs. 3.12 through 3.15 refer to the locations on the x-t plane. Substituting Eqs. 3.12 and 3.13 into Eq. 3.8 and Eqs. 3.14 and 3.15 into Eq. 3.10, computing the friction term at the points A and B, and multiplying throughout by Δt, we obtain

$$(Q_P - Q_A) + \frac{gA}{a}(H_P - H_A) + \frac{f\Delta t}{2DA} Q_A|Q_A| = 0 \tag{3.16}$$

and

$$(Q_P - Q_B) - \frac{gA}{a}(H_P - H_B) + \frac{f\Delta t}{2DA} Q_B|Q_B| = 0 \tag{3.17}$$

Equation 3.16 can be written as

$$Q_P = C_p - C_a H_P \tag{3.18}$$

and Eq. 3.17 as

$$Q_P = C_n + C_a H_P \tag{3.19}$$

in which

$$C_p = Q_A + \frac{gA}{a} H_A - \frac{f\Delta t}{2DA} Q_A|Q_A| \tag{3.20}$$

$$C_n = Q_B - \frac{gA}{a} H_B - \frac{f\Delta t}{2DA} Q_B|Q_B| \tag{3.21}$$

and

$$C_a = \frac{gA}{a} \tag{3.22}$$

Note that Eq. 3.18 is valid along the positive characteristic line AP and Eq. 3.19 along the negative characteristic line BP. The values of the *constants* C_p and C_n are known for each time step, and the constant C_a depends upon the conduit properties. We will refer to Eq. 3.18 as the *positive characteristic equation* and Eq. 3.19 as the *negative characteristic equation*. In Eqs. 3.18 and 3.19, we have two unknowns, namely, H_P and Q_P. The values of these unknowns can be determined by simultaneously solving these equations, i.e.,

$$Q_P = 0.5(C_p + C_n) \tag{3.23}$$

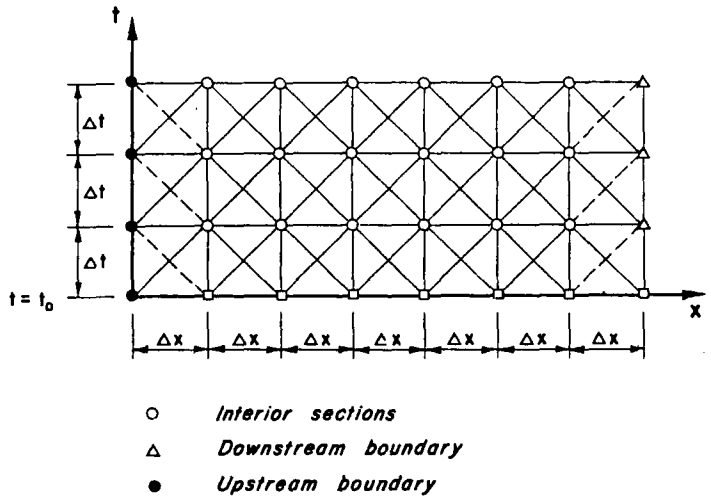

Figure 3.6. Characteristic grid.

Now the value of H_P can be determined either from Eq. 3.18 or Eq. 3.19. Thus, by using Eqs. 3.18 and 3.23, conditions at all interior points (see Fig. 3.6) at the end of the time step can be determined. However, at the boundaries, either Eq. 3.18 or 3.19 is available. Therefore, as discussed above, we need special boundary conditions to determine the condition at the boundaries at time $t_o + \Delta t$.

To illustrate how to use the above equations, we will again consider the single pipeline of Fig. 3.2. The pipeline is divided into n equal reaches (Fig. 3.6), and the steady-state conditions at the grid points at $t = t_o$ are first obtained. Then, to determine the conditions at $t = t_o + \Delta t$, Eqs. 3.18 and 3.23 are used for the interior points, and special boundary conditions are used for the end conditions. A close look at Fig. 3.6 shows that the conditions at the boundaries at $t = t_o + \Delta t$ must be known for calculating the conditions at $t = t_o + 2\Delta t$ at the interior points adjacent to the boundaries. Now conditions at $t = t_o + \Delta t$ are known at all the grid points, and the conditions at $t = t_o + 2\Delta t$ are determined by following the procedure just outlined. In this manner, the computations proceed step-by-step until transient conditions for the required time are determined.

3.3 BOUNDARY CONDITIONS

In the last section we discussed that special boundary conditions are required to determine the conditions at the boundaries. These are developed by solving Eq. 3.18, 3.19, or both, and the conditions imposed by the boundary. Equation

3.18 is used for the downstream boundaries and Eq. 3.19 for the upstream boundaries.

A number of simple boundary conditions are developed in this section while complex boundary conditions such as for pumps and turbines are derived in Chapter 4 and 5 and for waterhammer control devices, in Chapter 10.

Constant-Head Reservoir at Upstream End (Fig. 3.7)

If the entrance losses as well as the velocity head are negligible, then

$$H_P = H_{res} \tag{3.24}$$

in which H_{res} = height of the reservoir water surface above the datum. Equation 3.19 for the upper end thus becomes

$$Q_P = C_n + C_a H_{res} \tag{3.25}$$

However, if the velocity head or the entrance losses are not small, then these may be considered in the analysis as follows:

Let the entrance losses be given by the equation

$$h_e = \frac{kQ_P^2}{2gA^2} \tag{3.26}$$

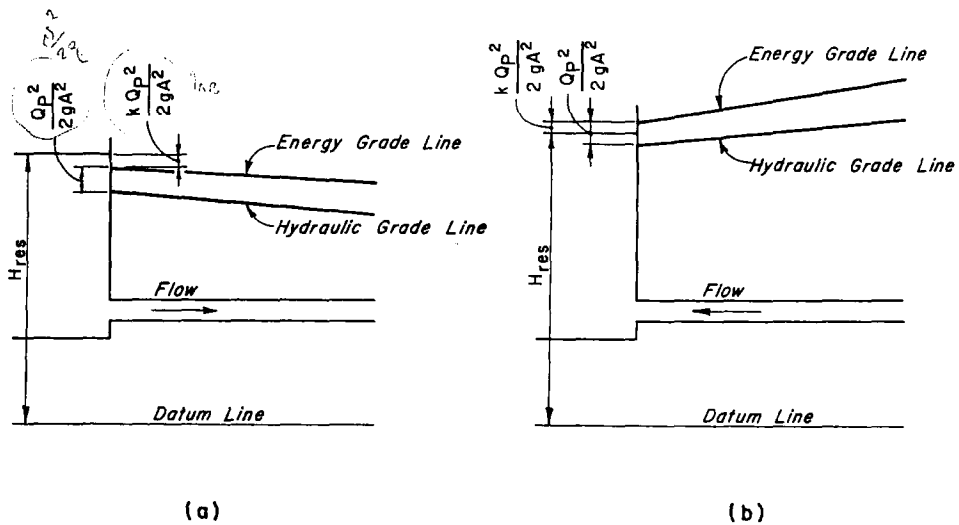

Figure 3.7. Constant-level upstream reservoir.

in which k is the coefficient of entrance loss. Referring to Fig. 3.7,

$$H_P = H_{res} - (1 + k)\frac{Q_P^2}{2gA^2} \tag{3.27}$$

Solving Eq. 3.27 and the negative characteristic equation (Eq. 3.19) simultaneously,

$$Q_P = \frac{-1 + \sqrt{1 + 4k_1(C_n + C_a H_{res})}}{2k_1} \tag{3.28}$$

in which

$$k_1 = \frac{C_a(1 + k)}{(2gA^2)} \tag{3.29}$$

Now H_P can be determined from Eq. 3.27.

For the reverse flow, k is assigned a negative value in Eqs. 3.27 and 3.29.

Constant-Head Reservoir at Downstream End (Fig. 3.8)

If the head losses at the entrance to the reservoir are

$$h_e = \frac{kQ_P^2}{2gA^2} \tag{3.30}$$

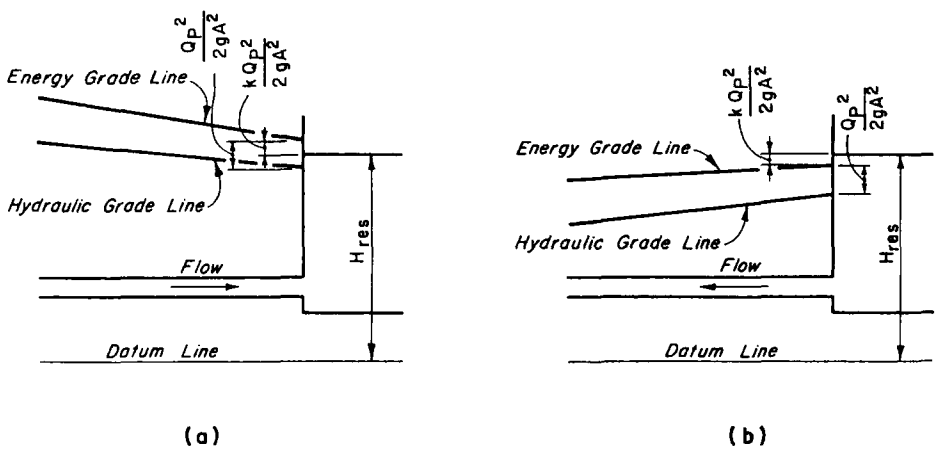

Figure 3.8. Constant-level downstream reservoir.

then referring to Fig. 3.8a

$$H_P = H_{res} - (1 - k)\frac{Q_P^2}{2gA^2} \tag{3.31}$$

In Eq. 3.30, k is assigned a negative value for the reverse flow.

Elimination of H_P from Eqs. 3.31 and 3.18 yields

$$k_2 Q_P^2 - Q_P + k_3 = 0 \tag{3.32}$$

in which

$$\left.\begin{aligned} k_2 &= \frac{C_a(1 - k)}{2gA^2} \\ \text{and} \\ k_3 &= C_p - C_a H_{res} \end{aligned}\right\} \tag{3.33}$$

Solving Eq. 3.32 for Q_P,

$$Q_P = \frac{1 + \sqrt{1 - 4k_2 k_3}}{2k_2} \tag{3.34}$$

Now H_P may be determined from Eq. 3.18. If the exit loss and the velocity head are negligible, then

$$H_P = H_{res} \tag{3.35}$$

and it follows from Eq. 3.18 that

$$Q_P = C_p - C_a H_{res} \tag{3.36}$$

Dead End at Downstream End (Fig. 3.9)

At the dead end, $Q_P = 0$. Hence, from the positive characteristic equation (Eq. 3.18), it follows that

$$H_P = \frac{C_p}{C_a} \tag{3.37}$$

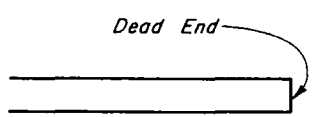

Figure 3.9. Dead end.

Valve at Downstream End (Fig. 3.10)

Steady-state flow through a valve can be written as

$$Q_o = (C_d A_v)_o \sqrt{2gH_o} \tag{3.38}$$

in which subscript o indicates steady-state conditions, C_d = coefficient of discharge, H_o = head upstream of the valve, and A_v = area of the valve opening.

An equation similar to Eq. 3.38 may be written for the transient state as

$$Q_P = (C_d A_v) \sqrt{2gH_P}. \tag{3.39}$$

Dividing Eq. 3.39 by Eq. 3.38, taking square of both sides and defining the relative valve opening $\tau = (C_d A_v)/(C_d A_v)_o$, we obtain

$$Q_P^2 = \frac{(Q_o \tau)^2}{H_o} H_P \tag{3.40}$$

Substitution for H_P from the positive characteristic equation (Eq. 3.18) into Eq. 3.40 yields

$$Q_P^2 + C_v Q_P - C_p C_v = 0 \tag{3.41}$$

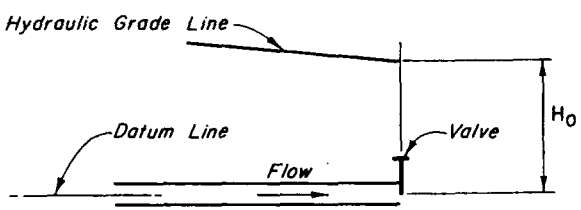

(a)

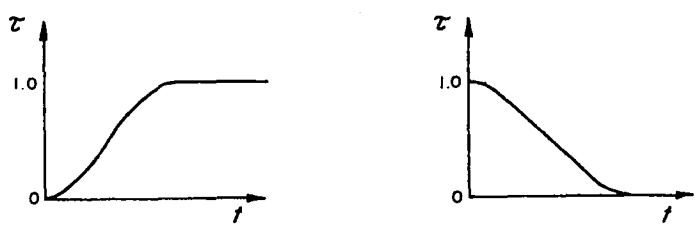

(b) Opening (c) Closing

Figure 3.10. Valve at downstream end.

in which $C_v = (\tau Q_o)^2/(C_a H_o)$. Solving for Q_P and neglecting the negative sign with the radical term

$$Q_P = 0.5(-C_v + \sqrt{C_v^2 + 4C_p C_v}) \tag{3.42}$$

Now H_P may be determined from Eq. 3.18.

To compute the transient-state conditions for an opening or a closing valve, τ versus t curves (Fig. 3.10b and c) may be specified either in a tabular form or by an algebraic expression. Note that $\tau = 1$ corresponds to a valve opening at which the flow through the valve is Q_o under a head of H_o.

Orifice at Lower End

For an orifice, the opening remains constant. Therefore, the above equations may be used with $\tau = 1$.

Series Junction (Fig. 3.11)

In the preceding discussion, we considered only one conduit, and the boundary was either at the upstream or at the downstream end. Therefore, no special care had to be taken to designate the variables at the boundary since there was only one conduit section under consideration. However, if the boundary is at the junction of two or more conduits, then the variables at different sections of various conduits have to be specified. For this purpose, we will use two subscripts. The first subscript will designate the conduit number, while the second will indicate the section number. For example, $Q_{P_{i,j}}$ indicates flow at the jth section of the ith conduit. For variables that have same value at all sections of a conduit, only one subscript will be used. For example, C_{a_i} refers to constant C_a (Eq. 3.22) for the ith conduit. Although C_p and C_n may have different values at different sections of a conduit, only one subscript will be used with them to indicate the conduit number. This simplifies presentation and at the same time does not result in any ambiguity since each conduit can have only one end-section at a boundary. As discussed previously, the subscript P will indicate the unknown variables at the end of the time step.

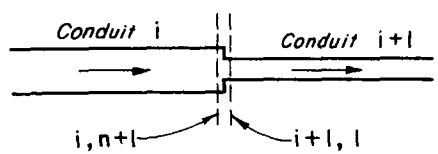

Figure 3.11. Series junction.

If the difference in the velocity heads at sections $(i, n+1)$ and $(i+1, 1)$ (Fig. 3.11) and the head losses at the junction are neglected, then

$$H_{P_{i,n+1}} = H_{P_{i+1,1}} \tag{3.43}$$

The positive and negative characteristic equations for sections $(i, n+1)$ and $(i+1, 1)$ are

$$Q_{P_{i,n+1}} = C_{p_i} - C_{a_i} H_{P_{i,n+1}} \tag{3.44}$$

$$Q_{P_{i+1,1}} = C_{n_{i+1}} + C_{a_{i+1}} H_{P_{i+1,1}} \tag{3.45}$$

The continuity equation at the junction is

$$Q_{P_{i,n+1}} = Q_{P_{i+1,1}} \tag{3.46}$$

It follows from Eqs. 3.43 through 3.46 that

$$H_{P_{i,n+1}} = \frac{C_{p_i} - C_{n_{i+1}}}{C_{a_i} + C_{a_{i+1}}} \tag{3.47}$$

Now $H_{P_{i+1,1}}$, $Q_{P_{i,n+1}}$, and $Q_{P_{i+1,1}}$ can be determined from Eqs. 3.43 through 3.45.

However, if the difference in the velocity heads at sections $(i, n+1)$ and $(i+1, 1)$ or the head losses at the junction are not negligible, then Eq. 3.43 is not valid. In such cases, the following equation for the total head may be used instead of Eq. 3.43:

$$H_{P_{i,n+1}} + \frac{Q^2_{P_{i,n+1}}}{2gA_i^2} = H_{P_{i+1,1}} + (1+k)\frac{Q^2_{P_{i+1,1}}}{2gA_{i+1}^2} \tag{3.48}$$

in which k = coefficient of head losses, h_l, at the junction

$$h_l = \frac{kQ^2_{P_{i+1,1}}}{2gA_{i+1}^2}$$

Simultaneous solution of Eqs. 3.44 through 3.46, and 3.48 yields

$$Q_{P_{i,n+1}} = \frac{b + \sqrt{b^2 - 4cd}}{2c} \tag{3.49}$$

in which

$$\left.\begin{aligned} b &= \frac{1}{C_{a_i}} + \frac{1}{C_{a_{i+1}}} \\ c &= \frac{1}{2g}\left(\frac{1}{A_i^2} - \frac{1+k}{A_{i+1}^2}\right) \\ d &= \frac{C_{p_i}}{C_{a_i}} + \frac{C_{n_{i+1}}}{C_{a_{i+1}}} \end{aligned}\right\} \tag{3.50}$$

Now $Q_{P_{i+1,1}}$, $H_{P_{i,n+1}}$, and $H_{P_{i+1,1}}$ can be determined from Eqs. 3.44 through 3.46.

Branching Junction (Fig. 3.12)

For the branching junction shown in Fig. 3.12, the following equations can be written:

1. Continuity equation

$$Q_{P_{i,n+1}} = Q_{P_{i+1,1}} + Q_{P_{i+2,1}} \tag{3.51}$$

2. Characteristic equations

$$Q_{P_{i,n+1}} = C_{p_i} - C_{a_i} H_{P_{i,n+1}} \tag{3.52}$$

$$Q_{P_{i+1,1}} = C_{n_{i+1}} + C_{a_{i+1}} H_{P_{i+1,1}} \tag{3.53}$$

$$Q_{P_{i+2,1}} = C_{n_{i+2}} + C_{a_{i+2}} H_{P_{i+2,1}} \tag{3.54}$$

3. Equation for total head

$$H_{P_{i,n+1}} = H_{P_{i+1,1}} = H_{P_{i+2,1}} \tag{3.55, 3.56}$$

In Eqs. 3.55 and 3.56, the head losses at the junction are neglected, and it is assumed that the velocity heads in all conduits are equal.

Simultaneous solution of Eqs. 3.51 through 3.55 yields

$$H_{P_{i,n+1}} = \frac{C_{p_i} - C_{n_{i+1}} - C_{n_{i+2}}}{C_{a_i} + C_{a_{i+1}} + C_{a_{i+2}}} \tag{3.57}$$

Now $H_{P_{i+1,1}}$ and $H_{P_{i+2,1}}$ can be determined from Eqs. 3.55 and 3.56, and $Q_{P_{i,n+1}}$, $Q_{P_{i+1,1}}$ and $Q_{P_{i+2,1}}$ from Eqs. 3.52 through 3.54.

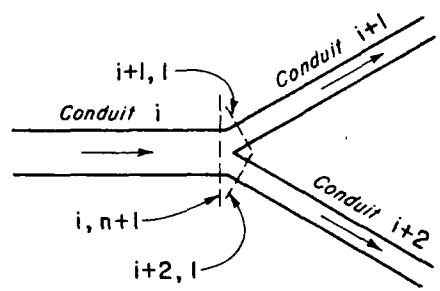

Figure 3.12. Branching junction.

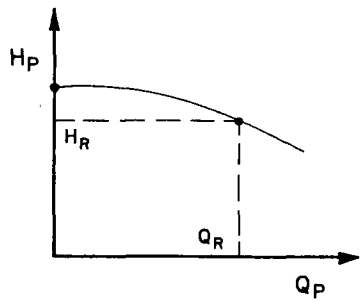

Figure 3.13. Head-discharge curve for a centrifugal pump.

Centrifugal Pump at Upstream End

The head-discharge curve for a centrifugal pump running at constant speed is shown in Fig. 3.13. This curve can be approximated by the equation

$$H_P = C_7 - C_8 Q_P^2 \tag{3.58}$$

Solving this equation simultaneously with Eq. 3.19,

$$Q_P = \frac{-1 + \sqrt{1 + 4C_aC_8(C_n + C_aC_7)}}{2C_aC_8} \tag{3.59}$$

Now H_P can be determined from Eq. 3.58.

Francis Turbine at Downstream End

The head-discharge curve for a Francis turbine running at constant speed (i.e., connected to a large system) and at constant gate opening can be approximated as

$$H_P = C_9 + C_{10} Q_P^2 \tag{3.60}$$

Solving this equation simultaneously with the positive characteristic equation (Eq. 3.18) yields

$$Q_P = \frac{-1 + \sqrt{1 + 4C_aC_{10}(C_p - C_aC_9)}}{2C_aC_{10}} \tag{3.61}$$

Now H_P can be determined from Eq. 3.60.

3.4 STABILITY AND CONVERGENCE CONDITIONS

The finite-difference scheme presented in Section 3.2 is termed *convergent* if the exact solution of the difference equations approaches that of the original differential equations as Δt and Δx approach zero. If the round-off error due to representation of the irrational numbers by a finite number of significant digits grows as the solution progresses, the scheme is called *unstable*; if this error decays, the scheme is *stable*. It has been proved that convergence implies stability and that stability implies convergence.[9,12]

Methods for determining the convergence or stability criteria for nonlinear equations are extremely difficult, if not impossible. Collatz[13] suggests that the convergence and stability may be studied by numerically solving the equations for a number of $\Delta x/\Delta t$ ratios and then examining the results. The convergence and stability may, however, be studied analytically by linearizing the basic equations. If the nonlinear terms are relatively small, it is reasonable to assume that the criteria applicable to the simplified equations are also valid for the original nonlinear equations.

Using the procedure proposed by O'Brien et al.[14] and considering the linearized equations, Perkins et al.[9] showed that for the finite-difference scheme of Section 3.2 to be stable,

$$\frac{\Delta t}{\Delta x} < \frac{1}{a} \tag{3.62}$$

This condition implies that the characteristics through point P in Fig. 3.1 should not fall outside the segment AB. For a neutral scheme,

$$\frac{\Delta t}{\Delta x} = \frac{1}{a} \tag{3.63}$$

The criteria for convergence indicate that the most accurate solutions are obtained if Eq. 3.63 is satisfied. Thus, the convergence and/or stability criterion for the finite-difference equations (Eqs. 3.16 and 3.17) is given by the expression

$$\frac{\Delta t}{\Delta x} \leqslant \frac{1}{a} \tag{3.64}$$

This is called *Courant's stability condition*.

3.5 SELECTION OF TIME INCREMENT FOR A COMPLEX PIPING SYSTEM

For a complex system of two or more conduits, it is necessary that the same time increment be used for all conduits so that boundary conditions at the junction may be used. This time increment should be selected such that Courant's stability condition (Eq. 3.64) is satisfied.

If the time interval, Δt, is such that the reach length for any conduit in the system is not equal to $a\Delta t$, then Δx must be greater than $a\Delta t$ to satisfy Courant's stability criteria. In other words, the characteristics through P pass through R

and S and not through the grid points A and B (Fig. 3.14). The conditions at every time step are, however, computed at the grid points only while conditions at R and S must be known to determine conditions at P.

Streeter and Lai in their pioneer paper[15] and Streeter and Wylie[10] proposed an interpolation procedure for computing conditions at R and S from the known conditions at A, B, and C. However, later investigations have shown that this procedure smooths the sharp transient peaks. To avoid this, Streeter[16] suggests that the original differential equations for short conduits may be written in an implicit form, whereas Kaplan et al.[17] propose a procedure called *zooming* in which Δt for longer conduits may be integral multiples of Δt for shorter conduits of the system.

In the author's opinion, the implicit method combined with the characteristic method should be used if a number of conduits in the system are very short relative to others; otherwise, simple adjustment of wave velocities to satisfy the following equation should give sufficiently accurate results.

$$\Delta t = \frac{L_i}{a_i n_i} \quad (i = 1 \text{ to } N) \tag{3.65}$$

in which n_i must be an integer and is equal to the number of reaches into which ith conduit is divided, and N = number of pipes in the system. As the wave velocity is not precisely known, minor adjustments in its value are acceptable.

Because of the limitations imposed on Δt by the Courant's stability condition, a large amount of computer time is required for analyzing systems having very slowly varying transients. For the analysis of such systems, Yow[18] has reported a technique that allows larger time steps and at the same time satisfies the Courant's condition. In this technique, the inertial term of the dynamic equation is multiplied by an arbitrary factor α^2. The resulting equation and the continuity equation are then converted into the characteristic form. Because of multiplication by α^2, a time step equal to $\alpha\Delta t$ is permissible, in which Δt is the time step given by the Courant's condition. Different values of α may be used for different conduits, and the value of α may be as large as 20. Yow's technique, however, is applicable only to those systems in which the inertial term is small as compared to the friction term such as gas flow in pipes,[18,21] flow in porous media,[19] and floods in rivers. The validity of this technique is questionable[20] because the original governing equations are arbitrarily altered; thus, extreme caution must be exercised while using this technique for the analysis of these systems.

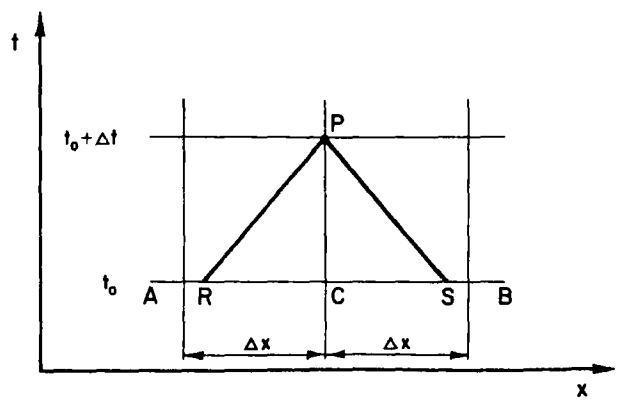

Figure 3.14. Notation for interpolation.

3.6 COMBINED IMPLICIT-CHARACTERISTIC METHOD

In the last section, it was pointed out that sometimes it is advantageous to use a combination of the implicit and characteristic methods while analyzing certain piping systems. Details of this follow.

Let us consider a piping system in which the ith reach of a conduit is to be analyzed using the implicit method. In this method, the derivatives of the continuity and dynamic equations (Eqs. 3.1 and 3.2) are replaced by the centered-implicit finite differences[16] as follows (Fig. 3.15):

$$\frac{\partial H}{\partial x} = \frac{(H_{P_{i+1}} + H_{i+1}) - (H_{P_i} + H_i)}{2\Delta x} \tag{3.66}$$

$$\frac{\partial H}{\partial t} = \frac{(H_{P_{i+1}} + H_{P_i}) - (H_{i+1} + H_i)}{2\Delta t} \tag{3.67}$$

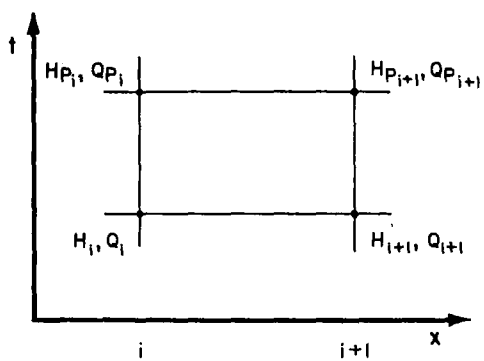

Figure 3.15. Notation for implicit method.

$$\frac{\partial Q}{\partial x} = \frac{(Q_{P_{i+1}} + Q_{i+1}) - (Q_{P_i} + Q_i)}{2\Delta x} \tag{3.68}$$

$$\frac{\partial Q}{\partial t} = \frac{(Q_{P_{i+1}} + Q_{P_i}) - (Q_{i+1} + Q_i)}{2\Delta t} \tag{3.69}$$

$$Q = 0.5(Q_{i+1} + Q_i) \tag{3.70}$$

To simplify presentation, only one subscript is used in this section to designate the variables. Substitution of Eqs. 3.66 to 3.70 into Eqs. 3.1 and 3.2 and simplification of the resulting equations yield

$$Q_{P_i} + Q_{P_{i+1}} - C_{11}H_{P_i} + C_{11}H_{P_{i+1}} + C_{12} = 0 \tag{3.71}$$

$$-Q_{P_i} + Q_{P_{i+1}} + C_{13}H_{P_i} + C_{13}H_{P_{i+1}} + C_{14} = 0 \tag{3.72}$$

in which

$$C_{11} = \frac{gA\Delta t}{\Delta x} \tag{3.73}$$

$$C_{12} = C_{11}(H_{i+1} - H_i) - (Q_i + Q_{i+1}) + \frac{f\Delta t}{4DA}(Q_i + Q_{i+1})|Q_i + Q_{i+1}| \tag{3.74}$$

$$C_{13} = \frac{gA\Delta x}{a^2\Delta t} \tag{3.75}$$

$$C_{14} = Q_{i+1} - Q_i - C_{13}(H_i + H_{i+1}) \tag{3.76}$$

Note that there are four unknowns in Eqs. 3.71 and 3.72, namely, Q_{P_i}, $Q_{P_{i+1}}$, H_{P_i}, and $H_{P_{i+1}}$. For a unique solution of these equations, there should be four equations. These other two equations, in addition to Eqs. 3.71 and 3.72, are provided by the end conditions of the reach. For example, if there is a conduit at the upstream end and a constant-head reservoir at the downstream end, then the negative characteristic equation (Eq. 3.19) and $H_{P_{i+1}} = H_{res}$ are the other two equations. For any other end conditions, similar equations are written. Thus, there are four equations in four unknowns, and their values are determined by simultaneously solving these equations.

Note that the conditions imposed by the boundary are used for the additional equations and not the boundary conditions developed in Section 3.3. Therefore, while selecting the conduit or the conduit reach for which the implicit method is being used, care should be taken that its end conditions are simple.

3.7 ANALYSIS OF A PIPING SYSTEM

To compute transient-state conditions in a piping system, the shortest conduit in the system is divided into a number of reaches so that a desired computational time interval, Δt, is obtained. According to Evangelisti,[2] a time interval of $\frac{1}{16}$ to $\frac{1}{24}$ of the transit time, i.e., wave-travel time from one end of the system to the other, should give sufficiently accurate results. In the author's opinion, however, this criterion should be used as a rough guide, and Δt should be increased or decreased depending upon the rate at which transients are produced. Having selected the value of Δt, the remaining conduits in the system are divided into reaches having equal lengths by using the procedure outlined in Section 3.5. If necessary, the wave velocities are adjusted to satisfy Eq. 3.65 or the procedure outlined in Section 3.6 is used so that characteristics pass through the grid points. The steady-state discharge and pressure head at all the sections are then computed, and their values are printed. The time is now incremented, and the transient conditions are computed at all the interior points from Eqs. 3.23 and 3.18 and at the boundaries from the appropriate boundary conditions. This process is continued until transient conditions for the required time are computed.

The flowchart of Fig. 3.16 shows the computational steps for determining the transient conditions in a series piping system. To illustrate this procedure, transient conditions in the piping system shown in Fig. 3.17a were determined. For this purpose, the computer program of Appendix B was developed in FORTRAN IV language. Transient conditions were caused by closing the valve according to the τ-t curve shown in Fig. 3.17b.

As the valve-closure time is rather large as compared to the wave-transit time in the system, pipe No. 2 was divided into two reaches, thus giving $\Delta t = 0.25$ s. Pipe No. 1 was also divided into two reaches to satisfy Eq. 3.65, and the initial steady-state conditions were computed. Time was incremented by Δt, and the conditions at the interior sections were determined using Eqs. 3.23 and 3.18. The boundary conditions for the reservoir (Eqs. 3.24 and 3.25) were used to determine the conditions at the upstream end, and Eqs. 3.43, 3.44, 3.46, and 3.47 were used to determine conditions at the junction of pipes No. 1 and No. 2. Seven points on the τ-t curve were stored in the computer, and the τ values at the intermediate times were parabolically interpolated. Equations 3.42 and 3.40 were used to determine the conditions at the valve.

Conditions at $t = \Delta t$ at all sections of the system were now known. These were stored as conditions at the beginning of the next time step. This procedure was repeated until transients for the desired duration were computed. The conditions were printed every second time step by specifying IPRINT = 2.

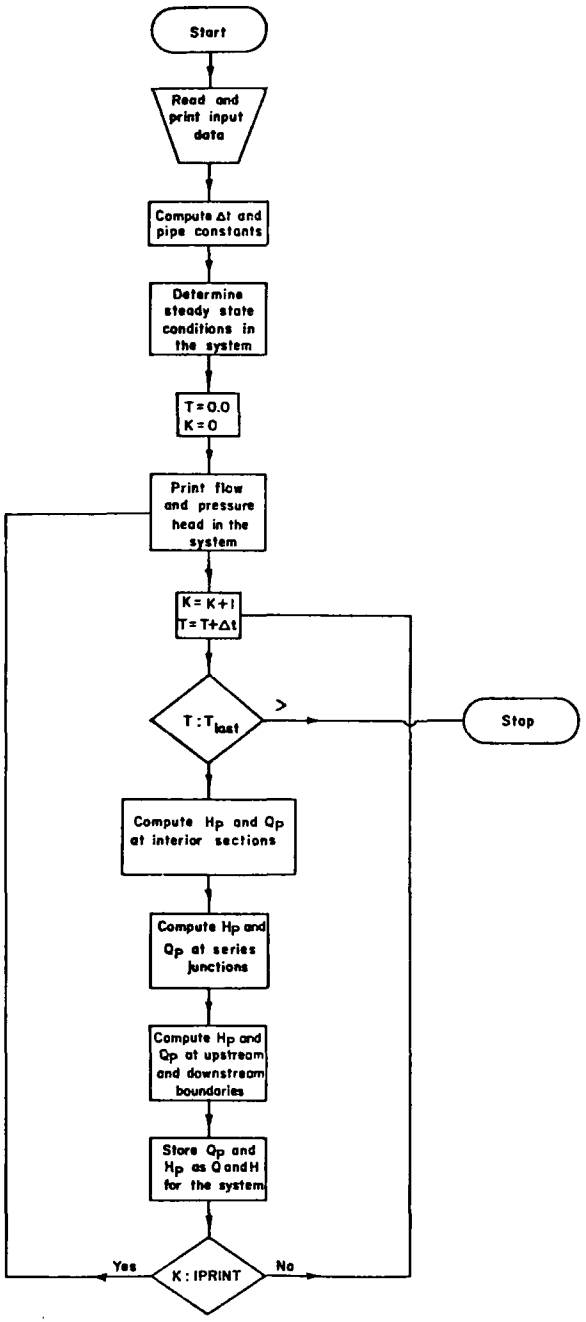

Figure 3.16. Flowchart for a series piping system.

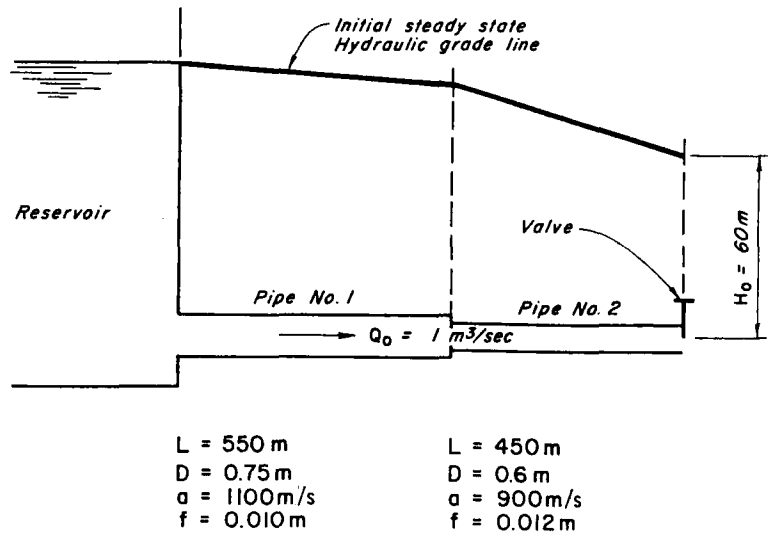

(a) Piping system

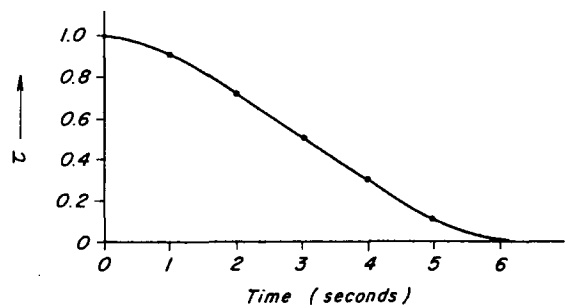

(b) Valve closure curve

Figure 3.17. Series piping system.

3.8 CASE STUDY

Figure 3.18 shows the schematic layout of the conduits of the Jordan River Redevelopment[22,23] located in British Columbia, Canada, and owned by the British Columbia Hydro and Power Authority. It is a peaking power plant.

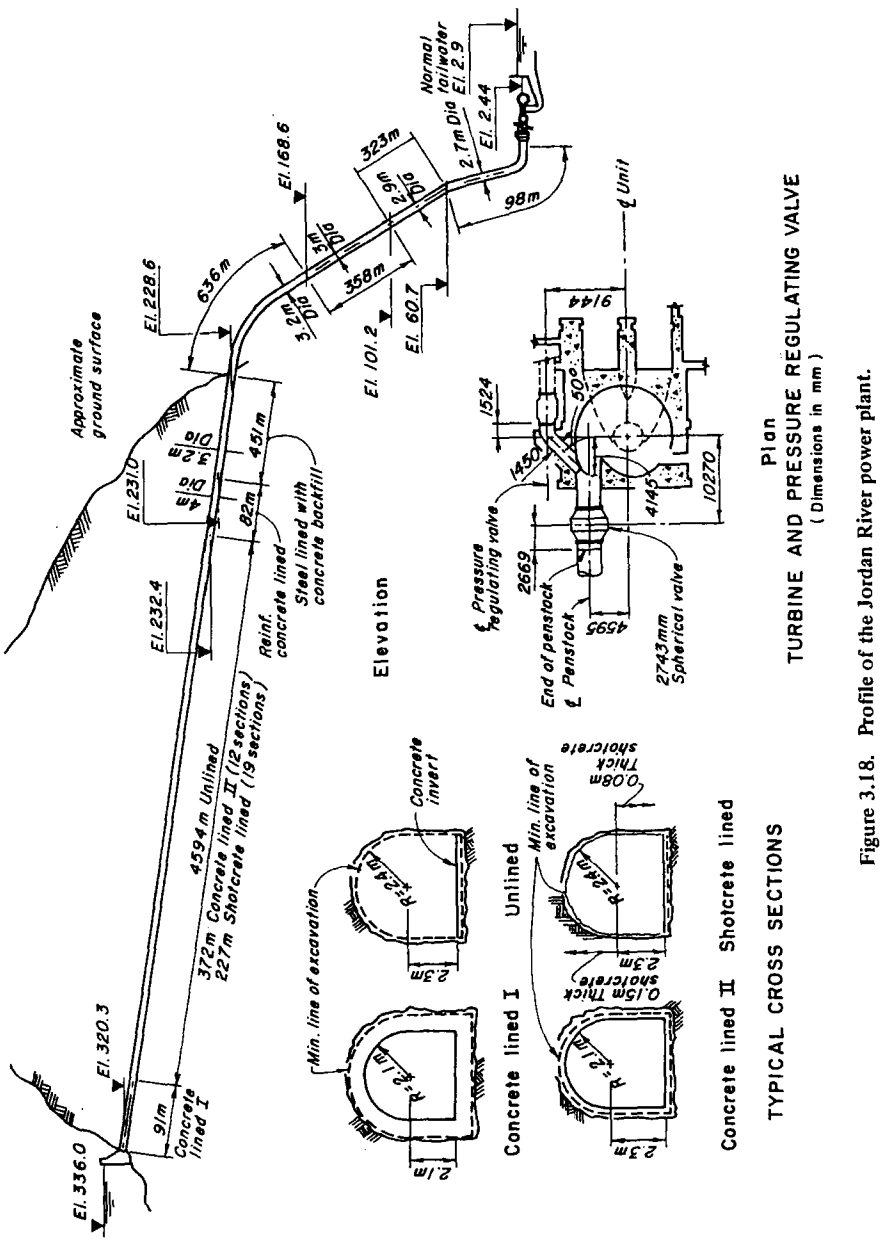

Figure 3.18. Profile of the Jordan River power plant.

The upstream conduit consists of a tunnel having a 5285-m-long, mainly D-shaped section; 82-m-long, 3.96-m-diameter, and 451-m-long, 3.2-m-diameter sections; and a 1400-m-long penstock reducing in diameter from 3.2 to 2.7 m. There is only one Francis turbine rated at 154 MW and 265.5-m rated head. To reduce the maximum transient-state pressures, a pressure-regulating valve (PRV) is provided. The rating curve for the PRV, at rated head (H_r) of 265.5 m as determined from the prototype tests, is shown in Fig. 3.19.

To determine the transient conditions caused by opening or closing of PRV, a computer program was developed by using the boundary conditions for the PRV derived in this section.* Analysis of transients caused by various turbine operations is discussed in Chapter 5. Points on the PRV rating curve (Fig. 3.19) were stored in the computer at 20 percent intervals of the valve stroke, and the discharge at the intermediate valve openings was determined by linear interpolation. Assuming that the valve characteristics obtained under steady-state operation are valid during the transient state, the PRV discharge under net head H_n is given by the equation

$$Q_v = Q_r \sqrt{\frac{H_n}{H_r}} \tag{3.77}$$

in which Q_v = PRV discharge under a net head of H_n, and Q_r = discharge under rated net head H_r, both at valve opening τ. Note that both H_r and H_n are total heads, i.e., $H_n = H_P + Q_v^2/(2gA^2)$, in which A = cross-sectional area of the conduit just upstream of the PRV.

To develop the boundary condition for the PRV, Eqs. 3.18 and 3.77 are simultaneously solved. Noting that $Q_P = Q_v$ and eliminating H_n from these equations,

$$Q_P = \frac{-C_{16} + \sqrt{C_{16}^2 + 4C_{15}C_{17}}}{2C_{15}} \tag{3.78}$$

in which

$$\left.\begin{aligned} C_{15} &= 1 - \frac{Q_r^2}{2gH_rA^2} \\ C_{16} &= \frac{Q_r^2}{C_aH_r} \\ C_{17} &= \frac{Q_r^2 C_p}{C_aH_r} \end{aligned}\right\} \tag{3.79}$$

Now H_P may be determined from Eq. 3.18.

*Boundary conditions for the simultaneous operation of the PRV and wicket gates are developed in Section 10.7.

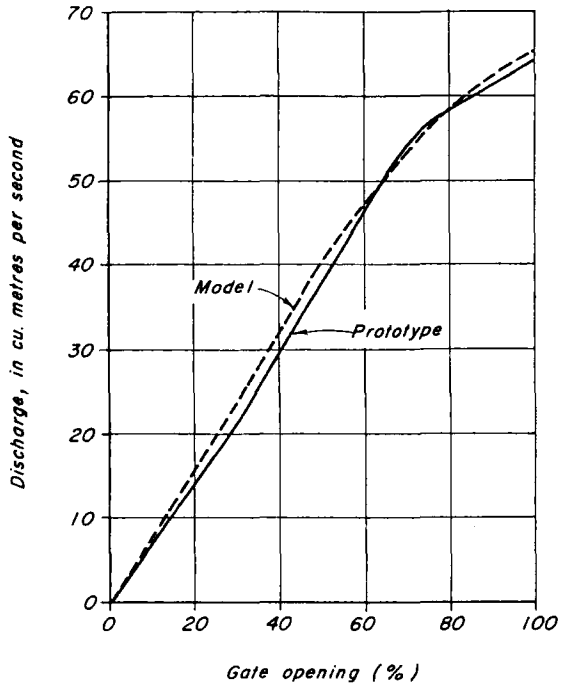

Figure 3.19. Discharge characteristics of pressure-regulating valve.

In the computer analysis, the upstream conduit was represented by 11 pipes while the conduit downstream of the PRV was neglected because of its short length. Lined and unlined segments of the tunnel were combined into two lined and unlined reaches, and the D-shaped tunnel was replaced by a circular conduit having the same cross-sectional area. The waterhammer wave velocity[24] was computed by taking the modulus of rigidity of the rock as 5.24 GPa, and assuming the penstock to be anchored at the lower end and free for longitudinal expansion at the upper end. The friction factor for various conduits were computed such that they included the friction and minor losses, such as expansion, contraction, and bend losses. Thus, although the minor losses are concentrated at various locations in the actual system, these are assumed to be distributed along the conduit length. In the author's opinion, this approximation should not introduce large errors in the analysis. The head losses computed using these values of friction factors and those measured on the prototype are in close agreement.

A number of transient-state tests were conducted on the prototype. Steady-state pressures were measured by a Budenberg deadweight gauge having a certified accuracy of 0.35 m. Transient-state pressures were measured with a strain-

gauge-type pressure cell, which delivered linear output within 0.6 percent over its entire range. The natural frequency of the cell was greater than 1000 Hz, and it was calibrated against the deadweight gauge. A multiturn potentiometer mechanically connected to the PRV-stroke mechanism was used to measure the PRV opening, and a Westinghouse leading-edge flowmeter[25] was used to measure the transient-state flows.

The computed and measured transient-state pressures and flows are shown in Fig. 3.20. In the prototype test, the PRV was first opened from 0 to 20 percent

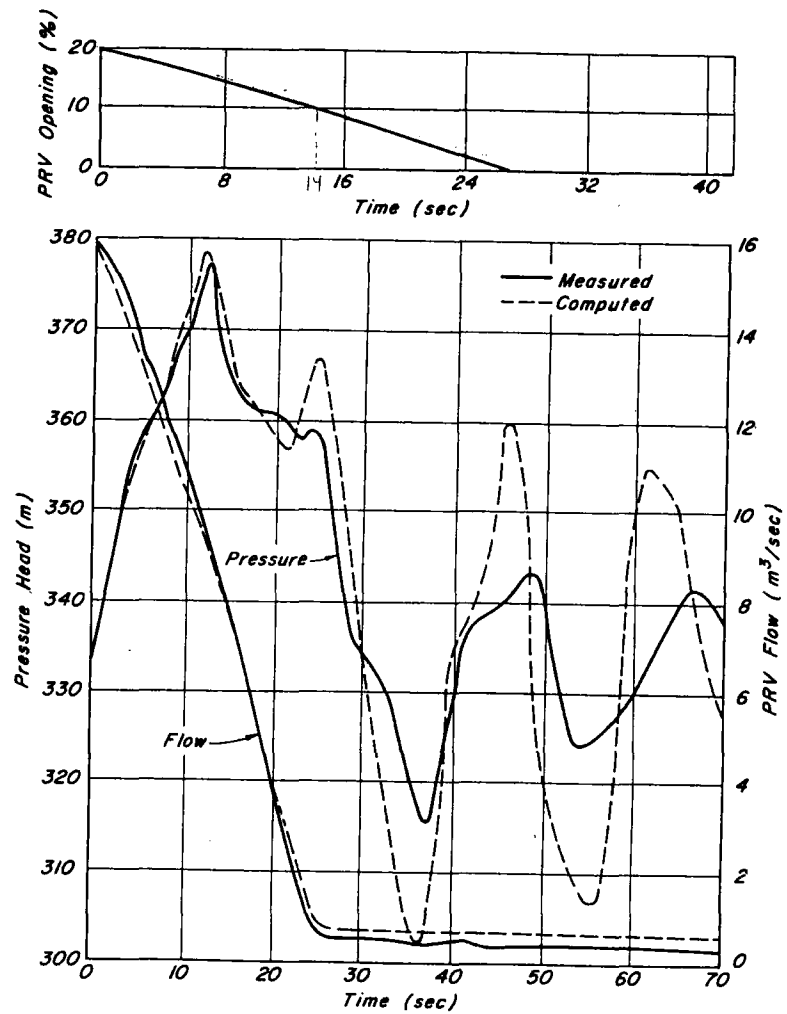

Figure 3.20. Comparison of computed and measured results.

at a very slow rate and was kept at this opening until steady flow was established in the upstream conduit. The PRV was then closed from 20 percent to 0 (Fig. 3.20). The wicket gates were kept closed throughout the test. In the computer analysis, however, the PRV was not completely closed but was held at 1 percent opening to simulate the leakage through the wicket gates.

As can be seen from Fig. 3.20, the computed and measured transient pressures agree closely up to an elapsed time of about 18 s; afterward, there is good agreement between the shapes of the pressure curves but the measured results show that the pressure waves are dissipated more rapidly than that indicated by the results of the mathematical model. In addition, the measured period of the pressure oscillations is less than the computed period. These differences may be due to using the steady-state friction formula for computing the transient-state friction losses and the reduction of wave velocity at low pressures as discussed in Section 2.6. The computed and measured discharge agree closely.

3.9 SUMMARY

In this chapter, the details of the method of characteristics were presented, and a number of simple boundary conditions were developed. Stability and convergence conditions for the finite-difference scheme were discussed, and a procedure was outlined for the selection of time interval for a complex system. For illustration purposes, a computational procedure for analyzing transient conditions caused by closing a valve in a series system was presented. The chapter was concluded by comparing the computed and measured results for the transient conditions caused by the closure of a pressure-regulating valve in a hydroelectric generating station.

PROBLEMS

3.1. Prove that the equations of the characteristic curves are $dx/dt = V \pm a$ if the term $V(\partial V/\partial x)$ of the dynamic equation (Eq. 2.10) is not neglected and there is an additional term $V(\partial H/\partial x)$ in the continuity equation.

3.2. Develop the boundary conditions for a centrifugal pump running at rated speed, taking into consideration transients in the suction line.

3.3. Write a computer program for the piping system shown in Fig. 3.17a. Run the program for various values of Δt and plot a graph between the computed pressure at the valve and Δt.

3.4. Develop the boundary conditions for an opening or closing valve located at the junction of two conduits (Fig. 3.21). (*Hint:* The following four equations are available: the positive characteristic equation for section $i, n + 1$; the negative characteristic equation for section $i + 1, 1$; the continuity equation, and the equation for flow through the valve. Solve these equations simultaneously to obtain an expression for $Q_{P_{i,n+1}}$.)

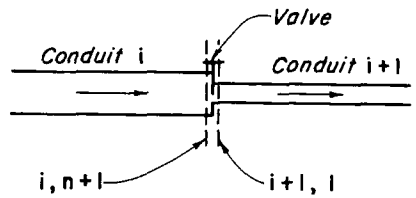

Figure 3.21. Valve at series junction.

3.5. Prove that if the valve in Fig. 3.21 is replaced by an orifice and the conduits i and $i + 1$ have the same diameter, wall thickness, and wall material, then

$$Q_{P_{i,n+1}} = Q_{P_{i+1,1}} = -C + \sqrt{C^2 + C(C_p + C_n)}$$

in which $C = Q_o^2/(C_a \Delta H_o)$ and ΔH_o is the orifice head loss for Q_o.

3.6. Is the equation for $Q_{P_{i,n+1}}$ given in Problem 3.5 valid for the reverse flow? If not, derive a similar equation for the reverse flow.

3.7. Develop the boundary conditions for the pressure-regulating valve and the Francis turbine shown in Fig. 3.18. The transient conditions are caused by opening or closing the valve. Assume that the turbine speed and the wicket-gate opening remain constant during the transient-state conditions.

3.8. Prepare a flowchart for programming the boundary conditions developed in Problem 3.7.

3.9. A procedure called *zooming* is presented in Ref. 17 in which the time step for the long pipes may be an integral multiple of that for short pipes. However, the procedure requires extrapolation at the junction of pipes having different time steps. Investigate the effect of extrapolation on the pressure peaks for the piping system shown in Fig. 3.17a. Assume that pipe No. 2 is 90-m-long instead of 450 m as shown in the figure. (*Hint:* Solve the system using the zooming procedure and then using the same Δt for the whole system as determined by the Courant's condition.)

REFERENCES

1. Ralston, A. and Wilf, H. S. (eds.), *Mathematical Methods for Digital Computers*, John Wiley & Sons, Inc., New York, 1960.
2. Evangelisti, G., "Waterhammer Analysis by the Method of Characteristics," *L'Energia Elettrica*, Nos. 10-12, 1969, pp. 673-692, 759-770, 839-858.
3. Webster, A. G., *Partial Differential Equations of Mathematical Physics*, Dover Publications, Inc., New York, 1950.
4. Stoker, J. J., *Water Waves*, Interscience, New York, 1965.

5. Abbott, M. B., *An Introduction to the Method of Characteristics*, American Elsevier, New York, 1966.
6. Mises, R., *Mathematical Theory of Compressible Fluid Flow*, Academic Press, New York, 1958.
7. Gray, C. A. M., "The Analysis of the Dissipation of Energy in Waterhammer," *Proc. Amer. Soc. Civil Engrs.*, vol. 119, 1953, pp. 1176–1194.
8. Courant, R., *Methods of Mathematical Physics*, Interscience, New York, 1962.
9. Perkins, F. E., Tedrow, A. C., Eagleson, P. S., and Ippen, A. T., *Hydro-Power Plant Transients*, Part II, Dept. of Civil Engineering, Hydrodynamics Lab. Report No. 71, Massachussetts Institute of Technology, Sept. 1964.
10. Streeter, V. L. and Wylie, E. B., *Hydraulic Transients*, McGraw-Hill Book Co., New York, 1967.
11. Lister, M., "The Numerical Solution of Hyperbolic Partial Differential Equations by the Method of Characteristics," chapter in *Ref. 1*, pp. 165–179.
12. Fox, P., "The Solution of Hyperbolic Partial Differential Equations by Difference Methods," chapter in *Ref. 1*.
13. Collatz, L., *The Numerical Treatment of Differential Equations*, Third ed., Springer, Berlin, 1960.
14. O'Brien, G. G., Hyman, M. A., and Kaplan, S. "A Study of the Numerical Solution of Partial Differential Equations," *Jour. Math. and Physics*, No. 29, 1951, pp. 223–251.
15. Streeter, V. L. and Lai, C., "Waterhammer Analysis Including Fluid Friction," *Jour. Hyd. Div., Amer. Soc. of Civ. Engrs.*, May, 1962, pp. 79–112.
16. Streeter, V. L., "Waterhammer Analysis," *Jour. Hyd. Div., Amer. Soc. of Civ. Engrs.*, Nov. 1969, pp. 1959–1971.
17. Kaplan, M., Belonogoff, G., and Wentworth, R. C., "Economic Methods for Modelling Hydraulic Transient Simulation," *Proc. First International Conference on Pressure Surges*, Canterbury, England, published by British Hydromechanic Research Assoc., Sept. 1972, pp. A4-33–A4-38.
18. Yow, W., "Numerical Error on Natural Gas Transient Calculations," *Trans. Amer. Soc. of Mech. Engrs.*, vol. 94, Series D, no. 2, 1972, pp. 422–428.
19. Wylie, E. B., "Transient Aquifer Flows by Characteristics Method," *Jour. Hyd. Div., Amer. Soc. of Civil Engrs.*, vol. 102, March 1976, pp. 293–305.
20. Rachford, H. H. and Todd, D., "A Fast, Highly Accurate Means of Modeling Transient Flow in Gas Pipeline Systems by Variational Methods," *Jour. Soc. of Petroleum Engrs.*, April 1974, pp. 165–175. (See also Discussion by Stoner, M. A., and Authors' Reply, pp. 175–178.)
21. Wylie, E. B., Streeter, V. L., and Stoner, M. A., "Unsteady-State Natural Gas Transient Calculations in Complex Pipe Systems," *Jour. Soc. of Petroleum Engrs.*, Feb. 1974, pp. 35–43.
22. Portfors, E. A. and Chaudhry, M. H., "Analysis and Prototype Verification of Hydraulic Transients in Jordan River Power Plant," *Ref. 17*, pp. E_4-57–E_4-72.
23. Chaudhry, M. H. and Portfors, E. A., "A Mathematical Model for Analyzing Hydraulic Transients in a Hydroelectric Power Plant," *Proc. First Canadian Hydraulic Conference*, published by the University of Alberta, Edmonton, Canada, May 1973, pp. 298–314.
24. Parmakian, J., *Waterhammer Analysis*, Dover Publications, Inc., New York, 1963.
25. Fischer, S. G., "The Westinghouse Leading Edge Ultrasonic Flow Measurement System," presented at the spring meeting, Amer. Soc. of Mech. Engrs., Boston, May 1973.

ADDITIONAL REFERENCES

Symposium, Waterhammer in Pumped Storage Projects, Chicago, Nov. 1965, published by Amer. Soc. of Mech. Engrs.

Evangelisti, G., "On the Numerical Solution of the Equations of Propagation by the Method of Characteristics," *Meccanica*, vol. 1, No. 1/2, 1966, pp. 29–36.

Contractor, D. N., "The Reflection of Waterhammer Pressure Waves from Minor Losses," *Trans. Amer. Soc. Mech. Engrs.*, vol. 87, Series D, June 1965.

Miyashiro, H., "Waterhammer Analysis of Pump System," *Bull. Japan Soc. of Mech. Engrs.*, vol. 10, No. 42, 1967, pp. 952–958.

Combes, G. and Zaoui, J., "Analyse des erreurs introduites par l'utilisation pratique de la methode des caracteristiques dans le calcul des coups de belier," *La Houille Blanche*, vol. 22, No. 2, 1967, pp. 195–202.

Fox, J. A., "The Use of the Digital Computer in the Solution of Waterhammer Problems," *Proc. Institution of Civil Engrs.*, Paper 7020, vol. 39, Jan. 1968, pp. 127–131.

Brown, F. T., "A Quasi Method of Characteristics with Application to Fluid Lines with Frequency Dependent Wall Shear and Heat Transfer," Amer. Soc. of Mech. Engrs., Paper No. 68-WA/Aut.-7, Dec. 1968.

Fox, J. A. and Henson, D. A., "The Prediction of the Magnitudes of Pressure Transients Generated by a Train Entering a Single Tunnel," *Proc., Institution of Civil Engrs.*, Paper 7365, vol. 49, May 1971, pp. 53–69.

Streeter, V. L., "Unsteady Flow Calculations by Numerical Methods," Amer. Soc. of Mech. Engrs., Paper No. 71-WA-FE-13, Nov. 1971, 9 pp.

Sheer, T. J., "Computer Analysis of Waterhammer in Power Station Cooling Water Systems," *Proc. First International Conference on Pressure Surges*, published by British Hydromechanics Research Assoc., Sept. 1972, pp. D1-1–D1-16.

Martin, C. S., "Method of Characteristics Applied to Calculation of Surge Tank Oscillations," *Proc. First International Conference on Pressure Surges*, published by British Hydromechanics Research Assoc., Sept. 1972, pp. E1-1–E1-12.

Proceedings, First International Conference on Pressure Surges, Canterbury England, Sept. 1972, published by British Hydromechanics Research Assoc., England.

Lai, C., "Some Computational Aspects of One and Two Dimensional Unsteady Flow Simulation by the Method of Characteristics," *Internat. Symposium on Unsteady Flow in Open Channels*, Newcastle-upon-Tyne, England, published by British Hydromechanics Research Assoc., April 1976.

Wylie, E. B. and Streeter, V. L., "One-Dimensional Soil Transients by Characteristics," *Proc., 2nd International Conference on Numerical Methods in Geomechanics*, Virginia Polytechnic Institute, Virginia, June 1976.

CHAPTER 4

TRANSIENTS CAUSED BY CENTRIFUGAL PUMPS

4.1 INTRODUCTION

The starting or stopping of pumps causes transients in pumping installations. To analyze these transients, the method of characteristics presented in Chapter 3 may be used. Since the pumping head and flow depend upon the pump speed, transient-state speed changes have to be taken into consideration in the analysis. For this purpose, special boundary conditions for the pump end of a pipeline have to be developed.

In this chapter, the analysis of transients caused by various pump operations is presented. A procedure for storing the pump characteristics in a digital computer is outlined, boundary conditions for a pump end are developed, and a typical problem is solved. Design criteria for designing pipelines are then presented, and the chapter concludes by a presentation of a case study.

4.2 TRANSIENT CONDITIONS CAUSED BY VARIOUS PUMP OPERATIONS

During a pump start-up, the discharge valve is usually kept closed to reduce the electrical load on the pump motor; and as the pump speed reaches the rated speed, the valve is gradually opened. Usually, in a normal pump-stopping procedure, the discharge valve is first closed slowly, and then the power supply to the pump motor is switched off. Transients caused by both of these operations may be analyzed by using the boundary conditions developed in Chapter 3 since the pump speed remains almost constant during the transients in the piping system. However, if the pumps are not started or stopped as previously outlined, then procedures outlined in this chapter should be used for the transient analysis.

Transients caused by emergency pump operations (e.g., sudden power failure) are usually severe, and the pipeline should be designed to withstand positive and

negative pressures caused by these operations. Following a power failure, the pump speed reduces since the pump inertia is usually small compared to that of the liquid in the discharge line. Because the flow and the pumping head at the pump are reduced, negative pressure waves propagate downstream in the discharge line, and positive pressure waves propagate upstream in the suction line. Flow in the discharge line reduces rapidly to zero and then reverses through the pump even though the latter may still be rotating in the normal direction. In this condition (i.e., when there is reverse flow through the pump while it is rotating in the normal direction), the pump is said to be operating in the *zone of energy dissipation.* Because of the reverse flow, the pump slows down rapidly, stops momentarily, and then reverses, i.e., the pump is now operating as a turbine. The pump speed increases in the reverse direction until it reaches the *runaway speed.* With the increase in the reverse speed, the reverse flow through the pump is reduced due to choking effect, and positive and negative pressure waves are produced in the discharge and suction lines, respectively.

If the pipeline profile is such that the transient-state hydraulic grade line falls below the pipeline at any point, vacuum pressure may occur, and the water column in the pipeline may separate at that point. Excessive pressure will be produced when the two columns later rejoin. During the design stages, the possibility of water-column separation should be investigated, and, if necessary, remedial measures should be taken. This will be discussed in detail in Chapter 9.

4.3 MATHEMATICAL REPRESENTATION OF A PUMP

As discussed in Chapter 3, the relationship between the discharge, Q, and the pressure head, H, at the boundary must be known in order to develop the boundary conditions. The discharge of a centrifugal pump depends upon the rotational speed, N, and the pumping head, H; and the transient-state speed changes depend upon torque, T, and the combined moment of inertia of the pump, motor, and liquid entrained in the pump impeller. Thus, four variables—namely, Q, H, N, and T—have to be specified for the mathematical representation of a pump. The curves showing the relationships between these variables are called the *pump characteristics.* Various authors have presented these curves in different graphical forms suitable for graphical[1-4] or computer[5-8] analysis. Of all the methods proposed for storing pump characteristics in a digital computer, the method used by Marchal et al.[6] appears to be the most suitable and is used herein.

Although pump-characteristics data in the pumping zone are usually available, little data, except that presented in Refs. 4 and 8, are available for either the zone of energy dissipation or the zone of turbine operation. If the complete characteristics data are not available, then the characteristics of a pump having about the same specific speed may be used as an approximation.

Data for prototype pump characteristics are obtained from model test results by using homologous relationships.[9] Two pumps (or turbines) are considered homologous if they are geometrically similar and the streamflow pattern through them is also similar. For homologous pumps, the following ratios are valid

$$\left.\begin{aligned} &\frac{H}{N^2D^2} = \text{Constant} \\ &\text{and} \\ &\frac{N}{QD^3} = \text{Constant} \end{aligned}\right\} \tag{4.1}$$

in which D = diameter of impeller. Since D is constant for a particular unit, it may be included in the constants of Eq. 4.1, i.e.,

$$\left.\begin{aligned} &\frac{H}{N^2} = \text{Constant} \\ &\text{and} \\ &\frac{N}{Q} = \text{Constant} \end{aligned}\right\} \tag{4.2}$$

Equation 4.2 may be nondimensionalized by using the quantities for the rated condition as reference values. Let us define the following dimensionless variables:

$$\left.\begin{aligned} v &= \frac{Q}{Q_R} \\ h &= \frac{H}{H_R} \\ \alpha &= \frac{N}{N_R} \\ \beta &= \frac{T}{T_R} \end{aligned}\right\} \tag{4.3}$$

In this equation, T = torque and the subscript R designates the value of the variables for the rated conditions. On the basis of Eq. 4.2, Eq. 4.3 may be written as

$$\left.\begin{aligned} &\frac{h}{\alpha^2} = \text{Constant} \\ &\frac{\alpha}{v} = \text{Constant} \end{aligned}\right\} \tag{4.4}$$

TABLE 4.1. Zones of pump operation.

Zone of Operation	Sign of v	Sign of α	Range of θ
Pump	+	+	$0° \leq \theta \leq 90°$
Energy dissipation	-	+	$90° \leq \theta \leq 180°$
Turbine	-	-	$180° \leq \theta \leq 270°$
Turbine energy dissipation	+	-	$270° \leq \theta \leq 360°$

Since α becomes zero while analyzing transients for all four zones of operation, h/α^2 becomes infinite. To avoid this, the parameter $h/(\alpha^2 + v^2)$ instead of h/α^2 may be used.*

The signs of v and α depend upon the zones of operation. In addition to the need to define a different characteristic curve for each zone of operation, α/v becomes infinite for $v = 0$. To avoid this, a new variable θ may be defined[6] as

$$\theta = \tan^{-1}\frac{\alpha}{v} \tag{4.5}$$

and then the characteristic curve may be plotted between θ and $h/(\alpha^2 + v^2)$. By definition, θ is always finite, and its value varies between 0° and 360° for the four zones of operation (see Table 4.1).

Similar to the pressure-head curve, the torque characteristic curve may be plotted between $\beta/(\alpha^2 + v^2)$ and θ.

Using the data presented by Thomas,[8] characteristic curves for pumps having specific speed** of 25,† 147, and 261 SI units (1276, 7600, and 13,500 gpm units, respectively) are presented in Fig. 4.1 and in Appendix E.

4.4 BOUNDARY CONDITIONS FOR PUMP FAILURE

As discussed in Chapter 3, the characteristic equation (equations *if* the boundary has pipes on both the upstream and downstream sides) and the conditions im-

*Marchal et al. suggest that sgn $(h)\sqrt{|h|/(\alpha^2 + v^2)}$ be used to increase accuracy for smaller values of this parameter (sgn designates sign of h). However, $h/(\alpha^2 + v^2)$ is used herein because it simplifies the derivation of the boundary conditions for the pump end (see Section 4.4).

**Specific speed = $N_R\sqrt{Q_R}/H_R^{3/4}$. In SI units, N_R is in rpm, Q_R is in m^3/s, and H_R is in m; in gpm units, N_R is in rpm, Q_R is in gpm, and H_R is in ft. For a double-suction pump, Q_R is divided by 2 while computing the specific speed.

†Some authors erroneously use a specific speed of 35 SI units for this pump. As the pump had a double suction, rated discharge should be divided by two to compute the specific speed (see Closure of Ref. 8, p. A-124 and A-127).

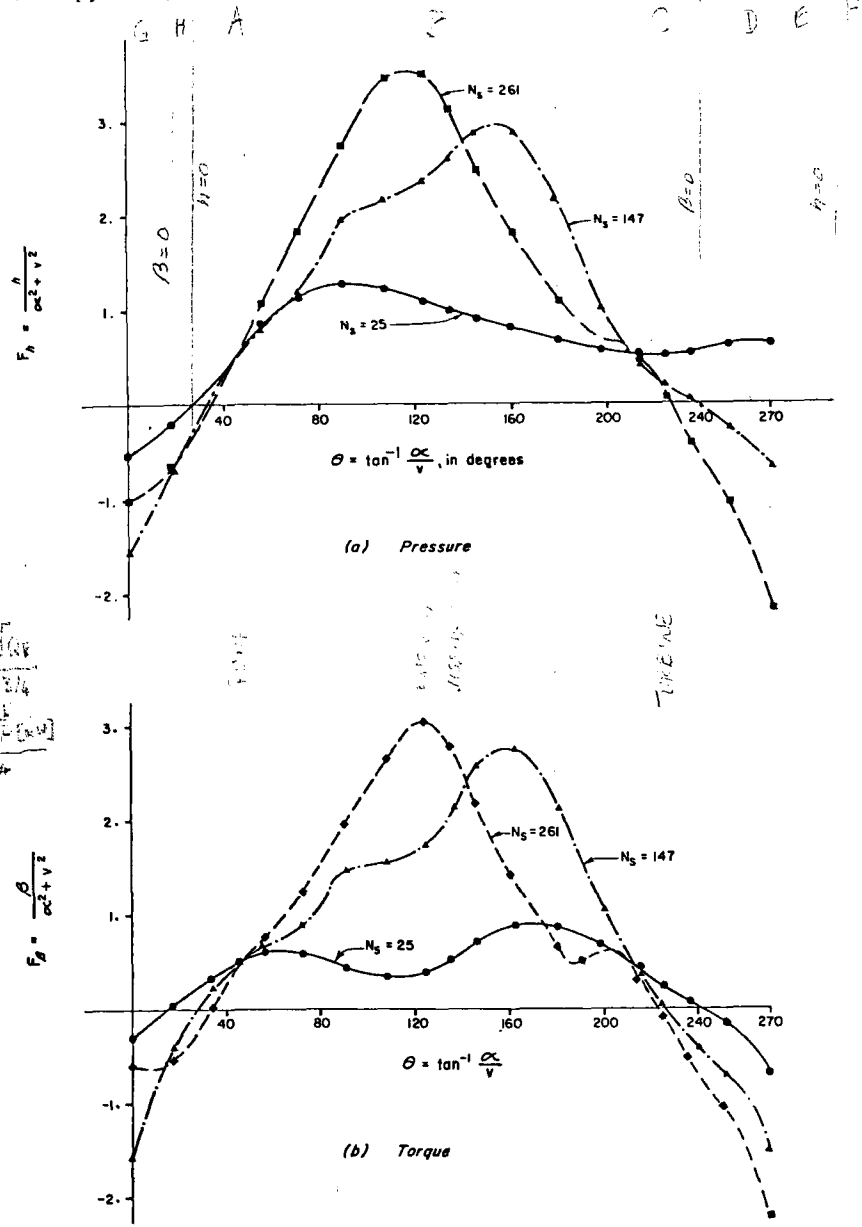

Figure 4.1. Characteristics of pumps of various specific speeds.

posed by the boundary are solved simultaneously to determine the boundary conditions. For a pump end, the pump characteristics define the conditions imposed by the boundary, and a differential equation defines the variation of the pump speed with time following power failure. Thus, we have to simultaneously solve these equations to develop the boundary conditions for the pump end.

To facilitate understanding of the derivation, let us first consider a simple system having only one pump and a very short suction line. We will develop the boundary conditions for more complex cases in the next section.

Equations of Conditions Imposed by Pump

As we outlined in Section 4.3, pump characteristics may be mathematically represented by curves between θ and $h/(\alpha^2 + v^2)$ and between θ and $\beta/(\alpha^2 + v^2)$, in which $\theta = \tan^{-1}(\alpha/v)$. To use these curves in a mathematical model, discrete points on these curves at equal intervals of θ, between the range $\theta = 0$ and $\theta = 360°$, are stored in the computer. Each segment of these curves between the points stored in the computer may be approximated by straight lines (Fig. 4.2). If a sufficient number of points (e.g., 73) are stored, then the error introduced by approximating the curves by segmental straight lines is negligible.

For any value of α and v (except when both α and v are simultaneously zero), the value of $\theta = \tan^{-1}(\alpha/v)$ may be determined by using IBM function ATAN2. However, this function computes the value of θ between 0 and π and between 0

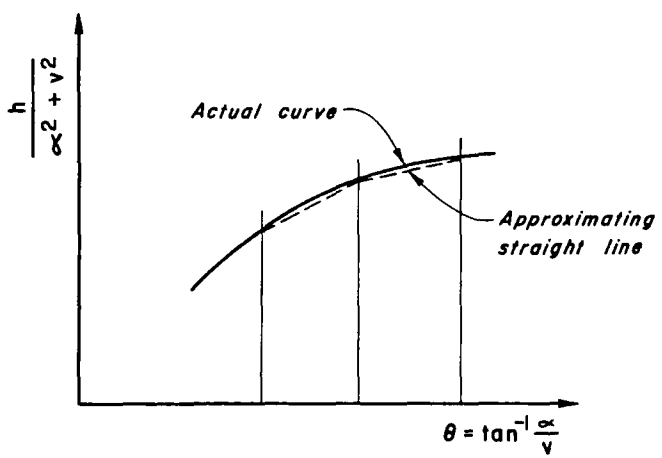

Figure 4.2. Approximation of pump characteristic curves by segmented straight lines.

and $-\pi$, whereas our range of interest is between 0 and 2π. This limitation can be circumvented by adding 2π to the computed value of θ if $\theta < 0$; e.g., if θ given by this function is $-30°$, then the value of θ to be used for determining the point on the pump characteristic curve is $360 - 30 = 330°$.

Let us assume that the calculation has progressed to the ith time step; that the variables α, v, h, and β at the beginning of this time step are known; and that we want to compute the values of these variables at the end of the time step. Let us denote these unknown variables by α_P, v_P, h_P, and β_P. To determine the value of these variables, we have to first of all determine the equation of the segment of pump characteristics corresponding to α_P and v_P. However, since the values of these variables are initially unknown, we may use, as a first estimate, their values determined by extrapolation from the known values for the previous time steps, i.e.,

$$\left.\begin{aligned} \alpha_e &= \alpha_i + \Delta\alpha_{i-1} \\ v_e &= v_i + \Delta v_{i-1} \end{aligned}\right\} \tag{4.6}$$

in which α_e and v_e are the estimated values at the end of ith time step, α_i and v_i refer to known values at the beginning of the ith time step, and $\Delta\alpha_{i-1}$ and Δv_{i-1} are the variation of these variables during the $(i-1)$th time step. Since the pump speed and the pump discharge vary gradually, the preceding linear extrapolation should yield sufficiently accurate estimates if the size of the computational time step, Δt, is small. Now, the grid points on either side of $\theta = \tan^{-1}(\alpha_e/v_e)$ are searched, and the ordinates $h/(\alpha^2 + v^2)$ and $\beta/(\alpha^2 + v^2)$ for these grid points are determined from the stored values. From these, the constants* for the equation of the segmental straight line are determined. Now, assuming that the points corresponding to α_P, v_P, h_P, and β_P lie on these straight lines, then

$$\frac{h_P}{\alpha_P^2 + v_P^2} = a_1 + a_2 \tan^{-1}\frac{\alpha_P}{v_P} \tag{4.7}$$

$$\frac{\beta_P}{\alpha_P^2 + v_P^2} = a_3 + a_4 \tan^{-1}\frac{\alpha_P}{v_P} \tag{4.8}$$

in which a_1 and a_2, and a_3 and a_4 are constants for the straight lines representing the head and torque characteristics, respectively.

Referring to Fig. 4.3, the following equation can be written for the total head at the pump:

$$H_{P_{i,1}} = H_{\text{suc}} + H_P - \Delta H_{P_v} \tag{4.9}$$

*If $y = a_1 + a_2 x$ is the equation of a straight line passing through the points (x_1, y_1) and (x_2, y_2), then $a_1 = (y_1 x_2 - y_2 x_1)/(x_2 - x_1)$ and $a_2 = (y_2 - y_1)/(x_2 - x_1)$.

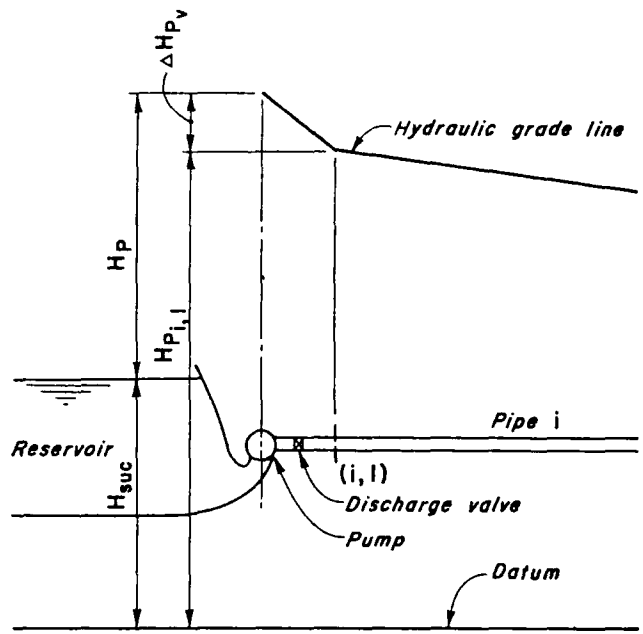

Figure 4.3. Notation of boundary conditions for pump.

in which H_{suc} = height of the liquid surface in the suction reservoir above datum, H_P = pumping head at the end of the time step, and ΔH_{P_v} = head loss in the discharge valve. Note that the velocity head in the discharge pipe, which is usually small, is not taken into consideration in Eq. 4.9. The valve head loss is given by the equation:

$$\Delta H_{P_v} = C_v Q_{P_{i,1}}^2 = C_v Q_{P_{i,1}} |Q_{P_{i,1}}| \tag{4.10}$$

in which C_v = coefficient of head losses in the valve. Note that in this equation, $Q_{P_{i,1}}^2$ is written as $Q_{P_{i,1}} |Q_{P_{i,1}}|$ to account for the reverse flow.

Equations 4.7 to 4.10 represent the conditions imposed by the boundary.

Differential Equation of Rotating Masses

The accelerating torque for a rotational system is equal to the product of the angular acceleration and the polar moment of inertia of the system. Since there is no external torque acting on the pump following power failure, the decelerat-

ing torque is the pump torque. Hence,

$$T = -WR^2 \frac{d\omega}{dt}$$

or

$$T = -WR^2 \frac{2\pi}{60} \frac{dN}{dt} \tag{4.11}$$

in which WR^2 = combined polar moment of inertia of the pump, motor, shaft, and liquid entrained in the pump impeller, and ω and N are rotational speed of the pump, in rad/s and in rpm, respectively. On the basis of Eq. 4.3, Eq. 4.11 may be written as:

$$\beta = -WR^2 \frac{2\pi N_R}{60\, T_R} \frac{d\alpha}{dt} \tag{4.12}$$

In this equation, $T_R = 60\ \gamma H_R Q_R/(2\pi N_R \eta_R)$ in which γ = specific weight of liquid, and η_R = pump efficiency at rated conditions. By using an average value of β during the time step, this equation may be written in a finite-difference form as:

$$\frac{\alpha_P - \alpha}{\Delta t} = -\frac{60\, T_R}{2\pi WR^2 N_R} \frac{\beta + \beta_P}{2} \tag{4.13}$$

which may be simplified to

$$\alpha_P - C_6 \beta_P = \alpha + C_6 \beta \tag{4.14}$$

in which

$$C_6 = \frac{-15\, T_R \Delta t}{\pi WR^2 N_R} \tag{4.15}*$$

Characteristic Equation for Discharge Pipe

As the suction line is short, it may be neglected in the analysis. Therefore, we need only the characteristic equation for the discharge line, i.e., for section (i, 1),

$$Q_{P_{i,1}} = C_n + C_a H_{P_{i,1}} \tag{4.16}$$

*In English units, the right-hand sides, of Eqs. 4.11 and 4.12 have to be divided by the acceleration of gravity, g. In SI units, WR^2 is in kg m^2 and T_R is in Nm; in the English units, WR^2 is in lb-ft^2, and T_R is in lb-ft. N_R in both SI and English units is in rpm. In English units, the right-hand side of Eq. 4.15 has to be multiplied by g.

Continuity Equation

Since there is no storage between the suction reservoir and section (i, 1)

$$Q_{P_{i,1}} = Q_P \tag{4.17}$$

in which Q_P = flow through the pump at the end of the time step.

Solution of Governing Equations

To develop the boundary conditions, we have to solve Eqs. 4.7 through 4.10, 4.14, 4.16, and 4.17 simultaneously. By eliminating $H_{P_{i,1}}$, ΔH_{P_v}, and $Q_{P_{i,1}}$ from Eqs. 4.9, 4.10, 4.16, and 4.17 and by using Q_R and H_R as reference values, the resulting equation may be written as

$$Q_R v_P = C_n + C_a H_{\text{suc}} + C_a H_R h_P - C_a C_v Q_R^2 v_P |v_P| \tag{4.18}$$

Now we have four equations—i.e., Eqs. 4.7, 4.8, 4.14, and 4.18—in four unknowns—α_P, v_P, h_P, β_P. To simplify the solution, we will first eliminate h_P and β_P from these equations as discussed in the following.

By substituting for h_P from Eq. 4.7 into Eq. 4.18 and for β_P from Eq. 4.8 into Eq. 4.14 and simplifying, we obtain

$$F_1 = C_a H_R a_1 (\alpha_P^2 + v_P^2) + C_a H_R a_2 (\alpha_P^2 + v_P^2) \tan^{-1} \frac{\alpha_P}{v_P} - Q_R v_P$$
$$- C_a C_v Q_R^2 v_P |v_P| + C_n + C_a H_{\text{suc}} = 0 \tag{4.19}$$

$$F_2 = \alpha_P - C_6 a_3 (\alpha_P^2 + v_P^2) - C_6 a_4 (\alpha_P^2 + v_P^2) \tan^{-1} \frac{\alpha_P}{v_P} - \alpha - C_6 \beta = 0 \tag{4.20}$$

Equations 4.19 and 4.20 are nonlinear equations in two unknowns, α_P and v_P. These equations can be solved by using the Newton-Raphson method in which a solution of the equations is first guessed, which is then refined to a required degree of accuracy by successive iterations.

Let $\alpha_P^{(1)}$ and $v_P^{(1)}$ be the initially estimated values of solution, which may be taken equal to α_e and v_e as determined from Eq. 4.6.* Then, a better estimate of the solution of Eqs. 4.19 and 4.20 is

$$\alpha_P^{(2)} = \alpha_P^{(1)} + \delta\alpha_P \tag{4.21}**$$

$$v_P^{(2)} = v_P^{(1)} + \delta v_P \tag{4.22}**$$

*Superscript (1) indicates estimated values and superscript (2) indicates values after first iteration.

**These equations may be deduced from the general derivation presented on p. 91.

in which

$$\delta\alpha_P = \frac{F_2 \dfrac{\partial F_1}{\partial v_P} - F_1 \dfrac{\partial F_2}{\partial v_P}}{\dfrac{\partial F_1}{\partial \alpha_P}\dfrac{\partial F_2}{\partial v_P} - \dfrac{\partial F_1}{\partial v_P}\dfrac{\partial F_2}{\partial \alpha_P}} \tag{4.23}$$

$$\delta v_P = \frac{F_2 \dfrac{\partial F_1}{\partial \alpha_P} - F_1 \dfrac{\partial F_2}{\partial \alpha_P}}{\dfrac{\partial F_1}{\partial v_P}\dfrac{\partial F_2}{\partial \alpha_P} - \dfrac{\partial F_1}{\partial \alpha_P}\dfrac{\partial F_2}{\partial v_P}} \tag{4.24}$$

In Eqs. 4.23 and 4.24, functions F_1 and F_2 and their derivatives with respect to α_P and v_P are evaluated at $\alpha_P^{(1)}$ and $v_P^{(1)}$. Differentiation of Eqs. 4.19 and 4.20 yields the following expressions for these derivatives:

$$\frac{\partial F_1}{\partial \alpha_P} = C_a H_R \left(2a_1\alpha_P + a_2 v_P + 2a_2\alpha_P \tan^{-1}\frac{\alpha_P}{v_P}\right) \tag{4.25}$$

$$\frac{\partial F_1}{\partial v_P} = C_a H_R \left(2a_1 v_P - a_2\alpha_P + 2a_2 v_P \tan^{-1}\frac{\alpha_P}{v_P}\right) - Q_R - 2C_a C_v Q_R^2 |v_P| \tag{4.26}$$

$$\frac{\partial F_2}{\partial \alpha_P} = 1 - C_6 \left(2a_3\alpha_P + a_4 v_P + 2a_4\alpha_P \tan^{-1}\frac{\alpha_P}{v_P}\right) \tag{4.27}$$

$$\frac{\partial F_2}{\partial v_P} = C_6 \left(-2a_3 v_P + a_4\alpha_P - 2a_4 v_P \tan^{-1}\frac{\alpha_P}{v_P}\right) \tag{4.28}$$

If $|\delta\alpha_P|$ and $|\delta v_P|$ are less than a specified tolerance (e.g., 0.001), then $\alpha_P^{(2)}$ and $v_P^{(2)}$ are solutions of Eqs. 4.19 and 4.20. Otherwise, $\alpha_P^{(1)}$ and $v_P^{(1)}$ are assumed equal to $\alpha_P^{(2)}$ and $v_P^{(2)}$, and the above procedure is repeated until a solution is obtained. Having determined α_P and v_P, it is verified whether the segment of the pump characteristic used in the computations corresponds to α_P and v_P. If it does not, then α_e and v_e are assumed equal to α_P and v_P, and the abovementioned procedure is repeated.

However, if the correct segment was used, then h_P and β_P are determined from Eqs. 4.7 and 4.8; H_P and Q_P from Eq. 4.3; and $H_{P_{i,1}}$ and $Q_{P_{i,1}}$ from Eqs. 4.9 and 4.17. The values of α and v are initialized for the next time step (i.e., $\alpha = \alpha_P$ and $\beta = \beta_P$), and the solution progresses to the next time step. To avoid an unlimited number of iterations in the case of divergence of solution, a counter may be used so that the computations are stopped if the number of iterations exceeds a specified value (e.g., 30). The flowchart of Fig. 4.4, illustrates this procedure.

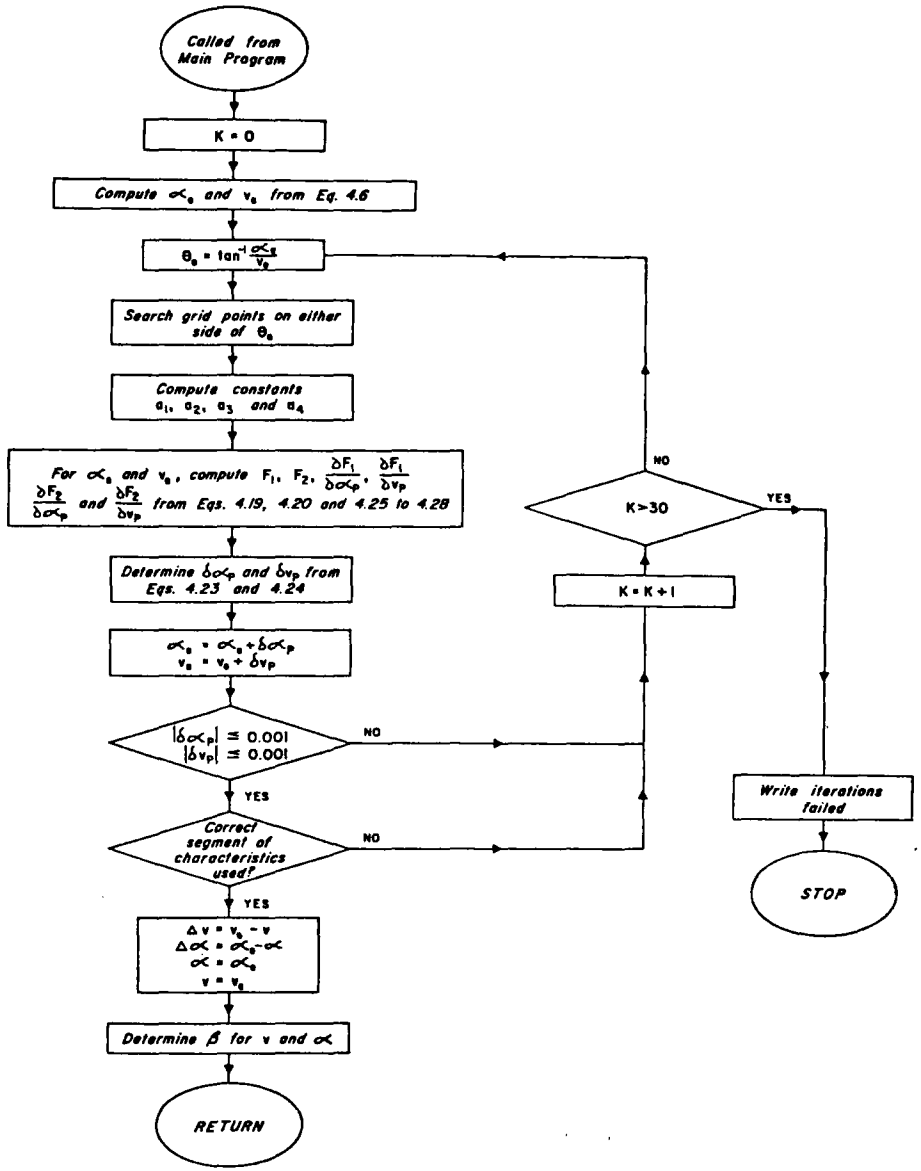

Figure 4.4. Flowchart for boundary conditions for pump.

4.5 BOUNDARY CONDITIONS FOR SPECIAL CASES

In Section 4.4, boundary conditions were developed for a system having only one pump and a short suction line. Because of the short length, the propagation of the waterhammer waves in the suction line was neglected. In this section, we will develop boundary conditions for complex systems often found in practice. Boundary conditions for systems not covered herein may be developed by following a similar procedure.

We will briefly describe the system configuration, and then present the governing equations and the expressions for F_1, F_2, $\partial F_1/\partial \alpha_P$, $\partial F_1/\partial v_P$, $\partial F_2/\partial \alpha_P$, and $\partial F_2/\partial v_P$. Using these expressions, the solutions may be determined as outlined in Section 4.4.

Parallel Pumps

Systems having parallel pumps to which power fails simultaneously may be analyzed as follows: If the length of pipe between each pump and the discharge manifold is long, then each pump may be handled as outlined in Section 4.4, and the parallel piping system may be analyzed using the boundary conditions presented in Chapter 3 (note that the discharge manifold will be considered as a junction of two or more pipes). However, if the pipe between each pump and the discharge manifold is short, then this pipe may be neglected in the analysis, and the combined discharge of all pumps may be considered as the flow at the upstream side of the discharge manifold. Boundary conditions for the latter case are developed in this section.

The continuity equation for this case is:

$$Q_{P_{i,1}} = n_P Q_P \tag{4.29}$$

in which n_P = number of parallel pumps.

Depending upon the length of the suction line, boundary conditions for parallel pumps may be divided into the following two cases:

1. *Short suction line.* If the suction line is short, then the waterhammer waves in this line may be neglected. On the basis of Eq. 4.29, Eq. 4.18 becomes

$$n_P Q_R v_P = C_n + C_a H_{\text{suc}} + C_a H_R h_P - C_a C_v Q_R^2 v_P |v_P| \tag{4.30}$$

Equations 4.7, 4.8, and 4.14 are valid for this case as well. Proceeding similarly as in Section 4.4, the following expressions are obtained:

$$F_1 = C_a H_R a_1(\alpha_P^2 + v_P^2) + C_a H_R a_2(\alpha_P^2 + v_P^2)\tan^{-1}\frac{\alpha_P}{v_P} - n_P Q_R v_P$$
$$- C_a C_v Q_R^2 v_P |v_P| + C_n + C_a H_{\text{suc}} = 0 \tag{4.31}$$

$$\frac{\partial F_1}{\partial v_P} = C_a H_R\left(2a_1 v_P - a_2\alpha_P + 2a_2 v_P \tan^{-1}\frac{\alpha_P}{v_P}\right) - n_P Q_R - 2C_a C_v Q_R^2 |v_P| \tag{4.32}$$

Expression for F_2, $\partial F_1/\partial \alpha_P$, $\partial F_2/\partial \alpha_P$, and $\partial F_2/\partial v_P$ are given by Eqs. 4.20, 4.25, 4.27, and 4.28, respectively.

2. *Long suction line* (Fig. 4.5). If the suction line is not short compared to the discharge line, then waterhammer in the former has to be considered in the analysis. Therefore, we have to include the characteristic equation for the suction line. Referring to Fig. 4.5,

$$H_P = H_{P_{i+1,1}} - H_{P_{i,n+1}} \tag{4.33}$$

$$Q_{P_{i,n+1}} = C_p - C_{a_i} H_{P_{i,n+1}} \tag{4.34}$$

$$Q_{P_{i+1,1}} = C_n + C_{a_{i+1}} H_{P_{i+1,1}} \tag{4.35}$$

$$Q_{P_{i,n+1}} = Q_{P_{i+1,1}} = n_P Q_P \tag{4.36}$$

In addition, Eqs. 4.7, 4.8, and 4.14 are valid for this case.

By multiplying Eq. 4.34 by $C_{a_{i+1}}$, Eq. 4.35 by C_{a_i}, substituting for $Q_{P_{i,n+1}}$, and $Q_{P_{i+1,1}}$ from Eq. 4.36, and adding the resulting equations, we obtain

$$n_P Q_P(C_{a_i} + C_{a_{i+1}}) = C_n C_{a_i} + C_p C_{a_{i+1}} + C_{a_i} C_{a_{i+1}} H_P \tag{4.37}$$

By using Q_R and H_R as reference values, Eq. 4.37 may be written as

$$h_P = \frac{n_P(C_{a_i} + C_{a_{i+1}})Q_R v_P - C_n C_{a_i} - C_p C_{a_{i+1}}}{C_{a_i} C_{a_{i+1}} H_R} \tag{4.38}$$

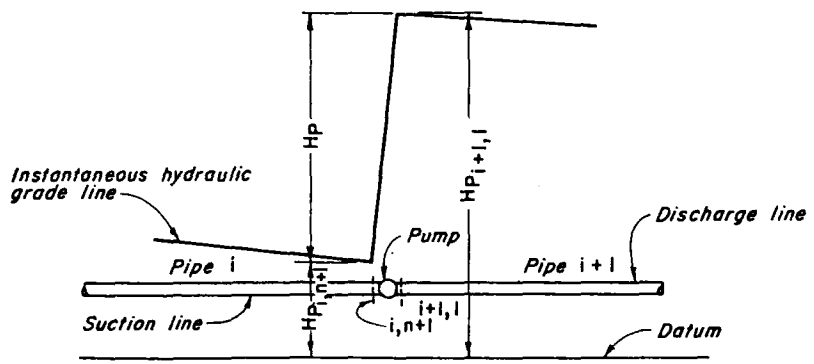

Figure 4.5. Pump with long suction line.

Elimination of h_P from Eqs. 4.7 and 4.38 yields

$$F_1 = a_1(\alpha_P^2 + v_P^2) + a_2(\alpha_P^2 + v_P^2)\tan^{-1}\frac{\alpha_P}{v_P} - C_7 v_P + C_8 = 0 \qquad (4.39)$$

in which

$$C_7 = \frac{n_P(C_{a_i} + C_{a_{i+1}})Q_R}{C_{a_i}C_{a_{i+1}}H_R} \qquad (4.40)$$

$$C_8 = \frac{C_n C_{a_i} + C_p C_{a_{i+1}}}{C_{a_i}C_{a_{i+1}}H_R} \qquad (4.41)$$

By differentiating Eq. 4.39 with respect to α_P and v_P, we obtain

$$\frac{\partial F_1}{\partial \alpha_P} = 2a_1\alpha_P + 2a_2\alpha_P\tan^{-1}\frac{\alpha_P}{v_P} + a_2 v_P \qquad (4.42)$$

$$\frac{\partial F_1}{\partial v_P} = 2a_1 v_P + 2a_2 v_P\tan^{-1}\frac{\alpha_P}{v_P} - a_2\alpha_P - C_7 \qquad (4.43)$$

Equations 4.20, 4.27, and 4.28 define the expressions for F_2, $\partial F_2/\partial\alpha_P$, and $\partial F_2/\partial v_P$.

Series Pumps (Fig. 4.6)

If the pipe length between the two pumping-sets is long, then each pumping-set may be analyzed individually assuming the downstream pumps have a long suction line. However, if the pipe length between the pumps is short, then this pipe may be neglected in the analysis, and the combined boundary conditions for both the pumping units may be developed as discussed in the following.

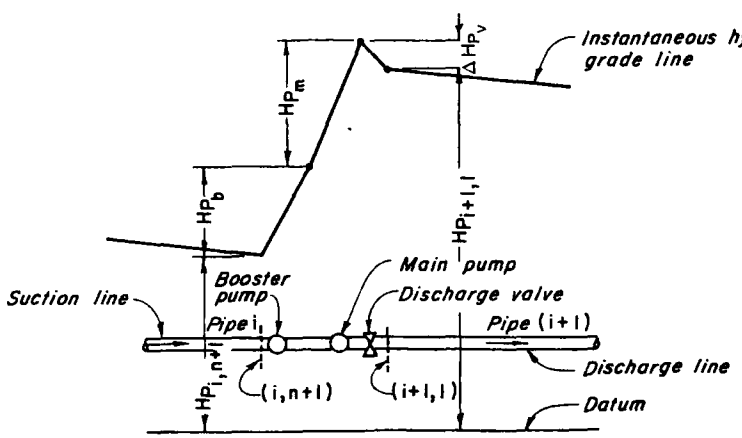

Figure 4.6. Notation for series pumps.

Referring to Fig. 4.6, the following equations may be written for the system:

1. Pumping head

$$H_{P_{i+1,1}} = H_{P_{i,n+1}} + H_{P_b} + H_{P_m} - \Delta H_{P_v} \qquad (4.44)$$

2. Continuity equations

$$Q_{P_{i,n+1}} = n_P Q_{P_b} \qquad (4.45)$$

$$Q_{P_b} = Q_{P_m} \qquad (4.46)$$

$$Q_{P_{i+1,1}} = n_P Q_{P_m} \qquad (4.47)$$

3. Positive characteristic equation for suction line

$$Q_{P_{i,n+1}} = C_p - C_{a_i} H_{P_{i,n+1}} \qquad (4.48)$$

4. Negative characteristic equation for discharge line

$$Q_{P_{i+1,1}} = C_n + C_{a_{i+1}} H_{P_{i+1,1}} \qquad (4.49)$$

5. Equation for head loss in the valve

$$\Delta H_{P_v} = C_v Q_{P_{i+1,1}} |Q_{P_{i+1,1}}| \qquad (4.50)$$

6. Equations for the pump characteristics

$$h_{P_m} = a_{1_m}(\alpha_{P_m}^2 + v_{P_m}^2) + a_{2_m}(\alpha_{P_m}^2 + v_{P_m}^2)\tan^{-1}\frac{\alpha_{P_m}}{v_{P_m}} \qquad (4.51)$$

$$h_{P_b} = a_{1_b}(\alpha_{P_b}^2 + v_{P_b}^2) + a_{2_b}(\alpha_{P_b}^2 + v_{P_b}^2)\tan^{-1}\frac{\alpha_{P_b}}{v_{P_b}} \qquad (4.52)$$

$$\beta_{P_m} = a_{3_m}(\alpha_{P_m}^2 + v_{P_m}^2) + a_{4_m}(\alpha_{P_m}^2 + v_{P_m}^2)\tan^{-1}\frac{\alpha_{P_m}}{v_{P_m}} \qquad (4.53)$$

$$\beta_{P_b} = a_{3_b}(\alpha_{P_b}^2 + v_{P_b}^2) + a_{4_b}(\alpha_{P_b}^2 + v_{P_b}^2)\tan^{-1}\frac{\alpha_{P_b}}{v_{P_b}} \qquad (4.54)$$

7. Equation for the rotating masses (i.e., equations similar to Eq. 4.14)

$$\alpha_{P_m} - C_{6_m}\beta_{P_m} = \alpha_m + C_{6_m}\beta_m \qquad (4.55)$$

$$\alpha_{P_b} - C_{6_b}\beta_{P_b} = \alpha_b + C_{6_b}\beta_b \qquad (4.56)$$

In the preceding equations, subscripts b, m, and v refer to the booster and main pump and to the valve, respectively; n_P = number of pumping-sets connected in parallel; and C_v = coefficient of head loss in the valve.

To solve these equations, let us first reduce the number of unknowns from 13 to three as follows:

Elimination of $H_{P_{i,n+1}}$, $Q_{P_{i,n+1}}$, $H_{P_{i+1,1}}$, $Q_{P_{i+1,1}}$, Q_{P_b}, and H_{P_v} from Eqs. 4.44 to 4.50 yields

$$H_{P_m} + H_{P_b} = \frac{n_P Q_{P_m} - C_n}{C_{a_{i+1}}} - \frac{C_p - n_P Q_{P_m}}{C_{a_i}} + C_v n_P Q_{P_m} |Q_{P_m}| \quad (4.57)$$

Using H_{R_m}, H_{R_b}, and Q_{R_m} as reference values, Eq. 4.57 may be written as

$$h_{P_m} H_{R_m} + h_{P_b} H_{R_b} = \frac{n_P Q_{R_m}}{C_{a_{i+1}}} v_{P_m} + \frac{n_P Q_{R_m}}{C_{a_i}} v_{P_m} + n_P C_v Q_{R_m}^2 v_{P_m} |v_{P_m}| - \frac{C_n}{C_{a_{i+1}}} - \frac{C_p}{C_{a_i}} \quad (4.58)$$

By substituting expressions for h_{P_m} and h_{P_b} from Eqs. 4.51 and 4.52 into Eq. 4.58 and simplifying the resulting equation, we obtain

$$F_1 = a_{1_m} H_{R_m} (\alpha_{P_m}^2 + v_{P_m}^2) + a_{2_m} H_{R_m} (\alpha_{P_m}^2 + v_{P_m}^2) \tan^{-1} \frac{\alpha_{P_m}}{v_{P_m}} + a_{1_b} H_{R_b} (\alpha_{P_b}^2 + v_{P_m}^2) + a_{2_b} H_{R_b} (\alpha_{P_b}^2 + v_{P_m}^2) \tan^{-1} \frac{\alpha_{P_b}}{v_{P_m}} - n_P C_v Q_{R_m}^2 v_{P_m} |v_{P_m}| - \frac{n_P Q_{R_m}}{C_{a_{i+1}}} v_{P_m} - \frac{n_P Q_{R_m}}{C_{a_i}} v_{P_m} + \frac{C_n}{C_{a_{i+1}}} + \frac{C_p}{C_{a_i}} = 0 \quad (4.59)$$

Note that in Eq. 4.59, we have replaced v_{P_b} by v_{P_m} since both are equal as the number of main and booster pumping-sets are equal.

By eliminating β_{P_m} from Eqs. 4.53 and 4.55 and β_{P_b} from Eqs. 4.54 and 4.56, we obtain

$$F_2 = \alpha_{P_m} - C_{6_m} \left[a_{3_m} (\alpha_{P_m}^2 + v_{P_m}^2) + a_{4_m} (\alpha_{P_m}^2 + v_{P_m}^2) \tan^{-1} \frac{\alpha_{P_m}}{v_{P_m}} \right] - \alpha_m - C_{6_m} \beta_m \quad (4.60)$$

$$F_3 = \alpha_{P_b} - C_{6_b} \left[a_{3_b} (\alpha_{P_b}^2 + v_{P_m}^2) + a_{4_b} (\alpha_{P_b}^2 + v_{P_m}^2) \tan^{-1} \frac{\alpha_{P_b}}{v_{P_m}} \right] - \alpha_b - C_{6_b} \beta_b \quad (4.61)$$

Now we have three nonlinear equations (Eqs. 4.59–4.61) in three unknowns, α_{P_m}, v_{P_m}, and α_{P_b}. To solve these equations by the Newton-Raphson method, we have to obtain a solution of the following equations:

$$\left(\frac{\partial F_1}{\partial \alpha_{P_m}} \delta\alpha_{P_m} + \frac{\partial F_1}{\partial v_{P_m}} \delta v_{P_m} + \frac{\partial F_1}{\partial \alpha_{P_b}} \delta\alpha_{P_b} \right)^{(1)} = -F_1^{(1)} \quad (4.62)$$

$$\left(\frac{\partial F_2}{\partial \alpha_{P_m}} \delta\alpha_{P_m} + \frac{\partial F_2}{\partial v_{P_m}} \delta v_{P_m} + \frac{\partial F_2}{\partial \alpha_{P_b}} \delta\alpha_{P_b} \right)^{(1)} = -F_2^{(1)} \quad (4.63)$$

$$\left(\frac{\partial F_3}{\partial \alpha_{P_m}} \delta\alpha_{P_m} + \frac{\partial F_3}{\partial v_{P_m}} \delta v_{P_m} + \frac{\partial F_3}{\partial \alpha_{P_b}} \delta\alpha_{P_b} \right)^{(1)} = -F_3^{(1)} \quad (4.64)$$

In these equations, the functions F_1, F_2, and F_3, and their derivatives, are evaluated for the estimated values of $\alpha_{P_m}^{(1)}$, $v_{P_m}^{(1)}$, and $\alpha_{P_b}^{(1)}$, and a better estimate of the solution is determined from the following equations:

$$\alpha_{P_m}^{(2)} = \alpha_{P_m}^{(1)} + \delta\alpha_{P_m} \quad (4.65)$$

$$v_{P_m}^{(2)} = v_{P_m}^{(1)} + \delta v_{P_m} \quad (4.66)$$

$$\alpha_{P_b}^{(2)} = \alpha_{P_b}^{(1)} + \delta\alpha_{P_b} \quad (4.67)$$

As before, the superscript in the parentheses refers to the number of the iteration. The expressions for the derivatives obtained by differentiating Eqs. 4.59 through 4.61 are

$$\frac{\partial F_1}{\partial \alpha_{P_m}} = 2a_{1_m} H_{R_m} \alpha_{P_m} + 2a_{2_m} H_{R_m} \alpha_{P_m} \tan^{-1} \frac{\alpha_{P_m}}{v_{P_m}} + a_{2_m} H_{R_m} v_{P_m} \quad (4.68)$$

$$\frac{\partial F_1}{\partial v_{P_m}} = 2a_{1_m} H_{R_m} v_{P_m} + 2a_{2_m} H_{R_m} v_{P_m} \tan^{-1} \frac{\alpha_{P_m}}{v_{P_m}} - a_{2_m} H_{R_m} \alpha_{P_m} + 2a_{1_b} H_{R_b} v_{P_m} + 2a_{2_b} H_{R_b} v_{P_m} \tan^{-1} \frac{\alpha_{P_b}}{v_{P_m}} - a_{2_b} H_{R_b} \alpha_{P_b} - 2n_P C_v Q_{R_m}^2 |v_{P_m}| - \frac{n_P Q_{R_m}}{C_{a_{i+1}}} - \frac{n_P Q_{R_m}}{C_{a_i}} \quad (4.69)$$

$$\frac{\partial F_1}{\partial \alpha_{P_b}} = 2a_{1_b} H_{R_b} \alpha_{P_b} + 2a_{2_b} H_{R_b} \alpha_{P_b} \tan^{-1} \frac{\alpha_{P_b}}{v_{P_m}} + a_{2_b} H_{R_b} v_{P_m} \tag{4.70}$$

$$\frac{\partial F_2}{\partial \alpha_{P_b}} = 0 \tag{4.71}$$

$$\frac{\partial F_2}{\partial \alpha_{P_m}} = 1 - 2C_{6_m} a_{3_m} \alpha_{P_m} - 2C_{6_m} a_{4_m} \alpha_{P_m} \tan^{-1} \frac{\alpha_{P_m}}{v_{P_m}} - C_{6_m} a_{4_m} v_{P_m} \tag{4.72}$$

$$\frac{\partial F_2}{\partial v_{P_m}} = -2C_{6_m} a_{3_m} v_{P_m} - 2C_{6_m} a_{4_m} v_{P_m} \tan^{-1} \frac{\alpha_{P_m}}{v_{P_m}} + C_{6_m} a_{4_m} \alpha_{P_m} \tag{4.73}$$

$$\frac{\partial F_3}{\partial \alpha_{P_m}} = 0 \tag{4.74}$$

$$\frac{\partial F_3}{\partial \alpha_{P_b}} = 1 - 2C_{6_b} a_{3_b} \alpha_{P_b} - 2C_{6_b} a_{4_b} \alpha_{P_b} \tan^{-1} \frac{\alpha_{P_b}}{v_{P_m}} - C_{6_b} a_{4_b} v_{P_m} \tag{4.75}$$

$$\frac{\partial F_3}{\partial v_{P_m}} = -2C_{6_b} a_{3_b} v_{P_m} - 2C_{6_b} a_{4_b} v_{P_m} \tan^{-1} \frac{\alpha_{P_b}}{v_{P_m}} + C_{6_b} a_{4_b} \alpha_{P_b} \tag{4.76}$$

If $|\delta\alpha_{P_m}|$, $|\delta\alpha_{P_b}|$, and $|\delta v_{P_m}|$, obtained by simultaneously solving Eqs. 4.62 through 4.64, are less than a specified tolerance (e.g., 0.001), then $\alpha_{P_m}^{(2)}$, $v_{P_m}^{(2)}$, and $\alpha_{P_b}^{(2)}$ are solutions of Eqs. 4.59 through 4.61; otherwise, $\alpha_{P_m}^{(1)}$, $v_{P_m}^{(1)}$, and $\alpha_{P_b}^{(1)}$ are assumed equal to $\alpha_{P_m}^{(2)}$, $v_{P_m}^{(2)}$, and $\alpha_{P_b}^{(2)}$, and the above procedure is repeated until a solution is obtained. Then, it is verified whether the segment of pump characteristics used in the computations corresponded to α_P and v_P. If it does not, then α_{e_m}, α_{e_b}, and v_{e_m} are assumed equal to $\alpha_{P_m}^{(2)}$, $\alpha_{P_b}^{(2)}$, and $v_{P_m}^{(2)}$, respectively, and the above procedure is repeated; otherwise, the values of the remaining variables are obtained from Eqs. 4.44 through 4.56, and the solution progresses to the next time step.

To avoid an unlimited number of iterations in the case of divergence of iterations, a counter should be used so that the computations are stopped if the number of iterations exceeds a specified value (e.g., 30).

4.6 EXAMPLE

To illustrate the use of the above procedure, the piping system shown in Fig. 4.7 is analyzed. Initially, both pumps are operating at rated conditions, and the

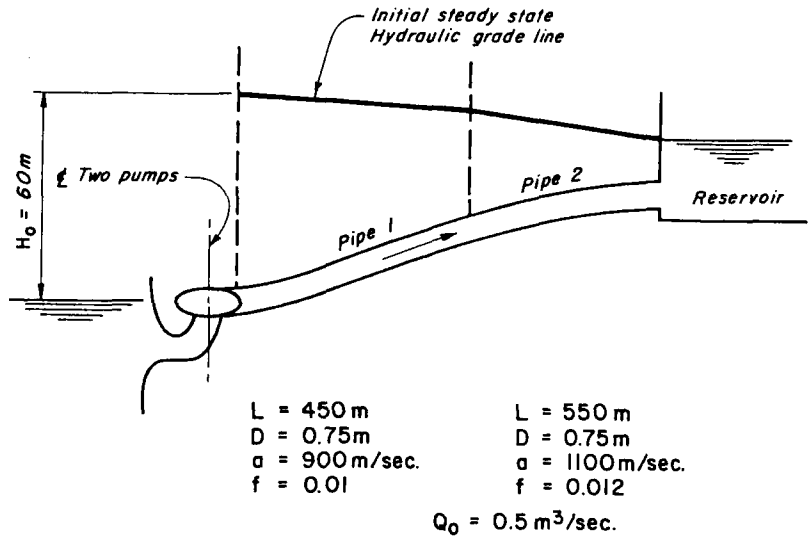

Figure 4.7. Piping system.

transient-state conditions are caused by simultaneous failure of power to both pumps.

A computer program (Appendix C) was developed using the boundary conditions derived in Section 4.5 for Parallel Pumps and the flowchart shown in Fig. 4.4. The method of characteristics discussed in Chapter 3 and the boundary conditions for the reservoir and series junction were used to analyze the transient conditions in the discharge line. The waterhammer wave velocity for various sections of the discharge line was determined using the equations presented in Section 2.6. The pump-characteristics data for N_s = 25 SI units (1276 gpm units) shown in Fig. 4.1 were used in the analysis. At rated discharge and rated pump speed, the pressure head at the upstream end of the discharge line would be equal to the rated head. Starting with this flow and pressure head at the upstream

end, the steady-state conditions in the discharge line were determined. Then, the power was assumed to fail, and the resulting transient conditions were computed. As the inertia of the liquid between the pump and the discharge manifold was small, the discharge of both pumps was lumped together and considered as the flow at the upstream end of the system.

Computed results are presented in Appendix C.

4.7 PUMP START-UP

In some piping systems, there is no control valve downstream of the pump; therefore start-up procedures outlined in Section 4.2 cannot be used. Pump start-up in such installations may produce very high pressures, especially if the motor is of the induction type and is started across the line (i.e., without reducing the voltage).

The transients caused by a pump start-up may be analyzed by selecting a start-up time, T_s, and by assuming that the pump speed increases linearly from zero to the rated speed in time T_s. The motor manufacturer can supply the time taken by the motor to reach the rated speed. The time specified by the motor manufacturer should be decreased by about 30 percent[11] to obtain a value for T_s.

Since the pump speed is known (it is assumed to increase from zero to N_R, in time T_s), the data for the torque characteristics and moment of inertia, WR^2, of the pump-motor are not required for the analysis. The pumping head and the pump discharge may be computed as outlined in the following.

Estimate the nondimensional pump discharge, v_e, at the end of the time step by extrapolation from the known values of v for the previous time steps. From the pump characteristics, determine h_P for the known value of α_P and for the estimated value of the pump discharge, v_e. Then, $H_{P_{1,1}} = h_P H_R$, in which the subscript (1, 1) refers to the first section on the discharge line just downstream of the pump. Now, using this value of $H_{P_{1,1}}$, compute the discharge at section (1, 1) from the negative characteristic equation (Eq. 3.19),

$$Q_{P_{1,1}} = C_n + C_a H_{P_{1,1}} \tag{4.77}$$

and then determine $v_P = Q_{P_{1,1}}/(n_p Q_R)$ in which n_P = number of parallel pumps. If $|v_P - v_e| \leqslant \epsilon$, in which ϵ is a specified tolerance (e.g., 0.001), proceed to the next time step. Otherwise, assume v_e equal to the mean of the computed value of v_P and the estimated value, v_e, during the previous iteration, and repeat the procedure.

If the discharge line is under a static head prior to the pump start-up, then there will be no flow into the discharge line until the pumping head exceeds this static head. This condition can be included in the above analysis by assuming that $Q_{P_{1,1}} = 0.0$ until $H_{P_{1,1}}$ exceeds the static head.

The pressure rise during a start-up may be reduced by having a slow start-up. This can be done by increasing the WR^2 of the pump motor, by reducing voltage, or by having a part-winding start. The overall economy of decreasing the maximum pressure to reduce the pipe-wall thickness by these methods should be investigated prior to their selection.

4.8 DESIGN CRITERIA FOR PIPELINES

Once the layout and dimensions of a piping system have been selected, the maximum and minimum pressures for various operating conditions can be determined by using the procedures outlined in Sections 4.4, 4.5, and 4.7. In the safest design, all components of the system would be designed for the possible maximum and minimum pressures with a liberal factor of safety. Such a design would, however, be uneconomical. Therefore, a factor of safety is chosen depending upon the risks and the probability of occurrence of a particular operating condition during the life of the project, i.e., the higher the probability of occurrence, the higher is the factor of safety.

Based upon the frequency of occurrence, various operating conditions may be classified as *normal*, *emergency*, or *catastrophic*. A discussion of the operating conditions included in each of these categories and the recommended factors of safety[12] follows.

Normal

All those operations that are likely to occur several times during the life of the pumping system are termed *normal*. Appurtenances or devices (e.g., surge tanks, surge suppressors, and air valves) provided in the system to reduce severe transients are assumed to be properly designed and to function as designed during these operations.

The following are considered to be normal operating conditions:

1. Automatic or manual starting or tripping of pumps throughout the entire range of pumping head. If there is more than one pump on the line, all are tripped simultaneously; however, only one may be started at a time.
2. If a check valve is present near the pump, it closes instantly upon flow reversal.
3. A surge tank does not drain and thus admit air into the pipeline, and it does not overflow unless an overflow spillway is provided.
4. If there is an air chamber, it is assumed to have a minimum air volume during a power failure.

As a result of any of the above operations, the water column does not separate at any point in the pipeline. However, if the water-column separation does occur, then appurtenances such as air chambers, surge tanks, etc. should be provided to avoid it. But, if it is impractical or too costly, then special devices will be provided to minimize the transient pressures when the columns subsequently rejoin.

A factor of safety of *three** based on the ultimate bursting strength of the member and a suitable factor of safety against collapse are recommended for the transient pressures caused by normal operations.

Emergency

The emergency operating conditions in pumping systems are those in which one of the pressure-control devices malfunctions during power failure. These conditions include:

1. One of the surge suppressors, surge tanks, or relief valves is inoperative.
2. Closure of one of the check valves provided for shutting off return flow through the pumps is delayed and occurs at the time of maximum reverse flow.
3. Air-inlet valves, if present in the system, are inoperative.

Since the probability of occurrence of these conditions is rather small, a factor of safety of *two* based on the ultimate bursting or collapsing strength is suggested.

Catastrophic

Catastrophic conditions are those in which the protective equipment malfunctions in the most unfavorable manner, such as loss of all air in the air chamber, very rapid abnormal opening or closing of a valve or a gate, and pump-shaft failure. Because the probability of occurrence of any of these conditions is extremely remote, a factor of safety of *slightly more than one*, based on the ultimate bursting or collapsing strength, may be used.

4.9 VERIFICATION OF MATHEMATICAL MODEL

The transient-state prototype test data obtained on the Wind Gap Pumping Plant by the Mechanical Design Unit of the Department of Water Resources, State of California, Sacramento, was used to verify a mathematical model based on the

*A factor of safety of four is recommended in Ref. 12.

boundary conditions developed in Sections 4.4 and 4.5. In this section, plant data are first presented; the tests, instrumentation, and mathematical model are then briefly described. This is followed by a comparison of the computed and measured results.

Plant Data

The Wind Gap Pumping Plant has five pumping units: three small units (Nos. 1-3) and two large units (Nos. 4, 5). Since test data for the large units only were used for verification purposes, we will only list the parameters of these units and of their discharge line. The large units (Nos. 4, 5) are manifolded together into a 3.81-m-diameter pipe. Each unit has a combined pump-motor WR^2 of 99,366 kg m^2, and is rated at 17.84 m^3/s at a total head of 159.7 m when operating at 360 rpm. The specific speed of the pump is 33.8 (SI units). The pipeline is 628 m long and varies in thickness from 11 to 27 mm. There is a discharge valve on the downstream side of each pumping unit. This valve closes in 22 ± 2 s following power failure to the unit. The minimum and maximum total pumping heads are 159.06 and 160.03 m, respectively, and the friction loss in the pipeline corresponding to a flow of both units is 1.8 m. To prevent backflow from the downstream canal, a siphon is provided near the downstream end of the pipeline, with the siphon having an air valve at its top. This valve opens as soon as power fails to the pump-motors.

Tests and Instrumentation

Single- and multiple-unit tests were conducted on both the small and large units. Runaway tests were conducted by subjecting the units to simulated power failure, with the discharge-valve closure delayed until after the units had reached the steady-state runaway speed.

The strain-gauge-type pressure transducers were used to measure the transient-state pressures on the upstream and downstream sides of the discharge valve. A valve position transducer (displacement) and an rpm (analog) transducer were installed on all units tested to record the discharge-valve closure and the unit speed.

Mathematical Model

A computer program was developed based on the boundary conditions for the pump end derived in Sections 4.4 and 4.5 and on the flowchart of Fig. 4.4. The closure of the discharge valve following power failure may be included in the

analysis, if desired. The pumping stations may have several parallel pumps, and the pumps may have long or short suction lines. To compute the transient conditions in the pipeline, the method of characteristics of Chapter 3 and the boundary conditions for the downstream and upstream reservoirs and for the series junction, derived in Section 3.3, were used in the program.

Comparison of Computed and Measured Results

The computed and measured results were compared for the tests simulating simultaneous power failure on Unit Nos. 4 and 5 with and without closure of the discharge valve. Results for the case when the discharge valve remained open are presented in Fig. 4.8a, and results for the case when the valve was closed are shown in Fig. 4.8b. As can be seen from the figure, the agreement between the

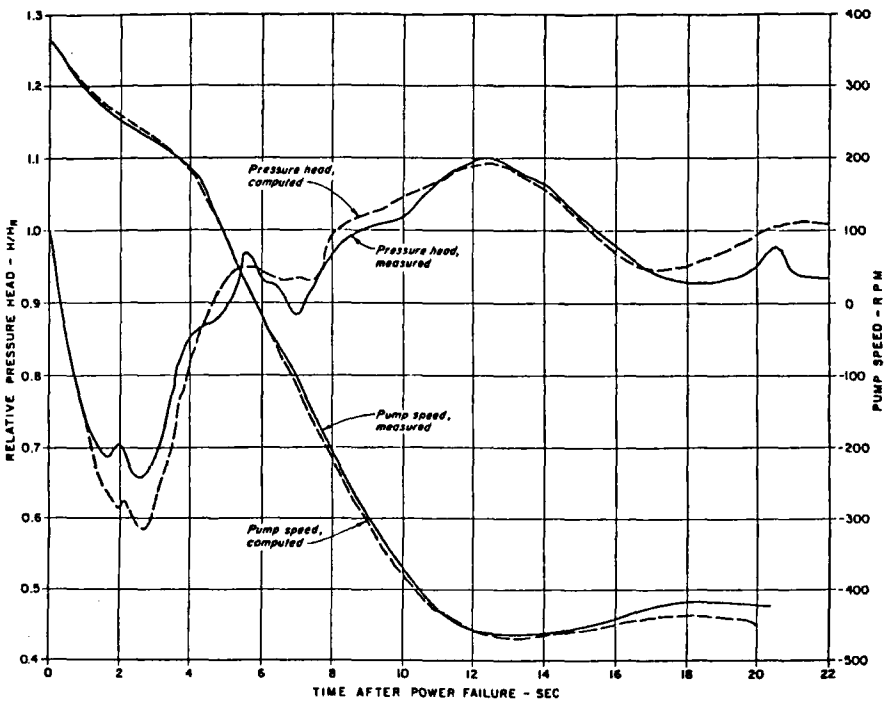

(a) Discharge valve remained open

Figure 4.8. Wind Gap Pumping Plant. Comparison of computed and measured results.

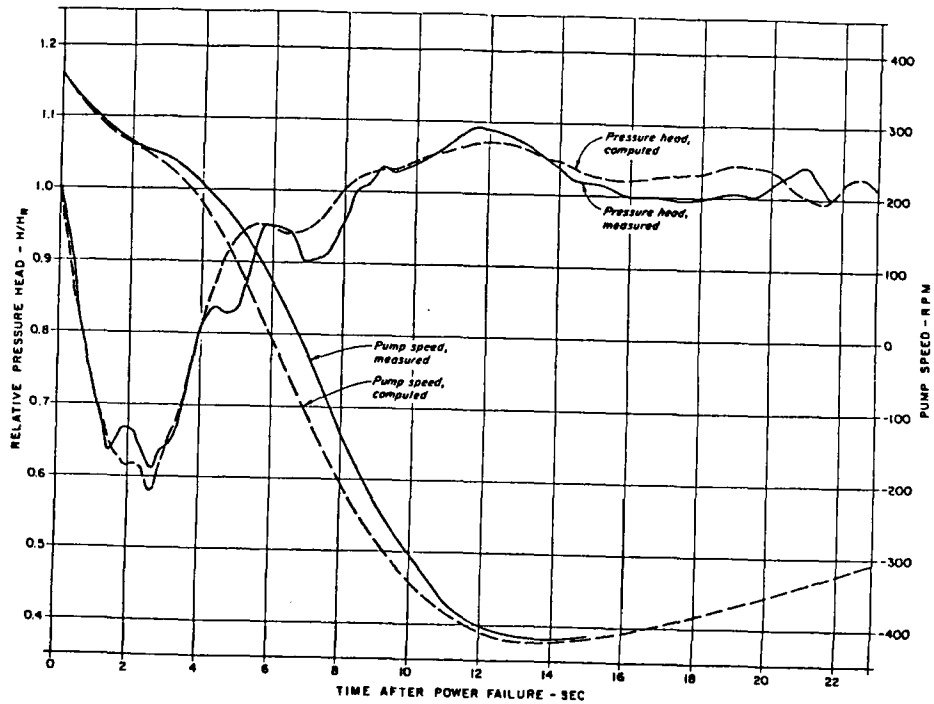

(b) Discharge valve closed gradually in 22 seconds

Figure 4.8. (*Continued*)

computed and measured results is satisfactory. However, the computed minimum pressure is lower than the measured minimum pressure. This difference is most probably due to the operation of the siphon valve, which was not simulated in the mathematical model.

4.10 CASE STUDY

The hydraulic transient studies,[13] carried out by the Hydroelectric Design Division of British Columbia Hydro and Power Authority for the water supply consultant* during the preliminary design of the makeup and cooling-water supply system for the Hat Creek Project of the Authority, are presented in this section.

*Sandwell and Company Limited (Sandwell), Vancouver, British Columbia, Canada.

Water-Supply System

As presently planned, the water-supply system (see Fig. 4.9) for pumping water from the Thompson River to the plant reservoir would be comprised of an 800-mm-diameter buried pipeline, approximately 23 km long; a pumping station with five pumping units at the river intake; two booster stations, each with four pumping units and a free-surface suction tank; and a reservoir near the power plant. Each booster station would have the free-surface tank on the suction side. The average and maximum discharges would be 0.725 and 1.60 m^3/s, respectively, and the maximum total static lift from the river intake to the plant reservoir would be 1083 m. The river intake would be located on the right bank of the Thompson River, 2.4 km northeast of Ashcroft, British Columbia.

Both booster stations have three-stage pumps, each rated at 0.4 m^3/s, 670 m, and 3580 rpm. The specific speed of each pump is 39.2 (SI units), and the moment of inertia of pump, motor, shaft, and entrained water in the impeller is equal to 62 kg m^2. If required, total inertia for each unit can be increased to 420 kg m^2 without exceeding the limits set by the pump start-up time. The pump manufacturer supplied the pump characteristics for the normal zone of pump operation only. Since no data were available for the other zones and since these characteristics agreed closely with those of Fig. 4.1 for $N_s = 25$ (SI units), the characteristics of Fig. 4.1 were used for all zones of operation.

Analysis

Computer Program

A computer program for analyzing the transient conditions in a pipeline caused by power failure and/or valve operation was developed. The boundary conditions and solution procedures presented in Chapters 3, 4, and 10 were used to solve the characteristic form of the dynamic and continuity equations. To avoid errors introduced by interpolations, wave velocities were adjusted slightly, if necessary, so that the characteristics passed through the grid points. Because there is a free-surface tank on the suction side of each booster station, transients in the discharge line were analyzed neglecting the effects of transients in the suction line.

The program was verified by comparing the computed results with those measured on a prototype (see Section 4.9) or those obtained by using other available, simpler, problem-oriented computer programs.

Selection of Control Devices

The procedure outlined on p. 102 was used to select appropriate waterhammer control devices:

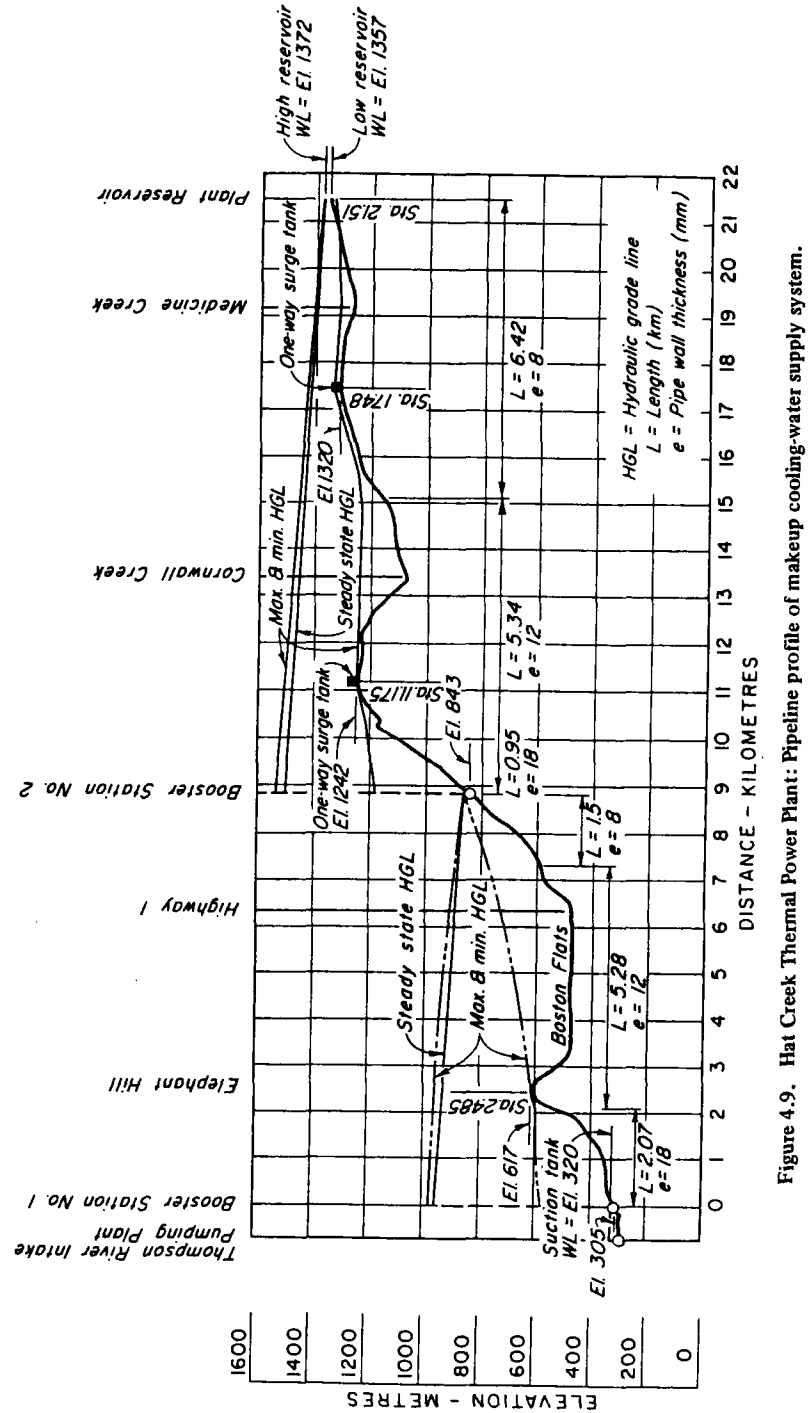

Figure 4.9. Hat Creek Thermal Power Plant: Pipeline profile of makeup cooling-water supply system.

1. *Column separation*. The system was analyzed for the case of simultaneous power failure to all pumps, assuming there were no control devices. Water-column separation occured in the pipeline between Booster Stations Nos. 1 and 2, and in the pipeline downstream of Booster Station No. 2. The provision of additional inertia at the pumps and one-way surge tanks prevented column separation. The data for these devices are listed subsequently.

2. *Maximum pressure*. It was assumed during the initial design of the pipeline that with appropriate control devices, the maximum pressure rise* at the pump end could be limited to 10 percent of the rated head. With check valves located downstream of the pumps, the pressure rise following power failure exceeded 10 percent. However, it could be reduced to less than 5 percent by slowly closing the pump-discharge valves.

Results

The maximum and minimum hydraulic grade lines following power failure are shown on Fig. 4.9 for the system containing suitable control equipment.

Column Separation

The following control devices would successfully prevent column separation in the various segments of the pipeline:

1. *Pipeline from Booster Station No. 1 to 2*. Two alternatives are available: (A) Increase the WR^2 of each pump motor to 115 kg m^2, and provide a 4-m-diameter one-way surge tank at the top of Elephant Ridge with the steady-state water level in tank at El. 627 (10 m above the ground surface); and (B) Increase the WR^2 of each pump motor to 390 kg m^2. With these controls, the minimum pressures in the pipeline remain above atmospheric pressure.

2. *Pipeline Downstream of Booster Station No. 2*. Increase the WR^2 of each pump motor to 370 kg m^2; provide a 4-m-diameter one-way surge tank at Station 11+175 with steady-state water level in the tank at El. 1252 (10 m above ground level); and provide a 4-m-diameter one-way surge tank at Station 17+480 with steady-state water level in the tank at El. 1345 (25 m above ground level).

With these measures, the minimum pressures along the pipeline were above atmospheric pressures.

Maximum Pressures

The pressure rise following power failure could be reduced by slowly closing the pump-discharge valves. With the closing times of about 100 s, the pressure rise

*Pressure rise = Maximum transient state pressure - Steady-state pressure.

at the pump following power failure was less than 5 percent of the rated head. A single rate closure was assumed in these computations. The maximum reverse pump speed following power failure for the cases when the discharge valve remained open and when the discharge valve was closed was less than the following maximum permissible limits specified by the pump manufacturer: 130 percent of rated speed for less than 30 s and 120 percent of rated speed for longer periods.

Emergency Conditions

As an emergency condition, the discharge valves were assumed to remain open following power failure. Because of the higher than normal inertia, the maximum pressure at the pump in all cases remained less than the steady-state pressure.

Discussion

The above results were obtained using assumed friction factors and assumed pump characteristics. In addition, both the topographic information and the data for the discharge valves were not precisely known. As the design operating conditions for each pumping station were different from the specified rated conditions for the pump, the water level in the suction reservoir had to be artificially lowered to obtain the correct downstream head for the given pump speed. Artificial lowering of the suction tank should have a negligible effect on the computed pressures in the discharge line. However, test runs using different pump characteristics showed that variation in the pump characteristics and/or in the data for the discharge valve could substantially change the computed maximum and minimum pressures. Similarly, significant changes in the ground topography would change the hydraulic grade line relative to the pipeline, thus possibly resulting in situations where column separation could occur. A difference in the friction losses could also affect the maximum and minimum pressures.

With the available data, the maximum pressures at the pump could be kept below 5 percent of the rated head. However, as discussed, the pressure rise may be higher due to significant variations in the data for the system. If necessary, the pressure rise could be decreased by increasing the discharge-valve closing time, which would result in an increase in the time period for which the pump runs in the reverse direction. Although the maximum reverse pump speed was within the limits specified by the pump manufacturer, reverse flow through the pumps for an extended period may partially drain the pipeline at high points. Therefore, it was recommended that, until better data were available and a sensi-

tivity analysis of the effects of changes in the variables affecting pressure rise was made, the maximum pressure rise at the pump end should be taken equal to 10 percent of the rated head, and the elevation of the maximum hydraulic grade line shown in Fig. 4.9 should be adjusted proportionately.

With the specified control measures, the minimum hydraulic grade line was always above the pipeline. At Elephant Ridge and at the summits downstream of Booster Station 2, the minimum hydraulic grade line was less than 5 m above the pipeline. During the final design, however, when better data should be available, this should be investigated in detail; if necessary, the safety margin could be increased.

Air valves should be provided at high points along the pipeline. These would be helpful during filling and draining of the line and would prevent collapse of a long length of the pipeline should a break occur in the pipeline at a lower elevation. In addition, valves could be provided along the line to isolate and drain segments of the line for inspection, repair, etc. Transients caused by the operation of these valves, if provided, would be studied during the final design.

The one-way surge tanks should have two pipes for water outflow. This should considerably reduce the possibility of a tank becoming inoperative due to the failure of a check valve to open.

Two alternatives are available to prevent column separation in the pipeline between Booster Stations Nos. 1 and 2. The alternative with increased inertia only is better from an operational point of view because the one-way surge tank is not as foolproof and in addition requires constant maintenance.

The inertia of the pump motors could be increased by adding flywheels or by a custom design of the electric motors. In order to provide operational flexibility and ease in exchanging spare parts, etc., it was decided that all units at both the booster stations should be identical and that each would have a WR^2 equal to 400 kg m^2.

4.11 SUMMARY

In this chapter, a procedure for storing the pump characteristics in a digital computer was presented, an iterative procedure for analyzing transients in piping systems caused by various pump operations was outlined, and boundary conditions for a number of cases usually found in practice were developed. Criteria for the design of pipelines were presented, and the chapter was concluded by a presentation of a case study.

PROBLEMS

4.1. Write a general-purpose computer program to determine the transient-state pressures in a discharge line caused by power failure. Using the pump characteristic of Appendix E, investigate the effect of increasing the value of WR^2 on the maximum and minimum pressures.

4.2. Using the program of Problem 4.1, prove that the maximum pressure at the pump does not exceed[14] the pumping head if the friction losses are greater than $0.7a\,V_o/g$, in which a = waterhammer wave velocity, V_o = steady-state flow velocity, and g = acceleration due to gravity.

4.3. Develop the boundary conditions for a system having n parallel pumps, in which power fails to n_f pumps and n_o pumps keep operating.

4.4. Draw a flowchart for the boundary condition derived in Problem 4.3, and develop a computer program.

4.5. To reduce maximum pressures following a power failure, a pressure-regulating valve is sometimes provided just downstream of the pump. This valve opens as the power fails and is closed slowly later. Develop the boundary conditions for such a system; write a computer program and investigate the effect of various rates of opening and closure of the pressure-regulating valve.

4.6. A check valve is provided in a discharge line to prevent reverse flows through the pumps. When power fails to the pump, water in the discharge line decelerates, and the check valve closes. A check valve having no dashpot and having negligible bearing friction losses closes[15] according to the equation

$$I\frac{d^2\theta}{dt^2} - W_s\bar{r}\sin\theta + \left(\frac{BV}{K_f} + \frac{C}{K_d}\frac{d\theta}{dt}\right)^2 + \left(\frac{G}{K_d}\frac{d\theta}{dt}\right)^2 + \left(\frac{FV}{K_f}\right)^2 = 0$$

in which θ = angle between the center of gravity of disk and vertical; I = moment of inertia of the disk; W_s = weight of disk in water; $\bar{r}$ = distance from pivot to weight-center of gravity of disk; V = mean pipeline velocity; k_f = flow coefficient for stationary disk in moving water (function of θ); k_d = flow coefficient for moving disk in still water (function of θ); and B, C, G, and F are constants. Expression for these constants are

$$B = \left(\frac{AR}{P^3}\right)^{0.25}$$

$$C = J\left(\frac{A^2P^3}{R}\right)^{0.25}$$

$$F = \left(AR - J^2\sqrt{\frac{A^2R}{P^3}}\right)^{0.5}$$

$$G = \left(AP^3 - J^2\sqrt{\frac{A^2P^3}{R}}\right)^{0.5}$$

in which A = area of disk; R = distance from pivot to center of disk; P = distance from pivot to the point of concentration of $\int r^3 dA$; J = distance from pivot to point of concentration of moment of inertia of disk area; and r = moment arm measured from disk pivot.

Develop the boundary conditions for the check valve, assuming that K_f and K_d are given in a tabular form.

4.7. Write a computer program for the check valve, and run it for the following data: $I = 0.235$ lb-ft-sec^2; $B = 0.548$; $C = 0.357$; $F = 0.11$; $G = 0.07$; $W_s\bar{r} = 10.74$ lb-ft; $\theta = 16.1^\circ + \alpha$; initial steady-state θ and α are 60.1° and 44°, respectively. K_f and K_d are listed in the following:

α (degrees)	k_f	k_d
0	0.	0.0
4	0.16	0.23
8	0.28	0.40
12	0.40	0.49
16	0.49	0.55
20	0.56	0.58
24	0.62	0.54
28	0.67	0.49
32	0.71	0.44
36	0.77	0.38
40	0.84	0.27
44	0.95	0.09

Use the pipeline and pump data given in Ex. 4.1 (Section 4.6), except that the diameter of the pipelines is 9 in.

REFERENCES

1. Knapp, R. T., "Complete Characteristics of Centrifugal Pumps and Their Use in Prediction of Transient Behaviour," *Trans. Amer. Soc. of Mech. Engrs.*, vol. 59, 1937, pp. 683–689.
2. Kittredge, J. P., "Hydraulic Transients in Centrifugal Pump Systems," *Trans. Amer. Soc. of Mech. Engrs.*, vol. 78, 1956, pp. 1307–1322.
3. Parmakian, J., *Waterhammer Analysis*, Dover Publications, 1963, pp. 78–81.
4. Donsky, B., "Complete Pump Characteristics and the Effect of Specific Speeds on Hydraulic Transients," *Jour. Basic Engineering, Trans. Amer. Soc. of Mech. Engrs.*, Dec. 1961, pp. 685–699.
5. Streeter, V. L., "Waterhammer Analysis of Pipelines," *Jour. Hydraulics Div., Proc. Amer. Soc. of Civ. Engrs.*, July 1964, pp. 151–171.
6. Marchal, M., Flesch, G., and Suter, P., "The Calculation of Waterhammer Problems by Means of the Digital Computer," paper presented at *International Symposium on Waterhammer in Pumped Storage Projects*, sponsored by Amer. Soc. of Mech. Engrs., 1965, pp. 168–188.
7. Streeter, V. L. and Wylie, E. B., *Hydraulic Transients*, McGraw-Hill Book Co., New York, 1967, pp. 151–159.
8. Thomas, G., "Determination of Pump Characteristics for a Computerized Transient Analysis," *Proc. First International Conference on Pressure Surges*, organized by British Hydromechanic Research Assoc. at Canterbury, England, Sept. 1972, pp. A3-21–A3-32.
9. Streeter, V. L., *Fluid Mechanics*, Third Edition, McGraw Hill Book Co., New York, pp. 466–468.
10. Miyashiro, H., "Waterhammer Analysis for Pumps Installed in Series," *Ref. 6*, pp. 123–133.
11. Joseph, I. and Hamill, F., "Start-Up pressures in Short Pump Discharge Lines," *Jour., Hyd. Div., Amer. Soc. of Civil Engrs.*, vol. 98, July 1972, pp. 1117–1125.
12. Parmakian, J., "Waterhammer Design Criteria," *Jour., Power Div., Amer. Soc. of Civil Engrs.*, April 1957, pp. 1216-1–1216-8.
13. Chaudhry, M. H., Cass, D. E., and Bell, W. W., "Hat Creek Project: Hydraulic Transient Analysis of Make-up Cooling Water Supply System," *Report No. DD 108, Hydroelectric Design Division, British Columbia Hydro and Power Authority*, Vancouver, Canada, February 1978.
14. Stephenson, D., *Pipeline Design for Water Engineers*, Elsevier Scientific Publishing Co., Amsterdam, The Netherlands, 1976, p. 58.
15. Parmley, L. J., "The Behaviour of Check Valves during Closure," Research report, Glenfield and Kennedy Ltd., Kilmarnock, England, Oct. 1965.

ADDITIONAL REFERENCES

Schnyder, O., "Comparison Between Calculated and Test Results on Waterhammer in Pumping Plant," *Trans. Amer. Soc. of Mech. Engrs.*, vol. 59, Nov. 1937, pp. 695–700.

Linton, P., "Pressure Surges on Starting Pumps with Empty Delivery Pipes," British Hydromechanic, Research Assoc., TN402, 1950.

Rich, G. R., *Hydraulic Transients*, McGraw-Hill Book Co., New York, 1951.

Parmakian, J., "Pressure Surges at Large Pump Installations," *Trans. Amer. Soc. of Mech. Engrs.*, vol. 75, Aug. 1953, pp. 995–1006.

Parmakian, J., "Pressure Surge Control at Tracy Pumping Plant," *Proc. Amer. Soc. of Civil Engrs.*, vol. 79, Separate No. 361, Dec. 1953.

Swanson, W. M., "Complete Characteristic Circle Diagrams for Turbo Machinery," *Trans. Amer. Soc. of Mech. Engrs.*, vol. 75, 1953, pp. 819–826.

Stepanoff, A. J., *Centrifugal and Axial Flow Pumps*, 2nd Edition, John Wiley & Sons, New York, 1957.

Jaeger, C., *Engineering Fluid Mechanics*, Blackie and Sons, London, 1959.

Jaeger, C., "Waterhammer Caused by Pumps," *Water Power*, London, July 1959, pp. 259–266.

Miyashiro, H., "Waterhammer Analysis of Pumps in Parallel Operation," *Bull. Japan Soc. of Mech. Engrs.*, vol. 5, No. 19, 1962, pp. 479–484.

Miyashiro, H., "Water Level Oscillations in a Surge Tank When Starting a Pump in a Pumped Storage Power Station," *Proc. International Assoc. for Hydraulic Research*, London, 1963, pp. 133–140.

Kinno, H. and Kennedy, J. F., "Waterhammer Charts for Centrifugal Pump Systems," *Proc. Amer. Soc. of Civil Engrs.*, vol. 91, HY3, May 1965, pp. 247–270.

Duc, J., "Negative Pressure Phenomena in Pump Pipelines," *Proc. International Symp. Waterhammer in Pumped Storage Projects,* Amer. Soc. of Mech. Engrs., 1965, pp. 154–157.

Miyashiro, H., "Waterhammer Analysis of Pump System," *Bull. Japan Soc. of Mech. Engrs.*, vol. 10, 1967, pp. 952–958.

Kinno, H., "Waterhammer Control in Centrifugal Pump Systems," *Proc. Amer. Soc. of Civil Engrs.*, vol. 94, HY3, 1968, pp. 619–639.

Brown, R. J., "Water-Column Separation at Two Pumping Plants," *Jour. Basic Engineering, Amer. Soc. of Mech. Engrs.*, Dec. 1968, pp. 521–531.

CHAPTER 5

HYDRAULIC TRANSIENTS IN HYDROELECTRIC POWER PLANTS

5.1 INTRODUCTION

In Chapter 3, boundary conditions for a Francis turbine connected to a large system were derived. In this chapter, a mathematical model is developed for analyzing hydraulic transients caused by various turbine operations, such as start-up, load acceptance, or load rejection.

The schematic representation of a typical hydroelectric power plant is first presented. Details of the mathematical simulation of the conduit system, turbogenerator, and governor are then outlined. Various turbine operations that produce hydraulic transients in the water passages of a power plant are discussed. Prototype test results used to verify the mathematical model are then presented, followed by a discussion of the governing stability of hydroturbines, and the selection of generator WR^2 and optimum governor settings. The chapter concludes with the case study of the governing stability studies carried out for a 500-MW hydroelectric generating station.

5.2 SCHEMATIC OF A HYDROELECTRIC POWER PLANT

Figure 5.1 shows the schematic diagram of a typical hydropower plant. As shown in the figure, the upstream conduits convey water from the upstream source, such as a reservoir, lake, or canal, to the turbine. Outflow from the turbine is carried downstream through the downstream conduit system. An electrical generator is mechanically coupled to the turbine, and the electrical output of the generator is carried by the transmission lines to the load centers. A governor is provided to correct any changes in the system frequency by opening or closing the wicket gates of the turbine.

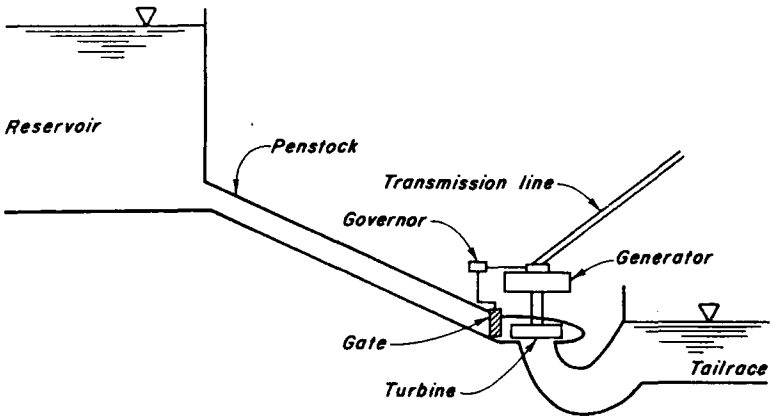

Figure 5.1. Schematic diagram of a hydroelectric power plant.

Thus, the following components have to be mathematically simulated to develop the mathematical model of a hydroelectric power plant:

1. upstream and downstream water conduits
2. turbine and generator
3. governor.

Details of the simulation of these components are presented in the following sections.

5.3 UPSTREAM AND DOWNSTREAM CONDUITS

As shown in Fig. 5.1, water is carried from the upstream reservoir or canal to the turbine scroll case through a tunnel and/or a penstock, and the outflow from the turbine is discharged through the draft tube to the downstream water passages, which may consist of either a free-surface flow or a pressurized tunnel, a tailrace canal, a river, or a downstream reservoir. Depending upon the conduit lengths, surge tanks may be provided to improve the governing characteristics or to reduce the maximum waterhammer pressures.*

The method of characteristics and the boundary conditions presented in Chapter 3 are used to simulate the upstream and downstream conduits. If the downstream conduit system is comprised of a free-surface flow tunnel, an open channel, or a short pressurized conduit, then the draft tube as well as the downstream conduit system may be neglected to simplify the analysis.

*This will be discussed in detail in Chapters 10 and 11.

Boundary conditions to analyze the turbine end of the conduit system are developed in the following section.

5.4 SIMULATION OF TURBINE

The relationship between the net head and discharge has to be specified to simulate a turbine in a hydraulic transient model. Flow through a turbine depends upon various parameters: for example, the flow through a Francis turbine depends upon the net head, rotational speed of the unit, and wicket-gate opening, while the flow through a Kaplan turbine depends upon these variables as well as the runner-blade angle. In an impulse turbine, however, the flow is a function of the head and the nozzle opening only. Curves representing the relationship between these parameters are called *turbine characteristics.*

To the author's knowledge, except for Krivehenko et al.,[1] no data have been reported in the literature for the turbine characteristics during transient-state conditions. Therefore, steady-state model test results are used to plot the expected prototype turbine characteristics and these are assumed to be valid during the transient state as well. As shown by Perkin et al.,[2] this is a valid assumption.

The data for the turbine flow and power output, obtained from the model tests, are presented in a graphical form known as *hill charts* (Fig. 5.2). The prototype efficiency is usually more than that determined from model tests because of scale effects. Therefore, while plotting the prototype output, this fact is taken into account by stepping up the model efficiency. Various empirical formulas have been proposed for this purpose, of which the Moody formula[3] appears to be the most suitable.

Usually very little data are available for small wicket-gate openings, and, to cover this range, the characteristic curves are extrapolated. To do this, flow should be known when the turbine rotational speed is zero, and the windage and friction losses should be known at wicket-gate openings below the speed-no-load gate (SNL). SNL gate is the lowest gate opening at which turbine rotates at synchronous speed with zero output.

Typical characteristics for a Francis turbine are shown in Fig. 5.3. In this figure, the abcissa is the unit speed, ϕ, and the ordinates are the unit flow, q, and the unit power, p. Definitions of ϕ, p, and q are given in Table 5.1.

In the expressions of Table 5.1, D = diameter of the runner; N = rotational speed; H_n = net head; Q = turbine discharge; and P = power output. In English units, D is expressed in in., N in rpm, H_n in ft, Q in ft^3/sec, and P in hp. In SI units, H_n and D are in m, N in rpm, P in kW, and Q in m^3/s.

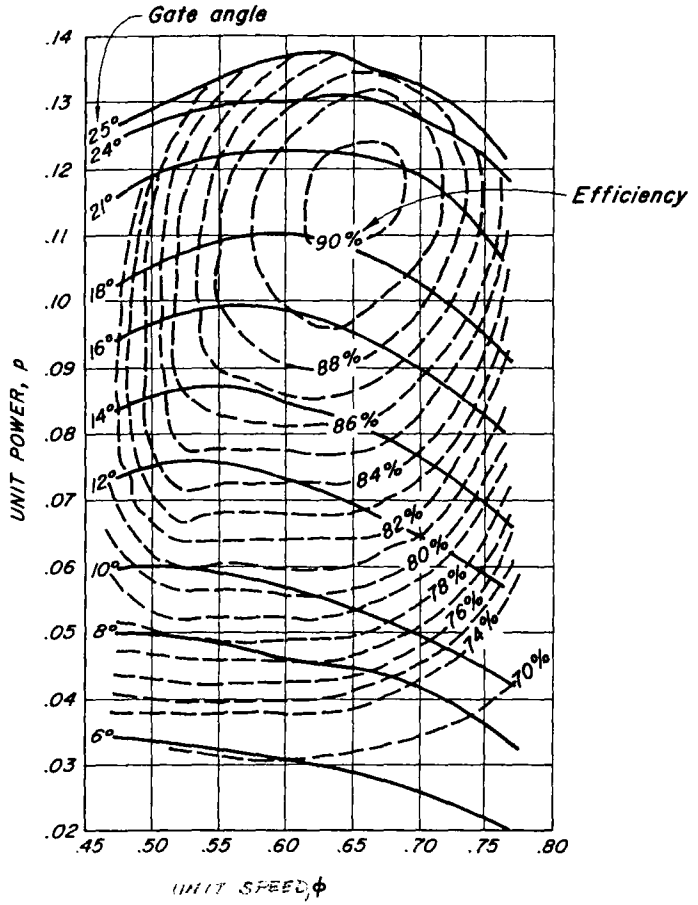

Figure 5.2. Typical hill chart for a Francis turbine (in ft-lb-sec units).

At SNL gate, the turbine output is equal to the turbogenerator windage and friction losses at the synchronous speed. Therefore, if the wicket gates are steadily open at the SNL gate opening, the unit rotates at the synchronous speed, and the net turbine output is zero. The abcissa axis on the unit power curves (Fig. 5.3b) represents the conditions at SNL gate. It is clear from this figure that the value of SNL gate varies with the net head. To keep the unit running at the synchronous speed when the wicket gates are open less than the SNL gate opening, power has to be supplied to the unit from an outside source

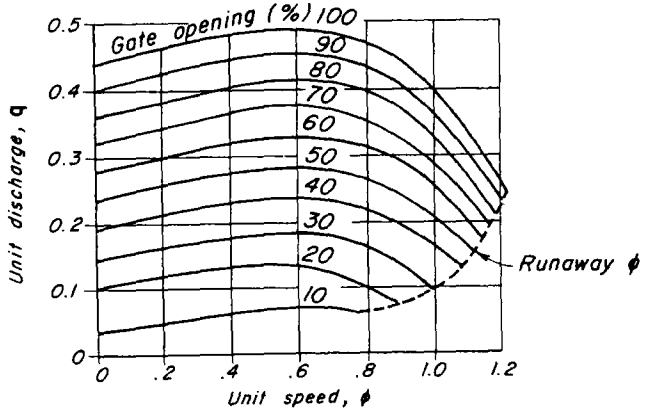

(a) Unit discharge vs unit speed

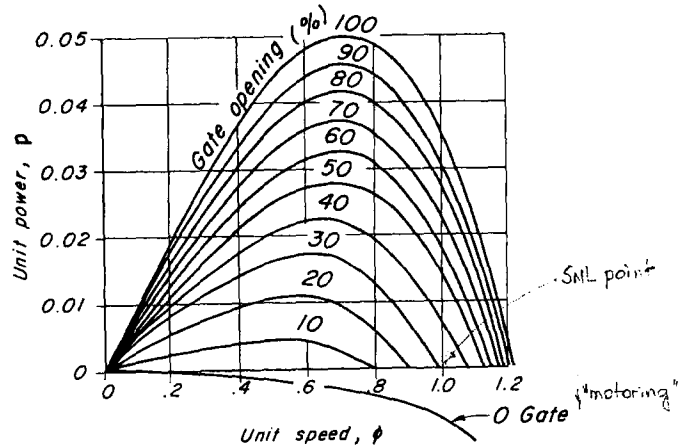

(b) Unit power vs unit speed

Figure 5.3. Characteristics of a Francis turbine (in ft-lb-sec units).

because the windage and friction losses are greater than the turbine output. This is called *motoring* of the unit.

During steady-state model tests, unit speed cannot exceed the runaway speed for a particular net head and gate opening. Therefore, model data are not obtained for ϕ higher than ϕ at runaway conditions (ϕ_{run}). However, during the transient state, the prototype speed may exceed the runaway speed for a short duration. To account for this, the curves are extended for ϕ values higher

Table 5.1. Definition of unit values.

	English Units	SI Units
ϕ	$\frac{DN}{1838\sqrt{H_n}}$	$\frac{DN}{84.45\sqrt{H_n}}$
q	$\frac{Q}{(D/12)^2\sqrt{H_n}}$	$\frac{Q}{D^2\sqrt{H_n}}$
p	$\frac{P}{(D/12)^2 H_n^{3/2}}$	$\frac{P}{D^2 H_n^{3/2}}$

than ϕ_{run} assuming that they follow the same trend as that at ϕ values less than ϕ_{run}.

A grid of points on the characteristic curves for various gate openings are stored in the computer, and the unit discharge and unit power at intermediate gate opening and ϕ values are determined by parabolic interpolation.

The boundary conditions for a Francis turbine[4] are derived below. For a Kaplan turbine, the variation of the turbine characteristics with the runner-blade angle would have to be considered. For a Pelton turbine, however, boundary conditions for a valve developed in Chapter 3 may be used.

Referring to Fig. 5.4,

$$H_P = H_n + H_{tail} - \frac{Q_P^2}{2gA^2} \tag{5.1}$$

in which H_P = instantaneous piezometric head at the scroll-case entrance; H_n = instantaneous net head; H_{tail} = tailwater level above datum; Q_P = instantaneous flow at entrance to the scroll case; and A = cross-sectional area of the pressure conduit at the turbine inlet. H_P, Q_P, and H_n are the values of these variables at the end of the time step under consideration. Note that the velocity head at the draft-tube exit has been neglected in Eq. 5.1 during computation of the net head. This is a valid assumption since the exit-velocity head is usually negligible. However, if the velocity head is not small as compared to H_n, it should be included in the analysis. Let the wicket-gate opening at the end of the time step be τ_P.

The values of four variables, namely, Q_P, H_P, τ_P, and N_P are unknown at the end of the time step under consideration and may be determined by the following iterative procedure. Because the transient-state turbine speed and gate opening vary gradually, these can be estimated as a first approximation by parabolic

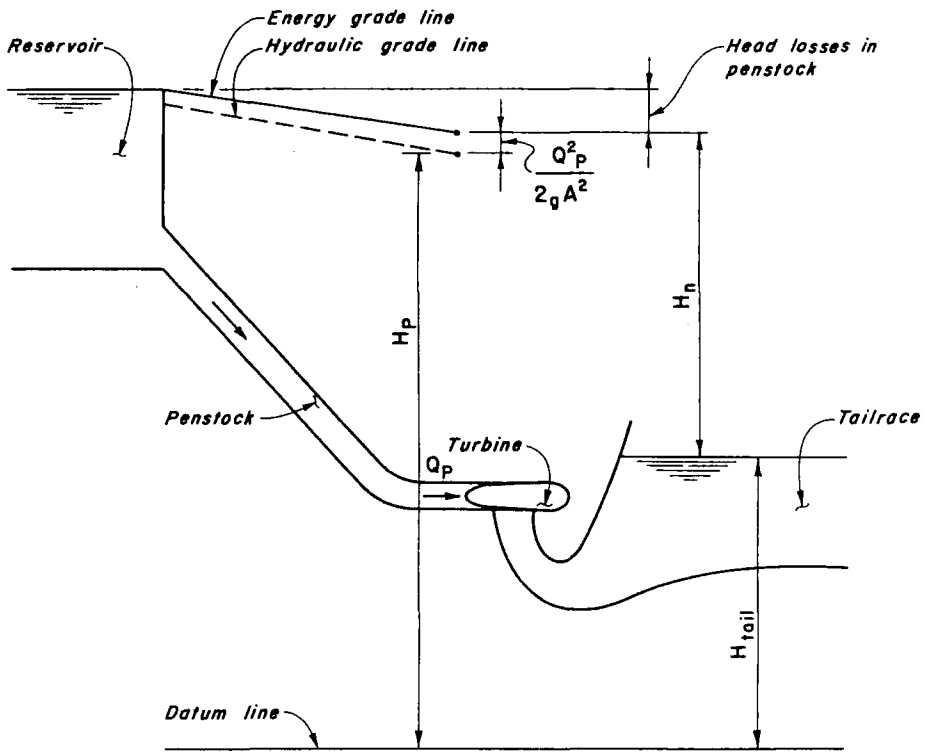

Figure 5.4. Notation for boundary conditions for a Francis turbine.

extrapolation. To determine the range of ϕ for which turbine characteristics have to be used during the time step, H_n is also extrapolated.

Let the values of τ_P, N_P, and H_n estimated by extrapolation be τ_e, N_e, and H_{ne} and the value of ϕ for the estimated values of N_e and H_{ne} be ϕ_e. The characteristics for τ_e for ϕ between ϕ_1 and ϕ_2 may be approximated by the straight line EF as shown in Fig. 5.5. The values at E are interpolated from the known values at the grid points A and B, and the values at F are interpolated from the known values at points C and D.

The equation of straight line EF may be written as

$$q = a_o + a_1 \phi \tag{5.2}$$

in which a_o and a_1 are determined from the known coordinates of E and F.

Substituting for q and ϕ from Table 5.1 (SI units) into Eq. 5.2 and simplifying

$$a_2 H_n^{1/2} = Q_P - a_3 \tag{5.3}$$

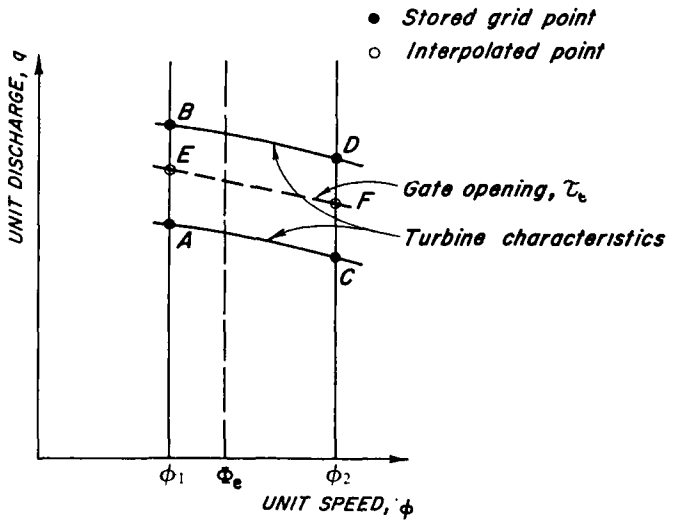

Figure 5.5. Interpolation of turbine characteristics.

in which

$$\left.\begin{aligned} a_2 &= a_o D^2 \\ \text{and} \qquad a_3 &= N_e D^3 a_1/84.45 \end{aligned}\right\} \qquad (5.4)^*$$

Combining Eqs. 3.18 and 5.1,

$$Q_P = (C_p - C_a H_{\text{tail}}) + \frac{C_a Q_P^2}{2gA^2} - C_a H_n \qquad (5.5)$$

Squaring both sides of Eq. 5.3, eliminating H_n from the resulting equation and Eq. 5.5, and simplifying,

$$a_4 Q_P^2 + a_5 Q_P + a_6 = 0 \qquad (5.6)$$

in which

$$a_4 = \frac{C_a}{2gA^2} - \frac{C_a}{a_2^2} \qquad (5.7)$$

$$a_5 = \frac{2a_3 C_a}{a_2^2} - 1 \qquad (5.8)$$

*In English units, $a_2 = a_o D^2/144$, and $a_3 = ND^3 a_1/264{,}672$.

$$a_6 = \left(C_p - C_a H_{\text{tail}} - \frac{C_a a_3^2}{a_2^2}\right) \qquad (5.9)$$

Solution of Eq. 5.6 yields

$$Q_P = \frac{-a_5 - \sqrt{a_5^2 - 4a_4 a_6}}{2a_4} \qquad (5.10)$$

Note that the positive sign with the radical term is neglected. Now H_n is determined from Eq. 5.3 and H_P from Eq. 5.1.

Because of the instantaneous unbalanced torque, $T_u = T_{\text{tur}} - T_{\text{gen}}$, the speed of the turbogenerator-set changes according to the equation

$$T_u = WR^2 \frac{d\omega}{dt} \qquad (5.11)^*$$

or

$$T_{\text{tur}} - T_{\text{gen}} = WR^2 \frac{2\pi}{60} \frac{dN}{dt} \qquad (5.12)^*$$

in which T_{tur} = instantaneous turbine torque; T_{gen} = instantaneous generator torque; ω = rotational speed of the turbogenerator, in rad/s; N = speed, in rpm; WR^2 = total moment of inertia of the turbine and generator, in kg m^2. If η_g = generator efficiency, and assuming that the load is only resistive, then Eq. 5.12 may be written as

$$P_{\text{tur}} - \frac{P_{\text{gen}}}{\eta_{\text{gen}}} = WR^2 \left(\frac{2\pi}{60}\right)^2 N \frac{dN}{dt} \qquad (5.13)^*$$

in which P_{gen} = generator load, and P_{tur} = power developed by the turbine, both in kW.

Integrating both sides of Eq. 5.13,

$$\int_{t_1}^{t_P} \left(P_{\text{tur}} - \frac{P_{\text{gen}}}{\eta_{\text{gen}}}\right) dt = 1.097 \times 10^{-2} WR^2 \int_{N_1}^{N_P} N\, dN \qquad (5.14)^*$$

Simplifying,

$$\left(\frac{P_{\text{tur}1} + P_{\text{tur}P}}{2} - \frac{P_{\text{gen}1} + P_{\text{gen}P}}{2\eta_{\text{gen}}}\right) \Delta t = 0.548 \times 10^{-2} WR^2 \left(N_P^2 - N_1^2\right) \qquad (5.15)$$

*If WR^2 is in lb-ft^2, replace WR^2 of Eqs. 5.11 through 5.13 by WR^2/g; if P_{tur} and P_{gen} are in horsepower, then divide the right-hand side of Eq. 5.13 by 550, and replace 1.097×10^{-2} of Eq. 5.14 and 0.548×10^{-2} of Eq. 5.15 by 0.619×10^{-6} and 0.3096×10^{-6}, respectively.

in which subscripts 1 and P indicate the values of the variables at the beginning and at the end of time step. Solving for N_P,

$$N_P = \left\{ N_1^2 + 182.38 \frac{\Delta t}{WR^2} \left[0.5(P_{\text{tur}1} + P_{\text{tur}P}) - \frac{0.5}{\eta_{\text{gen}}} (P_{\text{gen}1} + P_{\text{gen}P}) \right] \right\}^{0.5} \tag{5.16}*$$

In Eqs. 5.15 and 5.16, it is assumed that the generator load is gradually varied. However, if the transients are caused by a step change in the generator load, then the above equation may be simplified as

$$N_P = \left\{ N_1^2 + 182.38 \frac{\Delta t}{WR^2} \left[0.5(P_{\text{tur}1} + P_{\text{tur}P}) - \frac{P_{\text{genf}}}{\eta_{\text{gen}}} \right] \right\}^{0.5} \tag{5.17}*$$

in which P_{genf} = final generator load.

A computation procedure for using Eqs. 5.10 and 5.17 is presented in Section 5.6.

5.5 HYDRAULIC TURBINE GOVERNORS

As discussed in Section 5.2, a governor is provided to keep the speed of the turbogenerator at the synchronous speed. The main components of a governor are a speed-sensing device and a servomechanism for opening or closing the wicket gates.

Various mechanical and electrical speed-sensor devices[5] have been used. Of the mechanical devices, a centrifugal ballhead in various configurations has gained much popularity because of its simplicity, sensitivity, and ruggedness. The electrical speed sensors include a dc generator with permanent magnetic field, a permanent magnet alternator, a permanent magnet alternator feeding into a frequency-sensitive network, and a speed-signal generator. The output of these speed sensors is the deviation from the reference speed. This output is usually small and is amplified by means of a pilot valve before feeding it into the servo-mechanism provided for opening or closing the wicket gates. Since a large force is required to move the wicket gates, a hydraulic servo is provided for this purpose.

A governor, having a ballhead, pilot valve, and hydraulic servo, has only one equilibrium position in which the ports of the pilot valve are closed so that no oil is admitted into the servo. Such a governor is called an *isochronous governor* and is inherently unstable. Therefore, for stability, speed droop is provided.

*If WR^2 is in lb-ft^2, and P_{tur} and P_{gen} are both in hp, then replace 182.38 in these equations by 3.23×10^6.

The *speed droop* is a governor characteristic that requires a decrease in the speed to produce an increase in the wicket-gate opening (Fig. 5.6). For hydraulic turbines, a large value of speed droop is required for stability. However, this is not permissible from the point of view of system operation. Therefore, two types of speed droop are provided: permanent and temporary. Permanent speed droop is usually about 5 percent, is fixed during a transient, and is utilized for sharing loads on parallel units. The value of temporary droop may be large. It is made temporary by means of a dashpot.

Three types of governors are used for hydroelectric units: (1) *dashpot*, (2) *accelerometric*, and (3) *proportional-integral-derivative* (*PID*). The dashpot governors have been more commonly used in North America, and the accelerometric in Europe; the PID has been recently introduced. In the dashpot governor, the corrective action of the governor is proportional to the speed deviation, n; in the accelerometric governor, it is proportional to dn/dt; in the PID, it is proportional to n, dn/dt, and time integral of n (see Problem 5.3). We will discuss only the dashpot governor (Fig. 5.7) herein.

Following a load increase (decrease), the sequence of events is as follows: The speed of the unit decreases (increases) because of the load change, and the flyballs move inward (outward). This displaces the piston of the pilot valve, and the oil is admitted into the hydraulic servo that opens (closes) the wicket gates. As a result of the wicket-gate movement, the dashpot spring is compressed, which changes the position of the pilot valve. After some time, the dashpot spring returns to its original position because of oil flow through the small orifice in the dashpot, even though the servo and the wicket gates are now at a different position.

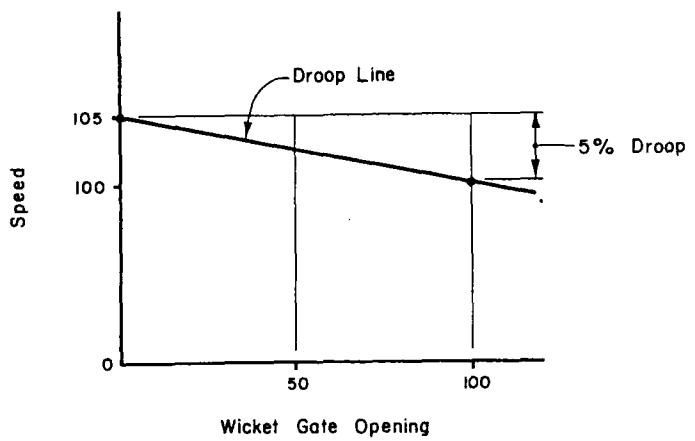

Figure 5.6. Speed droop.

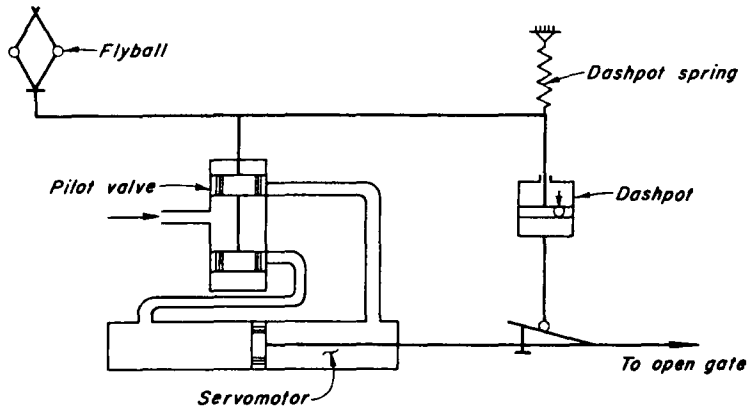

Figure 5.7. Dashpot governor (permanent speed droop not shown).

Figure 5.8 shows the block diagram for a dashpot governor. In this diagram, conventional notation of control systems[6] is used with different blocks representing various components of the governor. Input and output of various blocks is shown by means of arrows, and the transfer functions listed in the blocks show the relationship between the input and output of various components. In the transfer functions, s is the Laplace variable. If initial conditions are zero, then s is equivalent[7] to the time derivative d/dt.

The differential equations for different components of the governor can be written using the transfer functions listed in Fig. 5.8. Readers not interested in the derivation may proceed directly to Eqs. 5.31 through 5.34.

The following notation is used in the block diagram shown in Fig. 5.8:

T_a = actuator time constant
T_r = dashpot time constant
δ = temporary speed droop
σ = permanent speed droop
T_d = distributing valve time constant
k_d = distributing valve gain
k_s = gate-servomotor gain
n = normalized transient-state turbine speed.

The synchronous speed of the turbogenerator-set, N_R, is used to normalize the turbine speed, i.e., $n = N/N_R$. If τ_o = initial steady-state wicket-gate opening, then $n_{ref} = 1.0 + \sigma\tau_o$. The outputs of various governor components and their saturation limits are shown in Fig. 5.8. Typical values of these constants are:

T_a = 0.05 to 0.1s
σ = 0.3 to 0.5
0.03 to 0.05

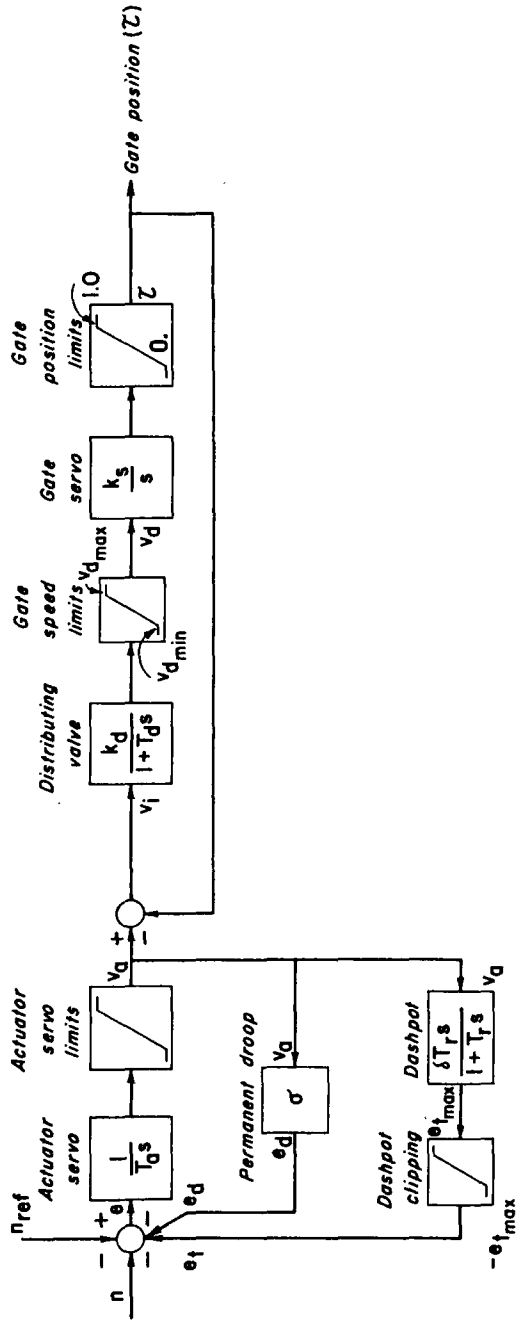

Figure 5.8. Block diagram for a dashpot governor.

T_d = 0.05 to 0.1 s
k_d = 10 to 15
k_s = 0.2
$e_{t_{max}}$ = 0.2 to 0.5

For a given set of power plant parameters, the optimum values of δ and T_r may be selected by using the procedures outlined in Section 5.11.

Actuator

$$v_a = \frac{1}{T_a s} e \tag{5.18}$$

or

$$e = T_a \frac{dv_a}{dt} \qquad 0 \leqslant v_a \leqslant 1.0 \tag{5.19}$$

Dashpot

$$e_t = \frac{\delta T_r s}{1 + T_r s} v_a \tag{5.20}$$

or

$$e_t + T_r \frac{de_t}{dt} - \delta T_r \frac{dv_a}{dt} = 0 \qquad -e_{t_{max}} \leqslant e_t \leqslant e_{t_{max}} \tag{5.21}$$

Permanent Drop

$$e_d - \sigma v_a = 0 \tag{5.22}$$

Distributing Valve

$$v_d = \frac{k_d}{1 + T_d s} v_i \tag{5.23}$$

$$T_d \frac{dv_d}{dt} + v_d - k_d v_i = 0 \qquad v_{d_{min}} \leqslant v_d \leqslant v_{d_{max}} \tag{5.24}$$

The gate-servomotor rate limits are often applied by restricting the maximum travel of the distributing valve in the positive and negative directions. Therefore, in the above inequality, we have

$$v_{d_{max}} = \frac{1}{k_s T_o} \tag{5.25}$$

and

$$v_{d_{min}} = \frac{-1}{k_s T_c} \tag{5.26}$$

in which T_o and T_c are the effective wicket-gate opening and closing times, which are defined as *twice the time taken by the wicket gates to open or close between 25 and 75 percent openings.*

Gate Servomotor

$$\tau = \frac{k_s}{s} v_d \tag{5.27}$$

or

$$\frac{d\tau}{dt} - k_s v_d = 0 \qquad 0 \leqslant \tau \leqslant 1.0 \tag{5.28}$$

The following equations may be written because of two feedbacks

$$e = n_{ref} - e_d - e_t - n \tag{5.29}$$

and

$$v_i = v_a - \tau \tag{5.30}$$

Note that the output of various components may saturate and that these saturation limits must be taken into consideration in the analysis of large load changes.

By eliminating e and e_d from Eqs. 5.19, 5.22, and 5.29, eliminating v_i from Eqs. 5.24 and 5.30, and rearranging Eqs. 5.24 and 5.28, we obtain

$$\frac{dv_a}{dt} = \frac{1}{T_a}(n_{ref} - n - e_t - \sigma v_a) \tag{5.31}$$

$$\frac{de_t}{dt} = \frac{1}{T_r}\left(\delta T_r \frac{dv_a}{dt} - e_t\right) \tag{5.32}$$

$$\frac{dv_d}{dt} = \frac{1}{T_d}[k_d(v_d - \tau) - v_d] \tag{5.33}$$

$$\frac{d\tau}{dt} = k_s v_d \tag{5.34}$$

The preceding four differential equations in four variables, namely, v_a, e_t, v_d, and τ, may be integrated by any standard numerical technique; a closed-form solution is not possible because of nonlinearities introduced by the saturation of

various variables. We have used the fourth-order Runge-Kutta method[8] in our analysis.

5.6 COMPUTATIONAL PROCEDURE

Boundary conditions for a Francis turbine and equations for a dashpot governor were derived in the preceding sections. A computational procedure for using these equations is presented in this section.

Let us assume that the transient-state conditions have been computed for $(i-1)$ time steps. The values of N_e, τ_e, and H_{ne} at the end of the ith time step may be estimated from the known values for the previous three time steps by parabolic extrapolation from the equation

$$y_i = 3y_{i-1} - 3y_{i-2} + y_{i-3} \tag{5.35}$$

in which y is the variable to be extrapolated[2] and the subscript indicates the time step. Note that this equation is valid only if the time steps are equal. Since there are no previous time steps at $t = 0$, the steady-state values may be used for previous time steps for extrapolation purposes. For the estimated values of H_{ne}, N_e, and τ_e, the grid points A through D (Fig. 5.5) are searched from the stored characteristic data. The coefficients a_0 and a_1 are computed, and the values of coefficients a_2 to a_6 are determined from Eqs. 5.4 and 5.7 through 5.9. Now Eq. 5.10 is used to determined Q_P, and Eq. 5.3 to determine H_n. The value of ϕ_e is computed using the estimated value of N_e and the computed value of H_n, and the turbine output, P_{turP}, is then determined from the turbine characteristic data for ϕ_e and τ_e. The turbine output, P_{turP}, and the generator load, P_{genP}, now being known, the value of N_P is determined from Eq. 5.16 or 5.17. If $|N_P - N_e| > 0.002\ N_R$, then N_e is assumed equal to N_P, and the above procedure is repeated; otherwise, the governor equations (Eqs. 5.31-5.34) are solved for τ_P by the fourth-order Runge-Kutta method. If $|\tau_P - \tau_e| > 0.005$, τ_e is assumed equal to τ_P, and the above procedure is repeated; otherwise, time is incremented, and the transient conditions are computed for the system. To avoid unlimited repetition of iterations in the case of a divergence in solution, a counter is introduced in both the iterative loops.

The flowchart of Fig. 5.9 illustrates the preceding computational procedure.

5.7 CAUSES OF TRANSIENTS

The following turbine operations produce transient-state conditions in the water conduits of a hydroelectric power plant:

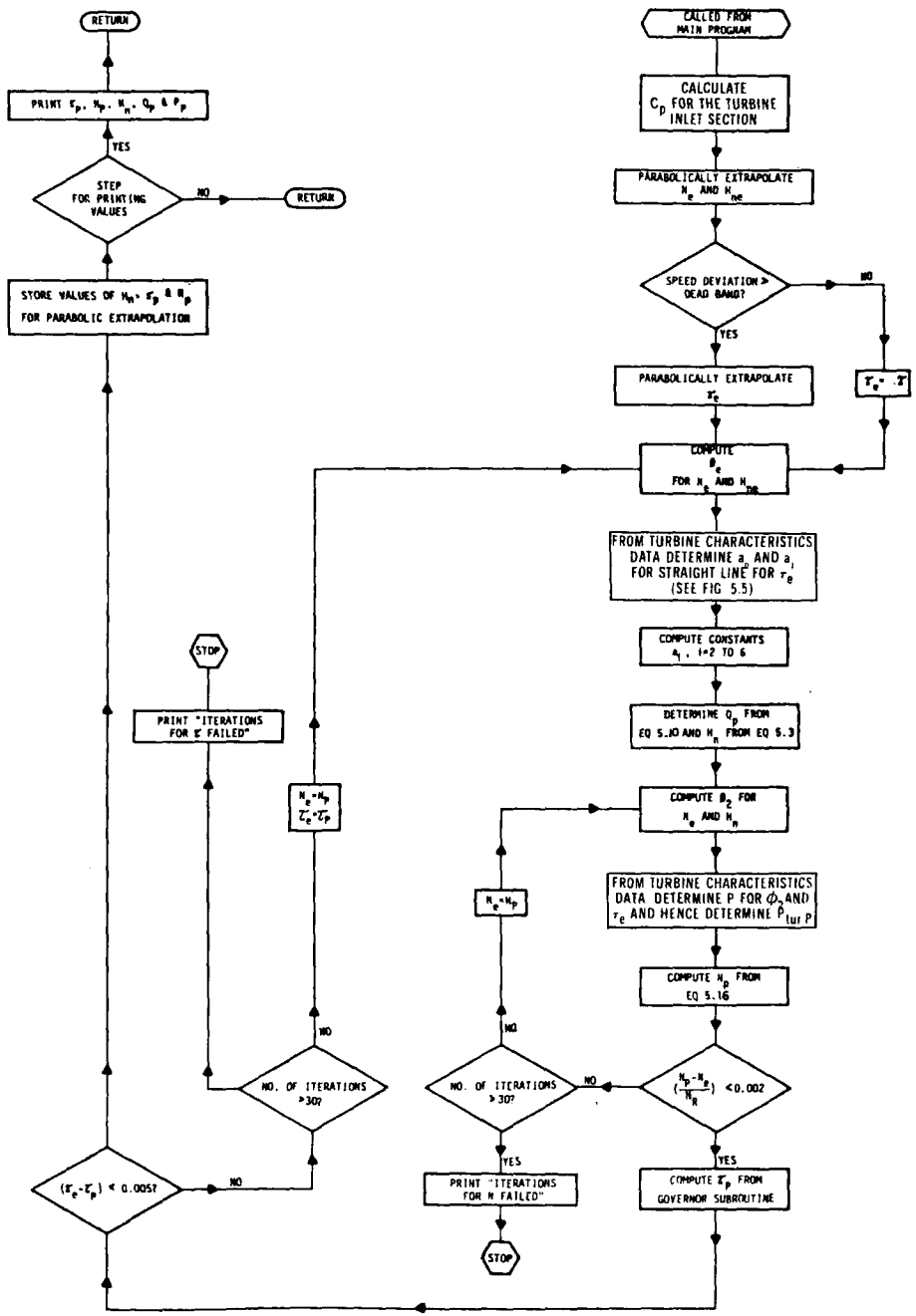

Figure 5.9. Flowchart for boundary conditions for a Francis turbine.

1. Unit synchronized to a large system
   a. load acceptance
   b. load reduction or total load rejection
2. Isolated unit
   a. unit start-up
   b. load acceptance
   c. load reduction or total load rejection.

A unit connected to a large system runs at the synchronous speed during load acceptance or rejection because of the large inertia of the system. However, the speed of an isolated unit rises during load rejection and decreases during load acceptance. For Kaplan and Francis turbines, the turbine speed has a considerable influence on the transients. Speed changes should therefore be taken into consideration in the transient-state computations for these turbines.

The boundary conditions and the computation procedure described in Sections 5.4 through 5.6 are for the isolated units only. These conditions can be used for units connected to a large system by keeping the speed constant and by bypassing the loop for computing the speed changes.

While starting a unit, the wicket gates are opened to the breakaway gate opening to give the unit a "kick" to overcome static friction. Gates are usually kept at this opening until the unit speed is about 60 percent of the rated speed; then the gates are closed to speed-no-load gate, and the unit is allowed to run at the synchronous speed for a short period of time. It is then synchronized to the system and is ready for load acceptance.

For load acceptance, the wicket gates are opened at the prescribed rate to the opening at which turbine output will be equal to the final output. Similarly, the gates are closed from one opening to another for a load reduction. Wicket-gate closure following total load rejection, however, depends upon the type of rejection.

5.8 VERIFICATION OF MATHEMATICAL MODEL

Prototype Tests

To obtain data for verifying the above mathematical model, load-rejection tests were conducted on Unit No. 4 of the G. M. Shrum Generating Station, owned and operated by British Columbia Hydro and Power Authority. The unit was loaded to the amount to be rejected, and was kept at this load until pressure and flow at the turbine inlet became steady. Then, to simulate an isolated load rejection, the speed-no-load solenoid was blocked, and the load was rejected. Five tests involving load rejections of 50, 115, 118, 202, and 250 MW were conducted. The upstream reservoir level during the tests was at an elevation of 671.0 m, and the downstream manifold level was at an elevation of 503.2 m.

The Westinghouse leading-edge flowmeter[9] was used to measure the steady as well as the transient-state flows. Locations of the flow transducers are shown in Fig. 5.10. The flowmeter display exhibited average flow every 2.1 s. As observing and recording the flowmeter readings at this rate was difficult, the flowmeter digital display along with clock time were recorded on a videotape. After each test, the tape was replayed at a slower speed in order to note the readings.

The speed of the turbogenerator was measured by a dc tachometer generator. A rubber-faced drive wheel was fastened to the shaft of the tachometer. The tachometer was mounted on a horizontal arm, which was free to turn about a vertical pivot anchored to the upper bearing of the turbine. A tensioning device held the drive wheel of the tachometer in contact with the turbogenerator shaft. The voltage output of the tachometer, which was proportional to the turbogenerator speed, was recorded on a Sanborn recorder.

The transient-state pressures were measured by a strain-gauge pressure cell attached to the turbine-inlet piezometer manifold. The output of the transducer, when appropriately conditioned through its strain-gauge amplifier, was recorded on a chart recorder.

The wicket-gate opening was recorded as follows. The motion of one of the servomotors of the wicket-gate moving mechanism activated a precision voltage divider (potentiometer). The change in voltage was then recorded on an oscillograph, which was calibrated against 0 and 100 percent gate openings.

Prototype Data

G. M. Shrum Generating Station is located on the Peace River in British Columbia, Canada. The power plant consists of 10 Francis units. Each unit has its individual power conduit (penstock and power intake). In the tailrace, five units discharge into one manifold, and a free-flow tunnel conveys water from each manifold to the tailrace channel. A schematic of the upstream water passages is shown in Fig. 5.10, and of the downstream water passages in Fig. 12.20.

Data for Unit No. 4, on which tests were conducted, are given in Table 5.2. The friction factors were calculated such that other minor losses were included in the friction losses. The conduit between the trashrack and the downstream end of the transition was replaced by an *equivalent* 5.49-m-diameter *pipe*.* The length of the scroll case was taken as one-half of the actual length to account for

*See Appendix A.

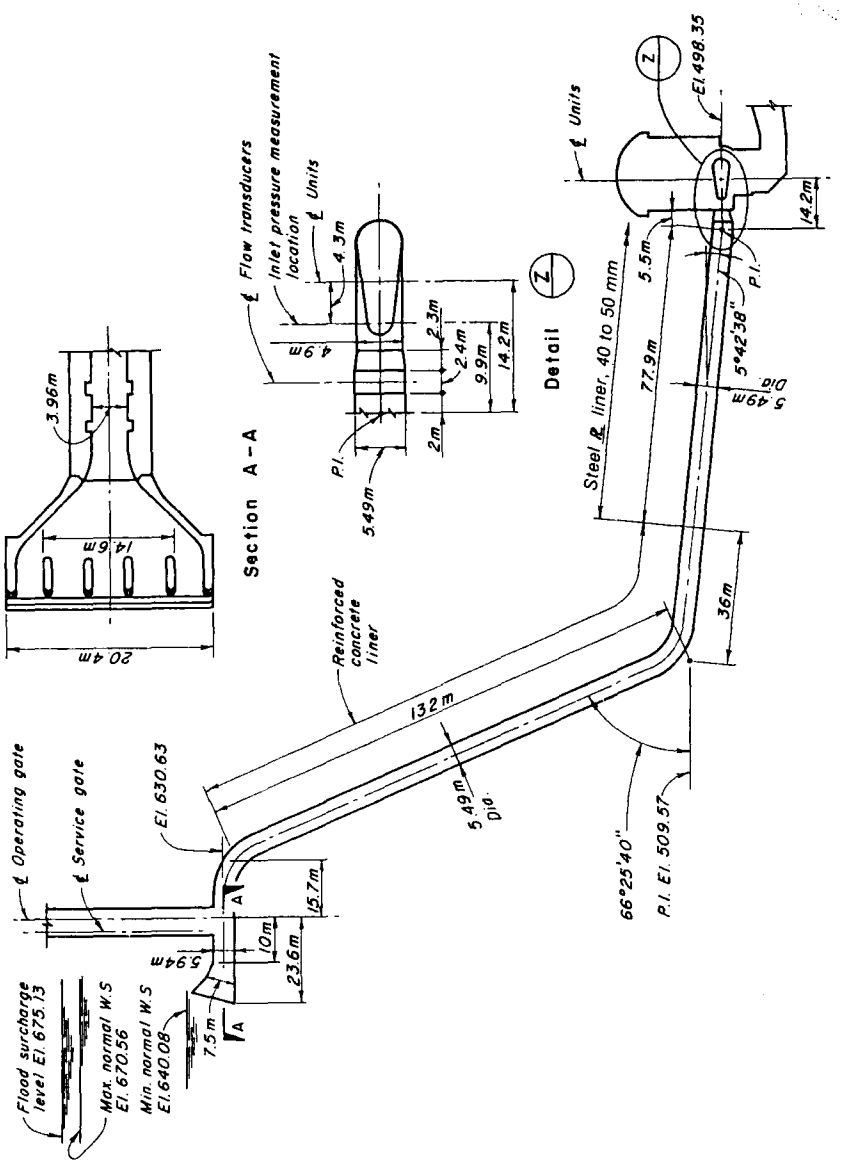

Figure 5.10. Profile and details of G.M. Shrum Generating Station.

Table 5.2. Data for Unit 4, G. M. Shrum Generating Station.

Turbine and Generator	
Rated turbine output	231 MW
Rated head	152.4 m
Synchronous speed	150 rpm
Flow at rated head for rated output	164 m^3/s
WR^2 of turbine and generator	9.27 Gg m^2 (i.e., 9.27×10^6 kg m^2)
Runner diameter	4.86 m

Governor Settings	
Dashpot time constant, T_r	8.0s
Temporary droop, δ	0.4
Permanent droop, σ	0.05
Dashpot saturation limit, $e_{r\max}$	0.25
Self-regulation constant, α	0.15

Conduits

Pipe No.	Diameter (m)	Length (m)	Wave Velocity (m/s)	Friction Factor
1	5.49	207	1244	0.016
2	5.49	78	1290	0.010
3	4.9	36.5	1300	0.009

reduction of flow along its length. Waterhammer wave velocities were computed using the equations presented in Section 2.6.

The draft tube was not included in the analysis because of its short length. This simplification should not introduce large errors. The downstream manifold, being a free-surface area, was assumed as a constant-level reservoir.

Comparison of Computed and Measured Results

A computer program based on the preceding mathematical model was developed. The flow in the conduit was analyzed using the method of characteristics of Chapter 3, and the turbogenerator and governor were simulated using the equations derived in Sections 5.4 and 5.5.

Pipe No. 3 was divided into two reaches. To satisfy the Courant's condition for stability of the finite-difference scheme, i.e., $\Delta t \leqslant \Delta x/a$, a time interval of 0.014 s was used. The wave velocities in the upper pipes were slightly adjusted so that there was no interpolation error. Static head and an estimated initial

steady-state gate opening were the input data to the program. Corresponding flow and turbine output were computed from the turbine characteristics. If the power output was different from the actual value, the initial gate opening was slightly changed, and the above procedure was repeated. By using this trial-and-error procedure, the initial steady-state gate opening, which gave the required turbine output, was determined.

Load was rejected at time, $t = 0$. As the unit was assumed to be isolated from the system following load rejection, it was allowed to overspeed, and the wicket gates were closed under governor control. Computed turbine speed, flow, gate opening, and pressure at the downstream end of each pipe were printed after every 35 time intervals, i.e., after every 0.5 s of prototype time.

Computed and measured results are plotted in Figs. 5.11 and 5.12. As can be seen, the computed and measured pressures agree closely. The computed and measured maximum unit speed agree closely; however, the computed results show a faster speed reduction than that shown by the measured results. It should be noted that this deviation starts when the wicket-gate opening is small. This difference may be due both to an error in the estimation of the windage and friction losses and due to lack of data for the turbine characteristics at small wicket-gate openings. The computed pressures show some oscillations that were not recorded during field measurements. The cause of this difference has not been explained.

5.9 DESIGN CRITERIA FOR PENSTOCKS

As discussed in Section 4.7, the factor of safety to be used during design depends upon the risks involved and the probability of occurrence of a particular operation during the life of the project. Based upon the frequency of occurrence, various operating conditions may be classified as *normal*, *emergency*, or *catastrophic*.[10,11] A discussion of the operating conditions included in each of these categories and recommended factors of safety[10] follows.

Normal

All operations that are likely to occur several times during the life of the penstock are termed *normal*. During these operations, appurtenances or devices—such as surge tanks, pressure-regulating valves, and cushioning stroke devices—provided for reducing excessive pressure-rise or pressure-drop function properly for which they are designed. The following are considered to be normal operations:

1. Full-load rejection and closure of the wicket gates in effective gate-closing time* with the static head on the turbine up to its maximum value.

*Effective wicket-gate opening and closing times are defined as *twice the time taken by the wicket gates to open or close between 25 and 75 percent openings.*

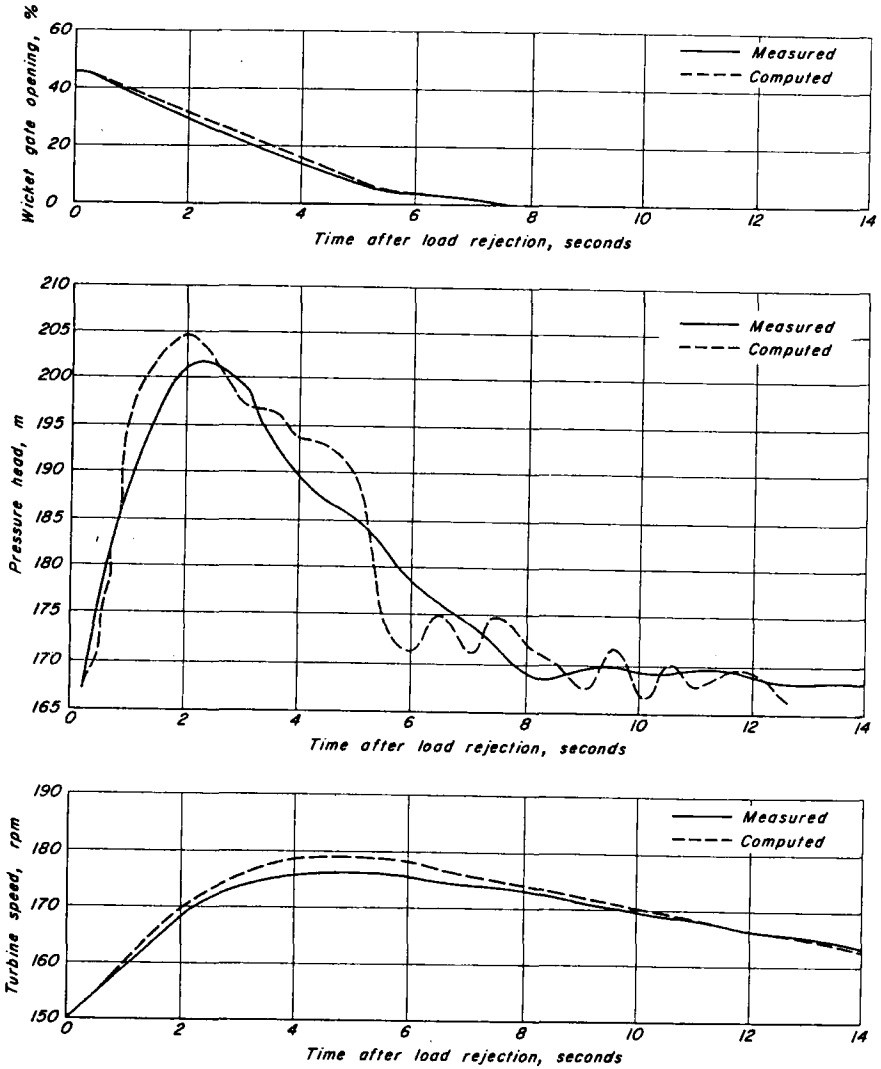

Figure 5.11. 150-MW load rejection: comparison of computed and measured results.

2. Opening of the wicket gates from the speed-no-load to full opening in effective gate-opening time, with the static head on the turbine as low as its minimum value.
3. The surge tanks do not overflow, unless an overflow weir is provided, nor do they drain.

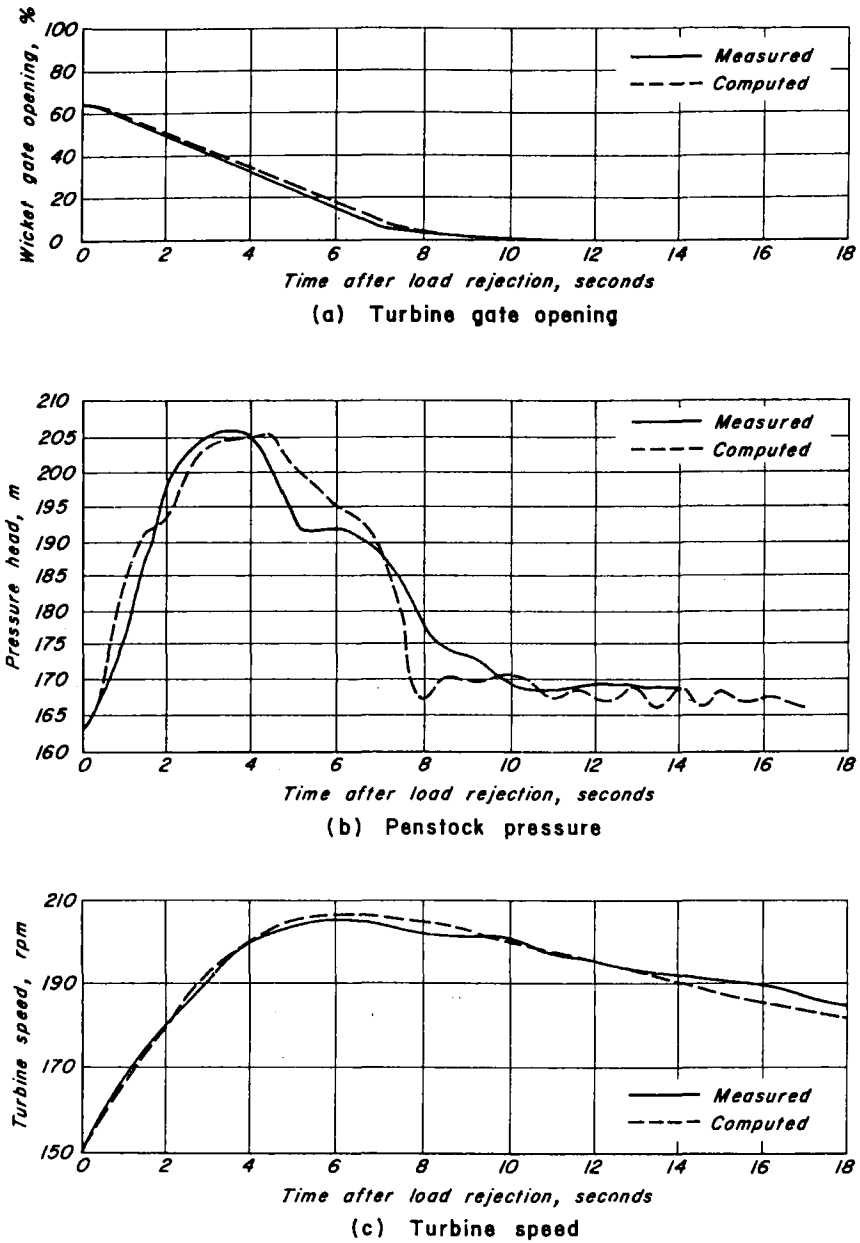

Figure 5.12. 250-MW load rejection: comparison of computed and measured results.

The penstock and scroll case are designed to withstand the maximum and minimum pressures caused by the preceding operations with a minimum factor of safety of *four*, based on the ultimate bursting and collapsing strength.

(Cold ASME)

Emergency

The *emergency* conditions are those in which one of the pressure-control equipment malfunctions. These conditions include:

1. The pressure-regulating valve is inoperative on one unit.
2. The cushioning stroke device is inoperative on one unit.

A factor of safety of *two*, based on the ultimate collapsing or bursting strength, is recommended for pressures produced by emergency operations.

Catastrophic

Catastrophic conditions are those in which various control devices malfunction in the most unfavorable manner. For example, if a pressure-regulating valve is provided, then the wicket-gate closing mechanism is designed such that the wicket gates will close at a very slow rate in case the pressure-regulating valve is inoperative during a load rejection. However, if the pressure regulating valve malfunctions following a load rejection and the wicket gates do not close at a slow rate, then this operation is considered catastrophic.[11]

Because of very low probability of occurrence, a factor of safety of *slightly more than one*, based upon the ultimate bursting or collapsing strength, is suggested.

5.10 GENERATOR INERTIA

For stable governing of a hydroelectric power plant and to keep the speed rise of the unit within permissible limits following a load rejection, it is necessary than an adequate amount of generator and turbine (unit) inertia be provided. Turbine inertia is small compared to the generator inertia; therefore, if necessary, only the latter is increased. Increasing the generator inertia increases the cost of the project. Although the increase in the generator cost due to increasing its inertia may not be large, other associated costs, such as increasing the crane capacity or increasing the powerhouse dimensions, are usually high. Therefore, the generator inertia is kept as small as possible while still maintaining acceptable governing characteristics.

The following factors are considered in selecting the generator inertia:

1. *Allowable frequency fluctuation*. The allowable frequency fluctuation depends upon the type of load. For example, a frequency deviation of 0.1

percent is not permissible for paper mills, while a deviation as large as 5 percent may be allowed for mining equipment.

2. *Size of the system.* A unit should be designed to be stable in isolated operation if it is supplying 40 percent or more of the system load, or if there are possibilities of the unit becoming isolated because of failure of the transmission line. The overall stability of the system is increased if the majority of the units in the system are stable in isolated operation.
3. *Type of load.* Periodically changing loads, such as electric trams and mining shovels, contribute to system instability. Therefore, more inertia should be provided if such loads are present in the system.
4. *Water passages.* One of the major factors in the selection of the inertia is the size, length, and layout of the water passages of the power plant. By increasing the size of the water passages, the generator inertia may be decreased. However, the former is usually more costly. Therefore, the size of the water passages is first selected based on the cost-benefit ratio of reducing the head losses, and the required generator inertia is then determined.
5. *Governor times.* By decreasing the governor opening and closing times, the stability of the system can be improved. However, they cannot be arbitrarily decreased since they are set so that the waterhammer pressure is within the design limits (Section 5.9), and so that the water column does not separate at high points of the penstock or in the draft tube.

No analytical method is available for determining the generator inertia required for a given set of plant parameters. Therefore, a number of empirical formulas and experience curves[12-14] have been proposed. The *normal or standard generator* inertia depends upon the unit rating[12] and is given by the equation,

$$\text{Normal generator } WR^2 = 15{,}970\left(\frac{kva}{N_r^{1.5}}\right)^{1.25} \qquad (5.36)^*$$

in which N_r = the synchronous speed, in rev/min; kva = the generator rated output; and WR^2 = moment of inertia, in kg m^2.

Depending upon the factors just outlined, the value of WR^2 may be increased or decreased. For good regulation, the United States Bureau of Reclamation recommends[12] that the ratio of the mechanical starting time, T_m, and the water-starting time, T_w, be greater than 8. Units with T_m/T_w of 5 or less may be integrated into a system but it may be necessary to compensate this deficiency on the other units of the system. T_m is the time in seconds for the rated torque to accelerate the rotating masses from zero to rated speed, and T_w is the time

*In English units, replace 15,970 by 379,000.

$GD^2 = 4 \cdot WR^2$

for the rated head to accelerate the flow from zero to rated velocity. Expressions for T_m and T_w are

$$T_m = \frac{WR^2 \times N_r^2}{90.4 \times 10^6\, MW} \qquad (5.37)^*$$

$$T_w = \frac{Q_r}{gH_r} \Sigma \frac{L}{A} \qquad (5.38)$$

in which g = acceleration due to gravity; Q_r and H_r are turbine flow and net head at rated conditions; L and A are the length and cross-sectional area of the water passages; N_r = synchronous speed; and $\Sigma\, L/A$ is computed from the upstream intake to the downstream end of the draft tube. The cross-sectional area of the scroll case at its upstream end is used for computing $\Sigma L/A$, and its length is taken as one-half to account for the reduction of flow along its length.

Experience curves proposed by the Tennesee Valley Authority relate T_m and T_w and show stability limits for various ratios of the unit size to that of the system. Gordon[14] has taken into consideration the effect of the governor times while plotting his curves (see Fig. 5.13), which are based on experience with 40 Kaplan, Francis, and propeller turbine installations. In the author's opinion, Gordon's stability curves should be used because they take into account most of the factors upon which the generator inertia depends. During the final design stages, however, the mathematical model developed in Sections 5.4 through 5.6 should be used to confirm the results of the preliminary analysis. To use these curves, the wicket-gate opening time, T_g, is computed by adding the time of the cushioning stroke (about 1.5 s) to the effective gate-opening time, T_o.

5.11 GOVERNING STABILITY

General Remarks

As discussed previously, a dashpot, a PID, or an accelerometric governor is provided to control the speed oscillations of a turbogenerator of a hydroelectric power plant. The speed oscillations are stable or unstable depending upon the values of the parameters of the hydro-unit, penstock, and governor.

Paynter[15] presented a stability limit curve and suggested optimum values of the governor settings by solving the problem on an analog computer. Hovey[16,17] derived a similar stability curve theoretically. However, both Paynter and Hovey neglected the permanent speed droop of the governor and the self-regulation of the turbine and of the load. In most cases, permanent speed droop σ is not zero

*If WR^2 is in lb ft^2 and the output is in hp, then $T_m = WR^2 \times N_r^2/(1.6 \times 10^6$ hp).

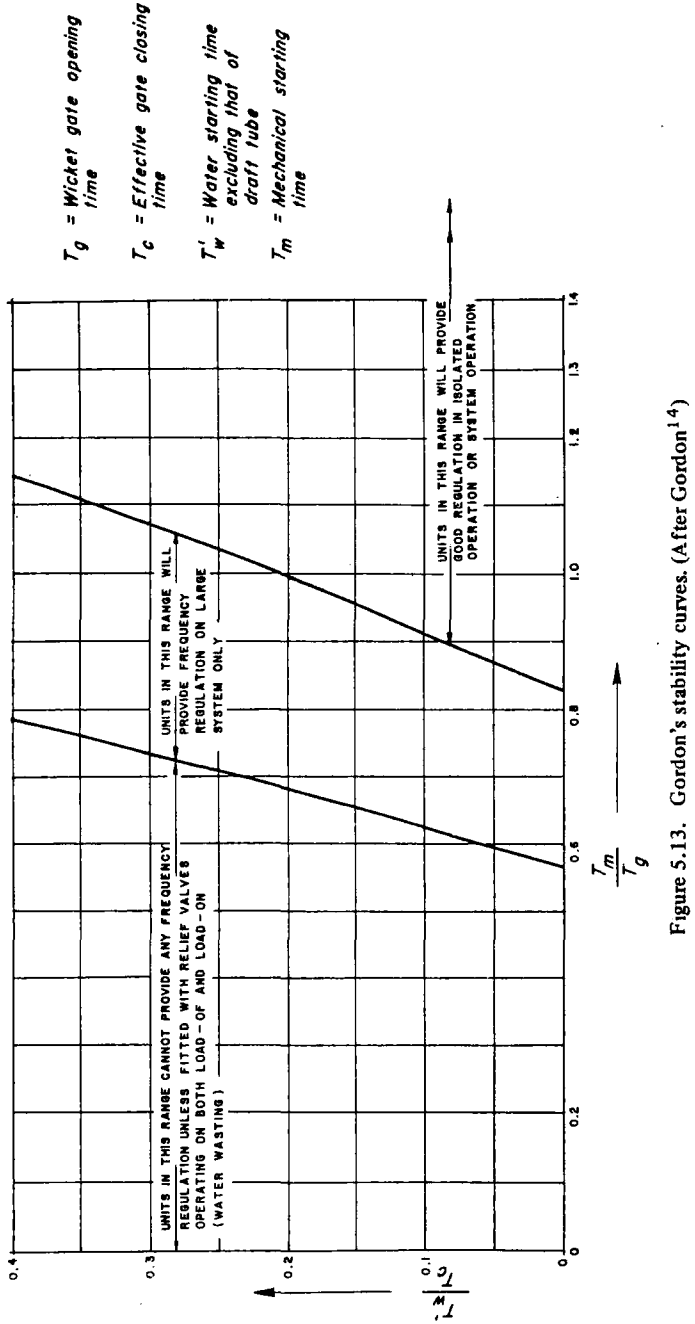

Figure 5.13. Gordon's stability curves. (After Gordon[14])

Table 5.3. Values of self-regulation coefficient.[a]

	α_l	α_{turb}	$\alpha = \alpha_l - \alpha_{turb}$
Turbine			
In general	–	about −1	–
High specific speed	–	up to −0.6	–
Load			
Grid loading: Motors only (constant torque)	0	–	+1
Ohmic resistance only with voltage regulation	−1	–	0.0
Ohmic resistance without voltage regulation	1 to 4	–	2 to 5

[a] Taken from Ref. 18.

while the self-regulation coefficient, α,[18] may or may not be zero depending upon the type of load.* (For values of α, see Table 5.3.)

The stability criteria are formulated herein[19] by taking into consideration the permanent speed droop and self-regulation. It is found that, if σ and α are allowed for, the stability is considerably increased, and the optimum values of the temporary speed droop, δ, and the dashpot time constant, T_r, are reduced.

Differential Equations of the System

In formulating the differential equations, the following *assumptions* are made:

1. The changes in the turbine speed, head, and gate opening are small; thus, nonlinear relationships can be assumed linear.
2. A single hydro-unit supplies power to an isolated load.
3. The governor has no dead band, backlash, or hysteresis.
4. The walls of the penstock, and the water in the penstock and scroll case are rigid. Thus, waterhammer pressure caused by changes in the gate opening can be computed by using the rigid water-column theory.

By making these assumptions, the following differential equations[15-18] can be written for the hydroelectric power plant shown in Fig. 5.1.

1. Machine acceleration

$$T_m \frac{dn}{dt} = g + 1.5h - \alpha n - \Delta m \tag{5.39}$$

*The turbine self-regulation coefficient, α_{tur}, is defined as *the slope of the graph relating the per unit deviation of the turbine torque from the rated value, to the per unit deviation of the turbine speed from the rated value.* The load self-regulation coefficient α_l, is defined as *the slope of the graph relating the per unit deviation of the torque of the electrical load from the rated value, to the per unit deviation of the frequency of the electrical load from the rated value.* The self-regulation coefficient is defined as *the algebraic difference between the load self-regulation coefficient and the turbine self-regulation coefficient.*

2. Water acceleration

$$-0.5\,T_w\frac{dh}{dt} = T_w\frac{dg}{dt} + h \tag{5.40}$$

3. Governor response

$$(\sigma+\delta)\,T_r\frac{dg}{dt} + \sigma g = -T_r\frac{dn}{dt} - n \tag{5.41}$$

in which n = relative speed deviation = $(N - N_o)/N_o$; h = relative pressure-head rise = $(H - H_o)/H_o$; g = relative gate-opening change = $(G - G_o)/G_o$; Δm = relative load-torque change = $\Delta M/M_o$; ΔM = step-load torque change (negative for load rejection); M_o = initial steady-state load torque; G = transient-state instantaneous gate opening; and N = transient-state instantaneous speed of the turbine, in rpm. The subscript o refers to the initial steady-state values.

Let $s = d/dt$. Then Eq. 5.41 may be written as

$$[(\sigma+\delta)\,T_r s + \sigma]\,g = -(T_r s + 1)n \tag{5.42}$$

or

$$g = \frac{-(T_r s + 1)n}{(\sigma+\delta)T_r s + \sigma} \tag{5.43}$$

It follows from Eq. 5.40 that

$$-(0.5\,T_w s + 1)h = T_w s g \tag{5.44}$$

or

$$h = \frac{T_w s(T_r s + 1)n}{[(\sigma+\delta)T_r s + \sigma]\,(0.5\,T_w s + 1)} \tag{5.45}$$

Substitution of Eqs. 5.43 and 5.45 into Eq. 5.39 yields

$$T_m p n = \frac{-(T_r s + 1)n}{(\sigma+\delta)T_r s + \sigma} + \frac{1.5\,T_w s(T_r s + 1)n}{[(\sigma+\delta)T_r s + \sigma]\,(0.5\,T_w s + 1)} - \alpha n - \Delta m \tag{5.46}$$

By simplifying and replacing s^3 by d^3/dt^3; s^2 by d^2/dt^2; and s by d/dt, Eq. 5.46 takes the form

$$0.5\,T_w T_m T_r(\sigma+\delta)\frac{d^3n}{dt^3} + [0.5\sigma T_w T_m + (\sigma+\delta)\,T_m T_r - T_w T_r + 0.5\alpha T_w T_r(\sigma+\delta)]\frac{d^2n}{dt^2} + [\sigma T_m + T_r - T_w + 0.5\sigma\alpha T_w + (\sigma+\delta)\alpha T_r]\frac{dn}{dt} + (1+\sigma\alpha)n = -\sigma\Delta m \tag{5.47}$$

Criteria for Stability

According to the Routh-Hurwitz criteria,[20] the oscillations represented by the third-order differential equation (Eq. 5.47) are stable if

1. $0.5\,T_w T_m T_r(\sigma+\delta) > 0$ (5.48)

2. $[0.5\sigma T_w T_m + (\sigma+\delta)\,T_m T_r - T_w T_r + 0.5\alpha T_w T_r(\sigma+\delta)] > 0$ (5.49)

3. $[\sigma T_m + T_r - T_w + 0.5\alpha\sigma T_w + (\sigma+\delta)\alpha T_r] > 0$ (5.50)

4. $(1+\alpha\sigma) > 0$ (5.51)

5. $[\sigma T_m + T_r - T_w + 0.5\,\sigma\alpha T_w + (\sigma+\delta)\alpha T_r]\,[0.5\,\sigma T_w T_m + (\sigma+\delta)\,T_m T_r - T_w T_r + 0.5\alpha T_w T_r(\sigma+\delta)] > [0.5\,T_w T_m T_r(\sigma+\delta)]\,(1+\sigma\alpha)$. (5.52)

The inequalities 5.48 and 5.51 are always satisfied. To plot the stability-limit curves, we have to consider the expressions given by inequalities 5.49, 5.50, and 5.52. There are six parameters in these expressions, namely, σ, δ, α, T_w, T_m, and T_r. To reduce the number of parameters and to present the criteria in a nondimensional form, the following nondimensional parameters are introduced:

$$\left.\begin{aligned}\lambda_1 &= \frac{T_w}{\delta T_m}\\ \lambda_2 &= \frac{T_w}{T_r}\\ \lambda_3 &= \frac{\alpha T_w}{T_m}\\ \lambda_4 &= \frac{\sigma T_m}{T_w}\end{aligned}\right\} \tag{5.52}$$

By substituting the above parameters into inequalities 5.49, 5.50, and 5.52 and simplifying the resulting expressions, we obtain the following equations for the limit of stability:

$$0.5\lambda_1\lambda_2\lambda_4 + 0.5\lambda_1\lambda_3\lambda_4 + \lambda_1\lambda_4 + 0.5\lambda_3 - \lambda_1 + 1 = 0. \tag{5.53}$$

$$0.5\lambda_1\lambda_2\lambda_3\lambda_4 + \lambda_1\lambda_3\lambda_4 + \lambda_1\lambda_2\lambda_4 - \lambda_1\lambda_2 + \lambda_1 + \lambda_3 = 0. \tag{5.54}$$

$$\lambda_1^2(\lambda_4 + 0.5\lambda_2^2\lambda_4^2 - 0.5\lambda_2^2\lambda_4 - 1 + \lambda_2 - 2\lambda_2\lambda_4 - 0.5\lambda_3\lambda_4 - \lambda_2\lambda_3\lambda_4 + \lambda_3\lambda_4^2 + \lambda_2\lambda_3\lambda_4^2 + 0.5\lambda_3^2\lambda_4^2 + 0.25\lambda_2\lambda_3^2\lambda_4^2 + 0.25\lambda_2^2\lambda_3\lambda_4^2 + \lambda_2\lambda_4^2) + \lambda_1(1 - 1.5\lambda_2 + \lambda_2\lambda_4 + 2\lambda_3\lambda_4 + \lambda_2\lambda_3\lambda_4 - 0.5\lambda_3 - 0.5\lambda_2\lambda_3 + \lambda_3^2\lambda_4 + 0.25\lambda_2\lambda_3^2\lambda_4) + (\lambda_3 + 0.5\lambda_3^2) = 0 \quad (5.55)$$

Equations 5.53 through 5.55 represent the stability criteria. Based on these equations, the stability limit curves for different values of $\lambda_1, \lambda_2, \lambda_3$, and λ_4 are plotted in Fig. 5.14. Speed oscillations corresponding to those values of λ_1 and λ_2, which lie in the region enclosed by the stability limit curve and the positive coordinate axes, are stable. For $\lambda_3 = 0$ and $\lambda_4 = 0$, Hovey's stability curve is obtained. This is shown as a dotted curve in Fig. 5.14.

The following example illustrates that the results obtained by neglecting σ and α are conservative.

Example 5.1

For the Kelsey hydroelectric plant, $T_w = 1.24$ s and $T_m = 9.05$ s. Hovey reported[21] that, according to his criteria, the speed oscillations caused by a step load change are unstable for $\delta = 0.28$ and $T_r = 2.25$ s. The following analysis shows that the oscillations are stable for these values of δ and T_r if the permanent speed droop and the self-regulation are taken into consideration.

The Kelsey plant supplies power to an isolated load consisting of furnaces, blowers, and compressors.[17] Thus, α may be taken equal to 1 (see Table 5.3). As reported by Hovey in another paper,[22] $\sigma = 0.035$. Stability calculations can be done as follows:

$$\lambda_1 = \frac{T_w}{\delta T_m} = \frac{1.24}{0.28 \times 9.05} = 0.49$$

$$\lambda_2 = \frac{T_w}{T_r} = \frac{1.24}{2.25} = 0.55$$

$$\lambda_3 = \frac{\alpha T_w}{T_m} = \frac{1 \times 1.24}{9.05} = 0.137$$

$$\lambda_4 = \frac{\sigma T_m}{T_w} = \frac{0.035 \times 9.05}{1.24} = 0.255.$$

From Fig. 5.14, it follows that, for $\lambda_1 = 0.49$, $\lambda_2 = 0.55$ and

1. $\lambda_3 = 0.0$ and $\lambda_4 = 0.0$, oscillations are unstable (Hovey's criteria)
2. $\lambda_3 = 0.0$ and $\lambda_4 = 0.255$, oscillations are stable

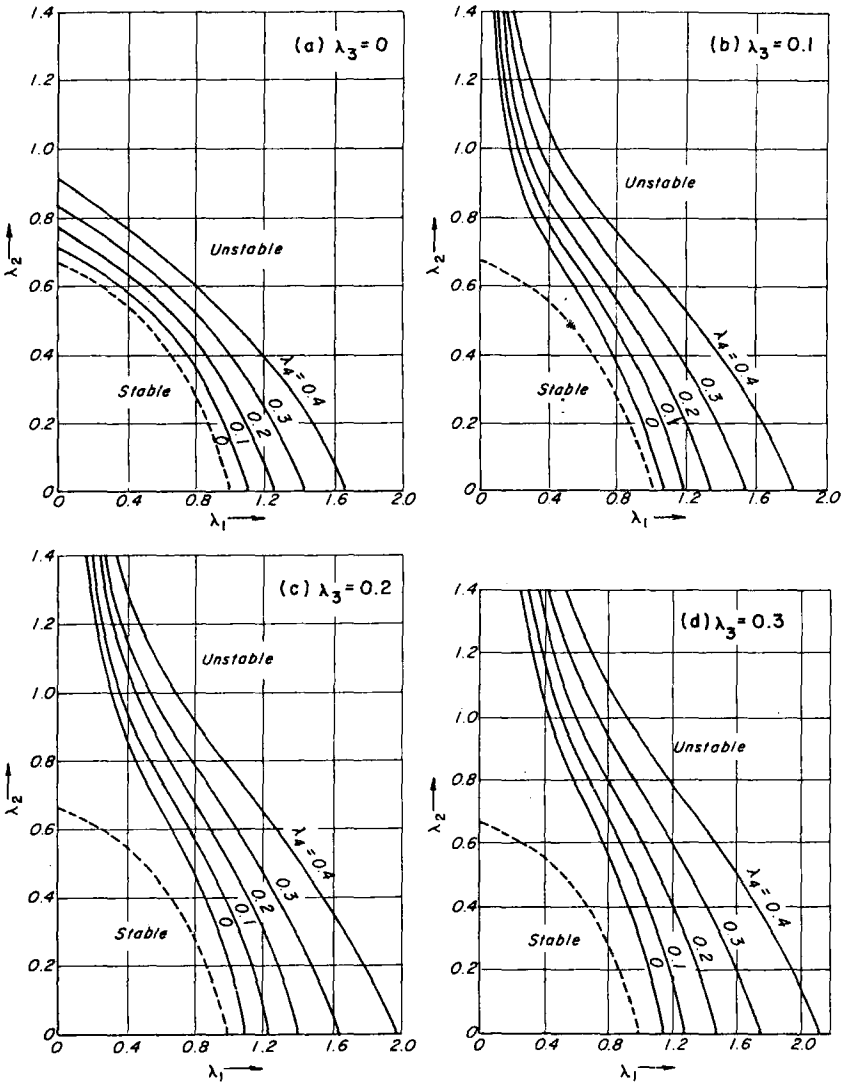

Figure 5.14. Stability limit curves.

3. $\lambda_3 = 0.1$ and $\lambda_4 = 0.0$, oscillations are stable
4. $\lambda_3 = 0.1$ and $\lambda_4 = 0.255$, oscillations are stable

To check the validity of these results, Eqs. 5.39 through 5.41 were solved on a digital computer. The plotter output obtained from the computer is presented

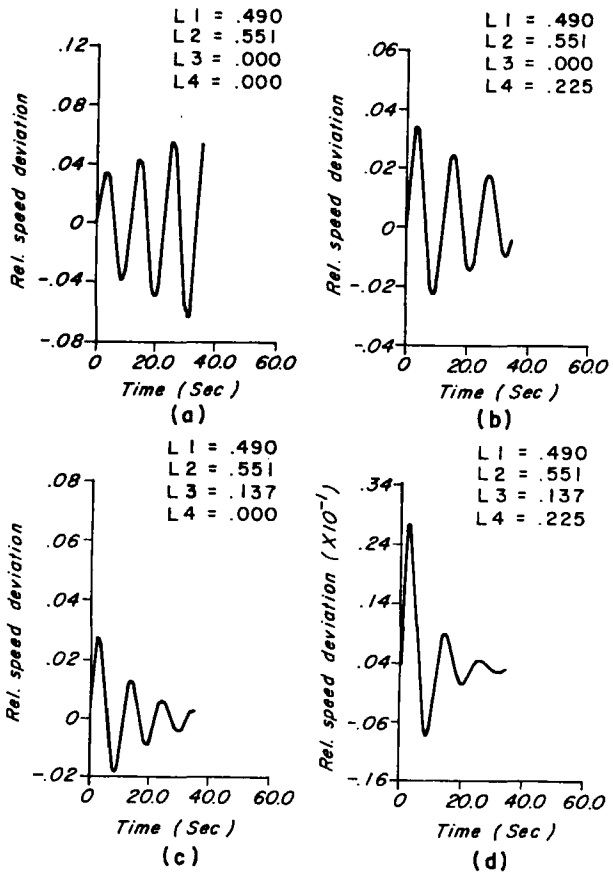

Figure 5.15. Unstable and stable speed oscillations.

in Fig. 5.15. In this figure, $L1$, $L2$, $L3$, and $L4$ denote λ_1, λ_2, λ_3, and λ_4, respectively.

Transient Speed Curve

The differential equation, Eq. 5.47, may be solved as follows to determine an expression for n:

Initial Conditions

At time $t = 0, N = N_o, G = G_o$, and $H = H_o$. Therefore,

$$n\big|_{t=0} = 0; \quad g\big|_{t=0} = 0; \quad h\big|_{t=0} = 0.0 \tag{5.56}$$

By substituting these values into Eq. 5.39, we obtain

$$T_m \left.\frac{dn}{dt}\right|_{t=0} = -\Delta m$$

or

$$\left.\frac{dn}{dt}\right|_{t=0} = -\frac{\Delta m}{T_m} \tag{5.57}$$

Note that for load-off condition, Δm is negative. Differentiation of Eq. 5.39 yields

$$T_m \frac{d^2n}{dt^2} = \frac{dg}{dt} + 1.5\frac{dh}{dt} - \alpha\frac{dn}{dt} \tag{5.58}$$

By substituting Eq. 5.56 into Eq. 5.41, we obtain

$$(\sigma + \delta)\, T_r \left.\frac{dg}{dt}\right|_{t=0} = -T_r \left.\frac{dn}{dt}\right|_{t=0} \tag{5.59}$$

which upon simplification becomes

$$\left.\frac{dg}{dt}\right|_{t=0} = \frac{-1}{(\sigma + \delta)} \left.\frac{dn}{dt}\right|_{t=0} \tag{5.60}$$

It follows from Eqs. 5.40 and 5.60 that

$$\left.\frac{dh}{dt}\right|_{t=0} = \frac{2}{(\sigma + \delta)} \left.\frac{dn}{dt}\right|_{t=0} \tag{5.61}$$

Substitution of Eqs. 5.57, 5.60, and 5.61 into Eq. 5.58 and simplification of the resulting equation yields

$$\left.\frac{d^2n}{dt^2}\right|_{t=0} = \frac{2 - \sigma\alpha - \delta\alpha}{\sigma + \delta} \frac{(-\Delta m)}{T_m^2} \tag{5.62}$$

Solution of the Differential Equation, Eq. 5.47

The general solution of the third-order differential equation, Eq. 5.47, is equal to the sum of the complementary function, n_c, and the particular integral, n_p (i.e., $n = n_p + n_c$). For Eq. 5.47, .

$$n_p = \frac{-\sigma\Delta m}{(1 + \sigma\alpha)} \tag{5.63}$$

To determine the complementary function, compute the roots of the characteristic equation,

$$0.5T_wT_mT_r(\delta+\sigma)\mu^3 + [0.5T_wT_m\sigma + (\delta+\sigma)T_rT_m - T_wT_r + 0.5\alpha T_wT_r(\delta+\sigma)]\mu^2 + [T_m\sigma + T_r - T_w + 0.5T_w\sigma\alpha + (\delta+\sigma)T_r\alpha]\mu + (1+\sigma\alpha) = 0 \quad (5.64)$$

Let the roots of Eq. 5.64 be $\alpha', \beta \pm i\gamma$. Then,

$$n_c = Ae^{\alpha' t} + De^{(\beta+i\gamma)t} + Ee^{(\beta-i\gamma)t} \quad (5.65)$$

where A, D, and E are arbitrary constants. Equation 5.65 can also be written as

$$n_c = Ae^{\alpha' t} + e^{\beta t}(B\sin\gamma t + C\cos\gamma t) \quad (5.66)$$

where A, B, and C are arbitrary constants. Therefore, the complete solution is

$$n = Ae^{\alpha' t} + e^{\beta t}(B\sin\gamma t + C\cos\gamma t) - \frac{\sigma\Delta m}{(1+\sigma\alpha)} \quad (5.67)$$

The values of the arbitrary coefficients are determined from the initial conditions

$$n|_{t=0} = A + C - \frac{\sigma\Delta m}{(1+\sigma\alpha)} = 0 \quad (5.68)$$

Hence,

$$A + C = \frac{\sigma\Delta m}{(1+\sigma\alpha)} \quad (5.69)$$

By differentiating Eq. 5.67, substituting $t = 0$, and using the initial condition given by Eq. 5.57, we obtain

$$\alpha' A + \gamma B + \beta C = -\frac{\Delta m}{T_m}. \quad (5.70)$$

By differentiating Eq. 5.67 twice, substituting $t = 0$, and using the initial condition given by Eq. 5.62, we obtain

$$\alpha'^2 A + 2\beta\gamma B + (\beta^2 - \gamma^2)C = \frac{2 - \sigma\alpha - \delta\alpha}{\sigma+\delta}\frac{(-\Delta m)}{T_m^2}. \quad (5.71)$$

Solution of Eqs. 5.69 to 5.71 for A, B, and C yields

$$\left.\begin{aligned} A &= \frac{\dfrac{-2\beta}{T_m} + \dfrac{2-(\sigma+\delta)\alpha}{(\sigma+\delta)T_m^2} - \dfrac{\sigma}{(1+\sigma\alpha)}(\gamma^2+\beta^2)}{(\alpha'-\beta)^2+\gamma^2}(-\Delta m) \\ B &= \left[\frac{-\Delta m}{T_m} - (\alpha'-\beta)A - \frac{\sigma\beta\Delta m}{1+\sigma\alpha}\right]\frac{1}{\gamma} \\ C &= \frac{\sigma\Delta m}{1+\sigma\alpha} - A. \end{aligned}\right\} \quad (5.72)$$

Optimum Values of the Governor Parameters

For a specific value of λ_3 and a specific value of λ_4, Eqs. 5.39 through 5.41 are solved for various values of λ_1 and λ_2. Those values of λ_1 and λ_2 are considered optimum values, which give the shortest settling time, but slightly underdamped response. This procedure is repeated for $\lambda_3 = 0.0$ and 0.25, and $\lambda_4 = 0.0$ to 0.4. The optimum values of λ_1 and λ_2 for different values of λ_3 and λ_4 are presented in Fig. 5.16. The following example illustrates the procedure to select the optimum values from this figure.

Example 5.2

Determine the optimum values of δ and T_r for Kelsey hydroelectric power plant. The following are the values of different parameters:

$T_w = 1.24$ s (computed from the dimensions and geometry of the penstock)
$T_m = 9.05$ s (computed from the known value of WR^2 and ratings of the turbine and generator)
$\alpha = 1.0$ (determined from Table 5.3 for the type of load)
$\sigma = 0.035$.

1. The optimum values of δ and T_r may be determined as follows:
   a. Compute λ_3 and λ_4:

$$\lambda_3 = \frac{\alpha T_w}{T_m} = \frac{1.0 \times 1.24}{9.05} = 0.137$$

$$\lambda_4 = \frac{\sigma T_m}{T_w} = \frac{0.035 \times 9.05}{1.24} = 0.255.$$

   b. Determine the optimum values of λ_1 and λ_2 from Fig. 5.16:
   From this figure, $\lambda_1 = 0.430$ and $\lambda_2 = 0.27$ for $\lambda_3 = 0.137$ and $\lambda_4 = 0.255$.

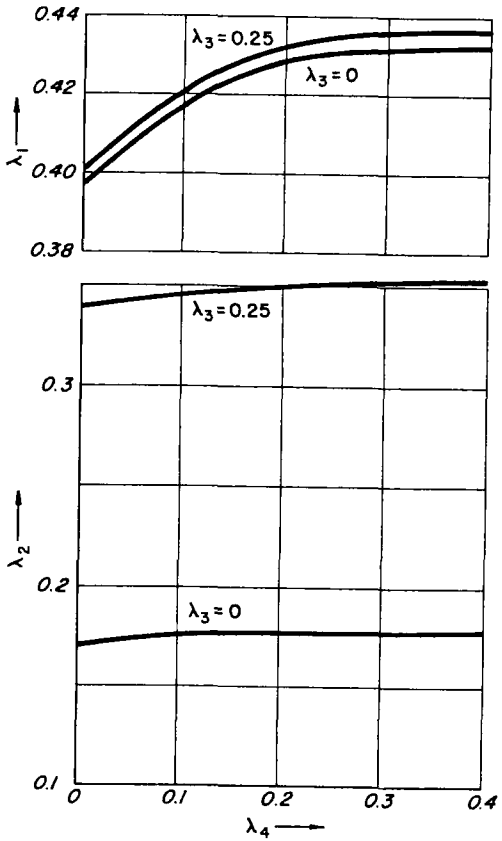

Figure 5.16. Optimum governor settings.

c. Compute δ and T_r from the values of λ_1 and λ_2 determined in step b:

$$\delta = \frac{T_w}{\lambda_1 T_m} = \frac{1.24}{0.430 \times 9.05} = 0.319$$

$$T_r = \frac{T_w}{\lambda_2} = \frac{1.24}{0.27} = 4.6 \text{ s}$$

2. Optimum values suggested by Hovey:

$$\delta = \frac{2T_w}{T_m} = \frac{2 \times 1.24}{9.05} = 0.274$$

$$T_r = 4\,T_w = 4 \times 1.24 = 4.96 \text{ s}$$

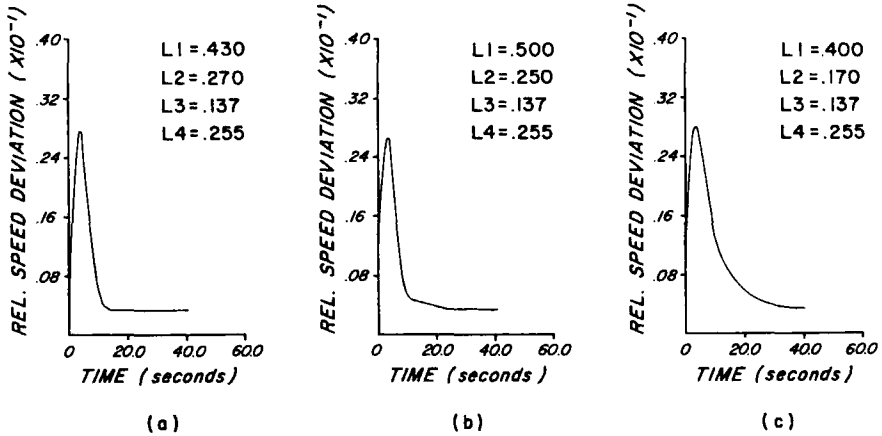

Figure 5.17. Speed deviation for various governor settings.

3. Optimum values according to Paynter's relationships:

$$\delta = \frac{T_w}{0.4\,T_m} = \frac{1.24}{0.4 \times 9.05} = 0.342$$

$$T_r = \frac{T_w}{0.17} = \frac{1.24}{0.17} = 7.3 \text{ s}$$

For cases 1 through 3, $n \sim t$ curves for $\Delta m = -0.1$ are presented in Fig. 5.17. It is clear that, if σ and α are taken into consideration, the optimum values suggested by the author give a better transient response.

5.12 CASE STUDY

For illustration purposes, governing stability studies carried out for the Kootenay Canal Development are presented in this section. Kootenay Canal Development is a 500-MW hydroelectric power plant owned by British Columbia Hydro and Power Authority. There are four units in the plant with each unit having its own power intake and penstock.

Data for the turbine, generator, and penstock follow:

1. Turbine

Type: Francis

Specific speed:* 55 (English units), 209 (SI units)

*Specific speed = $n\sqrt{P}/H^{1.25}$. In the English units, P is in hp, H in ft, and n in rpm; in SI units, P is in kW, H in m, and n in rpm.

Rated turbine output: 127.5 MW
Rated head: 74.6 m
Synchronous speed: 128.6 rpm
Flow at rated conditions: 191 m^3/s
Runner-throat diameter: 4.95 m

2. Generator
   Rated output: 125 MW
3. Penstock. The diameter of the penstock was determined from an economic analysis so that the incremental benefits from the decreased head losses were more than the increase in the penstock costs. The length, diameter, and wall thickness for various sections of the penstock are listed in Section 2.7.

Computations were done as follows:

1. *Mechanical starting time, T_m*

$$kva = \frac{\text{MW} \times 10^3}{\text{Power factor}}$$

$kva = 125{,}000/0.95 \quad = 131{,}579$

$$\text{Normal generator } WR^2 = 15{,}970\left(\frac{kva}{N_r^{1.5}}\right)^{1.25} \qquad \text{(Eq. 5.36)}$$

$$= 15{,}970\left(\frac{131{,}579}{(128.6)^{1.5}}\right)^{1.25}$$

$$= 4.44 \text{ Gg m}^2$$

$$\text{Turbine } WR^2 = 1446\left(\frac{kW}{N_r^{1.5}}\right)^{1.25}$$

$$= 1446\left(\frac{127{,}500}{(128.6)^{1.5}}\right)^{1.25}$$

$$= 0.39 \text{ Gg m}^2$$

$$\text{Total } WR^2 = 4.44 + 0.39 = 4.83 \text{ Gg m}^2$$

$$T_m = \frac{WR^2 \times N_r^2}{90.4 \times 10^6 \text{ MW}}$$

$$= \frac{4.83 \times 10^6 \times (128.6)^2}{90.4 \times 10^6 \times 127.5}$$

$$= 6.93 \text{ s}$$

2. *Water starting time, T_w*

Conduit	Length, L (m)	Cross-sectional Area, A (m^2)	$\Sigma \frac{L}{A}$ (m^{-1})	Remarks
Intake	7.6	$9.1 \times 9.1 = 82.8$	0.091	
	12.8	$4.9 \times 7.3 = 35.8$	0.357	
Penstock	244	$\frac{\pi}{4}(6.71)^2 = 35.4$	6.89	
	36.5	$\frac{\pi}{4}(5.55)^2 = 24.2$	1.51	
Scroll case	14.5	$\frac{\pi}{4}(5.55)^2 = 24.2$	0.60	Total length of scroll case = 29 m.
Draft tube	15.2	$\frac{\pi}{4}(4.88)^2 = 18.7$	0.81	
	13.7	$0.5(18.7 + 14.6 \times 5.33) = 48.3$	0.28	
			$\Sigma \frac{L}{A} = 10.54$;	
			$\Sigma \frac{L}{A}$ excluding draft tube = 9.45	

$$T_w = \frac{Q}{gH_r} \Sigma \frac{L}{A}$$

$$= \frac{191 \times 10.54}{9.81 \times 74.6}$$

$$= 2.75 \text{ s}$$

3. *Experience curves.* Since there is a strong possibility of this power plant being isolated from the system, the generator inertia was selected such that the units would be stable in isolated operation. For this purpose, the following empirical relationships and curves were used.

a. *U.S. Bureau of Reclamation criteria.*[12] For the normal WR^2 of the generator and turbine and for the selected conduit sizes, the values of T_m and T_w were computed above as 6.93 and 2.75 s, respectively. Hence,

$$\frac{T_m}{T_w} = \frac{6.93}{2.75} = 2.5.$$

As this ratio is less than 8, the unit would be unstable in isolated operation.

b. *Tennessee Valley Authority curves.*[13] The values of T_m and T_w computed in (a) were plotted on the TVA experience curves. It was found that the units would be unstable in isolated operation.

c. *Gordon's curves.*[14] As both the USBR criteria and the TVA experience curves indicated that the units would be unstable in isolated operation with the normal WR^2, total WR^2 of 7.2 and 8 Gg m^2, in addition to the normal WR^2 of 4.83 Gg m^2, were considered. The values of T_m for WR^2 of 7.2 and 8.0 Gg m^2 are 10.3 and 11.5 s, respectively. Water starting time, T'_w, excluding that for the draft tube, is

$$T'_w = \frac{191 \times 9.45}{9.81 \times 74.6} = 2.46 \text{ s}$$

Let us assume that the wicket-gate opening and closing times are equal. Then, allowing 1 sec for the cushioning stroke, $T_g = T_c + 1.0$, in which T_c = effective gate-closing time and T_g = total opening time. Now for different assumed values of T_c and for total WR^2 equal to 4.83, 7.2, and 8.0 Gg m^2, points were plotted on the Gordon's curves. Of these three curves, the curve for 4.83 Gg m^2 did not intersect the curve dividing the stable regions for the isolated and system operation. The values of T_c for WR^2 = 7.2 and 8.0 Gg m^2, which would result in stable isolated operation, were determined from the intersection of the other two curves. These values were 8.6 and 10.2 s, respectively.

4. *Speed rise.* Using the procedure outlined in Ref. 12 (p. 29), speed rise for full-load rejection was computed for various values of T_c and T_m. The computed values are listed in Table 5.4.

5. *Waterhammer pressure.* Waterhammer wave velocities in the penstock were computed in Section 2.7. Wave velocity and cross-sectional area for an equivalent 295-m-long (including half the length of scroll case) pipe[23] was computed as follows:

$$\frac{L}{a_e} = \Sigma \frac{L}{a}$$

Table 5.4. Speed rise.

T_c (s)	Speed rise, percent		
	T_m = 6.93 s	T_m = 10.27 s	T_m = 11.48 s
6	56.4	42.3	38.6
8	63.8	47	42.9
10	91.8	51.6	47.8

Therefore,

$$a_e = \frac{295}{\frac{244}{694} + \frac{51}{1410} + \frac{20}{1244}} = 730 \text{ m/s}$$

$$\frac{2L}{a_{eq}} = \frac{295}{730} = 0.81 \text{ s}$$

$$A_e = \frac{L}{\Sigma \frac{L}{A}}$$

$$= \frac{295}{9.45}$$

$$= 31.22 \text{ m}^2$$

$$V_o = \frac{191}{31.22} = 6.12 \text{ m/s}$$

Allievi's parameter, $\rho = \frac{aV_o}{2gH}$

$$= \frac{730 \times 6.12}{2 \times 9.81 \times 74.6} = 3.05$$

The waterhammer pressures for various values of T_c were computed from the charts presented in Appendix A. The computed values are as follows:

T_c	Pressure rise, $\frac{\Delta H}{H_r}$
6	0.48
8	0.36
10	0.27

6. *Selection of WR^2 and governor times.* From the preceding computations, the values of WR^2 and governor times were selected as follows:
   a. The maximum effective governor time was selected as the minimum of
      i. The governor time required for isolated stable governing from Gordon's stability curves.
      ii. The governor time so that the speed rise following total load rejection does not exceed 60 percent.
   b. The minimum value of the effective governor time is the maximum of
      i. The gate-opening time such that negative pressures do not occur in the penstock for the minimum forebay water level.
      ii. The waterhammer pressure rise following total load rejection does not exceed 50 percent of static head.

   Based on these criteria, the following values were selected:

   Total WR^2 of generator and turbine = 7.2 Gg m^2
   Turbine WR^2 = 0.2 Gg m^2 (specified by the turbine manufacturer)
   Generator WR^2 = 7.2 - 0.2 = 7.0 Gg m^2
   Governor closing time = 8 s
7. *Governor settings.* For the selected conduit sizes and WR^2 of the generator, T_w = 2.75 s and T_m = 10.27 s. Assuming the permanent speed droop, σ, equal to 5 percent and the self-regulation constant, α, equal to 0.5,

$$\lambda_3 = \frac{\alpha T_w}{T_m} = \frac{0.5 \times 2.75}{10.27} = 0.13$$

$$\lambda_4 = \frac{\sigma T_m}{T_w} = \frac{0.05 \times 10.27}{2.75} = 0.19$$

For these values of λ_3 and λ_4, optimum governor settings as determined from Fig. 5.16 are

$$\lambda_1 = 0.43$$

and

$$\lambda_2 = 0.27$$

Hence,

$$\text{Temporary speed droop, } \delta = \frac{T_w}{\lambda_1 T_m} = \frac{2.75}{0.43 \times 10.27} = 0.62$$

$$\text{Dashpot time constant, } T_r = \frac{T_w}{\lambda_2} = \frac{2.75}{0.27} = 10 \text{ s}$$

8. *Final check.* During the final design stages, the turbine characteristics were available from the model tests conducted by the turbine manufacturer. The mathematical model presented in Sections 5.3 through 5.6 was used to check the maximum and minimum transient-state pressures, maximum speed rise following total load rejection, and the speed deviation following large load changes. The maximum and minimum pressures and speed rise were found to be within the design limits, and the unit was stable following large load changes.

5.13 SUMMARY

In this chapter, the details of the mathematical simulation of the conduit system, hydraulic turbine, and governor were outlined. Various turbine operations that produce the hydraulic transients were discussed. Prototype test results to verify the mathematical model were presented. Procedures for the selection of the generator inertia and for determining the optimum governor settings were then described. The chapter was concluded by the presentation of a case study.

PROBLEMS

5.1. Develop the boundary conditions for a Francis turbine having a long pressurized downstream conduit.

5.2. How would the boundary conditions of Problem 5.1 be modified if there was a downstream surge tank?

5.3. The block diagram for a proportional-integral-derivative (PID) governor is shown in Fig. 5.18. Proceeding similarly as in Section 5.5, derive the differential equations for this governor.

5.4. Figure 3.18 shows the layout for the Jordan River Power Plant in which a pressure-regulating valve (PRV) is provided to reduce the transient pressures. In a load-rejection test on the prototype, the wicket gates closed, and the PRV opened as shown in Fig. 10.12. Develop a mathematical model to analyze the transients caused by a load rejection, and compare the computed results with those measured on the prototype (Fig. 10.13) Assume that the unit is isolated from the system, and that there is a delay of 0.4 s between the opening of the PRV and the closure of the wicket gates. Use the turbine characteristics shown in Fig. 5.3.

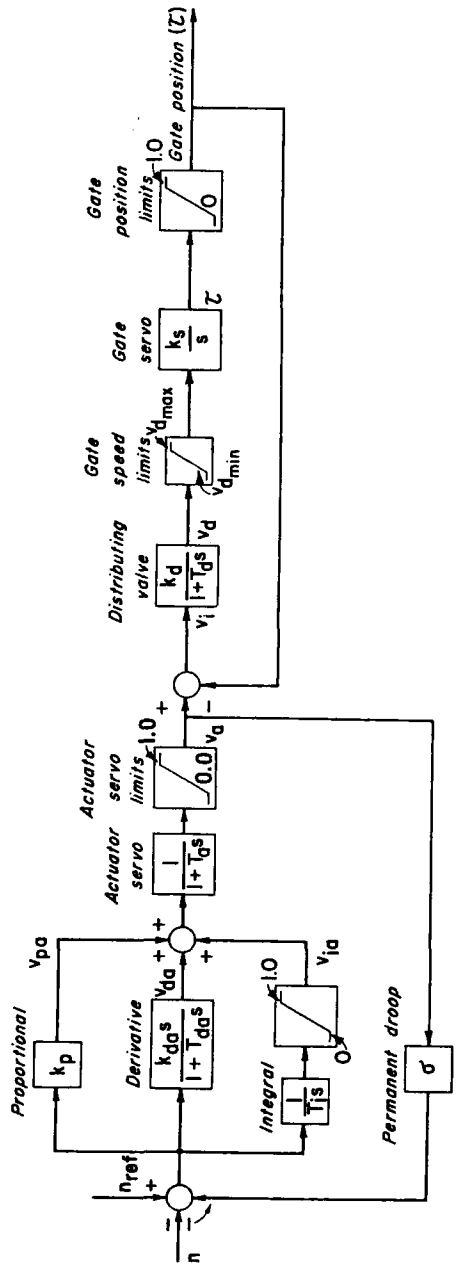

Figure 5.18. Block diagram for a PID governor.

5.5. Develop the boundary conditions for a Kaplan turbine taking into consideration the variation of the blade angle.

5.6. Determine the unit WR^2 required for stable governing of a hydroelectric power plant in isolated operation. The data for the power plant follow:

Rated output = 39 MW
Synchronous speed = 500 rpm
Rated head = 240 m
Turbine discharge at rated conditions = 38 m^3/s
Length of the penstock = 640 m
Length of the scroll case = 36 m
Cross-sectional areas of the penstock, and the scroll case at the upstream end = 7.9 m^2
Governor opening and closing time = 5 s

Neglect the length of the draft tube and assume a power factor of 0.95 while computing the *kva* of the unit.

5.7. What are the optimum governor settings for the unit of Problem 5.6?

REFERENCES

1. Krivehenko, G. I., Zolotov, L. A., and Klabukov, V. M., "Moment Characteristics of Cascades under Non-stationary Flow Conditions," *Proceeding, Annual Meeting, International Association for Hydraulic Research*, vol. 2, Paris, 1971, pp. B11-1-B11-9.
2. Perkins, F. E., et al., "Hydropower plant Transients," Part II and III, Dept. of Civil Engineering, Hydrodynamics Lab., Report 71, Massachusetts Inst. of Tech., Sept. 1964.
3. Streeter, V. L., *Fluid Mechanics*, 4th Edition, McGraw-Hill Book Co., New York, N.Y., 1966.
4. Chaudhry, M. H. and Portfors, E. A., "A Mathematical Model for Analyzing Hydraulic Transients in a Hydroelectric Powerplant," *Proceedings, First Canadian Hydraulic Conference*, published by the University of Alberta, Edmonton, Canada, May 1973, pp. 298-314.
5. "Speed Governor Fundamentals," Bulletin 25031, Wordward Governor Company, Rockford, Illinois.
6. D'Azzo, J. J. and Houpis, C. H., *Feedback Control System Analysis and Synthesis*, Second Edition, McGraw-Hill Book Co., New York, 1966.
7. Lathi, B. P., *Signals, Systems and Communications*, John Wiley & Sons, Inc., New York, 1965.
8. McCracken, D. D. and Dorn, W. S., *Numerical Methods and Fortran Programming*, John Wiley & Sons, Inc., New York, 1964.
9. Fischer, S. G., "The Westinghouse Leading Edge Ultrasonic Flow Measurement System," presented at the spring meeting, Amer. Soc. of Mech. Engineers, Boston, Massachusetts, May 15-16, 1973.
10. Parmakian, J., "Water Hammer Design Criteria," *Jour. Power Div., Amer. Soc. of Civil Engrs.*, April 1957, pp. 1216-1-1216-8.
11. Portfors, E. A. and Chaudhry, M. H., "Analysis and Prototype Verification of Hydraulic Transients in Jordan River Powerplant," *Proceedings, First International Conference on Pressure Surges*, Canterbury, England, published by British Hydromechanic Research Association, Sept. 1972, pp. E_4-57-E_4-72.

12. Krueger, R. E., "Selecting Hydraulic Reaction Turbines," *Engineering Monograph No. 20*, United States Bureau of Reclamation, 1966.
13. "Mechanical Design of Hydro Plants," Tennessee Valley Authority Projects, Technical Report No. 24, vol. 3, 1960.
14. Gordon, J. L., "Determination of Generator Inertia," presented to the Canadian Electrical Association, Halifax, January 1961.
15. Paynter, H. M. "A Palimpsest on the Electronic Analogue Art," A. Philbrick Researches, Inc., Boston, Mass., 1955.
16. Hovey, L. M., "Optimum Adjustment of Governors in Hydro Generating Stations," *The Engineering Journal, Engineering Inst. of Canada*, pp. 64-71, November 1960.
17. Hovey, L. M. "Speed Regulation Tests on a Hydrostation Supplying an Isolated Load," *Trans. Amer. Inst. of Elect. Engrs.*, 1962, pp. 364-368.
18. Stein, T., "The Influence of Self-Regulation and of the Damping Period on the WR^2 value of Hydroelectric Power Plant," *The Engineers' Digest*, May-June 1948. (Translated from *Schweizerische Bauzeitung*, Sept.-Oct. 1947.)
19. Chaudhry, M. H., "Governing Stability of a Hydroelectric Power Plant," *Water Power*, London, April 1970, pp. 131-136.
20. Wylie, C. R., *Advanced Engineering Mathematics*, McGraw-Hill Book Co., 3rd Edition, New York, p. 721.
21. Hovey, L. M., "The Use of an Electronic Analog Computer for Determining Optimum Settings of Speed Governors for Hydro Generating Units," Eng. Inst. of Canada, Annual General Meeting Paper No. 7, 1961, pp. 1-40.
22. Hovey, L. M., "Optimum Adjustment of Hydro Governors on Manitoba Hydro System," *Trans. Amer. Inst. of Elect. Engrs.*, Dec. 1962, pp. 581-586.
23. Parmakian, J., *Waterhammer Analysis*, Dover Publications, New York, 1963.

ADDITIONAL REFERENCES

Almeras, P., "Influence of Water Inertia on the Stability of Operation of a Hydroelectric System," *Engineer's Digest*, vol. 4, Jan. 1947, pp. 9-12, Feb. 1947, pp. 55-61.

"IEEE Recommended Practice for Preparation of Equipment Specifications for Speed Governing of Hydraulic Turbines Intended to Drive Electric Generators," *Amer. Inst. of Elect. and Electronics Engrs.*, April 1977.

Dennis, N. G., "Water-Turbine Governors and the Stability of Hydroelectric Plant," *Water Power*, Feb. 1953, pp. 65-76; Mar. 1953, pp. 104-109; Apr. 1953, pp. 151-154; May 1953, pp. 191-196.

Concordia, C. and Kirchmayer, L. K., "Tie-Line Power and Frequency Control of Electric Power Systems," Part I and II, *Trans., Amer. Inst. of Elect. Engrs.*, June 1953, pp. 562-572, April 1954, pp. 1-14. (See also discussion by H. M. Paynter.)

Sweiecicki, I., "Regulation of a Hydraulic Turbine Calculated by Step-by-Step Method," *Jour. Basic Engineering, Amer. Soc. of Mech. Engrs.*, Sept. 1961, pp. 445-455.

Oldenburger, R., "Hydraulic Speed Governor with Major Governor Problems Solved," *Jour. Basic Engineering, Amer. Soc. of Mech. Engrs.*, Paper No. 63-WA-15, 1964, pp. 1-8.

"Waterhammer in Pumped Storage Projects," *International Symposium, Amer. Soc. Mech. Engrs.*, Nov. 1965.

International Code of Testing of Speed Governing Systems for Hydraulic Turbines, Technical Committee No. 4, Hydraulic Turbines, *International Electrotechnical Commission*, Feb. 1965.

Lein, G. and Parzany, K., "Frequency Response Measurements at Vianden," *Water Power*, July 1967, pp. 283-286, Aug. 1967, pp. 323-328.

Newey, R. A., "Speed Regulation Study for Bay D'Espoir Hydroelectric Generating Station," Paper No. 67-WA/FE-17, presented at Winter Annual Meeting, *Amer. Soc. of Mech. Engrs.*, Dec. 1967.

Schleif, F. R. and Bates, C. G., "Governing Characteristics for 820,000 Horsepower Units for Grand Coulee Third Powerplant," *Trans., Inst. of Elect. and Electronics Engrs., Power Apparatus and Systems*, Mar.-April 1971, pp. 882-890.

Stein, T., "Frequency Control under Isolated Network Conditions," *Water Power*, Sept. 1970.

Araki, M. and Kuwabara, T, "Water Column Effect on Speed Control of Hydraulic Turbines and Governor Improvement," *Hitachi Review*, vol. 22, no. 2, pp. 50-55.

Chaudhry, M. H. and Ruus, E., "Analysis of Governing Stability of Hydroelectric Power Plants," *Trans., Engineering Inst. of Canada*, vol. 13, June 1970, pp. I-V.

Wozniak, L. and Fett, G. H., "Conduit Representation in Closed Loop Simulation of Hydroelectric Systems," *Jour. Basic Engineering, Amer. Soc. of Mech. Engrs.*, Sept. 1972, pp. 599-604. (See also discussion by Chaudhry, M. H., pp. 604-605).

Goldwag, E., "On the Influence of Water Turbine Characteristic on Stability and Response," *Jour. Basic Engineering, Amer. Soc. of Mech. Engrs.*, Dec. 1971, pp. 480-493.

Vaughan, D. R., "Speed Control in Hydroelectric Power Systems," thesis submitted to Massachusetts Institute of Technology in partial fulfillment of the requirements for the degree of doctor of philosophy, 1962.

Thorne, D. H. and Hill, E. F., "Field Testing and Simulation of Hydraulic Turbine Governor Performance," *Trans., Inst. of Elect. and Electronics Engrs. (U.S.A), Power Apparatus and Systems*, July -Aug. 1974, pp. 1183-1191.

Brekke, H., "Stability Studies for a Governed Turbine Operating under Isolated Load Conditions," *Water Power*, London, England, Sept. 1974, pp. 333-341.

Thorne, D. H. and Hill, E. F., "Extension of Stability Boundaries of a Hydraulic Turbine Generating Unit," *Trans., Inst. of Elect. and Electronics Engrs. (U.S.A)*, vol. PAS-94, July/Aug. 1975, pp. 1401-1409.

CHAPTER 6

HYDRAULIC TRANSIENTS IN NUCLEAR POWER PLANTS

6.1 INTRODUCTION

In nuclear power plants, various piping systems are used for cooling and for heat transfer. It is necessary for the design and for the safe operation of these systems that the transient-state conditions caused by various operating conditions be accurately known.

In this chapter, terminology is introduced first; various operations which may produce transients are then outlined. Different methods for analysis are discussed, and special boundary conditions for the method of characteristics are derived. The details of a numerical scheme, suitable for the analysis of two-phase transient flows, are then presented.

Since various types of reactors are available and each reactor type differs in details from one manufacturer to another, the analysis techniques are emphasized instead of the specifics of design details.

6.2 TERMINOLOGY

General

Figure 6.1 shows the schematic arrangement of a nuclear power plant. Thermal energy, generated in the nuclear reactor by splitting the atoms, is transferred from the reactor by a fluid medium called the *reactor coolant*. The reactor coolant may be a liquid (e.g., ordinary water, heavy water [D_2O], liquid sodium); it may be a liquid-vapor mixture, (e.g., boiling ordinary water); or it may be a gas (e.g., helium, carbon dioxide [CO_2]).

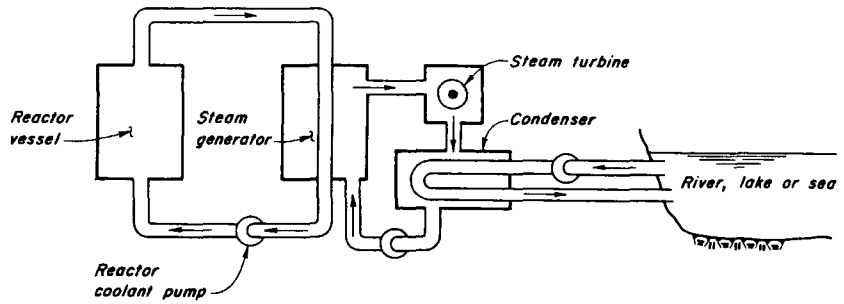

Figure 6.1. Schematic arrangement of a nuclear power plant.

Types of Reactors

Reactors are classified[1] according to the type of fuel, reactor coolant, and the type of medium, called *moderator*, used to slow down or moderate the high-energy neutrons produced by the fission process. Three main types of *liquid-cooled* reactors are:

1. *Pressurized water reactor (PWR).* In this reactor, ordinary water is used as a reactor coolant and as a moderator. Water coolant is circulated at high pressure (about 14 MPa) by the external pumps through the reactor vessel. Water flows upward through the fuel clusters, then from the vessel into the heat exchangers and back to the pumps. This loop is called the *primary loop.* A *pressurizer*[2] is provided in this loop to control the pressure of the coolant. The temperature of the coolant rises as it flows through the reactor vessel. Therefore, the pipe on the inlet side of the reactor is called the *cold leg*, and the pipe on the exit side is called the *hot leg* (Fig. 6.2). In the *secondary loop*, water is

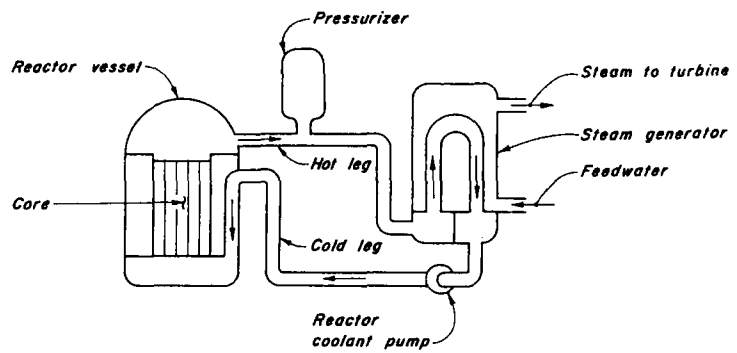

Figure 6.2. Pressurized water reactor.

boiled in the heat exchangers forming saturated steam, which is used to drive the steam turbine.

2. *Boiling water reactor (BWR).* This reactor is similar to the PWR except that ordinary (light) water coolant is permitted to boil in the reactor core. The steam thus produced is separated from the coolant by centrifugal separators (Fig. 6.3) located in the reactor vessel above the core. This steam is then directly fed into the turbine.

3. *Liquid-metal fast breeder reactor (LMFBR).* In this reactor, liquid sodium[1] is used as the reactor coolant, which is cooled in the intermediate heat exchangers (Fig. 6.4) and is returned to the reactor. The intermediate heat exchangers are cooled by a second flow of liquid sodium, which in turn is cooled in a second set of heat exchangers in which steam is produced for the turbine.

The steam exhausted from the turbine is condensed by means of a condenser, and the condensed water is pumped back into the heat exchangers. A large amount of water has to be pumped from a lake, river, or ocean to the condenser loop (Fig. 6.1) for this purpose.

Emergency Core Cooling Systems

The emergency core cooling (ECC) systems[2] are used to provide coolant for possible loss-of-coolant accident (LOCA). A number of subsystems are employed for this purpose:

1. *High-pressure coolant injection system.* This system employs high-head, low-capacity pumps and is intended to provide coolant during small-size breaks

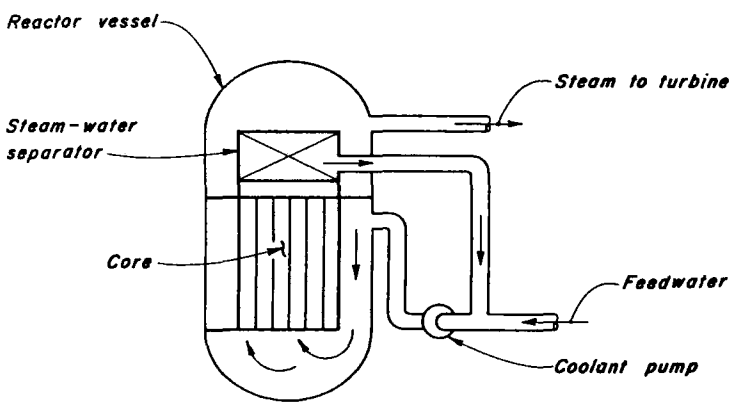

Figure 6.3. Boiling water reactor.

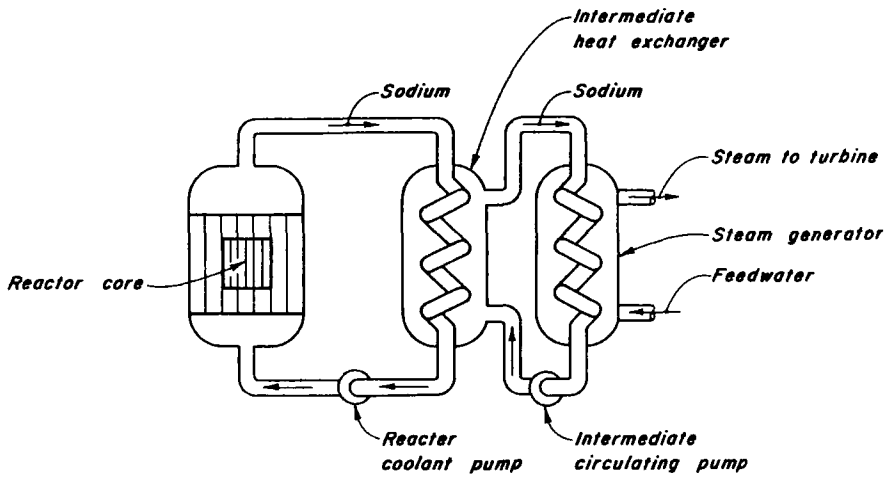

Figure 6.4. Liquid-metal fast-breeder reactor.

in the primary loop. This system is activated during the early stages of depressurization.

2. *Low-pressure coolant injection system.* This system employs low-head, high-capacity pumps; it is intended for supplying coolant following large-size breaks in the primary loop and provides coolant during later stages of LOCA.

3. *Accumulator System.* This is a passive system and is intended to provide large volumes for large-size breaks. A check valve, which isolates the accumulator from the reactor system during normal operation, opens whenever the pressure in the reactor system drops below the pressure of the accumulator and provides coolant to the primary loop.

6.3 CAUSES OF TRANSIENTS

Transients in the piping systems of a nuclear power plant are caused by the following (only events initiated in the hydraulic system are considered):[1-14]

1. Planned or accidental starting or stopping of pumps; power failure to pumps
2. Planned or accidental opening or closing of the control valves
3. Instability of pumps
4. Release of entrapped air or collapse of vapor bubbles
5. Wave action at the reservoir water surface (for the condenser piping system)
6. Rupture of pipeline.

The starting or stopping of the pumps, the opening or closing of control valves under controlled conditions, and power failure to the pumps are con-

sidered normal operations. Flow variations may be caused by pump instability due to abnormalities in the pump characteristics. If the pumps are started into an empty pipeline or into a partly drained discharge line, severe pressure oscillations may be produced.

Waterhammer pressure generated by air release or due to collapse of vapor or steam bubbles has resulted in damage to the pipelines of a number of nuclear power plants.[13,14]

Rupture of a pipe in the primary loop[2] and the loss of reactor coolant, i.e., loss-of-coolant accident, is one of the worst conditions to be considered in the design. Rupture of, or a leak in, the pipe in the secondary loop of a LMFBR will result in sodium-water reaction; transients produced by such an incident have to be considered in the design stages.

6.4 METHODS OF ANALYSIS

General Remarks

The following two approaches are available for the analysis of hydraulic transients in the piping systems of nuclear power plants:

1. Lumped-system approach
2. Distributed-system approach.

In a lumped-system approach, sometimes referred to as *control-volume* or *macroscopic* approach,[15] the system is divided into a number of control volumes, and an integrated form of the continuity and momentum equations (and the energy equation, if required) is used. Thus, there is no continuous spatial variation (i.e., with respect to distance x in a one-dimensional model) of various variables, and they vary with respect to time only. Therefore, a system of ordinary differential equations, instead of partial differential equations, describe the transients.[16] Since the initial steady-state conditions are specified, the transient analysis using a lumped-system approach may be considered as an initial value problem.

In a distributed-system approach, both the temporal and spatial variations of various variables are taken into consideration. Thus, a system of partial differential equations subject to appropriate boundary conditions describe the behavior of the system. If there is simultaneous flow of two phases (e.g., water and vapor, air and water), then the flow is called a *two-phase flow.*[17] Two-phase flows may be further classified as *homogeneous* or *separated flows.* We will consider only the homogenous two-phase flows in which the mixture of the two phases may be treated as a pseudofluid. The separated flows are beyond the scope of this book.

If heat is added or removed from the system during a transient, then the energy equation has to be considered in addition to the continuity and momentum equations.

Formulation of Mathematical Models

Extreme caution must be exercised in formulating a mathematical model since a model based on questionable simplifying assumptions may yield totally incorrect results no matter how sophisticated are the numerical techniques employed to solve the governing equations. Similarly, using too complex a model, where a simplified model would suffice, results in waste of manpower as well as computer time. A lumped-system one-dimensional model is one of the simplest, whereas a multidimensional, distributed-system, two-phase model with heat addition or removal is the most complicated.

The following factors are considered while selecting a model for the analysis of a particular system:

1. For a slow transient phenomenon, the compressibility effects may be neglected and the system may be analyzed by using a lumped-system approach. This approach may be used[18] for systems in which $\omega l/a << 1$ (see p. 219). In this expression ω = forcing frequency; l = length of the pipe, and a = wave velocity. As a rough rule of thumb, $\omega l/a = 0.05$ may be considered as the upper limit for the validity of the lumped-system approach.
2. If the void fraction, α (α = volume of the gas and vapors per total volume of the gas-vapor-liquid mixture), is small, then its effects can be totally neglected or may be taken into consideration by reducing the waterhammer wave velocity.
3. Flows having a large void fraction, have to be analyzed as two-phase flows. If the phases are not separated, then a homogeneous flow model may be used in which the gas-vapor-liquid mixture is treated as a pseudofluid and the continuity, momentum, and energy equations for a single-component flow are used in the analysis. However, if the phases are separated, then the continuity, momentum, and energy equation for each phase have to be used, and the transfer of mass, momentum, and energy between the phases has to be considered. Such a model is called a *separated flow* model.
4. If there is significant heat input or output from the system during the transient conditions under consideration, then it is necessary to include the energy equation in addition to the continuity and momentum equations in the analysis.

Numerical Solution

The numerical method to be used for the solution of the equations describing the system behavior depends upon whether a lumped-system or a distributed-

system approach is being used. Various available methods are discussed in the following paragraphs.

Lumped-System Approach

As discussed previously, a mathematical model based on a lumped-system approach is comprised of a system of ordinary differential equations. A number of finite-difference methods[19-20] are available to solve these equations. The author's experience with the solution of these equations indicates that the fourth-order Runge-Kutta method[20,21] is quite versatile and accurate. In addition, most computer installations have standard packages available for this method.

Distributed-System Approach

Distributed-system approaches may be further subdivided into two categories, depending upon whether the flow is single-phase or two-phase:

1. *Single-phase flows.* The method of characteristics presented in Chapter 3 may be used for single-phase flows. To account for a small amount of gaseous phase in the liquid, a reduced value of the waterhammer wave velocity (see Section 9.5) may be used in the analysis.

The transients caused by opening or closing of valves, by starting or stopping of pumps, or by power failure to the pump-motors may be analyzed by using the method of characteristics. A number of commonly used boundary conditions were derived in Chapters 3 and 4, and a few additional ones are developed in the next section and in Chapter 10.

2. *Two-phase flows.* The two-phase flows may be analyzed by considering them as homogeneous or separated flows. In the case of homogeneous flow, the liquid mixture is treated as a pseudofluid, and the averaged values of the various variables (such as pressure, flow velocity, and void fraction) over a cross section are used. The spatial variation of void fraction may be included in the analysis.

In the analysis of separated flows, each phase is treated separately, and the transfer of mass, momentum, and energy between each phase is taken into consideration. Analyses of these flows are beyond the scope of this book.

The following numerical methods have been used for the analysis of homogeneous two-phase flows:

1. Method of characteristics
2. Lax-Wendroff's two-step finite-difference method
3. Explicit finite-difference methods
4. Implicit finite-difference methods.

In the method of characteristics,[22-25] the discontinuities in the derivatives can be handled, and the boundary conditions are properly posed. The method, however, fails because of the convergence of characteristics curves if the wave velocity is highly dependent upon pressure, and a shock is formed in the solution. In addition, if an explicit finite-difference scheme is used to solve the total differential equations obtained by this method, the Courant-Fredrich-Levy condition[25] for the stability of the numerical scheme has to be satisfied. This condition requires the use of small computational time steps, thus making the method unsuitable for solving real-life large systems. The method may, however, be used to verify other numerical schemes by analyzing small, simple systems.

The Lax-Wendroff two-step finite-difference scheme[26] is the most suitable for analyzing systems in which a shock forms. However, the scheme produces oscillatory solution behind the wave front, and a smoothening parameter[27] has to be introduced to avoid this. This introduces numerical damping, which is not present in the actual system and which, if not properly taken care of, may smoothen the transient peaks. Because the Courant's stability condition has to be satisfied, the size of time steps is restricted, which makes the scheme uneconomical for general analyses.

Explicit finite-difference methods are very easy to program. However, as the step size is limited by the Courant's stability condition,[28] a large amount of computer time is required. Thus, the method is not suitable for analyzing large systems.

In the implicit finite-difference methods, the size of the time step is governed by accuracy only and not by the stability considerations.[29-32] These methods are therefore useful for the analysis of large systems. Details of this method are presented in Section 6.7.

6.5 BOUNDARY CONDITIONS

To analyze a piping system by the method of characteristics, the boundary conditions should be known. A number of boundary conditions commonly found in the piping systems of nuclear power plants are derived in this section. Note that these conditions are valid only for single-phase flows and are required if the method of characteristics of Chapter 3 is used for the analysis.

Condenser

A condenser is comprised of a large number of tubes with water boxes on the ends (Fig. 6.5). To derive the boundary condition, the cluster of tubes may be replaced by an equivalent pipe having a cross-sectional area, A_e, equal to the

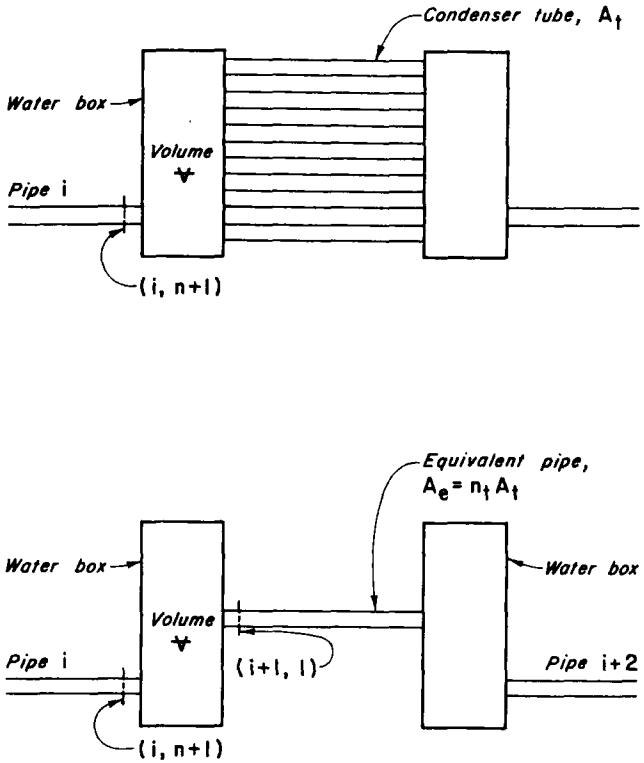

Figure 6.5. Condenser.

combined area of all the tubes, i.e., $A_e = n_t A_t$, in which A_t = cross-sectional area of one tube and n_t = number of tubes in the condenser (Fig. 6.5). The head loss in the equivalent pipe is, however, assumed equal to the head loss in an individual tube. The water boxes may be considered as lumped capacitances, and the compressibility of water and the elasticity of the walls of the boxes may be taken into consideration.

Equations for the upstream water box are derived below; equations for the downstream box may be derived in a similar manner.

Let the volume of water in the box be $\forall$, and let the combined effective bulk modulus of water inside the box and the vessel walls be K. Then, by definition,

$$K = \frac{\Delta p}{\frac{\Delta \forall}{\forall}} \tag{6.1}$$

in which $\Delta \forall$ is the change in volume due to change in pressure, Δp. For the pressure changes usually encountered in practice, $\Delta \forall$ is small, and therefore $\forall$ may be assumed constant. The change in volume, $\Delta \forall$, during a time step Δt, may be determined from the continuity equation

$$\Delta \forall = \tfrac{1}{2}\,\Delta t[(Q_{P_{i,n+1}} + Q_{i,n+1}) - (Q_{P_{i+1,1}} + Q_{i+1,1})] \tag{6.2}$$

in which Q and Q_P are discharges at the beginning and at the end of the time step, and subscripts $(i, n+1)$ and $(i+1, 1)$ refer to the section numbers (see Fig. 6.5). If it is assumed that the pressure is same throughout the box, then

$$H_{P_{i,n+1}} = H_{P_{i+1,1}} \tag{6.3}$$

in which H_P = piezometric head above the datum at the end of time step. Now,

$$\Delta p = \gamma \Delta H = \gamma(H_{P_{i,n+1}} - H_{i,n+1}) \tag{6.4}$$

in which γ = specific weight of water.

By substituting Eqs. 6.2 and 6.4 into Eq. 6.1 and simplifying the resulting equation, we obtain

$$H_{P_{i,n+1}} = H_{i,n+1} + \frac{K\Delta t}{2\gamma \forall}[(Q_{i,n+1} - Q_{i+1,1}) + (Q_{P_{i,n+1}} - Q_{P_{i+1,1}})] \tag{6.5}$$

The positive and negative characteristic equations (Eqs. 3.18, 3.19) for sections $(i, n+1)$ and $(i+1, 1)$ are

$$Q_{P_{i,n+1}} = C_p - C_{a_i} H_{P_{i,n+1}} \tag{6.6}$$

$$Q_{P_{i+1,1}} = C_n + C_{a_{i+1}} H_{P_{i+1,1}} \tag{6.7}$$

in which C_p, C_n, and C_a are as defined by Eqs. 3.20 through 3.22. Substitution of Eqs. 6.3, 6.6, and 6.7 into Eq. 6.5 yields

$$H_{P_{i,n+1}} = H_{i,n+1} + \frac{K\Delta t}{2\gamma \forall}[(Q_{i,n+1} - Q_{i+1,1}) + (C_p - C_n)] - \frac{K\Delta t}{2\gamma \forall}(C_{a_i} + C_{a_{i+1}}) H_{P_{i,n+1}} \tag{6.8}$$

Hence,

$$H_{P_{i,n+1}} = \frac{2\gamma \forall}{2\gamma \forall + K\Delta t(C_{a_i} + C_{a_{i+1}})}\left\{H_{i,n+1} + \frac{K\Delta t}{2\gamma \forall}[(Q_{i,n+1} - Q_{i+1,1}) + (C_p - C_n)]\right\} \tag{6.9}$$

Now, $H_{P_{i+1,1}}$, $Q_{P_{i,n+1}}$, and $Q_{P_{i+1,1}}$ may be determined from Eqs. 6.3, 6.6, and 6.7, respectively.

Entrapped Air

Let us consider a volume of air entrapped in a pipe having liquid on either side as shown in Fig. 6.6. If the entrapped air follows the polytropic law for perfect gases, then

$$H^*_{P_{air}} \forall^m_{P_{air}} = C \tag{6.10}$$

in which $H^*_{P_{air}}$ and $\forall_{P_{air}}$ are the absolute pressure head and volume of the entrapped air, respectively, and m = exponent in the polytropic gas law. The value of the constant, C, in Eq. 6.10 is determined from the initial steady-state conditions.

From the continuity equation, the following equation may be written for the volume of the air:

$$\forall_{P_{air}} = \forall_{air} + \tfrac{1}{2}\,\Delta t\,\{(Q_{i+1,1} + Q_{P_{i+1,1}}) - (Q_{i,n+1} + Q_{P_{i,n+1}})\} \tag{6.11}$$

The positive and negative characteristic equations (Eqs. 3.18, and 3.19) for sections $(i, n+1)$ and $(i+1, 1)$ are

$$Q_{P_{i,n+1}} = C_p - C_{a_i} H_{P_{i,n+1}} \tag{6.12}$$

$$Q_{P_{i+1,1}} = C_n + C_{a_{i+1}} H_{P_{i+1,1}} \tag{6.13}$$

in which C_p, C_n, C_{a_i}, and $C_{a_{i+1}}$ are as defined by Eqs. 3.20 through 3.22. If the pressure of air at any instant is assumed to be same throughout its volume, then

$$H_{P_{i,n+1}} = H_{P_{i+1,1}} \tag{6.14}$$

In addition,

$$H^*_{P_{air}} = H_b + H_{P_{i,n+1}} - z \tag{6.15}$$

in which H_b = barometric head, and z = height of the pipeline above datum.

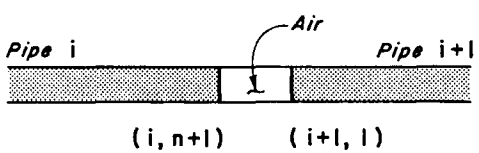

Figure 6.6. Entrapped air.

Now we have six equations (Eqs. 6.10-6.15) in six unknowns, namely, $H^*_{P_{air}}$, $\forall_{P_{air}}$, $Q_{P_{i,n+1}}$, $Q_{P_{i+1,1}}$, $H_{P_{i+1,1}}$, and $H_{P_{i,n+1}}$. Elimination of the first five unknowns from these equations yields

$$(H_{P_{i,n+1}} + H_b - z)\,[C_{air} + \tfrac{1}{2}\,\Delta t(C_{a_i} + C_{a_{i+1}})H_{P_{i,n+1}}]^m = C \tag{6.16}$$

in which

$$C_{air} = \forall_{air} + \tfrac{1}{2}\,\Delta t\,(Q_{i+1,1} - Q_{i,n+1} + C_n - C_p) \tag{6.17}$$

Equation 6.16 may be solved for $H_{P_{i,n+1}}$ by an iterative technique, such as the bisection method.[20] The values of the other unknowns may then be determined from Eqs. 6.10 through 6.15.

Pipe Rupture and Failure of Rupture Discs

Sometimes, rupture discs are installed, which fail if the pressure inside the pipeline exceeds a specified limit. Because of this controlled failure, extensive damage to the pipeline is avoided.

The ruptured discs or pipe-break may be analyzed as an orifice, and the boundary conditions derived in Chapter 3 may be used for this purpose. If there is back pressure from outside the pipeline, then ΔH is the difference between the pressure inside and outside the pipeline.

Total pipe-break may be analyzed considering it as a fixed-opening valve located at the ends of pipe at the location of the pipe-break.

6.6 LOSS-OF-COOLANT ACCIDENT

A sudden rupture of a pipe in the primary loop and the resulting loss of reactor coolant is referred to as loss-of-coolant accident. The size and location of the pipe-break in this hypothetical accident is selected, which results in the maximum cladding temperatures. In a PWR, a complete rupture of the pipe connecting the pump to the reactor (i.e., cold leg) is assumed.[2] In a BWR, a complete and instantaneous circumferential rupture is assumed[2] of the largest pipe in one of the suction lines of the recirculation system.

The analysis of LOCA is done by using a number of mathematical models, and the output of one model serves as input to the other model. For example, the average conditions in the core, such as flow, pressure, and temperature, are determined by a mathematical model of the primary loop. Using these computed conditions as input, the maximum cladding temperature is determined using another model. These two models are used in an iterative manner at every time step or after a number of time steps.

In the mathematical model of the primary loop, the continuity, dynamic, and

energy equations are solved. The heat addition in the core to the fluid of the primary loop and the heat loss in the heat exchangers from the primary loop to the secondary loop are assumed to be distributed along the pipe lengths representing the core and the heat exchangers. The secondary loop is considered as a heat sink and is therefore decoupled from the primary loop. Similarly, the containment vessel is decoupled by specifying a back pressure at the hypothetical pipe-break.

A numerical method is presented in the next section to solve the equations describing the flow conditions in the primary loop following a pipe-break.

6.7 IMPLICIT FINITE-DIFFERENCE METHOD FOR ANALYZING TWO-PHASE TRANSIENT FLOWS

General

In this section, the details of an implicit finite-difference method, presented by Hancox et al.[28,30,31] are outlined. In this method, the characteristic form of the equations governing the homogeneous two-phase flows are used. Therefore, the method is as similar as possible to the method of characteristics. However, as it is not necessary to satisfy the Courant's stability condition, a larger size of time steps can be used, thus making the method suitable for the analysis of large systems.

Governing Equations

The following equations describe[28,30] the homogeneous, two-phase flow in pipes including the heat addition or loss:

1. Momentum equation

$$\frac{\partial V}{\partial t} + V\frac{\partial V}{\partial x} + \frac{1}{\rho}\frac{\partial p}{\partial x} = c_1 \tag{6.18}$$

2. Energy equation

$$\frac{\partial h}{\partial t} + a^2\frac{\partial V}{\partial x} + V\frac{\partial h}{\partial x} = c_2 \tag{6.19}$$

3. Continuity equation

$$\frac{\partial p}{\partial t} + \rho a^2\frac{\partial V}{\partial x} + V\frac{\partial p}{\partial x} = c_3 \tag{6.20}$$

in which

$$c_1 = -F - g\cos\theta \tag{6.21}$$

$$c_2 = a^2\left[(q + VF)\left.\frac{\partial \rho}{\partial p}\right|_h - \frac{V}{A}\frac{dA}{dx}\right] \tag{6.22}$$

$$c_3 = -a^2\left[(q + VF)\left.\frac{\partial \rho}{\partial h}\right|_p + \frac{\rho V}{A}\frac{dA}{dx}\right] \tag{6.23}$$

$$a = \left(\left.\frac{\partial \rho}{\partial p}\right|_h + \frac{1}{\rho}\left.\frac{\partial \rho}{\partial h}\right|_p\right)^{-1/2} \tag{6.24}$$

$$q = \frac{k_w A_w}{\rho}(T_w - T_f) \tag{6.25}$$

$$F = \left(\frac{4f}{d}\tau^* + \frac{k}{l}\right)\frac{V|V|}{2} \tag{6.26}$$

and in which a = wave velocity in the fluid; q = wall-to-flow heat transfer; ρ = density of the fluid; F = friction force per unit mass; k_w = wall-heat transfer coefficient; T_w = wall temperature; T_f = temperature of the fluid; f = friction factor; k/l = distributed loss coefficient; A = cross-sectional area of the pipe; d_e = equivalent pipe diameter; g = acceleration due to gravity; h = mixture enthalpy; p = pressure; t = time; V = fluid velocity; x = distance along the pipe axis; and θ = angle between the pipe axis and horizontal.

In addition,

$$\left.\begin{aligned} &\tau^* = 1 \quad \text{for } x' < 0 \quad \text{and } x' > 1 \\ &\tau^* = \text{appropriate two-phase multiplier for } 0 < x' < 1 \end{aligned}\right\} \tag{6.27}$$

$$\left.\begin{aligned} f &= 0.046 R_N^{-0.2} \quad \text{for } R_N > 2000 \\ f &= \frac{64}{R_N} \qquad\quad \text{for } R_N < 2000 \end{aligned}\right\} \tag{6.28}$$

$$h = x'h_g + (1 - x')h_l \tag{6.29}$$

$$\rho = \alpha\rho_g + (1 - \alpha)\rho_l \tag{6.30}$$

In these equations, x' = thermodynamic quality; R_N = Reynolds number; α = void fraction = volume of vapor per total volume of the vapor-liquid mixture; and the subscripts g and l refer to the vapor and the liquid, respectively.

Conversion of Governing Equations into Characteristic Form

By following the procedure outlined in Section 2.4, it can be proved that Eqs. 6.18 through 6.20 form a set of hyperbolic partial differential equations. These equations can be converted into ordinary differential equations by the method of characteristics as follows:

Multiplying Eq. 6.18 by a linear multiplier, λ_1, adding the resulting equation to Eq. 6.20, and rearranging the terms, we obtain

$$\lambda_1\left[\frac{\partial V}{\partial t}+\left(V+\frac{\rho a^2}{\lambda_1}\right)\frac{\partial V}{\partial x}\right]+\left[\frac{\partial p}{\partial t}+\left(V+\frac{\lambda_1}{\rho}\right)\frac{\partial p}{\partial x}\right]=c_3+\lambda_1 c_1 \tag{6.31}$$

Let

$$V+\frac{\rho a^2}{\lambda_1}=\frac{dx}{dt}=V+\frac{\lambda_1}{\rho} \tag{6.32}$$

or

$$\lambda_1=\pm\rho a \tag{6.33}$$

Substitution of $\lambda_1=\rho a$ and $\lambda_1=-\rho a$ into Eqs. 6.31 and 6.32 yields

$$\rho a\left[\frac{\partial V}{\partial t}+(V+a)\frac{\partial V}{\partial x}\right]+\left[\frac{\partial p}{\partial t}+(V+a)\frac{\partial p}{\partial x}\right]=c_3+\rho a c_1 \tag{6.34}$$

if

$$\frac{dx}{dt}=V+a \tag{6.35}$$

and

$$-\rho a\left[\frac{\partial V}{\partial t}+(V-a)\frac{\partial V}{\partial x}\right]+\left[\frac{\partial p}{\partial t}+(V-a)\frac{\partial p}{\partial x}\right]=c_3-\rho a c_1 \tag{6.36}$$

if

$$\frac{dx}{dt}=V-a \tag{6.37}$$

Note that Eq. 6.34 is valid only if Eq. 6.35 is satisfied; i.e., Eq. 6.34 is valid along characteristic curve, $dx/dt=V+a$, in the x-t plane. Similarly, Eq. 6.36 is valid along the characteristic curve $dx/dt=V-a$.

Now, multiplying Eq. 6.20 by a linear multiplier (λ_2), adding the resulting equation to Eq. 6.19, and rearranging the terms, we obtain

$$\left(\frac{\partial h}{\partial t}+V\frac{\partial h}{\partial x}\right)+\lambda_2\left(\frac{\partial p}{\partial t}+V\frac{\partial p}{\partial x}\right)+a^2(1+\rho\lambda_2)\frac{\partial V}{\partial x}=\lambda_2 c_3+c_2 \tag{6.38}$$

Let

$$a^2(1+\rho\lambda_2)=0 \tag{6.39}$$

or

$$\lambda_2=-\frac{1}{\rho} \tag{6.40}$$

Substitution of Eq. 6.40 into Eq. 6.38 yields

$$\left(\frac{\partial h}{\partial t}+V\frac{\partial h}{\partial x}\right)-\frac{1}{\rho}\left(\frac{\partial p}{\partial t}+V\frac{\partial p}{\partial x}\right)=c_2-\frac{1}{\rho}c_3 \tag{6.41}$$

and

$$\frac{dx}{dt}=V \tag{6.42}$$

Equation 6.41 is valid if Eq. 6.42 is satisfied. Note that, unlike Eqs. 6.34 and 6.36, which were valid along the characteristic curves $dx/dt=V\pm a$, Eq. 6.41 is valid along the path of a particle in the x-t plane.

Equations 6.34, 6.36, and 6.41 can be written as:

1. Along $dx/dt=V+a$,

$$\rho a\,dV+dp=c_3+\rho a c_1 \tag{6.43}$$

2. Along $dx/dt=V-a$,

$$-\rho a\,dV+dp=c_2-\rho a c_1 \tag{6.44}$$

3. Along $dx/dt=V$,

$$\rho dh-dp=\rho c_2-c_3 \tag{6.45}$$

These ordinary differential equations (Eqs. 6.43-6.45) are called *compatibility equations*. Thus, Equations 6.34, 6.36, and 6.41 are in the so-called *characteristic form*. These equations can be combined into matrix form as

$$\mathbf{B}\frac{\partial \mathbf{U}}{\partial t}+C\frac{\partial \mathbf{U}}{\partial x}=\mathbf{D} \tag{6.46}$$

in which

$$\mathbf{U} = \begin{Bmatrix} V \\ h \\ p \end{Bmatrix} \tag{6.47}$$

$$\mathbf{B} = \begin{bmatrix} \rho a & 0 & 1 \\ 0 & 1 & -\frac{1}{\rho} \\ -\rho a & 0 & 1 \end{bmatrix} \tag{6.48}$$

$$\mathbf{C} = \begin{bmatrix} \rho a(V+a) & 0 & (V+a) \\ 0 & V & -\frac{V}{\rho} \\ -\rho a(V-a) & 0 & (V-a) \end{bmatrix} \tag{6.49}$$

$$\mathbf{D} = \begin{Bmatrix} c_3 + \rho a c_1 \\ c_2 - \frac{1}{\rho} c_3 \\ c_3 - \rho a c_1 \end{Bmatrix} \tag{6.50}$$

Formulation of Algebraic Equations

Referring to Fig. 6.7, Eq. 6.46 can be expressed in the finite-difference form as

$$\mathbf{B}_i^j \frac{\mathbf{U}_i^{j+1} - \mathbf{U}_i^j}{\Delta t} + \mathbf{C}_i^j \frac{\mathbf{U}_i^{j+1} - \mathbf{U}_{i-1}^{j+1}}{\Delta x_{i-1}} = \mathbf{D}_i^j \tag{6.51}$$

$$\mathbf{B}_i^j \frac{\mathbf{U}_i^{j+1} - \mathbf{U}_i^j}{\Delta t} + \mathbf{C}_i^j \frac{\mathbf{U}_{i+1}^{j+1} - \mathbf{U}_i^{j+1}}{\Delta x_i} = \mathbf{D}_i^j \tag{6.52}$$

Note that the spatial derivatives are approximated by the left-hand finite differences (Fig. 6.7) in Eq. 6.51 and by the right-hand finite differences in Eq. 6.52. Which of these two equations should be used, depends upon the flow direction and whether the flow is subsonic or supersonic. For subsonic flows, the left-hand finite differences are used for the positive characteristic ($V + a$ equation), and the right-hand finite differences for the negative characteristic ($V - a$ equation); in the V equation, the right- or left-hand finite differences are used depending upon the flow direction. This convention makes the finite-difference scheme as similar as possible to the method of characteristics.

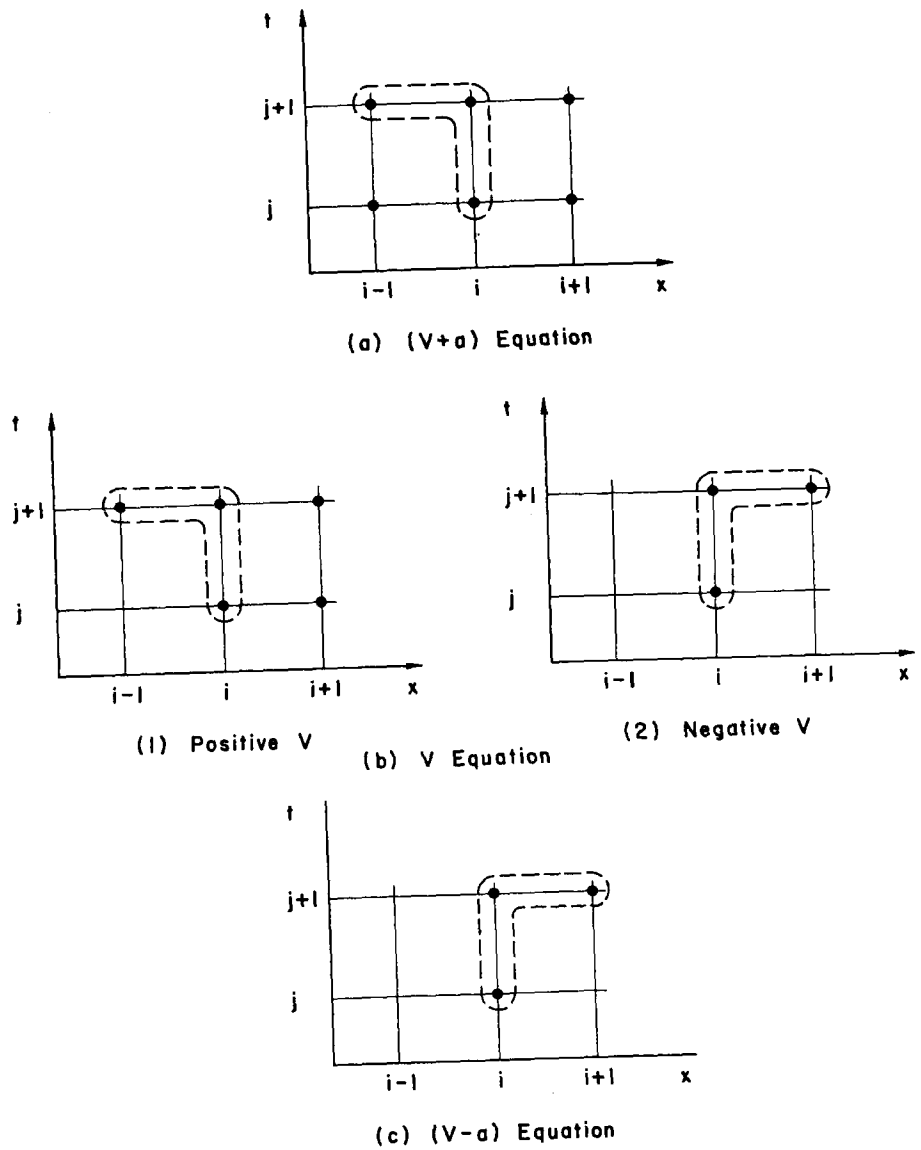

Figure 6.7. Notation for implicit finite-difference scheme (subsonic flow).

By introducing a weighting matrix, W, and by using the preceding convention for the finite-difference approximations, Eqs. 6.51 and 6.52 may be combined as

$$\mathbf{M}_{i,i-1}\,\mathbf{U}_{i-1}^{j+1} + \mathbf{M}_{i,i}\,\mathbf{U}_{i}^{j+1} + \mathbf{M}_{i,i+1}\,\mathbf{U}_{i+1}^{j+1} = \mathbf{N}_i \tag{6.53}$$

Usually, $\mathbf{W} = \mathbf{I}$, but where the property derivatives are changing rapidly, W may be used as a weighting matrix. The components of the 3 X 3 matrices $\mathbf{M}_{i,i-1}$, $\mathbf{M}_{i,i}$, and $\mathbf{M}_{i,i+1}$ and the column vector $\mathbf{N}_i$ are

$$\mathbf{M}_{i,i-1} = \mathbf{E}\left[-\mathbf{W}\mathbf{C}_i + (\mathbf{I} - \mathbf{W})\left(\frac{\Delta x_{i-1}}{\Delta t}\,\mathbf{I}\mathbf{B}_{i-1} - \mathbf{C}_{i-1}\right)\right] \tag{6.54}$$

$$\mathbf{M}_{i,i} = \mathbf{W}\left[(\mathbf{I} - \mathbf{E})\,\frac{\Delta x_i}{\Delta t}\,\mathbf{B}_i + \mathbf{E}\,\frac{\Delta x_{i-1}}{\Delta t}\,\mathbf{B}_i - (\mathbf{I} - 2\,\mathbf{E})\,\mathbf{C}_i\right] + (\mathbf{I} - \mathbf{W})\,[\mathbf{E}\mathbf{C}_{i-1} - (\mathbf{I} - \mathbf{E})\,\mathbf{C}_{i+1}] \tag{6.55}$$

$$\mathbf{M}_{i,i+1} = (\mathbf{I} - \mathbf{E})\left[\mathbf{W}\mathbf{C}_k + (\mathbf{I} - \mathbf{W})\left(\frac{\Delta x_i}{\Delta t}\,\mathbf{I}\mathbf{B}_{i+1} + \mathbf{C}_{i+1}\right)\right] \tag{6.56}$$

$$\mathbf{N}_i = \mathbf{W}\left[\left((\mathbf{I} - \mathbf{E})\,\Delta x_i + \mathbf{E}\,\Delta x_{i-1}\right)\mathbf{D}_i + \left((\mathbf{I} - \mathbf{E})\,\frac{\Delta x_i}{\Delta t} + \mathbf{E}\,\frac{\Delta x_{i-1}}{\Delta t}\right)\mathbf{B}_i\mathbf{U}_i^j\right] + (\mathbf{I} - \mathbf{W})\left[\mathbf{E}\mathbf{D}_{i-1}\,\Delta x_{i-1} + (\mathbf{I} - \mathbf{E})\,\mathbf{D}_{i+1}\,\Delta x_i + \frac{\Delta x_{i-1}}{\Delta t}\,\mathbf{E}\mathbf{B}_{i-1}\,\mathbf{U}_{i-1}^j + \frac{\Delta x_i}{\Delta t}\,(\mathbf{I} - \mathbf{E})\,\mathbf{B}_{i+1}\,\mathbf{U}_{i+1}^j\right] \tag{6.56}$$

The matrix E depends upon the type (subsonic or supersonic) and the direction of flow as follows:

1. Supersonic flow
   a. From left to right

$$\mathbf{E} = \mathbf{I} \tag{6.57}$$

   b. From right to left

$$\mathbf{E} = \mathbf{0} \tag{6.58}$$

2. Subsonic flow
   a. From left to right

$$\mathbf{E} = \begin{bmatrix} 1 & & \\ & 1 & \\ & & 0 \end{bmatrix} \tag{6.59}$$

   b. From right to left

$$\mathbf{E} = \begin{bmatrix} 1 & & \\ & 0 & \\ & & 0 \end{bmatrix} \tag{6.60}$$

Equation 6.53 is also used at the boundaries except that those finite-difference equations having subscripts of either 0 or $n + 2$ are dropped from the set and are replaced by the appropriate conditions imposed by the boundary.

Computational Procedure

The pipeline is divided into a number of reaches. Equation 6.53 is used at the interior points. This equation is also used at the boundaries except that the equations having the terms with subscripts 0 and $n + 2$ are dropped and are replaced by the conditions imposed by the boundary. (If these conditions are nonlinear, they are linearized.) Since the coefficients of these equations are expressed in terms of the known variables at the beginning of the time step, the resulting algebraic equations are linear. If the pipe is divided into n reaches, then writing Eq. 6.53 at the interior points and at the boundaries as described above results in $3(n + 1)$ linear equations in $3(n + 1)$ unknowns. These equations have a banded matrix structure as shown in Fig. 6.8. The structure of the band matrices, showing the flow direction dependence, is given in Fig. 6.9. Due to the banded structure, these equations can be efficiently solved using a special-purpose algorithm based on the Gauss elimination method, which takes advantage of the zero elements.

Verification

The preceding finite-difference scheme has been verified by comparing the results computed by using this scheme for standard problems with those computed by using the method of characteristics and with the experimental results.[28,30,31] Figure 6.10 shows the comparison with the experimental results reported by Edwards and O'Brien.[33] The experimental set-up was the blowdown of a closed-end, cylindrical pipe filled with high enthalpy water, which was suddenly opened to the atmosphere. The tube was 4 m long and had an inside diameter of 32 mm. The initial pressure was 7 MPa, and the initial temperature was 243°C. It is clear from Fig. 6.10 that the comparison between the computed and measured results is satisfactory.

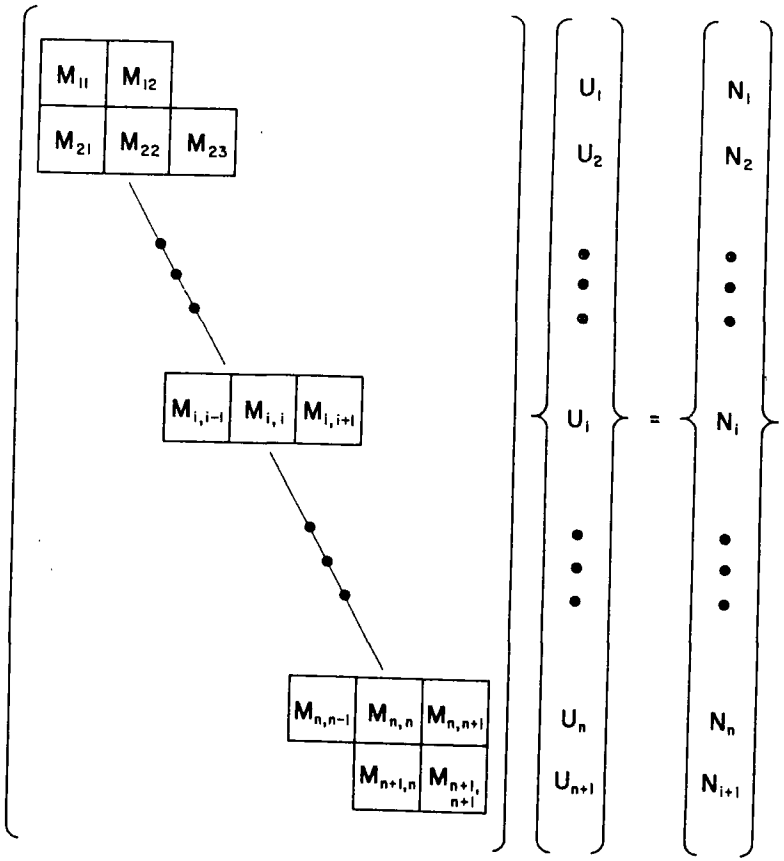

Figure 6.8. Structure of system of algebraic equations.

6.8 CASE STUDY

Studies undertaken by the Westinghouse Electric Corporation,[13,14] following the rupture of a pipe (0.46-m diameter, 25-mm wall thickness) due to waterhammer in the feedwater line of Unit No. 2, Consolidated Edison Company of New York's nuclear power plant at Indian Point, are summarized in this section.

Configuration of Feedwater Line

The Indian Point Unit No. 2 is equipped with a four-loop Westinghouse PWR steam supply system. There are two turbine-driven main-feed pumps, and two motor-driven and one turbine-driven auxiliary feedwater pumps. The schematic

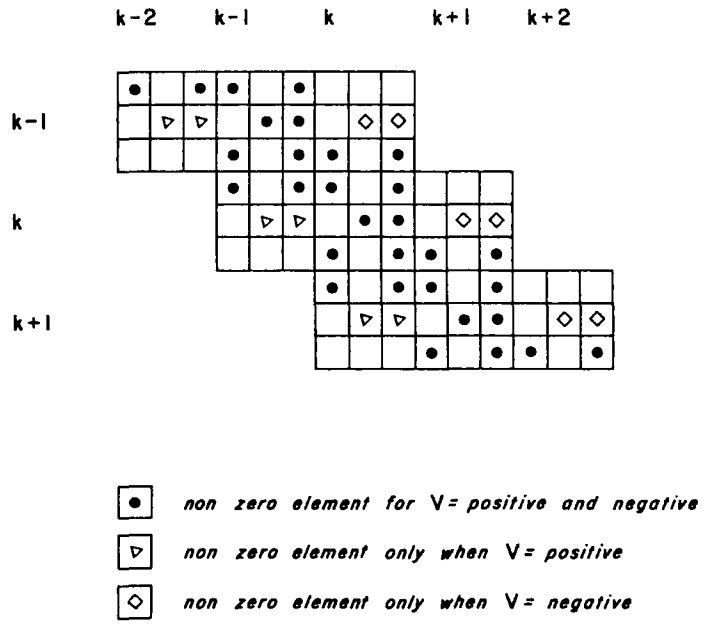

Figure 6.9. Structure of diagonal elements. (After Banerjee et al.[28])

layout of the motor-driven feedwater system is shown in Fig. 6.11; the turbine-driven auxiliary feedwater system is not shown. The pipe-break in feedline No. 22 occurred inside the containment near the containment penetration (Fig. 6.12).

Description of Incident

On November 13, 1973, the Indian Point Unit No. 2 was operating at about 8 percent power, with one main boiler feed pump in service and the main turbine running at 1750 rpm. At about 7:38 A.M., the main turbine and the operating main boiler feed pump were tripped due to high level in Steam Generator (SG) No. 23. Simultaneously, both motor-driven auxiliary pumps were started. At 7:44:41 A.M., the reactor tripped due to low-low level in SG No. 21. Several minutes after the reactor trip, there was a severe shock in the feedwater line No. 22, and water level in SG No. 22 could not be restored. At about 8:30 A.M., there were indications that the containment dew point and temperature were rising, and a second shock was observed when some adjustments were made to increase the auxiliary feedwater flow to SG No. 22. A third shock was observed at about 8:40 A.M. when the steam-driven auxiliary was started up to feed SG No. 22. Loop 22 was isolated, and cooldown was initiated at 10:10 A.M.

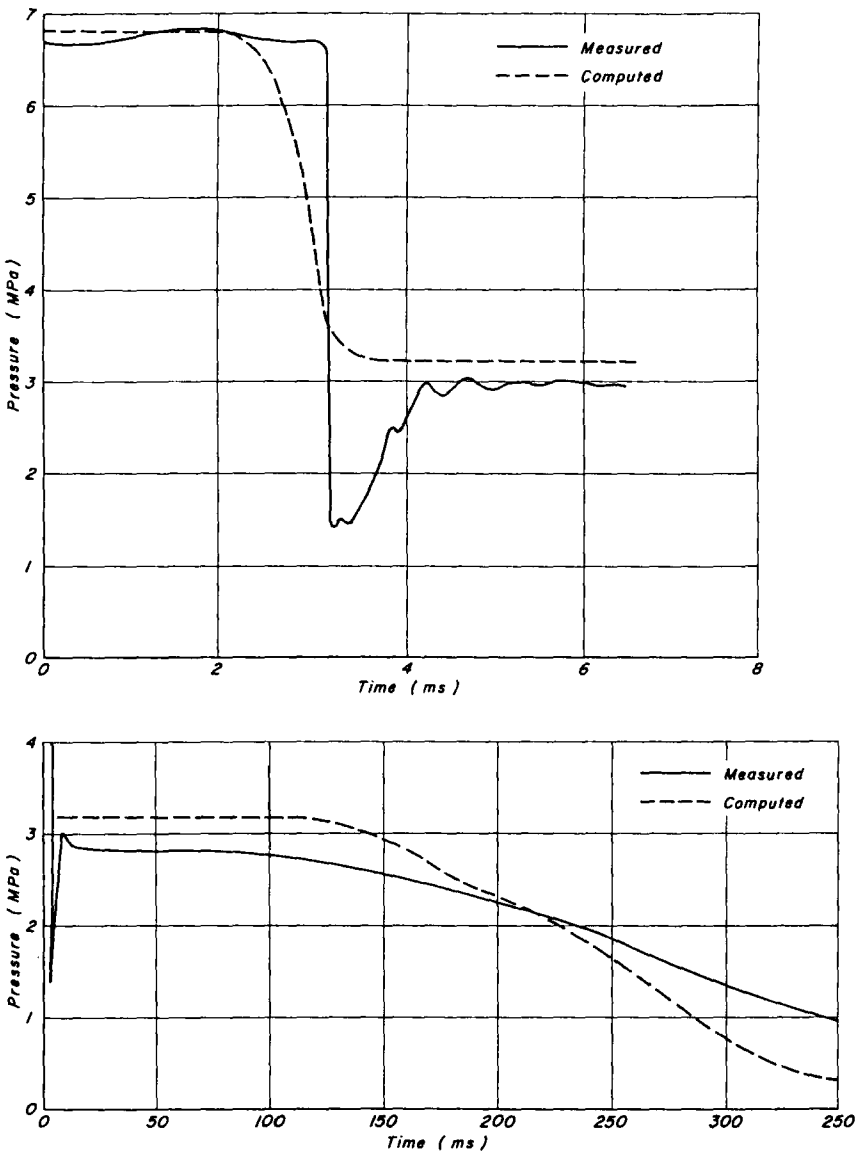

Figure 6.10. Comparison of computed and measured results. (After Hancox, and Banerjee[30])

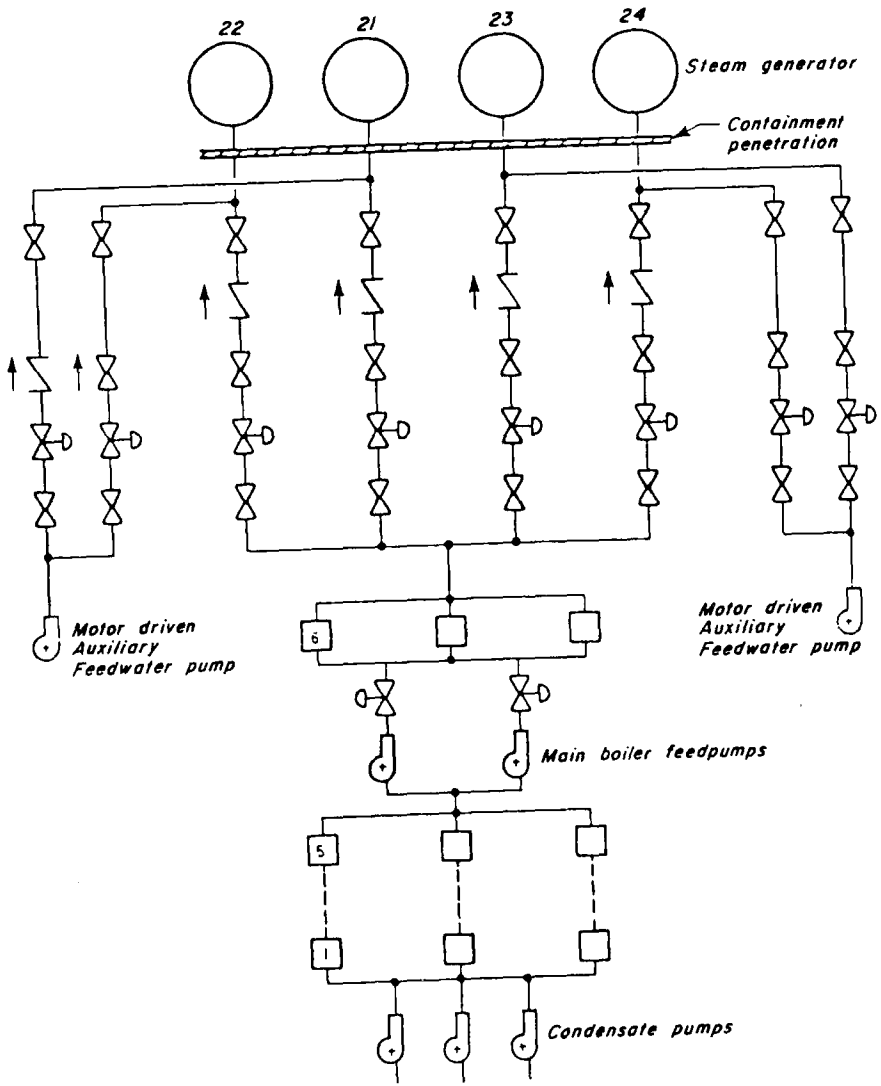

Figure 6.11. Schematic layout of feedwater system. (After Aanstad[13])

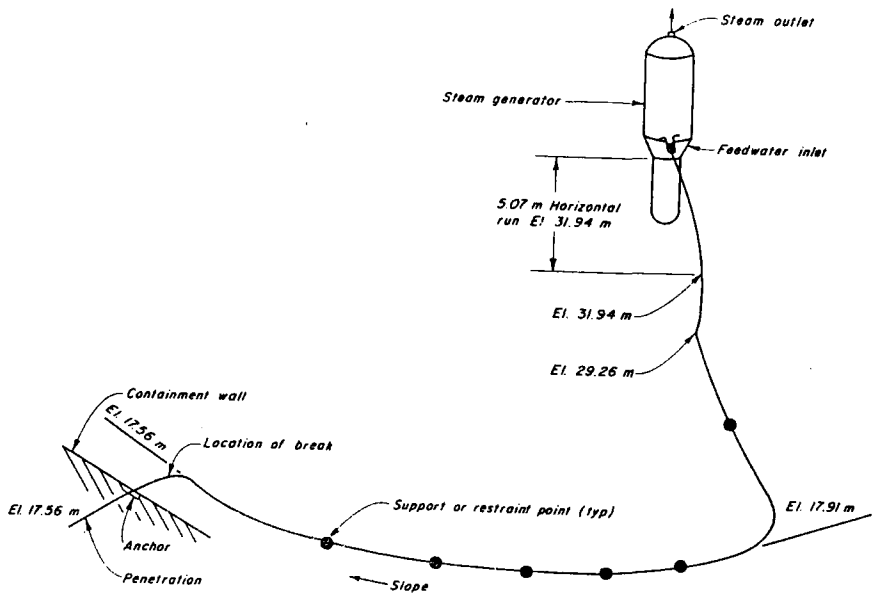

Figure 6.12. Feedwater piping of steam generator No. 22. (After Aanstad[13])

Possible Causes of Shock

Three possible shock mechanisms were considered:

1. Waterhammer due to quick closure of a feedwater regulating valve.
2. Shock due to backflow of hot water into the main feedline from SG No. 22.
3. Flow instability in the feedwater line when the feed ring was uncovered.

A brief description of the investigation for each of these causes follows.

Waterhammer

Since the line break occurred at about 8 percent power level, an instantaneous closure of a feedwater control valve or a feedwater check valve would not cause appreciable waterhammer. Thus, it would have to be assumed that the feedline was damaged during a previous incident and that the pipe finally ruptured during the incident on November 13. Actually, shocks had been noted during a previous plant trip from 360 MWe (30 percent power) due to low-low level in one steam generator.

A computer program was used to determine the maximum pressure due to:

1. instantaneous closure of the control valve with the check valve acting
2. control-valve closure in 50 ms with check valve acting
3. instantaneous control-valve closure without check valve.

Analytical investigations indicated that the maximum stress for 8 percent power could not cause pipe rupture; but for 30 percent power, the pipe stress at the containment penetration exceeded the specified minimum-yield strength of the pipe.

Backflow

Field investigations indicated that backflow from SG No. 22 could occur under conditions prevalent during the incident on November 13. The hot water could flow into line No. 22 for a period of time, and when the reactor tripped, the secondary side could have gradually depressurized, and the hot water could have flashed into steam and produced a trapped steam bubble in feedline No. 22. This trapped steam bubble could have collapsed abruptly when it came in contact with the cold auxiliary feedwater, and the resulting shock could have ruptured the line.

Steam-Header Flow Instability

Following the fall in the steam-generator liquid level below the feedring, the inlet sections of the feedline and the feedring could have been drained. If the auxiliary pump does not keep these sections full of water, a free surface will form, which will be available for condensation of counterflow steam moving up through the feedwater-ring injection holes. If the flow of steam is sufficient, ripples will form on the free surface, which will be followed by flooding of the cross-section. This local flooding will cause isolation of a condensing steam bubble, which will then collapse, causing a high-pressure pulse.

An analytical analysis of this phenomenon is impossible. Therefore, investigations were carried out on a 1 : 12-scale model in which the low pressure of the condensing steam was simulated by a vacuum line. These experiments revealed that a periodic slug of water would form within the horizontal section of the feedwater line.

Figure 6.13 shows the sequence of events. As the auxiliary feedwater is initiated to compensate for the falling steam pressure, cold water pours into the feedpipe, and a standing wave builds up at the juncture of the thermal sleeve to the feedring (Fig. 6.13a). Depending upon the flow rate, the standing wave

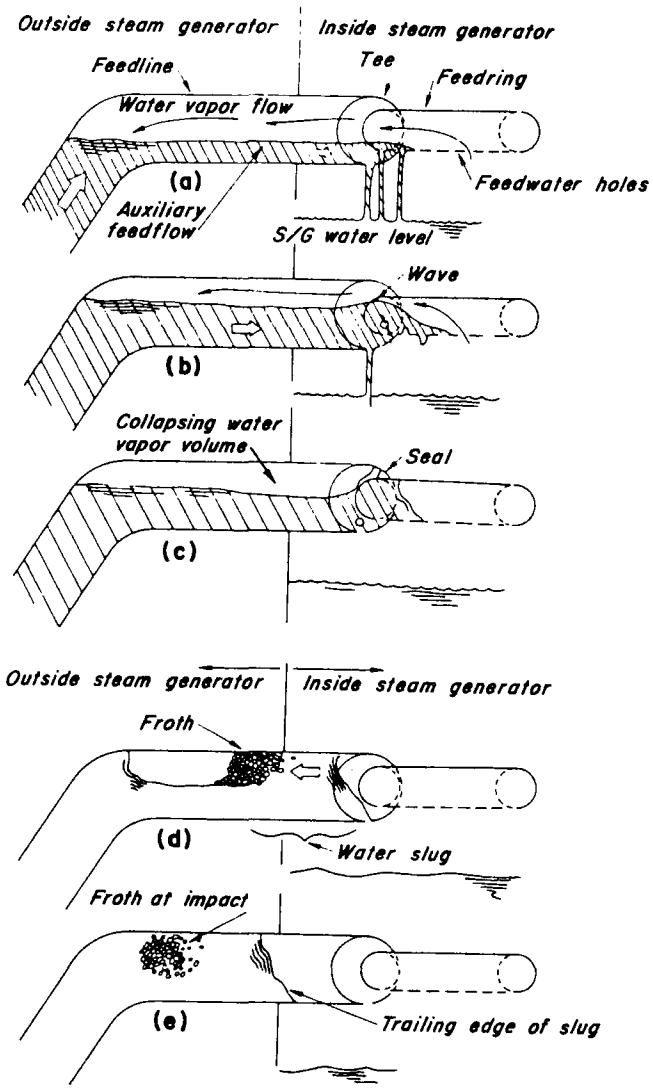

Figure 6.13. Schematic representation of a slugging mechanism. (After Pulling[14])

seals the feedring (Fig. 6.13b) yielding an entrapped steam bubble. This entrapped steam condenses due to rapid heat transfer, and a slug of water accelerates from the steam generator into the feedwater pipe (Fig. 6.13c) until it hits an obstruction, usually the first elbow in the feedpipe. A great amount of energy

is dissipated at the sleeve, and the remainder is transmitted into the pipe. The slug then returns to the steam generator, and the cycle is repeated with a diminishing energy (Fig. 6.13d and e).

Plant Modifications

Based on the results of the investigations, the following modifications were made to prevent recurrence of the November incident:

1. The feedwater control valves were equipped with snubbers to increase the closing time.
2. The main feedwater isolation valves were modified so that they will close by motor-operated actuators when the possibility of backflow exists.
3. The long horizontal run of feedwater line No. 22 was modified (Fig. 6.14) to reduce the entrapped steam volume in case the water level drops below the feedwater ring.

Verification Tests

To verify the effectiveness of the plant modifications, a systematic series of tests were conducted. It was found that low-intensity shocks still occurred in some cases. The tests indicated that the shock mechanism was related to the drainage

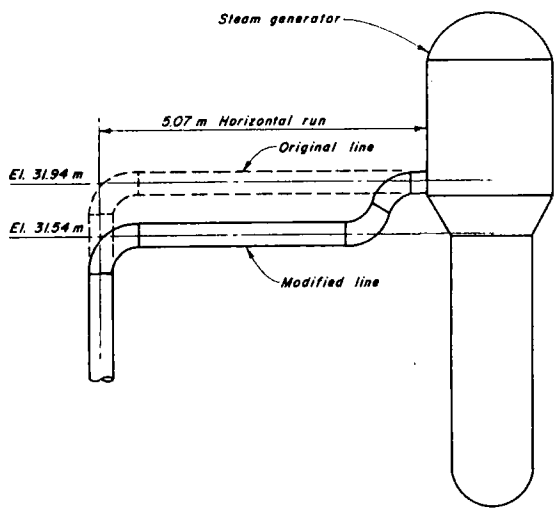

Figure 6.14. Modified feedwater piping of steam generator No. 22. (After Aanstad[13])

of the feedring and that the shocks occurred only at higher auxiliary feedwater flow rates. In addition, it was found that:

1. Prior to the shock, with the line partially drained, thermocouples located at the top and at the bottom of the feedwater line showed steam and auxiliary feedwater temperatures, respectively.
2. Shortly after the shock, the thermocouples located on the outside surface of the pipe showed that the temperature inside the pipe changed suddenly, which is indicative of a sudden condensation.

To reduce drainage of the feedwater ring following normal plant trips, the original nozzles in the bottom of the feedwater ring were plugged and then replaced with 35 larger holes in the top of the ring. A short J-bend pipe was welded to each hole to direct the feedwater vertically downward. Extensive tests conducted after making this modification showed that no shocks were observed.

6.9 SUMMARY

In this chapter, the terminology was first introduced, and causes that may produce transient conditions were then outlined. Various numerical methods available for the transient analysis were discussed. A number of boundary conditions commonly found in the piping systems of the nuclear power plants were derived. The loss-of-coolant accident was then briefly described. This was followed by the presentation of the details of an implicit finite-difference scheme that is suitable for analyzing transients in homogeneous two-phase flows.

PROBLEMS

6.1 Derive the boundary conditions for an air pocket entrapped in a pipeline. Assume that the air is released slowly through an air valve as the air pressure increases.

6.2 Develop the boundary conditions for a condenser in which the condenser tubes at higher level are unsubmerged as the water level in the water boxes falls. (*Hint:* Replace the condenser tubes with a number of parallel pipes located at different levels. Consider the flow through only those pipes that are submerged.)

6.3 For the implicit finite-difference method for analyzing two-phase flows presented in Section 6.7, write the end equations for:

1. a series junction
2. a valve
3. a junction of three pipes
4. a constant-head reservoir.

Neglect the form losses for cases 1, 3, and 4, and linearize the equation for case 2.

REFERENCES

1. Lecture Notes, Nuclear Power Symposium, Atomic Energy of Canada Ltd., Sheridan Park, Ontario, Canada, 1972.
2. Ybarrondo, L. J., Solbrig, C. W., and Isbin, H. S., "The Calculated Loss-of-Coolant Accident: A Review," *Monograph Series No. 7, Amer. Inst. of Chem. Engrs.*, New York, 1972, pp. 1–99.
3. Belonogoff, G., "Computer Simulation of Waterhammer Effects," *Jour., Transportation Engineering Div., Amer. Soc. of Civil Engrs.*, vol. 98, Aug. 1972, pp. 521–530.
4. Okrent, D., Holland, L. K., Moffette, T. R., and Moore, J. S., "On Calculational Methods in Power Reactor Safety," Amer. Nucl. Soc., Top. Meet., Univ. of Mich., Ann Arbor, April 1971 (published by U.S. Atomic Energy Commission, CONF-730414), April 1971, pp. D01–25.
5. Gwinn, J. M. and Wender, P. J., "Start-up Hammer in Service Water Systems," Paper No. 74-WA/PWR-8, presented at Winter Annual Meeting, Amer. Soc. of Mech. Engrs., Nov. 1974, 8 pp.
6. Pool, E. B., Porwit, A. J., and Carlton, J. L., "Prediction of Surge Pressure From Check Valves for Nuclear Loops," Paper No. 62-WA-219, presented at Winter Annual Meeting, Amer. Soc. of Mech. Engrs., Nov. 1962, 8 pp.
7. Harper, C. R., Hsieh, J. S., and Luk, C. H., "An Analysis of Waterhammer Loads in a Typical Nuclear Piping System," Paper No. 75-PVP-53, presented at Second National Congress on Pressure Vessels & Piping, San Francisco, Amer. Soc. of Mech. Engrs., June 1975, 8 pp.
8. Liebermann, P. and Brown, E. A., "Pressure Oscillations in a Water-Cooled Nuclear Reactor Induced by Water-Hammer Waves," *Jour., Basic Engineering, Amer. Soc. of Mech. Engrs.*, vol. 82, Dec. 1960, pp. 901–911.
9. Shin, Y. W. and Chen, W. L., "Numerical Fluid-Hammer Analysis by the Method of Characteristics in Complex Piping Networks," *Nucl. Engineering and Design*, vol. 33, 1975, pp. 357–369.
10. Penzes, L. E., "Theory of Pump-Induced Pulsating Coolant Pressure in Pressurized Water Reactors," *Nucl. Engineering and Design*, vol. 27, May 1974, pp. 176–188.
11. O'Leary, J. R. and Patel, Y. A., "Transient Analysis of a Class A Nuclear Piping System: A Comparative Study of Three Large Computer Codes," *Pressure Vessels & Piping Conf., Amer. Soc. of Mech. Engrs.*, Miami Beach, June 1974, pp. 51–58.
12. Bordelon, F. M., "Calculation of Flow Coastdown After Loss of Reactor Coolant Pump," Report No. WCAP-7973, Westinghouse Electric Corporation, Pittsburgh, Pennsylvania, Aug. 1970.
13. Aanstad, O., Investigation of a Feedwater Line Incident at Consolidated Edison Company of New York's Indian Point No. 2 Plant," Report No. WCAP-8433, Westinghouse Electric Corporation, Pittsburgh, Pennsylvania, Feb. 1975.
14. Pulling, W. T., "Literature Survey of Water Hammer Incidents in Operating Nuclear

Power Plants," Report No. WCAP-8799, Westinghouse Electric Corporation, Pittsburgh, Pennsylvania, Nov. 1976.
15. Esposito, V. J., "Mathematical Aspects of Reactor Blowdown," paper presented at Computational Methods in Nucl. Engineering Meeting, Charleston, South Carolina, Amer. Nucl. Soc., April 1975, 5 pp.
16. Wylie, C. R., *Advanced Engineering Mathematics*, Third Ed., McGraw-Hill Book Co., New York, 1965, p. M5.
17. Wallis, G. B., *One-Dimensional Two-Phase Flow*, McGraw-Hill Book Co., New York, 1969.
18. Chaudhry, M. H., "Resonance in Pressurized Piping Systems," thesis presented to the University of British Columbia, Vancouver, British Columbia, Canada, in 1970, in partial fulfillment for the degree of Doctor of Philosophy.
19. Richtmyer, R. D. and Morton, K. W., *Difference Methods for Initial Value Problems*, Interscience Publications, New York, 1967.
20. McCracken, D. D. and Dorn, W. S., *Numerical Methods and FORTRAN Programming*, John Wiley & Sons, Inc., New York, 1964.
21. Butcher, J. C., "On Runge-Kutta Procedures of High Order," *Jour. Austr. Math. Soc.*, vol. 4, 1964.
22. Hancox, W. T., Mathers, W. G., and Kawa, D., "Analysis of Transient Flow-Boiling; Application of the Method of Characteristics," paper presented at 15th National Heat Transfer Conference, San Francisco, Amer. Inst. of Chem. Engrs., Aug. 1975.
23. Martin, C. S. and Padmanabhan, M., "The Effect of Free Gases on Pressure Transients," *L'Energia Elettrica*, no. 5, 1975, pp. 262–267.
24. Martin, C. S., Padmanabhan, M., and Wiggert, D. C., "Pressure Wave Propagation in Two-Phase Bubbly Air-Water Mixtures," *Proc., 2nd Conference on Pressure Surges*, published by British Hydromechanics Research Association, England, Sept. 1976.
25. Abbott, M. B., *An Introduction to the Method of Characteristics*, American Elsevier, New York, 1966.
26. Lax, P. D. and Wendroff, B., "System of Conservation Laws," *Comm. on Pure and Applied Math.*, vol. 13, 1960, pp. 217–227.
27. Kranenburg, C., "Gas Release During Transient Cavitation in Pipes," *Jour., Hyd. Div., Amer. Soc. of Civ. Engrs.*, vol. 100, Oct. 1974, pp. 1383–1398.
28. Banerjee, S. and Hancox, W. T., "On the Development of Methods for Analysing Transient Flow-Boiling," paper submitted to *Inter. Jour. Multiphase Flow.*
29. Spencer, A. C. and Nakamura, S., "Implicit Characteristic Method for One-Dimensional Fluid Flows," *Trans. Amer. Nuclear Society*, vol. 17, Nov. 1973, pp. 247–249.
30. Hancox, W. T. and Banerjee, S., "Numerical Standards for Flow-Boiling Analysis," *Nuclear Science and Engineering*, 1978.
31. Mathers, W. G., Zuzak, W. W., McDonald, B. H., and Hancox, W. T., "On Finite-Difference Solutions to the Transient Flow-Boiling Equations," paper presented to Committee on the Safety of Nuclear Installations, Specialists Meeting on Transient Two-Phase Flow, Toronto, Ontario, Aug. 1976 (proceedings to be published by Pergamon Press).
32. Harlow, F. H. and Amsden, A. A., "Numerical Calculation of Almost Incompressible Flow," *Jour. Comp. Physics*, vol. 3, 1968, pp. 80–93.
33. Edwards, A. R. and O'Brien, T. P., "Studies of Phenomena Connected with the Depressurization of Water Reactors," *Jour. British Nuclear Energy Society*, vol. 9, 1970, pp. 125–135.

ADDITIONAL REFERENCES

Arker, A. J. and Lewis, D. G., "Rapid Flow Transients in Closed Loops," Reactor Heat Transfer Conference, U.S. Atomic Energy Commission, 1956.
Mori, Y., Hijikata, K., and Komine, A., "Propagation of Pressure Waves in Two-Phase Flow," *International Jour. Multiphase Flow*, vol. 2, 1957, pp. 139–152.
Standart, G., "The Mass, Momentum, and Energy Equations for Heterogeneous Flow Systems," *Chem. Eng. Sci.*, vol. 19, 1964, pp. 227–236.
Fabic, S., "BLODWN-2: Westinghouse APD Computer Program for Calculation of Fluid Pressure, Flow, and Density Transients during a Loss-of-Coolant Accident," *Trans. Amer. Nucl. Soc.*, vol. 12, 1969, p. 358.
Henry, R. E., Grolmes, M. A., and Fauske, H. K., "Propagation Velocity of Pressure Waves in Gas-Liquid Mixtures," *Concurrent Gas-Liquid Flow*, edited by Rhodes, E. and Scott, D. S., Plenum Press, New York, 1969, pp. 1–18.
Kalinin, A. V., "Derivation of Fluid-Mechanics Equations for a Two-Phase Medium with Phase Changes," *Heat Transfer, Soviet Research*, vol. 2, May 1970, pp. 83–96.
Boure, J., "Two-Phase Flow Transients and the Stability of Once-Through Steam Generators," International Heat Exchange Conf., Paris, France, no. 22, June 1971.
Albertson, M. L. and Andrews, J. S., "Transients Caused by Air Release," in *Control of Flow in Closed Conduits*, edited by Tullis, J. P., Colorado State University, Fort Collins, Colorado, 1971, pp. 315–340.
Rose, R. P. and Cooper, K. F., "Analysis of a PWR System for a Complete Loss of Feedwater Accident Without Reactor Trip," *Top Meet on Water Reactor Safety*, Salt Lake City, published by AEC (Conf. 730304), March 1973.
Gonzalez, S., "Exact Solutions for Flow Transients in Two-Phase Systems by the Method of Characteristics," *Jour. Heat Transfer, Amer. Soc. of Mech. Engrs.*, vol. 95, Nov. 1973, pp. 470–476.
Porsching, T. A., "Fluid Network Analysis," *Trans. Amer., Nucl. Soc.*, vol. 17, 1973, p. 242.
Hold, A., "Analytical One-Dimensional Frequency Response and Stability Model for PWR Nuclear Power Plant," *Nucl. Engineering and Design*, vol. 33, 1975, p. 336.
Martin, C. S., "Entrapped Air in Pipelines," *Proc., Second Conf. on Pressure Surge, London*, published by British Hydromech. Research Assoc., Cranfield, England, Sept. 1976.
Mikielewicz, J., Chan, T. C., Wilson, D. G., and Goldfish, A. L., "A Method for Correlating the Characteristics of Centrifugal Pumps in Two-Phase Flow," Paper No. 76-WA/FE-29, Amer. Soc. of Mech. Engrs., 1976, 11 pp.

CHAPTER 7

TRANSIENTS IN LONG OIL PIPELINES

7.1 INTRODUCTION

Cross-country pipelines transporting crude oil or refined products are usually several hundred kilometers long and have several pumping stations located along their length (Fig. 7.1), with each having a number of pumps in series. The pumping head of these stations is mainly used to overcome the friction losses in the pipeline; in a mountainous terrain, however, some gravity lift may be required in addition to the friction losses.

The analysis of transients in oil pipelines, sometimes called *oil-hammer analysis* or *surge analysis*, is rather complex because the pipeline friction losses are large compared to the instantaneous pressure changes caused by a sudden variation of the flow velocity. Prior to the availability of high-speed digital computers, these analyses were approximate, and a large factor of safety had to be used to allow for uncertainties in the computed results. Nowadays, pressures for various operating conditions can be accurately predicted, thus allowing a reduction in the factor of safety.

During the design of a pipeline, the maximum and minimum pressures are computed in order to select the pipe-wall thickness necessary to withstand these pressures. A small reduction in the pipe-wall thickness can result in significant savings in the initial cost of the project; therefore, a detailed analysis of the transients caused by various possible operating conditions is necessary for an economic design. A detailed analysis of an existing pipeline may indicate the possibility of increasing its throughput by increasing the normal working pressures, which in the original design might have been set too low to allow for uncertainties in the prediction of the maximum and minimum pressures.

A very important parameter in the design of an oil pipeline is the friction factor, f, which should be precisely known to determine the initial steady-state pressures along the pipeline and hence the required pumping heads of the

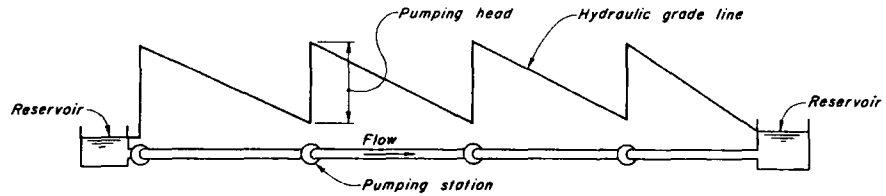

Figure 7.1. Schematic diagram of a long oil pipeline.

pumping units. In addition to f, the values of the bulk modulus of elasticity, K, and the density, ρ, of the oil should be known to compute the velocity of the pressure waves. The friction factors can usually be estimated closely during the design stages; the values of K and ρ, however, are unknown and may vary from one oil batch to another. Therefore, a range of the expected values of K and ρ should be used in the analysis during design, and the values that yield worst conditions should be selected. As soon as the pipeline is commissioned, the value of these variables should be determined by conducting prototype tests. Based on the results of these tests, operating guidelines should be prepared for a safe operation of the pipeline.

In this chapter, a number of terms commonly used in the oil industry are first defined. Different operations of vaious appurtenances and control devices that may produce transient conditions in the pipeline are discussed. A computational procedure to analyze the transient conditions in long pipelines by the method of characteristics is then presented.

7.2 DEFINITIONS

The following terms[1-6] are commonly used in the oil industry:

Potential Surge. The instantaneous pressure rise caused by instantaneously stopping the flow (i.e., reducing the flow velocity to zero) is defined as *potential surge*. The amplitude of the potential surge, Z, may be computed as follows: If V_o is the initial steady-state velocity, then $\Delta V = 0 - V_o = -V_o$. Substituting this value of ΔV into Eq. 1.8, we obtain

$$Z = \Delta H = -\frac{a}{g}\,\Delta V = \frac{a}{g}\,V_o \tag{7.1}$$

in which ΔH = instantaneous pressure rise due to reduction of flow velocity V_o to zero; a = velocity of pressure waves; and g = acceleration due to gravity. If V_o and a are in m/s, g is in m/s^2, then Z is in m.

Line Packing. The increase in the storage capacity of a pipeline due to an increase in pressure is called *line packing*. The following analogy will be helpful in the understanding of this phenomenon.

Let us assume that the flow velocity in the canal shown in Fig. 7.2 is suddenly reduced from V_o to zero at the downstream end by closing a sluice gate. This sudden reduction in the flow velocity produces a surge, which travels in the upstream direction. For simplification purposes, let us assume that the surge height does not change as it propagates in the upstream direction. If the water surface behind the wave front does not change, then it will be parallel to the initial steady-state water surface (line *cd* in Fig. 7.2), except that the water surface will be at a higher level. Because of slope in the water surface, water will keep on flowing toward the sluice gate even though the surge has passed a particular point in the canal. As the velocity at the sluice gate is zero, the water flowing behind the surge will be stored between the surge location and the sluice gate. Due to this storage, the water surface downstream of the wave will be almost horizontal. With further upstream movement of the surge from *bc* to *fh*, more water will flow behind the surge, and the water level at the sluice gate will rise from *e* to *j*. Thus, the shaded area in Fig. 7.2 is due to storage of water flowing downstream of the surge. At the downstream end, water level rose from *a* to *d* due to initial or potential surge, whereas it rose first from *d* to *e* and then from *e* to *j* due to storage of water between the surge location and the sluice gate.

Conditions are analogous in a long pipeline. Due to sudden closure of a downstream valve (Fig. 7.3), pressure rises instantaneously at the downstream end, and a wave having amplitude equal to the potential surge travels in the upstream direction. Just like the flow behind the surge in the canal, oil flows downstream of the wave front, pressure rises gradually at the downstream end, the hydraulic grade line becomes almost horizontal, and more oil is stored between the wavefront and the valve. This increase in storage is called *line*

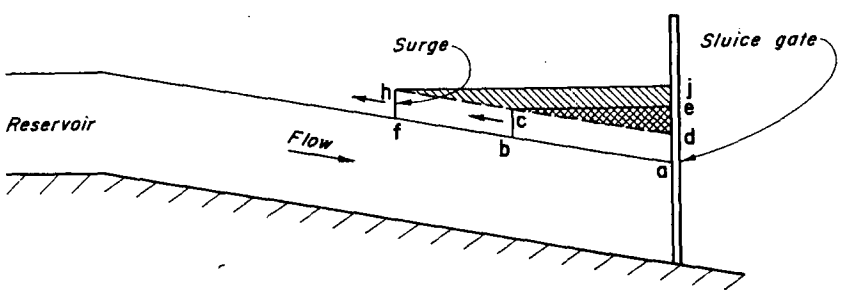

Figure 7.2. Propagation of surge in a canal.

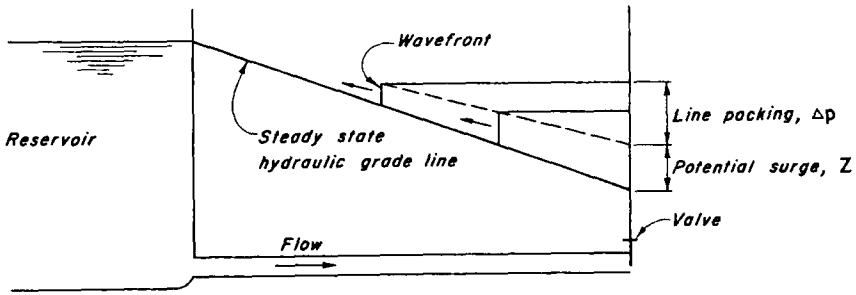

Figure 7.3. Potential surge and line packing.

packing. Referring to Fig. 7.3, the pressure rise at the valve is made up of two parts: (1) potential surge, Z, produced due to instantaneous closure of the valve, and (2) Δp, due to line packing.

Depending upon the length of the pipeline, the pressure rise due to line packing may be several times greater than the potential surge.

Attenuation. As discussed previously, the oil flows toward the valve even though the wave front has passed a particular location in the pipeline. In other words, the velocity differential (ΔV) across the wavefront is reduced as the wave propagates in the upstream direction. Hence, it follows from Eq. 7.1 that the amplitude of the surge is reduced as it propagates along the pipeline due to reduction in the velocity differential across the wave front. This reduction in the surge amplitude is referred to as *attenuation*.

The amplitude of the surge is also reduced due to friction losses. However, this reduction is usually small as compared to that due to decrease in the velocity differential across the wave front.

Pyramidal Effect. The superposition of one transient state pressure upon another is referred to as *pyramidal effect*. For example, if a line were packed due to closure of a downstream valve or due to power failure to the pumps of a downstream pumping station, and the pumps of an upstream station were started, then the pressure due to pump start-up will be superimposed on the pressure due to line packing.

Put-and-Take Operation. In a put-and-take station operation, each station pumps oil from a tank located on its suction side into a tank located on the suction side of the next station.

Float-Tank Operation. Float-tank operation is similar to the put-and-take station operation except that a float tank is open to the suction line of each

station. The size of the float tank is usually small compared to those in the put-and-take operation.

Tight-Line Operation. In tight-line station operation, each station pumps directly into the suction manifold of the downstream station, and no tanks are provided on the suction side. Such a system is called a *tight-line system* or a *closed system*.

Station Regulation. Maintenance of the pressures within the safe limits of the pipe and equipment by means of pressure controllers at each pumping station is called *station regulation*.

Line Regulation. Maintenance of an identical pumping rate at each pump station of a tight-line or closed system is referred to as *line regulation*.

Rarefaction Control. Planned reduction of flow at an upstream station to reduce pressure rise in the pipeline following a sudden accidental flow reduction at the downstream station is called *rarefaction control*. Flow at the pumping stations may be reduced by shutting down a pump or by closing a valve. By reducing flow at the upstream station, a negative wave is produced, which travels toward the downstream station. This wave nullifies part of the pressure rise caused by the upset at the downstream station.

7.3 CAUSES OF TRANSIENTS

The following operation of various appurtenances or control devices[1-3,7-9] produces transient conditions in oil pipelines:

1. Opening or closing the control valves
2. Starting or stopping the pumps
3. Power failure to the electric motors of pumping units
4. Change in the pumping rate and discharge pressure of pumping stations
5. Operation of the reciprocating pumps
6. Pipeline rupture.

Starting a pump or opening a valve at an intermediate station produces a pressure rise on the downstream side and a pressure drop on the upstream side, whereas a pump shutdown or closure of a valve produces a pressure rise on the upstream side and a pressure drop on the downstream side.

The flow and pressure on the suction and discharge sides of a reciprocating pump are periodic. If the period of the flow or pressure oscillations matches the natural period of the piping system, resonance will develop (see Chapter 8) resulting in high-amplitude pressure fluctuations, which may damage the pipeline.

Air entrapped during filling or following major repairs may produce surges of high magnitude.[10] In addition, if air is present in the pipeline, there is always a danger of an explosion, which may rupture the pipeline.

7.4 METHOD OF ANALYSIS

The dynamic and continuity equations (Eqs. 2.11, 2.30) derived in Chapter 2 describe the transient-state flows in oil pipelines. Note that these equations are not valid for a simultaneous flow of gas and oil in a pipeline for which equations for a two-phase flow will have to be used.

To determine the transient conditions in a pipeline, the dynamic and continuity equations are solved subject to appropriate boundary conditions. As discussed in Chapter 2, these equations can be integrated only by numerical methods since a closed-form solution is not possible because of the presence of nonlinear terms. The method of characteristics presented in Chapter 3 may be used for the numerical integration of these equations. However, as the friction losses in long oil pipelines are large compared to the potential surge, a first-order approximation* of the friction term, $fQ|Q|/(2DA)$, of Eqs. 3.8 and 3.10 may yield an incorrect and unstable solution. An examination of the computed results will reveal any instability, while the validity of the results may be checked by comparing the results obtained by using larger and smaller time steps. Since oil pipelines are usually very long, small time steps would require excessive amount of computer time. To avoid this, the friction term may be considered in the analysis by using either of the following procedures, which allow use of larger time steps:

1. Second-order approximation*,[4,11]
2. Predictor-corrector scheme.[12,13]

In a second-order approximation, an average value of the friction term computed at points P and A (Fig. 3.1) is used for Eq. 3.8, and an average value of the friction term computed at points P and B is used for Eq. 3.10. This results in two nonlinear algebraic equations in Q_P and H_P. These equations may be solved by the Newton-Raphson method. In the predictor-corrector scheme, presented by Evangelisti,[12,13] a first-order approximation is used to determine the discharge at the end of the time step. This predicted value of the discharge is then used in the corrector part to compute the friction term.

*$\int_{x_o}^{x_1} f(x)\,dx \approx f(x_o)\,(x_1 - x_o)$ is called a *first-order approximation*, and
$\int_{x_o}^{x_1} f(x)\,dx \approx \frac{1}{2}\,[f(x_o) + f(x_1)]\,(x_1 - x_o)$ is called a *second-order approximation*.

Because the predictor-corrector scheme is easy to program, requires less computer time than the second-order approximation, and yields sufficiently accurate results, details of this scheme are presented below.

Referring to Fig. 3.1, let us assume that the conditions (e.g., pressure and flow) are known at time t_o and that we have to determine the unknown conditions at point P. (If $t_o = 0$, these are initial steady-state conditions, and if $t_o > 0$, then these are computed values for the previous time step.)

For the predictor part, integration of Eqs. 3.8 and 3.10 by using a first-order approximation yields

$$Q_P^* - Q_A + C_a(H_P^* - H_A) + R Q_A |Q_A| = 0 \tag{7.2}$$

$$Q_P^* - Q_B - C_a(H_P^* - H_B) + R Q_B |Q_B| = 0 \tag{7.3}$$

in which $R = f\Delta t/(2DA)$. In these equations, the notation of Section 3.2 is used except that an asterisk is used to designate the predicted values of various variables.

Equations 7.2 and 7.3 can be written as

$$Q_P^* = C_p^* - C_a H_P^* \tag{7.4}$$

and

$$Q_P^* = C_n^* + C_a H_P^* \tag{7.5}$$

in which C_p^* and C_n^* are equal to the right-hand sides of Eqs. 3.20 and 3.21, respectively. Elimination of H_P^* from Eqs. 7.4 and 7.5 yields

$$Q_P^* = 0.5\,(C_p^* + C_n^*) \tag{7.6}$$

Now this value of Q_P^* may be used in the corrector part to calculate the friction term. Integration of Eqs. 3.8 and 3.10, by using a second-order approximation and by using Q_P^* for computing the friction term, yields

$$Q_P - Q_A + C_a(H_P - H_A) + 0.5\,R(Q_A|Q_A| + Q_P^*|Q_P^*|) = 0 \tag{7.7}$$

and

$$Q_P - Q_B - C_a(H_P - H_B) + 0.5\,R(Q_B|Q_B| + Q_P^*|Q_P^*|) = 0 \tag{7.8}$$

Equations 7.7 and 7.8 may be written as

$$Q_P = C_p - C_a H_P \tag{7.9}$$

and

$$Q_P = C_n + C_a H_P \tag{7.10}$$

in which

$$C_p = Q_A + C_a H_A - 0.5\,R\,(Q_A|Q_A| + Q_P^*|Q_P^*|) \tag{7.11}$$

$$C_n = Q_B - C_a H_A - 0.5\,R\,(Q_B|Q_B| + Q_P^*|Q_P^*|) \tag{7.12}$$

By eliminating H_P from Eqs. 7.9 and 7.10, we obtain

$$Q_P = 0.5\,(C_p + C_n) \tag{7.13}$$

Now H_P may be determined from either Eq. 7.9 or 7.10.

To determine conditions at the boundaries, the boundary conditions derived in Chapters 3 and 10 are first used to compute Q_P^* for the predictor part. Then, this value of Q_P^* is used to compute C_p and C_n from Eqs. 7.11 and 7.12, and the same boundary conditions are used again to determine Q_P and H_P in the predictor part before proceeding to the next time step. The other computational procedure is the same as described in Section 3.2.

7.5 DESIGN CONSIDERATIONS

General Remarks

With a proper design and provision of automatic-control and protective devices, such as pressure controllers, pump-shutdown switches, and relief valves, a pipeline can be safely operated to its maximum capacity. The main functions of these devices are to detect a severe upset in the system and to take appropriate corrective action so that the pipeline pressures remain within the design limits. The time lag between the detection of an upset and the corrective action should be as small as possible. In addition, the action of the protective facilities should be rapid.

The maximum pressure in a blocked line having a centrifugal pump is equal to the shutoff head. However, there is no such upper limit on the maximum pressure in a blocked line having a reciprocating pump; the pressure in this case keeps on rising until either the pipeline ruptures or the pump fails.

Power failure to the electric motors of a pumping station will shut down all pumping units simultaneously. Since this condition may occur a number of times during the life of the project, it should be considered as a normal operation during design. In an engine-powered pumping station, however, the probability of simultaneous shutdown of all pumping units is rather small under normal conditions although it is possible if some control equipment malfunctions.

While analyzing the controlling action of a valve, a proper flow versus valve-opening curve should be used since the flow in certain types of valves does not change until the valve has been opened or closed by approximately 20 to 30 percent. If it is assumed that the flow begins to change as soon as the valve opening is changed, it may yield incorrect results.

Since normal transient operating conditions are likely to occur several times during the life of the project, a factor of safety should be used that is larger than that for the emergency conditions, whose probability of occurrence is

rather small. Malfunctioning of the control equipment in the most unfavorable manner may be considered as an emergency condition.

Control and Surge Protective Devices

A discharge-pressure controller and a pump-shutdown switch are commonly provided in a pumping station having centrifugal pumps. A pressure controller controls the discharge pressure by reducing the pump speed or by closing a control valve. If the pressure exceeds the limits set on the controller, the pump-shutdown switch shuts down the entire station.

In pumping stations having reciprocating pumps, a pressure controller is also used to operate a bypass valve or to change the pump stroke or the pump speed. As an added protection, a relief valve with a capacity equal to the pump discharge should be installed. The resonance conditions may be avoided as follows: In a pumping station with two or three pumps operating at 20 cycles/s or less and having a discharge pressure of less than 6 MPa, tying the discharge lines a short distance from the pump headers or providing an air chamber has been reported[7] to be successful in reducing the pressure fluctuation by about 90 percent. On high-speed multiplex pumps operating at more than 20 cycles/s or having discharge pressures more than 6 MPa, the provision of air chambers does not adequately suppress the pressure fluctuations. In such cases, pulsation dampeners of special design have been found to be satisfactory.[10]

The pressure caused by line packing in a closed system may be several times greater than the potential surge, and it may stress the entire pipeline to the full discharge pressure of the upstream station. These pressures can be kept low by an advance action or rarefaction control, as discussed in the following. Pressure monitors, provided on the suction side of a pump station, detect any excessive pressure rise and transmit a signal to the supervisory control, which reduces the discharge pressure and/or outflow of the upstream station. Due to reduction of the discharge pressure or flow of the upstream station, a negative wave travels in the downstream direction and reduces pressure built up in the pipeline. Another method for reducing the pressure rise is to provide a relief valve at the downstream station.

Upon power failure to the pumping units of an intermediate pumping station, pressure rises on the suction side and decreases on the discharge side. Excessive pressure rise or drop may be prevented by providing a check valve in the pump bypass. As soon as the rising pressure on the suction side exceeds the falling pressure on the discharge side, oil begins to flow from the suction side to the discharge side of the pump. This flow through the check valve helps in preventing further increase and decrease in the pressure on the suction and discharge sides, respectively.

In a mountainous terrain, a surge tank may be provided at the peaks to avoid column separation following pump failure at the upstream station.

7.6 SUMMARY

In this chapter, a number of terms commonly used in the oil industry were defined, and different causes of transient conditions in oil pipelines were outlined. A computational procedure was presented to analyze transients in long pipelines by the method of characteristics. The chapter was concluded by discussing the use of various protective and control devices to keep the pressures within the design limits.

PROBLEMS

7.1 Write a computer program to analyze a long pipeline having a reservoir at the upstream end and a valve at the downstream end. Include the friction term of Eqs. 3.8 and 3.10 by using (1) a first-order finite-difference approximation outlined in Chapter 3 and (2) a predictor-corrector scheme of Section 7.4.

7.2 Use the computer program of Problem 7.1 to compute the potential surge, and the maximum transient-state pressures at the valve and at midlength of a 32,000-m-long, 2-m-diameter pipeline carrying 3.14 m^3/s of crude oil. Assume that the downstream valve is instantaneously closed.

7.3 Compare the maximum pressures of Problem 7.2, obtained by including the friction term, by using: (1) a first-order, finite-difference approximation and (2) a predictor-corrector scheme.

7.4 Develop the boundary conditions for a pumping station having a bypass line fitted with a check valve. The check valve opens as soon as the pressure on the suction side exceeds the pressure on the discharge side.

REFERENCES

1. Ludwig, M. and Johnson, S. P., "Prediction of Surge Pressures in Long Oil Transmission Line," *Proc. Amer. Petroleum Inst.*, Annual Meeting, New York, Nov. 1950.
2. Kaplan, M., Streeter, V. L., and Wylie, E. B., "Computation of Oil Pipeline Transients," *Jour., Pipeline Div., Amer. Soc. of Civil Engrs.*, Nov. 1967, pp. 59-72.
3. Streeter, V. L. and Wylie, E. B., *Hydraulic Transients*, McGraw-Hill Book Co., New York, 1967.
4. Streeter, V. L., "Transients in Pipelines Carrying Liquids or Gases," *Jour., Transportation Engineering Div., Amer. Soc. of Civil Engrs.*, Feb. 1971, pp. 15-29.
5. Burnett, R. R., "Predicting and Controlling Transient Pressures in Long Pipelines," *Oil and Gas Jour., U.S.A.*, vol. 58, no. 10, May 1960, pp. 153-160.
6. *Oil Pipeline Transportation Practices*, issued by Univ. of Texas in cooperation with Amer. Petroleum Inst., Division of Transportation, vol. 1 and 2, 1975.

7. Lundberg, G. A., "Control of Surges in Liquid Pipelines," *Pipeline Engineer*, March 1966, pp. 84-88.
8. Bagwell, M. U. and Phillips, R. D., "Pipeline Surge: How It is Controlled," *Oil and Gas Jour., U.S.A.*, May 5, 1969, pp. 115-120.
9. Bagwell, M. U. and Phillips, R. D., "Liquid Petroleum Pipe Line Surge Problems (Real and Imaginary)," Transportation Div., Amer. Petrol. Inst., April 1969.
10. Ludwig, M., "Design of Pulsation Dampeners for High Speed Reciprocating Pumps," *Conference of the Transportation Div., Amer. Petroleum Inst.*, Houston, Texas, May, 1956.
11. Lister, M., "The Numerical Solution of Hyperbolic Partial Differential Equations by the Method of Characteristics," in Ralston, A. and Wilf, H. S. (eds.), *Mathematical Methods for Digital Computers*, John Wiley & Sons, Inc., New York, 1960, pp. 165-179.
12. Evangelisti, G., "Waterhammer Analysis by the Method of Characteristics," *L'Energia Elettrica*, nos. 10, 11, and 12, 1969, pp. 673-692, 759-771, and 839-858.
13. Evangelisti, G., Boari, M., Guerrini, P., and Rossi, R., "Some Applications of Waterhammer Analysis by the Method of Characteristics, " *L'Energia Elettrica*, nos. 1 and 6, pp. 1-12, 309-324.

ADDITIONAL REFERENCES

Green, J. E., "Pressure Surge Tests on Oil Pipelines," *Proc. Amer. Petroleum Inst.*, vol. 29, Section 5, 1945.
Kerr, S. L., "Surges in Pipelines, Oil and Water," *Trans. Amer. Soc. of Mech. Engrs.*, 1950, p. 667.
Binnie, A. M., "The Effect of Friction on Surges in Long Pipelines," *Jour. Mechanics and Applied Mathematics*, vol. IV, Part 3, 1951.
Kersten, R. D. and Waller, E. J., "Prediction of Surge Pressures in Oil Pipelines," *Jour., Pipeline Div., Amer. Soc. of Civil Engrs.*, vol. 83, no. PL 1, March 1957, pp. 1195-1-1195-22.
Wostl, W. J. and Dresser, T., "Velocimeter Measures Bulk Moduli," *Oil and Gas Jour.*, Dec. 7, 1970, pp. 57-62.
Wylie, E. B., Streeter, V. L., and Bagwell, M. U., "Flying Switching on Long Oil Pipelines," *Amer. Inst. Chem. Engrs. Symposium Series*, vol. 135, no. 69, 1973, pp. 193-194.
Techo, R., "Pipeline Hydraulic Surges are Shown in Computer Simulations," *Oil and Gas Jour.*, November 22, 1976, pp. 103-111.
Kaplan, M., "Analyzing Pipeline Transients by Method of Characteristics," *Oil and Gas Journal*, Jan. 15, 1968, pp. 105-108.

CHAPTER 8

RESONANCE IN PRESSURIZED PIPING SYSTEMS

8.1 INTRODUCTION

In Chapters 4 to 6, we considered transient-state flows that represented the intermediate-flow conditions when the flow is changed from one steady state to another. However, sometimes when a disturbance is introduced into a piping system, it is amplified with time instead of decaying and results in severe pressure and flow oscillations. This condition, which depends upon the characteristics of the piping system and of the excitation, is termed *resonance*.

In this chapter, the development of resonating conditions and the available methods for their analysis are discussed. The details of the transfer matrix method, derivation of the field and point matrices, and procedures for determining the natural frequencies and frequency response of piping systems are then presented. To verify the transfer matrix method, its results are compared with those of the characteristics and impedance methods and with those measured in the laboratory and on the prototype installations.

8.2 DEVELOPMENT OF RESONATING CONDITIONS

We know from fundamental mechanics[1] that the natural frequency, ω_n, of the spring-mass system shown in Fig. 8.1 is equal to $\frac{1}{2\pi}\sqrt{k/m}$, in which ω_n = natural frequency of the system in rad/s, m = mass, and k = spring constant. If a sinusoidal force having frequency ω_f (Fig. 8.1b) is applied to the mass, initially a beat develops (transient state) and then the system starts to oscillate (Fig. 8.1c) at the forcing frequency ω_f and with a constant amplitude. These oscillations, having a constant amplitude, are called *steady vibrations*. The amplitude of the

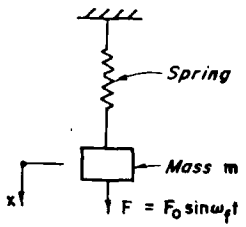

(a) Spring - mass system

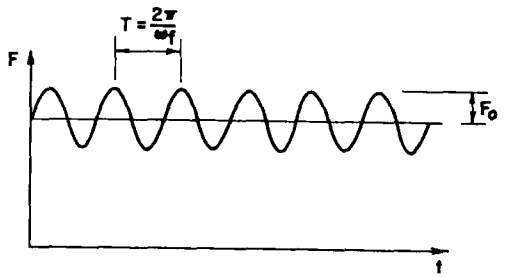

(b) Periodic force

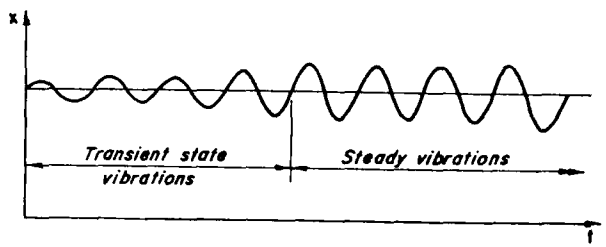

(c) Vibration of mass

Figure 8.1. Vibrations of a spring mass system.

vibrations depends upon the ratio $\omega_r = \omega_f/\omega_n$. If the forcing frequency ω_f is equal to the natural frequency ω_n and the system is frictionless, then the amplitude of steady vibrations becomes infinite. The reason for this is that the total energy of the system keeps on increasing with each cycle because no energy is

dissipated in the system. Hence, the oscillations are amplified without any upper bound. However, if the system is not frictionless, the amplitude of the oscillations grows until the energy input and energy dissipation during a cycle are equal. Since at that time there is no additional energy input per cycle, the system oscillates with a finite amplitude.

Now let us consider a pipeline having a reservoir at the upstream end and a valve at the downstream end (Fig. 8.2a). Let us assume that the valve is initially in a closed position but that we open and close it sinusoidally at frequency ω_f starting at time $t = 0$ (Fig. 8.2b). Similar to our spring-mass system, a beat develops first (transient state), and then the flow and pressure oscillate at a constant amplitude but with frequency ω_f (Fig. 8.2c). Such a periodic flow is termed *steady-oscillatory flow*.

Let us compare the characteristics of the steady-oscillatory flow in our simple hydraulic system with the steady vibrations of the spring-mass system. The displacement of the spring at the fixed end in our spring-mass system is zero. Similarly, the water level in the upstream reservoir of the hydraulic system is constant. Therefore, the amplitude of pressure oscillations at the reservoir is zero, or, in other words, there is a pressure node at the reservoir. In the spring-mass system, there is only one mass and one spring; therefore, there is only one mode of vibrations or one degree of freedom, and hence the system has only one natural frequency (or natural period). If the compressibility of the fluid is taken into consideration, the fluid in the pipeline of our hydraulic system is comprised of an infinite number of masses and springs. Therefore, our hydraulic system has infinite modes of oscillations or degrees of freedom* and hence has infinite natural periods: the first is termed as *fundamental*, and the others are called *higher harmonics*.

Figure 8.3 shows the variation of the amplitude of the pressure oscillations at various harmonics along the piping system of Fig. 8.2. Since the reservoir level is constant, a pressure node always exists at the reservoir end. At the valve, however, there is a pressure node during even harmonics and an antinode during odd harmonics. The location of the nodes and antinodes along a pipeline depends upon the harmonic at which the system is oscillating.

Let us now consider another significant difference between our spring-mass, and hydraulic systems. In the former, the source of energy is the external periodic force acting on the mass. In the hydraulic system, although the valve is the forcing function, it is not the source of energy. The valve is just controlling the efflux of energy from the system, whereas the upstream reservoir is the source of

**Distributed systems*[2] represented by partial differential equations have infinite degrees of freedom, whereas *lumped systems* represented by ordinary differential equations have finite degrees of freedom.

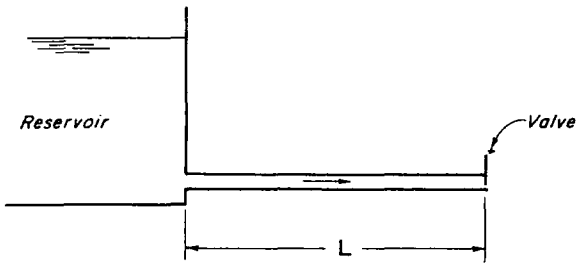

(a) Single pipeline

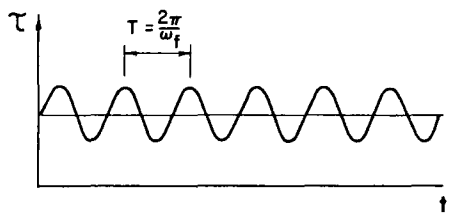

(b) Periodic valve operation

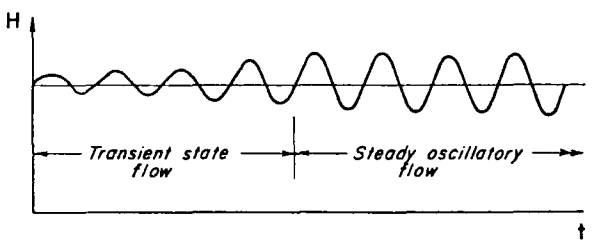

(c) Pressure oscillations at valve

Figure 8.2. Development of steady-oscillatory flow in a single pipeline.

energy. Since the volume of the fluid in the pipeline is constant, the outflow per cycle at the valve must be equal to the inflow per cycle at the reservoir. The reservoir level being constant, the energy input into the system is at a constant head. However, there is no such restriction on the energy efflux at the valve. If

the valve operation is such that there is outflow when the pressure at the valve is low and there is little or no outflow when the pressure is high, net influx of energy occurs during each cycle. This causes the pressure oscillations to grow. When the steady-oscillatory flow is fully developed, a discharge node exists at the valve during oscillations at odd harmonics if the head losses in the system are neglected. Once a discharge node is formed at the valve, opening or closing of

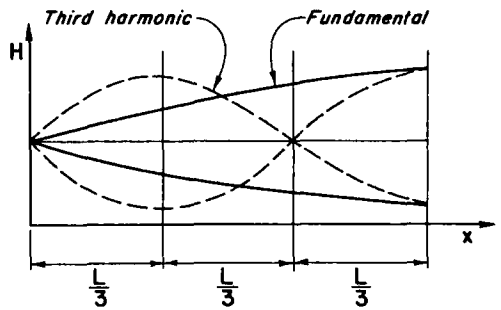

(a) Odd harmonics

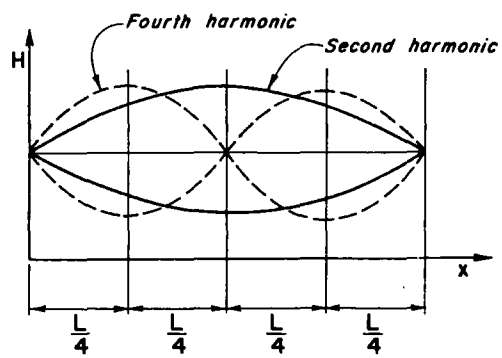

(b) Even harmonics

Figure 8.3. Pressure oscillations along pipeline at various harmonics.

the valve has no effect on the energy efflux, and thus the amplitude of the pressure oscillations does not increase further even though it is assumed that there is no energy dissipation in the system.

Allievi[3] was the first to prove that the maximum possible amplitude of the pressure oscillations at the valve was equal to the static head. However, later on, Bergeron[4] proved graphically that for large values of Allievi's parameter, $\rho = (aV_o)/(2gH_o)$, it is possible to have amplitude greater than the static head. Also, Camichel[5] demonstrated that doubling of the pressure head is not possible unless $H_o > (aV_o)/g$. In the preceding expressions, a = waterhammer wave velocity; g = acceleration due to gravity; H_o = static head; and V_o = steady-state flow velocity.

8.3 FORCED AND SELF-EXCITED OSCILLATIONS

Steady-oscillatory flows in piping systems may be caused by a boundary that acts as a periodic forcing function or by a self-excited excitation. The system oscillates at the frequency of the forcing function during forced oscillations and at one of the natural frequencies of the system during self-excited oscillations.

Forcing Functions

There are three common types of forcing functions in hydraulic systems: periodic variation of the pressure, flow, and the relationship between the pressure and the flow.

A typical example of the periodic pressure variation is a standing wave on the reservoir water surface at a pipe intake. If the period of the surface waves corresponds to one of the natural periods of the piping system, steady-oscillatory conditions are developed in the system in just a few cycles.

A reciprocating pump has periodic inflow and outflow. If the period of a predominant harmonic of either the inflow or of the outflow corresponds to a natural period of the suction or discharge lines, severe flow oscillations will develop.

A periodically opening and closing valve is an example of a periodic variation of the relationship between the pressure and the flow. The development of steady-oscillatory flows by a periodic valve operation was discussed in Section 8.2.

Self-Excited Oscillations

In the *self-excited* or *auto- oscillations*, a component of the system acts as an exciter, which causes the system energy to increase following a small disturbance in the system. Resonance develops when the net energy influx to the system per cycle is more than the energy dissipated per cycle.

A typical example of an exciter is a leaking valve or a leaking seal.[6] Let us examine how the oscillations develop. Figure 8.4 shows the valve characteristics for a normal and for a leaking valve (Fig. 8.4a and b). For a normal valve, the flow increases as the pressure increases; for a leaking valve, the flow decreases as the pressure increases. In Chapter 1, we derived the following equation for the change in pressure caused by a flow variation, i.e.,

$$\Delta H = -\frac{a}{g}\Delta V \tag{1.8}$$

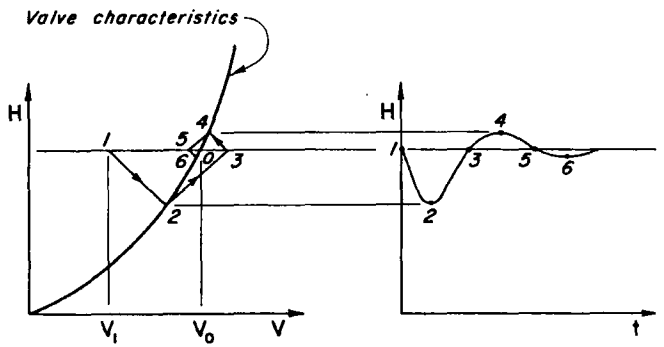

(a) Normal valve

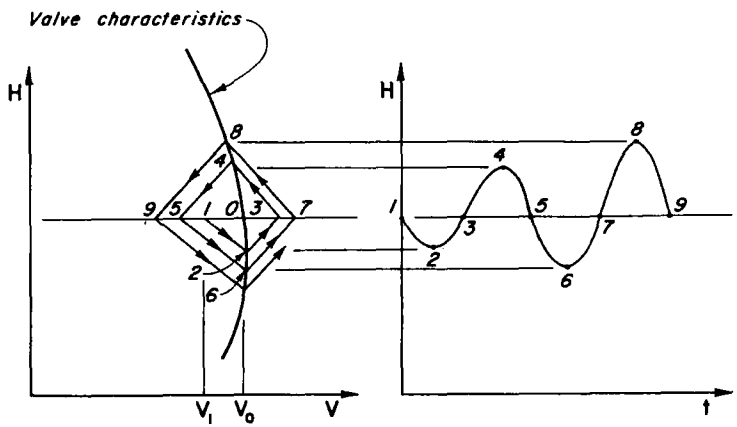

(b) Leaking valve

Figure 8.4. Self-excited oscillations.

On the $H \sim V$ diagram, this equation plots as straight lines having slopes $\pm a/g$ for a decrease or increase in velocity, respectively. Let us assume that the initial steady-state velocity is V_o and that, due to a disturbance, it is decreased to V_1. The decay or amplification of this disturbance using the graphical waterhammer analysis is shown in Fig. 8.4.[7] It can be seen that the disturbance decays in a few cycles for a normal valve whereas it amplifies for a leaking valve. As the flow through a leaking valve cannot be less than zero and it cannot increase infinitely, the amplification of the pressure oscillations is therefore finite.

Den Hartog[8] reported self-excited penstock vibrations caused by the disturbances produced by the runner blades passing the guide vanes of a Francis turbine. Based on a simplified theoretical analysis, which was confirmed by observations on eight hydroelectric installations, he concluded that such vibrations are to be expected if the number of the runner blades is one less than the number of the guide vanes. Self-excited vibrations of the guide vanes of a centrifugal pump is considered to be the cause of the accident at the Lac Blanc-Lac Noir pumped storage plant,[9] in which several testing personnel died.

The possibility of the self-excited vibrations in a liquid rocket-engine-propellant feed system were determined by a computer analysis;[10] experimental determination of such a possibility in the piping system of a control system is described by Saito.[11]

Improper settings of a hydraulic turbine governor can result in self-excited oscillations called *governor hunting*.

Abbot et al.[6] measured self-excited vibrations in Bersimiss II power plant. A slight leak in a 3.7-m-diameter penstock valve due to a reduction of seal pressure resulted in the vibrations of the valve. The valve vibrations and pressure oscillations were sinusoidal and were eliminated by opening a bypass valve.

McCaig and Gibson[12] reported vibrations in a pump-discharge line caused by a leak under the static head in a 0.25-m-diameter spring-cushioned check valve. Measurements showed that the pressure oscillations were approximately sinusoidal with sharp impulses of large magnitude every third cycle. The vibrations were prevented by installing a weaker cushioning spring in the check valve and removing the air valves from the pipeline.

8.4 METHODS OF ANALYSIS

The steady-oscillatory flows in a hydraulic system may be analyzed either in the time domain or in the frequency domain[13] by using the following methods:

1. Time domain: method of characteristics
2. Frequency domain: (a) Impedance method and (b) Transfer matrix method.

A discussion of the advantages and disadvantages of each method follows.

Analysis in Time Domain–Method of Characteristics

As discussed in Chapter 3, in this method, the partial differential equations describing the unsteady flow are converted into ordinary differential equations, which are then solved by a finite-difference technique. Nonlinear friction losses and the nonlinear boundary conditions may be included in the analysis.

To analyze the steady-oscillatory flows by this method,[14] the initial steady-state discharge and pressure head in the piping system are assumed equal to their mean values or equal to zero-flow conditions. The specified forcing function is then imposed as a boundary condition, and the system is analyzed by considering one frequency at a time. When the initial transients are vanished and a steady-oscillatory regime is established, the amplitudes of the pressure and discharge fluctuation are determined. The process of convergence to the steady-oscillatory conditions is slow (it takes about 150 cycles) and requires a considerable amount of computer time, thus making the method uneconomical for general studies. The main advantage is that the nonlinear relationships can be included in the analyses.

Analysis in Frequency Domain

By assuming a sinusoidal variation of the pressure head and the flow, the dynamic and continuity equations describing the unsteady flow in the time domain are converted into the frequency domain. The friction term and the nonlinear boundary conditions are linearized for solution by these methods. If the amplitude of oscillations is small, the error introduced by linearization is negligible.

Any periodic forcing function can be handled by these methods. The forcing function is decomposed into various harmonics by Fourier analysis,[15] and each harmonic is analyzed separately. Since all the equations and relationships are linear, the system response is determined by superposition[16] of individual responses.

As the frequency response is determined directly, the computer time required for the analysis is small. Therefore, these methods are suitable for general studies. The following two methods of analysis in the frequency domain are available:

Impedance Method

The concept of impedance was introduced by Rocard[9] and was used later by Paynter[17] and Waller.[18] Wylie[19,20] extended and systemized this method for the analysis of complex systems.

In this method, the *terminal impedance*, Z_s, which is the ratio of the oscillatory pressure head and the discharge, is computed by using the known boundary conditions. An impedance diagram between ω_f and $|Z_s|$ is plotted. The frequencies at which $|Z_s|$ is maximum are the resonant frequencies of the system.

Because of the lengthy algebraic equations involved, the method is suitable for digital computer analysis only. For a parallel piping system, a procedure is suggested that requires solution of a large number of simultaneous equations. This becomes cumbersome if the system has many parallel loops. For example, eight simultaneous equations have to be solved for systems having only two parallel loops.[19]

Transfer Matrix Method

The transfer matrix method has been used for analyzing structural and mechanical vibrations[21,22] and for analyzing the electrical systems.[23] This method was introduced[24-27] by the author for the analysis of steady-oscillatory flows and for determining the frequency response of hydraulic systems.

Similar to the impedance method, the transfer matrix method is based on the linearized equations and on sinusoidal flow and pressure fluctuations. However, in the author's opinion, transfer matrix method is simpler and more systematic than the impedance method. Other advantages of the transfer matrix method are (1) the analysis of the parallel systems does not require any special treatment; (2) the method is suitable for both hand and digital computations; (3) the stability of a system can be checked by the root locus technique;[28] and (4) systems, in which oscillations of more than two variables (e.g., pressure, flow, density, temperature) have to be considered, can be analyzed.

Details of the transfer matrix method are presented herein. Any reader having an elementary knowledge of the matrix algebra should be able to follow the derivation of matrices and their application. Block diagrams are used to achieve an orderly and concise formulation and analysis of problems involving complex systems.

8.5 TERMINOLOGY

The terminology established by Camichel et al.[5] and later used by Jaeger[30,31] and Wylie[19,20] is followed herein.

Steady-Oscillatory Flow

A flow in which a permanent regime is established such that the conditions at a point (e.g., pressure, discharge) are periodic functions of time is called *steady-oscillatory flow*. In the theory of vibrations, the steady-state oscillations refer to the oscillations that have constant amplitude. However, the term *steady-oscillatory* is used herein to avoid confusion with the steady flow in which conditions at a point are constant with respect to time.

Instantaneous and Mean Discharge and Pressure Head

In a steady-oscillatory flow, the instantaneous discharge, Q, and the instantaneous pressure head, H, can be divided into two parts:

$$Q = Q_o + q^* \tag{8.1}$$

$$H = H_o + h^* \tag{8.2}$$

in which Q_o = average, or mean, discharge; q^* = discharge deviation from the mean (see Fig. 8.5); H_o = average, or mean, pressure head; and h^* = pressure head deviation from the mean. Both h^* and q^* are functions of time, t, and distance, x. It is assumed that h^* and q^* are sinusoidal in time, which, in practice, is often true or a satisfactory approximation.[6,12,30,31] Hence, by using complex algebra, we can write

$$q^* = \mathrm{Re}\,(q(x)e^{j\omega t}) \tag{8.3}$$

$$h^* = \mathrm{Re}\,(h(x)e^{j\omega t}) \tag{8.4}$$

in which ω = frequency in rad/s; $j = \sqrt{-1}$; h and q are complex variables and are functions of x only; and "Re" stands for real part of the complex variable.

Theoretical Period

For a series piping system,

$$T_{th} = 4\sum_{i=1}^{n} \frac{l_i}{a_i} \tag{8.5}$$

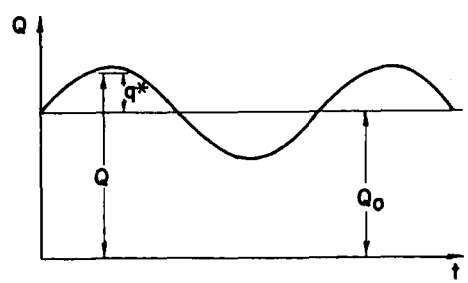

Figure 8.5. Instantaneous, mean, and oscillatory discharge.

and

$$\omega_{th} = \frac{2\pi}{T_{th}} \tag{8.6}$$

in which T_{th} = theoretical period; ω_{th} = theoretical frequency; n = number of pipes; and a = velocity of the waterhammer waves. The subscript i denotes quantities for the ith pipe. In a branch system, l_i/a_i is calculated along the main pipeline.

Resonant Frequency

The frequency corresponding to the fundamental or one of the higher harmonics of the system is called the *resonant frequency*.

State Vectors and Transfer Matrices

Let us consider a general system (Fig. 8.6) whose input variables $x_1, x_2, \cdots x_n$ and output variables $y_1, y_2, \cdots, y_n$ are related by the following n simultaneous equations:

$$\left.\begin{aligned} y_1 &= u_{11}x_1 + u_{12}x_2 + \cdots + u_{1n}x_n \\ y_2 &= u_{21}x_1 + u_{22}x_2 + \cdots + u_{2n}x_n \\ &\cdots\cdots\cdots\cdots\cdots\cdots \\ &\cdots\cdots\cdots\cdots\cdots\cdots \\ &\cdots\cdots\cdots\cdots\cdots\cdots \\ y_n &= u_{n1}x_1 + u_{n2}x_2 + \cdots + u_{nn}x_n \end{aligned}\right\} \tag{8.7}$$

In the matrix notation, these equations can be written as

$$\mathbf{y} = \mathbf{U}\,\mathbf{x} \tag{8.8}$$

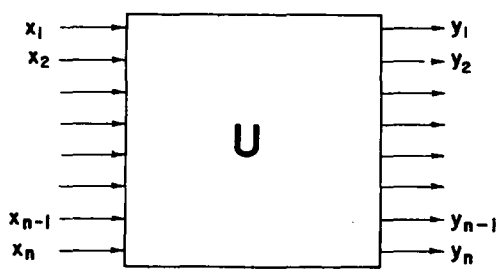

Figure 8.6. Block diagram for one-component system.

in which the input variables are combined into a single column vector, x, and the output variables are combined into a column vector, y. In other words, it can be said that the system converts, or transfers, the input variables x into the output variables y, and the transfer takes place in accordance with Eq. 8.8. The matrix U in Eq. 8.8 is called the *transfer matrix*, and x and y are called the *state vectors*.

In the previous example, the system has only one component. The physical systems, however, are usually made up of several subsystems or components. In such cases, each component is represented by a transfer matrix, and the overall transfer matrix for the system is obtained by multiplying the individual transfer matrices in a proper sequence (see pp. 214-215).

The general system of Fig. 8.6 has n input and output variables. In hydraulic systems, however, the quantities of interest at the section i of a pipeline are usually h and q, which can be combined in the matrix notation as

$$\mathbf{z}_i = \begin{Bmatrix} q \\ h \end{Bmatrix}_i \tag{8.9}$$

The column vector $\mathbf{z}_i$ is called the state vector at section i. The state vectors just to the left and to the right of a section are designated by the superscripts L and R, respectively. For example, $\mathbf{z}_i^L$ refers to the state vector just to the left of the ith section (Fig. 8.7).

To combine the matrix terms in some cases (see p. 229) the state vector is defined as

$$\mathbf{z}_i' = \begin{Bmatrix} q \\ h \\ 1 \end{Bmatrix}_i \tag{8.10}$$

Because of the additional element with unit value, the column vector $\mathbf{z}_i'$ is called the *extended state vector*. A prime is used herein to designate an extended state vector.

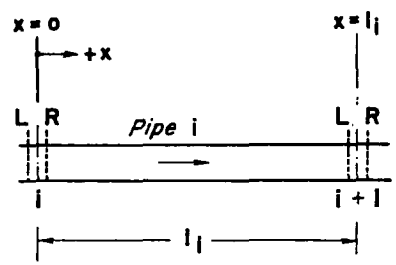

Figure 8.7. Single pipeline.

A matrix relating two state vectors is called a *transfer matrix*. The upper-case letters **F**, **P**, and **U** are used to designate the transfer matrices; the corresponding lower-case letters with the double subscripts refer to the elements of the matrix: the first subscript represents the row, and the second subscript represents the column of the element. For example, the element in the second row and the first column of the matrix **U** is represented by u_{21}.

Transfer matrices are of three types:

1. *Field transfer matrix, or field matrix,* **F**. A field-transfer relates the state vectors at two adjacent sections of a pipe. For example, in Fig. 8.7,

$$\mathbf{z}_{i+1}^{L} = \mathbf{F}_i \mathbf{z}_i^{R} \tag{8.11}$$

in which $\mathbf{F}_i$ = field matrix for the ith pipe.

2. *Point transfer matrix, or point matrix*, **P**. The state vectors just to the left and to the right of a discontinuity, such as at a series junction (Fig. 8.8) or at a valve, are related by a point-transfer matrix. The type of the discontinuity is designated by specifying a subscript with the letter P. For example, in Fig. 8.8,

$$\mathbf{z}_{i+1}^{R} = \mathbf{P}_{sc} \mathbf{z}_{i+1}^{L} \tag{8.12}$$

in which $\mathbf{P}_{sc}$ = point matrix for a series junction.

3. *Overall transfer matrix,* **U**. The overall transfer matrix relates the state vector at one end of a system, or a side branch, to that at the other end. For example if $n + 1$ is the last section, then

$$\mathbf{z}_{n+1}^{L} = \mathbf{U} \mathbf{z}_1^{R} \tag{8.13a}$$

in which **U** = overall transfer matrix. This is obtained by an ordered multiplication of all the intermediate field and point matrices as follows:

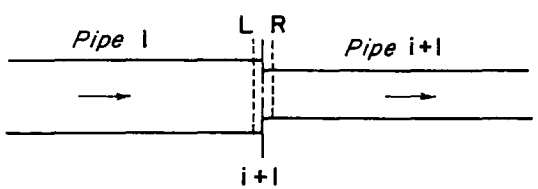

Figure 8.8. Series junction.

The intermediate field and point matrices are:

$$\left.\begin{aligned}
\mathbf{z}_2^{L} &= \mathbf{F}_1 \mathbf{z}_1^{R} \\
\mathbf{z}_2^{R} &= \mathbf{P}_2 \mathbf{z}_2^{L} \\
\mathbf{z}_3^{L} &= \mathbf{F}_2 \mathbf{z}_2^{R} \\
&\cdots\cdots \\
&\cdots\cdots \\
&\cdots\cdots \\
\mathbf{z}_i^{L} &= \mathbf{F}_{i-1} \mathbf{z}_{i-1}^{R} \\
\mathbf{z}_i^{R} &= \mathbf{P}_i \mathbf{z}_i^{L} \\
&\cdots\cdots \\
&\cdots\cdots \\
\mathbf{z}_n^{R} &= \mathbf{P}_n \mathbf{z}_n^{L} \\
\mathbf{z}_{n+1}^{L} &= \mathbf{F}_n \mathbf{z}_n^{R}
\end{aligned}\right\} \tag{8.13b}$$

Elimination of $\mathbf{z}_2^{L}, \mathbf{z}_2^{R}, \ldots, \mathbf{z}_n^{L}$, and $\mathbf{z}_n^{R}$ from Eq. 8.13b yields

$$\mathbf{z}_{n+1}^{L} = (\mathbf{F}_n \mathbf{P}_n \ldots \mathbf{F}_i \mathbf{P}_i \ldots \mathbf{F}_3 \mathbf{P}_3 \mathbf{F}_2 \mathbf{P}_2 \mathbf{F}_1) \mathbf{z}_1^{R} \tag{8.13c}$$

Hence, it follows from Eqs. 8.13a and 8.13c that

$$\mathbf{U} = \mathbf{F}_n \mathbf{P}_n \ldots \mathbf{F}_i \mathbf{P}_i \ldots \mathbf{F}_3 \mathbf{P}_3 \mathbf{F}_2 \mathbf{P}_2 \mathbf{F}_1 \tag{8.14d}$$

8.6 BLOCK DIAGRAMS

A block diagram is a schematic representation of a system in which each component, or a combination of components, of the system is represented by a "black box." The box representing a pipeline of constant cross-sectional area, wall thickness, and wall material is characterized by a field matrix, while that representing a discontinuity in the system geometry is represented by a point matrix. The block diagram for a system can be simplified by representing a block of individual boxes by a single box. This procedure is illustrated in the following sections by a number of typical examples.

A section on a block diagram is shown by a small circle on the line joining the two boxes. The number of the section is written below the circle and the left- and right-hand sides of the section are designated by writing the letters L and R

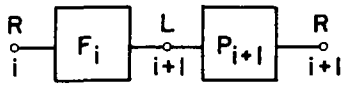

Figure 8.9. Block diagram.

above the circle. For example, in Fig. 8.9, i and $i + 1$ denote the number of the sections, and L and R denote the left- and right-hand sides of the section. In the case of a branch pipe, the number of the section is written to the right of the circle, and the left- and right-hand sides of the sections are identified by writing the letters BL and BR to the left of the circle (see Fig. 8.13b).

The block diagrams are of great help for (1) the concise and orderly formulation and analysis of problems involving complex systems, (2) an easy understanding of the interaction of different parts of the system, and (3) determining the sequence of multiplication of transfer matrices while doing the calculations by hand or while writing a computer program.

8.7 DERIVATION OF TRANSFER MATRICES

To analyze the steady-oscillatory flows and to determine the resonating characteristics of a piping system by the method presented herein, it is necessary that the transfer matrices of the elements of the system be known. In this section, field matrices for a simple pipeline and for a system of parallel loops are derived. A numerical procedure is presented to determine the field matrix for a pipe having variable characteristics along its length. The point matrices for a series junction, for valves and orifices, and for the junction of a branch (branch with various end conditions) and the main are developed.

Field Matrices

Single Conduit

The field matrix for a conduit having a constant cross-sectional area, constant wall thickness, and the same wall material is derived in this section. In the derivation, the system is considered to be distributed, and the friction-loss term is linearized.

The continuity and dynamic equations describing the flow through closed conduits were derived in Chapter 2. For an easy reference, let us rewrite these equations as

1. Continuity equation

$$\frac{\partial Q}{\partial x} + \frac{gA}{a^2}\frac{\partial H}{\partial t} = 0 \tag{8.14}$$

2. Dynamic equation

$$\frac{\partial H}{\partial x} + \frac{1}{gA}\frac{\partial Q}{\partial t} + \frac{fQ^n}{2gDA^n} = 0 \tag{8.15}$$

in which A = cross-sectional area of the pipeline; g = acceleration due to gravity; D = inside diameter of the pipeline; f = Darcy-Weisbach friction factor; n = exponent of velocity in the friction loss term; x = distance along the pipeline, measured positive in the downstream direction (see Fig. 8.7); and t = time.

As the mean flow and pressure head are time-invariant and as the mean flow is constant along a pipeline, $\frac{\partial Q_o}{\partial x}$, $\frac{\partial Q_o}{\partial t}$, and $\frac{\partial H_o}{\partial t}$ are all equal to zero. Hence, it follows from Eqs. 8.1 and 8.2 that

$$\left.\begin{aligned} \frac{\partial Q}{\partial x} &= \frac{\partial q^*}{\partial x}; \quad \frac{\partial Q}{\partial t} = \frac{\partial q^*}{\partial t} \\ \frac{\partial H}{\partial t} &= \frac{\partial h^*}{\partial t}; \quad \frac{\partial H}{\partial x} = \frac{\partial H_o}{\partial x} + \frac{\partial h^*}{\partial x} \end{aligned}\right\} \tag{8.16}$$

However, since we are considering the friction losses, $\frac{\partial H_o}{\partial x}$ is not equal to zero.

For turbulent flow,

$$\frac{\partial H_o}{\partial x} = -\frac{fQ_o^n}{2gDA^n} \tag{8.17}$$

and for laminar flow,

$$\frac{\partial H_o}{\partial x} = -\frac{32\nu Q_o}{gAD^2} \tag{8.18}$$

in which ν = kinematic viscosity of the fluid. If $q^* << Q_o$, then

$$Q^n = (Q_o + q^*)^n \simeq Q_o^n + n\,Q_o^{n-1}\,q^* \tag{8.19}$$

in which higher-order terms are neglected.

It follows from Eqs. 8.14 through 8.19 that

$$\frac{\partial q^*}{\partial x} + \frac{gA}{a^2}\frac{\partial h^*}{\partial t} = 0 \tag{8.20}$$

$$\frac{\partial h^*}{\partial x} + \frac{1}{gA}\frac{\partial q^*}{\partial t} + R\,q^* = 0 \tag{8.21}$$

in which $R = (nfQ_o^{n-1})/(2gDA^n)$ for turbulent flow and $R = (32\nu)/(gAD^2)$ for laminar flow.

The field matrix for a pipe can be derived by using the separation-of-variable technique[2] or by using the Cayley-Hamilton theorem.[21] The former is used herein because of its simplicity.†

Elimination of h^* from Eqs. 8.20 and 8.21 yields

$$\frac{\partial^2 q^*}{\partial x^2} = \frac{1}{a^2}\frac{\partial^2 q^*}{\partial t^2} + \frac{gAR}{a^2}\frac{\partial q^*}{\partial t} \tag{8.22}$$

Now, if it is assumed that the variation of q^* is sinusoidal with respect to t, then on the basis of Eq. 8.3, Eq. 8.22 takes the form

$$\frac{d^2 q}{dx^2} = \left(-\frac{\omega^2}{a^2} + \frac{jgA\omega R}{a^2}\right) q \tag{8.23}$$

or

$$\frac{d^2 q}{dx^2} - \mu^2 q = 0 \tag{8.24}$$

in which

$$\mu^2 = -\frac{\omega^2}{a^2} + \frac{jgA\omega R}{a^2} \tag{8.25}$$

The solution of Eq. 8.24 is

$$q = c_1 \sinh \mu x + c_2 \cosh \mu x \tag{8.26}$$

in which c_1 and c_2 are arbitrary constants.

If h^* is also assumed sinusoidal in t, then by substituting Eqs. 8.26 and 8.4 into Eq. 8.20 and solving for h, we obtain

$$h = -\frac{a^2 \mu}{jgA\omega}(c_1 \cosh \mu x + c_2 \sinh \mu x) \tag{8.27}$$

The field matrix relating the state vectors at the ith and at the $(i+1)$th section of the ith pipe (see Fig. 8.7) of length l_i is to be derived. It is known that at the ith section (at $x = 0$), $h = h_i^R$ and $q = q_i^R$. Hence, it follows from Eqs. 8.26 and 8.27 that

$$\left.\begin{aligned} c_1 &= -\frac{jgA_i\omega}{a_i^2 \mu_i} h_i^R \\ \text{and} \qquad & \\ c_2 &= q_i^R \end{aligned}\right\} \tag{8.28}$$

†For the derivation using the Cayley-Hamilton theorem, interested readers should see Ref. 24 or 26.

In addition, at the $(i+1)$th section (at $x = l_i$), $h = h_{i+1}^L$ and $q = q_{i+1}^L$. The substitution of these values of h and q, and c_1 and c_2 from Eq. 8.28 into Eqs. 8.26 and 8.27 yields

$$q_{i+1}^L = (\cosh \mu_i l_i) q_i^R - \frac{1}{Z_c}(\sinh \mu_i l_i) h_i^R \tag{8.29}$$

$$h_{i+1}^L = -Z_c (\sinh \mu_i l_i)\, q_i^R + (\cosh \mu_i l_i)\, h_i^R \tag{8.30}$$

in which *characteristic impedance*[14] for the pipe $Z_c = (\mu_i a_i^2)/(j\omega g A_i)$.

Equations 8.29 and 8.30 can be expressed in the matrix notation as

$$\begin{Bmatrix} q \\ h \end{Bmatrix}_{i+1}^{L} = \begin{bmatrix} \cosh \mu_i l_i & -\frac{1}{Z_c}\sinh \mu_i l_i \\ -Z_c \sinh \mu_i l_i & \cosh \mu_i l_i \end{bmatrix} \begin{Bmatrix} q \\ h \end{Bmatrix}_{i}^{R} \tag{8.31}$$

or

$$\mathbf{z}_{i+1}^L = \mathbf{F}_i \mathbf{z}_i^R. \tag{8.32}$$

Hence, field matrix for the ith pipe is

$$\mathbf{F}_i = \begin{bmatrix} \cosh \mu_i l_i & -\frac{1}{Z_c}\sinh \mu_i l_i \\ -Z_c \sinh \mu_i l_i & \cosh \mu_i l_i \end{bmatrix} \tag{8.33}$$

If friction is neglected, i.e., $R_i = 0$, then $\mathbf{F}_i$ becomes

$$\mathbf{F}_i = \begin{bmatrix} \cos b_i\omega & -\frac{j}{C_i}\sin b_i\omega \\ -jC_i \sin b_i\omega & \cos b_i\omega \end{bmatrix} \tag{8.34}$$

in which $b_i = l_i/a_i$ and $C_i = a_i/(gA_i)$. Note that b_i and C_i are constants for a pipe and are not functions of ω, and that C_i is the characteristic impedance[14] for the ith pipe if friction is neglected.

If $\omega l_i/a_i \ll 1$, then the system may be analyzed as a *lumped* system. In this case, for a frictionless system, field matrix $\mathbf{F}_i$ becomes

$$\mathbf{F}_i = \begin{bmatrix} 1 & -\frac{gA_i l_i \omega j}{a_i^2} \\ -\frac{l_i \omega j}{gA_i} & 1 \end{bmatrix} \tag{8.35}$$

which follows from Eq. 8.34 since $\cos(\omega l_i/a_i) \approx 1$ and $\sin(\omega l_i/a_i) \approx \omega l_i/a_i$ for small values of $\omega l_i/a_i$.

While doing the analysis, one first calculates the elements of the field matrix for each pipe. A comparison of the field matrices of Eqs. 8.34 and 8.35 shows

that this idealization of a distributed system as a lumped system does not greatly simplify the computations.

Example 8.1

For $\omega = 2.0$ rad/s, compute the elements of the field matrix for a pipe that is 400-m-long and has a diameter of 0.5 m. The velocity of waterhammer waves in the pipe is 1000 m/s. Assume

1. The liquid inside the pipe as a lumped mass.
2. The liquid inside the pipe as distributed, and consider the system is frictionless.

Solution

Data:

$$l = 400 \text{ m}$$
$$D = 0.5 \text{ m}$$
$$a = 1000 \text{ m/s}$$
$$g = 9.81 \text{ m/s}^2$$
$$\omega = 2 \text{ rad/s}$$

1. *Lumped System*

$$A = \frac{\pi}{4}(0.5)^2 = 0.196 \text{ m}^2$$

From Eq. 8.35,

$$f_{12} = -\frac{gAl\omega j}{a^2}$$
$$= -\frac{9.81 \times 0.196 \times 400 \times 2j}{(1000)^2}$$
$$= -0.00154\,j$$
$$f_{21} = -\frac{l\omega}{gA} j$$
$$= -\frac{400 \times 2}{9.81 \times 0.196} j$$
$$= -416.07\,j$$

2. *Distributed System*

$$b = l/a = 400/1000 = 0.4 \text{ s}$$

$$C = \frac{a}{gA}$$
$$= \frac{1000}{9.81 \times 0.196} = 520.08 \text{ s m}^{-2}$$
$$b\omega = 0.4 \times 2 = 0.8$$

Substituting these values into Eq. 8.34,

$$f_{11} = f_{22} = \cos b\omega$$
$$= \cos 0.8 = 0.697$$
$$f_{12} = -\frac{j}{C} \sin b\omega$$
$$= -\frac{j}{520.08} \sin 0.8 = -0.0014\,j$$
$$f_{21} = -jC \sin b\omega$$
$$= -j \times 520.08 \times \sin 0.8 = 373.08\,j$$

Conduit Having Variable Characteristics Along Its Length

A conduit is said to have variable characteristics if, A, a, wall thickness, or wall material vary along its length. Equations 8.14 and 8.15 describe the transient flow through such conduits; the only difference is that A and/or a are functions of x instead of being constants, i.e.,

$$\frac{\partial Q}{\partial x} + \frac{gA(x)}{a^2(x)} \frac{\partial H}{\partial t} = 0 \tag{8.36}$$

$$\frac{\partial H}{\partial x} + \frac{1}{gA(x)} \frac{\partial Q}{\partial t} = 0 \tag{8.37}$$

in which $A(x)$ and $a^2(x)$ denote that A and a^2 are functions of x. In these equations, nonlinear terms of higher order and friction are neglected. By substituting Eqs. 8.1 through 8.4 into the preceding equations and simplifying, we obtain

$$\frac{\partial q}{\partial x} + \frac{jgA(x)\omega}{a^2(x)} h = 0 \tag{8.38}$$

$$\frac{\partial h}{\partial x} + \frac{j\omega}{gA(x)} q = 0 \tag{8.39}$$

These equations can be expressed in the matrix notation as

$$\frac{dz}{dx} = \mathbf{B}z \tag{8.40}$$

in which z is the column vector as defined in Eq. 8.9 and

$$\mathbf{B} = \begin{bmatrix} 0 & -\dfrac{jgA(x)\omega}{a^2(x)} \\ -\dfrac{j\omega}{gA(x)} & 0 \end{bmatrix} \tag{8.41}$$

Since the elements of the matrix B are functions of x, the procedure that has been outlined to determine the field matrix for the conduit fails. To analyze such cases, recourse is made to either of the following procedures[27]:

1. The actual pipeline is replaced by a substitute pipeline having piecewise constant elements (see Fig. 8.10), and the system is analyzed by using the field matrices given by Eq. 8.34. This gives satisfactory results at low frequencies.[27]
2. A numerical procedure is adopted to determine the elements of the field matrix.

The determination of the field matrix for a pipeline having variable characteristics is equivalent to integrating the differential equation, Eq. 8.40. This may be done by the Runge-Kutta method[29] as follows.

The pipeline is divided into n reaches as shown in Fig. 8.10. First, the field matrix for each reach is computed, and then the field matrix for the pipe is

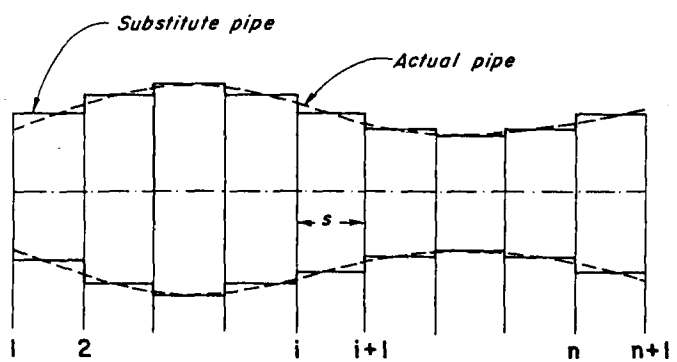

Figure 8.10. Actual and substitute pipe for a pipe having variable characteristics along its length.

determined by multiplying these matrices in a proper sequence. If the length of the reach between the sections i and $i+1$ is s, then the fourth-order Runge-Kutta method gives[29]

$$\mathbf{z}_{i+1} = \mathbf{z}_i + \tfrac{1}{6}(\mathbf{k}_0 + 2\mathbf{k}_1 + 2\mathbf{k}_2 + \mathbf{k}_3) \tag{8.42}$$

in which

$$\left.\begin{aligned} \mathbf{k}_0 &= s\mathbf{B}(x_i)\mathbf{z}_i \\ \mathbf{k}_1 &= s\mathbf{B}(x_i + s/2)(\mathbf{z}_i + \mathbf{k}_0/2) \\ \mathbf{k}_2 &= s\mathbf{B}(x_i + s/2)(\mathbf{z}_i + \mathbf{k}_1/2) \\ \mathbf{k}_3 &= s\mathbf{B}(x_{i+1})(\mathbf{z}_i + \mathbf{k}_2) \end{aligned}\right\} \tag{8.43}$$

in which $\mathbf{B}(x_i)$, $\mathbf{B}(x_{i+1})$, and $\mathbf{B}(x_i + s/2)$ are, respectively, the values of the matrix $\mathbf{B}(x)$ at section i, at $i+1$, and at the middle of sections i and $i+1$.

By substituting Eqs. 8.43 into Eq. 8.42, we obtain

$$\mathbf{z}_{i+1} = \mathbf{F}_{vc}\mathbf{z}_i \tag{8.44}$$

in which the field matrix for a pipe having variable characteristics along its length is

$$\begin{aligned} \mathbf{F}_{vc} = \mathbf{I} &+ \frac{s}{6}[\mathbf{B}(x_i) + 4\mathbf{B}(x_i + s/2) + \mathbf{B}(x_{i+1})] \\ &+ \frac{s^2}{6}[\mathbf{B}(x_i + s/2)\mathbf{B}(x_i) + \mathbf{B}(x_{i+1})\mathbf{B}(x_i + s/2) + \mathbf{B}^2(x_i + s/2)] \\ &+ \frac{s^3}{12}[\mathbf{B}^2(x_i + s/2)\mathbf{B}(x_i) + \mathbf{B}(x_{i+1})\mathbf{B}^2(x_i + s/2)] \\ &+ \frac{s^4}{24}[\mathbf{B}(x_{i+1})\mathbf{B}^2(x_i + s/2)\mathbf{B}(x_i)] \end{aligned} \tag{8.45}$$

in which I = identity or unit matrix.

Parallel System

Let there be n loops in parallel (Fig. 8.11) whose overall transfer matrices are

$$\mathbf{U}^{(m)} = \mathbf{F}_{n'_m}^{(m)}\mathbf{P}_{n'_m}^{(m)} \ldots \mathbf{P}_{2'_m}^{(m)}\mathbf{F}_{1'_m}^{(m)} \quad m = 1, 2, \ldots, n \tag{8.46}$$

The superscript in the parentheses refers to the number of the loop. The matrix $\mathbf{U}^{(m)}$ relates the state vectors at the $1'_m$st and at the $(n'_m + 1)$th section of the mth loop (see Fig. 8.11b), i.e.,

$$\mathbf{z}_{n'_m+1}^{(m)L} = \mathbf{U}^{(m)}\mathbf{z}_{1'_m}^{(m)R} \tag{8.47}$$

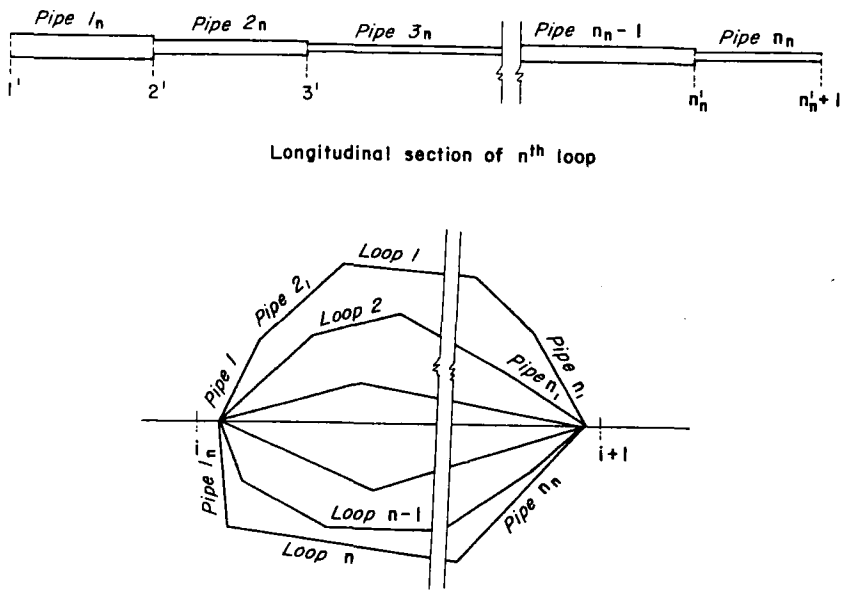

Figure 8.11. Parallel system.

A prime on the subscript denotes a section on the parallel loop.

The elements of the field matrix, $\mathbf{F}_p$, for the parallel loops relating the state vectors $\mathbf{z}_{i+1}^R$ and $\mathbf{z}_i^L$ (Fig. 8.11b) can be determined from the following equations:[22]

$$\left.\begin{aligned} f_{11} &= \frac{\xi}{\eta} \\ f_{12} &= \frac{\xi\zeta}{\eta} - \eta \\ f_{21} &= \frac{1}{\eta} \\ f_{22} &= \frac{\zeta}{\eta} \end{aligned}\right\} \tag{8.48}$$

in which

$$\left.\begin{aligned} \xi &= \sum_{m=1}^{n} \frac{u_{11}^{(m)}}{u_{21}^{(m)}} \\ \eta &= \sum_{m=1}^{n} \frac{1}{u_{21}^{(m)}} \\ \zeta &= \sum_{m=1}^{n} \frac{u_{22}^{(m)}}{u_{21}^{(m)}} \end{aligned}\right\} \tag{8.49}$$

In deriving the above expressions, use has been made of the relation that

$$|\mathbf{U}^{(m)}| = 1 \qquad m = 1, 2, \ldots, n \tag{8.50a}$$

i.e.,

$$u_{11}^{(m)} u_{22}^{(m)} - u_{12}^{(m)} u_{21}^{(m)} = 1 \qquad m = 1, 2, \ldots, n. \tag{8.50b}$$

Note that Eq. 8.48 is valid only if the elements of the overall transfer matrix for each parallel loop satisfy Eq. 8.50b. It is known from the theory of matrices that, for square matrices, the determinant of the product of matrices is equal to the product of the determinants of matrices. Hence, if $|\mathbf{P}_k^{(m)}| = 1$, $k = 2, 3, \ldots, n_m$, and $|\mathbf{F}_k^{(m)}| = 1, k = 1, 2, \ldots, n_m$, for $m = 1, 2, \ldots, n$, then $|\mathbf{U}^{(m)}| = 1$. It is clear from Eqs. 8.33 and 8.34 that $|\mathbf{F}| = 1$. Furthermore, the determinants of the point matrices for series junctions and for valves and orifices are also unity (see the point matrices derived in the following paragraphs). Thus, if there is a discontinuity other than a series junction, valve, or orifice in any of

the parallel loops, the determinant of the point matrix for the discontinuity should be checked to ensure that it has unit value before using Eq. 8.48.

Point Matrices

When there is a discontinuity in the geometry of the system at a section (e.g., series junction, orifice, valve, branch junction), we have to derive a point matrix relating the state vector to the left of the discontinuity with that to the right. This point matrix is required in the calculation of the overall transfer matrix for the system, which is then used to determine the resonant frequencies and/or frequency response of the system.

Point matrices for various boundary conditions usually found in hydropower and in water-supply schemes are derived in the following sections.

Series Junction

A junction of two pipes having different diameters (see Fig. 8.8), wall thicknesses, wall materials, or any combination of these variables is called a *series junction.*

It follows from the continuity equation that

$$q_i^R = q_i^L \tag{8.51}$$

In addition,

$$h_i^R = h_i^L \tag{8.52}$$

if the losses at the junction are neglected. These two equations can be expressed in the matrix notation as

$$\mathbf{z}_i^R = \mathbf{P}_{sc}\mathbf{z}_i^L \tag{8.53}$$

in which the point matrix for the series junction is

$$\mathbf{P}_{sc} = \begin{bmatrix} 1 & 0 \\ 0 & 1 \end{bmatrix} \tag{8.54}$$

Since $\mathbf{P}_{sc}$ is a unit matrix, it can be incorporated into the field matrix while doing the calculations.

Valves and Orifices

The point matrix for a valve or an orifice can be derived by linearizing the gate equation. This linearization does not introduce large errors if the pressure rise at

the valve is small as compared to the static head. For an oscillating valve, a sinusoidal valve motion is assumed. It is possible, however, to analyze nonsinusoidal periodic valve motions by this method. The periodic motion is decomposed into a set of harmonics by Fourier analysis,[2] and the system response is determined for each harmonic. The individual responses are then superimposed to determine the total response for the given valve motion (since all the equations are linear, the principle of superposition[2,16] can be applied).

Oscillating Valve Discharging into Atmosphere. The instantaneous and mean discharge through a valve (Fig. 8.12a) are given by the equations

$$Q_{n+1}^L = C_d A_v (2gH_{n+1}^L)^{1/2} \tag{8.55}$$

$$Q_o = (C_d A_v)_o (2gH_o)^{1/2} \tag{8.56}$$

in which C_d = coefficient of discharge, and A_v = area of the valve opening. Division of Eq. 8.55 by Eq. 8.56 yields

$$\frac{Q_{n+1}^L}{Q_o} = \frac{\tau}{\tau_o}\left(\frac{H_{n+1}^L}{H_o}\right)^{1/2} \tag{8.57}$$

in which the instantaneous relative gate opening $\tau = (C_d A_v)/(C_d A_v)_s$, and the mean relative gate opening $\tau_o = (C_d A_v)_o/(C_d A_v)_s$. The subscript s denotes steady-state reference, or index, values.

The relative gate opening may be considered to be made up of two parts, i.e.,

$$\tau = \tau_o + \tau^* \tag{8.58}$$

in which τ^* = deviation of the relative gate opening from the mean (Fig. 8.12b). Substitution of Eqs. 8.1, 8.2, and 8.58 into Eq. 8.57 yields

$$\left(1 + \frac{q_{n+1}^{*L}}{Q_o}\right) = \left(1 + \frac{\tau^*}{\tau_o}\right)\left(1 + \frac{h_{n+1}^{*L}}{H_o}\right)^{1/2} \tag{8.59}$$

If the valve motion is assumed sinusoidal, then

$$\tau^* = \mathrm{Re}\,(ke^{j\omega t}) \tag{8.60}$$

in which k = amplitude of valve motion. The phase angle between any other forcing function in the system and the oscillating valve can be taken into consideration by making k a complex number; otherwise, k is real.

By expanding Eq. 8.59, neglecting terms of higher order (this is valid only if $|h_{n+1}^{*L}| \ll H_o$), and substituting Eqs. 8.3, 8.4, and 8.60 into the resulting equation, we obtain

$$h_{n+1}^L = \frac{2H_o}{Q_o} q_{n+1}^L - \frac{2H_o k}{\tau_o} \tag{8.61}$$

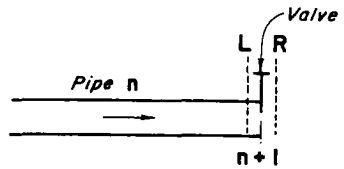

(a) Valve at downstream end of pipeline

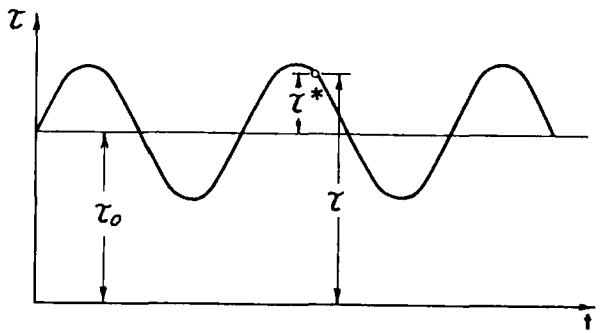

(b) Sinusoidal valve motion

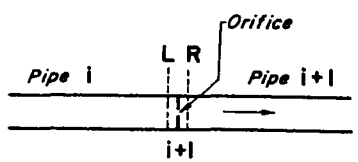

(c) Orifice at intermediate section

Figure 8.12. Valves.

Since $h^R_{n+1} = 0$, on the basis of Eq. 8.61, we can write

$$h^R_{n+1} = h^L_{n+1} + \frac{2H_o k}{\tau_o} - \frac{2H_o}{Q_o} q^L_{n+1} \tag{8.62}$$

In addition, from the continuity equation it follows that

$$q^R_{n+1} = q^L_{n+1} \tag{8.63}$$

Equations 8.62 and 8.63 may be expressed in the matrix notation as

$$\begin{Bmatrix} q \\ h \end{Bmatrix}^R_{n+1} = \begin{bmatrix} 1 & 0 \\ -\frac{2H_o}{Q_o} & 1 \end{bmatrix} \begin{Bmatrix} q \\ h \end{Bmatrix}^L_{n+1} + \begin{Bmatrix} 0 \\ \frac{2H_o k}{\tau_o} \end{Bmatrix} \tag{8.64}$$

The two matrix terms on the right-hand side may be combined as follows:

$$\begin{Bmatrix} q \\ h \\ 1 \end{Bmatrix}^R_{n+1} = \begin{bmatrix} 1 & 0 & 0 \\ -\frac{2H_o}{Q_o} & 1 & \frac{2H_o k}{\tau_o} \\ 0 & 0 & 1 \end{bmatrix} \begin{Bmatrix} q \\ h \\ 1 \end{Bmatrix}^L_{n+1} \tag{8.65}$$

Note that the expansion of Eq. 8.65 yields Eqs. 8.62 and 8.63, and 1 = 1. Thus, the additional element 1 in the column vector aids in writing the right-hand side of Eq. 8.64 in a compact form. As defined in Section 8.5 (Eq. 8.10), the column vector with 1 as an additional element is called an *extended-state vector*, $\mathbf{z}'$. The extended-state vectors and extended-transfer matrices are denoted by a prime.

On the basis of Eq. 8.10, Eq. 8.65 may be written as

$$\mathbf{z}'^R_{n+1} = \mathbf{P}'_{ov} \mathbf{z}'^L_{n+1} \tag{8.66}$$

in which $\mathbf{P}'_{ov}$ = the extended point matrix for an oscillating valve and is given by

$$\mathbf{P}'_{ov} = \begin{bmatrix} 1 & 0 & 0 \\ -\frac{2H_o}{Q_o} & 1 & \frac{2H_o k}{\tau_o} \\ 0 & 0 & 1 \end{bmatrix} \tag{8.67}$$

Valve Having Constant Gate Opening Discharging into Atmosphere. In this case, $k = 0$. Hence, Eq. 8.64 takes the form

$$\begin{Bmatrix} q \\ h \end{Bmatrix}^R_{n+1} = \begin{bmatrix} 1 & 0 \\ -\frac{2H_o}{Q_o} & 1 \end{bmatrix} \begin{Bmatrix} q \\ h \end{Bmatrix}^L_{n+1} \tag{8.68}$$

or

$$\mathbf{z}^R_{n+1} = \mathbf{P}_v \mathbf{z}^L_{n+1} \tag{8.69}$$

in which P_v = the point matrix for a valve or orifice discharging into atmosphere, and is given by

$$\mathbf{P}_v = \begin{bmatrix} 1 & 0 \\ -\dfrac{2H_o}{Q_o} & 1 \end{bmatrix} \tag{8.70}$$

Note that $\mathbf{P}_v$ is *not* an extended-point matrix.

If a valve of constant gate opening, or an orifice, is at an intermediate section (Fig. 8.12c) then Eq. 8.70 becomes

$$\mathbf{P}_{vi} = \begin{bmatrix} 1 & 0 \\ -\dfrac{2\Delta H_o}{Q_o} & 1 \end{bmatrix} \tag{8.71}$$

in which ΔH_o = the mean head loss across the valve corresponding to the mean discharge, Q_o.

Branch Pipelines

In the piping systems shown in Fig. 8.13a, pipeline *abc* is the main branch, and *bd* is the side branch. The transfer matrix for the pipeline *ab* can be computed

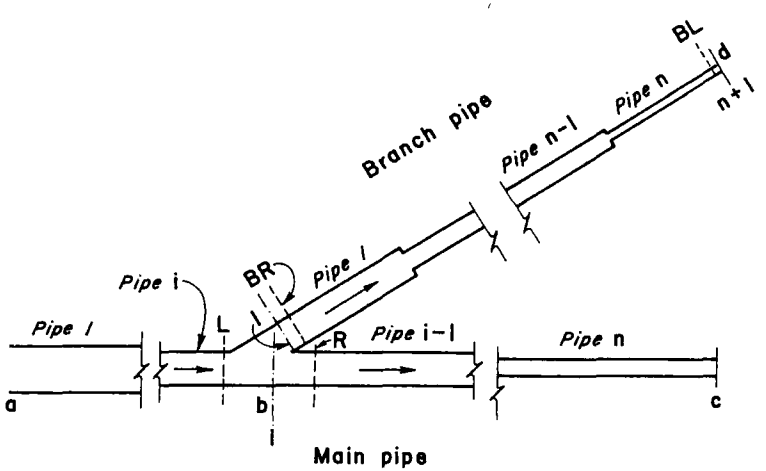

(a) Piping system

Figure 8.13. Branch system.

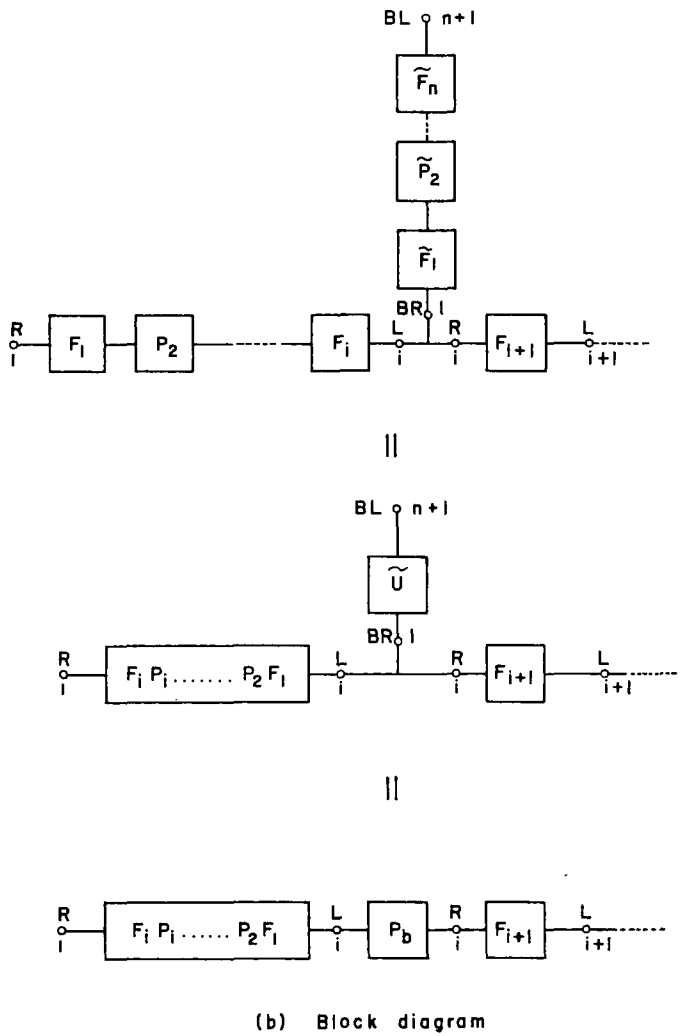

(b) Block diagram

Figure 8.13. (*Continued*)

by using the field and point matrices derived previously. To calculate the overall transfer matrix for *abc*, the point matrix at the junction *b*, relating the state vectors to the left and to the right of the junction, must be known. This matrix can be obtained if the boundary conditions at point *d* are specified.

Point matrices for the junction of the main and the branch having various boundary conditions are derived in this section.

Let $\tilde{\mathbf{U}}$ be the overall transfer matrix for the branch (refer to Fig. 8.13b), i.e.,

$$\tilde{\mathbf{z}}^L_{n+1} = \tilde{\mathbf{U}}\,\tilde{\mathbf{z}}^R_1 \tag{8.72}$$

or

$$\begin{Bmatrix} \tilde{q} \\ \tilde{h} \end{Bmatrix}^L_{n+1} = \begin{bmatrix} \tilde{u}_{11} & \tilde{u}_{12} \\ \tilde{u}_{21} & \tilde{u}_{22} \end{bmatrix} \begin{Bmatrix} \tilde{q} \\ \tilde{h} \end{Bmatrix}^R_1 \tag{8.73}$$

in which $\tilde{\mathbf{U}} = \tilde{\mathbf{F}}_n \tilde{\mathbf{P}}_n \ldots \tilde{\mathbf{P}}_3 \tilde{\mathbf{F}}_2 \tilde{\mathbf{P}}_2 \tilde{\mathbf{F}}_1$. The quantities relating to the branch are designated by a tilde (~).

Expansion of Eq. 8.73 yields

$$\tilde{q}^L_{n+1} = \tilde{u}_{11}\tilde{q}^R_1 + \tilde{u}_{12}\tilde{h}^R_1 \tag{8.74}$$

$$\tilde{h}^L_{n+1} = \tilde{u}_{21}\tilde{q}^R_1 + \tilde{u}_{22}\tilde{h}^R_1 \tag{8.75}$$

If the flow direction is assumed positive as shown in Fig. 8.13a and the losses at the junction are neglected, then the following equations can be written

$$q^L_i = q^R_i + \tilde{q}^R_1 \tag{8.76}$$

$$h^L_i = h^R_i = \tilde{h}^R_1 \tag{8.77}$$

By substituting appropriate boundary conditions into Eqs. 8.74 and 8.75 and making use of Eqs. 8.76 and 8.77, the point matrices at the junction of the main and the branch can be derived. The following examples illustrate the procedure.

Dead-End Branch. In this case, $\tilde{q}^L_{n+1} = 0$. Hence, it follows from Eqs. 8.74 and 8.77 that

$$\tilde{q}^R_1 = -\frac{\tilde{u}_{12}}{\tilde{u}_{11}}\,\tilde{h}^L_i\,. \tag{8.78}$$

Substitution of this equation into Eq. 8.76 yields

$$q^R_i = q^L_i + \frac{\tilde{u}_{12}}{\tilde{u}_{11}}\,h^L_i\,. \tag{8.79}$$

Equation 8.77 can be written as

$$h^R_i = 0\ q^L_i + h^L_i \tag{8.80}$$

Equations 8.79 and 8.80 can be expressed in the matrix notation as

$$\begin{Bmatrix} q \\ h \end{Bmatrix}^R_i = \begin{bmatrix} 1 & \dfrac{\tilde{u}_{12}}{\tilde{u}_{11}} \\ 0 & 1 \end{bmatrix} \begin{Bmatrix} q \\ h \end{Bmatrix}^L_i \tag{8.81}$$

or

$$\mathbf{z}^R_i = \mathbf{P}_{bde}\,\mathbf{z}^L_i \tag{8.82}$$

in which $\mathbf{P}_{bde}$ = the point matrix for the side branch with dead end and is given by

$$\mathbf{P}_{bde} = \begin{bmatrix} 1 & \dfrac{\tilde{u}_{12}}{\tilde{u}_{11}} \\ 0 & 1 \end{bmatrix} \tag{8.83}$$

Branch with Constant-Head Reservoir. In this case, $\tilde{h}^L_{n+1} = 0$. Hence, it follows from Eqs. 8.74 through 8.77 that

$$q^R_i = q^L_i + \frac{\tilde{u}_{22}}{\tilde{u}_{21}}\,h^L_i \tag{8.84}$$

Equations 8.84 and 8.80 can be expressed in the matrix notation as

$$\begin{Bmatrix} q \\ h \end{Bmatrix}^R_i = \begin{bmatrix} 1 & \dfrac{\tilde{u}_{22}}{\tilde{u}_{21}} \\ 0 & 1 \end{bmatrix} \begin{Bmatrix} q \\ h \end{Bmatrix}^L_i \tag{8.85}$$

or

$$\mathbf{z}^R_i = \mathbf{P}_{bres}\,\mathbf{z}^L_i \tag{8.86}$$

in which $\mathbf{P}_{bres}$ = the point matrix for the branch with constant-head reservoir and is given by

$$\mathbf{P}_{bres} = \begin{bmatrix} 1 & \dfrac{\tilde{u}_{22}}{\tilde{u}_{21}} \\ 0 & 1 \end{bmatrix} \tag{8.87}$$

Branch with Oscillating Valve at the Downstream End. If the frequency of the oscillating valve on the branch is the same as that of the forcing function on the main (these may not be in phase), the system can be analyzed by using the point matrix derived in this section. However, if the frequencies of the forcing functions are not the same, then the system is analyzed considering each forcing function at a time and the results are then superimposed to determine the total response.

Since an extended overall transfer matrix relating the state vector at the first and at the last section on the branch is required, the extended transfer matrices will also have to be used for the main. Let the extended overall transfer matrix

for the branch be

$$\tilde{\mathbf{U}}' = \begin{bmatrix} \tilde{u}_{11} & \tilde{u}_{12} & 0 \\ \tilde{u}_{21} & \tilde{u}_{22} & 0 \\ 0 & 0 & 1 \end{bmatrix} \tag{8.88}$$

In writing $\tilde{\mathbf{U}}'$ in Eq. 8.88, it is assumed that there is no other forcing function on the branch. If this is not the case, then at least one of the elements $\tilde{u}_{13}$, $\tilde{u}_{23}$, $\tilde{u}_{31}$, and $\tilde{u}_{32}$ is not equal to zero, and the point matrix derived in this section should be modified accordingly.

For the branch pipeline,

$$\tilde{\mathbf{z}}'^{R}_{n+1} = \tilde{\mathbf{P}}'_{ov}\tilde{\mathbf{z}}'^{L}_{n+1} \tag{8.89}$$

and

$$\tilde{\mathbf{z}}'^{L}_{n+1} = \tilde{\mathbf{U}}'\tilde{\mathbf{z}}'^{R}_{1} \tag{8.90}$$

By substituting $\tilde{\mathbf{P}}_{ov}$ from Eq. 8.67 and $\tilde{\mathbf{z}}^{L}_{n+1}$ from Eq. 8.90 into Eq. 8.89 and expanding the resulting equation, we obtain

$$\tilde{q}^{R}_{n+1} = \tilde{u}_{11}\tilde{q}^{R}_{1} + \tilde{u}_{12}\tilde{h}^{R}_{1} \tag{8.91}$$

$$\tilde{h}^{R}_{n+1} = \left(\tilde{u}_{21} - \frac{2\tilde{H}_o}{\tilde{Q}_o}\tilde{u}_{11}\right)\tilde{q}^{R}_{1} + \left(\tilde{u}_{22} - \frac{2\tilde{H}_o}{\tilde{Q}_o}\tilde{u}_{12}\right)\tilde{h}^{R}_{1} + \frac{2\tilde{H}_o\tilde{k}}{\tilde{\tau}_o} \tag{8.92}$$

All the notations defined in the previous sections apply except that the tilde (~) refers to the branch. For example, $\tilde{\tau}_o$ = the mean relative gate opening of the valve on the branch. Any phase shift between the valve on the branch and the forcing function on the main can be taken into consideration by making $\tilde{k}$ a complex number; otherwise, $\tilde{k}$ is real.

Since $\tilde{h}^{R}_{n+1} = 0$, and $\tilde{h}^{R}_{1} = h^{L}_{i}$, it follows from Eq. 8.92 that

$$\tilde{q}^{R}_{1} = -p_{12}h^{L}_{i} - p_{13} \tag{8.93}$$

in which

$$p_{12} = \frac{\tilde{u}_{22} - \dfrac{2\tilde{H}_o\tilde{u}_{12}}{\tilde{Q}_o}}{\tilde{u}_{21} - \dfrac{2\tilde{H}_o\tilde{u}_{11}}{\tilde{Q}_o}} \tag{8.94}$$

and

$$p_{13} = \frac{2\tilde{H}_o\tilde{k}/\tilde{\tau}_o}{\tilde{u}_{21} - \dfrac{2\tilde{H}_o\tilde{u}_{11}}{\tilde{Q}_o}} \tag{8.95}$$

By substituting $\tilde{q}^{R}_{1}$ from Eq. 8.93 into Eq. 8.76, we obtain

$$q^{R}_{i} = q^{L}_{i} + p_{12}h^{L}_{i} + p_{13} \tag{8.96}$$

Moreover, we can write

$$1 = 0\ q^{L}_{i} + 0\ h^{L}_{i} + 1 \tag{8.97}$$

Equations 8.80, 8.96, and 8.97 can be expressed in the matrix notation as

$$\begin{Bmatrix} q \\ h \\ 1 \end{Bmatrix}^{R}_{i} = \begin{bmatrix} 1 & p_{12} & p_{13} \\ 0 & 1 & 0 \\ 0 & 0 & 1 \end{bmatrix} \begin{Bmatrix} q \\ h \\ 1 \end{Bmatrix}^{L}_{i} \tag{8.98}$$

or

$$\mathbf{z}'^{R}_{i} = \mathbf{P}'_{bov}\mathbf{z}'^{L}_{i} \tag{8.99}$$

in which $\mathbf{P}'_{bov}$ = the transfer matrix at the junction of the side branch having an oscillating valve and is given by

$$\mathbf{P}'_{bov} = \begin{bmatrix} 1 & p_{12} & p_{13} \\ 0 & 1 & 0 \\ 0 & 0 & 1 \end{bmatrix} \tag{8.100}$$

If there is an orifice, or a valve having constant-gate opening at the downstream end of the branch, then $k = 0$. Hence, $p_{13} = 0$, and the point matrix for the branch can be written as

$$\mathbf{P}_{borf} = \begin{bmatrix} 1 & p_{12} \\ 0 & 1 \end{bmatrix} \tag{8.101}$$

Note that this is not an extended-point matrix.

8.8 FREQUENCY RESPONSE

The transfer matrix method can be used to determine the frequency response of a system having one or more periodic forcing functions. The equations derived in this section can be directly used if the forcing functions are sinusoidal. Nonharmonic periodic functions are decomposed into different harmonics by Fourier analysis.[2] By considering each harmonic at its particular frequency, the system response is determined, and the results are then superimposed to determine the total response.

Systems having more than one exciter may be analyzed as follows: If all exciters have the same frequency, then the system oscillates at this particular frequency. To analyze such a system, the extended transfer matrices are used,

which allows all the exciters to be considered simultaneously. The concept of extending the matrices facilitates the development of a point matrix, which includes the effect of the forcing function. If, however, the forcing functions have different frequencies, then the system response for each forcing function has to be determined separately, and the concept of extended transfer matrices becomes invalid. The following explanation will further clarify this point. Systems having more than one exciter can be classified into three categories as shown in Fig. 8.14. The system of Fig. 8.14a can be analyzed considering all the exciters simultaneously by using the extended transfer matrices with frequency ω_1. For the system of Fig. 8.14b, the exciters are divided into groups, with each group comprised of exciters that have the same frequency. Considering one group of exciters at a time, the system is analyzed by using the extended-transfer matrices with the frequency of the group. The results are then superimposed to determine the total response of the system. For the system of Fig. 8.14c, the system response for each exciter is determined separately, and the total response is then

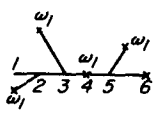

(a) All exciters have same frequency

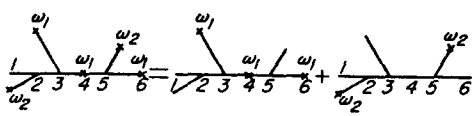

(b) Exciters divided into two groups, according to frequency

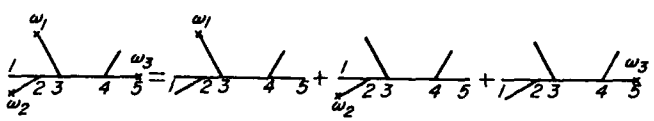

(c) Each exciter has a different frequency

Figure 8.14. Systems having more than one exciter.

calculated by superposition. As in this case only one forcing function is considered at a time, and ordinary transfer matrices (i.e., 2 X 2) are used.

Expressions to determine the frequency response of typical piping systems for the following exciters are derived in this section: fluctuating pressure head, oscillating valve, and fluctuating discharge. By proceeding in a similar manner, expression for other exciters can be derived.

Fluctuating Pressure Head

Consider the system shown in Fig. 8.15, which has a dead end at the right end. A wave on the surface of the reservoir produces pressure oscillations in the system. Due to the wave, the pressure head at section 1 fluctuates sinusoidally about the mean-pressure head. Let this pressure-head variation be given by

$$h_1^{*R} = \mathrm{Re}\,(h_1^R e^{j\omega t}) = K\cos\omega t = \mathrm{Re}\,(Ke^{j\omega t}) \tag{8.102}$$

and let **U** be the transfer matrix relating the state vectors at the 1st and $(n+1)$th section, i.e.,

$$\mathbf{z}_{n+1}^L = \mathbf{U}\mathbf{z}_1^R \tag{8.103}$$

It is assumed that there is no other forcing function in the system; otherwise, an extended-transfer matrix, $\mathbf{U}'$, will have to be used. Expansion of Eq. 8.103 yields

$$q_{n+1}^L = u_{11}\,q_1^R + u_{12}\,h_1^R \tag{8.104}$$

$$h_{n+1}^L = u_{21}\,q_1^R + u_{22}\,h_1^R \tag{8.105}$$

Since $q_{n+1}^L = 0$ (dead end), it follows from Eq. 8.104 that

$$q_1^R = -\frac{u_{12}}{u_{11}}\,h_1^R \tag{8.106}$$

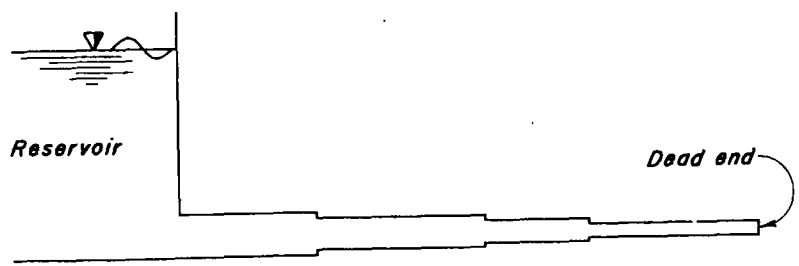

Figure 8.15. Series system with dead end.

which on the basis of Eq. 8.102 becomes

$$q_1^R = -\frac{u_{12}K}{u_{11}} \tag{8.107}$$

Substitution of Eq. 8.107 into Eq. 8.105 and simplification of the resulting equation gives

$$h_{n+1}^L = \left(u_{22} - \frac{u_{12}u_{21}}{u_{11}}\right)K \tag{8.108}$$

Hence, the amplitude of the pressure-head fluctuation at the dead end is

$$h_a = |h_{n+1}^L| = \left|\left(u_{22} - \frac{u_{12}u_{21}}{u_{11}}\right)K\right| \tag{8.109}$$

The amplitude of the pressure head at the dead end may be nondimensionalized by dividing the amplitude of the pressure fluctuations at the reservoir end, i.e.,

$$h_r = \left|\frac{h_a}{K}\right| = \left|u_{22} - \frac{u_{12}u_{21}}{u_{11}}\right| \tag{8.110}$$

Fluctuating Discharge

Flows are periodic on the suction and on the discharge side of a reciprocating pump. These fluctuations can be decomposed into a set of harmonics. Severe pressure oscillations may develop if any of these harmonics has a period equal to one of the natural periods of either the suction or discharge pipeline.

Expressions are derived below to determine, by the transfer matrix method, the frequency response of systems having a reciprocating pump. The suction and the discharge pipeline may have stepwise changes in diameter and/or wall thickness and may have branches with reservoirs, dead ends, or orifices.

Suction Line

Let the transfer matrix relating the state vectors at the 1st and $(n+1)$th section of the suction line (Fig. 8.16) be **U**, i.e.,

$$\mathbf{z}_{n+1}^L = \mathbf{U}\mathbf{z}_1^R \tag{8.111}$$

By expanding Eq. 8.111 and noting that $h_1^R = 0$, we obtain

$$q_{n+1}^L = u_{11}\,q_1^R \tag{8.112}$$

and

$$h_{n+1}^L = u_{21}\,q_1^R \tag{8.113}$$

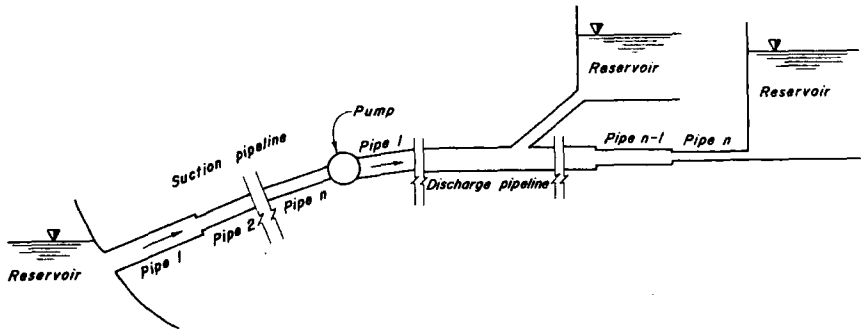

Figure 8.16. Suction and discharge pipelines.

Hence,

$$h_{n+1}^L = \frac{u_{21}}{u_{11}}\,q_{n+1}^L \tag{8.114}$$

The inflow-versus-time curve for one period can be decomposed into a set of harmonics by Fourier analysis.[2] Let the discharge for the mth harmonic be

$$q_{n+1}^{*L} = A'_m \sin(m\omega t + \psi_m) \tag{8.115}$$

or

$$q_{n+1}^{*L} = \mathrm{Re}\,(A_m e^{j\,m\omega t}) \tag{8.116}$$

in which $A_m = A'_m \exp[j(\psi_m - \frac{1}{2}\pi)]$; A'_m and ψ_m are the amplitude and the phase angle, respectively, for the mth harmonic; and ω = frequency of the fundamental. It follows from Eqs. 8.3 and 8.116 that $q_{n+1}^L = A_m$ in which A_m is a complex constant. Substitution of this relationship into Eq. 8.114 yields

$$h_{n+1}^L = \frac{u_{21}}{u_{11}}A_m \tag{8.117}$$

Hence, the amplitude of pressure-head fluctuation at the suction flange is

$$h_m = |h_{n+1}^L|_m = \left|\frac{u_{21}A_m}{u_{11}}\right| \tag{8.118}$$

and the phase angle for the pressure head is

$$\phi_m = \tan^{-1}\left[\frac{\mathrm{Im}(h_{n+1}^L)_m}{\mathrm{Re}(h_{n+1}^L)_m}\right] \tag{8.119}$$

The head-versus-time curve may be obtained by vectorially adding the head-versus-time curve for each harmonic. For the mth harmonic,

$$h_{n+1}^{*L} = \mathrm{Re}\,[h_m e^{j(m\omega t+\phi_m)}] \tag{8.120}$$

or

$$h^{*L}_{n+1} = h_m \cos(m\omega t + \phi_m) \tag{8.121}$$

Hence, the pressure-head-versus-time curve may be computed from the equation

$$h^{*L}_{n+1} = \sum_{m=1}^{M} h_m \cos(m\omega t + \phi_m) \tag{8.122}$$

in which M = number of harmonics into which the inflow-versus-time curve for the pump is decomposed.

Discharge Line

By proceeding in a similar manner and noting that $h^L_{n+1} = 0$, the following equation is obtained for the pressure-head-versus-time curve at the discharge side of the pump:

$$h^{*R}_1 = \sum_{m=1}^{M} h'_m \cos(m\omega t + \phi'_m) \tag{8.123}$$

in which

$$h'_m = |(h^R_1)_m| = \frac{|u_{21} A_m|}{|u_{12}u_{21} - u_{11}u_{22}|} \tag{8.124}$$

$$\phi'_m = \tan^{-1}\left[\frac{\mathrm{Im}(h^R_m)}{\mathrm{Re}(h^R_m)}\right] \tag{8.125}$$

and A_m = complex amplitude of mth harmonic of the discharge-time curve of the pump.

Oscillating Valve

In oscillating valves, the area of the opening of the gate or valve is varied periodically. Since the gate equation (Eq. 8.55) relating the head, discharge, and the gate area is nonlinear, this case is more difficult to analyze than the preceding ones. However, as discussed in Section 8.7, this equation can be linearized if $h \ll H_o$. In the derivation of expressions in this section, the point matrix of Eq. 8.67 is used. This matrix is derived by assuming the valve movement as sinusoidal and by linearizing the gate equation. Thus, to use the expression derived herein for the nonharmonic periodic valve movements, the valve motion is decomposed into a set of harmonics by Fourier analysis, the system response is determined considering each harmonic at its frequency, and then the total system response is calculated by superimposing the individual responses.

Let $\mathbf{U}'$ be the extended overall transfer matrix relating the state vectors at the

1st and the $(n+1)$th section of the system, i.e.,

$$\mathbf{z}'^L_{n+1} = \mathbf{U}'\mathbf{z}'^R_1 \tag{8.126}$$

In addition,

$$\mathbf{z}'^R_{n+1} = \mathbf{P}'_{ov}\mathbf{z}'^L_{n+1} \tag{8.127}$$

Hence,

$$\mathbf{z}'^R_{n+1} = \mathbf{P}'_{ov}\mathbf{U}'\mathbf{z}'^R_1 \tag{8.128}$$

By substituting $\mathbf{P}'_{ov}$ from Eq. 8.67; multiplying the matrices $\mathbf{P}'_{ov}$ and $\mathbf{U}'$; and expanding and noting that $h^R_1 = 0, h^R_{n+1} = 0$, and $q^L_{n+1} = q^R_{n+1}$; we obtain

$$q^R_1 = -\frac{u_{23} - \dfrac{2H_o}{Q_o}u_{13} + \dfrac{2H_o k}{\tau_o}u_{33}}{u_{21} - \dfrac{2H_o}{Q_o}u_{11} + \dfrac{2H_o k}{\tau_o}u_{13}} \tag{8.129}$$

$$q^L_{n+1} = u_{11}q^R_1 + u_{13} \tag{8.130}$$

in which $u_{11}, u_{12}, \ldots, u_{33}$ are the elements of the matrix, $\mathbf{U}'$. By expanding Eq. 8.126 and noting that $h^R_1 = 0$, we obtain

$$h^L_{n+1} = u_{21}q^R_1 + u_{23} \tag{8.131}$$

To determine the frequency response, the extended field and point matrices are first computed. Then, the extended overall transfer matrix is determined by multiplying the field and point matrices starting at the downstream end, i.e.,

$$\mathbf{U}' = \mathbf{F}'_n\mathbf{P}'_n \ldots \mathbf{P}'_2\mathbf{F}'_1 \tag{8.132}$$

The value of q^R_1 is determined from Eq. 8.129, and q^L_{n+1} and h^L_{n+1} are computed from Eqs. 8.130 and 8.131. The absolute values of h^L_{n+1} and q^L_{n+1} are the amplitudes of pressure head and discharge fluctuations at the valve, and their arguments are, respectively, the phase angles between head and τ^* and between discharge and τ^*.

If there is no other forcing function except the oscillating valve at the downstream end of the system, ordinary field and point matrices may be used instead of the extended ones. In this case, $u_{13} = u_{23} = u_{31} = 0$ and $u_{33} = 1$ in Eqs. 8.129 through 8.131.

Procedure for Determining the Frequency Response

The frequency response of piping systems may be determined as follows:

1. Draw the block diagram and then the simplified block diagram for the system. In the case of simple systems, this step may be omitted.

2. If the forcing function is nonharmonic, decompose it into a set of harmonics by Fourier analysis, and consider one harmonic at a time. For the specified frequency, compute the point and field matrices. To write an extended transfer matrix, simply add the following elements to the ordinary transfer matrix derived in Section 8.7: $u_{13} = u_{23} = u_{31} = u_{32} = 0$ and $u_{33} = 1$. Note that extended transfer matrices are used only if there is more than one forcing function in the system and each has the same frequency.

3. Calculate the overall transfer matrix by an ordered multiplication of the point and field matrices, starting at the downstream end. For this calculation, the block diagram of step 1 is very helpful. For multiplication of matrices, the scheme outlined in Example 8.2 may be followed if the calculations are being done by hand, slide rule, or desk calculator. This scheme reduces the amount of computations.

4. Use the expressions developed in this section to determine the frequency response.

5. If a frequency-response diagram is to be plotted, repeat steps 3 and 4 by taking different frequencies.

The following example illustrates the preceding procedure for determining the frequency response at the valve end of a branch system having an oscillating valve at the downstream end.

Example 8.2

Plot a frequency-response diagram for the valve end of the branch system shown in Fig. 8.17a and for the following data:

$$Q_o = 0.314 \text{ m}^3/\text{s} \qquad T_{th} = 3.0 \text{ s}$$
$$R = 0.0 \qquad k = 0.2$$
$$\tau_o = 1.0 \qquad H_o = 100 \text{ m}$$

Do the calculations by using a slide rule or a desk calculator.

Computations for $\omega_r = 2.0$ are summarized in the following. By taking different values of ω_r and proceeding similarly as for $\omega_r = 2.0$, the frequency-response diagram shown in Fig. 8.17c can be plotted.

Components of Transfer Matrices

from 18.6) $\omega_{th} = 2\pi/3 = 2.094$ rad/s

$\omega = \omega_r \omega_{th} = 2 \times 2.094 = 4.189$ rad/s

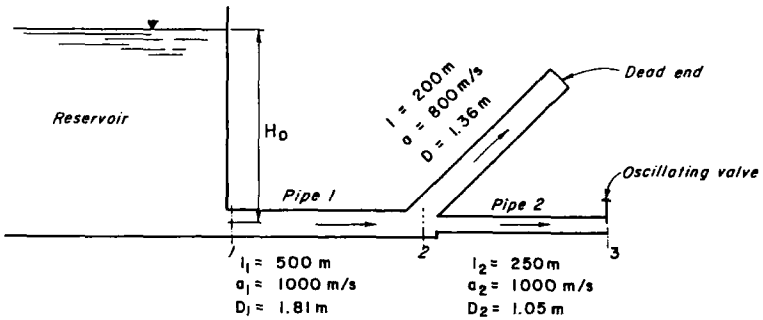

(a) Piping system

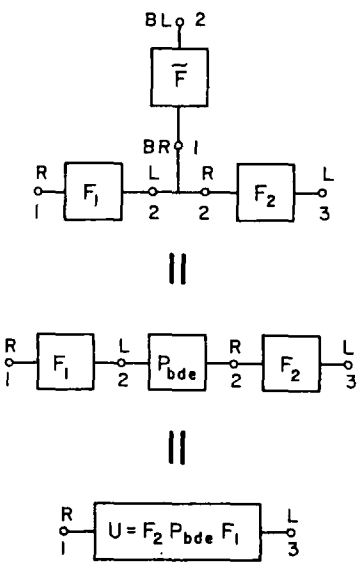

(b) Block diagram

Figure 8.17. Frequency response of a branch piping system. Branch with dead end.

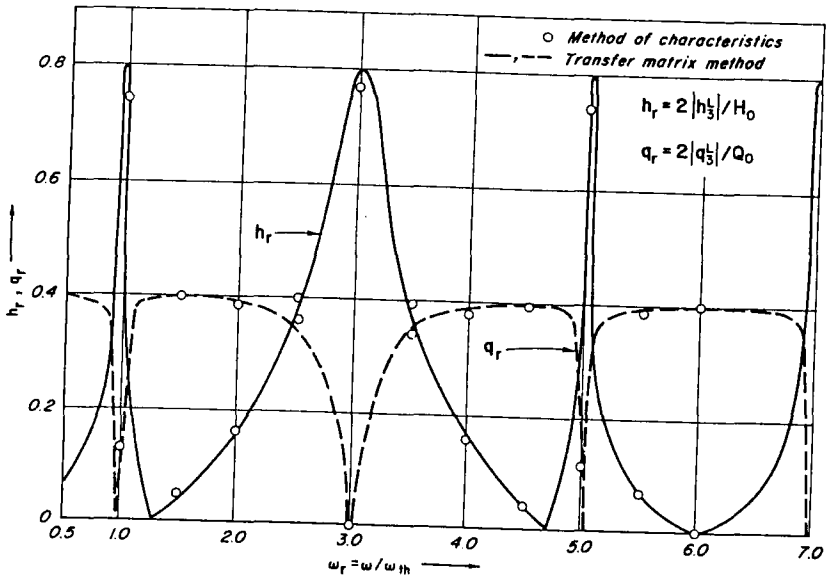

(c) Frequency response diagram

Figure 8.17. (*Continued*)

Pipe 1:

$$b_1 = l_1/a_1 = 500/1000 = 0.5 \text{ s}$$
$$A_1 = \pi D_1^2/4 = \pi(1.81)^2/4 = 2.578 \text{ m}^2$$
$$C_1 = a_1/(gA_1) = 1000/(9.81 \times 2.578) = 39.542 \text{ s m}^{-2}$$

Substitution of these values into Eq. 8.34 yields

$$f_{11} = f_{22} = \cos(0.5 \times 4.189) = -0.5$$
$$f_{21} = -39.542 \sin(0.5 \times 4.189)\, j = -34.244j$$
$$f_{12} = -j \sin(0.5 \times 4.189)/39.542 = -0.022j$$

Proceeding in a similar manner, the following field matrix, $\mathbf{F}_2$, for pipe 2 is obtained:

$$\mathbf{F}_2 = \begin{bmatrix} 0.500 & -0.007j \\ -102.732j & 0.500 \end{bmatrix}$$

Branch pipe:

Since the branch pipe is made up of a single pipe, $\tilde{\mathbf{U}} = \tilde{\mathbf{F}}$.

Proceeding similarly, the following values of the elements of the field matrix for the branch are obtained:

$$\tilde{u}_{11} = 0.5$$
$$\tilde{u}_{12} = -0.0154j$$

Substitution of these values into Eq. 8.83 yields the following point matrix for the junction of the branch and the main:

$$\mathbf{P}_{bde} = \begin{bmatrix} 1.0 & -0.0308j \\ 0.0 & 1.0 \end{bmatrix}$$

It is clear from the block diagram shown in Fig. 8.17b that

$$\mathbf{U} = \mathbf{F}_2 \mathbf{P}_{bde} \mathbf{F}_1$$

These matrices may be multiplied in a schematic manner as shown in Table 8.1. Since $h_1^R = 0$ (constant-head reservoir), the second column in the matrices $\mathbf{F}_1$, $\mathbf{P}_{bde}\mathbf{F}_1$, and $\mathbf{F}_2\mathbf{P}_{bde}\mathbf{F}_1$ is multiplied by zero. Thus, the elements in the second column of these matrices are unnecessary and therefore may be dropped. The unnecessary elements in Table 8.1 are indicated by a horizontal dash.

Note that ordinary transfer matrices have been used because there is only one forcing function. Hence, u_{13}, u_{23}, and u_{31} are zero, and u_{33} is unity in Eqs. 8.129 through 8.131. Substitution of these values and those for u_{11} and u_{21} calculated in Table 8.1 into Eq. 8.129 yields

$$q_1^R = -0.584 + 0.0127j$$

Hence, it follows from Eqs. 8.130 and 8.131 that

$$q_3^L = 0.0600 - 0.0131j$$

Table 8.1. Scheme for multiplication of transfer matrices.

	$\begin{bmatrix} -0.500 & - \\ -34.244j & - \end{bmatrix}$	$\begin{Bmatrix} q \\ 0 \end{Bmatrix}_1^R = z_2^L$
$\mathbf{P}_{bde}\begin{bmatrix} 1.000 & -0.031j \\ 0.000 & 1.000 \end{bmatrix}$	$\begin{bmatrix} -1.555 & - \\ -34.244j & - \end{bmatrix}$	$\begin{Bmatrix} q \\ h \end{Bmatrix}_1^R = z_2^R$
$\mathbf{F}_2\begin{bmatrix} 0.500 & -0.0073j \\ -102.732j & 0.500 \end{bmatrix}$	$\begin{bmatrix} -1.0273 & - \\ 142.595j & - \end{bmatrix}$	$\begin{Bmatrix} q \\ h \end{Bmatrix}_1^R = z_3^L$

and

$$h_3^L = -1.8134 - 8.3215j$$

Hence,

$$h_r = 2\,|h_3^L|/H_o = 0.170$$
$$q_r = 2\,|q_3^L|/Q_o = 0.390$$

The phase angle between the pressure head and the relative gate opening

$$= \tan^{-1}\left[\frac{-8.3215}{-1.8134}\right]$$
$$= -102.29^\circ$$

The phase angle between the discharge and the relative gate opening

$$= \tan^{-1}\left[\frac{-0.0131}{0.0600}\right]$$
$$= -12.29^\circ$$

8.9 PRESSURE AND DISCHARGE VARIATION ALONG A PIPELINE

The previous sections dealt with the determination of the pressure and discharge oscillations at the end sections of a system. However, sometimes it is necessary to determine the amplitudes of the discharge and pressure fluctuations along the length of the pipeline. In this section, a procedure to determine the amplitudes of the discharge and pressure fluctuations along the length of the pipeline is outlined.

To analyze a piping system, two of the four quantities—discharge and pressure or their relationship at either end of the system—must be known. The other two quantities can then be calculated by using the equations derived in the last section. The amplitudes of the discharge and pressure fluctuations at the upstream end being known, their amplitudes along the pipeline may then be determined. The procedure is illustrated by discussing a system that has a reservoir at the upstream end and an oscillating valve at the downstream end. Similarly, equations for other systems having different boundary conditions can be developed.

Suppose that the amplitudes of the discharge and pressure oscillations at the kth section on the ith pipe (see Fig. 8.18a) are to be determined. Let the transfer matrix relating the state vectors at the first section of the first pipe and the first section of the ith pipe be designated by $\mathbf{W}$, i.e.,

$$(\mathbf{z}_1^R)_i = \mathbf{W}(\mathbf{z}_1^R)_1 \tag{8.133}$$

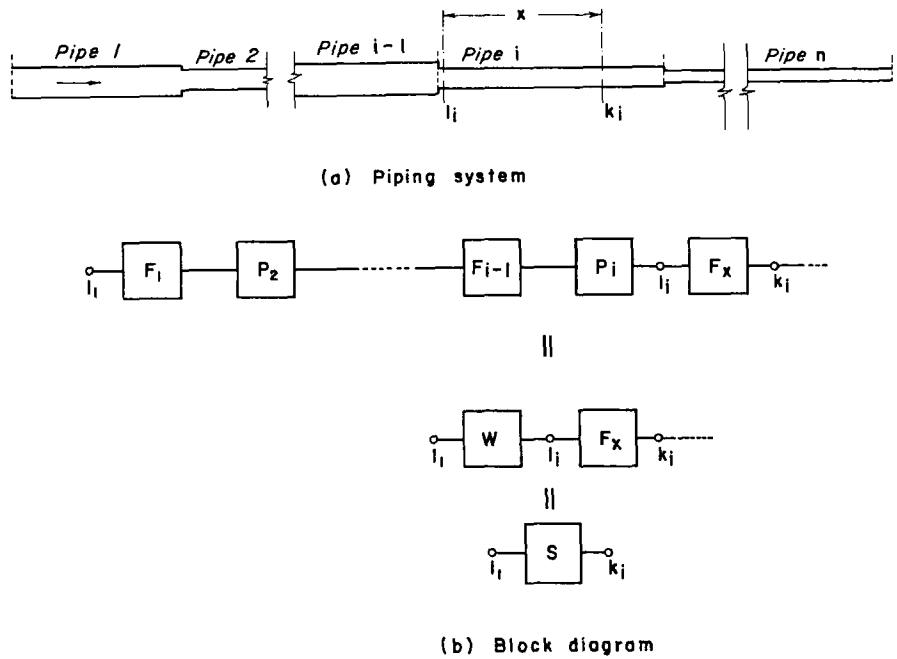

Figure 8.18. Designation of kth section on ith pipe.

and the field matrix relating the state vectors at the first and the kth section of the ith pipe by $\mathbf{F}_x$, i.e.,

$$(\mathbf{z}_k^L)_i = \mathbf{F}_x(\mathbf{z}_1^R)_i \tag{8.134}$$

In these equations, the subscript within the parentheses refers to the pipe number. The matrix $\mathbf{W}$ is computed by multiplying the point and field matrices for the first $(i-1)$ pipes (see the block diagram of Fig. 8.18b), i.e.,

$$\mathbf{W} = \mathbf{P}_i\mathbf{F}_{i-1}\mathbf{P}_{i-1}\ \ldots\ \mathbf{F}_1 \tag{8.135}$$

and the matrix $\mathbf{F}_x$ is calculated by replacing l with x in Eq. 8.33. Note that the elements of the matrix $\mathbf{W}$ for a specified frequency are constants, while those of the matrix $\mathbf{F}_x$ depend upon the value of x as well.

It follows from Eqs. 8.133 and 8.134 that

$$(\mathbf{z}_k^L)_i = \mathbf{S}(\mathbf{z}_1^R)_1 \tag{8.136}$$

in which

$$\mathbf{S} = \mathbf{F}_x\mathbf{W} = \mathbf{F}_x\mathbf{P}_i\mathbf{F}_{i-1}\mathbf{P}_{i-1}\ \ldots\ \mathbf{F}_1 \tag{8.137}$$

The value of $(q_1^R)_1$ is calculated from Eq. 8.129. Furthermore, it is known that $(h_1^R)_1 = 0$. Substitution of these values into the expanded form of Eq. 8.136 yields

$$(q_k^L)_i = s_{11}(q_1^R)_1 \tag{8.138}$$

and

$$(h_k^L)_i = s_{21}(q_1^R)_1 \tag{8.139}$$

The amplitudes of the discharge and pressure fluctuations at any other section can be determined by proceeding in a similar manner.

8.10 LOCATION OF PRESSURE NODES AND ANTINODES

The location of pressure nodes and antinodes is an important aspect of the analysis of resonance in pipelines at higher harmonics. The amplitude of the pressure fluctuation is a minimum at a node and a maximum at an antinode. For a frictionless system, the amplitude of the pressure fluctuation at a node is zero.

The pipelines may be subjected to severe pressure fluctuations at the antinodes. Thus, the pipe may burst due to pressure in excess of the design pressure or may collapse due to subatmospheric pressure. A surge tank becomes inoperative in preventing the transmission of pressure waves upstream of the tank if a node is formed at its base. Jaeger explained the development of fissures in the Kandergrund tunnel[30,31] due to the establishment of a pressure node at the tank, which made the tank inoperative although it was overdesigned.

The locations of the nodes and antinodes may be determined as follows:

Equation 8.139 gives the amplitude of the pressure fluctuation at a point. By making use of the fact that for a frictionless system, the amplitude of the pressure fluctuations at a node is zero and $q_1^R \neq 0$ for nontrivial solutions, we obtain

$$s_{21}(x) = 0 \tag{8.140}$$

The solution of this equation for x gives the location of the nodes on the ith pipe.

The amplitude of the pressure fluctuation is a maximum at the antinodes. The location of these points may be determined by differentiating Eq. 8.140 with respect to x, equating the result to zero, and then solving for x, i.e., the roots of the equation

$$\frac{d}{dx} s_{21}(x) = 0 \tag{8.141}$$

give the location of the antinodes.

By making use of Eqs. 8.140 and 8.141, expressions for the location of nodes and antinodes in simple systems can be derived. The procedure is illustrated in the following by deriving expressions for a single pipe and for two pipes in series. Expressions for other systems may be derived in a similar manner. However, for complex systems, it is better to solve Eq. 8.140 and 8.141 numerically rather than to derive the expressions and then solve them.

On the basis of Eq. 8.34, for a frictionless single pipeline having constant cross-sectional area, Eq. 8.140 becomes

$$-jC_1 \sin(\omega x/a_i) = 0 \tag{8.142}$$

or

$$\sin(\omega x/a_i) = 0 \tag{8.143}$$

whose solution gives

$$x = n\pi a_i/\omega \quad (n = 0, 1, 2, \ldots.) \tag{8.144}$$

The values of $x > l_i$ represent the locations of the imaginary nodes, which are discarded. It follows from Eqs. 8.141 and 8.143 that

$$\cos(\omega x/a_i) = 0 \tag{8.145}$$

The solution of this equation gives the locations of the antinodes, i.e.,

$$x = (n + \tfrac{1}{2})\pi a_i/\omega \quad (n = 0, 1, 2, \ldots.) \tag{8.146}$$

Again, the values of $x > l_i$ are the locations of the imaginary nodes and are discarded.

Equations 8.143 and 8.145 show that a standing wave is formed along the length of the pipeline.

Series System

In a series system having two pipes (Fig. 8.7), the locations of nodes and antinodes in the pipe leading from the reservoir are given by Eqs. 8.143 and 8.145. However, their location in the second pipe can be determined by using Eqs. 8.140 and 8.141.

By substituting the expressions for $\mathbf{F}_x$, $\mathbf{F}_1$, and $\mathbf{P}_2$ into Eq. 8.135, multiplying the matrices, and using Eq. 8.140, we obtain

$$-C_2 \sin\left(\frac{\omega x}{a_2}\right)\cos\left(\frac{\omega l_1}{a_1}\right) - C_1 \cos\left(\frac{\omega x}{a_2}\right) \sin\left(\frac{\omega l_1}{a_1}\right) = 0 \tag{8.147}$$

which upon simplification becomes

$$\tan \frac{\omega x}{a_2} = - \frac{a_1 A_2}{a_2 A_1} \tan \frac{\omega l_1}{a_1} \tag{8.148}$$

Note that Eqs. 8.147 and 8.148 are valid for a frictionless system only. Solution of Eq. 8.148 for x gives the location of the nodes.

8.11 DETERMINATION OF RESONANT FREQUENCIES

To reduce the possibility of resonance in piping systems, it is important to know their resonant frequencies so that possible forcing functions or exciters having similar frequencies can be avoided. However, if it is not possible to avoid these frequencies, then remedial measures can be taken. As the forcing function is usually unknown in the case of self-excited systems, the frequency response of the system cannot be determined. For the investigation of such systems, resonant frequencies can be calculated using the procedure presented by Zielke and Rösl[32] or by using the transfer matrix method[33] as follows.

The transfer matrices for the system components are written for the free-damped oscillations. This is done by replacing $j\omega$ by the complex frequency $s = \sigma + j\omega$ in the transfer matrices presented in Section 8.7. By multiplying these matrices, the overall-transfer matrix is obtained. Then, applying the free-end conditions (e.g., constant-head reservoirs, dead ends, orifices), two homogeneous equations in two unknowns are obtained. For a nontrivial solution, the determinant of the coefficients of these equations should be zero. A trial-and-error technique is used to solve the determinant equation to determine the resonant frequencies of the system.

The following example of a dead-end system having a constant-head reservoir at the upper end is presented for illustration purposes:

Let U be the overall transfer matrix for the system, i.e.,

$$z_{n+1}^R = \mathbf{U}\, z_1^R \tag{8.149}$$

By substituting the free-end conditions, i.e., $h_1^R = 0$ and $q_{n+1}^L = 0$, Eq. 8.149 becomes

$$u_{11} q_1^R = 0 \tag{8.150}$$

Note that u_{11} and q_1^R are complex variables. By using the superscripts r and i to represent the real and imaginary parts of a complex variable, i.e., $u_{11} = u_{11}^r + j u_{11}^i$ and simplifying, Eq. 8.150 takes the form

$$(u_{11}^r q_1^{rR} - u_{11}^i q_1^{iR}) + j(u_{11}^i q_1^{rR} + u_{11}^r q_1^{iR}) = 0 \tag{8.151}$$

For a complex number to be zero, the real and imaginary parts must be zero.

Hence,

$$u_{11}^r q_1^{rR} - u_{11}^i q_1^{iR} = 0 \tag{8.152}$$

$$u_{11}^i q_1^{rR} + u_{11}^r q_1^{iR} = 0 \tag{8.153}$$

For a nontrivial solution of Eqs. 8.152 and 8.153,

$$\begin{vmatrix} u_{11}^r & -u_{11}^i \\ u_{11}^i & u_{11}^r \end{vmatrix} = 0 \tag{8.154}$$

which upon simplification becomes

$$(u_{11}^r)^2 + (u_{11}^i)^2 = 0 \tag{8.155}$$

Equation 8.155 can be satisfied if and only if

$$u_{11}^r = 0 \tag{8.156}$$

and

$$u_{11}^i = 0 \tag{8.157}$$

The Newton-Rapson method[29] may be used to determine the values of σ and ω that satisfy Eqs. 8.156 and 8.157. If σ_k and ω_k are the values after kth iteration, then a better estimate of the solution, σ_{k+1} and ω_{k+1} of Eqs. 8.156 and 8.157 is

$$\sigma_{k+1} = \sigma_k - \frac{u_{11}^r \dfrac{\partial u_{11}^i}{\partial \omega} - u_{11}^i \dfrac{\partial u_{11}^r}{\partial \omega}}{\dfrac{\partial u_{11}^r}{\partial \sigma}\dfrac{u_{11}^i}{\partial \omega} - \dfrac{u_{11}^r}{\partial \omega}\dfrac{\partial u_{11}^i}{\partial \sigma}} \tag{8.158}$$

$$\omega_{k+1} = \omega_k - \frac{u_{11}^r \dfrac{\partial u_{11}^i}{\partial \sigma} - u_{11}^i \dfrac{\partial u_{11}^r}{\partial \sigma}}{\dfrac{\partial u_{11}^r}{\partial \omega}\dfrac{\partial u_{11}^i}{\partial \sigma} - \dfrac{\partial u_{11}^r}{\partial \sigma}\dfrac{\partial u_{11}^i}{\partial \omega}} \tag{8.159}$$

In Eqs. 8.158 and 8.159, u_{11}^r and u_{11}^i and their partial derivatives are computed for σ_k and ω_k. If $|\sigma_{k+1} - \sigma_k|$ and $|\omega_{k+1} - \omega_k|$ are less than a specified tolerance, then σ_{k+1} and ω_{k+1} are solutions of Eqs. 8.156 and 8.157; otherwise, σ_k and ω_k are assumed equal to σ_{k+1} and ω_{k+1} and this process is continued until the difference between the two successive values of σ and ω is less than the specified tolerance.

This procedure is general and is not limited to simple and frictionless systems.

Also, note that the intermediate-state vectors have been eliminated by multiplying the transfer matrices, and only a second-order determinant has to be solved as compared to an $n \times n$ determinant (value of n depends upon the number of pipes and appurtenances in the system) in Zielke and Rösl's method.

The above procedure is simplified considerably for a frictionless system since u is a function of ω only. In a frictionless system having a constant-head reservoir at the upstream end and an oscillating valve at the downstream end, the amplitude of the discharge fluctuation at the valve is zero during resonating conditions at the fundamental or one of the higher odd harmonics. This was observed by Camichel et al.[5] and reported to be true by Jaeger.[30,31] The frequency-response diagrams obtained by theoretical analysis of a number of series, parallel, and branch systems (a branch system with a side branch having an orifice or an oscillating valve being an exception) done by Wylie[19,20] and by the author[24] confirm this result. Expressions for the resonant frequencies of the simple frictionless systems and their numerical values for the simple or complex systems can be determined by using this result as follows:

Let U be the overall transfer matrix for a system having a constant-head reservoir at the upstream end (section 1) and an oscillating valve at the downstream end (section $n + 1$), i.e.,

$$\mathbf{z}_{n+1}^{L} = \mathbf{U}\,\mathbf{z}_{1}^{R} \tag{8.160}$$

By expanding Eq. 8.160 and noting that $h_1^R = 0$ (constant-head reservoir), and $q_{n+1}^L = 0$ (discharge fluctuation node) at a resonant frequency, we obtain

$$u_{11} q_1^R = 0 \tag{8.161}$$

Recall that u_{11} is the element in the first row and the first column of the matrix U. For a nontrivial solution, $q_1^R \neq 0$; therefore,

$$u_{11} = 0 \tag{8.162}$$

To determine the resonant frequencies, we have to solve Eq. 8.162. To do this, u_{11} is computed for different trial values of ω, and the u_{11}-versus-ω curve is plotted. If the chosen value of ω is equal to one of the resonant frequencies, then $u_{11} = 0$. This requirement is not normally met by the first guess for ω, and the resulting numerical value of u_{11} is referred to as the *residual*. The points of intersection of the u_{11}-versus-ω curve and the ω-axis are the resonant frequencies.

Example 8.3

Derive an expression for the frequencies of the fundamental and odd harmonics of the system shown in Fig. 8.19. Assume that the system is frictionless.

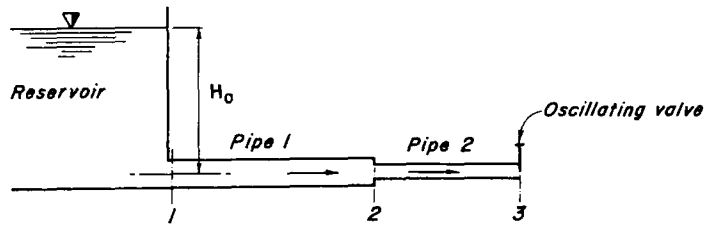

Figure 8.19. Series piping system.

For the series system shown in Fig. 8.19,

$$\mathbf{U} = \mathbf{F}_2\mathbf{P}_2\mathbf{F}_1 \tag{8.163}$$

By substituting $\mathbf{F}_2$ and $\mathbf{F}_1$ from Eq. 8.34 and $\mathbf{P}_2$ from Eq. 8.54, multiplying the matrices, and using Eq. 8.162, we obtain

$$\cos b_1\omega . \cos b_2\omega - \frac{a_1}{a_2}\left(\frac{D_2}{D_1}\right)^2 \sin b_1\omega \sin b_2\omega = 0 \tag{8.164}$$

in which b_1 and b_2 are constants for pipe No. 1 and No. 2, respectively, as defined in Eq. 8.34.

Example 8.4

Determine the frequencies of the fundamental and odd harmonics of the Toulouse pipeline shown in Fig. 8.20.

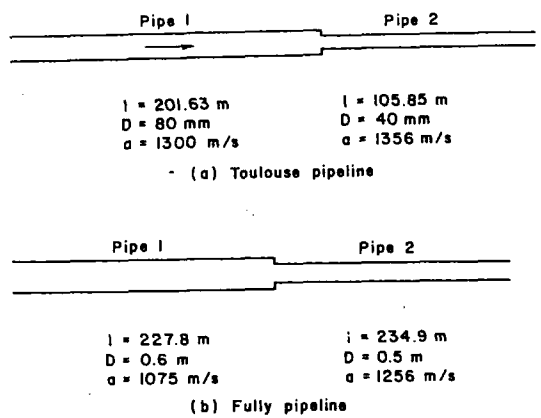

Figure 8.20. Longitudinal profile. (After Camichel et al.[5])

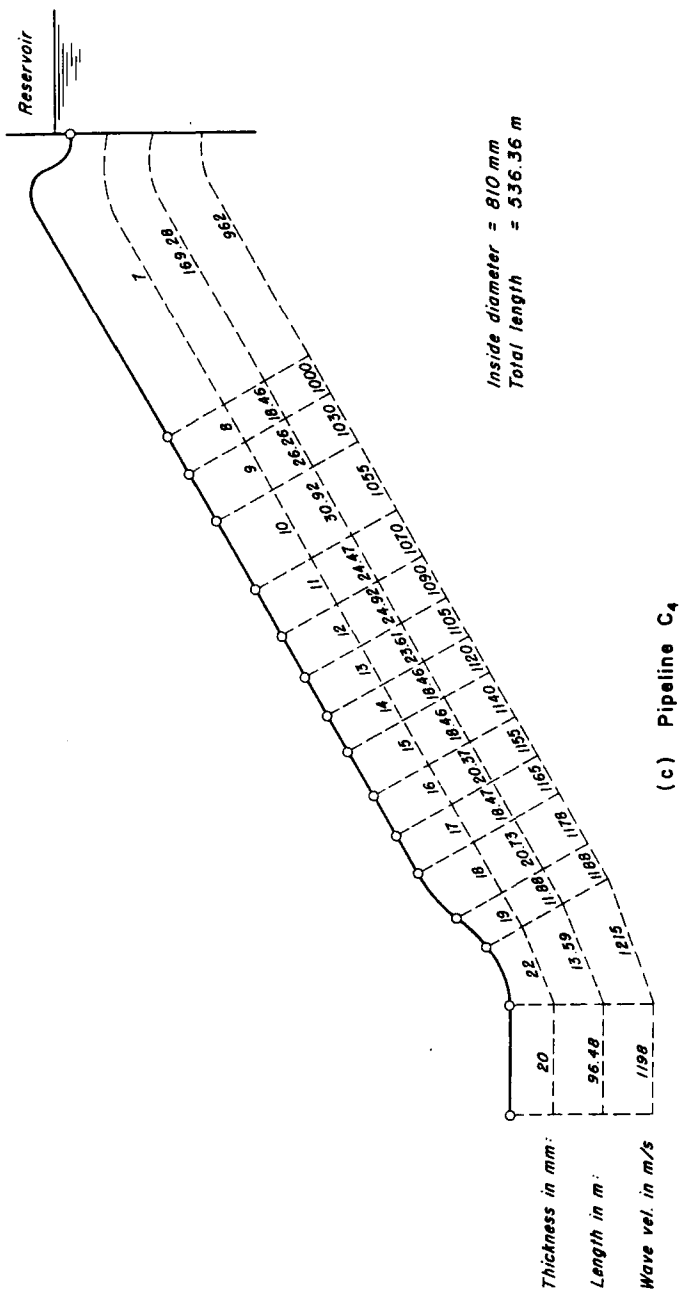

(c) Pipeline C_4

Figure 8.20. (*Continued*)

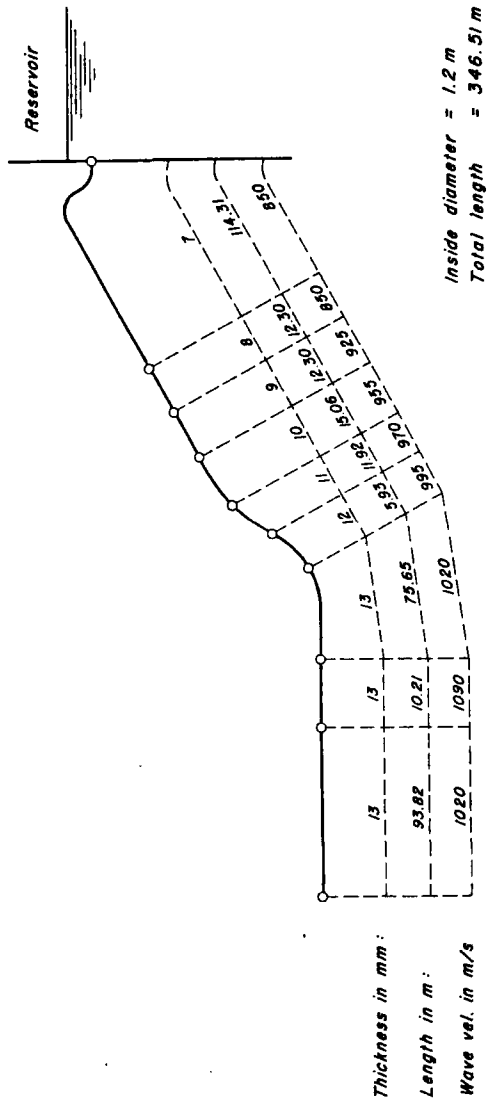

(d) Pipeline P_3

Figure 8.20. (*Continued*)

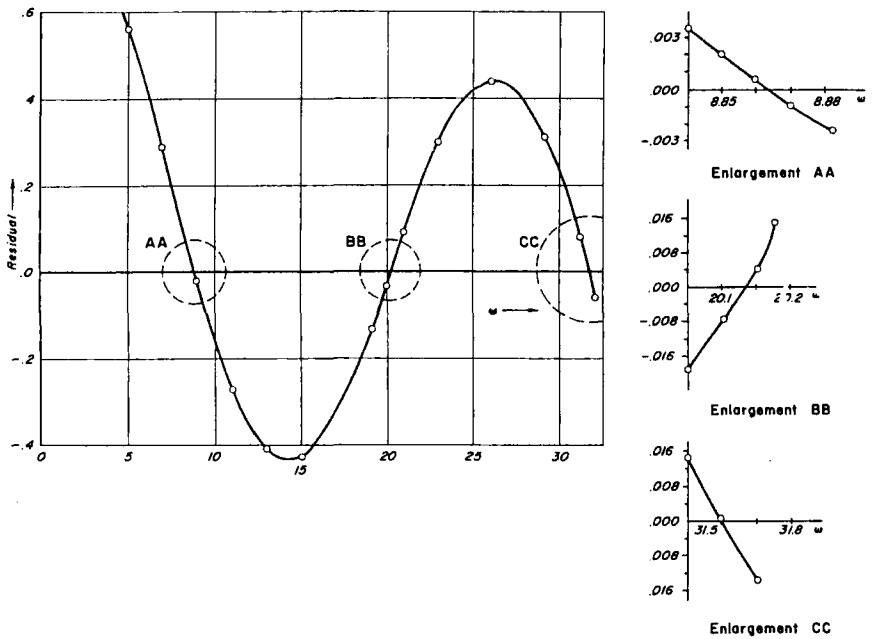

Figure 8.21. Plot of residual versus ω for Toulouse system.

The overall transfer matrix, **U**, for the system of Fig. 8.20 is given by Eq. 8.163. For an assumed value of ω, the elements of the matrices $\mathbf{F}_2$, $\mathbf{P}_2$, and $\mathbf{F}_1$ are computed from Eqs. 8.34 and 8.54 using the system dimensions shown in Fig. 8.20, and these matrices are multiplied to compute the elements of **U** matrix. The value of u_{11} is the residual. By assuming different values of ω, the values of the residual are determined, and the residual-versus-ω curve is plotted as shown in Fig. 8.21. The intersection of this curve with the ω-axis yields the following frequencies in rad/s:

1. Fundamental: 8.863
2. Third harmonic: 20.14
3. Fifth harmonic: 31.6

8.12 VERIFICATION OF TRANSFER-MATRIX METHOD

To demonstrate the validity of the method presented herein, the results obtained by the transfer matrix method are compared with the experimental values and with those determined by the method of characteristics, by the impedance theory, and by energy concepts.

Experimental Results

Except for the laboratory and field tests reported by Camichel et al.,[5] few experimental results on the resonating characteristics of pipes are available in the literature. In the tests reported by Camichel et al., the resonating conditions in series pipes were established by a rotating cock located at the downstream end of the pipeline. Each system had a constant-head reservoir at the upstream end. The data for these systems are given in Fig. 8.20.

The values of the periods of the fundamental and higher harmonics determined experimentally and by the procedure outlined in Section 8.11 are listed in Table 8.2. As can be seen, close agreement is found between the experimental values and those determined by the transfer matrix method.

Method of Characteristics

A number of systems—series, parallel, and branch systems with the side branch having various boundary conditions—were analyzed using the transfer-matrix method and the method of characteristics. The data for four of these systems and the frequency-response diagrams are presented in Figs. 8.22 through 8.25.

The frequency-response diagrams are presented in a nondimensional form. The frequency ratio, ω_r, is defined as ω/ω_{th}; the pressure head ratio, h_r, as $2|h^L_{n+1}|/H_o$; and the discharge ratio, q_r, as $2|q^L_{n+1}|/Q_o$. The values of h_r and q_r determined by the method of characteristics represent the amplitude of the swing from the minimum to the maximum value. The frequency of the forcing function is designated by ω.

The oscillating valves are the forcing functions in all the systems except the dead-end series system of Fig. 8.22 in which the fluctuating pressure head at the upstream end is the forcing function. The valve movement is taken as sinusoidal with $\tau_o = 1.0$ and $k = 0.2$. The fluctuating pressure head in Fig. 8.22 is also sinusoidal with $K = 1.0$. In the branch systems of Fig. 8.25, $\tilde{\tau}_o = 1.0$ and $\tilde{k} = 0.2$.

If the friction losses are taken into consideration, the analysis of various systems by the method of characteristics showed that the amplitudes of the positive swing of pressure head and negative swing of the discharge are larger than the corresponding negative and positive swings. This is caused by the friction loss term of the governing differential equations. In the transfer matrix method, however, the amplitudes of the positive and negative oscillations are equal because a sinusoidal solution is assumed.

To check the values of the phase angles between different quantities of interest, the oscillatory discharge and pressure head at the valve are computed by using the method of characteristics. The $q_r^* \sim t$, $h_r^* \sim t$, and $\tau^* \sim t$ curves are plotted

Table 8.2. Calculated and measured periods.

System	No. Pipes	Theoretical Period (s)	Period (s)											
			Fundamental		3rd Harmonic		5th Harmonic		7th Harmonic		9th Harmonic		11th Harmonic	
			Calc.	Meas.	Calc.	Meas.	Calc.	Meas.	Calc.	Meas.	Calc.	Meas.	Calc.	Meas.
Toulouse	2	0.932	0.708	0.69	0.311	0.31	0.198	0.19	[a]	–	–	–	–	–
Fully	2	15.96	13.719	13.50	–	–	–	–	–	–	–	–	–	–
C_4	15	2.008	1.887	1.882	–	–	–	–	–	–	–	–	–	–
F_3	9	1.464	1.405	1.368	0.502	0.505	0.296	0.310	0.2117	0.2150	0.1650	0.1667	0.1338	0.1420

[a] Not available.

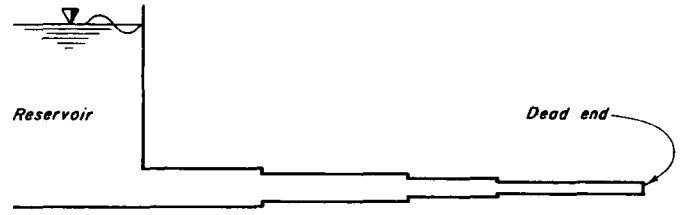

(a) Piping system

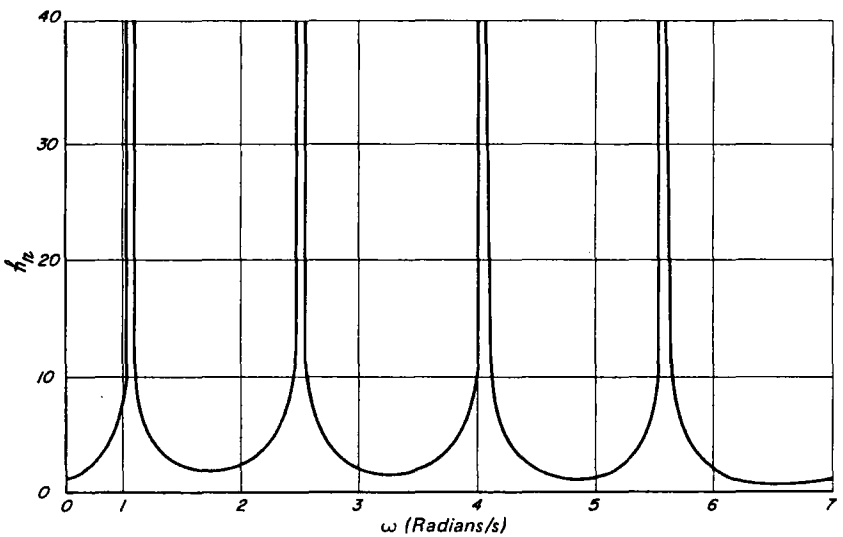

(b) Frequency response diagram

Figure 8.22. Frequency response of a series piping system with dead end.

in Fig. 8.26. In this diagram, $h_r^* = h^*/H_o$ and $q_r^* = q^*/Q_o$. The phase angles determined by the transfer matrix method and by the method of characteristics are presented in Table 8.3. Close agreement is found between the results obtained by the two methods.

Impedance Method

The data and the solution, by the impedance method, of examples used for comparison purposes in this study have been taken from the literature.[17,19] The first example is that of a 490.7-m-long, 0.61-m-diameter, simple pipeline connected

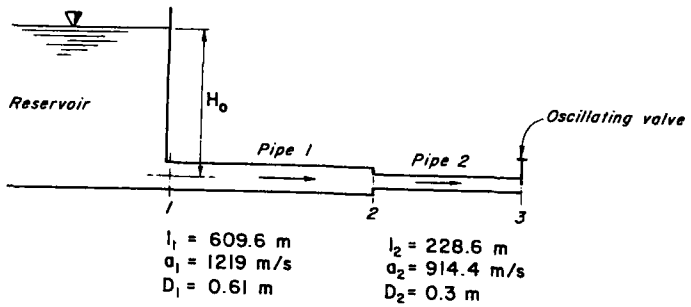

(a) Piping system

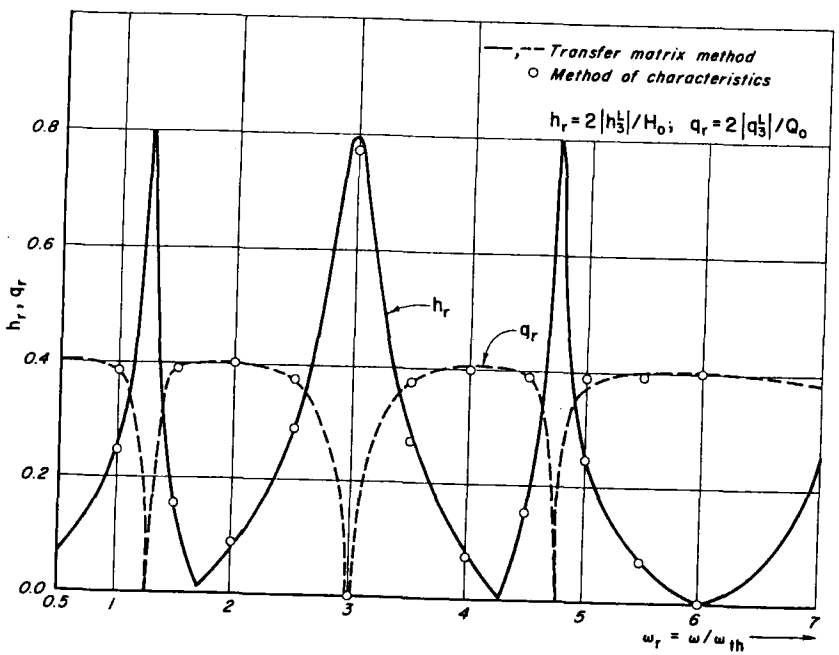

(b) Frequency response diagram

Figure 8.23. Frequency response of a series piping system.

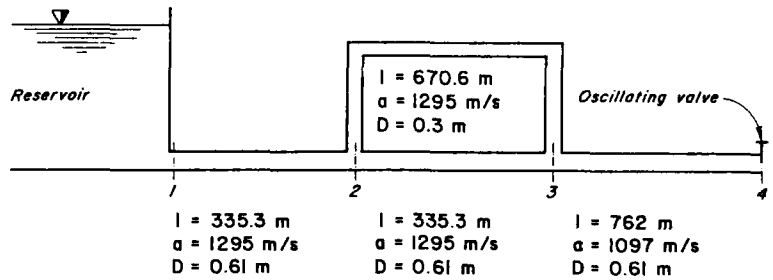

(a) Piping system

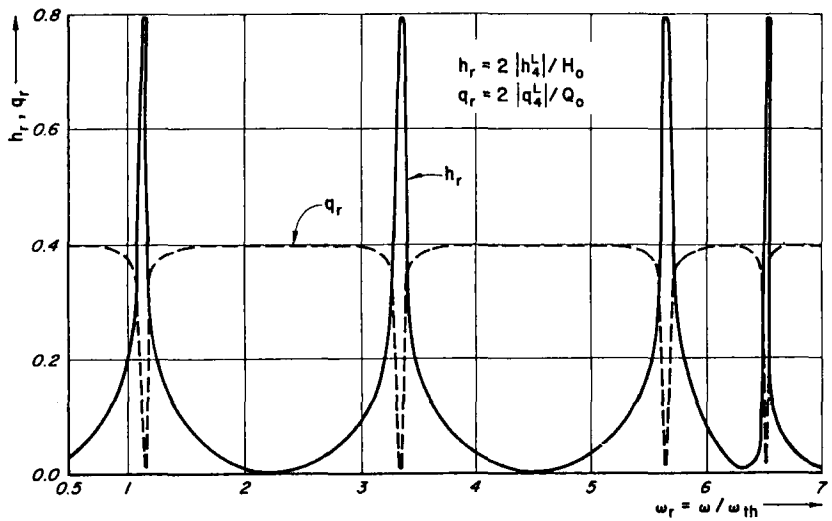

(b) Frequency response diagram

Figure 8.24. Frequency response of a parallel piping system.

to a reservoir. There is an oscillating valve at the downstream end with $\tau_o = 0.5$ and $k = 0.5$. The steady-state mean discharge is 0.89 m^3/s; the wave speed, a = 981.5 m/s; and the static head, 30.5 m. Using the Paynter's diagram,[17] the following values are obtained: $h_r = 1.92$, and the phase angle between the pres-

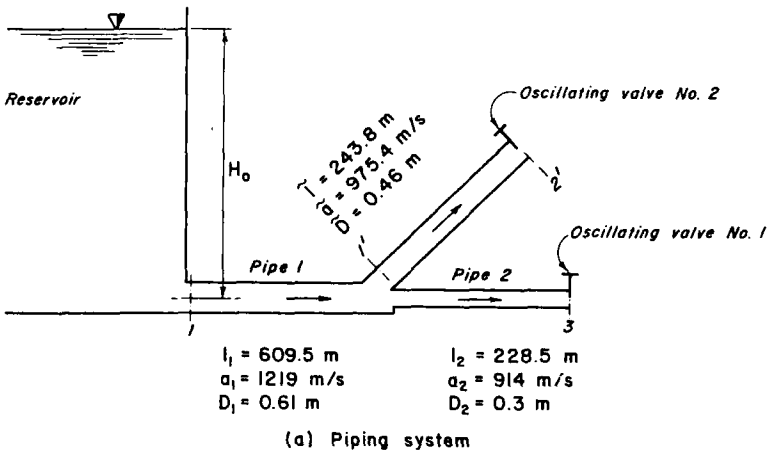

(a) Piping system

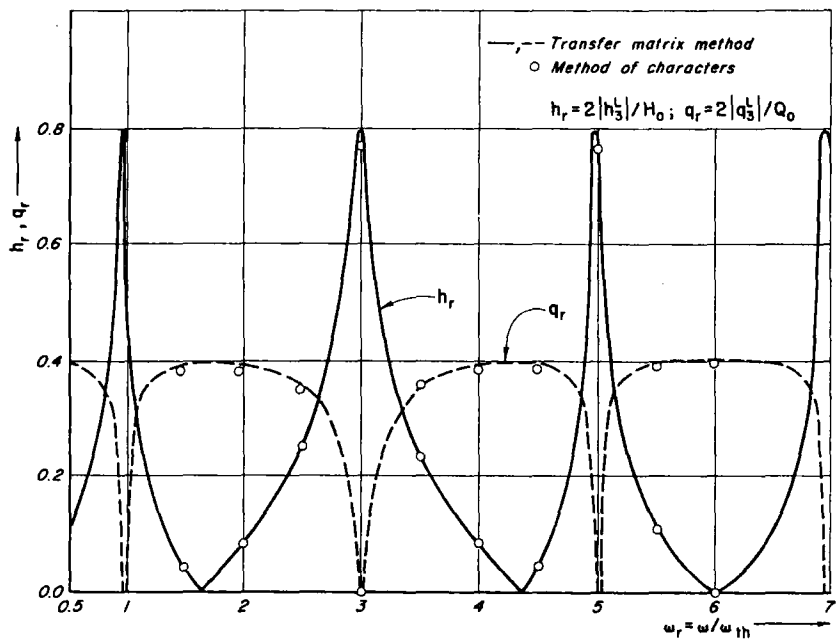

(b) Frequency response diagram (valves No. 1 and No. 2 are in phase)

Figure 8.25. Frequency response of a branch piping system. Branch with oscillating valve.

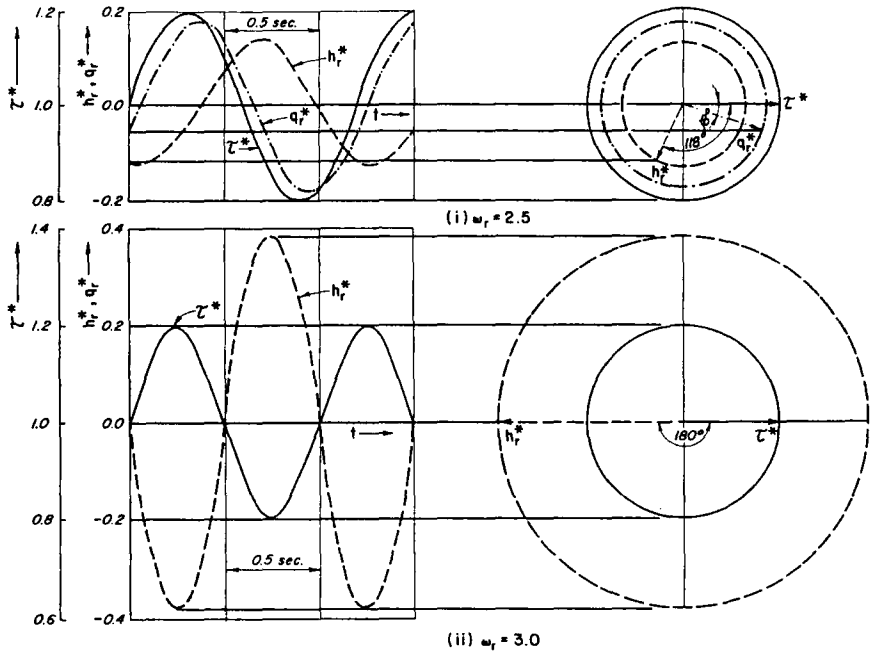

(c) Branch system of Fig. 5.8a (Valve No. 1 and 2 in phase)

Figure 8.26. Time history of h_r^*, q_r^*, and τ^*.

Table 8.3. Phase angles.

System	Frequency Ratio, ω_r	Phase Angles, ϕ (in degrees) Between h and τ^*: Transfer Matrix Method	Between h and τ^*: Method of Characteristics	Between q and τ^*: Transfer Matrix Method	Between q and τ^*: Method of Characteristics
Series (Fig. 8.23a)	2.5	-110.99	-110.50	-20.99	-20.5
	3.0	-180.01	-180.00	-270.01	–
Branch (Fig. 8.17a)	2.5	-117.90	-119.00	-27.90	-29.50
(Side branch with dead end)	3.0	-180.01	-180.00	-270.01	–
Branch (Fig. 8.25a)	2.5	-117.13	-118.00	-18.17	-18.00
(Side branch with oscillating valve)	3.0	-180.01	-180.00	-270.01	–

sure head and the relative-gate opening, $\phi_h = 164°$. The analysis by the transfer matrix method gives $h_r = 1.929$ and $\phi_h = 164.5°$, which are in close agreement with those obtained from the Paynter's diagram. The piping systems presented by Wylie in Ref. 19 are solved by the transfer-matrix method. The impedance, Z, at the valve is determined by computing the ratio h^L_{n+1}/q^L_{n+1}. Approximately the same values of the impedance are obtained as those given by Wylie. Two of these piping systems and the impedance diagrams are presented in Figs. 8.27 and 8.28. The normalized impedance, z_r, was computed by dividing $|Z|$ by the characteristic impedance, Z_c, at the valve, i.e., $z_r = |Z|/Z_c$.

Energy Concepts

In steady-oscillatory flows in piping systems, the energy input during a cycle is equal to the energy output plus the losses in the system. If the losses in the system are neglected, then the energy input is equal to the energy output during one period. This result may be used as follows to verify the numerical values of the amplitudes of the pressure head and discharge oscillations, and of the phase angles obtained by the transfer-matrix method.

The energy entering the system during time interval Δt is

$$E_{in} = \gamma Q H \Delta t \tag{8.165}$$

in which γ = specific weight of the fluid and the subscript *in* refers to the input quantities. Substitution of Eqs. 8.1 and 8.2 into Eq. 8.165 and expansion of the resulting equation yield

$$E_{in} = \gamma(Q_o H_o + q^*_{in} H_o + h^*_{in} Q_o + q^*_{in} h^*_{in})\Delta t \tag{8.166}$$

Let q^*_{in} and h^*_{in} be sinusoidal, i.e.,

$$h^*_{in} = h'_{in} \cos \omega t \tag{8.167}$$

$$q^*_{in} = q'_{in} \cos (\omega t - \phi_{in}) \tag{8.168}$$

in which ϕ_{in} = phase angle between q^*_{in} and h^*_{in} and h'_{in} and q'_{in} are the amplitudes of the pressure and discharge fluctuations. Note that both h'_{in} and q'_{in} are real quantities. The energy input during one cycle may be calculated by substituting Eqs. 8.167 and 8.168 into Eq. 8.166 and by integrating the resulting equation over period, T. This process gives

$$E_{in} = \gamma Q_o H_o T + \gamma q'_{in} h'_{in} \int_0^T \cos \omega t \cos (\omega t - \phi_{in}) dt \tag{8.169}$$

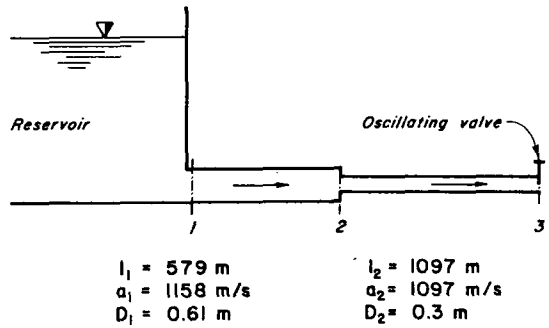

(a) Piping system

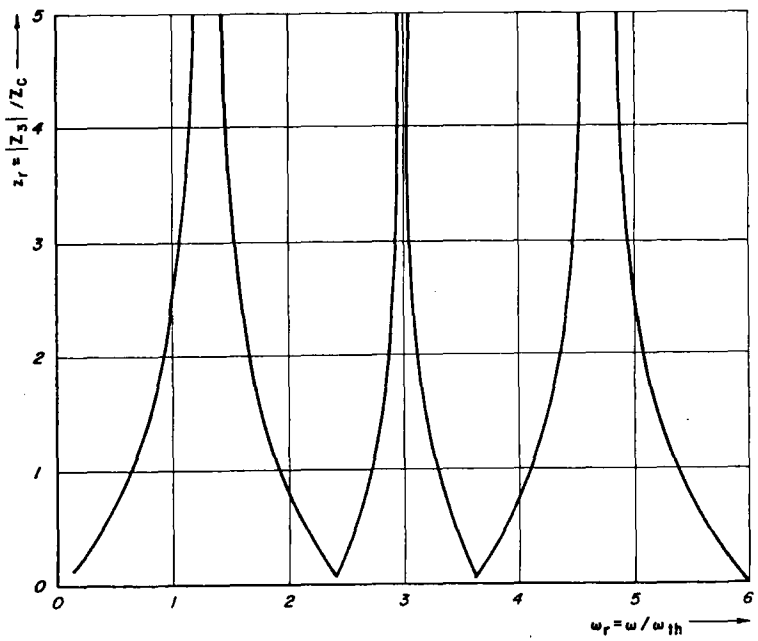

(b) Impedance diagram

Figure 8.27. Impedance diagram for series piping system.

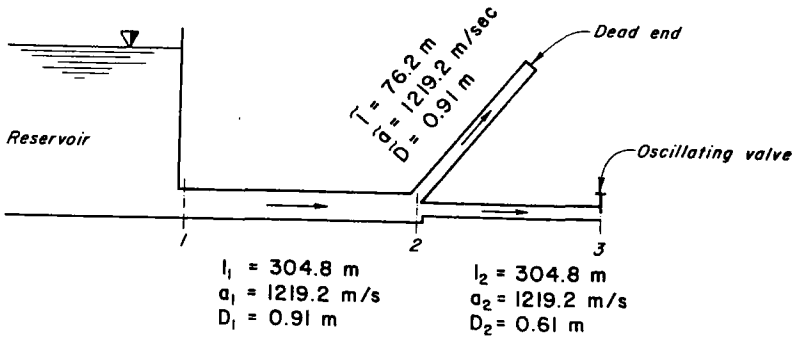

(a) Piping system

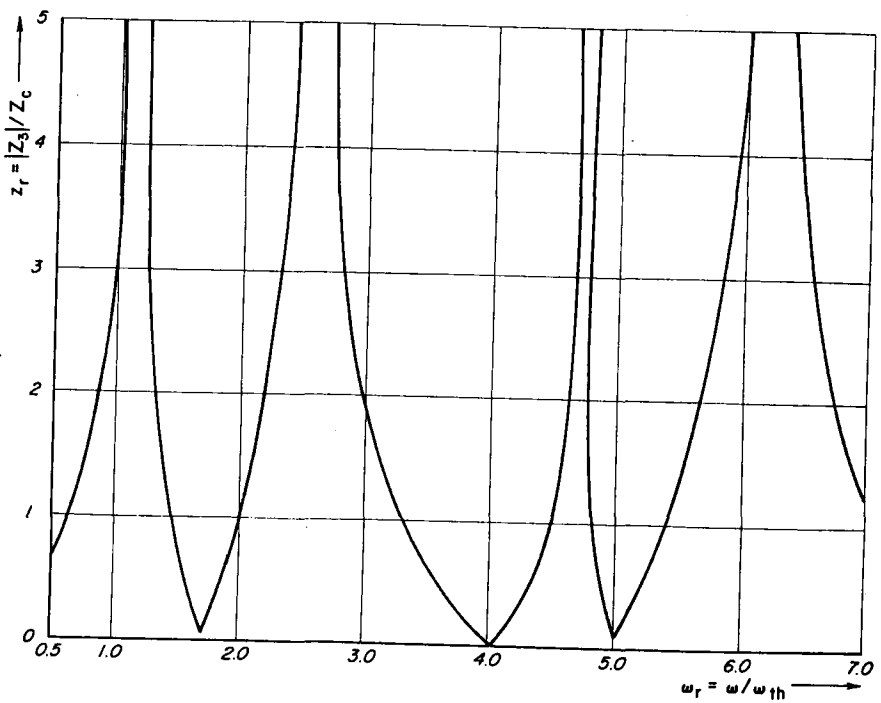

(b) Impedance diagram

Figure 8.28. Impedance diagram for branch piping system. Branch has dead end.

If there is a constant-level reservoir at the upstream end, then $h'_{in} = 0$. Hence, Eq. 8.169 becomes

$$E_{in} = \gamma Q_o H_o T \tag{8.170}$$

By proceeding in a similar manner,

$$E_{out} = \gamma Q_o H_o T + \gamma h'_{out} q'_{out} \int_0^T \cos \omega t \cos (\omega t - \phi_{out}) dt \tag{8.171}$$

The subscript *out* designates output quantities.

If the losses in the system are neglected, then $E_{in} = E_{out}$. Hence, it follows from Eqs. 8.170 and 8.171 that

$$\int_0^T \cos \omega t \cos (\omega t - \phi_{out})\, dt = 0 \tag{8.171}$$

which yields

$$\phi_{out} = 90^\circ \tag{8.172}$$

For all the systems analyzed in this study, ϕ_{out} was 90°. The only exceptions were the branch systems in which the side branch had an orifice or an oscillating valve. Equations 8.171 and 8.172 do not hold in these cases because there is energy output at more than one point (see Problem 8.6).

8.13. STUDIES ON PIPELINE WITH VARIABLE CHARACTERISTICS

The resonating characteristics of a pipeline with *linearly* variable characteristics—A and a—along its length, a constant-head reservoir at the upstream end, and an oscillating valve at the downstream end (Fig. 8.29a) are studied by using the transfer matrix method. Frequency response is determined by using the transfer matrix given in Eq. 8.45. Then the actual pipe is replaced by a substitute pipe having stepwise changes in characteristics, as shown in Fig. 8.29a. The expressions presented in Section 8.8 are used to determine the frequency response. To compute ω_r, the theoretical period is calculated from the equation

$$T_{th} = \frac{4l}{a_m} \tag{8.173}$$

in which a_m = velocity of waterhammer waves at the midpoint of the pipeline, and l = length of the pipeline. The results for both these cases are presented in Fig. 8.29b.

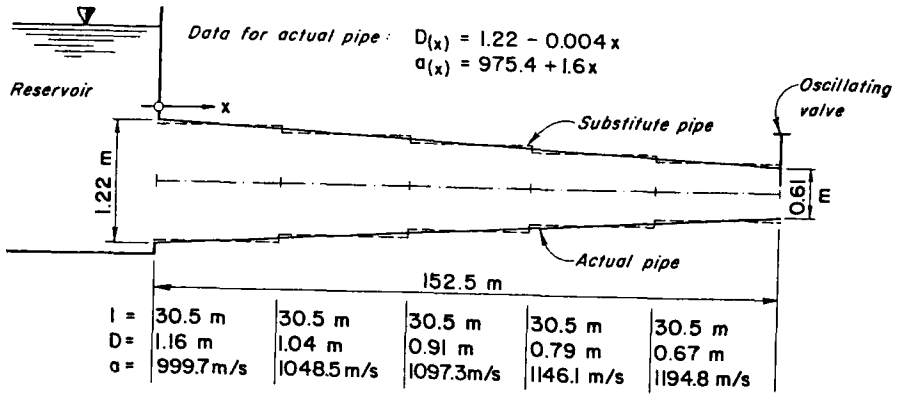

(a) Piping system

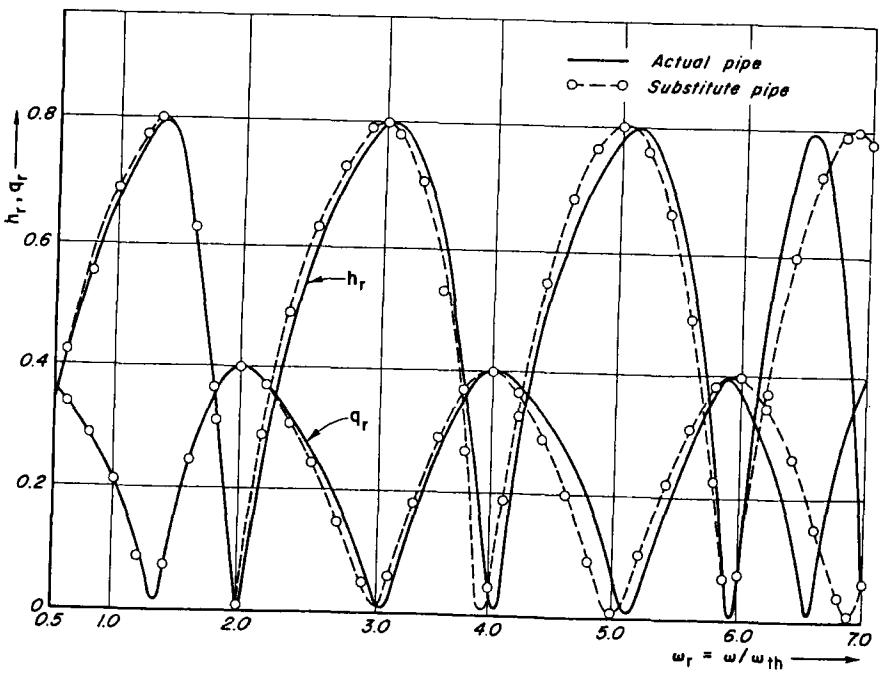

(b) Frequency response diagram

Figure 8.29. Frequency response of pipeline having variable characteristics.

Table 8.4. Resonant frequencies of piping system of Fig. 8.29a.

	Resonant Frequencies (rad/s)		
		Transfer Matrix Method	
Mode	Favre's Expression	Actual Pipe	Substitute Pipe
Fundamental	15.127	15.075	14.905
Third	35.683	35.702	35.001
Fifth	57.647	57.856	56.375
Seventh	79.963	74.130	77.749

Resonant frequencies for the system of Fig. 8.29a were determined by considering the pipe *per se* and then replacing it with a substitute pipe (shown by dotted lines in Fig. 8.29a), and by using the following expression for the resonant frequencies of a pipeline having linearly variable characteristics derived by Favre[34]:

$$\tan \frac{\omega l}{a_m} = -\frac{\omega l}{a_m \sigma} \tag{8.174}$$

in which $\sigma = (1 + \psi/2)\,[\mu(1 + \psi/2) + \psi]$; $\psi = (a_o - a_m)/a_m$; and $\mu = (D_A - D_o)/D_o$. The subscripts o, m, and A refer to the values at the valve, at the midpoint, and at the reservoir end of the pipe, respectively. The results are tabulated in Table 8.4. Close agreement is found between the results obtained in these cases up to the fifth harmonic. The higher harmonics can be predicted to a reasonable degree of accuracy by increasing the number of reaches into which the pipeline is divided.

8.14 SUMMARY

In this chapter, the development of the resonating conditions in piping system was discussed; available methods for determining the frequency response and the resonant frequencies were presented; and the details of the transfer matrix method were outlined. The transfer matrix method was verified by comparing its results with those of the characteristics and impedance methods and with those measured in the laboratory and on the prototype installations.

PROBLEMS

8.1 Prove that if $(\omega l/a) \ll 1$, then the system may be analyzed as a lumped system. Assume the system is frictionless. (*Hint:* Compute and compare

the elements of the field matrix for a lumped system [Eq. 8.35] and for a distributed system [Eq. 8.34] for $\omega l/a \simeq 0.01$.)

8.2 Derive the point matrix for an orifice located at the junction of ith and $(i+1)$th pipe (Fig. 8.12c). The mean head loss, ΔH_o, across the orifice corresponds to the mean discharge, Q_o.

8.3 Compute the elements of the field matrices for the pipes of the system shown in Fig. 8.22 for $\omega_r = 2.0$, and compute the overall transfer matrix.

8.4 Derive expressions for the location of the nodes and antinodes for a system having three pipes in series, a constant-level reservoir at the upstream end, and an oscillating valve at the downstream end. Assume the system to be frictionless. (*Hint:* Proceed as in Section 8.10.)

8.5 Derive an expression for the natural frequencies corresponding to the odd harmonics of a frictionless system having three pipes in series, a constant-level reservoir at the upstream end, and an oscillating valve at the downstream end.

8.6 Prove that for a branch system having an oscillating valve or an orifice on the branch

$$h'_{out} q'_{out} \cos \phi_{out} + \tilde{h}'_{out} \tilde{q}'_{out} \cos \tilde{\phi}_{out} = 0$$

in which h'_{out} and q'_{out} are the amplitudes of the pressure and discharge oscillations, and ϕ_{out} is the phase angle between the pressure head and discharge. A tilde (~) on various variables refers to the branch; other variables are for the main. (*Hint:* $E_{in} = E_{out} + \tilde{E}_{out}$. Substitute expressions for E_{in}, E_{out}, and $\tilde{E}_{out}$ in terms of the mean and oscillatory parts, integrate over the period T, and simplify the resulting equation.)

8.7 Derive a point matrix for a simple surge tank and for an air chamber.

8.8 Figure 8.30 shows a Helmholtz resonator. Derive a point matrix for the resonator.

8.9 A short dead-end pipe, called *tuner*, is sometimes connected to a pipeline to change its frequency response at a particular frequency. Determine

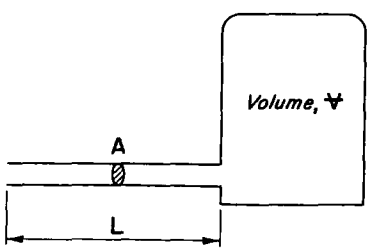

Figure 8.30. Helmholtz resonator.

the length, diameter, and wave velocity of a tuner to be connected at the junction of pipes No. 1 and No. 2 of the series system of Fig. 8.23 so that the resonating conditions do not occur at $\omega_r = 3.0$. (*Hint:* Select arbitrarily the length, diameter, and wave velocity of a tuner, and analyze the system as a branch system with the branch having a dead end. If the resonating conditions still occur at $\omega_r = 3.0$, change the characteristics of the tuner, and repeat the above procedure until a suitable tuner is obtained.)

REFERENCES

1. Thomson, W. T., *Vibration Theory and Applications*, Prentice-Hall, Inc., Englewood Cliffs, New Jersey, 1965, p. 5.
2. Wylie, C. R., *Advanced Engineering Mathematics*, Third Ed., McGraw-Hill Book Co., New York, 1965, p. 145.
3. Allievi, L., *Theory of Water Hammer* (translated by E. E. Halmos), Riccardo Garoni, Rome, Italy, 1925.
4. Bergeron, L., "Etude des variations de regime dans les conduits d'eau: Solution graphique generale," *Revue hydraulique*, Vol. 1, 1935, Paris, pp. 12–25.
5. Camichel, C., Eydoux, D., and Gariel, M., "Etude Théorique et Expérimentale des Coups de Bélier," Dunod, Paris, France, 1919.
6. Abbot, H. F., Gibson, W. L., and McCaig, I. W., "Measurements of Auto-Oscillations in a Hydroelectric Supply Tunnel and Penstock System," *Trans. Amer. Soc. of Mech. Engrs.*, vol. 85, Dec. 1963, pp. 625–630.
7. Parmakian, J., *Water Hammer Analysis*, Dover Publications, Inc., New York, 1963.
8. Den Hartog, J. P., "Mechanical Vibrations in Penstocks of Hydraulic Turbine Installations," *Trans., Amer. Soc. of Mech. Engrs.*, vol. 51, 1929, pp. 101–110.
9. Rocard, Y., Les Phénomèns d'Auto-Oscillation dans les Installations Hydrauliques, Paris, 1937.
10. Fashbaugh, R. H. and Streeter, V. L., "Resonance in Liquid Rocket Engine System," *Jour., Basic Engineering, Amer. Soc. of Mech. Engrs.*, vol. 87, Dec. 1965, p. 1011.
11. Saito, T., "Self-excited Vibrations of Hydraulic Control Valve Pipelines," *Bull., Japan Soc. of Mech. Engrs.*, vol. 5, No. 19, 1962, pp. 437–443.
12. McCaig, I. W. and Gibson, W. L., "Some Measurements of Auto-Oscillations Initiated by Valve Characteristics," *Proceedings, 10th General Assembly, International Association for Hydraulic Research*, London, 1963, pp. 17–24.
13. Hovanessian, S. A. and Pipes, L. A., *Digital Computer Methods in Engineering*, McGraw-Hill Book Co., New York, Chapter 4, 1969.
14. Streeter, V. L. and Wylie, E. B., *Hydraulic Transients*, McGraw Hill Book Co., Inc., New York, 1967.
15. Blackwall, W. A., *Mathematical Modelling of Physical Networks*, Macmillan Co., New York, 1968, Chapter 14.
16. Lathi, B. P., *Signals, Systems and Communication*, John Wiley & Sons, 1965, pp. 2, 13.
17. Paynter, H. M., "Surge and Water Hammer Problems," *Trans. Amer. Soc. of Civ. Engrs.*, vol. 118, 1953, pp. 962–1009.
18. Waller, E. J., "Prediction of Pressure Surges in Pipelines by Theoretical and Experimental Methods," *Publication No. 101*, Oklahoma State University, Stillwater, Oklahoma, June 1958.

19. Wylie, E. B., "Resonance in Pressurized Piping Systems," thesis presented to the University of Michigan, Ann Arbor, Michigan, in 1964, in partial fulfillment of the requirements for the degree of doctor of philosophy.
20. Wylie, E. B., "Resonance in Pressurized Piping Systems," *Jour., Basic Engineering, Trans., Amer. Soc. of Mech. Engrs.*, vol. 87, No. 4, Dec, 1965, pp. 960-966.
21. Pestel, E. C. and Lackie, F. A., *Matrix Methods in Elastomechanics*, McGraw-Hill Book Co., New York, 1963.
22. Molloy, C. T., "Use of Four-Pole Parameters in Vibration Calculations," *Jour. Acoustical Society of America*, vol. 29, No. 7, July 1957, pp. 842-853.
23. Reed, M. B., *Electrical Network Synthesis*, Prentice-Hall, Inc., New York, 1955, Chapter 2.
24. Chaudhry, M. H., "Resonance in Pressurized Piping Systems," thesis presented to the University of British Columbia, Vancouver, British Columbia, Canada, in 1970, in partial fulfillment of the requirements for the degree of doctor of philosophy.
25. Chaudhry, M. H., "Resonance in Pipe Systems," *Water Power*, London, July/August 1970, pp. 241-245.
26. Chaudhry, M. H., "Resonance in Pressurized Piping Systems," *Jour., Hydraulics Div., Amer. Soc. of Civil Engrs.*, vol. 96, Sept. 1970, pp. 1819-1839.
27. Chaudhry, M. H., "Resonance in Pipes Having Variable Characteristics," *Jour., Hydraulics Div., Amer. Soc. of Civil Engrs.*, vol. 98, Feb. 1972, pp. 325-333.
28. Thorley, A. R. D., Unpublished lecture notes, course on Hydraulic Transients arranged by British Hydromechanics Research Assoc., England, Sept. 1972.
29. McCraken, D. D. and Dorn, W. S., *Numerical Methods and FORTRAN Programming*, John Wiley & Sons, New York, 1964, p. 156.
30. Jaeger, C., "Water Hammer Effects in Power Conduits," *Civil Engineering and Public Works Review*, vol. 23, No. 500-503, London, England, Feb.-May 1948.
31. Jaeger, C., "The Theory of Resonance in Hydropower Systems, Discussion of Incidents and Accidents Occuring in Pressure Systems," *Jour. of Basic Engineering, Trans., Amer. Soc. of Mech. Engrs.*, vol. 85, Dec. 1963, pp. 631-640.
32. Zielke, W. and Rösl, G., Discussion of *Ref. 26, Jour., Hydraulics Div., Amer. Soc. of Civ. Engrs.*, July 1971, pp. 1141-1146.
33. Chaudhry, M. H., Closure of *Ref. 26, Jour., Hydraulics Div., Amer. Soc. of Civ. Engrs.*, April 1972, pp. 704-707.
34. Favre, H., "La Résonance des Conduites à charactéristiques Linéairement Variables," *Bulletin Technique de la Suisse Romande*, vol. 68, No. 5, Mar. 1942, pp. 49-54. (Translated into English by Sinclair, D. A., "Resonance of Pipes with Linearly Variable Characteristics," Tech. Translation 1511, National Research Council of Canada, Ottawa, Canada, 1972.)

ADDITIONAL REFERENCES

Jaeger, C., "Theory of Resonance in Pressure Conduits," *Trans. Amer. Soc. of Mech. Engrs.*, vol. 61, Feb. 1939, pp. 109-115.
Evangelisti, G., "Determinazione Operatoria Delle Frequenze di Risonanza Nei Sistemi Idraulici in Pressione," *Letta Alla R. Accademia Della Scienze Dell'Istituto di Bologne*, Feb. 1940.
Deriaz, P., "Contributions to the Understanding of Flow in Draft Tubes in Francis Turbines," *Symposium, International Assoc. for Hydraulic Research*, Paper N-1, Sept. 1960.

Katto, Y., "Some Fundamental Nature of Resonant Surge," *Japan Soc. of Mech. Engrs.*, 1960, pp. 484-495.
Blade, R. J. and Goodykootz, J., "Study of Sinusoidally Perturbed Flow in a Line Including a 90° Elbow with Flexible Supports," NASA Report No. TN-D-1216, 1962.
Oldenburger, R. and Donelson, J., "Dynamic Response of Hydroelectric Plant," *Trans. Amer. Inst. of Elect. Engrs., Power App. and Systems*, vol. 81, Oct. 1962, pp. 403-418.
Roberts, W. J., "Experimental Dynamic Response of Fluid Lines," *M.S. Thesis*, Purdue University, 1963.
Lewis, W. and Blade, R. J., "Study of the Effect of a Closed-End Side Branch on Sinusoidally Perturbed Flow of a Liquid in a Line," NASA Report TN-D-1876, 1963.
D'Souza, A. F. and Oldenburger, R., "Dynamic Response of Fluid Lines," *Trans. Amer. Soc. of Mech. Engrs.*, Series D, Sept. 1964, pp. 589.
Vibrations in Hydraulic Pumps and Turbines, Symposium, Inst. of Mech. Engrs., Proc. V, pt. 3A, 1966-67.
Weng, C., "Transmission of Fluid Power by Pulsating Flow Concept in Hydraulic Systems," *Jour., Basic Engineering, Amer. Soc. of Mech. Engrs.*, June 1966.
Tadaya, I. et al., "Study of Self-Sustained Oscillations of a Piston-Type Valving System," *Japan Soc. of Mech. Engrs.*, 1967, pp. 793-807.
Florio, P. J. and Mueller, W. K., "Development of a Periodic Flow in a Rigid Tube," *Jour. Basic Engineering*, Sept. 1968, p. 395.
Holley, E. R., "Surging in a Laboratory Pipeline with Steady Inflow," *Jour. Hyd. Div., Amer. Soc. of Civ. Engrs.*, May 1969, pp. 961-980.
Chaudhry, M. H., Discussion of preceding paper by Holley, E. R., Jan. 1970, pp. 294-296.
Moshkov, L. V., "Natural Frequencies of Water Pulsations in a Pipe of Uniform Cross Section in the Case of Aerated Flow," *Trans. Vedeneev All Union Scientific Res. Inst. of Hyd. Engineering*, vol. 88, 1969, pp. 46-54 (translated from Russian Israel Program Sci. Trans., Jerusalem, 1971).

CHAPTER 9

TRANSIENT CAVITATION AND COLUMN SEPARATION

9.1 INTRODUCTION

In the previous chapters, we assumed that the transient-state pressures throughout the system remained above the vapor pressure of the liquid. However, this is not always the case. In many low-head systems or systems in which transients are produced rapidly, the pressure may be reduced to the vapor pressure of the liquid. This may produce vapor cavities in the flow or may cause the liquid column to separate. Rejoining of the separated columns or collapse of the cavities results in a large pressure rise, which may damage the piping system.

The term *transient cavitation* is used herein to refer to the phenomenon of the formation and growth of cavities within a liquid due to reduction of transient-state pressures to the vapor pressure of the liquid. Depending upon the pipeline geometry and the velocity gradient, the cavity may become so large as to fill the entire cross section of the pipe. This is called *column separation*. The liquid is divided into two columns at the location of column separation (see Fig. 9.1). Some authors also refer to the formation of a large cavity at the top of a pipe as *column separation*.

In this chapter, column separation and transient cavitation are briefly described. Various causes that may reduce the liquid pressures to the vapor pressure are then discussed. Expressions for the dissipation and for the velocity of pressure waves in a gas-liquid mixture are presented. Various methods available for the analysis of cavitating flows or flows in which column separation may occur are listed, and the details of two of these methods are presented. The chapter concludes with a case study.

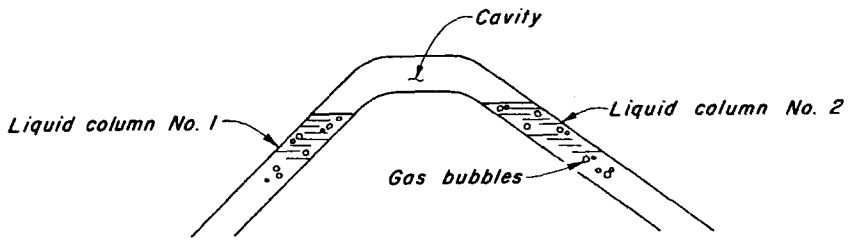

Figure 9.1. Column separation.

9.2 GENERAL REMARKS

Almost all industrial liquids and especially natural water contain a small gaseous phase either in the form of free bubbles or as nuclei adhering to or hidden in the fissures of solids. The solids may form a boundary containing the liquid, or they may be present as contaminants in the liquid. The nuclei grow in size when the liquid pressure is reduced to the vapor pressure and may become bubbles of sufficient size to act as nuclei for cavitation. The growth of a bubble depends upon the force acting on the bubble due to surface tension, the ambient liquid pressure, the vapor pressure of the liquid, the gas pressure inside the bubble, and the time-pressure history to which the bubble has been exposed. Furthermore, the molecules of free gases may enter the bubble, and two or more bubbles may coalesce to form a large cavity. The size of this cavity increases until the difference between its internal pressure and the decreasing external pressure is sufficient to offset the surface tension. Once this critical size is reached, the vapor-filled cavity becomes unstable and expands explosively. This hypothesized sequence of events, i.e., from the pressure reduction to the onset of explosive cavitation, occurs in a very short time period, probably in a few milliseconds.[1]

Depending upon the system geometry and the velocity gradient, the cavity may become so large as to fill the entire cross section of the pipe and thus divide the liquid into two columns. This usually occurs in vertical pipes, pipes having steep slopes, or pipes having "knees" in their profile. Experimental investigations[2-6] have shown that bubbles are dispersed in the pipeline over a considerable distance on either side of the location of the column separation.

In horizontal pipes or pipes having mild slopes, a thin cavity confining to the top of the pipe and extending over a long distance may be formed. In addition, in this case, cavitation bubbles are produced over a considerable length of the pipe. Such a flow is referred to as *cavitating flow*.

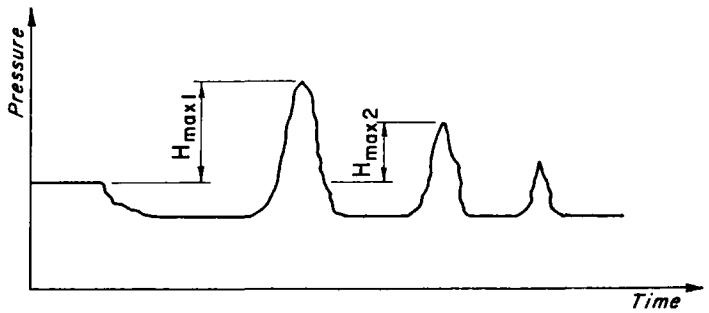

Figure 9.2. Time history of pressure following column separation.

The low pressures that may lead to column separation or cavitating flows are produced by negative or rarefaction waves. These waves are reflected as positive waves from various boundaries (e.g., a reservoir) in the system, and compress the bubbles in the cavitation-flow region and progressively reduce the size of the cavity where column separation had occurred. When the cavities collapse or when the separated columns rejoin, very high pressures are produced. These pressures may burst the pipe if they are not allowed for in the design.

The pressure inside a cavity is equal to the sum of the partial pressures of the liquid vapors and the released gases. If the temperature of the liquid is assumed constant, the partial pressure of the liquid vapors is constant. The partial pressure of the gases can, however, increase or decrease if their mole fraction in the cavity increases or decreases. If a cavity forms and collapses several times during a transient, Weyler's experimental measurements[3] show that the pressure within the cavity increases with successive cavity formations.

If water-column separation occurs at more than one location, Tanahashi and Kasahara's experimental results[2] show that the second pressure peak may be higher than the first pressure peak, i.e., $H_{max_2} > H_{max_1}$ (Fig. 9.2), although generally the first pressure peak is the highest.

9.3 CAUSES OF REDUCTION OF PRESSURE TO VAPOR PRESSURE

The transient-state pressure in a pipeline may be reduced to vapor pressure by power failure to a pump or by rapid closure of a valve. The sequence of events for these cases follows.

Upon power failure, negative-pressure waves generated at the pump travel in the downstream direction. If the pumping head is small and the pump has a small moment of inertia, the pressure in the pipeline may be reduced to vapor pressure. For high-head pumping systems, the pressure at a high point of the pipeline may be reduced to vapor pressure (Fig. 9.3a).

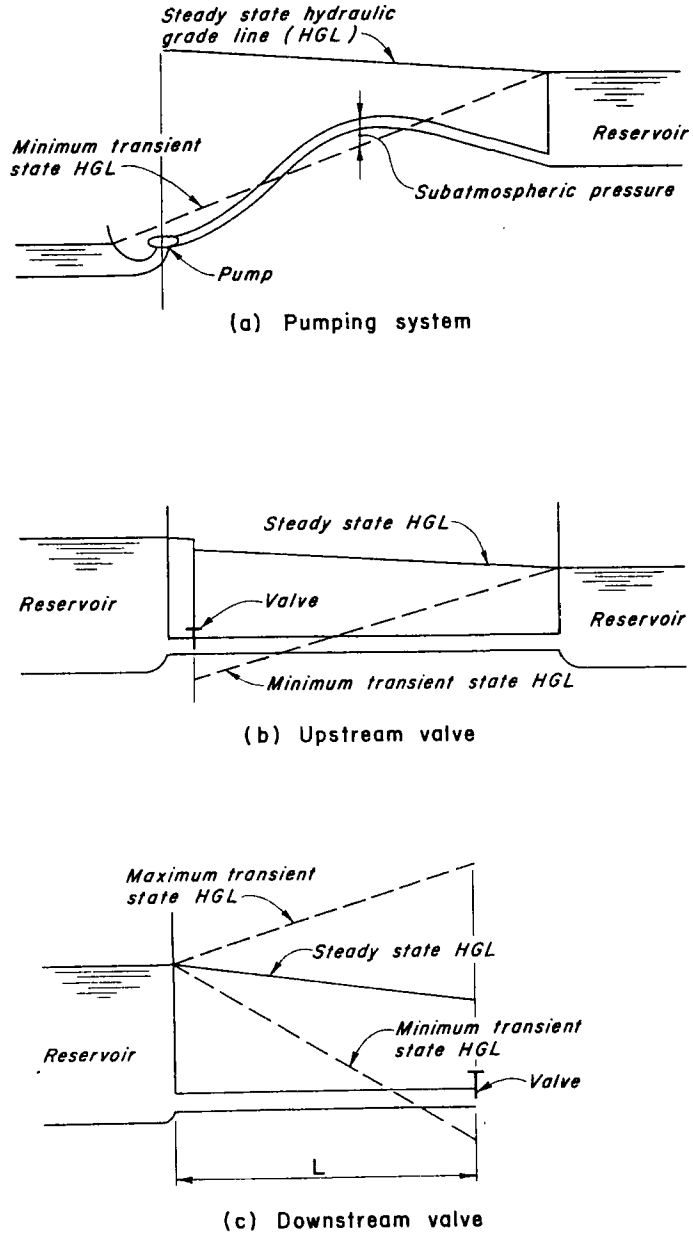

Figure 9.3. Reduction of transient-state pressure to vapor pressure.

If a valve is closed rapidly at the upstream end of a pipeline (Fig. 9.3b), the pressure downstream of the valve may be reduced to vapor pressure. Similarly, the pressure upstream of a rapidly closing valve located at the downstream end of a pipeline may be reduced to vapor pressure $2L/a$ s after the valve closure (a = velocity of waterhammer waves, and L = length of the pipeline). The sequence of events is as follows: A positive pressure wave produced by the closure of the valve travels in the upstream direction. It is reflected as a negative wave from the reservoir. This negative wave is again reflected as a negative wave at the valve. If the initial steady-state pressure were low or if the magnitude of the pressure waves were large, the pressures at the valve may be reduced to vapor pressure.

A rapid opening of a valve at the downstream end of a pipeline may reduce the pipeline pressures to vapor pressure.

9.4 ENERGY DISSIPATION IN CAVITATING FLOWS

Because of the presence of the bubbles, the liquid in a cavitating flow is a mixture of the released gases and the liquid. Experimental investigations have shown that there is more dissipation of the pressure waves in a gas-liquid mixture than in a pure liquid. This additional dissipation is due to the heat transfer to the liquid when the bubbles are expanded and compressed. Bernardis et al.[7] showed how mechanical work is transferred in the form of heat energy into the liquid during each compression-and-expansion cycle of a single spherical bubble containing a perfect gas, confined in an unbound incompressible liquid, and subjected to a sudden pressure impulse of short duration.

Weyler[3] developed the following equation for the shear stress due to nonadiabatic behavior of a spherical bubble

$$\tau_b = C\alpha_o \rho g D |\Delta H| \frac{V}{\Delta x |V|} \tag{9.1}$$

in which α_o = void fraction at reservoir pressure; ρ = mass density of the liquid; g = acceleration due to gravity; D = inside diameter of the pipe; Δx = fixed length of the pipe; ΔH = change in the piezometric head; V = flow velocity; and C = an unknown constant. The void fraction, α, for a gas-liquid mixture is defined as

$$\alpha = \frac{\mathcal{V}_g}{\mathcal{V}_g + \mathcal{V}_l} \tag{9.2}$$

in which $\mathcal{V}_g$ and $\mathcal{V}_l$ are the volumes of the gas and the liquid in the mixture. Weyler determined the value of C by trial and error by comparing his computed

results with Baltzer's experimental data.[1] It was found that $C\alpha_o$ varied slightly for a wide range of α_o, thus allowing the use of a mean value of $C\alpha_o = 225$.

To compute energy dissipation in the cavitating flows, the total shear stress, τ, is determined by adding τ_b to the wall shear stress, τ_o, i.e., $\tau = \tau_b + \tau_o$.

9.5 WAVE VELOCITY IN A GAS-LIQUID MIXTURE

The wave velocity in a liquid having a small quantity of undissolved gases is considerably less[8–13] than in the pure liquid. Pearsall, based on measurements taken on two sewage plants,[11] reported that this reduction in the wave velocity[12] can be as much as 75 percent depending upon the gas content.

By making the following *assumptions*, we can derive[12,14] an expression for the wave velocity in a gas-liquid mixture:

1. The gas-liquid mixture is homogeneous, i.e., the gas bubbles are uniformly distributed in the liquid.
2. The gas bubbles follow an isothermal law.
3. The pressure within the bubbles is independent of the surface tension and the vapor pressure.

Let us consider a volume of gas-liquid mixture at pressure p_o confined in an elastic conduit, and assume that the pressure is instantaneously increased by dp. Then,

$$d\mathcal{V}_m = d\mathcal{V}_g + d\mathcal{V}_l + d\mathcal{V}_c \tag{9.3}$$

in which the subscripts m, g, l, and c, respectively, refer to the quantities for the gas-liquid mixture, gas, liquid, and conduit. The symbol $\mathcal{V}$ denotes volume, and the letter d in front of $\mathcal{V}$ indicates the change in the volume due to increase in pressure, dp. For example, $d\mathcal{V}_g$ is the change in the volume of gas, $\mathcal{V}_g$. Now,

$$\mathcal{V}_m = \mathcal{V}_l + \mathcal{V}_g \tag{9.4}$$

Hence, Eq. 9.2 becomes

$$\alpha = \frac{\mathcal{V}_g}{\mathcal{V}_m} \tag{9.5}$$

Since $\mathcal{V}_g$ is a function of pressure p, α is also a function of p. If the bubble expansion follows an isothermal law, then

$$\alpha p = \alpha_o p_o \tag{9.6}$$

in which subscript o indicates initial conditions, and variables without any subscript refer to conditions at pressure p.

If M and ρ refer to the mass and the mass density, then

$$M_m = M_l + M_g \tag{9.7}$$

It follows from Eq. 9.4 and 9.5 that

$$\mathcal{V}_l = (1 - \alpha)\,\mathcal{V}_m \tag{9.8}$$

Dividing Eq. 9.7 by $\mathcal{V}_m$ and making use of Eqs. 9.5 and 9.8, we can write

$$\rho_m = \rho_l (1 - \alpha) + \alpha\rho_g \tag{9.9}$$

On the basis of Eq. 9.6 and the fact that $p\mathcal{V}_g = p_o\mathcal{V}_{g_o}$, Eq. 9.9 becomes

$$\rho_m = \rho_l \left(1 - \frac{\alpha_o p_o}{p}\right) + \rho_{g_o}\alpha_o \tag{9.10}$$

Let us now write expressions for $d\mathcal{V}_g$, $d\mathcal{V}_l$, and $d\mathcal{V}_c$. If the conduit walls are thin, then

$$d\mathcal{V}_c = -\frac{D_c\,\mathcal{V}_m}{E_c e}\,dp \tag{9.11}$$

in which E_c = modulus of elasticity of the conduit walls, and D_c = diameter of the conduit. If the void fraction is small and K_l = bulk modulus of elasticity of the liquid, then

$$d\mathcal{V}_l = -\mathcal{V}_m \frac{dp}{K_l} \tag{9.12}$$

Since the gas bubbles are assumed to follow the isothermal law, $p\mathcal{V}_g = p_o\mathcal{V}_{g_o}$. Differentiating this equation, we obtain

$$d\mathcal{V}_g = -\mathcal{V}_g \frac{dp}{p} \tag{9.13}$$

Making use of the fact that $\mathcal{V}_g = p_o V_{g_o}/p$ and $\mathcal{V}_{g_o} = \alpha_o\mathcal{V}_m$, Eq. 9.13 becomes

$$d\mathcal{V}_g = -\frac{\alpha_o p_o}{p^2}\,\mathcal{V}_m\,dp \tag{9.14}$$

The bulk modulus of the gas-liquid mixture, K_m, may be defined as

$$K_m = \frac{dp}{-\dfrac{d\mathcal{V}_m}{\mathcal{V}_m}} \tag{9.15}$$

Substituting expressions for $d\mathcal{V}_c$, $d\mathcal{V}_l$, and $d\mathcal{V}_g$ from Eqs. 9.11, 9.12, and 9.14 into 9.3, substituting the resulting expression for $d\mathcal{V}_m$ into Eq. 9.15, and

simplifying, we obtain

$$K_m = \frac{1}{\dfrac{\alpha_o p_o}{p^2} + \dfrac{1}{K_l} + \dfrac{D_c}{E_c e}} \tag{9.16}$$

In Chapter 1, we derived the following expression for the wave velocity (subscript m is added to denote values for the gas-liquid mixture)

$$a_m = \sqrt{\frac{K_m}{\rho_m}} \tag{9.17}$$

Substituting expression for ρ_m from Eq. 9.10 and for K_m from Eq. 9.16 into Eq. 9.17, we obtain

$$a_m = \sqrt{\frac{1}{\left[\rho_l \left(1 - \dfrac{\alpha_o p_o}{p}\right) + \rho_{g_o} p_o\right]\left(\dfrac{\alpha_o p_o}{p^2} + \dfrac{1}{K_l} + \dfrac{D_c}{E_c e}\right)}} \tag{9.18}$$

If the compressibility of the liquid, the elasticity of the conduit walls, and the terms of smaller magnitude are neglected, then the preceding expression, on the basis of Eq. 9.6, may be written as

$$a_m = \sqrt{\frac{p}{\rho_l (1 - \alpha)\,\alpha}} \tag{9.19}$$

In this derivation, we assumed that the pressure inside the bubble did not depend upon the surface tension as well as on the vapor pressure. Raiteri and Siccardi[14] derived an expression for the wave velocity without making this assumption. Kalkwijk and Kranenburg[15] presented a similar, but simplified expression.

9.6 ANALYSIS OF CAVITATING FLOWS AND COLUMN SEPARATION

From the preceding discussion, it is clear that a system in which cavitating flow and column separation occur can be divided into three regions or phases: (1) waterhammer, (2) cavitation, and (3) column separation.

In the waterhammer region, the void fraction is so small that it can be neglected. Hence, the velocity of the pressure waves does not depend upon the pressure. In the cavitation region, gas bubbles are dispersed throughout the liquid. Thus, the liquid behaves like a gas-liquid mixture. In such flows, there is additional damping due to thermodynamic effects (see Section 9.4). In addi-

tion, the velocity of waterhammer waves depends upon the void fraction, which in turn depends upon the pressure.

The three regions may be present simultaneously in a piping system. In such a case, cavitation occurs in one part of the system, column separates at some critical location, and the remaining system can be considered as the waterhammer region. These phases can occur in a sequence as well. For example, the system can be considered initially as waterhammer region, then the void fraction increases due to the reduction of pressure and so the flow becomes a cavitating flow. With further reduction of pressure, the column may separate at a critical point. Then, as the transient-state pressure increases due to wave reflections, the separated columns rejoin, the cavities collapse, and the whole system becomes a waterhammer region again.

In the analysis of systems in which liquid column separates or cavitating flow occurs, there are many unknowns such as the variation of the void fraction along the pipeline and hence the variation of the wave velocity, the energy dissipation, gas release, and so on. Based on various simplifying assumptions, a number of methods for the analysis of column separation and cavitating flows have been reported in the literature. We will briefly discuss some of these methods and present details of two of them.

In the graphical methods,[16–19] the cavitation region is neglected, and the liquid column is assumed to separate over the whole pipe cross section as soon as the pressure at that location drops below the liquid vapor pressure. The volume of the cavity is calculated from the continuity equation using the velocities of the liquid columns on either side of the cavity. The pressure inside the cavity is assumed to be equal to the liquid vapor pressure, and the remaining system is analyzed as for a normal waterhammer analysis.

Streeter and Wylie[20] used a similar procedure in which the method of characteristics was used for the waterhammer analysis and the development, growth, and collapse of a cavity was considered as an internal boundary condition. Pressures following rejoining of the separated columns computed by using this approach were found to be higher than those measured on a prototype.[21] Swaffield[22] showed that a better agreement was obtained, between the computed and measured results for column separation behind a closing valve in a short pipeline, when the gas release was considered than when no gas release was assumed. In the latter case, referred to as a *vapor-only* case, the pressure inside the cavity was assumed equal to the vapor pressure. When gas release was considered, the pressure inside the cavity was assumed equal to the vapor pressure plus the partial pressure of the gas. Similar results were obtained by Kranenburg.[23] Brown[19] reported that the maximum pressures in the pipelines of two pumping systems computed by assuming that column separation occurred at only one critical location were less than those measured on the prototype. However, he obtained better agreement between the computed and measured results when discrete air cavities were assumed along the pipeline.

For horizontal pipes, Baltzer,[1] Dijkman and Vreugdenhil,[24] and Siemons[25] assumed that a thin cavity was formed at the top of the pipe, and analyzed the flow below the cavity, considering it as an open-channel flow. Vreugdenhil et al.[26] presented two mathematical models for the analysis of cavitation in long horizontal pipelines: In the first model, a homogeneous gas-liquid mixture was assumed in the cavitation region, while the regular continuity and dynamic equations of waterhammer were used for the waterhammer region. In the second model, called *separated flow model*, a thin cavity was assumed at the top of the pipe in the cavitation region. Gas release into the cavities was neglected in both the models. Based on experimental observations, Weyler et al.[3] developed a semiempirical formula for predicting additional momentum loss in the cavitation region.

Kranenburg[27] presented a mathematical model in which all three regions—namely, column separation, cavitation, and waterhammer—were considered. Equations were derived such that they are valid both in the cavitation region and in the waterhammer region. A finite-difference scheme was outlined that is suitable for the analysis of shocks. Comparison of the computed and measured results showed good agreement.

Of all the methods listed previously, Kranenburg's mathematical model[27] appears to be the best because of the inclusion of gas release, consideration of all three possible regions, and its suitability for the analysis of shocks without isolating them. (A shock is a steep wave front.) We will present the details of this model in Section 9.8. In addition, the procedure outlined by Brown[19] is very simple, and the comparison of the computed results with those measured on the pipeline of two pumping stations has shown good agreement. Details of this method will be presented in Section 9.10.

9.7 DERIVATION OF EQUATIONS

In this section, we will present the continuity and momentum equations that describe the flow in the cavitation region, and the equations of state for the gas release. These equations were derived by Kranenburg in Ref. 27.

The continuity and momentum equations presented in this section become the continuity and momentum equations for the waterhammer region if the void fraction, α, approaches zero. Hence, these equations can be used for both the cavitation and the waterhammer regions.

Assumptions

The following assumptions are made in the derivation of the equations:

1. The flow is one-dimensional.
2. The gas-vapor-liquid mixture is homogeneous.
3. The vapor pressure and the gas temperature in the cavities are constant. This is a valid assumption since the heat-transfer processes related to the cavities are fast processes compared to the time span of the pressure changes.
4. The momentum of the gas and vapor phases is small compared to that of the liquid phase and may be neglected.
5. The gravity term for the density gradient of the fluid along the pipeline is small and may be neglected.
6. The bubbles are spherical.

Continuity Equation

Applying the law of conservation of mass to a control volume comprising of a segment of the pipe yields

$$\frac{\partial}{\partial t}\int_A (1-\alpha)\,\rho_l\,dA + \frac{\partial}{\partial x}\int_A (1-\alpha)\,\rho_l\,V\,dA = 0 \qquad (9.20)$$

in which α = local void fraction; x = distance along the pipeline; t = time; V = liquid velocity; and A = cross-sectional area of the pipe. Note that α is a function of x, t, and the position in the cross section.

The mean void ratio, $\bar{\alpha}$, for a cross section may be written as

$$\bar{\alpha} = \frac{1}{A}\int_A \alpha\,dA \qquad (9.21)$$

The equations of state for the liquid phase and for a circular pipe are

$$\frac{d\rho_l}{dp} = \frac{\rho_l}{K_l}$$

and

$$\frac{dA}{dp} = \frac{\psi A}{eE/D} \qquad (9.22)$$

in which K_l = modulus of compressibility of the liquid; E = modulus of elasticity of pipe-wall material; e = wall thickness of the pipe; and ψ = a coefficient accounting for the anchorage system of the pipeline. By substituting Eqs. 9.21 and 9.22 into Eq. 9.20, neglecting higher-order terms, and simplifying, we obtain

$$\frac{\partial}{\partial t}\left[(1-\bar{\alpha})\left(1+\frac{p}{\rho_l a_l^2}\right)\right] + \frac{\partial}{\partial x}\left[(1-\bar{\alpha})\left(1+\frac{p}{\rho_l a_l^2}\right)V\right] = 0 \qquad (9.23)$$

in which a_l = wave velocity in the liquid (assuming no gas release) and is given by the expression

$$a_l = \sqrt{\frac{K_l/\rho_l}{1+\frac{\psi D K_l}{eE}}} \qquad (9.24)$$

and p = absolute pressure in the top of the cross section of the pipe.

Momentum Equation

Applying the law of conservation of momentum in the positive x-direction

$$\frac{\partial}{\partial t}\int_A (1-\alpha)\,\rho_l\,V\,dA + \frac{\partial}{\partial x}\int_A (1-\alpha)\,\rho_l\,V^2\,dA + \int_A \frac{\partial p}{\partial x}\,dA = -\int_A (1-\alpha)\left(\rho_l g\sin\theta + \frac{\lambda}{2D}V|V|\right)dA \qquad (9.25)$$

in which θ = angle of inclination of the pipeline, and λ = friction parameter. By substituting Eqs. 9.21 and 9.22 into Eq. 9.25, neglecting higher-order terms, and simplifying, we obtain

$$\frac{\partial}{\partial t}\left[(1-\bar{\alpha})\left(1+\frac{p}{\rho_l a_l^2}\right)V\right] + \frac{\partial}{\partial x}\left[(1-\bar{\alpha})\left(1+\frac{p}{\rho_l a_l^2}\right)V^2 + \frac{p}{\rho_l}\right] = -(1-\bar{\alpha})\left(g\sin\theta + \frac{\lambda}{2D}V|V|\right) \qquad (9.26)$$

Note that Eqs. 9.23 and 9.26 are in the conservation form.

Cavitating Flow

As discussed previously, small bubbles or cavities are present in the region of cavitating flow. Assuming the gas inside the cavity follows the perfect gas law and neglecting surface tension, we can write for the dynamic equilibrium of a

spherical bubble,

$$(p - p_v)\frac{4}{3}\pi R^3 = N_b kT \tag{9.27}$$

in which p_v = vapor pressure of the liquid; R = radius of the bubble; k = universal gas constant; T = absolute temperature; and N_b = quantity of gas in a bubble.

Let us assume that the bubbles are spherical, uniformly distributed, and of the same size. Then, the average void fraction

$$\bar{\alpha} = \frac{n_b}{A}\frac{4}{3}\pi R^3 \tag{9.28}$$

in which n_b = number of bubbles per unit length of the pipeline.

Because of release or re-solution, the quantity of gas, N_b, in a bubble is a function of time, i.e.,

$$\frac{dN_b}{dt} = \gamma (p_s - p)\sqrt{\beta}\, F\left[R(\tau), \frac{dR(\tau)}{dt}, U(\tau)\right] \tag{9.29}$$

in which γ = proportionality constant in Henry's law relating the gas pressure and equilibrium concentration of the dissolved gas; p_s = saturation pressure of the liquid; β = diffusion coefficient; τ = dummy variable with respect to time; and U = bubble velocity with respect to the surrounding liquid.

If $|dR/dt| << U$ and $UR/\beta >> 1$, then the function F may be approximated[28] as

$$F \simeq 4R(t)\sqrt{2\pi U(t)R(t)} \tag{9.30}$$

The value of the bubble velocity, U, may be selected[27] as follows: If the bubble is not influenced by the wall of the pipe, then U may be assumed equal to the rise velocity of the bubble. If the bubble is attached to the wall, U is approximately equal to the liquid velocity V; but, if the bubble is in the topmost part of the pipe without being attached, then U is considerably less. Experimental measurements show that $U \simeq 0.01$ m/s.

Column Separation

As previously discussed, liquid column separates only at the critical sections, such as sharp vertical bends, of a pipeline. Thus, it is a local phenomenon and is governed by the continuity equation only, i.e.,

$$\frac{d\mathcal{V}_c}{dt} = A(V_{c2} - V_{c1}) \tag{9.31}$$

in which $\mathcal{V}_c$ = volume of the cavity at the location of column separation; V_{c1} and V_{c2} are the velocities of the liquid column on the upstream and downstream sides of the cavity, respectively. According to the perfect gas law,

$$(p_c - p_v)\mathcal{V}_c = N_c kT \tag{9.32}$$

in which p_c = pressure at column separation and N_c = quantity of the released gas at the column separation. Gas release or re-solution is represented by

$$\frac{dN_c}{dt} = n_c \frac{dN_b}{dt} \tag{9.33}$$

in which n_c = number of bubbles that together form the column separation and dN_b/dt is determined from Eq. 9.29, assuming $p = p_c$.

9.8 NUMERICAL SOLUTION

Wave Equations

In the last section, we developed equations that describe the transient conditions in the cavitating flows. If the transient-state pressure is significantly higher than the vapor pressure, then the bubble size, and hence the void fraction, become so small that the free-gas content may be neglected. In this case, Eqs. 9.23 and 9.26 reduce to equations describing the transient-state conditions in closed conduits without cavitation. Hence, Eqs. 9.23 and 9.26 may be used in both the waterhammer and cavitation regions.

Equations 9.23, and 9.26 through 9.29 form a nonlinear, second-order, hyperbolic system. The following numerical methods are available for the solution of Eqs. 9.23 and 9.26:

1. Method of characteristics.
2. Finite-difference methods.

As the velocity of waterhammer waves in the cavitation region depends upon the pressure, a fixed grid cannot be used in the method of characteristics, since a fixed grid requires interpolations at each time step which smoothen the sharp peaks. Interpolations can be eliminated by using a flexible grid. However, if a shock is formed, the method fails because of the convergence of the characteristic curves.[29] This difficulty can be circumvented by isolating the shock in the computations. Although, isolation of the shock may be feasible for the analysis of a simple system,[15] the procedure is too cumbersome to be practical.

Only those finite-difference methods are suitable for the numerical integration of Eqs. 9.23 and 9.26, in which isolation of the shock is not necessary and which

add some numerical dissipation terms[30] so that the nonlinear instability due to the pressure dependence of the waterhammer wave velocity is damped. Two such schemes are available: Lax's diffusive scheme and Lax-Wendroff's two-step scheme. Lax's scheme[31] is of first-order accuracy and introduces additional diffusion terms, which are not present in the original differential equations. This may result in reducing the maximum pressures. Lax-Wendroff's scheme[32] is of second-order accuracy. It can be shown that the resulting difference equations, based on this scheme, are consistent with the original differential equations. Details of this scheme are presented herein.

To apply the Lax-Wendroff's scheme, it is necessary that the governing equations be in the so-called conservation or divergence form. The continuity and momentum equations, Eqs. 9.23 and 9.26, are in conservation form and may be written as

$$\frac{\partial y_{1i}}{\partial t} + \frac{\partial y_{2i}}{\partial x} = y_{3i} \tag{9.34}$$

in which y_{ji} ($j = 1, 2, 3$ and $i = 1, 2$) is a function of the pressure, velocity, and void fraction. By replacing the partial derivatives of Eq. 9.34 by finite differences (Fig. 9.4a) as given by the Lax scheme, we obtain

$$y_{1i}(x + \Delta x, t + \Delta t) = 0.5[y_{1i}(x + 2\Delta x, t) + y_{1i}(x, t)] + \left\{\frac{-\Delta t}{2\Delta x}[y_{2i}(x + 2\Delta x, t) - y_{2i}(x, t)] + \frac{\Delta t}{2}[y_{3i}(x + 2\Delta x, t) + y_{3i}(x, t)]\right\} \tag{9.35}$$

in which Δx = length of a reach into which a pipeline is divided and Δt = computational time step. By adding the following second step to Eq. 9.35, a second-order accuracy can be obtained:

$$y_{1i}(x, t + 2\Delta t) = y_{1i}(x, t) - \frac{\Delta t}{\Delta x}[y_{2i}(x + \Delta x, t + \Delta t) - y_{2i}(x - \Delta x, t + \Delta t)] + \Delta t[y_{3i}(x + \Delta x, t + \Delta t) + y_{3i}(x - \Delta x, t + \Delta t)] \tag{9.36}$$

Equations 9.35 and 9.36 are known as *Lax-Wendroff's two-step scheme*. The numerical damping introduced by this scheme is acceptable[33] provided Δx is small.

The above finite-difference scheme is stable if

$$\Delta x \geq \Delta t(a_l + |V|) \tag{9.37}$$

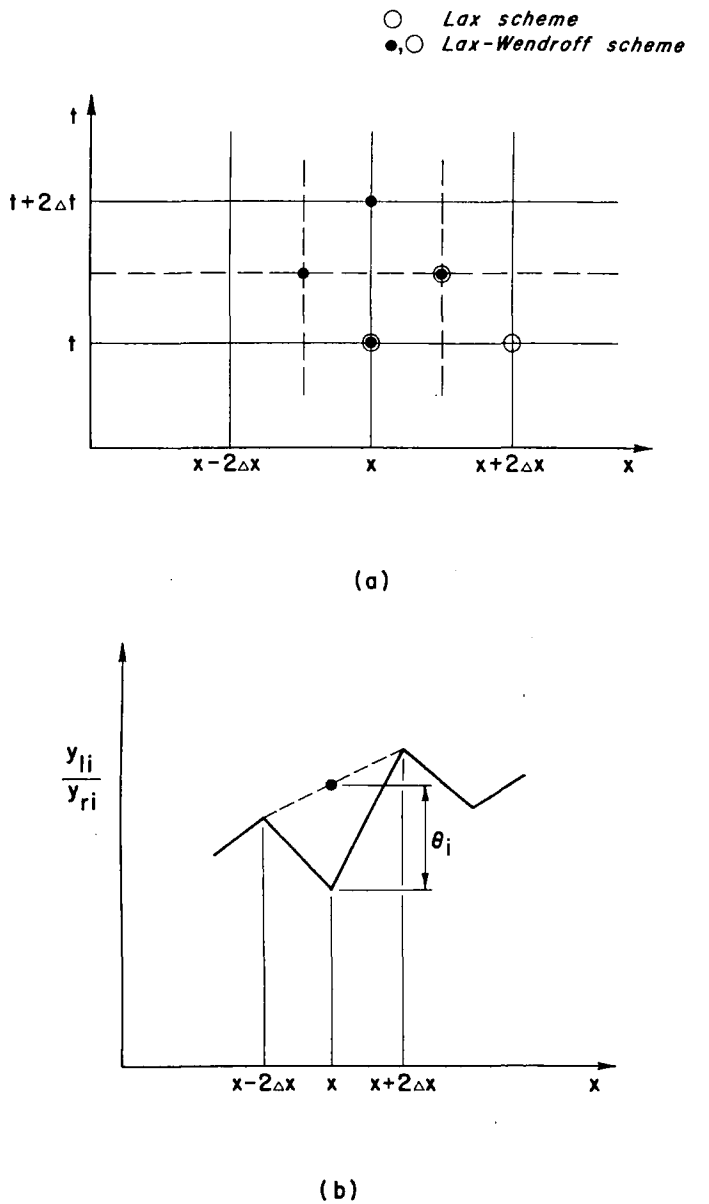

Figure 9.4. Notation for Lax-Wendroff's two-step scheme. (After Kranenburg[27])

and

$$\Delta t < \frac{D}{\lambda |V|} \tag{9.38}$$

If the transient-state pressures drop to the vapor pressure of the liquid, then the solution obtained by using the Lax-Wendroff's scheme show some oscillations, which are caused by the nonlinearities of the governing equations. These oscillations can be suppressed by applying a smoothing operator at those grid points at which a parameter, θ_i, characterizing the oscillations in the variable y_{1i}, exceeds a prescribed value, θ_r. The parameter θ_i is defined as

$$\theta_i(x, t) = \frac{0.5[y_{1i}(x + 2\Delta x, t) + y_{1i}(x - 2\Delta x, t)] - y_{1i}(x, t)}{y_{ri}} \tag{9.39}$$

in which y_{ri} = reference interval of the variable $y_{1i}(x, t)$. (See Fig. 9.4b.) If $|\theta_i| > \theta_r$, the smoothened value of y_{1i} is determined from the equation

$$\bar{y}_{1i}(x, t) = y_{1i}(x, t) + 0.5 y_{ri} \theta_i(x, t) \tag{9.40}$$

However, if $|\theta_i| < \theta_r$, the value of $y_{1i}(x, t)$ is not smoothened. Kranenburg used $|\theta_r| = 0.01$ in his computations.

Column Separation

As discussed previously, liquid column separates only at the critical locations of a pipeline. This can, therefore, be explicitly taken into account at the points where it is expected to occur. The differential equations describing the column separation, Eqs. 9.31 and 9.32, can be integrated by using an explicit finite-difference scheme. However, the time steps required for such a scheme for small amounts of free gas, N_c, is considerably less than that given by Eq. 9.37. This difficulty can be overcome by eliminating V_{c1} and V_{c2} by using the compatibility equations[27,33,34] for the characteristic directions following from Eqs. 9.23 and 9.26.

$$V_{c1} + \frac{1}{\rho_l a_R}(p_c - p_v) = B_1 = \left[V + \frac{1}{\rho_l a}(p - p_v) + \Delta t \left(\frac{-\lambda}{2D} V|V| - g \sin\phi + \frac{a n_b k T}{A(p - p_v)} \frac{dN_b}{dt} \right) \right]_R \tag{9.41}$$

$$V_{c2} - \frac{1}{\rho_l a_S}(p_c - p_v) = B_2 = \left[V - \frac{1}{\rho_l a}(p - p_v) + \Delta t \left(\frac{-\lambda}{2D} V|V| - g \sin\phi - \frac{a n_b k T}{A(p - p_v)} \frac{dN_b}{dt} \right) \right]_S \tag{9.42}$$

in which the subscripts R and S denote conditions at points R and S, which are assumed equal to those at the grid points A and B on either side of column separation (Fig. 9.5). By eliminating V_{c1}, V_{c2}, and p_c from Eqs. 9.31, 9.32, 9.41, and 9.42 and integrating over a time step, $2\Delta t$, assuming N_c to be constant, we obtain

$$\forall_c(t + 2\Delta t) = \forall_c(t) + 2\Delta t(B_1 - B_2) A + \frac{C_w}{\rho_l(B_1 - B_2)} \ln\left[\frac{C_w + \rho_l(B_1 - B_2) \forall_c(t + 2\Delta t)}{C_w + \rho_l(B_1 - B_2) \forall_c(t)} \right] \tag{9.43}$$

in which

$$C_w = \left(\frac{1}{a_1} + \frac{1}{a_2} \right) N_c k T \tag{9.44}$$

Equation 9.43 allows larger time steps without leading to instability.

Gas Release

A simple explicit finite-difference scheme may be used to integrate Eqs. 9.29 and 9.33 describing the gas release and re-solution.

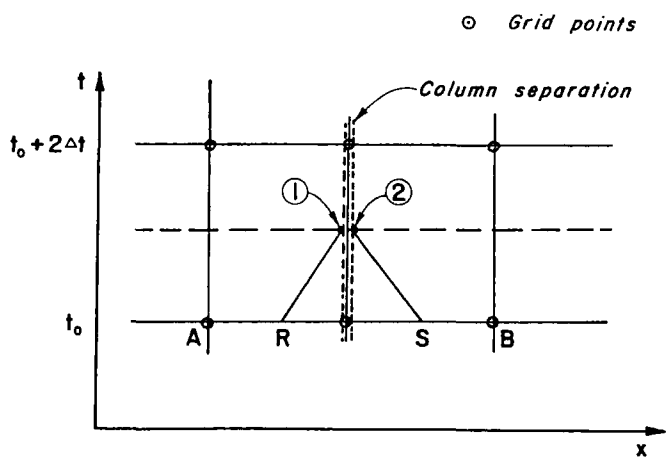

Figure 9.5. Notation for liquid-column separation.

Results

Kranenburg[27] compared the results computed by using the mathematical model of Sections 9.7 and 9.8 with Baltzer's experimental results[1] and with those measured on a laboratory pipeline.[26] The agreement between the computed and measured results was satisfactory.

Based on the results of his studies, Kranenburg concluded that:

1. Including the gas release has insignificant influence in cases where only cavitating flow occurs; however, the influence is considerable in cases in which both column separation and cavitating flow occur.
2. Gas release in the cavitating flow adjacent to the column separation reduces the duration of the subsequent column separations and hence the maximum pressures following column separation.
3. Gas release at the separation cavity increases the duration of column separation and slightly increases the pressure.
4. For a quantitative prediction of the gas release, further investigations, probably on prototypes, are required of various parameters, such as number of bubbles, n_b and n_c, and relative bubble velocity.

9.9 DESIGN CONSIDERATIONS

If the analysis of transient conditions shows that the liquid column will separate or transient cavitation will occur in a pipeline, then it has to be decided whether the pressures generated when the separated columns rejoin or when the cavities collapse are acceptable. Of course, it is possible to design a pipeline to withstand any pressure. Such a design will, however, be uneconomical. Therefore, provision of various control devices or appurtenances should be investigated to obtain an overall economic design.

The following are some of the common appurtenances usually employed to prevent column separation or to reduce the pressure rise when the separated columns rejoin:

1. Air chambers
2. Surge tanks
3. One-way surge tanks
4. Flywheel
5. Air-inlet valves
6. Pressure-relief or pressure-regulating valve.

Providing an air chamber or a surge tank is usually costly. Increasing the WR^2 of the pump-motor by means of a flywheel increases the space requirements and may require a separate starter for the motor, thus increasing the initial costs. Caution must be exercised if air-inlet valves are used, because once air is admitted into a pipeline, it has to be removed from the line prior to refilling since entrapped air can result in very high pressures. By providing a pressure-relief valve or a pressure-regulating valve, the pressure rise can be reduced by letting the columns rejoin under controlled conditions.

In addition to the initial costs, the cost and ease of maintenance should be taken into consideration while selecting any of the preceding appurtenances for a particular installation.

9.10 CASE STUDY

Brown[19] reported analytical studies and prototype test results on the water-column separation in the discharge lines of two pumping plants designed by the United States Bureau of Reclamation. Details of the mathematical model and comparison of the computed and measured results for one of the pumping plants are presented in this section.

Project Details

The pipeline profile for the 7.2 Mile Pumping Plant is shown in Fig. 9.6. Other data for the pumping plant are:

Type of pump:	Single stage, double suction
Rated head:	72.24 m
Flow at rated head:	0.237 m^3/s
Rated speed:	1770 rpm
Peak efficiency:	86 percent
Specific speed of equivalent single suction pump:	1270 (gpm units); 25 (SI units)
Length of pipeline:	1078 m
Diameter of pipeline:	0.61 m
Thickness of steel pipe:	4.8 mm
Output of motors:	224 kW
WR^2 of one motor:	10.11 kg m^2
WR^2 of one pump:	1.59 kg m^2
No. pumping units:	2

The pump characteristics were obtained from a double suction-type pump,[35,36] and therefore its equivalent, single-suction, specific speed is 1270 (gpm units) instead of the listed value of 1800.

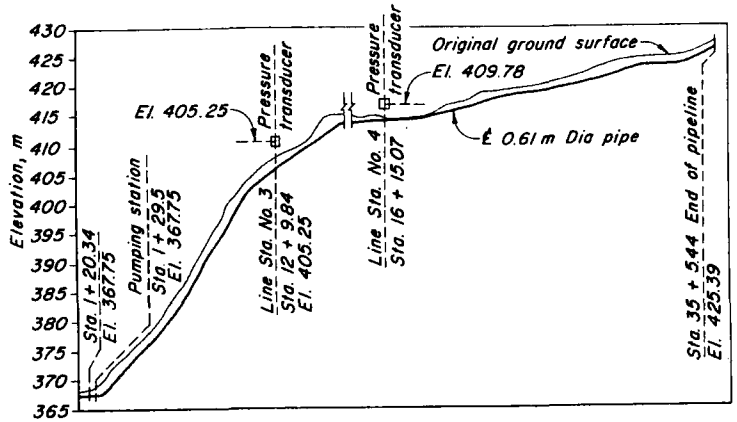

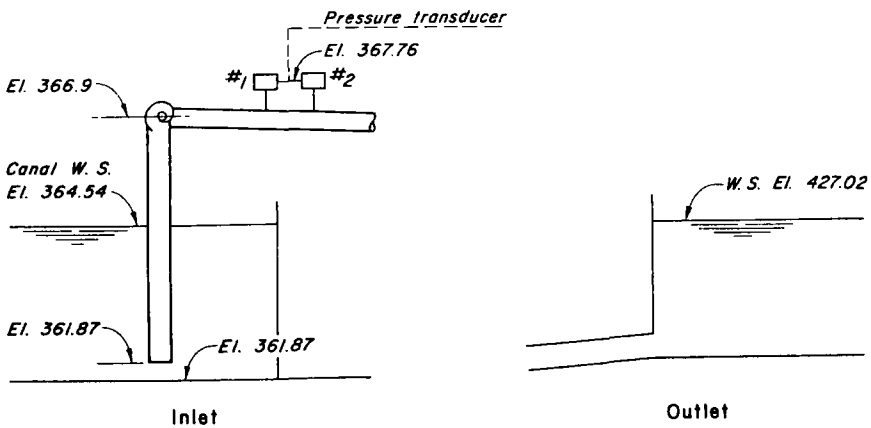

Figure 9.6. Profile of 7.2-mile pumping plant. (After Brown[19])

Field Tests

The locations of the test stations are marked in Fig. 9.6. The pumping-plant station is located essentially at the pumping units, and station 3 and 4 bracket the "knee" in the pipeline where the water column was expected to separate. The resistance-type pressure cells were used to measure the pressure, and a photoelectric revolution counter was used to measure the pump speed. High-speed oscillographs were used to record the data.

Mathematical Model

A mathematical model was developed based on the method of characteristics. The upstream boundary condition was a centrifugal pump. The pump characteristics for all four zones of operation were stored in the computer. The downstream boundary condition was a constant-head reservoir. The effect of the entrained air and column separation was taken into consideration as outlined below. In order to be compatible with the text, the notation used herein is different from that of Ref. 19.

The total volume of the entrained air in the pipeline is assumed to be concentrated at discrete air cavities. Let us consider the air cavity located at the ith junction (see Fig. 9.7). The volume of this air cavity is

$$\forall_i = \alpha A_i L_i \tag{9.45}$$

in which α = void fraction and L_i and A_i are the length and cross-sectional area of the ith pipe, respectively.

The expansion and contraction of the air pocket is assumed to follow the

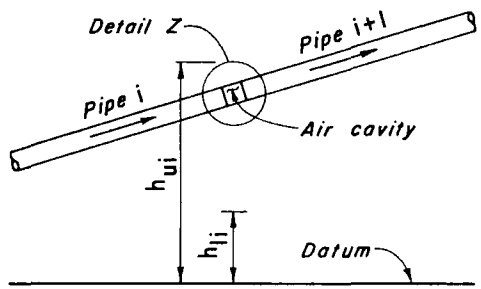

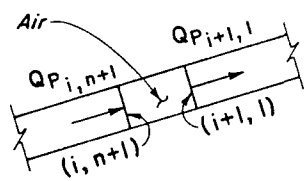

Figure 9.7. Notation for air cavity. (After Brown[19])

polytropic equation for a perfect gas

$$(H_{P_{i,n+1}} - h_{li})\, \forall_{P_i}^m = C \tag{9.46}$$

in which $\forall_{P_i}$ = volume of the air pocket at the end of time step; $H_{P_{i,n+1}}$ = piezometric head above the datum at section $(i, n+1)$ at the end of time step; C = a constant determined from the initial steady-state conditions for the air pocket; and h_{li} = pressure head between the datum and the lowest possible absolute-pressure head level that a gauge at the top of the pipe at junction i could measure (Fig. 9.7). The value of exponent m is equal to 1.0 for a slow isothermal process, and it is equal to 1.4 for a fast adiabatic process. An average value of $m = 1.2$ may be used.

The continuity equation at the cavity may be written as

$$\forall_{P_i} = \forall_i + \tfrac{1}{2}\,\Delta t[(Q_{P_{i+1,1}} + Q_{i+1,1}) - (Q_{P_{i,n+1}} + Q_{i,n+1})] \tag{9.47}$$

in which Δt = size of the time step; $\forall_i$ and $\forall_{P_i}$ are the volumes of the air cavity at the beginning and at the end of the time step; $Q_{i,n+1}$ and $Q_{P_{i,n+1}}$ are the flow rates at the upstream end of the air cavity at the beginning and at the end of the time step; and $Q_{i+1,1}$ and $Q_{P_{i+1,1}}$ are the flow rates at the downstream end of the air cavity at the beginning and at the end of the time step. Note that the values of the variables at the beginning of the time step are known.

If the method of characteristics (see Chapter 3) is used for the analysis of transient conditions, then the positive and negative characteristic equations (Eqs. 3.18 and 3.19) for the $(i, n+1)$ and $(i+1, 1)$ section are

$$Q_{P_{i,n+1}} = C_p - C_{a_i} H_{P_{i,n+1}} \tag{9.48}$$

and

$$Q_{P_{i+1,1}} = C_n + C_{a_{i+1}} H_{P_{i+1,1}} \tag{9.49}$$

If the head losses at the junction are neglected, then

$$H_{P_{i,n+1}} = H_{P_{i+1,1}}. \tag{9.50}$$

There are five unknowns, namely, $\forall_{P_i}, Q_{P_{i,n+1}}, Q_{P_{i+1,1}}, H_{P_{i,n+1}}$ and $H_{P_{i+1,1}}$, in Eqs. 9.46 through 9.50, which can be solved by an iterative technique.

Comparison of Computed and Measured Results

In the computations done by Brown, α at an absolute pressure head of 10.4 m was assumed equal to $1.x\ 10^{-4}$, and the value of exponent, m, was taken equal to 1.2. The pipeline was divided into 30 pipes, and an air cavity was assumed at the end of each pipe. The effects of the entrained air were considered only in the effective head range, $h_{ui} - h_{li}$ in which h_{ui} is defined as the upper limit of

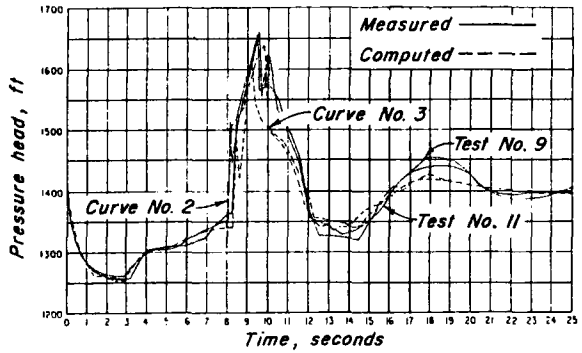

(a) Pumping plant station

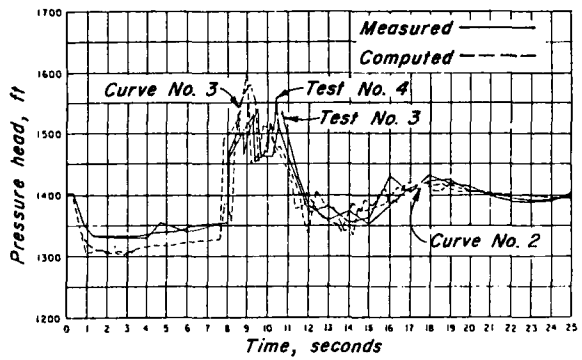

(b) Line station 3 – one pump operation

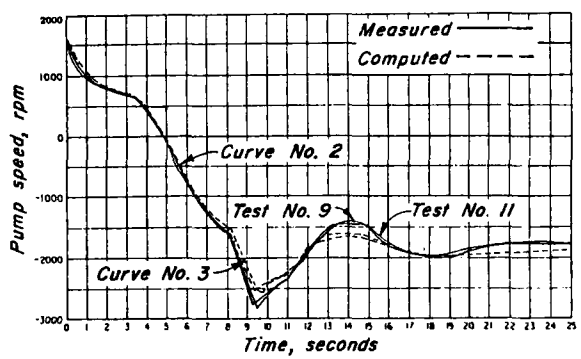

(c) Pump speed

Figure 9.8. Comparison of computed and measured results. (After Brown[19])

the effective head range. If the hydraulic grade line was above h_{ui}, the effects of the air at that location were neglected. An effective head range, $h_{ui} - h_{li}$, of 10.4 m was used in the computations.

The measured and computed results are shown in Fig. 9.8. In one case, shown as Curve No. 2, a very small amount of air was considered only at the critical point, i.e., at the knee in the pipeline profile. This was done to determine the effects of the air entrainment. For Curve No. 3, $\alpha = 0.0001$ was assumed. It is clear from these figures that a better agreement is obtained between the computed and measured results if the effects of entrained air are taken into consideration.

9.11 SUMMARY

In this chapter, flows in which liquid-column separation and cavitating flows may occur were considered, and the causes of the reduction of pressure that may produce these flows were outlined. The continuity and momentum equations describing the cavitating flows were derived, and the methods available for their solution were listed. Details of one of these methods were presented. The chapter concluded with a case study.

PROBLEMS

9.1 Derive Eq. 9.19 from first principles.

9.2 At low pressures and temperatures, the expansion of the entrained gases in a gas-liquid mixture is isothermal, and thus the bulk modulus of the gas, K_g, is equal to the absolute pressure of the gas, p_g.[16] From first principles, prove that, for a low gas content (i.e., void fraction, $\alpha < 0.001$),

$$\frac{a}{a_o} = \sqrt{\frac{p_g}{\alpha K_l + p_g}}$$

in which a_o = wave velocity in a gas-free liquid. Neglect the effect of the pipeline anchorage system. (*Hint:* For small values of α, $\alpha\rho_g \ll (1 - \alpha)\rho_l$ and $(1 - \alpha)\rho_l \simeq \rho_l$.)

9.3 Assuming different values of α, compute the wave velocity, a, in an air-water mixture at atmospheric pressure. Plot a graph between a and α.

9.4 Write a computer program for the analysis of the piping system shown in Fig. 9.3a. Transient conditions are produced by power failure to the pump-motors. Assume that the water-column separation occurs as soon as the pressure at the summit of the pipeline is reduced to the vapor pressure of the liquid.

9.5 By using the program of Problem 9.4, investigate the effect of increasing the WR^2 of the pump-motors on the duration of column separation and on the maximum pressures in the pipeline.

REFERENCES

1. Baltzer, R. A., "Column Separation Accompanying Liquid Transients in Pipes," *Jour. of Basic Engineering*, Amer. Soc. of Mech. Engrs., Dec. 1967, pp. 837–846.
2. Tanahashi, T. and Kasahara, E., "Comparison between Experimental and Theoretical Results of the Waterhammer with Water Column Separations," *Bull. Japan Soc. of Mech. Engrs.*, vol. 13, no. 61, July 1970, pp. 914–925.
3. Weyler, M. E., Streeter, V. L., and Larsen, P. S., "An Investigation of the Effect of Cavitation Bubbles on the Momentum Loss in Transient Pipe Flow," *Jour. Basic Engineering*, Amer. Soc. of Mech. Engrs., March 1971, pp. 1–7.
4. Sharp, B. B., Discussion of Ref. 3, *Jour. Basic Engineering*, Amer. Soc. of Mech. Engrs., March 1971, pp. 7–10.
5. Safwat, H. H., "Photographic Study of Water Column Separation," *Jour., Hyd. Div., Amer. Soc. of Civ. Engrs.*, vol. 98, April 1972, pp. 739–746.
6. Safwat, H. H., "Water-Column Separation and Cavitation in Short Pipelines," Paper No. 75-FE-33, presented at the Joint Fluid Engineering and Lubrication Conference, Minneapolis, Minn., organized by *Amer. Soc. of Mech. Engrs.*, May 1975.
7. Bernardinis, B. D., Federici, G., Siccardi, F., "Transient with Liquid Column Separation: Numerical Evaluation and Comparison with Experimental Results," *L'Energia Elettrica*, no. 9, 1975, pp. 471–477.
8. Wood, A. B., *A Textbook of Sound*, Bell & Sons, London, 1955.
9. Ripken, J. F. and Olsen, R. M., "A Study of the Gas Nuclei on Cavitation Scale Effects in Water Tunnel Tests," *St. Anthony Falls Hyd. Lab. Proj., Report No. 58*, Minneapolis, Univ. of Minnesota, 1958.
10. Silberman, E., "Some Velocity Attenuation in Bubbly Mixtures Measured in Standing Wave Tubes," *Jour. Accoust. Soc. of Amer.*, vol. 29, 1957, p. 925.
11. Whiteman, K. J. and Pearsall, I. S., "Reflex-Valve and Surge Tests at a Station," *Fluid Handling*, vol. XIII, Sept. and Oct. 1962, pp. 248–250 and 282–286.
12. Pearsall, I. S., "The Velocity of Water Hammer Waves," *Symposium on Surges in Pipelines, Institution of Mech. Engrs.*, vol. 180, part 3E, Nov. 1965, pp. 12–20 (see also discussions, pp. 21–27 and author's reply, pp. 110–111).
13. Kobori, T., Yokoyama, S., and Miyashiro, H., "Propagation Velocity of Pressure Waves in Pipe Line," *Hitachi Hyoron*, vol. 37, no. 10, Oct. 1955.
14. Raiteri, E. and Siccardi, F., "Transients in Conduits Conveying a Two-phase Bubbly Flow: Experimental Measurements of Celerity," *L'Energia Elettrica*, no. 5, 1975, pp. 256–261.
15. Kalkwijk, J. P. Th. and Kranenburg, C., "Cavitation in Horizontal Pipelines due to Water Hammer," *Jour., Hyd. Div., Amer. Soc. Civ. Engrs.*, vol. 97, Oct. 1971, pp. 1585–1605.
16. Bergeron, L., *Waterhammer in Hydraulics and Wave Surges in Electricity*, John Wiley & Sons, New York, 1961 (translated from original French text published by Dunod, Paris, 1950).

17. Parmakian, J., "One-Way Surge Tanks for Pumping Plants," *Trans. Amer. Soc. of Mech. Engrs.*, vol. 80, 1958, pp. 1563-1573.
18. Sharp, B. B., "Rupture of the Water Column," *Proc. Second Australian Conf. of Hydraulics, Fluid Mech.*, Auckland, New Zealand, 1965, pp. A 169-176.
19. Brown, R. J., "Water-Column Separation at Two Pumping Plants," *Jour. Basic Engineering*, Amer. Soc. of Mech. Engrs., Dec. 1968, pp. 521-531.
20. Streeter, V. L. and Wylie, E. B., *Hydraulic Transients*, McGraw-Hill Book Co., New York, 1967.
21. Joseph, I., "Design of Protective Facilities for Handling Column Separation in a Pump Discharge Line," in *Control of Flow in Closed Conduits*, edited by Tullis, J. P., Fort Collins, Colorado, 1971, pp. 295-313.
22. Swaffield, J. A., "Column Separation in an Aircraft Fuel System," *Proc. First International Conference on Pressure Surges*, British Hydromechanics Research Assoc., England, 1972, pp. (C2) 13-28.
23. Kranenburg, C., "The Effects of Free Gas on Cavitation in Pipelines," *Proc. First International Conference on Pressure Surges*, British Hydromechanics Research Assoc., England, 1972, pp. (C4) 41-52.
24. Dijkman, H. K. M. and Vreugdenhil, C. B., "The Effect of Dissolved Gas on Cavitation in Horizontal Pipe-Lines," *Jour. Hyd. Research*, International Assoc. of Hyd. Research, vol. 7, no. 3, 1969, pp. 301-314.
25. Siemons, J., "The Phenomenon of Cavitation in a Horizontal Pipe-line due to Sudden Pump-Failure," *Jour. Hyd. Research*, International Assoc. for Hyd. Research, vol. 5, no. 2, 1967, pp. 135-152.
26. Vreugdenhil, C. B., de Vries, A. H., Kalkwijk, J. P. Th., and Kranenburg, C., "Investigation into Cavitation in Long Horizontal Pipeline Caused by Water-Hammer," *6th Symposium, International Assoc. for Hyd. Research*, Rome, Italy, Sept. 1972, 13 pp.
27. Kranenburg, C., "Gas Release During Transient Cavitation in Pipes," *Jour., Hyd. Div., Amer. Soc. of Civ. Engrs.*, vol. 100, Oct. 1974, pp. 1383-1398.
28. Boussinesq, J., "Calcul du Pouvoir Refroidissant des Courants Fluides," *Journal de Mathématiques Pures et Appliquées*, Paris, France, vol. 6, no. 1, 1905, pp. 285-332.
29. Martin, C. S. and Padmanabhan, M., "The Effect of Free Gases on Pressure Transients," *L'Energia Elettrica*, no. 5, 1975, pp. 262-267.
30. Richtmeyer, R. D. and Morton, K. W., *Difference Methods for Initial-Value Problems*, Interscience Publications, New York, 1967.
31. Lax, P. D., "Weak Solutions of Nonlinear Hyperbolic Equations and Their Numerical Computation," *Communications on Pure and Applied Mathematics*, vol. 7, 1954, pp. 159-163.
32. Lax, P. D. and Wendroff, B., "System of Conservation Laws," *Communications on Pure and Applied Mathematics*, vol. 13, 1960, pp. 217-237.
33. Kranenburg, C., "Transient Cavitation in Pipelines," *Report No. 73-2, Laboratory of Fluid Mechanics*, Dept. of Civil Engineering, Delft University of Technology, Delft, The Netherlands, 1973.
34. Streeter, V. L., "Transients in Pipelines Carrying Liquids or Gases," *Jour., Transp. Div., Amer. Soc. of Civ. Engrs.*, vol. 97, Feb. 1971, pp. 15-29.
35. Stepanoff, A. M., *Centrifugal and Axial Flow Pumps*, John Wiley & Sons, New York, 1948, pp. 271-295.
36. Swanson, W. M., "Complete Characteristic Circle Diagrams for Turbomachinery," *Trans. Amer. Soc. of Mech. Engrs.*, vol. 75, 1953, pp. 819-826.

ADDITIONAL REFERENCES

de Haller, P. and Bedue, A., "The Break-away of Water Columns as a Result of Negative Pressure Shocks," *Sulzer Tech. Review*, vol. 4, pp. 18-25, 1951.
Duc, J., "Water Column Separation," *Sulzer Tech. Review*, vol. 41, 1959.
Lupton, H. R., "Graphical Analysis of Pressure Surges in Pumping Systems," *Jour Inst. of Water Engrs.*, vol. 7, 1953, p. 87.
Richards, R. T. et al., "Hydraulic Design of the Sandow Pumping Plant," *Jour., Power Div., Amer. Soc. of Civ. Engrs.*, April 1956.
Richards, R. T., "Water Column Separation in Pump Discharge Lines," *Trans. Amer. Soc. of Mech. Engrs.*, vol. 78, 1956, pp. 1297-1306.
Kephart, J. T. and Davis, K., "Pressure Surge Following Water-Column Separation," *Jour., Basic Engineering, Amer. Soc. of Mech. Engrs.*, vol. 83, Sept. 1961, pp. 456-460.
Li, W. H., "Mechanics of Pipe Flow Following Column Separation," *Trans. Amer. Soc. of Civ. Engrs.*, vol. 128, part 2, 1963, pp. 1233-1254.
Li, W. H. and Walsh, J. P., "Pressure Generated in a Pipe," *Jour. Engineering Mech. Div., Amer. Soc. of Civ. Engrs.*, vol. 90, no. EM6, 1964, pp. 113-133.
Carstens, H. R. and Hagler, T. W., "Water Hammer Resulting from Cavitating Pumps," *Jour., Hyd. Div., Amer. Soc. of Civ. Engrs.*, vol. 90, 1964.
Duc, J., "Negative Pressure Phenomena in Pump Pipelines," *International Symposium on Waterhammer in Pumped Storage Projects, Amer. Soc. of Mech. Engrs.*, Nov. 1965.
Walsh, J. P. and Li, W. H., "Water Hammer Following Column Separation," *Jour., Applied Mech. Div., Amer. Soc. of Mech. Engrs.*, vol. 89, 1967, pp. 234-236.
Tanahashi, T. and Kasahara, E., "Analysis of Water Hammer with Water Column Separation," *Bull. Japan Soc. of Mech. Engrs.*, vol. 12, no. 50, 1969, pp. 206-214.
Knapp, R. T., Daily, J. W., and Hammitt, F. G., *Cavitation*, McGraw-Hill Book Co., New York, 1970.
Proc. Meeting on Water Column Separation, Organized by ENEL, Milan, Italy, Oct. 1971.

CHAPTER 10

METHODS FOR CONTROLLING TRANSIENTS

10.1 INTRODUCTION

A piping system can be designed with a liberal factor of safety to withstand the maximum and minimum pressures caused by any possible operating condition expected to occur during the life of the system. Such a design in most cases will, however, be very uneconomical. Therefore, various devices and/or control procedures are used to reduce or eliminate undesirable transients, e.g., excessive pressure rise or drop, column separation, pump or turbine overspeed. Such devices are usually costly, and there is no single device that is suitable for all systems or for all operating conditions. Therefore, while designing a piping system, a number of alternatives should be considered. The alternative that gives an acceptable system response and an overall economical system should be selected. An acceptable system response may be defined by specifying limits on the maximum and minimum pressures, maximum turbine speed following full-load rejection, or maximum reverse pump speed following power failure.

In Chapter 1, we derived the following equation for pressure change, ΔH, as a result of an instantaneous change in the flow velocity, ΔV,

$$\Delta H = -\frac{a}{g}\Delta V \tag{10.1}$$

in which a = waterhammer wave velocity and g = acceleration due to gravity. This equation indicates that the main function of a device used for the reduction of the magnitude of pressure rise or pressure drop would be to reduce ΔV and/or a. In addition, the flow velocity, V, may be varied in such a manner that the pressures are kept within the prescribed limits. Such a controlled variation of the flow conditions, which results in a required system response,

is referred to as *optimal control of transient flows*. A discussion of the optimal control of transient flows will be presented in Section 10.6.

In this chapter, we will first present various devices available to reduce or to eliminate undesirable transients. Boundary conditions for these devices will be developed, which are required for the analysis of a system by the method of characteristics presented in Chapter 3. The chapter concludes with a case study.

10.2 AVAILABLE DEVICES AND METHODS FOR CONTROLLING TRANSIENTS

The following devices are commonly used to reduce or to eliminate the undesirable transients, such as excessive pressures, column separation, and pump or turbine overspeed following a power failure or a load rejection: (1) surge tanks, (2) air chambers, and (3) valves.

In addition, the severity of undesirable transients may be reduced by changing the pipeline profile, by increasing the diameter of the pipeline, or by reducing the waterhammer wave velocity.

A brief description of and the boundary conditions for the three devices are presented in the following sections.

In the derivation of the boundary conditions, the notation of Chapter 3 is used. Two subscripts are used with the variables to designate their values at a section of a pipe: the first subscript refers to the pipe, while the second refers to the section. The subscript P is used to designate an unknown variable at the end of the time step under consideration, i.e., at time $t_o + \Delta t$, while a variable without the subscript P refers to its known value at the beginning of the time step, i.e., at time, t_o (see Fig. 3.1).

10.3 SURGE TANKS

Description

A surge tank is an open chamber or a tank connected to the pipeline. This tank reflects the pressure waves, and supplies or stores excess liquid. Various types of surge tanks are presented in Section 11.2.

The transients in a piping system having a surge tank may be analyzed by using the method of characteristics if the transients are rapid and are of short duration—e.g., waterhammer. However, for slow transients—e.g., oscillations of the water level in a surge tank following a load rejection on a turbine—this method requires an excessive amount of computer time and is not suitable. In such cases, the system may be analyzed as a lumped system, details of which are given in Chapter 11. In this section, we will derive the boundary conditions

for a surge tank. These boundary conditions are required for the analysis of a system having a surge tank by the method of characteristics.

Boundary Conditions

Let us consider a surge tank having a standpipe, as shown in Fig. 10.1. The length of the standpipe is usually short as compared to the lengths of the pipes of the system. Therefore, the liquid inside the standpipe may be considered as a lumped mass.

The following equations may be written for the junction of the standpipe with the pipeline (see Fig. 10.1a):

1. Positive characteristic equation (Eq. 3.18) for section $(i, n+1)$

$$Q_{P_{i,n+1}} = C_p - C_{a_i} H_{P_{i,n+1}} \tag{10.2}$$

2. Negative characteristic equation (Eq. 3.19) for section $(i+1, 1)$

$$Q_{P_{i+1,1}} = C_n + C_{a_{i+1}} H_{P_{i+1,1}} \tag{10.3}$$

3. Continuity equation

$$Q_{P_{i,n+1}} = Q_{P_{i+1,1}} + Q_{P_{sp}} \tag{10.4}$$

in which $Q_{P_{sp}}$ = flow in the standpipe (flow in the upward direction is considered positive) at the end of the time step; Q_P = discharge at the end of time step; H_P = piezometric head above datum; C_p, C_n and C_a are constants as defined by Eqs. 3.20 through 3.23. The subscripts i and $i+1$ refer to the pipe numbers, and the subscripts 1 and $n+1$ refer to the section numbers.

4. If the losses at the junction are neglected, then

$$H_{P_{i,n+1}} = H_{P_{i+1,1}}. \tag{10.5}$$

5. Referring to the freebody diagram of Fig. 10.1b, the following differential equation may be written for the acceleration of the liquid in the standpipe at the end of the time step:

$$\gamma A_{sp} \frac{L_{sp}}{g A_{sp}} \frac{dQ_{sp}}{dt} = \gamma A_{sp} [H_{P_{i,n+1}} - (z_P - L_{sp})] - W - F_f \tag{10.6}$$

in which γ = specific weight of the liquid; W = weight of the liquid in the standpipe = $\gamma A_{sp} L_{sp}$; F_f = force due to friction = $\gamma A_{sp} f L_{sp} Q_{P_{sp}} |Q_{P_{sp}}| / (2g D_{sp} A_{sp}^2)$; and D_{sp} = diameter of the standpipe. Substituting expressions for W and F_f into Eq. 10.6 and dividing by γA_{sp}, we obtain

$$\frac{L_{sp}}{g A_{sp}} \frac{dQ_{sp}}{dt} = H_{P_{i,n+1}} - z_P - \frac{f L_{sp}}{2g A_{sp}^2 D_{sp}} Q_{P_{sp}} |Q_{P_{sp}}| \tag{10.7}$$

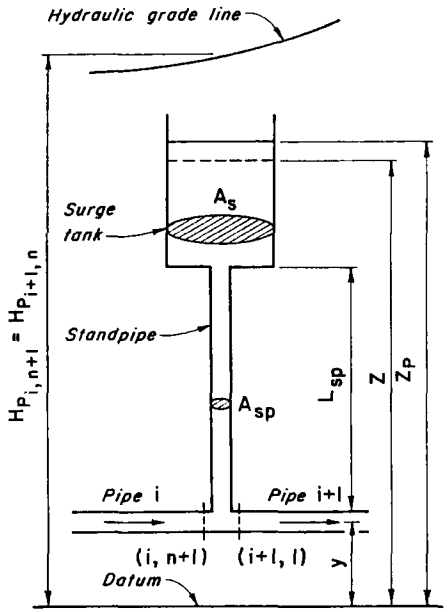

(a) Notation

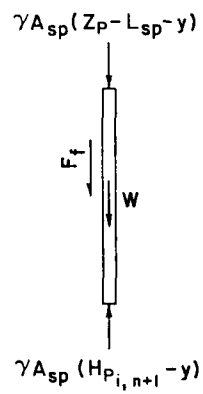

(b) Freebody diagram

Figure 10.1. Notation for surge tank with standpipe.

6. Let z and z_P be the heights of the liquid surface in the tank above the datum at the beginning and at the end of the time step. Then,

$$z_P = z + \frac{0.5\,\Delta t}{A_s}\,(Q_{P_{sp}} + Q_{sp}) \tag{10.8}$$

in which A_s = horizontal cross-sectional area of the tank; Q_{sp} = flow in the standpipe at the beginning of the time step; and Δt is the size of the computational time step.

If the size of the time step is small, then $dQ_{sp}/dt \simeq (Q_{P_{sp}} - Q_{sp})/\Delta t$. In addition, since the variation of the flow in the standpipe is usually gradual, the friction term may be approximated as $f L_{sp} Q_{sp} |Q_{sp}|/(2gD_{sp}A_{sp}^2)$. Substitution of these relationships into Eq. 10.7 yields

$$Q_{P_{sp}} = \frac{g\Delta t A_{sp}}{L_{sp}}\,(H_{P_{i,n+1}} - z_P - C_{sp}) + Q_{sp} \tag{10.9}$$

in which $C_{sp} = f L_{sp} Q_{sp} |Q_{sp}|/(2gA_{sp}^2 D_{sp})$.

Now we have six linear equations, i.e., Eqs. 10.2 to 10.5, 10.8, and 10.9, in six unknowns–namely, $Q_{P_{i,n+1}}$, $Q_{P_{i+1,1}}$, $H_{P_{i,n+1}}$, $Q_{P_{sp}}$, $H_{P_{i+1,1}}$, and z_P. These equations may be solved simultaneously by any standard numerical method.

Note that if we had not written the friction term in terms of the known discharge at the beginning of the time step, we would have a nonlinear system of equations. In that case, the Newton-Raphson method may be used to solve the system of equations.

10.4 AIR CHAMBERS

Description

An air chamber (Fig. 10.2) is a vessel having compressed air at its top and having liquid in its lower part. To restrict the inflow into or outflow from the chamber, an orifice is usually provided between the chamber and the pipeline. An orifice, which is shaped such that it produces more head loss for inflow into the chamber than for a corresponding outflow from the chamber, is referred to as *differential orifice* (Fig. 10.2). To prevent very low minimum pressures in the pipeline and hence column separation, the outflow from the chamber should be as free as possible, while the inflow may be restricted to reduce the size of the chamber. A ratio of 2.5:1 between the orifice head losses for the same inflow and outflow is commonly used.[1] As the air volume may be reduced due to leakage or due to solution in the liquid, an air compressor is used to keep the volume of the air within the prescribed limits.

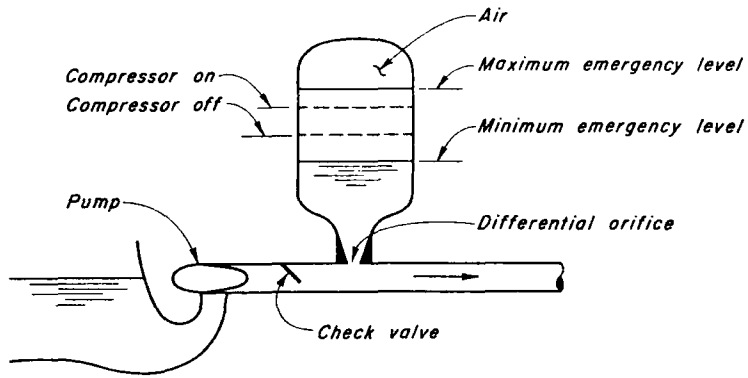

Figure 10.2. Air chamber.

It is a common practice to provide a check valve between the pump and the air chamber (see Fig. 10.2). Upon power failure, the pressure in the pipeline drops, and the liquid is supplied from the chamber into the pipeline. When the flow in the pipeline reverses, the check valve closes instantaneously, and the liquid flows into the chamber. Because of the inflow or outflow from the chamber, the air in the chamber contracts or expands, and the magnitude of the pressure rise and drop are reduced due to gradual variation of the flow velocity in the pipeline.

An air chamber has the following *advantages* over a surge tank:

1. The volume of an air chamber required for keeping the maximum and minimum pressures within the prescribed limits is smaller than that of an equivalent surge tank.
2. An air chamber can be installed with its axis parallel to the ground slope. This reduces the foundation costs and provides better resistance to both wind and earthquake loads.
3. An air chamber can be provided near the pump, which may not be practical in the case of a surge tank because of excessive height. This reduces the pressure rise and the pressure drop in the pipeline.
4. To prevent freezing in cold climates, it is cheaper to heat the liquid in an air chamber than in a surge tank because of smaller size and because of proximity to the pumphouse.

The main *disadvantage* of an air chamber is the necessity to provide air compressors and auxiliary equipment, which require constant maintenance.

Engler,[2] Allievi,[3] and Angus[4] discussed the use of air chambers in pumping systems to control transients generated by power failure to the pumps. Charts (see Appendix A) to determine the size of an air chamber for a pipeline to keep the maximum and minimum pressures within design limits are reported in the

literature.[1,5-8] These charts may be used to determine the approximate size of a chamber for a pipeline. During the final design stages, however, a detailed transient analysis should be carried out. The method of characteristics incorporating the following boundary conditions may be used for this analysis.

Boundary Conditions

Referring to Fig. 10.3, the following equations are available at the junction of the chamber with the pipeline:

1. Positive characteristic equation (Eq. 3.18) for section $(i, n+1)$:

$$Q_{P_{i,n+1}} = C_p - C_{a_i} H_{P_{i,n+1}} \tag{10.10}$$

2. Negative characteristic equation (Eq. 3.19) for section $(i+1, 1)$:

$$Q_{P_{i+1,1}} = C_n + C_{a_{i+1}} H_{P_{i+1,1}} \tag{10.11}$$

3. If the losses at the junction are neglected, then

$$H_{P_{i,n+1}} = H_{P_{i+1,1}} \tag{10.12}$$

4. Continuity equation

$$Q_{P_{i,n+1}} = Q_{P_{i+1,1}} + Q_{P_{\text{orf}}} \tag{10.13}$$

in which $Q_{P_{\text{orf}}}$ = flow through the orifice (considered positive into the chamber).

Assuming that the air enclosed at the top of the chamber follows the polytropic relation for a perfect gas, i.e.,

$$H^*_{P_{\text{air}}} \forall^m_{P_{\text{air}}} = C \tag{10.14}$$

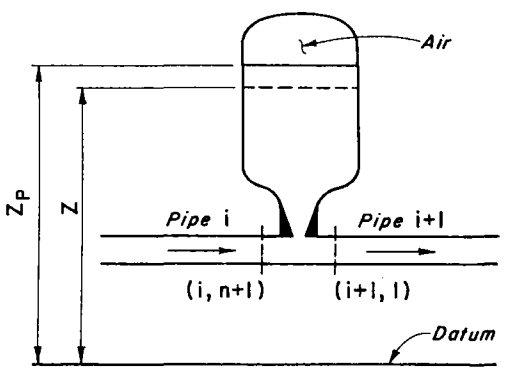

Figure 10.3. Notation for air chamber.

in which $H^*_{P_{\text{air}}}$ and $\forall_{P_{\text{air}}}$ are the absolute pressure head and the volume of the enclosed air at the end of the time step; m is the exponent in the polytropic gas equation; C is a constant whose value is determined from the initial conditions, i.e., $C = \forall^m_{o_{\text{air}}} H^*_{o_{\text{air}}}$; and the subscript o refers to the initial steady-state conditions. The values of m are equal to 1.0 and 1.4 for an isothermal and for an adiabatic expansion or contraction of the air. The expansion or contraction process is almost adiabatic for small-size chambers and rapid transients, and it is almost isothermal for slow transients and large air volumes. For design calculations, an average value of $m = 1.2$ may be used because the transients are usually rapid at the beginning and they are slow at the end.

For modeling the behavior of the air volume, Graze[9-11] recommends using a differential equation based on rational heat transfer rather than using the polytropic equation, Eq. 10.14. The main difficulty in using the equation recommended by Graze is that the rate of heat transfer is not precisely known and has to be assumed.

The orifice losses may be expressed as

$$h_{P_{\text{orf}}} = C_{\text{orf}} Q_{P_{\text{orf}}} |Q_{P_{\text{orf}}}| \tag{10.15}$$

in which C_{orf} = coefficient of orifice losses, and $h_{P_{\text{orf}}}$ = head loss in the orifice for a flow of $Q_{P_{\text{orf}}}$. Note that if the orifice is of differential type, then C_{orf} has different values for the inflow into and outflow from the chamber.

The following equations may be written for the enclosed air volume:

$$H^*_{P_{\text{air}}} = H_{P_{i,n+1}} + H_b - z_P - h_{P_{\text{orf}}} \tag{10.16-a}$$

$$\forall_{P_{\text{air}}} = \forall_{\text{air}} - A_c (z_P - z) \tag{10.16-b}$$

$$z_P = z + 0.5 (Q_{\text{orf}} + Q_{P_{\text{orf}}}) \frac{\Delta t}{A_c} \tag{10.16-c}$$

in which H_b = barometric pressure head; A_c = horizontal cross-sectional area of the chamber; z and z_P are the heights of the liquid surface in the chamber above the datum at the beginning and at the end of the time step (measured positive upwards); Q_{orf} = orifice flow at the beginning of time step; and $\forall_{\text{air}}$ = volume of air at beginning of time step.

We have nine equations, Eq. 10.10 to 10.16 in nine unknowns–namely, $Q_{P_{i,n+1}}$, $Q_{P_{i+1,1}}$, $Q_{P_{\text{orf}}}$, $H_{P_{i,n+1}}$, $H_{P_{i+1,1}}$, $h_{P_{\text{orf}}}$, $\forall_{P_{\text{air}}}$, $H^*_{P_{\text{air}}}$, and z_P. A number of these unknowns may be eliminated as follows: Substituting Eqs. 10.10 through 10.12 into Eq. 10.13, we obtain

$$Q_{P_{\text{orf}}} = (C_p - C_n) - (C_{a_i} + C_{a_{i+1}}) H_{P_{i,n+1}} \tag{10.17}$$

It follows from Eqs. 10.14 through 10.16b that

$$(H_{P_{i,n+1}} + H_b - z_P - C_{\text{orf}} Q_{P_{\text{orf}}} |Q_{P_{\text{orf}}}|) [\forall_{\text{air}} - A_c (z_P - z)]^m = C \tag{10.18}$$

In Eqs. 10.16c through 10.18, we have three unknowns, namely, $Q_{P_{\text{orf}}}$, $H_{P_{i,n+1}}$, and z_P. The value of these three unknowns may be determined by solving these equations by an iterative technique, such as the Newton-Raphson method. The known values of these variables at the beginning of the time step may be used as a first estimate for starting the iterations.

Sometimes, the air chamber is connected to the pipeline by a standpipe as shown in Fig. 10.4. In such a case, the length of the standpipe should be as short as possible, and it should be sized so that there is little delay between the pressure change in the pipeline and the start of inflow or outflow from the chamber. To account for the liquid in the standpipe, the preceding equations for an air chamber having a standpipe are modified as discussed in the following.

Let us consider the flow in the standpipe in the upward direction as positive (Fig. 10.4) and assume the liquid inside the standpipe as a lumped mass. Then, the dynamic equation for the standpipe may be written as

$$\frac{\gamma L_{sp} A_{sp}}{g A_{sp}} \frac{dQ_{sp}}{dt} = \gamma A_{sp} [H_{P_{i,n+1}} - (H^*_{P_{\text{air}}} - H_b) - (z_P - L_{sp})] - F_f - W \tag{10.19}$$

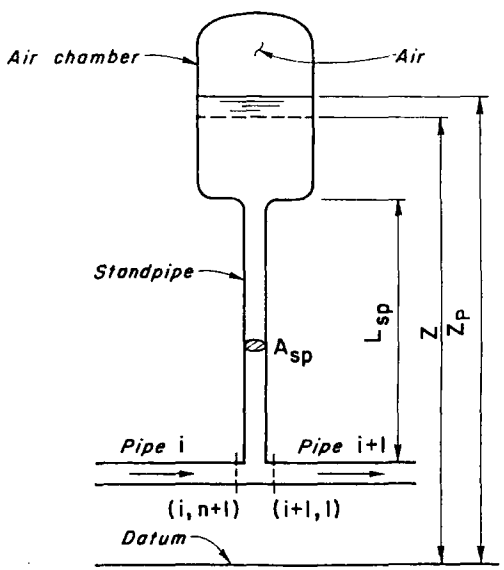

Figure 10.4. Notation for air chamber with standpipe.

in which W = weight of the liquid in the standpipe; L_{sp} and A_{sp} are the length and cross-sectional area of standpipe, respectively; z_P = height of the liquid surface in the chamber above the datum; and F_f = frictional force in the standpipe including the entrance or exit losses from the chamber into the standpipe and is equal to $\gamma A_{sp} h_{P_f}$. In this expression,

$$h_{P_f} = \left(\frac{f L_{sp}}{2 g D_{sp} A_{sp}^2} + C_{\text{orf}} \right) Q_{P_{sp}} |Q_{P_{sp}}| \tag{10.20}$$

in which D_{sp} = diameter of the standpipe and C_{orf} = coefficient of the orifice head losses. If the size of the time step, Δt, is small, then h_{P_f} may be approximated as

$$h_{P_f} = k Q_{sp} |Q_{sp}| \tag{10.21}$$

in which $k = (f L_{sp})/(2 g D_{sp} A_{sp}^2) + C_{\text{orf}}$. Substituting $W = \gamma L_{sp} A_{sp}$ and the expression for h_{P_f} from Eq. 10.21 into Eq. 10.19, approximating $dQ_{sp}/dt = (Q_{P_{sp}} - Q_{sp})/\Delta t$, and simplifying the resulting equation, we obtain

$$Q_{P_{sp}} = Q_{sp} + \frac{g \Delta t A_{sp}}{L_{sp}} (H_{P_{i,n+1}} - H^*_{P_{\text{air}}} - z_P) + \frac{g \Delta t A_{sp}}{L_{sp}} (H_b - k Q_{sp} |Q_{sp}|) \tag{10.22}$$

The continuity equation at the junction of the standpipe and the pipeline, and the equation for the liquid level in the chamber, may be written as

$$Q_{P_{i,n+1}} = Q_{P_{sp}} + Q_{P_{i+1,1}} \tag{10.23}$$

$$z_P = z + 0.5 (Q_{P_{sp}} + Q_{sp}) \frac{\Delta t}{A_c} \tag{10.24}$$

Elimination of $Q_{P_{i,n+1}}$, $Q_{P_{i+1,1}}$, and $H_{P_{i+1,1}}$ from Eqs. 10.10 through 10.12 and 10.23 yields

$$H_{P_{i,n+1}} = \frac{C_p - C_n}{C_{a_i} + C_{a_{i+1}}} - \frac{1}{C_{a_i} + C_{a_{i+1}}} Q_{P_{sp}} \tag{10.25}$$

It follows from Eqs. 10.14 and 10.16b that

$$H^*_{P_{\text{air}}} [\forall_{\text{air}} - (z_P - z) A_c]^m = C \tag{10.26}$$

Now we have four equations (i.e., Eqs. 10.22, 10.24, 10.25, and 10.26) in four unknowns, namely, $Q_{P_{sp}}$, $H^*_{P_{\text{air}}}$, z_P, and $H_{P_{i,n+1}}$. Because Eq. 10.26 is nonlinear, the Newton-Raphson method may be used to solve these equations. The value of $H_{P_{i+1,1}}$, $Q_{P_{i,n+1}}$, $Q_{P_{i+1,1}}$, and $\forall_{P_{\text{air}}}$ may then be determined from Eqs. 10.12, 10.10, 10.11, and 10.16b, respectively.

10.5 VALVES

Description

Depending upon the type, a valve is used to control the transients by either of the following operations:

1. The valve opens or closes to reduce the rate of net change in the flow velocity in the pipeline.
2. It allows rapid outflow of the liquid from the pipeline if the pressure exceeds a set limit. This outflow causes a pressure drop, thus reducing the maximum pressure.
3. The valve opens to admit air into the pipeline, thus preventing the pressure from dropping to the liquid vapor pressure.

A number of valves commonly used to control transients are:

1. Safety valves
2. Pressure-relief valves
3. Pressure-regulating valves
4. Air-inlet valves
5. Check valves.

A *safety valve* or an *overpressure pop-off valve* (Fig. 10.5a) is a spring or weight-loaded valve, which opens as soon as the pressure inside the pipeline exceeds the pressure head set on the valve. The valve closes abruptly when the pressure drops below the limit set on the valve (Fig. 10.6a). A safety valve is either fully open or fully closed.

The operation of a *pressure-relief valve* or *surge suppressor* (Fig. 10.5b) is similar to that of a safety valve except that its opening is proportional to the amount by which the pressure in the pipeline just upstream of the valve exceeds the prescribed limits. The valve closes when the pipeline pressure drops and is fully closed when the pressure is below the limit set on the valve. There is usually some hysteresis in the opening and the closing of the valve, as shown in Fig. 10.6b.[12]

For a pumping system having more than one pump discharging into a common header, a battery of smaller-size relief valves or surge suppressors may be used[13] instead of one large surge suppressor. A suppressor may be installed on each pump or the entire battery of the suppressors may be mounted on the main discharge line. In the latter arrangement, the overpressure setting of each valve should be set such that the valves open in sequence one after the other rather than simultaneously.

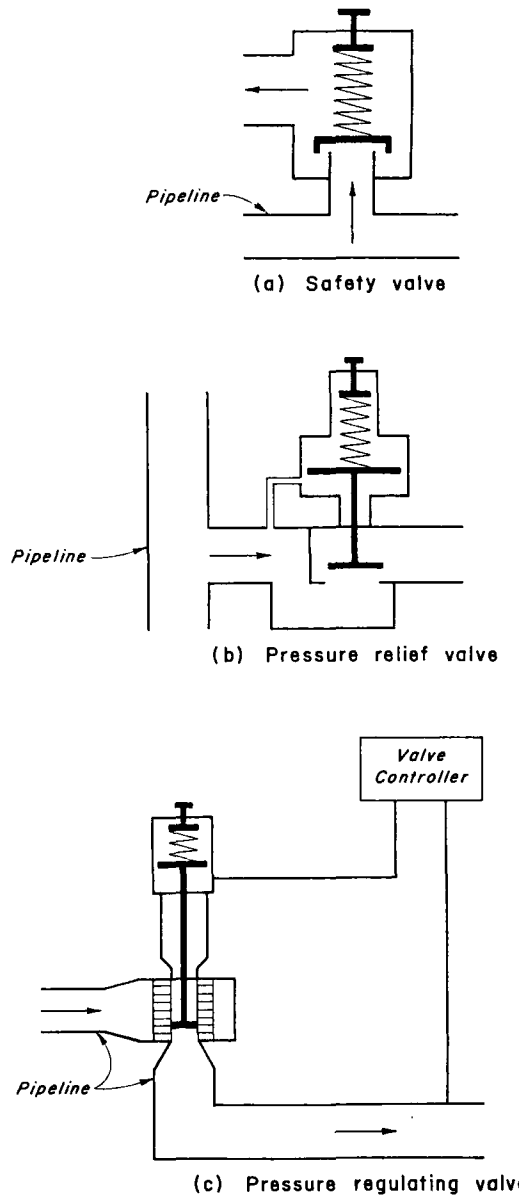

Figure 10.5. Schematic diagrams of safety, relief, and pressure-regulating valves.

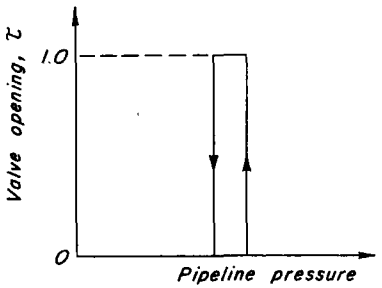

(a) Safety valve

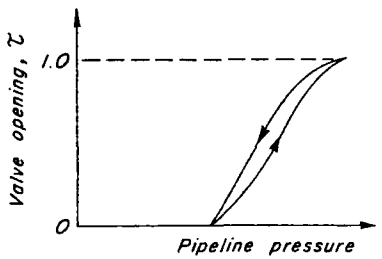

(b) Pressure relief valve

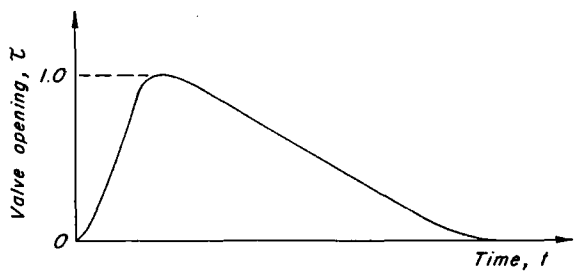

(c) Pressure regulating valve

Figure 10.6. Discharge characteristics of safety, relief, and pressure-regulating valves. (After Evangelisti[12])

A *pressure-regulating valve* (PRV) is a pilot-controlled throttling valve, which is opened or closed by a servomotor, and the opening and closing times of this valve can be individually set. It is installed just downstream of a pump in a pumping system and upstream of a turbine in a hydropower scheme. Following power failure to the pump-motor, this valve rapidly opens and then gradually closes (Fig. 10.6c) to reduce the pressure rise. The operation of this valve in a hydropower scheme is as follows: If the power plant is isolated from the grid system, the PRV is kept partly open to provide for the maximum anticipated rapid load increase. When accepting rapid load changes, the PRV is closed in approximate synchronism with the turbine wicket gates to maintain an essentially constant flow velocity in the penstock. Following a load rejection, the PRV is opened as the wicket gates are closed, and then the PRV is closed at a slow rate. In such an operation, some water is wasted. However, as isolated operation is an emergency condition, the amount of water wasted is insignificant.

Upon full-load rejection, either in the normal or isolated operation of the turbine, all the turbine flow is switched from the turbine to the PRV, which is then closed slowly.

Figure 10.7 illustrates the synchronous operation of a PRV and a turbine. Figs. 10.7a and b are for a turbine isolated from the grid system. Figure 10.7c is for a turbine connected to or isolated from the grid system.

Ideally, the net change in the penstock flow may be reduced to zero by matching the discharge characteristics of the PRV with that of the turbine. However, this is usually not possible because of the nonlinear flow characteristics of the turbines and valves and because of the dead or delay time between the opening (closing) of the pressure regulator and the closing (opening) of the wicket gates. This dead time should be as small as possible to minimize pressure rise or drop in the penstock.

Air-inlet valves are installed to admit air into the pipeline whenever the pressure inside the pipeline drops below the atmospheric pressure. Therefore, the pressure differential between the outside atmospheric pressure and the pressure inside the pipeline is reduced, thus preventing the collapse of the pipeline. Air-inlet valves are also used to reduce the generation of high pressures when the liquid columns rejoin following column separation by providing an air cushion in the pipe.

Once air has been admitted into the pipeline, extreme care must be exercised while refilling the line. The air pockets should be eliminated gradually from the line because the entrapped air can result in very high pressures.[14-17]

Check valves are used to prevent reverse flow through a pump and to prevent inflow into a one-way surge tank from the pipeline. They are installed imme-

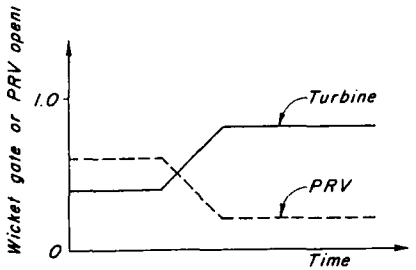

(a) Partial load acceptance in isolated operation

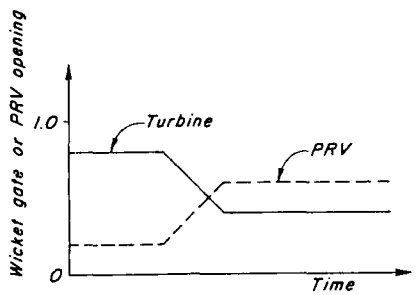

(b) Partial load rejection in isolated operation

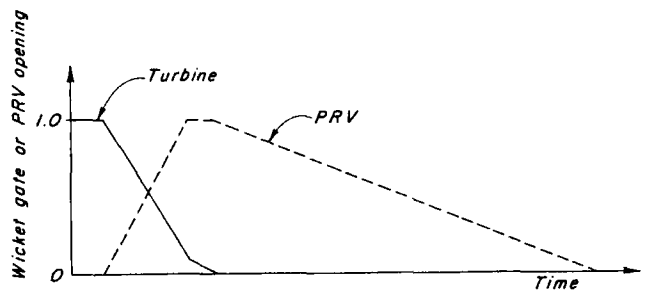

(c) Total load rejection in normal or isolated operation

Figure 10.7. Synchronous operation of turbine and pressure-regulating valve.

diately downstream of a pump or at the bottom of a one-way surge tank (see Section 11.2). A check valve in its simplest form is a flap valve, although sometimes dashpots and springs are provided to prevent slamming of the valve.

Boundary Conditions

For the analysis of a system in which a valve is used to control transients, the boundary conditions and the time history of the valve opening, τ, should be known.

Boundary conditions for a valve (developed in Section 3.3) may be used for safety and relief valves, and for a PRV if the pump is isolated from the pipeline following power failure by means of a check valve. The boundary conditions for a PRV become slightly more complex if simultaneous flow is permitted through the valve as well as through the pump or the turbine. Boundary conditions for a pump and a PRV are derived in this section; and for a Francis turbine and a PRV in Section 10.6.

A check valve may be considered as a dead end for negative flows, while its presence may be ignored for positive flows. For a more elaborate analysis, however, the differential equation of Problem 4.6 for the closure of a check valve when the flow in the discharge line decelerates may be used.

To use the boundary conditions, the variation of valve opening, τ, with time should be known. For a pressure relief valve or surge suppressor, τ is a function of the pressure in the pipeline just upstream of the valve. Therefore, the value of τ is determined as the calculations progress. The τ-versus-time curve for a PRV is specified. Discrete values on this τ-t curve may be stored in the computer, and the τ values at intermediate times may be determined by parabolic interpolation.

PRV and a Pump

Let us consider the PRV and pump arrangement shown in Fig. 10.8 in which the pipes between the pump and section $(i, 1)$ and between the valve and section $(i, 1)$ are very short and therefore may be neglected. Assuming the downstream flow direction as positive, the continuity equation at section $(i, 1)$ may be written as

$$Q_{P_{i,1}} = n_p Q_{P_p} - Q_{P_v} \tag{10.27}$$

in which Q_P = discharge at the end of the time step; the subscripts p, v, and $(i, 1)$ refer to the pump, PRV, and section $(i, 1)$; and n_p = number of parallel pumps.

Referring to Fig. 10.8,

$$H_{P_{i,1}} = H_{P_p} + H_{\text{suc}} - \Delta H_{P_d} \tag{10.28}$$

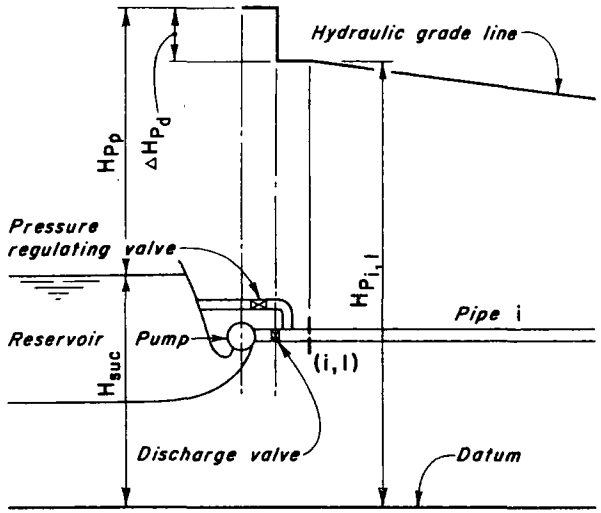

Figure 10.8. Notation for a pressure-regulating valve–centrifugal pump system.

in which H_{suc} = height of the suction reservoir above the datum; $H_{P_{i,1}}$ = piezometric head at section $(i, 1)$ above datum; ΔH_{P_d} = head loss at the discharge valve; and H_{P_p} = pumping head.

The flow through the PRV, Q_{P_v}, is given by the equation

$$Q_{P_v} = C_{pv}\tau_P\sqrt{H_{P_{i,1}} - z_o} \tag{10.29}$$

in which $C_{pv} = Q_{ov}/\sqrt{H_o - z_o}$; Q_{ov} = flow through the fully open valve under a head of $(H_o - z_o)$; τ_P = effective valve opening at the end of time step = $(C_dA_v)/(C_dA_v)_o$; C_d = coefficient of discharge; A_v = area of valve opening; z_o = height above the datum of the reservoir into which PRV is discharging; and the subscript o refers to steady-state conditions. If the PRV is discharging into the suction reservoir, then $z_o = H_{suc}$, and if the PRV is discharging into atmosphere, then z_o = height of PRV above datum.

The following equations are available for the pump-PRV end:

1. negative characteristic equation for section $(i, 1)$, Eq. 4.16
2. equations for the head and torque characteristics, Eqs. 4.7 and 4.8
3. equation for the rotating masses, Eq. 4.14.

Now, we have seven equations in seven unknowns, i.e., $Q_{P_p}, Q_{P_{i,1}}, Q_{P_v}, H_{P_{i,1}}$, α_P, h_P, and β_P. To simplify their solution, let us eliminate all other variables except two so that we have two equations in two unknowns. Then, we can use the Newton-Raphson method to solve these equations. In this section, we will

only derive the expressions for F_1 and F_2 and for their derivatives; the procedure for using these expressions in the Newton-Raphson method was outlined in Section 4.4.

By eliminating $Q_{P_{i,1}}$ and Q_{P_v} from Eqs. 10.27, 10.29, and 4.16, and writing $\Delta H_{P_d} = C_vQ_{P_p}|Q_{P_p}|$, we obtain

$$n_pQ_{P_p} = C_{pv}\tau_P\sqrt{H_{P_p} + H_{suc} - C_vQ_{P_p}|Q_{P_p}| - z_o} + C_n + C_{a_i}(H_{P_p} + H_{suc} - C_vQ_{P_p}|Q_{P_p}|) \tag{10.30}$$

By using the relationships, $v_P = Q_P/Q_R$ and $h_P = H_P/H_R$, Eq. 10.30 may be written as

$$n_pQ_Rv_P = C_{pv}\tau_P\sqrt{H_Rh_P + H_{suc} - C_vQ_R^2v_P|v_P| - z_o} + C_n + C_{a_i}(H_Rh_P + H_{suc} - C_vQ_R^2v_P|v_P|) \tag{10.31}$$

By eliminating h_P from Eqs. 4.7 and 10.31, and simplifying the resulting equation, we obtain

$$F_1 = C_{pv}\tau_P \times \sqrt{a_1H_R(\alpha_P^2 + v_P^2) + a_2H_R(\alpha_P^2 + v_P^2)\tan^{-1}\frac{\alpha_P}{v_P} - C_vQ_R^2v_P|v_P| + H_{suc} - z_o} + C_{a_i}H_Ra_1(\alpha_P^2 + v_P^2) + C_{a_i}H_Ra_2(\alpha_P^2 + v_P^2)\tan^{-1}\frac{\alpha_P}{v_P} - C_{a_i}C_vQ_R^2v_P|v_P| - n_pQ_Rv_P + C_n + C_aH_{suc} = 0 \tag{10.32a}$$

Differentiation of Eq. 10.32a with respect to α_P and v_P yields

$$\frac{\partial F_1}{\partial \alpha_P} = \frac{1}{2}\tau_PC_{pv}\left[a_1H_R(\alpha_P^2 + v_P^2) + a_2H_R(\alpha_P^2 + v_P^2)\tan^{-1}\frac{\alpha_P}{v_P} - C_vQ_R^2v_P|v_P| + H_{suc} - z_o\right]^{-1/2}\left(2a_1\alpha_PH_R + a_2H_Rv_P + 2a_2H_R\alpha_P\tan^{-1}\frac{\alpha_P}{v_P}\right) + 2a_1C_{a_i}H_R\alpha_P + 2a_2C_{a_i}H_R\alpha_P\tan^{-1}\frac{\alpha_P}{v_P} + a_2C_{a_i}H_Rv_P \tag{10.32b}$$

$$\frac{\partial F_1}{\partial v_P} = \frac{1}{2}\tau_P C_{pv}\left[a_1 H_R(\alpha_P^2 + v_P^2) + a_2 H_R(\alpha_P^2 + v_P^2)\tan^{-1}\frac{\alpha_P}{v_P} - C_v Q_R^2 v_P|v_P| + H_{suc} - z_o\right]^{-1/2} \times \left[2v_P H_R\left(a_1 + a_2\tan^{-1}\frac{\alpha_P}{v_P}\right) - a_2 H_R\alpha_P - 2C_v Q_R^2|v_P|\right] + 2a_1 C_{a_i} H_R v_P + 2a_2 C_{a_i} H_R v_P \tan^{-1}\frac{\alpha_P}{v_P} - a_2 C_{a_i} H_R \alpha_P - 2C_{a_i} C_v Q_R^2 |v_P| - n_p Q_R \quad (10.32c)$$

Expressions for F_2, $\partial F_2/\partial\alpha_P$, and $\partial F_2/\partial v_P$ are given by Eqs. 4.20, 4.27, and 4.28, respectively.

The value of τ_P is determined from the specified valve-opening-versus-time curve, and then Eqs. 10.32a-c, 4.20, 4.27, and 4.28 are used to determine the values of α_P and v_P by following the procedure outlined in Section 4.4 (see Fig. 10.9).

Air-Inlet Valve

Let the air-inlet valve be located at the junction of the ith and $(i+1)$th pipe as shown in Fig. 10.10. Then the positive and negative characteristic equations for sections $(i, n+1)$ and $(i+1, 1)$ are

$$Q_{P_{i,n+1}} = C_p - C_{a_i} H_{P_{i,n+1}} \quad (10.33)$$

$$Q_{P_{i+1,1}} = C_n + C_{a_{i+1}} H_{P_{i+1,1}} \quad (10.34)$$

In addition, if the head losses in the pipeline at the valve are neglected, then

$$H_{P_{i,n+1}} = H_{P_{i+1,1}} \quad (10.35)$$

In the subsequent discussion, we will use $H_{P_{i,n+1}}$ as the piezometric head at the valve location.

When $H_{P_{i,n+1}}$ drops below a predetermined value, y, set on the valve,[18] the valve opens, and the air flows into the pipeline. Later, when $H_{P_{i,n+1}} > y$, the valve closes and entraps air inside the pipeline. Thus, depending upon the history of the pressure at the valve location, the valve may open or close several times during a transient. The mass of the entrapped air will increase with each opening of the valve.

We will make the following *assumptions* in the derivation of the boundary conditions:

1. The airflow into the pipeline is isentropic.
2. The entrapped air remains at the valve location and is not carried away by the flowing liquid.
3. The expansion or contraction of the entrapped air is isothermal.

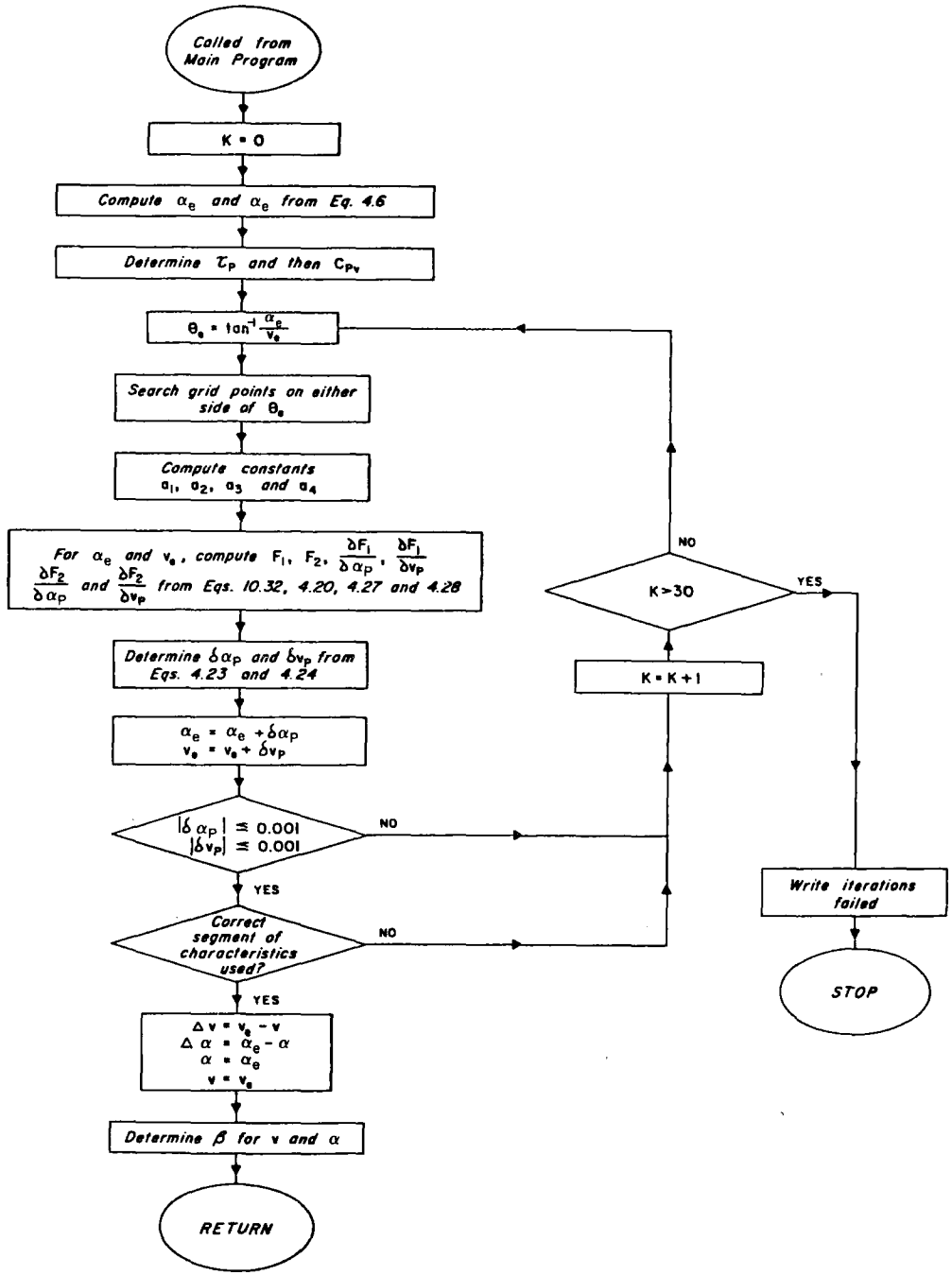

Figure 10.9. Flowchart for boundary conditions for a pressure-regulating valve—centrifugal

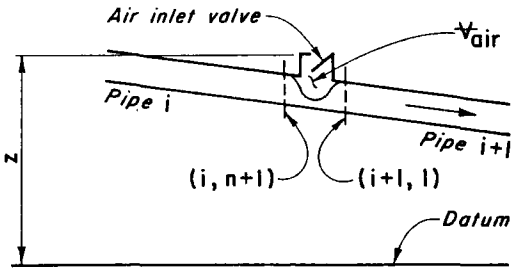

Figure 10.10. Notation for air-inlet valve.

If Δt is small and m_a is the mass of the air entrapped in the pipeline at the beginning of the time step, then the mass of air, m_{P_a} at the end of time step is

$$m_{P_a} = m_a + \frac{dm_a}{dt}\Delta t \tag{10.36}$$

in which dm_a/dt is the time rate of mass inflow of air through the valve into the pipeline.

The entrapped air volume should satisfy the continuity equation, i.e.,

$$\forall_{P_{air}} = \forall_{air} + 0.5\,\Delta t\,[(Q_{P_{i+1,1}} + Q_{i+1,1}) - (Q_{P_{i,n+1}} + Q_{i,n+1})] \tag{10.37}$$

By substituting Eqs. 10.33 through 10.35 into Eq. 10.37, we obtain

$$\forall_{P_{air}} = C_{air} + 0.5\,\Delta t\,(C_{a_i} + C_{a_{i+1}})H_{P_{i,n+1}} \tag{10.38}$$

in which $C_{air} = \forall_{air} + 0.5\,\Delta t\,(C_n + Q_{i+1,1} - C_p - Q_{i,n+1})$.

If the expansion and contraction of the air volume inside the pipeline is isothermal, then

$$p\forall_{P_{air}} = m_{P_a}RT \tag{10.39}$$

in which R = universal gas constant; and p and T are the absolute pressure and temperature of the air volume inside the pipeline. The absolute pressure, p, is related to $H_{P_{i,n+1}}$ through the equation

$$p = \gamma(H_{P_{i,n+1}} - z + H_b) \tag{10.40}$$

in which z = height of the valve throat above the datum; γ = specific weight of the liquid inside the pipeline; and H_b = barometric pressure head.

Substituting $H_{P_{i,n+1}}$ from Eq. 10.40 into Eq. 10.38, eliminating $\forall_{P_{air}}$ from the resulting equation and Eq. 10.39, we obtain

$$m_{P_a}RT = p\left[C_{air} + 0.5\,\Delta t\,(C_{a_i} + C_{a_{i+1}})\left(\frac{p}{\gamma} + z - H_b\right)\right] \tag{10.41}$$

Elimination of m_{P_a} from Eqs. 10.36 and 10.41 yields

$$\left(m_a + \frac{dm_a}{dt}\Delta t\right)RT = p\left[C_{air} + 0.5\,\Delta t\,(C_{a_i} + C_{a_{i+1}})\left(\frac{p}{\gamma} + z - H_b\right)\right] \tag{10.42}$$

In this equation, all variables are known except p and dm_a/dt. If the absolute pressure, p, inside the pipeline is less than 0.53 p_a (p_a = barometric pressure), then the airflow through the valve is at sonic velocity, and, if p is greater than 0.53 p_a but less than p_a, then the air velocity through the valve is subsonic. The expressions for dm_a/dt are:[19]

1. Subsonic air velocity through the valve ($p_a > p > 0.53\,p_a$)

$$\frac{dm_a}{dt} = C_d A_v \sqrt{7p_a\rho_a\left(\frac{p}{p_a}\right)^{1.43}\left[1 - \left(\frac{p}{p_a}\right)^{0.286}\right]} \tag{10.43}$$

2. Sonic air velocity through the valve ($p \leq 0.53\,p_a$)

$$\frac{dm_a}{dt} = 0.686\,C_d A_v \frac{p_a}{\sqrt{RT_a}} \tag{10.44}$$

in which C_d = coefficient of discharge of the valve; A_v = area of the valve opening at its throat; ρ_a = mass density of air at absolute atmospheric pressure, p_a, and absolute temperature, T_a, outside the pipeline. Equations 10.43 and 10.44 are obtained by substituting $k = 1.4$ into the equations presented in Ref. 19 in which k is the ratio of the specific heats for air.

Substitution of Eq. 10.43 or 10.44 into Eq. 10.42 yields a nonlinear equation in p, which may be solved by an iterative technique such as the Newton-Raphson method. The values of $H_{P_{i,n+1}}$, $\forall_{P_{air}}$, m_{P_a}, $H_{P_{i+1,1}}$, $Q_{P_{i,n+1}}$, and $Q_{P_{i+1,1}}$ may then be determined from Eqs. 10.40, 10.38, 10.39, 10.35, 10.33, and 10.34, respectively.

Prior to the time the air-inlet valve opens for the first time, $m_a = 0$. Afterward, however, the value of m_a increases with subsequent valve openings.

Note that in the development of above boundary conditions, it was assumed that there is no air outflow through the valve. However, if the air is allowed to escape through the air-inlet valve when the pressure inside the pipeline exceeds the outside pressure, then this should be taken into consideration in the derivation of the boundary conditions (see Problem 10.6).

10.6 OPTIMAL CONTROL OF TRANSIENT FLOWS

The mode of operation of various appurtenances and control devices such that a desired system response is obtained is called *optimal flow control.* A desired system response may be keeping the maximum and minimum transient-state

pressures within specified limits, changing the flow conditions from one steady state to another steady state in a minimum of time, changing the flow conditions from one steady state to another without flow oscillations, and so on. For example, a valve at the downstream end of a pipeline may be closed such that the pressure does not exceed a specified limit and the transients in the pipeline are vanished as soon as the valve movement ceases. Such a valve operation has been referred to as *optimum valve closure*[20] and *valve stroking*.[21–25]

Optimal flow control is a design or synthesis approach in which the variations of boundary conditions are determined to obtain a desired system response. This approach is different from the usual analysis approach in which the variations of the boundary conditions are specified and the system response is computed.

Following are some of the practical applications of optimal control of transient flows:

1. Changing the outflow at different locations in water supply or oil pipelines without affecting the outflow to other clients.
2. Establishing flow in the conduits of a pumped-storage scheme in minimum time while switching from generation to pumping mode or vice versa.
3. Opening or closing the control valves in a piping system without violating the upper or lower pressure limits.
4. Closing the wicket gates of hydraulic turbines to minimize pressure and speed rise following load rejection.
5. Accepting or rejecting load on hydraulic turbines in a minimum of time without exceeding the specified pressure drop or pressure rise.
6. Utilizing the storage capacity of sewer systems to obtain constant outflow for treatment by properly operating the control devices.[26]

To conserve space, we are not presenting details of computational procedures for determining optimal flow control; interested readers should see Refs. 15 and 20 through 25 for problem-oriented procedures, and Refs. 25 and 26 for application of various operations-research techniques.

10.7 CASE STUDY

Studies carried out for the analysis of transients in the power conduit of the Jordan River Redevelopment, reported earlier by the author,[27,28] are presented in this section.

Design

During the design of this power plant, a number of plant layouts were considered.[29] The project layout as shown in Fig. 3.18 was selected because it was the most economic.

In the optimization studies, a waterhammer pressure rise equal to 30 percent of the static head was assumed. However, subsequent studies indicated that substantial savings would result from a reduction in the pressure rise without greatly affecting the plant regulation. Therefore, a 20 percent pressure rise was adopted for the final design.

To keep the maximum transient pressures within the design limits, the following two alternatives were considered:

1. Provision of an upstream surge tank.
2. Provision of a PRV.

The topography at Jordan River does not favor locating a surge tank near the powerhouse, as the cost of a tower-type surge tank would be very high. In addition, computer studies indicated that, with a surge tank more than 1585 m away from the powerhouse, the plant would not be stable under isolated operation up to its full generating capacity.

In comparison to a surge tank, it was found that a PRV operating in synchronous operation with the turbine would provide good governing characteristics. The estimated cost of the PRV was about the same as that of a 90-m-high surge tank. However, the PRV was selected because it alone would meet the operational requirements.

Mathematical Model

A mathematical model was developed[27,28] to analyze the transient conditions in the power conduit of the power plant. The method of characteristics was used for the analysis. Special boundary conditions, which are presented hereafter, were developed for the synchronous operation of the turbine and the PRV. (Boundary conditions for the PRV acting alone are presented in Section 3.8.)

Let us designate the last section on the penstock adjacent to the turbine as $(i, n+1)$. Then, referring to Fig. 10.11, the continuity equation may be written as

$$Q_{P_{i,n+1}} = Q_{P_{tur}} + Q_{P_v} \tag{10.45}$$

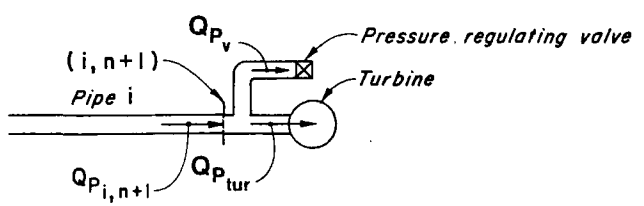

Figure 10.11. Notation for pressure-regulating valve and Francis turbine.

in which $Q_{P_{tur}}$ and Q_{P_v} are the turbine and PRV discharge at the end of time step. The positive characteristic equation for section $(i, n+1)$ is

$$Q_{P_{i,n+1}} = C_p - C_a H_{P_{i,n+1}}. \tag{10.46}$$

Equation 10.46 may be written in terms of the net head, H_n, as

$$Q_{P_{i,n+1}} = C_p - C_a \left(H_n - \frac{Q^2_{P_{i,n+1}}}{2gA_i^2} \right) \tag{10.47}$$

in which A_i = cross-sectional area of the penstock at turbine inlet.

If the turbine characteristics are used in the analysis as outlined in Section 5.4, then

$$Q_{P_{tur}} = a_3 + a_2 \sqrt{H_n} \tag{10.48}$$

in which a_2 and a_3 are constants as defined by Eq. 5.4

The flow through the PRV is

$$Q_{P_v} = Q_r \sqrt{\frac{H_n}{H_r}} \tag{10.49}$$

in which Q_r and Q_{P_v} are the PRV discharges, both for valve opening, τ_P, under net heads of H_r and H_n, respectively; and the subscript r refers to the rated conditions.

Substituting Eqs. 10.48 and 10.49 into Eq. 10.45, we obtain

$$Q_{P_{i,n+1}} = a_3 + a_4 \sqrt{H_n} \tag{10.50}$$

in which $a_4 = a_2 + Q_r/\sqrt{H_r}$.

Elimination of H_n from Eqs. 10.47 and 10.50 yields

$$a_5 Q^2_{P_{i,n+1}} + a_6 Q_{P_{i,n+1}} + a_7 = 0 \tag{10.51}$$

in which $a_5 = C_a[1/(2gA_i^2) - 1/a_4^2]$; $a_6 = 2a_3 C_a/a_4^2 - 1$; and $a_7 = C_p - C_a a_3^2/a_4^2$. Solution of Eq. 10.51 gives

$$Q_{P_{i,n+1}} = \frac{-a_6 - \sqrt{a_6^2 - 4a_5 a_7}}{2a_5} \tag{10.52}$$

Now the values of H_n, $Q_{P_{tur}}$, Q_{P_v}, and $H_{P_{i,n+1}}$ are determined from Eqs. 10.50, 10.48, and 10.49, and 10.46, respectively.

The iterative procedure of Section 5.6 was used to refine the solution and to determine the turbine speed.

Results

The transient-state pressures computed by using the preceding mathematical model were compared with those measured on the prototype following 150-MW load rejection. The PRV and the turbine wicket-gate-opening-versus-time curves (Fig. 10.12) recorded during the prototype tests were used in the analysis. The turbine and generator WR^2 was taken equal to 1.81×10^6 kg m^2 to compute the transient-state turbine speed.

The computed and measured transient-state pressures at the turbine inlet are shown in Fig. 10.13. There is close agreement between the computed and mea-

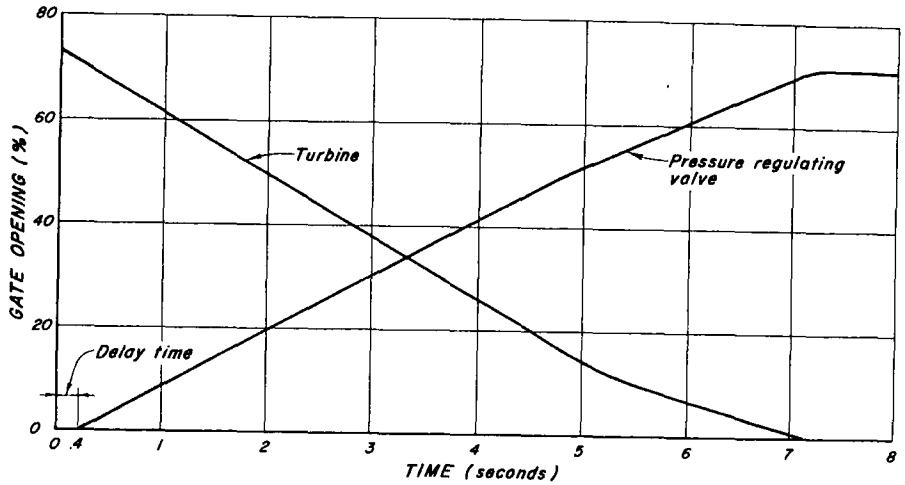

Figure 10.12. Time history of wicket gates and pressure-regulating valve opening following 150-MW load rejection.

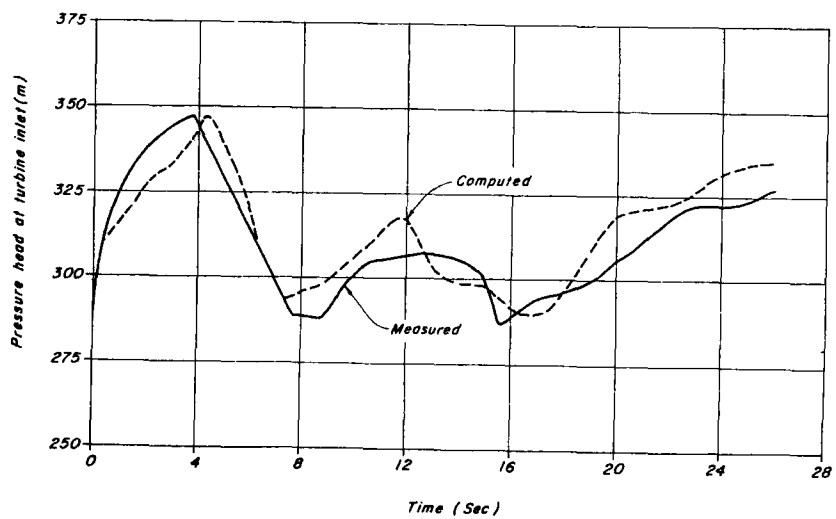

Figure 10.13. Comparison of computed and measured pressure head at turbine inlet.

sured maximum pressures; however, there is some phase shift, and the measured results show more rapid dissipation of transient pressure than that indicated by the computed results. Probably, the phase shift is caused by incorrect values of the wave velocity, and the difference in the dissipation is due to computing the transient-state head losses by using the steady-state friction formula.

10.7 SUMMARY

In this chapter, a number of devices and methods were presented to control the transient conditions in pipelines. A brief description of the operation of these devices was given, and the boundary conditions for these devices were developed. The chapter concluded with a case study.

PROBLEMS

10.1 Derive the boundary condition for an orifice surge tank. In this tank, an orifice is provided between the pipeline and the surge tank.

10.2 How would the boundary conditions for the simple surge tank of Fig. 10.1 be modified if there were no standpipe?

10.3 Write a computer program for the analysis of a piping system having an air chamber as shown in Fig. 10.2. Assume that the check valve closes as soon as power fails. The pipeline has a constant-head reservoir at the downstream end.

10.4 Prove that an air chamber behaves like a virtual surge tank[12] having a cross-sectional area

$$A_s = \frac{1}{m} \frac{\forall_{o_{air}} H_o^{*\frac{1}{m}}}{[H_{P_{i,n+1}} + H_b]^{\frac{m+1}{m}}}$$

in which the variables are as defined in Section 10.4.

10.5 Develop the boundary conditions for the centrifugal-pump–PRV system shown in Fig. 10.8. Assume that the PRV is discharging into the suction line of the pump. (*Hint:* Equation 10.29 will be modified to $Q_{P_v} = \tau_P Q_o \sqrt{(H_{P_{1,1}} - H_{P_s})/H_o}$ in which H_{P_s} is the piezometric head on the suction side of the pump, and H_o = steady-state pumping head.)

10.6 Develop the boundary conditions for an air-inlet valve that allows outflow of air, but not of liquid, from the pipeline when the pressure inside the pipeline exceeds the outside atmospheric pressure. (*Hint:* Use expressions similar to Eqs. 10.43 and 10.44 for the time rate of mass outflow of air through the valve. As the air inflow was assumed positive in Eqs. 10.36 and 10.42, dm_a/dt for air outflow should be considered negative in these equations.)

REFERENCES

1. Evans, W. E. and Crawford, C. C., "Design Charts for Air Chambers on Pump Lines," *Trans. Amer. Soc. of Civil Engrs.*, vol. 119, 1954, pp. 1025–1045.
2. Engler, M. L., "Relief Valves and Air Chambers," *Symposium on Waterhammer, Amer. Soc. of Mech. Engrs. and Amer. Soc. of Civil Engrs.*, 1933, pp. 97–115.
3. Allievi, L., "Air Chamber for Discharge Lines," *Trans. Amer. Soc. of Mech. Engrs.*, vol. 59, Nov. 1937, pp. 651–659.
4. Angus, R. W., "Air Chambers and Valves in Relation to Waterhammer," *Trans. Amer. Soc. of Mech. Engrs.*, vol. 59, Nov. 1937, pp. 661–668.
5. Combes, G. and Borot, G., "New Chart for the Calculation of Air Vessels Allowing for Friction Losses," *LaHouille Blanche*, 1952, pp. 723–729.
6. Tucker, D. M. and Young, G. A. J., "Estimation of the Size of Air Vessels," *British Hydromechanics Research Assoc.*, Report SP 670, 1962.
7. Graze, H. R. and Forrest, J. A., "New Design Charts for Air Chambers," *Fifth Australasian Conference on Hydraulics and Fluid Mechanics*, Christchurch, New Zealand, 1974, pp. 34–41.
8. Ruus, E., "Charts for Waterhammer in Pipelines with Air Chamber," *Canadian Jour. of Civil Engineering*, vol. 4, no. 3, Sept. 1977, pp. 293–313.
9. Graze, H. R., "A Rational Thermodynamic Equation for Air Chamber Design," *Proc. Third Australasian Conference on Hydraulics and Fluid Mechanics*, Sydney, Australia, 1968, pp. 57–61.
10. Graze, H. R., Discussion of "Pressure Surge Attenuation Utilizing an Air Chamber," by Wood, D. J., *Jour., Hyd. Div., Amer. Soc. of Civil Engrs.*, vol. 97, March 1971, pp. 455–459.
11. Graze, H. R., "The Importance of Temperature in Air Chamber Operations," *Proc. First International Conference on Pressure Surges, British Hydromechanic Research Assoc.*, England, 1972, pp. F2-13–F2-21.
12. Evangelisti, G., "Waterhammer Analysis by the Method of Characteristics," *L'Energia Elettrica*, no. 12, 1969, pp. 839–858.
13. Lescovich, J. E., "The Control of Water Hammer by Automatic Valves," *Jour. Amer. Water Works Assoc.*, May 1967, pp. 832–844.
14. Gadenberger, W., "Grundlagen der graphischen Ermittlung der Druckschwankungen in Wasserversorgungsleitungen," R. Oldenbourg Verley, 1950.
15. Streeter, V. L. and Wylie, E. B., *Hydraulic Transients*, McGraw-Hill Book Co., New York, 1967.
16. Albertson, M. L. and Andrews, J. S., "Transients Caused by Air Release," in *Control of Flow in Closed Conduits*, edited by Tullis, J. P., Colorado State University, 1971.
17. Martin, C. S., "Entrapped Air in Pipelines," *Proc. Second Conference on Pressure Surges, British Hydromechanic Research Assoc.*, England, 1976.
18. Papadakis, C. N. and Hsu, S. T., "Transient Analysis of Air Vessels and Air Inlet Valves," *Jour., Fluid Engineering, Amer. Soc. of Mech. Engrs.*, 1977.
19. Streeter, V. L., *Fluid Mechanics*, McGraw-Hill Book Co., 4th edition, 1966, p. 304.
20. Ruus, E., "Optimum Rate of Closure of Hydraulic Turbine Gates," presented at Amer. Soc. of Mech. Engrs.–Engineering Inst. of Canada Conference, Denver, Colorado, April 1966.
21. Streeter, V. L., "Valve Stroking to Control Water Hammer," *Jour., Hyd. Div., Amer. Soc. of Civil Engineers*, vol. 89, March 1963, pp. 39–66.
22. Streeter, V. L., "Valve Stroking for Complex Piping Systems," *Jour., Hyd. Div., Amer. Soc. of Civ. Engrs.*, vol. 93, May 1967, pp. 81–98.

23. Driel, M., "Valve Stroking in Separated Pipe Flow," *Jour., Hyd. Div., Amer. Soc. of Civ. Engrs.*, vol. 100, Nov. 1974, pp. 1549–1563.
24. Ikeo, S. and Kobori, T., "Waterhammer Caused by Valve Stroking in Pipeline With Two Valves," *Bull. Japan Soc. of Mech. Engrs.*, vol. 18, October 1975, pp. 1151–1157.
25. Driels, M., "Predicting Optimum Two-Stage Valve Closure," Paper No. 75-WA/FE-2, *Amer. Soc. of Mech. Engrs.*, 1975, 7 pp.
26. Bell, W. W., Johnson, G., and Winn, C. B., "Control Logic for Real Time Control of Flow in Combined Sewers," *Proc., 9th Canadian Symp., Water Poll. Res.*, Canada, 1974, pp. 217–234.
27. Portfors, E. A. and Chaudhry, M. H., "Analysis and Prototype Verification of Hydraulic Transients in Jordan River Power Plant," *Proc. First Conference on Pressure Surges*, published by British Hydromechanics Research Assoc., England, Sept. 1972, pp. E4-57–E4-72.
28. Chaudhry, M. H. and Portfors, E. A., "A Mathematical Model for Analyzing Hydraulic Transients in a Hydro Power Plant," *Proc. First Canadian Hydraulic Conference*, published by the University of Alberta, Edmonton, Alberta, Canada, May 1973, pp. 298–314.
29. Forster, J. W., Kadak, A., and Salmon, G. M., "Planning of the Jordan River Redevelopment," *Engineering Jour., Engineering Inst. of Canada*, Oct. 1970, pp. 34–43.

ADDITIONAL REFERENCES

Strowger, E. B., "Relation of Relief Valve and Turbine Characteristics in the Determination of Waterhammer," *Trans. Amer. Soc. of Mech. Engrs.*, vol. 59, Nov. 1937, pp. 701–705.
Parmakian, J., "Air Inlet Valves for Steel Pipe Lines," *Trans. Amer. Soc. of Civ. Engrs.*, vol. 115, 1950, pp. 438–443.
Jacobson, R. S., "Charts for Analysis of Surge Tanks in Turbine or Pump Installations," *Special Report 104*, Bureau of Reclamation, Denver, Colorado, Feb. 1952.
Parmakian, J., "Pressure Surge Control at Tracy Pumping Plant," *Proc. Amer. Soc. of Civil Engrs.*, vol. 79, Separate No. 361, Dec. 1953.
Parmakian, J., "Pressure Surge at Large Installations," *Trans. Amer. Soc. of Mech. Engrs.*, 1953, p. 995.
Lindros, E., "Grand Coulee Model–Pump Investigation of Transient Pressures and Methods for Their Reduction," *Trans. Amer. Soc. of Mech. Engrs.*, 1954, p. 775.
Parmakian, J., "One-Way Surge Tanks for Pumping Plants," *Trans. Amer. Soc. of Mech. Engrs.*, 1958, pp. 1563–1573.
Kerr, S. L., "Effect of Valve Operation on Waterhammer," *Jour. Amer. Water Works Assoc.*, vol. 52, Jan. 1960.
Lundgren, C. W., "Charts for Determining Size of Surge Suppressors for Pump-Discharge Lines," *Jour. Engineering for Power, Amer. Soc. of Mech. Engrs.*, Jan. 1961, pp. 43–46.
Whiteman, K. J., and Pearsall, I. S., "Reflex Valve and Surge Tests at a Pumping Station," *Fluid Handling*, vol. 152, Sept. and Oct. 1962, pp. 248–250, 282–286.
Widmann, R., "The Interaction Between Waterhammer and Surge Tank Oscillations," *International Symposium on Waterhammer in Pumped Storage Projects, Amer. Soc. of Mech. Engrs.*, Chicago Nov., 1965, pp. 1–7.
Bechteler, W., "Surge Tank and Water Hammer Calculations on Digital and Analog Computers," *Water Power*, vol. 21, no. 10, Oct. 1969, pp. 386–390.
Ruus, E., and Chaudhry, M. H., "Boundary Conditions for Air Chambers and Surge Tanks," *Trans., Engineering Inst. of Canada, Engineering Jour.*, Nov. 1969, pp. I–VI.

Meeks, D. R. and Bradley, M. J., "The Effect of Differential Throttling on Air Vessel Performance," *Symposium on Pressure Transients*, The City University, London, Nov. 1970.
Wood, D. J., "Pressure Surge Attenuation Utilizing an Air Chamber," *Jour., Hyd. Div., Amer. Soc. of Civil Engrs.*, vol. 96, May 1970, pp. 1143–1156.
Kinno, H., "Waterhammer Control in Centrifugal Pump Systems," *Jour., Hyd. Div., Amer. Soc. of Civ. Engrs.*, May 1968, pp. 619–639.
Chaudhry, M. H., "Boundary Conditions for Waterhammer Analysis," thesis submitted to the Univ. of British Columbia, Vancouver, Canada, in partial fulfillment of the requirements of M.A.Sc., April 1968.

CHAPTER 11

SURGE TANKS

11.1 INTRODUCTION

A *surge tank* is an open standpipe or a shaft connected to the conduits of a hydroelectric power plant or to the pipeline of a piping system. This is also referred to as a *surge shaft* or *surge chamber*.

The main functions of a surge tank are:

1. It reduces the amplitude of pressure fluctuations by reflecting the incoming pressure waves. For example, the waterhammer waves produced in a penstock by load changes on a turbine (Fig. 11.1) are reflected back at the surge tank. Thus, the conduit length to be used in the waterhammer analysis is between the turbine and the surge tank rather than between the turbine and the upstream reservoir. Due to this reduction in the conduit length, the pressure rise or drop is less than if the surge tank were not provided. In addition, if a surge tank were not present at the junction of the penstock and the tunnel, then the tunnel would have to be designed to withstand the waterhammer pressures.
2. A surge tank improves the regulating characteristics of a hydraulic turbine. Because of the surge tank, the length of the power conduit to be used for determining the water-starting time (see Section 5.10) is up to the surge tank rather than up to the upstream reservoir. The water-starting time of a hydropower scheme is therefore reduced, thus improving the regulating characteristics of the power plant.
3. A surge tank acts as a storage for excess water during load reduction in a hydropower plant and during start-up of the pumps in a pumping system. Similarly, it provides water during load acceptance in a hydropower plant and during power failure in a pumping system. Therefore, the water is accelerated or decelerated in the pipeline slowly, and the amplitude of the pressure fluctuations in the system is reduced.

In this chapter, various types of surge tanks are reviewed. Differential equations describing the oscillations of the water level in a simple surge tank are derived, and methods available for their solution are presented. The phase plane method is then used to study the stability of a simple surge tank. This is followed by the analysis of orifice, differential, and a system of surge tanks. The chapter is concluded by summarizing the studies carried out for the design of the Chute-des-Passes surge-tank system.

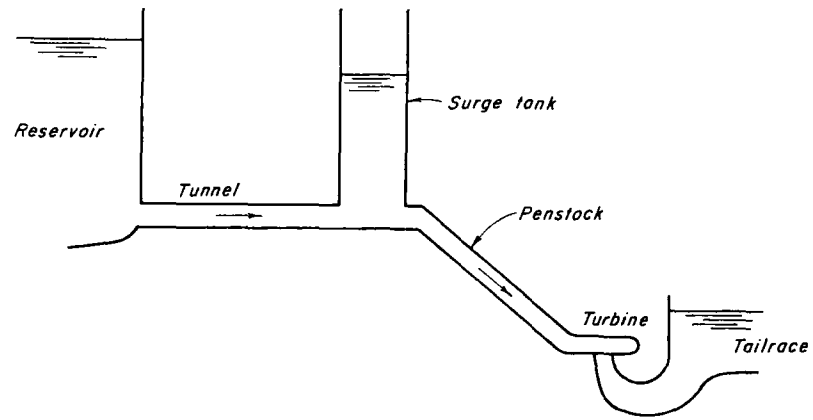

Figure 11.1. Schematic diagram of a hydroelectric power plant.

11.2 TYPES OF SURGE TANKS

Depending upon its configuration, a surge tank may be classified as *simple*, *orifice*, *differential*, *one-way*, or *closed*. A brief description of each follows.

A *simple surge tank* is just a shaft or standpipe connected to the pipeline. If the entrance to the surge tank is restricted by means of an orifice, it is called an *orifice tank*. An orifice tank having a riser is termed *differential*. In a *one-way surge tank*, the liquid flows from the tank into the pipeline only when the pressure in the pipeline drops below the liquid level in the surge tank. Following the transient-state conditions, the tank is filled from the pipeline. If the top of the tank is closed or if there is a valve or orifice in the vent stack connecting the tank to the outer atmosphere, the tank is called a *closed surge tank*. Depending upon the requirement that the tank must fulfill, a simple tank may have upper or lower galleries. Figure 11.2 shows a number of typical surge tanks.

If necessary, a combination of different types of surge tanks may be provided in an installation.

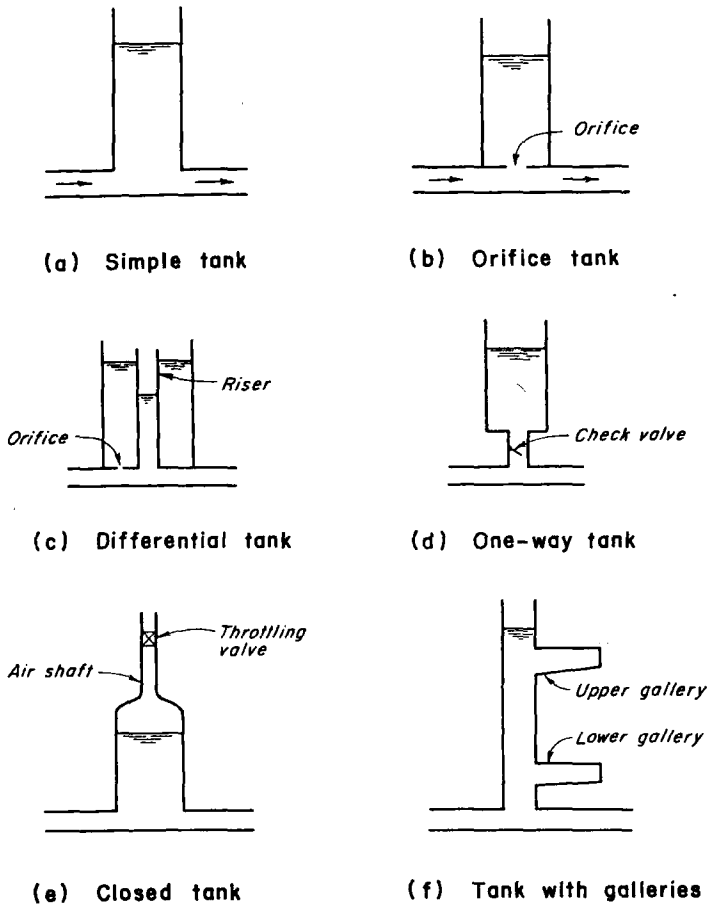

(a) Simple tank (b) Orifice tank

(c) Differential tank (d) One-way tank

(e) Closed tank (f) Tank with galleries

Figure 11.2. Types of surge tanks.

11.3 DERIVATION OF EQUATIONS

Figure 11.3a shows a typical surge-tank system in which a control valve is used to represent a pump or a hydraulic turbine. A change in the valve opening causes the flow variation, which results in the oscillations of the liquid level in the surge tank.

To simplify the derivation of the dynamic and continuity equations, let us make the following *assumptions:*

1. The conduit walls are rigid, and the liquid is incompressible. This means that a flow change is felt throughout the system instantaneously and that the liquid in the conduit is moving like a solid slug.
2. The inertia of the liquid in the surge tank is small compared to that of the liquid in the tunnel and can therefore be neglected.
3. The head losses in the system during the transient state can be computed by using the steady-state formulas for the corresponding flow velocities.

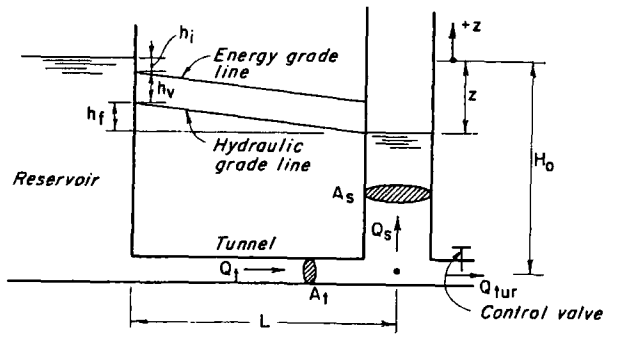

(a)

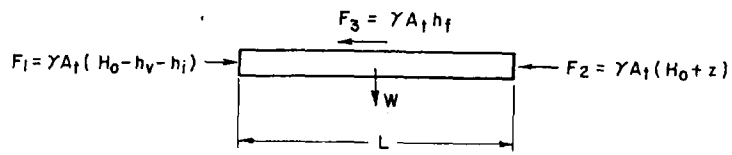

(b) Freebody diagram

Figure 11.3. Simple surge tank: notation for dynamic and continuity equations.

Dynamic Equation

A freebody diagram of a horizontal conduit having constant cross-sectional area is shown in Fig. 11.3b. Forces acting on the liquid are:

$$F_1 = \gamma A_t(H_o - h_v - h_i) \tag{11.1}$$

$$F_2 = \gamma A_t(H_o + z) \tag{11.2}$$

$$F_3 = \gamma A_t h_f \tag{11.3}$$

In these equations, A_t = cross-sectional area of the tunnel; H_o = static head; γ = specific weight of liquid; h_v = velocity head at the intake; h_i = intake head losses; h_f = friction and form losses in the tunnel between the intake and the surge tank; and z = water level in the surge tank above the reservoir level (positive upward). Considering the downstream flow direction as positive, the net force acting on the liquid element in the positive direction is $\Sigma F = F_1 - F_2 - F_3$. Hence, from Eqs. 11.1 to 11.3,

$$\Sigma F = \gamma A_t(-z - h_v - h_i - h_f) \tag{11.4}$$

The mass of the liquid element is $\gamma A_t L/g$, in which L = length of the tunnel and g = acceleration due to gravity. If Q_t is the tunnel flow and t = time, then the rate of change of momentum of the element may be written as

$$\frac{\gamma A_t L}{g} \frac{d}{dt}\left(\frac{Q_t}{A_t}\right)$$

or

$$\frac{\gamma L}{g} \frac{dQ_t}{dt}$$

According to Newton's second law of motion, the rate of change of momentum is equal to the net applied force. Therefore,

$$\frac{\gamma L}{g} \frac{dQ_t}{dt} = \gamma A_t(-z - h_v - h_i - h_f). \tag{11.5}$$

By defining $h = h_v + h_i + h_f = cQ_t|Q_t|$, in which c is a coefficient, Eq. 10.5 may be written as

$$\frac{dQ_t}{dt} = \frac{gA_t}{L}(-z - cQ_t|Q_t|) \tag{11.6}$$

Note that h is expressed as $cQ_t|Q_t|$ to account for the reverse flow.

In the preceding derivation, the tunnel was assumed to be horizontal and to have constant cross-sectional area throughout its length. Equation 11.6 is also valid for a sloping tunnel (see Problem 11.3). However, for a tunnel having different cross-sectional areas for various lengths, the term A_t/L of Eq. 11.6 is replaced by $\Sigma(A_t/L)_i$ (see Problem 11.5).

Continuity Equation

Referring to Fig. 11.3, the continuity equation for the junction of the tunnel and the surge tank may be written as

$$Q_t = Q_s + Q_{tur} \tag{11.7}$$

in which Q_s = flow into the surge tank (positive into the tank), and Q_{tur} = turbine flow. Note that Eq. 11.7 is equally valid for the pumping system if the flow of the pump is designated as Q_{tur}. Writing Q_s as $A_s(dz/dt)$, Eq. 11.7 becomes

$$\frac{dz}{dt} = \frac{1}{A_s}(Q_t - Q_{tur}) \tag{11.8}$$

Note that Eqs. 11.6 and 11.8 are for a surge tank located at the upstream side of a turbine. These equations are valid for a tailrace surge tank (i.e., a tank located on the downstream of the turbine), provided the velocity head, h_v, is properly taken into consideration.

11.4 AVAILABLE METHODS FOR SOLVING DYNAMIC AND CONTINUITY EQUATIONS

Due to the assumption that the tunnel and the liquid inside are rigid, we do not have spatial derivatives (i.e., variation with respect to x) in the dynamic and continuity equations, and the flow and the liquid level in the tank vary with respect to time only. Therefore, Eqs. 11.6 and 11.8 are a set of ordinary differential equations. Because of the presence of the term $cQ_t|Q_t|$, Eq. 11.6 is nonlinear. Also, note that turbine flow may be a function of time.

A closed-form solution of Eqs. 11.6 and 11.8 is available only for a few special cases.[1] Therefore, graphical[2,3] and arithmetical methods suitable for hand computations[4,5] have been used in the past to integrate these equations. However, with the invention of the analog and digital computers, graphical and arithmetical methods of integration have been superseded by analog simulation or digital computation. When a large number of parameters have to be optimized, analog computers are very handy[6,7]; with these, once the required circuitry has been wired, it is just a matter of twisting various knobs to change various parameters. As compared to the analog, digital computers are more readily accessible. Therefore, we will discuss only the methods suitable for digital computer analysis.

A number of finite-difference techniques are available[8,9] to solve the dynamic and continuity equations on a digital computer. Although more sophisticated and accurate methods[10,11] are reported in the literature, in the author's opinion,

the fourth-order Runge-Kutta method[12] may be used, which yields sufficiently accurate results that are of the same order of accuracy as that of the input data. In addition to being simpler to program than other methods, subroutines are available as a standard package for this method at most of the computer installations.

11.5 PERIOD AND AMPLITUDE OF OSCILLATIONS OF A FRICTIONLESS SYSTEM

The head losses were taken into consideration while deriving the dynamic equations. If the system is considered frictionless, i.e., $c = 0$, then Eq. 11.6 becomes

$$\frac{dQ_t}{dt} = -\frac{gA_t}{L} z \tag{11.9}$$

Let us assume that an initial steady-state turbine flow, Q_o, is instantaneously reduced to zero at $t = 0$, i.e.,

$$\text{at } t < 0, \quad Q_{\text{tur}} = Q_o \tag{11.10}$$

and

$$\text{at } t \geqslant 0, \quad Q_{\text{tur}} = 0 \tag{11.11}$$

On the basis of Eq. 11.11, Eq. 11.8 can be written as

$$\frac{dz}{dt} = \frac{1}{A_s} Q_t \tag{11.12}$$

Differentiating Eq. 11.12 with respect to t and eliminating dQ_t/dt from the resulting equation and Eq. 11.9, we obtain

$$\frac{d^2z}{dt^2} + \frac{gA_t}{LA_s} z = 0 \tag{11.13}$$

As the coefficient of z in Eq. 11.13 is a positive real constant, we know from the theory of ordinary differential equations[13] that a general solution of Eq. 11.13 is

$$z = C_1 \cos \sqrt{\frac{gA_t}{LA_s}}\, t + C_2 \sin \sqrt{\frac{gA_t}{LA_s}}\, t \tag{11.14}$$

in which C_1 and C_2 are arbitrary constants and are determined from the initial conditions. For this case, at $t = 0$,

$$z = 0 \tag{11.15}$$

and

$$\frac{dz}{dt} = \frac{Q_o}{A_s} \tag{11.16}$$

Substituting these conditions into Eq. 11.14,

$$\left.\begin{aligned} C_1 &= 0 \\ \text{and} \\ C_2 &= Q_o \sqrt{\frac{L}{gA_sA_t}} \end{aligned}\right\} \tag{11.17}$$

Hence, it follows from Eq. 11.14 and 11.17 that

$$z = Q_o \sqrt{\frac{L}{gA_sA_t}} \sin \sqrt{\frac{gA_t}{LA_s}}\, t \tag{11.18}$$

Equation 11.18 describes the oscillations of the water surface in the surge tank. The period, T, and the amplitude, Z, of these oscillations (Fig. 11.4) are

$$T = 2\pi \sqrt{\frac{L}{g}\frac{A_s}{A_t}} \tag{11.19}$$

and

$$Z = Q_o \sqrt{\frac{L}{gA_sA_t}} \tag{11.20}$$

The amplitude, Z, is referred to as *free surge* for load rejection.

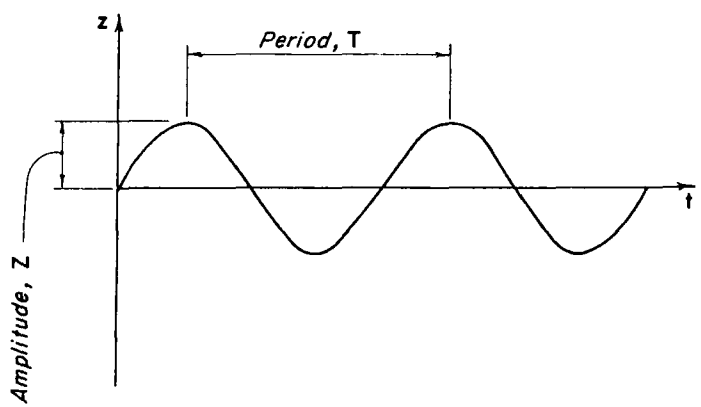

Figure 11.4. Period and amplitude of oscillations of a frictionless system.

11.6 STABILITY

If the hydraulic system of Fig. 11.3 is disturbed (e.g., by changing the turbine flow), the water level in the surge tank begins to oscillate. These oscillations are stable or unstable depending upon the parameters of the power plant and the type and magnitude of the disturbance. Oscillations are said to be *stable* if they dampen to the final steady state in a reasonable time and *unstable* if their magnitude increases with time (see Fig. 11.5).

In addition to oscillatory instability, a condition called *tank drainage* has to be avoided. In this case, following a large load increase, the water in the tunnel does

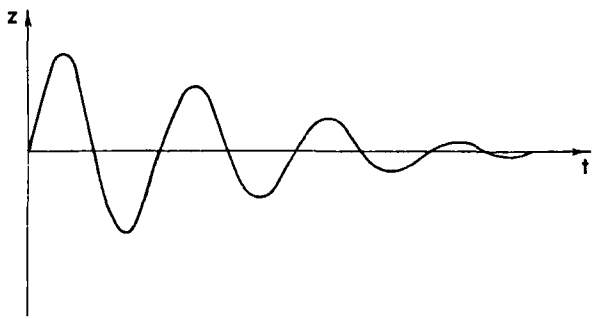

(a) Stable oscillations

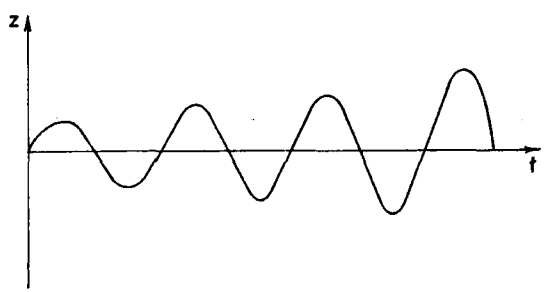

(b) Unstable oscillations

Figure 11.5. Stable and unstable oscillations.

not accelerate fast enough to meet the turbine demand. Therefore, the surge tank supplies the water, and its water level keeps on falling until the tank drains. This condition usually occurs if the tunnel losses are large.

The following four cases of change in the turbine flow are of interest:

1. *Constant Flow.* The turbine flow is changed from one steady-state value Q_1 to another steady-state value, Q_2. Since the turbine flow varies with the change in the surge-tank level, constant flow is possible only on very high head installations where oscillations in the surge tank are small compared to the static head.

2. *Constant-Gate Opening.* Constant-gate opening occurs when the plant is under manual control after a load change, or when the governor is inoperative due to malfunctioning of some of its parts, or when the turbine gates are opened to the maximum position following a load increase while the governor is trying to maintain constant power.

3. *Constant Power.* In this case, it is assumed that an ideal governor maintains constant power input to the turbine or maintains constant turbine output if the turbine efficiency is considered constant. Following a load increase, the governor opens the wicket gates to increase the flow. As a result, the water level in the surge tank is lowered, and the net head on the turbine is reduced. Therefore, the governor has to open the gates further to keep the power constant. No restriction on the turbine-gate opening is assumed, which implies that the turbine discharge can be increased to any required amount to maintain constant power. Thus, it can be seen that the action of the governor is destabilizing.

4. *Constant Power Combined with Full Gate Opening.* In case 3, we assumed that the turbine gates can be opened to any value to maintain constant power. On actual installations, however, gates cannot be opened to more than their fully open position. Therefore, the governor maintains constant power if the net head on the turbine is more than or equal to the rated head. When the net head is less than the rated head, the case of constant-gate opening applies. Note that for the net heads less than the rated head, the turbine power output decreases with the lowering of the surge-tank level, and, as a result, the system frequency decreases if the plant is isolated. Usually the load is tripped if the system frequency drops below a prescribed value. In our analysis, however, we are assuming that the load is not tripped, and the turbine keeps on generating power irrespective of the system frequency.

By integrating Eqs. 11.6 and 11.8 graphically, Frank and Schüller[2] demonstrated that the oscillations are always stable in case 2 and stable in case 1 if the tunnel friction losses are taken into consideration. Case 3 has been studied by a number of investigators: Thoma[14] linearized the governing differential equations and demonstrated that the oscillations are unstable if the tank area is less

than a minimum. This minimum area is now called the *Thoma area*, A_{th}. Paynter[15,16] solved the equations analytically and on an analog computer and presented a stability diagram. Using the phase-plane method,[17,18] Marris[19,20] and Sideriades[21,22] demonstrated that Thoma's stability criteria do not hold for large oscillations. Ruus[23] analyzed case 4 on a digital computer and showed that small, rather than large, oscillations are critical for the stability of a tank. The author and Ruus[24] used the phase-plane method to investigate the stability for all four cases listed. These studies are presented herein. A number of quantitative results are obtained from the analysis of the singularities, and a number of phase portraits are presented to show the effect of the changes in different parameters on the qualitative behavior of the system.

11.7 NORMALIZATION OF EQUATIONS

In order to reduce the number of parameters, we will normalize Eqs. 11.6 and 11.8 as follows:

Let

$$\left.\begin{aligned} y &= z/Z \\ x &= Q_t/Q_o \\ q &= Q_{tur}/Q_o \\ \tau &= 2\pi t/T \end{aligned}\right\} \tag{11.21}$$

By substituting these variables into Eqs. 11.8 and 11.6, and simplifying the resulting equations, we obtain

$$\frac{dy}{d\tau} = x - q \tag{11.22}$$

$$\frac{dx}{d\tau} = -y - \tfrac{1}{2}Rx^2 \tag{11.23}$$

in which $R = 2h_{fo}/Z = 2cQ_o^2/Z$; and h_{fo} = head loss corresponding to flow Q_o, in the tunnel.

11.8 PHASE-PLANE METHOD*

To facilitate discussion in the following section, a summary of the necessary equations follows; for a detailed description of the method, see Ref. 17.

*Readers who are not interested in the mathematical details may proceed directly to the conclusions summarized at the end of Section 11.9, p. 360.

Let the differential equations describing a system be

$$\frac{dx}{d\tau} = P(x,y) \tag{11.24}$$

and

$$\frac{dy}{d\tau} = Q(x,y) \tag{11.25}$$

in which the functions $P(x, y)$ and/or $Q(x, y)$ may be nonlinear. By combining Eqs. 11.24 and 11.25, we obtain

$$\frac{dy}{dx} = \frac{Q(x,y)}{P(x,y)} \tag{11.26}$$

The points (x_s, y_s) for which $\frac{dy}{dx} = \frac{0}{0}$ are called *singular points.* The location of these points is obtained by simultantously solving the equations $P(x, y) = 0$, and $Q(x, y) = 0$. The type of singularity may be determined by substituting $x = x_s + u$ and $y = y_s + v$ into Eq. 11.26, which after simplification yields

$$\frac{dv}{du} = \frac{Q(x_s,y_s) + c'u + d'v + c''u^2 + d''v^2}{P(x_s,y_s) + a'u + b'v + a''u^2 + b''v^2} \tag{11.27}$$

in which a', a'', b', b'', c', c'', d', and d'' are real constants. If both the linear terms and the higher-power terms in u and v are present in the denominator and in the numerator, the singularity is called a *simple* singularity. For such a singularity, the higher-power terms can be neglected because their effect on the solution in the neighborhood of the singularity is small compared to that of the linear terms. However, if the linear terms are missing, the singularity is *nonsimple*, and the higher-power terms cannot be neglected.

To study the properties of the solution in the neighborhood of a simple singularity, Eq. 11.27 may be written as

$$\frac{dv}{du} = \frac{c'u + d'v}{a'u + b'v} \tag{11.28}$$

The characteristic roots, λ_1 and λ_2, of the two equations equivalent to the above equation, i.e.,

$$\frac{dv}{dt} = c'u + d'v \tag{11.29}$$

and

$$\frac{du}{dt} = a'u + b'v \tag{11.30}$$

are

$$\lambda_1, \lambda_2 = \tfrac{1}{2}\left[(a' + d') \pm \sqrt{(a' + d')^2 + 4(b'c' - a'd')}\right] \tag{11.31}$$

The roots, λ_1 and λ_2, determine the type of a singularity as follows:

1. *Node*, if both roots are real and have the same sign.
2. *Saddle*, if both roots are real and have the opposite signs.
3. *Vortex*, if both roots are imaginary.
4. *Focus*, if the roots are complex conjugates.

If the real part of the roots is negative, the singularity of node and focus is termed *stable*; if positive, it is called *unstable*. Note that Eqs. 11.28 through 11.31 are valid only for simple singularities.

11.9 ANALYSIS OF DIFFERENT CASES OF FLOW DEMAND

For the cases discussed in Section 11.6, the normalized flow demand characteristics are shown in Fig. 11.6. Stability of these cases may be studied as discussed in the following.

Constant Flow

Let the initial steady-state flow be Q_1, and the final steady-state flow, Q_2. Then in normalized form, $q = x^*$, in which $x^* = Q_2/Q_o$. By substituting this into Eq. 11.22, and dividing the resulting equation by Eq. 11.23, we obtain

$$\frac{dy}{dx} = \frac{x - x^*}{-y - \frac{1}{2}Rx^2} \tag{11.32}$$

The coordinates of the singularity are obtained by solving the equations

$$x - x^* = 0 \tag{11.33}$$

and

$$-y - \tfrac{1}{2}Rx^2 = 0 \tag{11.34}$$

simultaneously. This yields $x_s = x^*$ and $y_s = -\frac{1}{2}Rx^{*2}$.

Substitution of $x = x^* + u$ and $y = -\frac{1}{2}Rx^{*2} + v$ into Eq. 11.32 and following

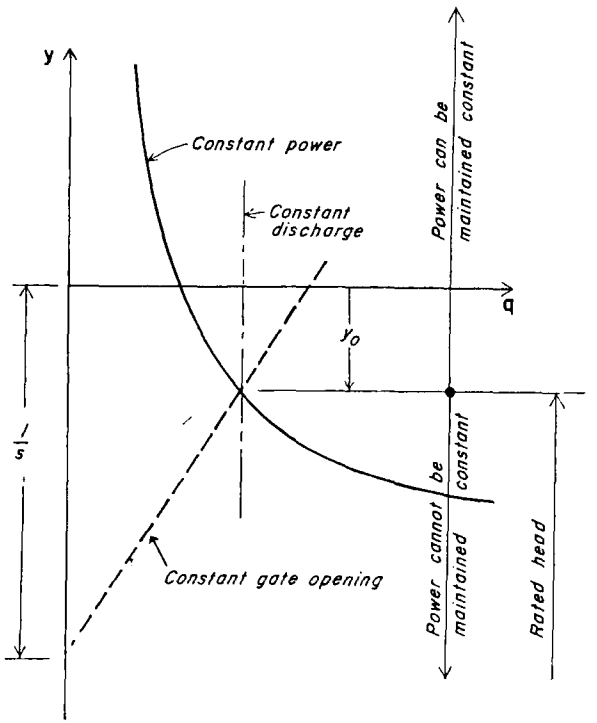

Figure 11.6. Flow demand characteristics.

the procedure outlined in Section 11.8 yield

$$\frac{dv}{du} = \frac{u}{-Rx^*u - v} \tag{11.35}$$

By comparing this equation with Eq. 11.28, $a' = -Rx^*$, $b' = -1$, $c' = 1$, and $d' = 0$ are obtained. Therefore, it follows from Eq. 11.31 that

$$\lambda_1, \lambda_2 = \tfrac{1}{2}\left[-Rx^* \pm \sqrt{(Rx^*)^2 - 4}\right] \tag{11.36}$$

Both roots are real and negative if $Rx^* > 2$. The singularity is then a *stable node* (Fig. 11.7a). If the final steady-state flow, Q_2, is used as the reference flow, ($Q_2 \neq 0$), then $Rx^* > 2$ impiles that $h_{fo} > Z$. If $Rx^* < 2$, then the roots are complex conjugates with negative real parts. Therefore, the singularity is a *stable focus* (Fig. 11.7b). If the friction losses are neglected, i.e., $R = 0$, then the roots are imaginary, and the singularity is a *vortex*.

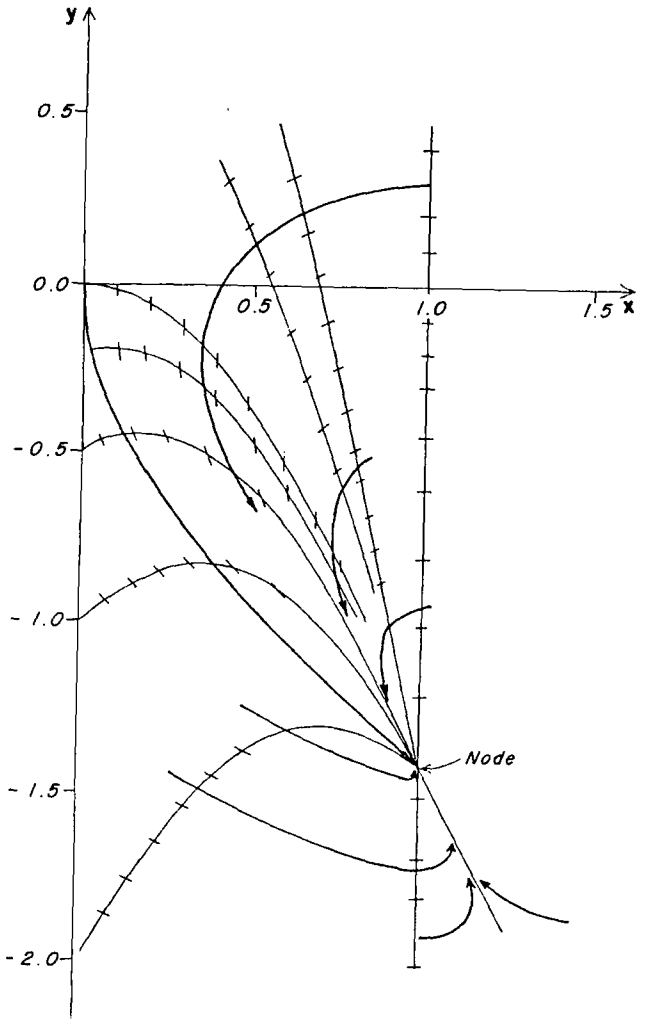

(a) k = 0.35, R = 2.8

Figure 11.7. Phase portrait for constant discharge.

This analysis confirms the results obtained by Frank and Schüller[2] who solved the differential equations by graphical integration.

In the equation corresponding to Eq. 11.27 for the case of total rejection (i.e., $x^* = 0$), there is a u^2 term in the denominator, but there is no linear term in

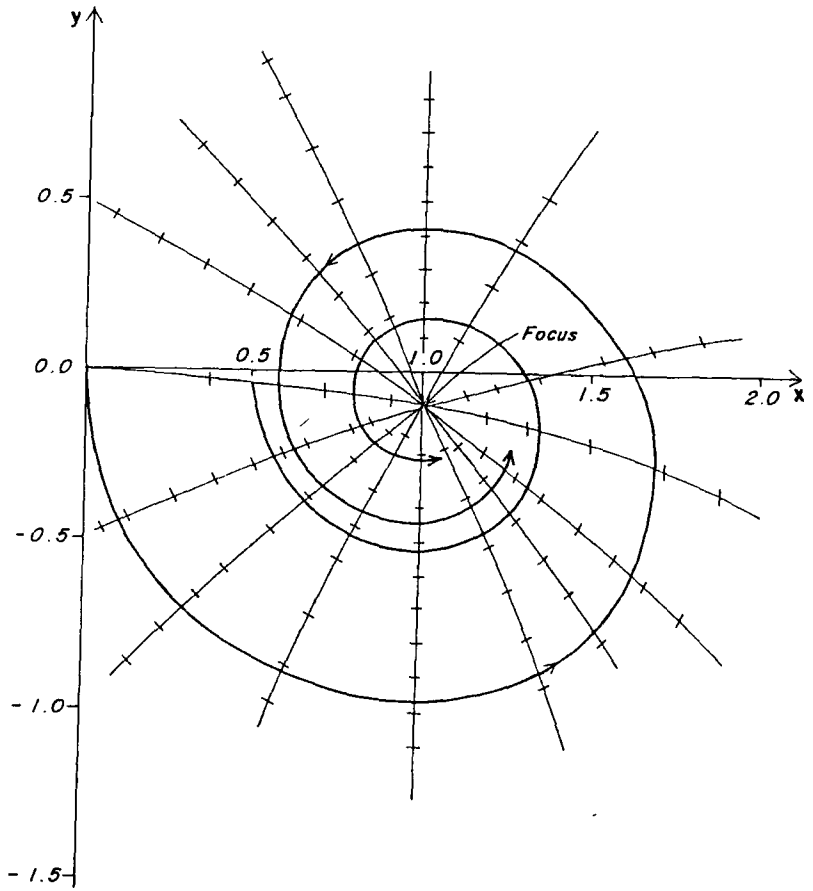

(b) k = 0.025, R = 0.2

Figure 11.7. (*Continued*)

u. Thus, the equation represents a nonsimple singularity. To solve this case, *isoclines* may be plotted as described subsequently, and thereafter the solution trajectories may be drawn. From the shape of the trajectories, the type of the singularity can be ascertained.

The phase portraits may be plotted by the method of isoclines.[17] An *isocline* is the locus of the points at which the solution trajectories have the same slope. Let m be the slope of the solution trajectories for an isocline.

Then, it follows from Eq. 11.32 that

$$\frac{dy}{dx} = \frac{x - x^*}{-y - \frac{1}{2}Rx^2} = m \tag{11.37}$$

or

$$y = -\frac{1}{2}Rx^2 - \frac{x - x^*}{m} \tag{11.38}$$

is the equation of the isocline. To obtain a graphical solution, the isoclines are first plotted for different values of m. Once this has been done, the solution trajectories for any initial conditions can be drawn. This procedure is illustrated by the phase portraits of Figs. 11.7 through 11.10. The data for plotting the phase portraits have been selected to illustrate the different types of singularities.

Constant-Gate Opening

The head-discharge relationship for a reaction turbine running at constant speed cannot be represented by a simple mathematical function. As can be seen from the turbine characteristics given in Ref. 25, the net head acting on and the discharge through the turbine are approximately linearly related for a constant-gate opening. To simplify the analysis, the head-discharge relationship is assumed as indicated in Fig. 11.6.

The equation for the flow through a reaction turbine may be written as

$$q = b(1 + sy) \tag{11.39}$$

in which $b = 1/(1 - k)$; $s = Z/H_o$; $k = h_{fo}/H_o$; and H_o = static head.

From Eqs. 11.22, 11.23, and 11.39, it follows that

$$\frac{dy}{dx} = \frac{x - b(1 + sy)}{-y - \frac{1}{2}Rx^2} \tag{11.40}$$

The coordinates of the singular points are determined by solving simultaneously

$$x - b(1 + sy) = 0 \tag{11.41}$$

and

$$-\frac{1}{2}Rx^2 - y = 0 \tag{11.42}$$

The solution of these two equations give the coordinates of two singular points: $(1, -\frac{1}{2}R)$ and $[-1/k, -1/(ks)]$. The second singular point is virtual because Eqs. 11.22 and 11.23 are valid only for $x > 0$. A singular point is *virtual* if it does not lie in the region to which it belongs. The effect of a virtual singular point on the stability of the system depends upon its distance from the stable singularities.

Singularity $(1, -\frac{1}{2}R)$

By substituting $x = 1 + u$ and $y = -\frac{1}{2}R + v$ into Eq. 11.40, and following the procedure outlined previously for determining the type of a singular point, the following equation is obtained:

$$\frac{dv}{du} = \frac{u - bsv}{-Ru - v} \tag{11.43}$$

Comparison of Eqs. 11.43 and 11.28 yields $a' = -R$; $b' = -1$; $c' = 1$; and $d' = -bs$. Thus,

$$\lambda_1, \lambda_2 = \tfrac{1}{2}\left[-(R + bs) \pm \sqrt{(R + bs)^2 - 4(1 + Rbs)}\right] \tag{11.44}$$

Since R, b, and s are all positive constants, both roots are real and negative if $(R + bs)^2 > 4(1 + Rbs)$—i.e., $(R - bs) > \pm 2$. The roots are complex conjugates with negative real part if $(R - bs) < \pm 2$. In the former case, the singular point is a *stable node* (Fig. 11.8a); in the latter, it is a *stable focus* (Fig. 11.8b).

Note that the singular point is a *stable node* for $bs > \pm 2$, and a *stable focus* (Fig. 11.8c) for $bs > \pm 2$, even if flow is considered frictionless, i.e., $R = 0$. This is because of the damping effect of the turbine gates being held in a fixed position.

Singularity $[-1/k, -(1/ks)]$

Substitution of $x = -(1/k) + u$, and $y = -1/(ks) + v$ into Eq. 11.40 results in

$$\frac{dv}{du} = \frac{u - bsv}{(R/k)u - v} \tag{11.45}$$

Comparison of Eqs. 11.45 and 11.28 yields $a' = R/k$; $b' = -1$; $c' = 1$; and $d' = -bs$. Hence,

$$\lambda_1, \lambda_2 = \frac{1}{2}\left[\left(\frac{R}{k} - bs\right) \pm \sqrt{\left(\frac{R}{k} - bs\right)^2 + 4\left(-1 + \frac{Rbs}{k}\right)}\right] \tag{11.46}$$

which upon simplification becomes

$$\lambda_1, \lambda_2 = \frac{1}{2}\left[\left(\frac{R}{k} - bs\right) \pm \sqrt{\left(\frac{R}{k} - bs\right)^2 + 4(2b - 1)}\right] \tag{11.47}$$

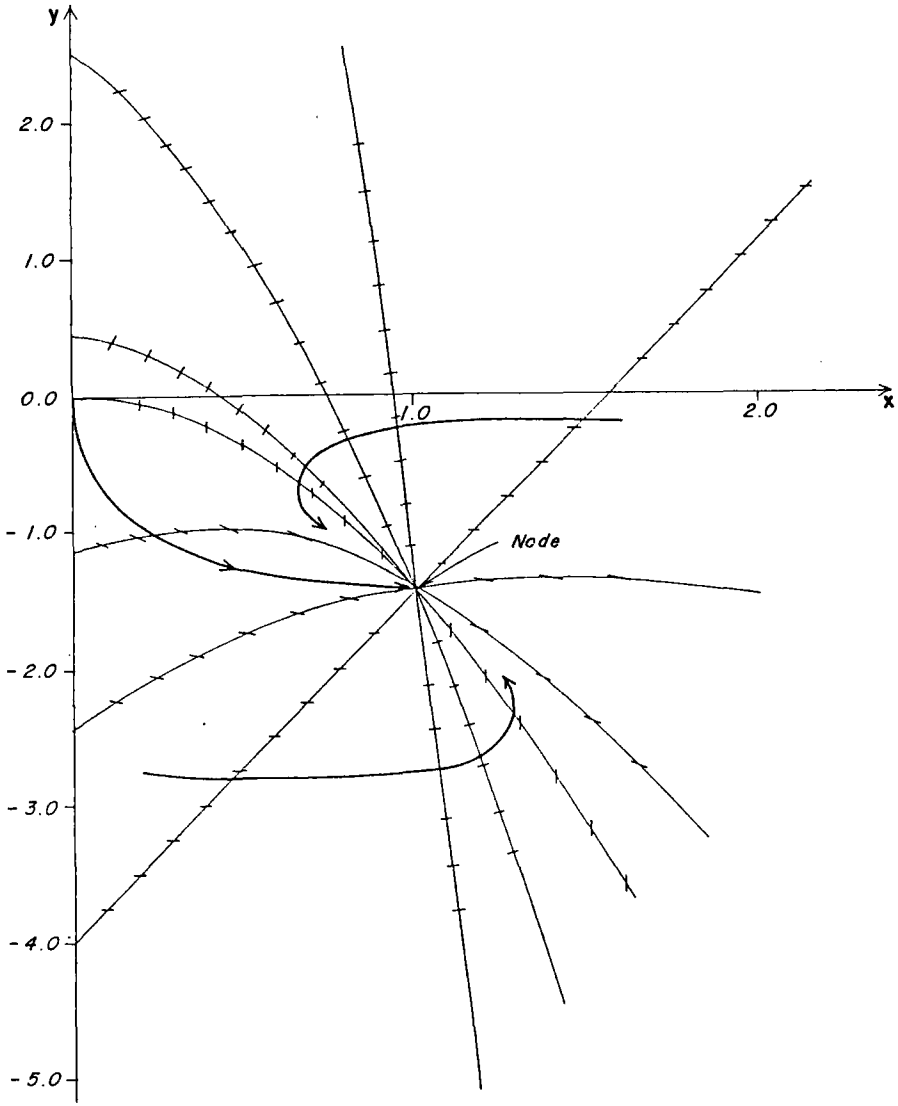

(a) k = 0.35, R = 2.8

Figure 11.8. Phase portrait for constant gate opening.

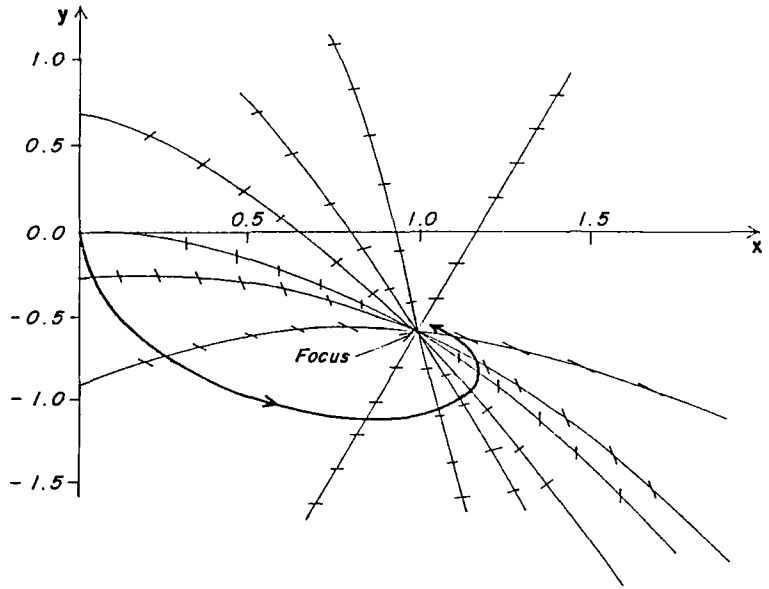

(b) k = 0.15, R = 1.2

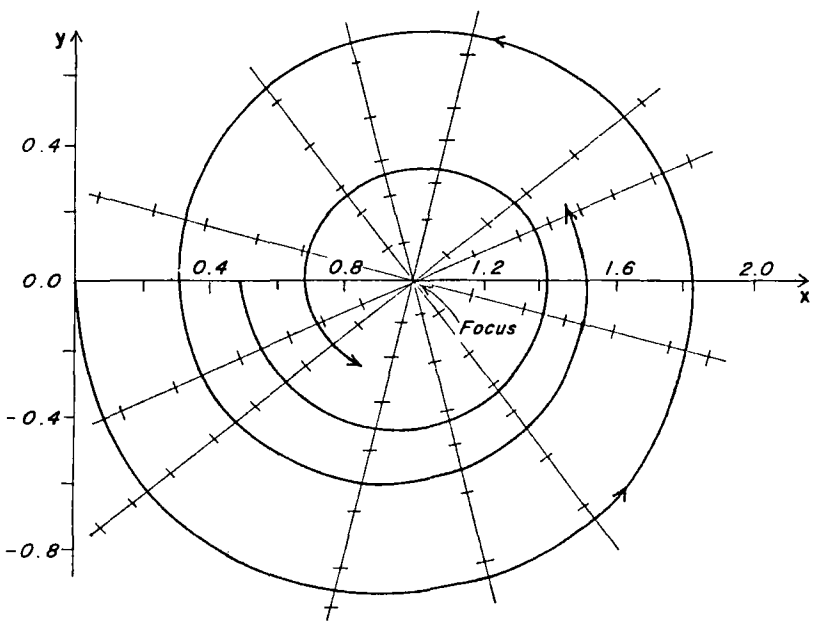

(c) k = 0, R = 0

Figure 11.8. (*Continued*)

Since $2b > 1$, both the roots are real with opposite signs. Hence, the singular point is a *saddle* point. It is a *virtual singularity* because Eqs. 11.22 and 11.23 are not valid for $x < 0$. The effect of this singular point on the stability of oscillations depends upon its location. For small friction losses, $1/k$ and $1/ks$ are large quantities, and thus the point lies at a substantial distance from the stable singular point $(1, -\frac{1}{2}R)$. Hence, its destabilizing effect is negligible. For large friction losses, however, this virtual singularity affects the stability of the system because of its proximity to the stable singularity $(1, -\frac{1}{2}R)$. For a frictionless flow, the singular point $[-1/k, -1/(ks)]$ lies at an infinite distance from the origin and thus has no destabilizing effect on the system.

Constant Power

In this case, it is assumed that an "ideal governor" ensures constant power input to the turbine. From Fig. 11.6, it can be seen that, as the water level in the tank is lowered, the governor has to open the gates to increase the discharge for maintaining constant hydraulic power. No restriction on turbine-gate opening is assumed, which implies that the turbine discharge can be increased to any required amount to maintain constant hydraulic power.

The variables of interest are x and y. Therefore, instead of using the $y - dy/d\tau$ plane, as done by Marris,[19,20] the $x - y$ plane is used herein. In addition to giving the variables of interest, the use of the $x - y$ plane has the advantage that one can clearly see the region in which Eqs. 11.22 and 11.23 are valid.

If the efficiency of the turbine is assumed constant and the penstock friction losses are neglected, then, for constant hydraulic power,

$$Q_{tur}(H_o + z) = Q_o(H_o - h_{fo}) \tag{11.48}$$

From Eq. 11.48, it follows that

$$q = \frac{Q_{tur}}{Q_o} = \frac{H_o - h_{fo}}{H_o + z} \tag{11.49}$$

which upon simplification becomes

$$q = \frac{1 - k}{1 + sy} \tag{11.50}$$

in which k and s have the same meaning as defined previously. By substituting Eq. 11.50 into Eq. 11.22, dividing the resulting equation by Eq. 11.23, and simplifying,

$$\frac{dy}{dx} = \frac{x + sxy - 1 + k}{-sy^2 - (1 + kx^2)y - \frac{1}{2}Rx^2} \tag{11.51}$$

To determine the coordinates of the singular points, the following two equations,

$$x + sxy - 1 + k = 0 \tag{11.52}$$

$$sy^2 + (1 + kx^2)y + \tfrac{1}{2}Rx^2 = 0 \tag{11.53}$$

are solved simultaneously. The solution of these equations gives the coordinates of the following three singular points:

1. $(1, -\frac{1}{2}R)$
2. $[-\frac{1}{2} + c_1, -\frac{1}{2}R(c_2 - c_1)]$
3. $[-\frac{1}{2} - c_1, -\frac{1}{2}R(c_2 + c_1)]$

in which $c_1 = \sqrt{(1/k) - \frac{3}{4}}$, and $c_2 = (1/k) - \frac{1}{2}$.

By substituting $x = x_s + u$ and $y = y_s + v$ into Eq. 11.51, and neglecting the terms in u and v of power higher than one, the equation

$$\frac{dv}{du} = \frac{(1 + sy_s)u + sx_s v}{-(R + 2ky_s)x_s u - (kx_s^2 + 2sy_s + 1)v} \tag{11.54}$$

is obtained. Comparison of Eqs. 11.28 and 11.54 yields

$$\left.\begin{aligned} a' &= -(R + 2ky_s)x_s \\ b' &= -(kx_s^2 + 2sy_s + 1) \\ c' &= (1 + sy_s) \\ d' &= sx_s. \end{aligned}\right\} \tag{11.55}$$

Singularity $(1, -\frac{1}{2}R)$

Substituting $x_s = 1$ and $y_s = -\frac{1}{2}R$ into Eq. 11.55, noting that $k = \frac{1}{2}Rs$, and simplifying, we obtain: $a' = R(k - 1)$; $b' = k - 1$; $c' = 1 - k$; and $d' = s$. Hence,

$$\lambda_1, \lambda_2 = \tfrac{1}{2}\{R(k - 1) + s \pm \sqrt{[R(k - 1) + s]^2 + 4[-(k - 1)^2 - sR(k - 1)]}\} \tag{11.56}$$

or

$$\lambda_1, \lambda_2 = \tfrac{1}{2}[R(k - 1) + s \pm \sqrt{D_1}] \tag{11.57}$$

in which $D_1 = [R(k - 1) + s]^2 + 4[2k(1 - k) - (k - 1)^2]$. If $2k(1 - k) - (k - 1)^2 > 0$ (i.e., $k > \frac{1}{3}$), then the singularity is a *saddle* (Fig. 11.9a). For $k < \frac{1}{3}$, the singularity is a node if $D_1 > 0$, and a spiral if $D_1 < 0$. The node or spiral is stable if $R(k - 1) + s < 0$. For small friction, this inequality takes the form $s < R$, or $2h_{f_o}H_o > Z^2$. The following expression for the Thoma area,

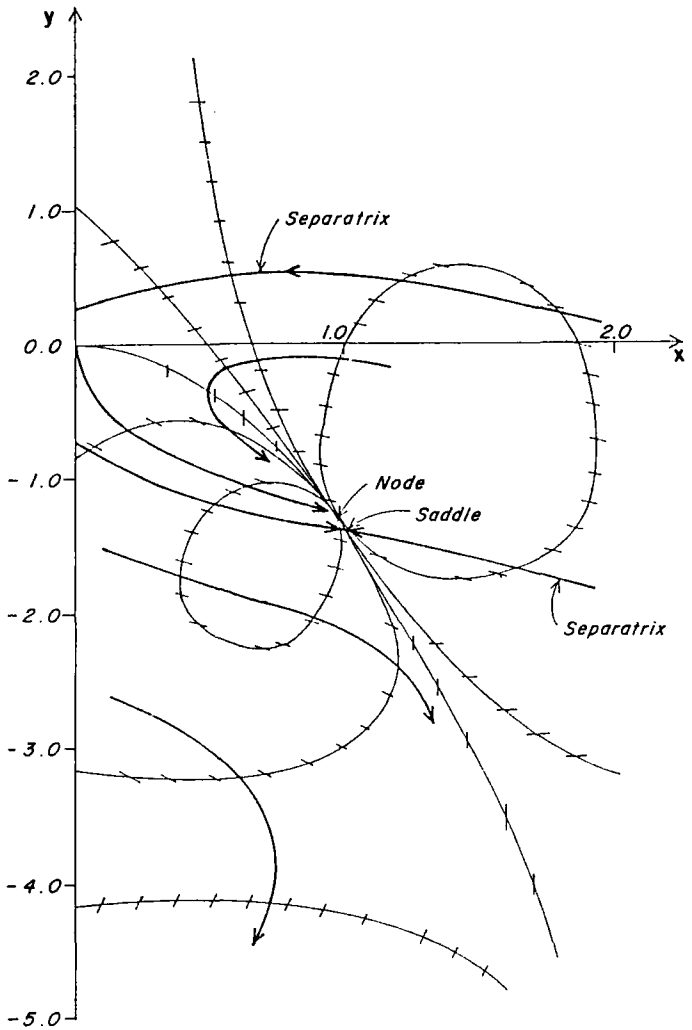

(a) k = 0.35, R = 2.8

Figure 11.9. Phase portrait for constant power.

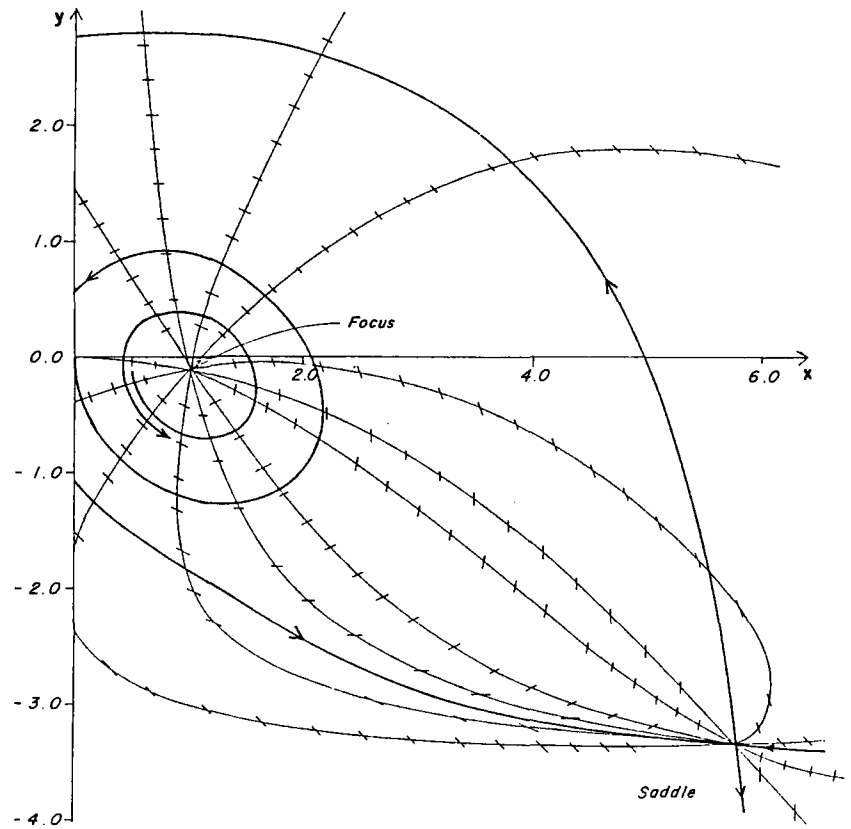

(b) k = 0.025, R = 0.2

Figure 11.9. (*Continued*)

A_{th}, may be obtained from $s = R$:

$$A_{th} = \frac{L}{2cgA_t} \tag{11.58}$$

If $2h_{f_o}H_o < Z^2$, the singularity is unstable (Fig. 11.9b).

Singularity $[c_1 - \frac{1}{2}, -\frac{1}{2}R(c_2 - c_1)]$

Substitution of the coordinates of the singularity into Eq. 11.55 and simplification of the resulting expressions give: $a' = -R(1 - k)$; $b' = -k(\frac{1}{2} + c_1)$; $c' =$

$k(\frac{1}{2} + c_1)$; and $d' = s(c_1 - \frac{1}{2})$. Hence,

$$\lambda_1, \lambda_2 = \tfrac{1}{2}\left[-R(1-k) + s(c_1 - \tfrac{1}{2}) \pm \sqrt{D_2}\right] \qquad (11.59)$$

in which $D_2 = [-R(1-k) + s(c_1 - \frac{1}{2})]^2 + 4[-k^2(c_1 + \frac{1}{2})^2 + 2k(1-k)(c_1 - \frac{1}{2})]$. The singularity is a *saddle* if $2k(1-k)(c_1 - \frac{1}{2}) > k^2(c_1 + \frac{1}{2})^2$, which reduces to $k < \frac{1}{3}$ (Fig. 11.9b). Note that for $k = \frac{1}{3}$, this singularity shifts to the previous point, i.e., to $(1, -\frac{1}{2}R)$. For $k > \frac{1}{3}$, the singular point is a *node* if $D_2 > 0$, and a *focus* if $D_2 < 0$. The node or focus is stable if $R(1-k) > s(c_1 - \frac{1}{2})$, and *unstable* if $R(1-k) < s(c_1 - \frac{1}{2})$.

It is apparent from Fig. 11.9a that all trajectories starting inside the separatrix reach the stable node. For initial conditions such that the corresponding point on the phase portrait lies outside the separatrix, the tank will *drain*.

Singularity $[(-c_1 - \frac{1}{2}), -\frac{1}{2}R(c_2 + c_1)]$

Because Eqs. 11.22 and 11.23 are not valid for $x < 0$, the singularity is virtual. By substituting the coordinates of the singularity into Eq. 11.55, we obtain $a' = R(k-1)$; $b' = -k(\frac{1}{2} - c_1)$; $c' = k(\frac{1}{2} - c_1)$; and $d' = -s(c_1 + \frac{1}{2})$. Hence,

$$\lambda_1, \lambda_2 = \tfrac{1}{2}\left[-R(1-k) - s(\tfrac{1}{2} + c_1) \pm \sqrt{D_3}\right] \qquad (11.60)$$

in which $D_3 = [R(1-k) + s(\frac{1}{2} + c_1)]^2 - 4[k^2(\frac{1}{2} - c_1)^2 + 2k(1-k)(\frac{1}{2} + c_1)]$. Since $0 \leqslant k < 1$, $s > 0$, and $R > 0$, both roots are real and negative if $D_3 > 0$, and complex conjugates with negative real part if $D_3 < 0$. In the former case, the singularity is a *stable node*; in the latter, a *stable focus*.

Constant Power Combined With Constant-Gate Opening

In the last section, it was assumed that the turbine gates can be opened to any value to maintain constant power. On an actual installation, however, the gates cannot be opened beyond their fully open position, and therefore the discharge cannot be increased indefinitely to maintain constant power as the level in the surge tank falls.

Referring to Fig. 11.6, for heads greater than the rated head–i.e., for $y > -y_0$, in which y_0 = final steady-state water level in the tank–the governor operates the gates in such a manner that turbine discharge corresponding to constant power is obtained. For heads less than the rated head, i.e., for $y < -y_0$, the governor keeps the gate open at the maximum value, and the discharge through the gate is determined by the maximum gate characteristics (Fig. 11.6). The flow in this case is less than that required for constant power. Thus, power output cannot be maintained constant for $y < -y_0$, and the oscillations for this condition should be analyzed considering the gate opening as constant.

For this combined governing case, the phase plane is divided into two regions: (1) constant power region for $y > -y_0$, and (2) constant-gate-opening region for $y < -y_0$. There are five singular points: two in the constant gate, two in the constant power region, and the singular point at $(1, -\frac{1}{2}R)$, which is common to both the constant-gate and constant-power regions. The latter is called a *compound singularity*. All the singular points have been analyzed above for constant-gate opening and constant power, and the results are summarized in Table 11.1.

For $k < \frac{1}{3}$, there is only one real singular point at $(1, -\frac{1}{2}R)$, hereafter called the *first singularity*. This is a compound singular point: for $y < -y_0$ (region of maximum gate opening), it is always stable; for $y > -y_0$ (region of constant power), it may be stable or unstable depending upon whether the Thoma criterion is satisfied or not (see Table 11.1). Thus, if the Thoma criterion is satisfied, the oscillations are stable *whether they are large or small.* In the case of the sub-Thoma area, the oscillations may be stable, unstable, or of constant

Table 11.1. Characteristics of singular points.

Coordinates of Singularity	Type	Stable or Unstable	Required Conditions	Miscellaneous
Constant gate opening ($y < -\frac{1}{2}R$):				
$(1, -\frac{1}{2}R)$	Node	Stable	$(R - bs) > 2$	Real
	Focus	Stable	$(R - bs) < 2$	Real
$(-1/k, -1/ks)$	Saddle	–	Always	Virtual
Constant power ($y > -\frac{1}{2}R$):				
$(1, -\frac{1}{2}R)$	Saddle	–	$k > \frac{1}{3}$	Real
	Node	–	$k < \frac{1}{3}$, and $D_1 > 0$	Real
		Stable	$R(k-1) + s < 0$	
		Unstable	$R(k-1) + s > 0$	
	Focus		$k < \frac{1}{3}$, and $D_1 < 0$	Real
		Stable	$R(k-1) + s < 0$	
		Unstable	$R(k-1) + s > 0$	
$[c_1 - \frac{1}{2},$	Saddle	–	$k < \frac{1}{3}$	Virtual
$-\frac{1}{2}R(c_2 - c_1)]$	Node	–	$k > \frac{1}{3}$, and $D_2 > 0$	Real
		Stable	$R(1-k) > s(c_1 - \frac{1}{2})$	
	Focus	–	$k > \frac{1}{3}$, and $D_2 < 0$	Real
		Stable	$R(1-k) > s(c_1 - \frac{1}{2})$	
		Unstable	$R(1-k) < s(c_1 - \frac{1}{2})$	
$[-c_1 - \frac{1}{2},$	Node	Stable	$D_3 > 0$	Virtual
$-\frac{1}{2}R(c_2 + c_1)]$	Focus	Stable	$D_3 < 0$	Virtual

magnitude (called the *limit cycle* in phase-plane terminology) depending upon the stabilizing action of the gate and the point from which the trajectory emanates. The trajectories emanating inside the limit cycle are unstable, and their amplitude increases until it is equal to that of the limit cycle. The oscillations

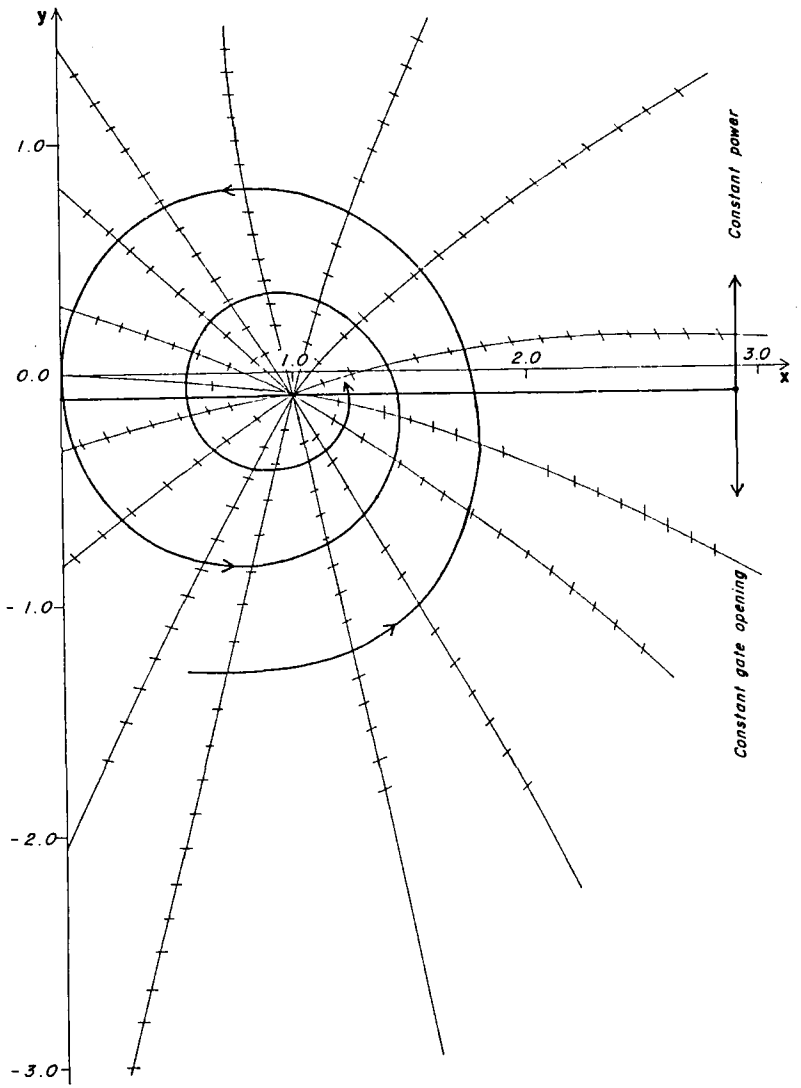

(a) k = 0.025, R = 0.2

Figure 11.10. Phase portrait for constant power combined with constant gate opening.

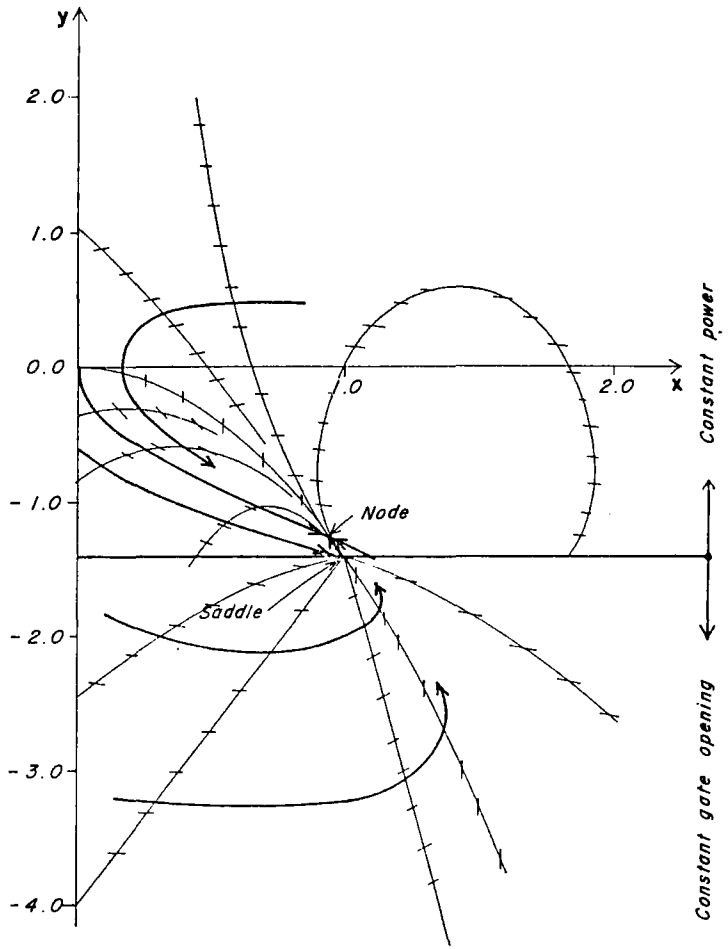

(b) k = 0.35, R = 2.8

Figure 11.10. (*Continued*)

outside the limit cycle are stable and their amplitude decreases until it is equal to that of the limit cycle.

For $k > \frac{1}{3}$, the second singularity becomes real and is either a stable or unstable *node* or *focus*, while the first singularity is a *saddle* (see Table 11.1). Since such a high value of friction loss is not economical, this case is usually of little practical importance.

Phase portraits for $k = 0.35$ and $R = 2.8$, and $k = 0.025$ and $R = 0.2$ are pre-

sented in Fig. 11.10. Oscillations in the latter case are unstable (Fig. 11.9b) as given by Paynter's stability diagram,[6] if it is assumed that the constant power is always maintained. If, however, it is considered that the governor can open the gates up to a maximum limit, and then the gates remain fully open as long as $y < -y_0$, then the oscillations are stable as shown in Fig. 11.10a.

Conclusions

From the preceding analysis of the oscillations in a simple surge tank by the phase-plane method, the following *conclusions* can be drawn:

1. Oscillations are always stable in the cases of constant-discharge and constant-gate opening. This conclusion has been drawn by earlier investigators by using other methods.

2. For the case of an ideal governor, which ensures constant power but can open the gates only to their specified maximum limit, the phase plane is divided into two regions: (1) The region in which power can be maintained constant, i.e., $y > -y_0$, and (2) the region of maximum gate opening in which power cannot be maintained constant, i.e., $y < -y_0$. The solution trajectories in the former region correspond to the stable oscillations if $A_s > A_{th}$, and to the unstable oscillations if $A_s < A_{th}$, while in the latter region they are always stable. Hence, the oscillations, large or small, are stable if $A_s > A_{th}$. For $A_s < A_{th}$, the solution trajectories in the phase plane correspond to stable oscillations for $y < -y_0$ and to unstable oscillations for $y > -y_0$. Due to these stabilizing and destabilizing effects, a solution trajectory corresponding to perpetual oscillations is obtained, which in the phase-plane terminology is called a *limit cycle*. The region enclosed by the limit cycle depends upon the stabilizing effect of the constant-gate opening and upon the destabilizing effect of the governor. The oscillations inside the limit cycle are unstable, and their amplitude increases until it is equal to that of the limit cycle. The oscillations outside the limit cycle are stable, and their amplitude decreases until it is equal to that of the limit cycle.

3. The danger of drainage of the tank for the case of constant power combined with constant-gate opening is considerably less than that indicated by the stability analysis assuming constant power only.

11.10. ORIFICE TANK

Description

In an orifice tank, there is an orifice between the tunnel and the tank (Fig. 11.2b). As this orifice restricts the inflow into the tank or outflow from it, the amplitude of the oscillations of the liquid level in the tank is less than

that of an equivalent simple tank, and the development of the accelerating or decelerating head on the tunnel is more rapid than in the case of a simple tank. If the orifice area is the same as that of the tunnel, then the orifice losses are negligible and the tank acts like a simple surge tank. However, if the orifice size is very small, then there is very little inflow or outflow, and the system behaves as if there were no surge tank.

Because of the restrictive effects of the orifice, the volume of inflow or outflow from the tank is small compared to a simple tank, and therefore the tank size can be reduced. This reduction in the tank area, however, depends upon the orifice size. Disadvantages of an orifice tank are: (1) the waterhammer waves are not completely reflected back at the tank and are partly transmitted into the tunnel (this must be taken into consideration while designing the tunnel), and (2) the governing of turbines with an orifice tank is not as good as with a simple surge tank because of the more rapid development of accelerating and decelerating heads following a change in the turbine flow.

Derivation of Dynamic Equation

Let us consider the orifice tank shown in Fig. 11.11a in which the orifice friction loss, $h_{orf} = c_{orf} Q_s|Q_s|$. The following forces are acting on the liquid in the conduit (see the freebody diagram of Fig. 11.11b):

$$F_1 = \gamma A_t(H_o - h_i - h_v) \tag{11.61}$$

$$F_2 = \gamma A_t(H_o + z + h_{orf}) \tag{11.62}$$

$$F_3 = \gamma A_t h_f \tag{11.63}$$

In the above equations, the notation of Section 11.3 is used. Considering the downstream direction as positive, the net force acting on the liquid element in the positive direction is $\Sigma F = F_1 - F_2 - F_3$. As shown in Section 11.3, the rate of change of momentum of the liquid in the tunnel is $(\gamma L/g)\,(dQ_t/dt)$. Applying Newton's second law of motion and substituting expressions for F_1, F_2, and F_3 from Eqs. 11.61 to 11.63, we obtain

$$\frac{\gamma L}{g}\frac{dQ_t}{dt} = \gamma A_t(-z - h_v - h_i - h_f - h_{orf}) \tag{11.64}$$

By defining $h = h_v + h_i + h_f = cQ_t|Q_t|$ in which c is a coefficient, substituting expression for h_{orf}, and simplifying, Eq. 11.64 becomes

$$\frac{dQ_t}{dt} = \frac{gA_t}{L}(-z - cQ_t|Q_t| - c_{orf} Q_s|Q_s|) \tag{11.65}$$

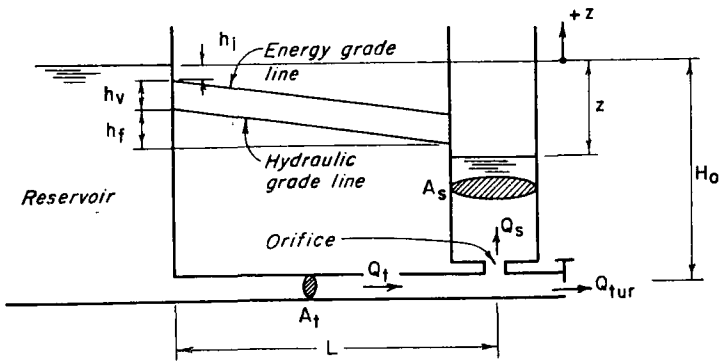

(a)

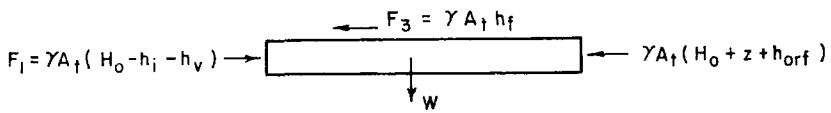

(b) Freebody diagram

Figure 11.11. Orifice tank: notation for dynamic equation.

The continuity equation for the simple tank (Eq. 11.8) is also valid for the orifice tank.

The fourth-order Runge-Kutta method may be used to solve the dynamic and continuity equations for an orifice tank.

11.11. DIFFERENTIAL SURGE TANK

Description

In a differential tank (Fig. 11.2c), the riser acts like a simple tank while the main tank acts like an orifice tank. Thus, a differential tank is a compromise between a simple tank and an orifice tank. In this tank, following a change in the penstock flow, the accelerating or decelerating head on the tunnel develops slower than in an orifice tank but faster than in a simple tank. Because of this, the area

of the outer tank can be reduced as compared to that of an equivalent simple tank, and the regulation capabilities of the turbine are not as adversely affected as in an orifice tank.

As shown in Fig. 11.2c, an orifice is provided between the tunnel and the outer tank. During initial steady state, the water surface in the riser and that in the tank are at the same level. If the turbine gates are opened to accept load on the turbogenerator set, the water is initially provided by the riser. Because of small cross-sectional area, the water level in the riser falls rapidly, thus creating an accelerating head on the tunnel in a short period. The water level in the tank falls slowly to supply additional water. If the turbine gates are closed to reject load, then the water level in the riser rises rapidly to store water, thus creating in a short period a decelerating head on the tunnel and a differential head on the orifice of the outer tank. The water rejected by the turbine is then forced through the orifice into the tank.

Depending upon the terrain, the riser and the main tank may not be as close to each other as shown in Fig. 11.2c.

Derivation of Equations

Referring to Fig. 11.12 and proceeding similarly as for the simple and orifice tanks, the dynamic equation may be written as

$$\frac{L}{gA_t}\frac{dQ_t}{dt} = -z_r - cQ_t|Q_t| \tag{11.66}$$

in which z_r = water level in the riser above the reservoir level (positive upwards) and c is a coefficient as defined in Section 11.3. The continuity equation at the junction of the tunnel and the tank is

$$Q_t = Q_s + Q_r + Q_{tur} \tag{11.67}$$

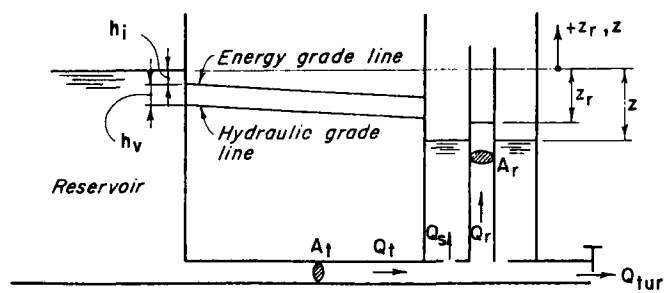

Figure 11.12. Differential tank: notation for dynamic equation.

in which Q_r = flow into or outflow from the riser, and Q_s = flow into or outflow from the outer tank. The value of Q_s depends upon the difference of water levels in the riser and in the tank, and upon the size and characteristics of the orifice at the bottom of the tank, and may be computed from the following equation:

$$Q_s = \pm C_d A_{\text{orf}} \sqrt{2g|z_r - z|} \tag{11.68}$$

in which C_d = coefficient of discharge of the orifice, and A_{orf} = cross-sectional area of the orifice. If $z_r > z$, the flow is into the tank and Q_s is positive; if $z_r < z$, then Q_s is negative. The coefficient of discharge may have different values for flow into or out of the tank. In addition, note that in the Eq. 11.68, it is assumed that there is no spill from the riser into the tank.

To compute the variation of the level in the riser and in the tank, the following equations are available:

$$A_s \frac{dz}{dt} = Q_s \tag{11.69}$$

and

$$A_r \frac{dz_r}{dt} = Q_t - Q_s - Q_{\text{tur}} \tag{11.70}$$

11.12. MULTIPLE SURGE TANKS

The hydraulic system of a turbine or pump may have more than one surge tank. Such a system is referred to as a *multiple surge tank system* or a *system of surge tanks*. Multiple surge tanks are used in the following situations:

1. To provide additional water into the tunnel upstream of the main surge tank through adits.
2. To increase the cross-sectional area of the tank in order to increase the output of the turbogenerator. This increase may be accomplished more easily by adding another tank than by increasing the area of the existing tank.
3. To provide a tank on the tailrace tunnel of an underground hydroelectric power plant or a pumped storage project to reduce waterhammer pressures and/or to improve the governing characteristics of the turbogenerators.
4. To split the main surge tank into two or more shafts for the economy of construction or to suit the rock conditions.

To conserve space and due to a large number of possible configurations of the multiple-surge-tank systems, the equations describing the tank oscillations are not derived in this section. Two typical systems usually found in practice are

presented in the problems at the end of the chapter. Equations for these systems may be easily derived in a manner similar to that used for a simple or an orifice tank.

11.13. DESIGN CONSIDERATIONS

Necessity of a Tank

The first question that arises is whether a surge tank is required. For this purpose, the following criteria[25] may be used:

1. Surge tanks should be provided where the resulting reduction in the waterhammer pressure provides a more economical penstock-surge-tank installation.
2. A surge tank should be provided if the maximum speed rise following rejection of the maximum turbine output cannot be reduced to less than 45 percent of the rated speed by other practical methods, such as increasing the generator inertia or penstock diameter or decreasing the effective wicket-gate closing time. The speed rise will be computed assuming one unit operating alone if there is more than one unit on the penstock.
3. As a rough rule of thumb, the provision of a surge tank should be investigated if

$$\frac{\Sigma L_i V_i}{H_n} > 3 \text{ to } 5 \qquad \text{(SI units)*}$$

in which $\Sigma L_i V_i$ is computed from the intake to the turbine, and H_n is the minimum net head. In general, a surge tank should be preferred to a pressure regulator although the latter may be preferred for high-head plants for economic reasons.

Location

A surge tank should be located as near to the turbine as the local topography permits.

Size

The cross-sectional area of a tank is determined to satisfy the following criteria:

1. The tank is stable.
2. The tank does not drain (i.e., the water level does not fall to the tunnel

*In the English units, $\frac{\Sigma L_i V_i}{H_n} > 10$ to 20.

crown) following maximum possible load acceptance with the reservoir at its minimum level.

3. The tank does not overflow following load rejection unless an overflow weir is provided.

The minimum cross-sectional area required for stability has been a matter of great discussion. Jaeger[26,27] proposed a safety factor n such that the area of the surge tank should be n times the Thoma area, A_{th}, with $n > 1$. As a rough guide for preliminary design, n may be taken as 1.5 for a simple tank, and 1.25 for an orifice and a differential tank. During the final design when various plant parameters have been selected, detailed investigations should be conducted to check the stability of the tank by using digital or analog computers or by arithmetical or graphical integration. In these investigations, the variation of the turbine efficiency with head and gate opening and the fact that the turbine gates cannot be opened more than their maximum opening should be taken into consideration. If these calculations show that the tank is unstable or that the dissipation of the tank oscillations is very slow, then the tank area may be increased and the above procedure repeated. If, however, the tank is stable, and the oscillations are dissipated at a faster than an acceptable rate, then the possibility of decreasing the tank area should be investigated.

Figure 11.13 may be used to determine the type of instability to be expected, i.e., oscillatory or drainage. In this figure, compiled by Forster[28] using results of various investigators, the abcissa, h, is h_{fo}/H_o, and the ordinate, y, is h_{fo}/Z; the curves represent the condition of critical stability where oscillations, once begun, continue with constant amplitude. This figure should be used for the most critical operating conditions, i.e., minimum reservoir level and maximum possible turbine output at that level. In general, if h and y for a system plot above the upper envelope of curves, the system will be free of both oscillatory instability and tank drainage for all conditions including full-load acceptance from zero load. A system plotting below the lower envelope will be subject to instability or tank drainage, or both.

To determine the maximum tank level, the turbine should be assumed to reject maximum possible load. If there is more than one unit on the penstock, then all units should be assumed to reject load simultaneously. Such unloading conditions are possible if there is a fault on the transmission line. Experience with the operation of large grid systems shows that such severe unloading conditions occur a number of times during the life of the project.

The selection of the critical loading conditions is more complex and difficult than the unloading conditions. Some authors suggest that a load acceptance of 50 to 100 percent of the rated load be used for determining the maximum downsurge. In the author's opinion, however, no set criteria can be recommended be-

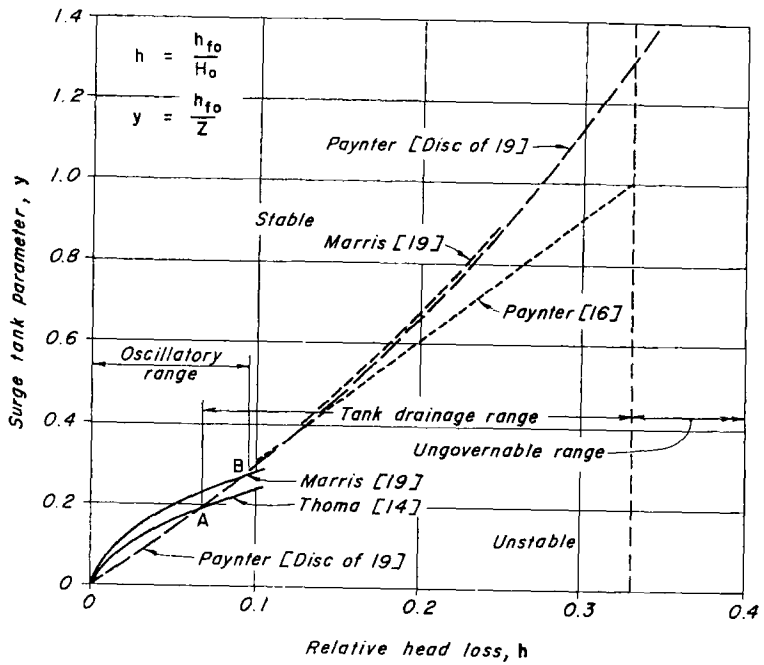

Figure 11.13. Types of instability for various values of h and y. (After Forster[28])

cause they depend upon the size of the grid system, the amount and the rate of maximum load that the plant may be required to accept because of isolation from the grid system, and the maximum load that can be added to the system at a given rate. Therefore, the maximum load and the rate of acceptance for which the tank should be designed should be decided in consultation with the engineers responsible for operating the grid system.

If the tunnel head losses are not precisely known, then the *minimum probable* value of friction factor should be used for computing the *maximum upsurge*, and the *maximum probable* value of friction factor for computing the *maximum downsurge.*

If the tank area has to be increased to keep the maximum upsurge or the minimum downsurge within acceptable limits, then the provision of upper or lower gallery may be economical instead of increasing the area of the tank.

The size of the orifice of an orifice tank or a differential tank should be selected with care. For the orifice tank, the orifice is usually designed[29] so that the initial retarding head for full-load rejection is approximately equal to the maximum upsurge. Johnson's charts[30,31] may be used to determine the approximate dimensions of the tank, riser, and the ports.

11.14. CASE STUDY

Design studies, carried out for the Chute-des-Passes surge-tank system and reported in Ref. 28 by Forster, are presented herein for illustration purposes.

Project Details

Figures 11.14 and 11.15 show the plant layout and the details of the hydraulic elements. The upstream tunnel is 9.82-km long, is concrete-lined, and has a diameter of 10.46 m. The 2.73-km-long downstream tunnel is also pressurized, is unlined, and has a diameter of 14.63 m. The maximum and minimum reservoir elevations are 378.2 m and 347.7 m, respectively. There are five units rated at 149.2 MW each at a net head of 164.6 m.

The plant supplies power to electric smelters that have a capacity of 746 MW or more and that are used for the production of aluminum. The nature of the smelters is such that power shutdown of a few hours could impose great operating difficulties in addition to large monetary losses. The plant could be isolated from the system due to major system disturbances, although the possibility of such an event occurring was considered remote.

At the upstream end of the tailrace tunnel, the 144.9-by-14.64-m tailrace manifold running parallel to the 144.9-m-long powerhouse served as the downstream surge tank.

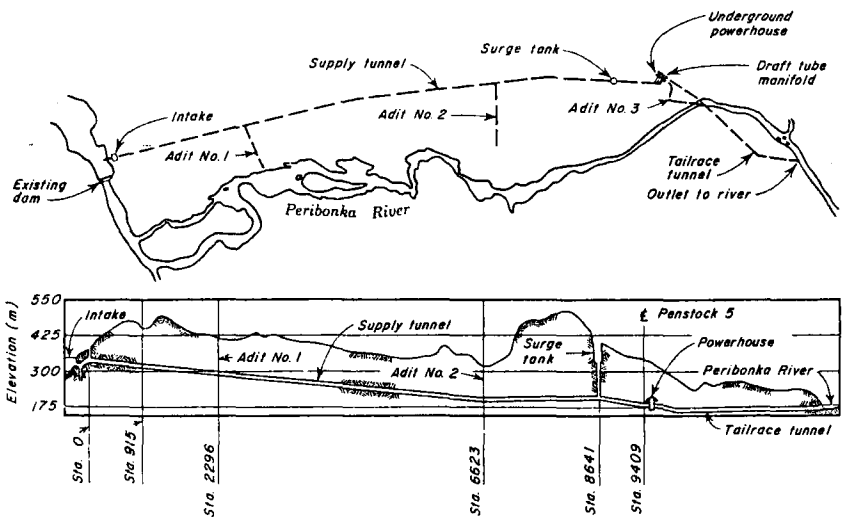

Figure 11.14. Project layout of Chute-Des-Passes development (After Forster[28])

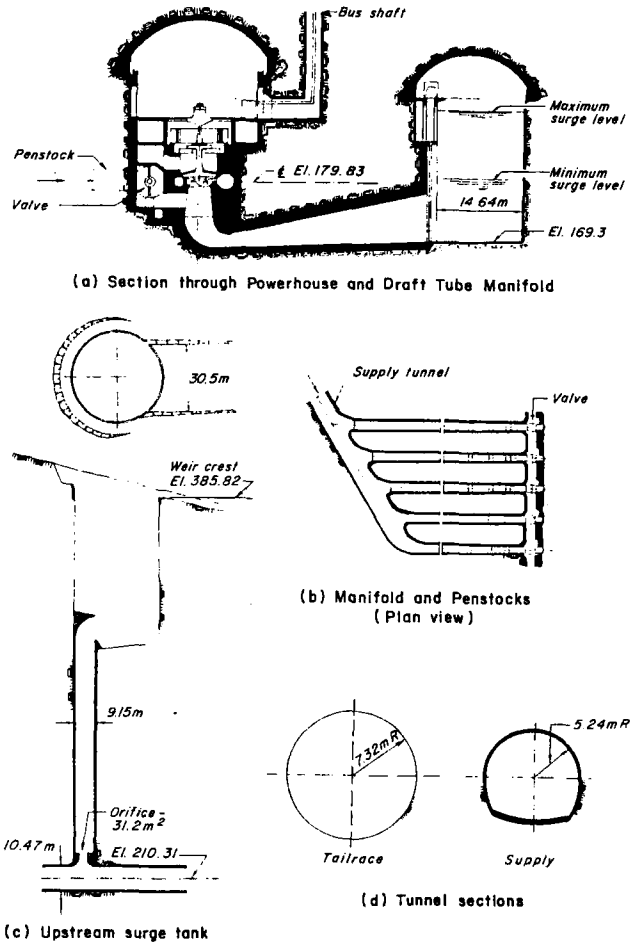

Figure 11.15. Details of hydraulic elements. (After Forster[28])

Preliminary Investigations

1. As the downstream surge tank is about seven times the Thoma area, the variation of water level of the tank was considered to be of secondary importance and could be neglected in the preliminary analysis. Similarly, the losses in the orifice of the upstream tank could be neglected, and the tank could be considered a simple tank.

For full plant output and at the minimum reservoir level, the value of h was

computed as 0.065 for the minimum expected head losses and 0.091 for the maximum expected losses. On Fig. 11.13, these values lie within the range where the oscillatory and the drainage types of instability overlap, thus indicating that both types of instability were possible.

2. Analysis using the procedure outlined by Jaeger[32] for a double surge-tank system showed that if the system was to be stable, the area of either tank could not be reduced significantly below its corresponding Thoma area even if the area of the other tank were enlarged.

3. Preliminary analysis showed that, for a stable system and for a 144.9-by-14.64-m downstream surge tank, the diameter of the upstream tank would range from 33.5 to 52 m, and detailed studies were necessary for determining the most economical tank diameter.

Selection of Method of Analysis

The following methods were available for a detailed investigation:

1. Arithmetical or graphical integration methods
2. Hydraulic model studies
3. Digital computer simulation
4. Analog computer simulation.

Because of a large number of cases to be studied, the arithmetical or graphical integration methods would have been time-consuming and were therefore rejected. In the hydraulic model studies, regulating the turbine flow for maintaining constant power is difficult. Such studies are desirable for those systems in which the velocity head and the form losses are comparable in magnitude to the tunnel friction losses. Since this was not the case for the Chute-des-Passes system, hydraulic model studies were not considered suitable. Digital computer simulations were rather rare at that time, and difficulties had been reported by Barbarossa[33] for the analysis of tank oscillations following small load changes. However, the use of analog computers for such studies had been demonstrated by Paynter.[6,16] Since a large number of cases involving variation of many variables had to be analyzed, this method was considered to be the most economic and was selected for the detailed investigations.

Program of Investigations

For the assumed values of various variables, the following information had to be obtained:

1. Maximum and minimum water levels in the upstream and in the downstream surge tank

2. Stability of the system and the rate of surge damping
3. Discharge and volume of overflow over the spillway of the upstream tank
4. Permissible load acceptance for different tank sizes over full operating range of the reservoir.

Selection of Range of Various Variables

Size of Upstream and Downstream Tanks

For the downstream surge tank comprising the tailrace manifold, the area was assumed to be fixed at 144.9 by 14.64 m.

Preliminary analysis had indicated that upstream tank diameters should range from 33.5 to 52 m. Based on preliminary computer investigations, three tank diameters, 33.5, 39.7 m, and 45.75 m, were selected for a detailed analysis.

Tunnel Resistance

From the data published* on the Niagara Falls Development,[35] Appalachia tunnel,[36] and Swedish unlined tunnels,[37] the following maximum and minimum values for Manning's n were selected:

Tunnel	*Maximum*	*Minimum*
Concrete-lined upstream tunnel	0.013	0.011
Unlined downstream tunnel	0.038	0.035

Orifice Size

The orifice size was selected such that the waterhammer pressure head in the tunnel did not exceed 0.5 of the rock cover.

The orifice loss coefficient for the flow into the tank was computed from the expansion losses for the flow from the orifice into the standpipe and from the standpipe into the tank. The loss coefficient for the outflow from the tank was determined from the contraction losses for the flow from the tank into the standpipe, from the standpipe into the orifice, and a 45° cone-diffuser expansion. Doubling these estimated loss coefficients or assuming them equal to zero had a negligible effect on the stability of the system.

Reservoir Levels

Four reservoir levels—El. 347.7, 356.8, 366 and 378.2 m—were selected for determining the permissible amounts of load acceptance.

*For more up-to-date data on head losses in tunnels, see Ref. 34.

Table 11.2. Assumed conditions.

Critical Condition	Assumption	
	Tunnel Loss Coefficient	Reservoir Level
Stability	Minimum	Minimum
Possibility of drainage of upstream tank following load acceptance	Maximum	Minimum
Maximum upstream tank level following full load rejection	Minimum	Maximum

Table 11.2 summarizes the assumptions made regarding the reservoir level and the tunnel losses for determining different critical conditions.

Derivation of Equations

The following equations were derived for the double-surge-tank system:

1. The dynamic equation for the upstream tunnel
2. The dynamic equation for the tailrace tunnel
3. Continuity equation at the upstream tank
4. Continuity equation at the downstream tank
5. Equation for turbine flow to maintain constant power at various net heads, taking into consideration the variation of the turbine efficiency and the reaction time of the wicket gates
6. Equation for the net head on the turbine.

Analog Simulation

A model-400 Reeves "REAC" electronic analog computer was used. Changes in the value of the tank area, reservoir elevation, and losses in the tunnels and in the tank orifice could be made easily and quickly. The variation of six variables–namely, z_1, Q_1, z_2, Q_2, and Q_{tur}*–and net head on the turbine with time were recorded on a Sanborn recorder. In addition, plots of z_1 versus Q_1 and z_2 versus Q_2 were recorded by an oscillographic recorder. These were similar to the phase portrait presented in Fig. 11.10a and were especially useful in showing the stability of the system.

*For notation, see Fig. 11.18a.

Results

Permissible Load Acceptance

Figure 11.16 shows curves between the permissible amount of load, ΔP_{max}, that may be accepted and the initial load, P. Figure 11.16a is for minimum reservoir level of El. 347.7 m and a range of tank diameters, and Fig. 11.16b is for 39.65-m tank diameter and a range of reservoir levels. These curves were determined by trial and error so that the maximum permissible load, ΔP_{max}, for the given initial load, P, yielded critical stable oscillations, i.e., surges of constant amplitude, or tank drainage, whichever occurred first.

From these curves, the following observations can be made:

1. At low reservoir level, an undersized tank reduces the effective plant capacity. For example, for 33.55-m tank diameter, the maximum permissible base load (i.e., load increment, ΔP_{max}, approaches zero) is 582 MW, whereas with a 45.75-m diameter tank, the plant is stable to full output.
2. The tank drainage condition becomes critical at low base load and with large load increments, whereas instability becomes critical at large base load and with small load increments.

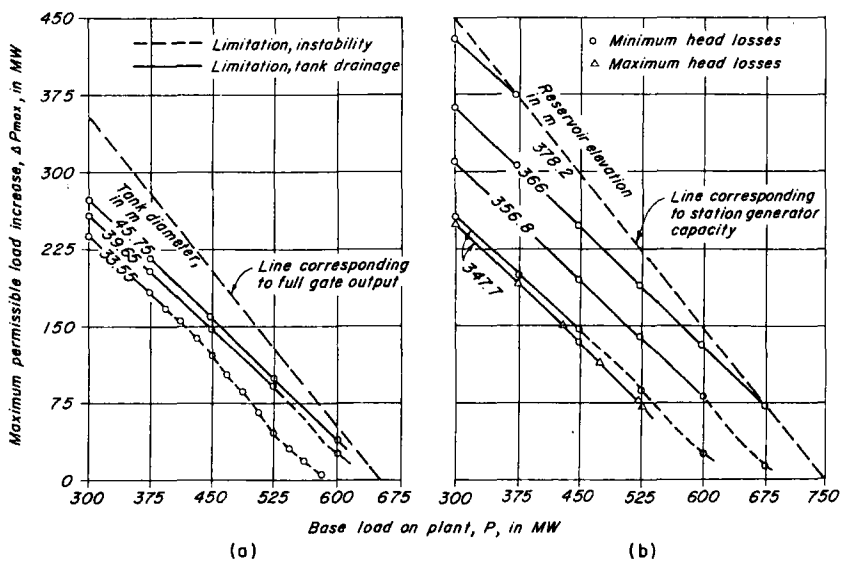

Figure 11.16. Variation of plant operating flexibility. (After Forster[28])

3. The advantages of larger tank diameter decreases as the reservoir level increases.
4. As the reservoir level increases, the limitation on the load increment gradually changes from instability to tank drainage.

Effect of Tank Area on Damping

Data listed in Table 11.3 show the effect of the tank diameter on surge damping for the critical case of minimum reservoir level and minimum tunnel losses. For each tank diameter, the number of surge cycles, the period of each cycle, and the time for the surge to be damped to one tenth of the amplitude of the first cycle are listed. It is clear from this table that, for full-load rejection, the time for surge damping is independent of tank diameter since the turbine gates are not reacting to the changes in the tank level. For normal load changes, however, increasing the tank size reduces the time required for damping and hence increases stability.

Effect of Tank Area on Overflow

Table 11.4 shows the maximum overflow rate and the volume of overflow for various tank diameters. It is clear that increasing the tank size does not significantly reduce the overflow volume.

Effect of Tank Area on Excavation

Because the range between the maximum and minimum surge levels decreases with increase in the horizontal tank area, the volume of excavation is not proportional to the tank area. Due to overflow, the maximum water level was unaffected by variation in the tank area. The minimum water level, however, varied with increase in the tank diameter. Table 11.5 lists the required volume of excavation for various tank diameters.

Table 11.3. Variation of surge damping with tank size.

	149-MW Load Increase				Full-Load Rejection		
Tank Diameter (m)	Base Load (MW)	No. Cycles	Period (s)	Time[a] (s)	No. Cycles	Period (s)	Time[a] (s)
33.55	407	7.6	630	4860	13.7	580	8400
39.65	425	4.0	770	3060	11.8	700	8400
45.75	440	2.8	930	2580	10.1	800	8400

[a] Time required for surge to be damped down to one-tenth of the amplitude of first cycle.

Table 11.4. Volume of overflow.[a]

Tank Diameter (m)	Maximum Water Level in Tank (m)	Maximum Overflow Rate (m^3/s)	Volume of Overflow ($\times 10^3$ m^3)
33.55	388.94	358	53.5
39.65	388.78	328	50.7
45.75	388.57	300	47.0

[a] Following full-load rejection (746 MW) at maximum reservoir level (El. 378.2 m) and assuming minimum tunnel losses.

Selection of Tank Size

Upstream Tank

As discussed previously, increasing the tank diameter from 33.55 to 39.65 m increases the firm capacity of the isolated plant at low reservoir levels by about 37.3 MW. This advantage decreases rapidly as the tank diameter is increased above 39.65 m and disappears entirely at higher reservoir levels. Considering such factors as permissible amount of load acceptance, degree of surge damping, and effective plant capacity, a tank diameter of 39.65 m was selected. The bottom elevation of the tank was set at El. 321.5 m. This level allowed sudden acceptance of one unit or a small amount of load acceptance following full-load

Table 11.5. Effect of tank area on required excavation volumes.

	Full Load Rejection[a]		149-MW Load Acceptance[b]	
Tank Diameter (m)	Minimum Water Level (m)	Tank Volume (m^3)	Minimum Water Level (m)	Tank Volume (m^3)
33.55	320.34	63,200	325.07	59,000
39.65	325.0	82,500	326.81	80,200
45.75	329.4	102,700	328.45	104,300

[a] At minimum reservoir level and assuming minimum tunnel losses.
[b] From maximum permissible base load at minimum reservoir level and assuming maximum tunnel losses.

rejection. A surge-tank-level indicator was installed in the control room so that the operators could avoid accepting the load during that part of the surge cycle that would cause excessive downsurge.

Overflow from the tank would have been carried by a stream course through the permanent town site for the project. Because of the potential danger associated with sudden rushes of water through an inhabited area, it was later decided[38] to excavate a basin in rock at the upper level to retain the overflow until it could discharge back into the surge tank.

Downstream Tank

As outlined above, the tailrace manifold was selected to act as the tailrace surge tank. For normal operation, the maximum and minimum water levels in this tank were computed to be at El. 192.15 m and El. 181.2 m, respectively. The floor was set at El. 170.5 m. To avoid letting the water level fall so low as to unwater the draft tubes following total-load rejection, a weir was constructed in the tailrace tunnel downstream of the manifold.

11.15 SUMMARY

In this chapter, the description and analysis of various types of surge tanks were presented. The phase-plane method was used to investigate the stability of a simple surge tank. Design criteria for determining the necessity of a surge tank and for selecting the tank size were presented, and the details of the studies carried out for the design of the Chute-des-Passes surge-tank system were outlined.

PROBLEMS

11.1. Compute the free surge and the period of oscillations of a simple surge tank following sudden total rejection if the initial steady flow is 1200 m^3/s. The length of the tunnel is 1760 m, and the cross-sectional area of the tunnel and of the tank are 200 m^2 and 600 m^2, respectively.

11.2. Prove that dynamic equation (Eq. 11.6) is valid for an inclined surge tank (Fig. 11.17) if A_s = horizontal area of the tank.

11.3. Derive the dynamic equations for simple, orifice, and differential tanks assuming that the tunnel is inclined at an angle θ to the horizontal. (*Hint:* Draw a freebody diagram of the tunnel, and apply Newton's second law of motion. Because of the cancellation of the component of the weight of water in the tunnel by the difference in the datum head on the ends of tunnel, Eqs. 11.6, 11.65, and 11.66 are valid.)

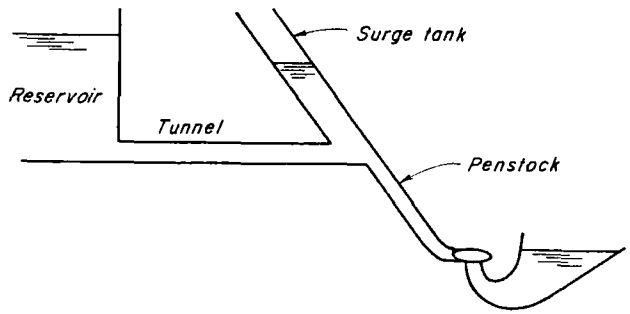

Figure 11.17. Inclined surge tank.

11.4. Prove that the oscillations of the tunnel flow and the water level in a simple tank following load rejection are 90° out of phase. Is the flow leading the water level or vice versa? Assume that the system is frictionless.

11.5. If the cross-sectional area of a tunnel varies in steps along its length, prove that the actual tunnel may be replaced by an equivalent tunnel having length, L_e, and area, A_e, such that

$$\frac{L_e}{A_e} = \sum_{i=1}^{n} \frac{L_i}{A_i}$$

in which L_i and A_i are the length and the cross-sectional area of the ith section of the tunnel (i = 1 to n).

11.6. If the inertia of the water in the tank is taken into consideration, prove that the expression for the free surge (Eq. 11.20) for a simple tank is valid; however, the expression for the period, T, becomes

$$T = 2\pi \sqrt{\frac{\lambda}{g}\frac{A_s}{A_t}}$$

in which $\lambda = L + H_a A_t/A_s$, and H_a = height of the tank.

11.7. Figure 11.18 shows two multiple-surge-tank systems usually found in practice. Derive the dynamic and continuity equations for these systems.

11.8. Prove that the critical area, A_{cr}, for perpetual oscillations in a closed surge tank (Fig. 11.19) is

$$A_{cr} = A_{sc}\left(1 + n\frac{p_o}{\gamma z_{a_o}}\right)$$

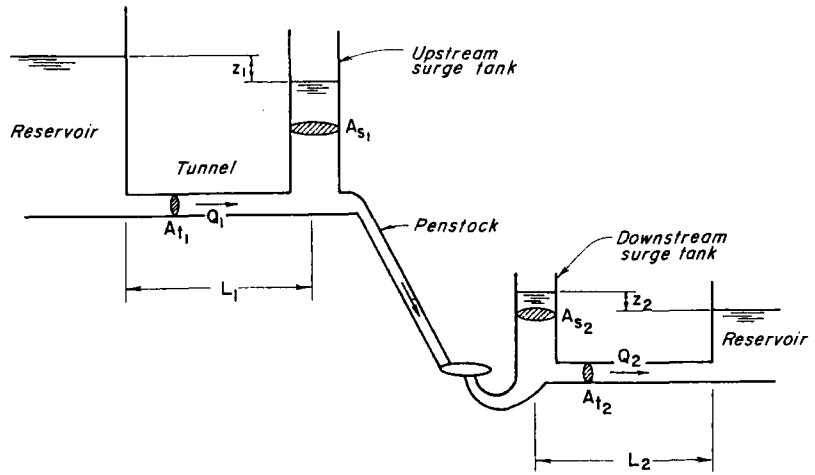

(a)

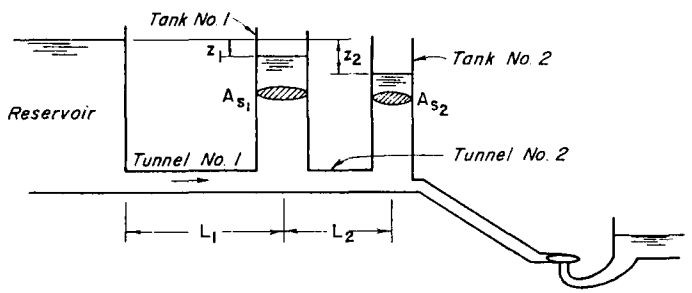

(b)

Figure 11.18. Multiple surge tanks.

in which A_{sc} is critical area for an open surge tank and is given by the expression

$$A_{sc} = \frac{L A_t}{2g\left(\frac{h_{f_o}}{V_o^2} + \frac{1}{2g}\right)\left(H_o - h_{f_o} + \frac{V_o^2}{2g}\right) + 2\frac{V_o^2}{2g}}$$

p_o = steady-state air pressure, and z_{a_o} = distance between the roof of the tank and the initial steady-state water surface in the tank. Assume that

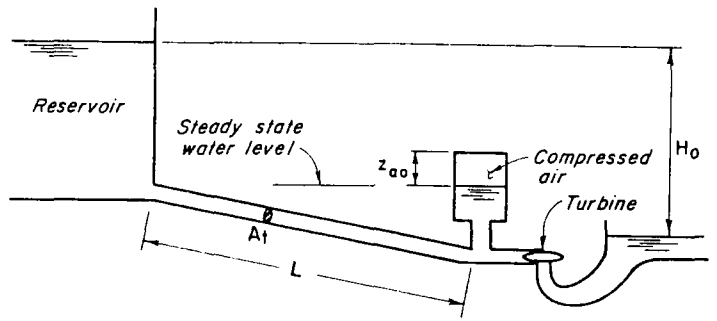

Figure 11.19. Closed surge tank.

the expansion and contraction of the air follow the law, $p\, v_{air}^n$ = constant; the governor maintains constant power; and the efficiency of turbine is constant. (*Hint:* Write the dynamic equation for the tunnel, the continuity equation, and the governor equation in terms of small deviations, Δz, ΔQ_t, and ΔQ_{tur}, from the steady-state values; neglect terms of second and higher order, and combine the resulting equations by eliminating ΔQ_t and ΔQ_{tur}. For perpetual oscillations, the coefficient of the term $d[\Delta z]/dt$ of this equation should be equal to zero.)

11.9. Write a computer program for determining the water-level oscillations in a simple tank following a load acceptance or rejection. Using this program, compute the minimum downsurge for a surge-tank system in which flow is suddenly increased from 56 to 112 m^3/s. The length of the tunnel is 1964 m, the cross-sectional area of the tunnel and the surge tank are 23.25 and 148.8 m^2, and the initial steady-state tunnel losses are equal to 1.22 m.

Answers

11.1. Free surge, $Z = 46.42$ m; period $T = 145.84$ s.
11.9. 16.05 m below the reservoir level.

REFERENCES

1. Jaeger, C., *Engineering Fluid Mechanics*, translated from German by Wolf, P. O., Blackie and Sons Ltd., London, 1961.
2. Frank, J. and Schüller, J., *Schwingungen in den Zuleitungs–und Ableitungskanalen von Wasserkraftanlagen*, Springer, Berlin, 1938.
3. Mosonyi, E., *Water Power Development*, Vol. I and II, Publishing House of Hungarian Academy of Sciences, Budapest, Hungary, 1957, 1960.
4. Rich, G. R., *Hydraulic Transients*, Dover Publications, New York, 1963.
5. Pickford, J., *Analysis of Surge*, MacMillan and Co. Ltd., London, England, 1969.

6. Paynter, H. M., "Transient Analysis of Certain Nonlinear Systems in Hydroelectric Plants," thesis presented to Massachusetts Institute of Technology, Cambridge, Mass. in partial fulfillment of the requirements of degree of doctor of philosophy, 1951.
7. Paynter, H. M., "A Palimpsest on the Electronic Analogue Art," A. Philbrick, Researches, Inc., Boston.
8. Gear, C. W., *Numerical Initial Value Problems in Ordinary Differential Equations*, Prentice-Hall, Inc., Englewood Cliffs, New Jersey, 1966.
9. McCalla, T. R., *Introduction to Numerical Methods and FORTRAN Programming*, John Wiley & Sons, New York, 1967.
10. Butcher, J. C., "On Runge-Kutta Procedures of High Order," *Jour. Austr. Math. Soc.*, Vol. 4, 1964.
11. Fehlberg, E., "Classical 5th, 6th, 7th and 8th Order Runge-Kutta Formula with Step Size Control," *N.A.S.A. Tech. Report* R-287, Oct. 1968.
12. McCracken, D. D. and Dorn, W. S., *Numerical Methods and FORTRAN Programming*, John Wiley & Sons, Inc., New York, 1964.
13. Wylie, C. R., *Advanced Engineering Mathematics*, 3rd Edition, McGraw-Hill Book Co., New York, 1967.
14. Thoma, D., *Zur Theorie des Wasserschlosses bei Selbsttaetig Geregelten Turbinenanlagen*, Oldenburg, Munchen, Germany, 1910.
15. Paynter, H. M., "The Stability of Surge Tanks," thesis presented to Massachusetts Institute of Technology, Cambridge, Mass., in partial fulfillment of the requirements of degree of master of science, 1949.
16. Paynter, H. M., "Surge and Water Hammer Problems," Electrical Analogies and Electronic Computers Symposium, *Trans. Amer. Soc. Civ. Engrs.*, vol. 118, 1953, pp. 962–1009.
17. Cunningham, W. J., *Introduction to Nonlinear Analysis*, McGraw-Hill Book Company, Inc., New York, 1958.
18. Li, Wen-Hsiung, *Differential Equations of Hydraulic Transients, Dispersion, and Groundwater Flow*, Prentice-Hall, Inc., Englewood Cliffs, New Jersey, pp. 22–36.
19. Marris, A. W., "Large Water Level Displacements in the Simple Surge Tank," *Jour. Basic Engineering*, Amer. Soc. of Mech. Engrs., vol. 81, 1959.
20. Marris, A. W., "The Phase-Plane Topology of the Simple Surge Tank Equation," *Jour. Basic Engineering*, Amer. Soc. of Mech. Engrs., 1961, pp. 700–708.
21. Sideriades, L., "Qualitative Topology Methods: Their Applications to Surge Tank Design," *La Houille Blanche*, Sept. 1962, pp. 569–80.
22. Sideriades, L., Discussion of "A Review of Surge Tank Stability Criteria," *Jour. Basic Engineering*, Amer. Soc. of Mech. Engrs., Dec. 1960, pp. 778–781.
23. Ruus, E., "Stability of Oscillation in Simple Surge Tank," *Jour., Hyd. Div., Amer. Soc. of Civ. Engrs.*, Sept. 1969, pp. 1577–1587.
24. Chaudhry, M. H., and Ruus, E., "Surge Tank Stability by Phase Plane Method," *Jour., Hyd. Div., Amer. Soc. of Civ. Engrs.*, April 1971, pp. 489–503.
25. Krueger, R. E., "Selecting Hydraulic Reaction Turbines," *Engineering Monograph No. 20*, Bureau of Reclamation, Denver, Colorado, 1966.
26. Jaeger, C., "Present Trends in Surge Tank Design," *Proc., Inst. of Mech. Engrs.*, England, vol. 168, 1954, pp. 91–103.
27. Jaeger, C., "A Review of Surge Tank Stability Criteria," *Jour. Basic Engineering*, Amer. Soc. of Mech. Engrs., Dec. 1960, pp. 765–775.
28. Forster, J. W., "Design Studies for Chute des-Passes Surge-Tank System," *Jour., Power Div., Amer. Soc. of Civ. Engrs.*, vol. 88, May 1962, pp. 121–152.

29. Ruus, E., "The Surge Tank," mimeographed lecture notes, University of British Columbia, Vancouver, Canada.
30. Johnson, R. D., "The Surge Tank in Water Power Plants," *Trans. Amer. Soc. of Mech. Engrs.*, vol. 30, 1908, pp. 443–501.
31. Johnson, R. D., "The Differential Surge Tank," *Trans. Amer. Soc. of Civ. Engrs.*, vol. 78, 1915, pp. 760–805.
32. Jaeger, C., "Double Surge Tank System," *Water Power*, July-August, 1957.
33. Barbarossa, N. L., "Hydraulic Analysis of Surge Tanks by Digital Computer," *Jour., Hyd. Div., Amer. Soc. of Civ. Engrs.*, vol. 85, April 1959, pp. 39–78.
34. "Factors Influencing Flow in Large Conduits," Report of the Task Force on Flow in Large Conduits of the Committee on Hydraulic Structures, *Jour., Hyd. Div., Amer. Soc. of Civ. Engrs.*, vol. 91, Nov. 1965, pp. 123–152.
35. Bryce, J. B. and Walker, R. A., "Head Loss Coefficients for Niagara Water Supply Tunnels," *Engineering Journal*, Engineering Inst. of Canada, July 1959.
36. Elder, R. A., "Friction Measurements in Appalachia Tunnel," *Jour., Hyd. Div., Amer. Soc. of Civ. Engrs.*, vol. 82, June 1956.
37. Rahm, L., "Flow Problems with Respect to Intake and Tunnels of Swedish Hydroelectric Power Plants," *Bulletin No. 36*, Inst. of Hydraulics, Royal Inst. of Tech., Stockholm, Sweden, 1953.
38. Matthias, F. T., Travers, F. J., and Duncan, J. W. L., "Planning and Construction of the Chute-des-Passes Hydroelectric Power Project," *Engineering Jour.*, Engineering Inst. of Canada, vol. 43, Jan. 1960.

CHAPTER 12

TRANSIENT FLOWS IN OPEN CHANNELS

12.1 INTRODUCTION

In the previous chapters, we considered transient-state flows in the closed conduits. In this chapter, we will discuss the transient flows in open channels. A flow having a free surface is considered open-channel flow even though the channel may be closed at the top, e.g., a tunnel flowing partially full.

In this chapter, a number of commonly used terms are first defined, and the causes of transient flows are discussed. The dynamic and continuity equations describing such flows are then derived, and various methods available for their solution are discussed. Details of two of these—the *explicit finite-difference method* and the *implicit finite-difference method*—are then presented. This is followed by a discussion of a number of special topics on open-channel transients. The chapter concludes with a case study.

12.2 DEFINITIONS

If the depth and/or velocity varies at a point with time, the flow is termed *unsteady flow*. Examples of unsteady flow are: floods in rivers, tides in oceans and in estuaries, surges in power canals, and storm runoff in sewers.

Depending upon the rate of variation of the flow and the depth, the unsteady flows may be classified as *rapidly varied* or *gradually varied* flow.[1] In the case of rapidly varied flows, the water-surface variation is rapid; and usually, the water surface has a discontinuity called *bore* or *shock*. Examples of such flows are surges in power canals that are caused by load changes on turbines or tidal bores in estuaries. In the gradually varied flows, the variation of the free surface is gradual—e.g., river floods, tides without bore formation.

Transient flows in the open channels are usually associated with the propagation of waves. A *wave* is defined as a temporal (i.e., with respect to time) or spatial (i.e., with respect to distance) variation of flow or water surface. The

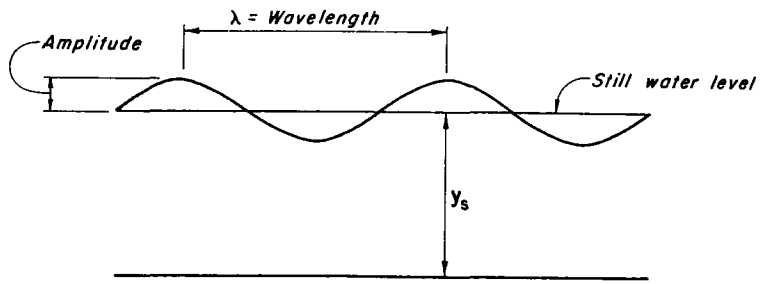

Figure 12.1. Wavelength and amplitude.

wavelength, λ, is the distance from one crest to the next, and the *amplitude* of a wave is the difference between the maximum level and the still water level (see Fig. 12.1).

The wave speed *relative* to the medium in which it is traveling is called *wave celerity*, c. Note that it is different from the flow velocity, V, with which the particles of the fluid move as a result of the wave propagation. The *absolute wave velocity*, $\mathbf{V}_w$, is equal to the vectorial sum of the wave celerity and the flow velocity, i.e.,

$$\mathbf{V}_w = \mathbf{V} + \mathbf{c} \tag{12.1}$$

in which boldface type indicates that the variables are vectors. In a one-dimensional flow, there is only one flow direction. Therefore, the wave celerity is either in the direction of the flow (downstream), or it is opposite to the flow (upstream). Considering the downstream direction as positive, Eq. 12.1 may be written as

$$V_w = V \pm c \tag{12.2}$$

In this equation, the positive sign is used for a wave traveling in the downstream direction, and the negative sign is used for a wave traveling upstream.

By using different characteristics as the criterion of classification, the waves may be classified as described in the following.

A wave having a wavelength more than twice the flow depth is termed a *shallow-water wave*, and a wave having a wavelength less than twice the flow depth is called a *deep-water wave*. Note that it is the ratio of the wavelength, λ, to the depth, y_s, and not the flow depth alone, which defines the type of wave.[2] For example, depending upon the ratio of the wavelength to the flow depth, a short wave, such as a ripple, can be a deep-water wave in otherwise shallow water; a long wave, such as a tide, in the deepest part of an ocean can be a shallow-water wave.

In a shallow-water wave, the fluid particles at a cross-section have the same flow velocity; the wave celerity depends upon the flow depth, and the vertical acceleration of the fluid particles is usually negligible compared to the horizontal acceleration. The wave celerity of a deep-water wave depends upon the wavelength; the particle motion is negligible at depths equal to the wavelength from the surface; and the horizontal and vertical accelerations are comparable in magnitude and decrease rapidly with distance from the surface.

If the wave surface is higher than the initial steady-state surface, the wave is called a *positive wave*, while if the wave surface is lower than the steady-state surface, it is called a *negative wave*.

If the fluid particles translate spatially with the wave, the wave is called *translatory* (e.g., surges, tides, floods), while, if their is no such translation, the wave is called a *stationary wave* (e.g., a sea wave).

A wave having just one rising or falling limb is called a *monoclinal wave*. A *solitary wave* has gradually rising and falling (or recession) limbs. A number of waves traveling in succession are called a *wave train*.

12.3 CAUSES OF TRANSIENTS

Transient-state conditions are produced in open channels whenever either the flow or the depth of flow or both are changed at a section. These changes may be planned or accidental; they may be natural or produced by human action. Following are some of the most common examples and causes of open-channel transients:

1. Floods in the rivers, streams, and lakes caused by snow-melt, rainstorm, or opening or closing of control gates
2. Surges in the channels caused by loading or unloading the turbines, starting or stopping the pumps, opening or closing the control gates
3. Surges in the navigation canals caused by the operation of locks
4. Waves in a river or a reservoir created by a dam-break
5. Lake and reservoir circulation caused by wind or density currents
6. Storm-runoff in sewers
7. Tides in estuaries or inlets.

Depending upon the rate at which the flow or the depth changes, a bore or shock may be formed during the transient-state conditions.

12.4 SURGE HEIGHT AND CELERITY

In the last section, *celerity* was defined as the wave speed relative to the fluid in which it is traveling. Let us now derive expressions for the celerity and height of a surge.

Referring to Fig. 12.2a, let the flow in the channel be steady at time $t = 0$ when a sluice gate located at the upstream end of the channel is suddenly opened and the flow is suddenly increased from Q_1 to Q_2. This increase in flow produces a wave of height, z, which travels in the downstream direction.

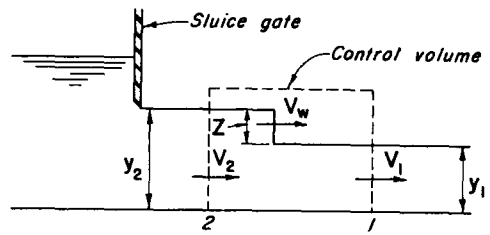

(a) Unsteady flow

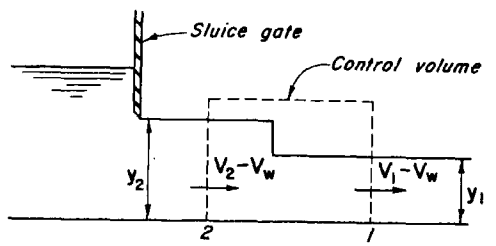

(b) Equivalent steady flow

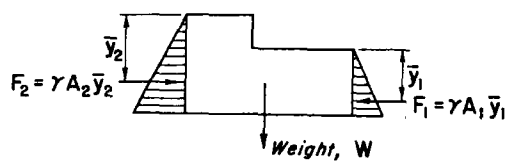

(c) Freebody diagram of control volume

Figure 12.2. Wave height and celerity.

Let us designate the flow depth and the flow velocity to the right of the wave front (i.e., undisturbed conditions) by y_1 and V_1, and the corresponding variables to the left of the wave front by y_2 and V_2 (Fig. 12.2a). If V_w is the *absolute wave velocity*, then the unsteady flow (Fig. 12.2a) can be converted into a steady flow by superimposing velocity V_w on the control volume in the upstream direction (Fig. 12.2b). The velocity in the downstream flow direction is considered positive.

Referring to Fig. 12.2b, the continuity equation may be written as

$$A_1(V_1 - V_w) = A_2(V_2 - V_w) \tag{12.3}$$

Assuming that the pressure distribution at section 1 and 2 is hydrostatic and that the channel is horizontal, and neglecting friction, the forces acting on the control volume (Fig. 12.2c) are:

$$\text{Force in the upstream direction, } F_1 = \gamma \bar{y}_1 A_1 \tag{12.4}$$

$$\text{Force in the downstream direction, } F_2 = \gamma \bar{y}_2 A_2 \tag{12.5}$$

in which $\bar{y}_1$ and $\bar{y}_2$ are the depths of the centroids of areas A_1 and A_2.

The rate of change of momentum of the water in the control volume

$$= \frac{\gamma}{g} A_1(V_1 - V_w)\,[(V_1 - V_w) - (V_2 - V_w)]$$

$$= \frac{\gamma}{g} A_1(V_1 - V_w)(V_1 - V_2) \tag{12.6}$$

The resultant force, F, acting on the water in the control volume in the downstream direction, is

$$F = F_2 - F_1 = \gamma(A_2\bar{y}_2 - A_1\bar{y}_1) \tag{12.7}$$

Applying Newton's second law of motion,

$$\frac{\gamma}{g} A_1(V_1 - V_w)(V_1 - V_2) = \gamma(A_2\bar{y}_2 - A_1\bar{y}_1) \tag{12.8}$$

Eliminating V_2 from Eqs. 12.3 and 12.8 and rearranging the resulting equation, we obtain

$$(V_1 - V_w)^2 = \frac{gA_2}{A_1(A_2 - A_1)}(A_2\bar{y}_2 - A_1\bar{y}_1) \tag{12.9}$$

Since the wave is moving in the downstream direction, its velocity must be greater than the initial flow velocity V_1. Hence, it follows from Eq. 12.9 that

$$V_w = V_1 + \sqrt{\frac{gA_2}{A_1(A_2 - A_1)}(A_2\bar{y}_2 - A_1\bar{y}_1)} \tag{12.10}$$

If there is no initial flow in the channel (i.e., $V_1 = 0$), then the absolute wave velocity V_w is equal to the radical term of Eq. 12.10. Transposing V_1 to the left-hand side,

$$V_w - V_1 = \sqrt{\frac{gA_2}{A_1(A_2 - A_1)}(A_2\bar{y}_2 - A_1\bar{y}_1)} \tag{12.11}$$

We previously defined the *celerity*, c, of a wave as its velocity relative to the medium in which it is traveling. Since $V_w - V_1$ is the velocity of the wave relative to the initial flow velocity V_1, the following general expression for c is obtained from Eq. 12.11:

$$c = \pm\sqrt{\frac{gA_2}{A_1(A_2 - A_1)}(A_2\bar{y}_2 - A_1\bar{y}_1)} \tag{12.12}$$

A positive sign is used if the wave is traveling in the downstream direction, and a negative sign is used if it is traveling upstream.

The relationship between the velocities and the depths of flow at sections 1 and 2 is obtained by eliminating V_w from Eqs. 12.3 and 12.8, i.e.,

$$A_2\bar{y}_2 - A_1\bar{y}_1 = \frac{A_1A_2}{g(A_2 - A_1)}(V_1 - V_2)^2 \tag{12.13}$$

The height of the wave, z, is equal to $y_2 - y_1$. If $y_2 > y_1$, then the wave is a *positive wave*, and if $y_2 < y_1$, then it is a *negative wave*.

There are five variables–namely, y_1, V_1, y_2, V_2, and V_w–in Eqs. 12.3 and 12.13. The value of V_2 or y_2 may be determined by trial and error from these equations if the values of other three independent variables are known.

Note that Eqs. 12.12 and 12.13 are general and may be used for channels having any cross-sectional shape. Let us see how these equations are simplified for a rectangular channel.

Rectangular Channel

For a rectangular channel having width B, $\bar{y}_1 = \frac{1}{2}y_1$; $\bar{y}_2 = \frac{1}{2}y_2$; $A_1 = By_1$; and $A_2 = By_2$. Substituting these expressions into Eq. 12.12 and simplifying the resulting equation,

$$c = \sqrt{\frac{gy_2}{2y_1}(y_1 + y_2)} \tag{12.14-a}$$

If the wave height is small as compared to the flow depth, y, then $y_1 \simeq y_2 \simeq y$. Hence, it follows from Eq. 12.14a that

$$c = \sqrt{gy} \tag{12.14-b}$$

For a rectangular channel, the continuity equation (Eq. 12.3) may be written as

$$By_1(V_1 - V_w) = By_2(V_2 - V_w) \tag{12.15}$$

from which it follows that

$$V_w = \frac{y_1V_1 - y_2V_2}{y_1 - y_2} \tag{12.16}$$

Noting that for a wave traveling in the downstream direction, $V_w = V_1 + c$, substituting expression for c from Eq. 12.14a and eliminating V_w from the resulting equation and Eq. 12.16, we obtain

$$(V_1 - V_2)^2 = \frac{g(y_1 - y_2)}{2y_1y_2}(y_1^2 - y_2^2) \tag{12.17}$$

This equation[3,4] was derived by Johnson and may be solved by trial and error to determine the surge height.

Figure 12.3 shows a positive wave. Because the depth at the leading edge of

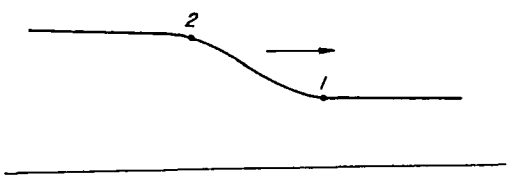

(a)

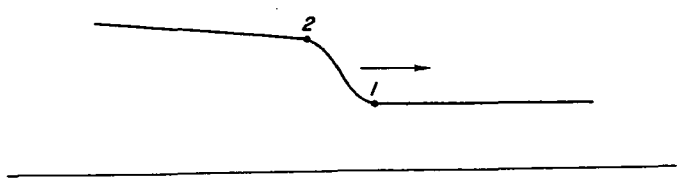

(b)

Figure 12.3. Variation of the wave front of a positive wave.

the wave front (point 1) is smaller than at the trailing edge (point 2), it follows from Eq. 12.14b that the wave celerity is higher at point 2 than that at point 1. Thus, as the wave travels, the trailing edge of the wave front tends to overtake the front edge. Therefore, the wave front gradually becomes steeper until a bore forms. Using a similar argument, it is clear that a negative wave front flattens as it travels in a channel.

We know that for the subcritical flows, the Froude number, $F < 1$, i.e.,

$$\frac{V}{\sqrt{gy}} < 1 \tag{12.18}$$

or

$$V < \sqrt{gy} \tag{12.19}$$

On the basis of Eq. 12.14b, Eq. 12.19 can be written as

$$V < c \tag{12.20}$$

Hence, it follows from Eq. 12.2 and 12.20 that V_w is negative if the wave is traveling in the upstream direction. In other words, a disturbance travels both in the upstream and in the downstream direction. For supercritical flows ($F > 1$), however, a wave can travel only in the downstream direction, since the flow velocity is more than the wave celerity and V_w is always positive.

12.5 DERIVATION OF EQUATIONS

The dynamic and continuity equations* describing the one-dimensional transient flows are derived in this section.

The following *assumptions* are made in deriving these equations:

1. The slope, θ, of the channel bottom is small so that $\sin\theta \simeq \tan\theta \simeq \theta$ and $\cos\theta \simeq 1$.
2. The pressure distribution at a section is hydrostatic. This is true if the vertical acceleration is small, i.e., if the water-surface variation is gradual.
3. The transient-state friction losses may be computed using formulas for the steady-state friction losses.
4. The velocity distribution at a channel cross section is uniform.
5. The channel is straight and prismatic.

Let us consider the control volume shown in Fig. 12.4. The x-axis lies along the bottom of the channel and is positive in the downstream direction. The depth of flow, y, is measured vertically from the channel bottom. Thus, the

*These equations are usually referred to as *Saint-Venant equations*.[5] For a general derivation of these equations, see Refs. 6 through 8.

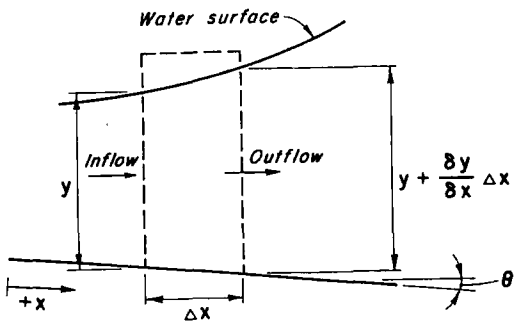

(a)

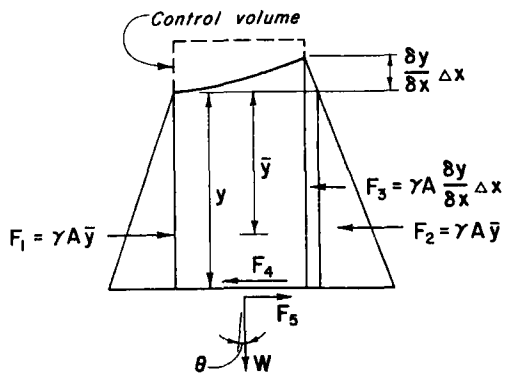

(b) Freebody diagram

Figure 12.4. Notation for dynamic and continuity equations.

x and y axes are not orthogonal. However, as the channel is assumed to have a small bottom slope, this discrepancy does not introduce significant errors.

Continuity Equation

If γ is the specific weight of the water, then referring to Fig. 12.4:

The rate of mass inflow into the control volume

$$= \frac{\gamma}{g} AV \tag{12.21}$$

The rate of mass outflow from the control volume

$$= \frac{\gamma}{g}\left(A + \frac{\partial A}{\partial x}\Delta x\right)\left(V + \frac{\partial V}{\partial x}\Delta x\right) \tag{12.22}$$

Hence, the net rate of mass inflow

$$= \frac{\gamma}{g} AV - \frac{\gamma}{g}\left(A + \frac{\partial A}{\partial x}\Delta x\right)\left(V + \frac{\partial V}{\partial x}\Delta x\right)$$

Neglecting second-order terms,

$$\text{Net rate of mass inflow} = -\frac{\gamma}{g} V \frac{\partial A}{\partial x}\Delta x - \frac{\gamma}{g} A \frac{\partial V}{\partial x}\Delta x \tag{12.23}$$

The rate of increase of the mass of the control volume

$$= \frac{\gamma}{g}\frac{\partial A}{\partial t}\Delta x \tag{12.24}$$

As the time rate of increase of the mass of the control volume must equal the net rate of mass inflow into the control volume, it follows from Eqs. 12.23 and 12.24 that

$$\frac{\gamma}{g}\frac{\partial A}{\partial t}\Delta x = -\frac{\gamma}{g} V \frac{\partial A}{\partial x}\Delta x - \frac{\gamma}{g} A \frac{\partial V}{\partial x}\Delta x \tag{12.25}$$

Dividing both sides by $(\gamma/g)\Delta x$ and rearranging, Eq. 12.25 becomes

$$\frac{\partial A}{\partial t} + V\frac{\partial A}{\partial x} + A\frac{\partial V}{\partial x} = 0 \tag{12.26}$$

Since the channel is assumed prismatic, the flow area, A, is a known function of depth, y. Therefore, the derivatives of A may be expressed in terms of y as follows:

$$\left.\begin{aligned} \frac{\partial A}{\partial x} &= \frac{dA}{dy}\frac{\partial y}{\partial x} = B(y)\frac{\partial y}{\partial x} \\ \frac{\partial A}{\partial t} &= \frac{dA}{dy}\frac{\partial y}{\partial t} = B(y)\frac{\partial y}{\partial t} \end{aligned}\right\} \tag{12.27}$$

For a channel having continuous side slopes, dA/dy is equal to the channel width B at depth y. If the values of $A(y)$ and $B(y)$ are obtained by independent measurements, the measurement error may cause $B(y)$ to be different from the values of channel width obtained by differentiating area $A(y)$ with respect to depth, y. For numerical stability,[9] it is important that $A(y)$ and $B(y)$ should be compatible—i.e., if either $A(y)$ or $B(y)$ is obtained by measurement, then the other should be determined by calculus.

Substituting Eq. 12.27 into Eq. 12.26, we obtain

$$\frac{\partial y}{\partial t} + \frac{A}{B}\frac{\partial V}{\partial x} + V\frac{\partial y}{\partial x} = 0 \tag{12.28}$$

Since discharge $Q = VA$, we can write

$$\frac{\partial Q}{\partial x} = V\frac{\partial A}{\partial x} + A\frac{\partial V}{\partial x} \tag{12.29}$$

On the basis of Eq. 12.27, Eq. 12.29 becomes

$$\frac{\partial Q}{\partial x} = BV\frac{\partial y}{\partial x} + A\frac{\partial V}{\partial x} \tag{12.30}$$

Hence, it follows from Eqs. 12.28 and 12.30 that

$$\frac{\partial Q}{\partial x} + B\frac{\partial y}{\partial t} = 0 \tag{12.31}$$

Dynamic Equation

The following forces are acting on the water in the control volume shown in Fig. 12.4b:

$$F_1 = F_2 = \gamma A\bar{y} \tag{12.32}$$

$$F_3 = \gamma A\frac{\partial y}{\partial x}\Delta x \tag{12.33}$$

$$F_4 = \gamma A S_f \Delta x \tag{12.34}$$

Note that the pressure force acting on the downstream face is divided into two components, F_2 and F_3, and the terms of higher order are not included in the expression for F_3. In Fig. 12.4b, F_1, F_2, and F_3 are forces due to pressure; F_4 = force due to friction; F_5 = x-component of the weight of the water in the control volume; θ = angle between the channel bottom and horizontal axis (positive downward); and S_f = slope of the energy grade line.

The value of S_f may be computed using any standard formula for the steady-state losses. such as Manning's or Chezy's formula. Since θ is assumed small, $\sin\theta \simeq \theta = S_o$ in which S_o = bottom slope. Hence,

$$F_5 = \gamma A \Delta x S_o \tag{12.35}$$

Referring to Fig. 12.4b, the resultant force acting on the water in the control volume in the positive x-direction is $F = \Sigma F = F_1 - F_2 - F_3 - F_4 + F_5$. Substituting expressions for F_1 to F_5 from Eqs. 12.32 to 12.35, we obtain

$$F = -\gamma A\frac{\partial y}{\partial x}\Delta x + \gamma A S_o \Delta x - \gamma A S_f \Delta x \tag{12.36}$$

$$\text{Momentum entering the control volume} = \frac{\gamma}{g}AV^2 \tag{12.37}$$

$$\text{Momentum leaving the control volume} = \frac{\gamma}{g}\left[AV^2 + \frac{\partial}{\partial x}(AV^2)\Delta x\right] \tag{12.38}$$

Therefore, net influx of momentun into the control volume

$$= -\frac{\gamma}{g}\frac{\partial}{\partial x}(AV^2)\Delta x \tag{12.39}$$

The time rate of increase of momentum

$$= \frac{\partial}{\partial t}\left(\frac{\gamma}{g}AV\Delta x\right) \tag{12.40}$$

According to the law of conservation of momentum, the time rate of increase of momentum is equal to the net rate of momentum influx plus the sum of the forces acting on the water in the control volume. Hence, it follows from Eqs. 12.36, 12.39, and 12.40 that

$$\frac{\partial}{\partial t}\left(\frac{\gamma}{g}AV\Delta x\right) = -\frac{\gamma}{g}\frac{\partial}{\partial x}(AV^2)\Delta x - \gamma A\frac{\partial y}{\partial x}\Delta x + \gamma A S_o \Delta x - \gamma A S_f \Delta x \tag{12.41}$$

Dividing throughout by $(\gamma/g)\Delta x$ and simplifying, Eq. 12.41 becomes

$$\frac{\partial}{\partial t}(AV) + \frac{\partial}{\partial x}(AV^2) + gA\frac{\partial y}{\partial x} = gA(S_o - S_f) \tag{12.42}$$

Expansion of two terms on the left-hand side, division by A, and rearrangement of the terms yields

$$g\frac{\partial y}{\partial x} + V\frac{\partial V}{\partial x} + \frac{\partial V}{\partial t} + \frac{V}{A}\left(\frac{\partial A}{\partial t} + V\frac{\partial A}{\partial x} + A\frac{\partial V}{\partial x}\right) = g(S_o - S_f) \tag{12.43}$$

On the basis of the continuity equation, Eq. 12.26, the sum of the terms within the brackets on the left-hand side of Eq. 12.43 is equal to zero. Hence, Eq. 12.43 becomes

$$g\frac{\partial y}{\partial x} + \frac{\partial V}{\partial t} + V\frac{\partial V}{\partial x} = g(S_o - S_f) \tag{12.44}$$

By expanding the terms and making use of the fact that $Q = VA$, Eq. 12.42 may be expressed[6,10] in the following form

$$\frac{\partial Q}{\partial t} + 2V\frac{\partial Q}{\partial x} + (1 - F^2)gA\frac{\partial y}{\partial x} = gA(S_o - S_f) \qquad (12.45)$$

in which $F^2 = V^2/(gA/B)$.

Equations 12.28 and 12.44 are referred to as *St. Venant equations*.

Note that Equations 12.31 and 12.44 are derived assuming that the channel is prismatic and that there is no lateral inflow or outflow. Proceeding as before, the dynamic and continuity equations can be derived for nonprismatic channels having lateral inflow or outflow (Problem 12.8).

12.6 METHODS OF SOLUTION

The following numerical methods suitable for a computer analysis are available to solve the continuity and dynamic equations describing the unsteady flow in open channels:

1. Method of characteristics[11-22]
2. Finite-difference methods[9,12-14,20,22-33]
3. Finite-element method.[34-36]

In the method of characteristics, the equations are first converted into characteristic form, which are then solved by a finite-difference scheme. In the finite-difference methods, the partial derivatives are replaced by finite-difference quotients, and the resulting algebraic equations are then solved to determine the transient conditions. In the finite-element method, the system is divided into a number of elements, and the partial differential equations are integrated at the nodal points of the elements.

The finite-element method is in the infancy stage for application to open-channel transients and will not be discussed further herein. The method of characteristics fails due to convergence of the characteristic curves once a bore forms. Therefore, the bore has to be isolated and treated separately in the computational procedures. Using the advances made in gas dynamic and the fact that the equations of gas dynamics and St. Venant equations are analogous, a number of finite-difference schemes have been proposed in which it is not necessary to isolate the bore.

The isolation of a bore in automatic computations is very cumbersome and complex, especially if there are several geometrical changes in the system since the transmission and reflection of the bore at each change has to be considered. Therefore, it is highly desirable to have a computational procedure in which no special treatment is required if a bore forms during the transient conditions. Such a scheme is presented in Section 12.9.

12.7 METHOD OF CHARACTERISTICS

As described previously, in the method of characteristics, the St. Venant equations are converted into characteristic equations, which are then solved by a finite-difference scheme. This method is not suitable for systems having numerous geometrical changes, and it fails because of the convergence of the characteristic curves whenever a bore or a shock forms. Although this method was quite popular in the 1960s, it is being replaced by the finite-difference methods. However, in the latter methods and especially in the explicit finite-difference methods, the characteristic equations are required to develop the boundary conditions. Herein, we will not present the details of the method but will develop only those equations that will be used in the next section. Readers interested in the details of the method should see Refs. 11 through 15; and for its application to the open-channel transients, they should see Refs. 16 through 19.

Multiplying Eq. 12.28 by $\pm cB/A$, adding it to Eq. 12.44, and rearranging the terms, we obtain the following so-called characteristic equations

$$\left[\frac{\partial V}{\partial t} + (V + c)\frac{\partial V}{\partial x}\right] + \frac{g}{c}\left[\frac{\partial y}{\partial t} + (V + c)\frac{\partial y}{\partial x}\right] = g(S_o - S_f) \qquad (12.46)$$

and

$$\left[\frac{\partial V}{\partial t} + (V - c)\frac{\partial V}{\partial x}\right] - \frac{g}{c}\left[\frac{\partial y}{\partial t} + (V - c)\frac{\partial y}{\partial x}\right] = g(S_o - S_f) \qquad (12.47)$$

in which $c = \sqrt{gA/B}$. Equation 12.46 can be converted into an ordinary differential equation by defining $dx/dt = V + c$; similarly, Eq. 12.47 can be converted into an ordinary differential equation by defining $dx/dt = V - c$. Since $dx/dt = V + c$ is the equation of a positive characteristic curve in the x-t plane, Eq. 12.46 is called the *forward or positive characteristic equation*. Similarly, $dx/dt = V - c$ is the equation of a negative characteristic curve in the x-t plane, and Eq. 12.47 is called the *negative characteristic equation*. Referring to Fig. 12.5, these equations may be expressed[1] in the finite-difference form as

$$\frac{V_P - V_M}{\Delta t} + (V_M + c_M)\frac{V_M - V_L}{\Delta x} + \frac{g}{c_M}\left[\frac{y_P - y_M}{\Delta t} + (V_M + c_M)\frac{y_M - y_L}{\Delta x}\right] = g(S_o - S_{f_M}) \qquad (12.48)$$

and

$$\frac{V_P - V_M}{\Delta t} + (V_M - c_M)\frac{V_R - V_M}{\Delta x} - \frac{g}{c_M}\left[\frac{y_P - y_M}{\Delta t} + (V_M - c_M)\frac{y_R - y_M}{\Delta x}\right] = g(S_o - S_{f_M}) \qquad (12.49)$$

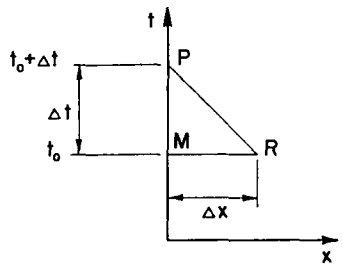

(a) Upstream boundary

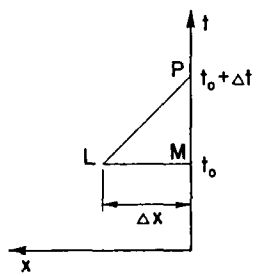

(b) Downstream boundary

Figure 12.5. Notation for positive and negative characteristic equations.

In these equations, the subscripts L, M, P, and R refer to the variables at various points in the x-t plane (Fig. 12.5).

The terms of Eqs. 12.49 and 12.48 can be rearranged to yield the following equations:

1. Negative characteristic equation (Fig. 12.5a):

$$V_P = C_n + C_a y_P \tag{12.50}$$

in which

$$C_n = V_M + \frac{\Delta t}{\Delta x}(V_M - c_M)(V_M - V_R) - \frac{g}{c_M}\left[y_M - \frac{\Delta t}{\Delta x}(V_M - c_M)(y_R - y_M)\right] + g(S_o - S_{f_M})\Delta t \tag{12.51}$$

$$C_a = \frac{g}{c_M} \text{ and } c_M = \sqrt{\frac{gA_M}{B_M}} \tag{12.52}$$

2. Positive characteristic equation (Fig. 12.5b)

$$V_P = C_p - C_a y_p \tag{12.53}$$

in which

$$C_p = V_M - \frac{\Delta t}{\Delta x}(V_M + c_M)(V_M - V_L) + \frac{g}{c_M}\left[y_M - \frac{\Delta t}{\Delta x}(V_M + c_M)(y_M - y_L)\right] + g(S_o - S_{f_M})\Delta t \tag{12.54}$$

In Eq. 12.50 through 12.54, conditions at M are those at the boundary at the beginning of the time step. Since the values of all variables are known at L, M, and R, the value of constants C_n and C_p can therefore be computed. In Eq. 12.50 or Eq. 12.53, there are two unknowns (i.e., y_P and V_P). These equations and the conditions imposed by a boundary will be solved simultaneously in Section 12.9 and 12.12 to develop boundary conditions for the finite-difference schemes.

12.8 EXPLICIT FINITE-DIFFERENCE METHOD

In the explicit finite-difference method, the partial derivatives of the St. Venant equations are replaced by finite differences such that the unknown conditions at a point at the end of a time step are expressed in terms of the known conditions at the beginning of the time step. The following explicit finite-difference schemes are available to solve the St. Venant equations:

1. diffusive scheme
2. two-step Lax-Wendroff scheme
3. Dronker's scheme.

Of these, the diffusive scheme is the simplest and easiest to program, and it gives satisfactory results.[7,20,29,30,31,33] In addition, a bore does not have to be isolated in the computations. Details of this scheme are presented here. Readers interested in the other schemes should see Refs. 7, 23, 31, and 37 for the Lax-Wendroff scheme, and Refs. 7 and 38 for Dronker's scheme.

12.9. DIFFUSIVE SCHEME

Formulation of Algebraic Equations

In this scheme, the partial derivatives of the St. Venant equations are replaced by the following finite differences (Fig. 12.6):

$$\frac{\partial y}{\partial t} = \frac{y_P - y_M}{\Delta t}; \quad \frac{\partial V}{\partial t} = \frac{V_P - V_M}{\Delta t} \tag{12.55}$$

$$\frac{\partial y}{\partial x} = \frac{y_R - y_L}{2\Delta x}; \quad \frac{\partial V}{\partial x} = \frac{V_R - V_L}{2\Delta x} \tag{12.56}$$

and S_f is replaced by S_{fm}. The conditions at point M are calculated from

$$\left.\begin{aligned} V_M &= \tfrac{1}{2}(V_L + V_R) \\ y_M &= \tfrac{1}{2}(y_L + y_R) \\ S_{fM} &= \tfrac{1}{2}(S_{fL} + S_{fR}) \end{aligned}\right\} \tag{12.57}$$

Substituting Eqs. 12.55 and 12.56 into Eqs. 12.31 and 12.44 and solving for V_P and y_p, we obtain:

$$V_P = V_M + \tfrac{1}{2}\frac{\Delta t}{\Delta x}[V_M(V_L - V_R) + g(y_L - y_R)] + g\Delta t[S_o - \tfrac{1}{2}(S_{fL} + S_{fR})] \tag{12.58}$$

$$y_P = y_M + \tfrac{1}{2}\frac{\Delta t}{\Delta x}\frac{1}{B_M}(Q_L - Q_R) \tag{12.59}$$

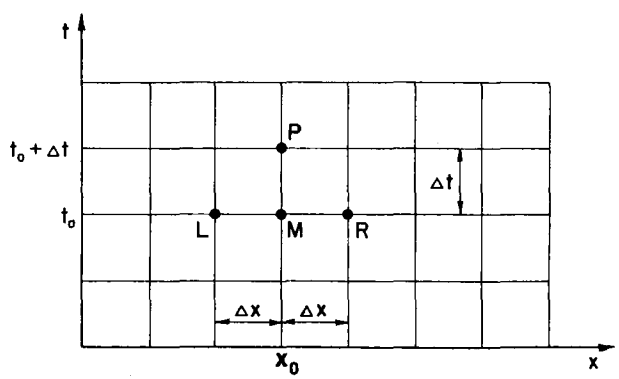

Figure 12.6. Notation for diffusive scheme.

Note that the unknown conditions at point P are expressed in terms of the known conditions at points L and R. These two equations, Eq. 12.58 and 12.59, are used to determine V_P and y_P at the interior sections.

It is clear from Fig. 12.6 that the coordinates of points P, M, L, and R are $(x_o, t_o + \Delta t)$, (x_o, t_o), $(x_o - \Delta x, t_o)$, and $(x_o + \Delta x, t_o)$. By expanding the terms of Eqs. 12.58 and 12.59 into a Taylor series—e.g., $y_P = y(x_o, t_o) + \Delta t(\partial y/\partial t) + \{[(\Delta t)^2/2!]\,(\partial^2 y/\partial t^2)\}$—and comparing with Eqs. 12.31 and 12.44, it can be proved that this difference scheme introduces additional diffusionlike terms, $\frac{1}{2}[(\Delta x)^2/\Delta t]\,(\partial^2 y/\partial x^2)$ and $\frac{1}{2}[(\Delta x)^2/\Delta t]\,(\partial^2 y/\partial x^2)$. Therefore, this scheme is called a *diffusive scheme*.

Boundary Conditions

As discussed above, Eqs. 12.58 and 12.59 are used to determine the conditions at the interior sections. At the boundaries, however, special boundary conditions are developed by solving the positive or negative characteristic equations, or both, simultaneously with the conditions imposed by the boundary. The positive characteristic equation, Eq. 12.53, is used for a downstream boundary, and the negative characteristic equation, Eq. 12.50, is used for an upstream boundary.

Two subscripts are used in this section to designate variables at various sections. The first subscript refers to the channel, and the second refers to the section number. For example, subscripts $(i, 1)$ refer to the first section on the ith channel. To designate the last section on the ith channel, which is assumed to be divided into n reaches, subscripts $(i, n + 1)$ are used. Note that subscript P is used for the unknown quantities at time $t_o + \Delta t$ (Fig. 12.6).

Four common boundary conditions are derived in this section; other boundary conditions may be developed similarly.

Constant-Head Reservoir at Upstream End

If the entrance loss at the reservoir is $k\,V_{P_{i,1}}^2/(2g)$, then, referring to Fig. 12.7a,

$$y_{\text{res}} = y_{P_{i,1}} + (1 + k)\frac{V_{P_{i,1}}^2}{2g}. \tag{12.60}$$

Substituting for $y_{P_{i,1}}$ from Eq. 12.50 into Eq. 12.60 and solving for $V_{P_{i,1}}$, we obtain

$$V_{P_{i,1}} = \frac{-1 + \sqrt{1 + 4C_r(C_n + C_a y_{\text{res}})}}{2C_r} \tag{12.61}$$

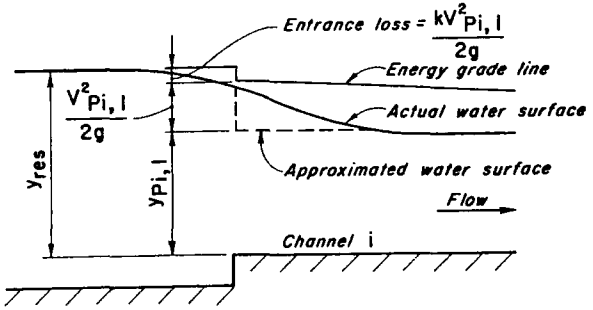

(a) Upstream reservoir

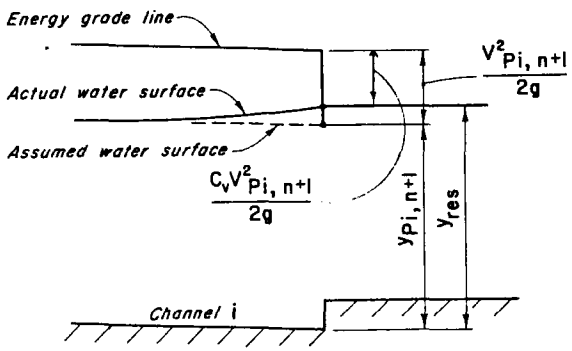

(b) Downstream reservoir

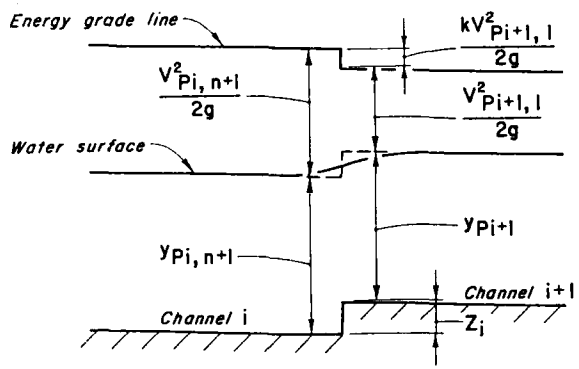

(c) Junction of two channels

Figure 12.7. Notation for boundary conditions.

in which

$$C_r = C_a(1 + k)/(2g) \tag{12.62}$$

Now $y_{P_{i,1}}$ can be determined from Eq. 12.50.

If the head losses and the velocity head at the entrance are negligible, then $y_{P_{i,1}} = y_{res}$; $V_{P_{i,1}}$ may be computed from Eq. 12.50.

Note that Eqs. 12.60 and 12.61 are valid for the positive flows only; similar equations may be written for the negative flows.

Constant-Head Reservoir at Downstream End

If the head loss is $C_vV^2_{P_{i,n+1}}/2g$, then, referring to Fig. 12.7b,

$$y_{P_{i,n+1}} = y_{res} + \frac{(1 - C_v)\,V^2_{P_{i,n+1}}}{2g} \tag{12.63}$$

in which y_{res} = water depth in the reservoir, and C_v = coefficient of head loss. Simultaneous solution of Eqs. 12.53 and 12.63 yields

$$V_{P_{i,n+1}} = \frac{1 + \sqrt{1 - 4C_r(C_p - C_{res})}}{2C_r} \tag{12.64}$$

in which $C_r = (1 - C_v)\,C_a/2g$.

If the total velocity head is lost, then $C_v = 1$, and Eq. 12.64 cannot be used since it will involve division by zero. In such a case, the following equation should be used:

$$y_{P_{i,n+1}} = y_{res} \tag{12.65}$$

$V_{P_{i,n+1}}$ is then determined from Eq. 12.53.

Discharge Change at Upstream or Downstream End

Discharge changes may result from load acceptance or rejection by hydraulic turbines, starting or stopping of pumps, or opening or closing of control gates.

Discharge is specified as a function of time, i.e., the function $Q = Q(t)$ is known. Hence,

$$Q_{P_{i,j}} = A(y_{P_{i,j}})\,V_{P_{i,j}} = Q(t_P) \tag{12.66}$$

Note that $A(y_{P_{i,j}})$ denotes area at depth $y_{P_{i,j}}$ and $Q(t_P)$ denotes discharge at time t_P. To determine $y_{P_{i,j}}$ and $V_{P_{i,j}}$, Eqs. 12.53 and 12.66 are solved by an iterative procedure for the downstream end and Eqs. 12.50 and 12.66 for the upstream end.

Junction of Two Channels

At the junction of the channels (Fig. 12.7c), the energy equation can be written as

$$y_{P_{i,n+1}} + \frac{V^2_{P_{i,n+1}}}{2g} = z_i + y_{P_{i+1,1}} + (1+k)\frac{V^2_{P_{i+1,1}}}{2g} \tag{12.67}$$

in which k is the coefficient of head losses at the junction, and z_i = rise or drop in the channel bottom = [invert elevation of the $(i+1)$th channel] - (invert elevation of the ith channel).

The following other equations are available:

$$V_{P_{i+1,1}} = C_n + C_{a_{i+1}} y_{P_{i+1,1}} \tag{12.68}$$

$$V_{P_{i,n+1}} = C_p - C_{a_i} y_{P_{i,n+1}} \tag{12.69}$$

$$A(y_{P_{i,n+1}})\, V_{P_{i,n+1}} = A(y_{P_{i+1,1}})\, V_{P_{i+1,1}} \tag{12.70}$$

There are four unknowns—namely, $y_{P_{i,n+1}}$, $y_{P_{i+1,1}}$, $V_{P_{i,n+1}}$, and $V_{P_{i+1,1}}$—in Eqs. 12.67 to 12.70. These unknowns may be determined by solving these equations by the Newton-Raphson method[39,40] as follows:

To simplify the notation, let us designate

$$\left.\begin{aligned} y_{P_{i,n+1}} &= x_1 \\ y_{P_{i+1,1}} &= x_2 \\ V_{P_{i,n+1}} &= x_3 \\ V_{P_{i+1,1}} &= x_4 \end{aligned}\right\} \tag{12.71}$$

Equations 12.67 to 12.70 may then be written as

$$F_1 = x_1 - x_2 + \frac{x_3^2}{2g} - (1+k)\frac{x_4^2}{2g} - z_i = 0 \tag{12.72}$$

$$F_2 = -C_{a_{i+1}} x_2 + x_4 - C_n = 0 \tag{12.73}$$

$$F_3 = C_{a_i} x_1 + x_3 - C_p = 0 \tag{12.74}$$

$$F_4 = A_i(x_1)\, x_3 - A_{i+1}(x_2)\, x_4 = 0 \tag{12.75}$$

in which F_1, F_2, F_3, and F_4 are functions of x_1, x_2, x_3, and x_4, and $A_i(x_1)$ and $A_{i+1}(x_2)$ denote that A_i and A_{i+1} are functions of x_1 and x_2, respectively.

Neglecting the second- and higher-order terms, F may be expanded in the Taylor series as

$$F = F^{(o)} + \left\{ \frac{\partial F}{\partial x_1}\Delta x_1 + \frac{\partial F}{\partial x_2}\Delta x_2 + \frac{\partial F}{\partial x_3}\Delta x_3 + \frac{\partial F}{\partial x_4}\Delta x_4 \right\}^{(o)} = 0 \tag{12.76}$$

or

$$\left\{ \frac{\partial F}{\partial x_1}\Delta x_1 + \frac{\partial F}{\partial x_3}\Delta x_2 + \frac{\partial F}{\partial x_3}\Delta x_3 + \frac{\partial F}{\partial x_4}\Delta x_4 \right\}^{(o)} = -F^{(o)} \tag{12.77}$$

in which the derivatives $\partial F/\partial x_1$, $\partial F/\partial x_2$, $\partial F/\partial x_3$, $\partial F/\partial x_4$, and the function $F^{(o)}$ are evaluated for the estimated values of x_1 to x_4.

On the basis of Eq. 12.77, Eqs. 12.72 through 12.75 may be written as

$$\Delta x_1 - \Delta x_2 + \frac{x_3^{(o)}}{g}\Delta x_3 - \frac{(1+k)x_4^{(o)}}{g}\Delta x_4 = -F_1^{(o)} \tag{12.78}$$

$$-C_{a_{i+1}}\Delta x_2 + \Delta x_4 = -F_2^{(o)} \tag{12.79}$$

$$C_{a_i}\Delta x_1 + \Delta x_3 = -F_3^{(o)} \tag{12.80}$$

$$B_i x_3^{(o)}\Delta x_1 - B_{i+1}x_4^{(o)}\Delta x_2 + A_i\Delta x_3 - A_{i+1}\Delta x_4 = -F_4^{(o)} \tag{12.81}$$

In Eq. 12.81, areas A_i and A_{i+1} are computed for $x_1^{(o)}$ and $x_2^{(o)}$, and it is assumed that

$$\frac{\partial A_i}{\partial x_1} \simeq B_i \quad \text{and} \quad \frac{\partial A_{i+1}}{\partial x_2} \simeq B_{i+1}$$

The coefficients of Eq. 12.81 are much larger than the coefficients of Eq. 12.78 through 12.80. To reduce their magnitude, both the left- and the right-hand sides of Eq. 12.81 may be divided by B_i. Thus, Eq. 12.81 becomes

$$x_3^{(o)}\Delta x_1 - \frac{B_{i+1}}{B_i}x_4^{(o)}\Delta x_2 + \frac{A_i}{B_i}\Delta x_3 - \frac{A_{i+1}}{B_i}\Delta x_4 = -\frac{1}{B_i}F_4^{(o)} \tag{12.82}$$

Equations 12.78 to 12.80 and 12.82 are a set of four linear equations in four unknowns—namely, Δx_1 to Δx_4. These equations may be solved by any standard numerical technique, such as the Gauss elimination scheme.[39] Then,

$$\left.\begin{aligned} x_1^{(1)} &= x_1^{(o)} + \Delta x_1 \\ x_2^{(1)} &= x_2^{(o)} + \Delta x_2 \\ x_3^{(1)} &= x_3^{(o)} + \Delta x_3 \\ x_4^{(1)} &= x_4^{(o)} + \Delta x_4 \end{aligned}\right\} \tag{12.83}$$

in which $x_1^{(1)}$ to $x_4^{(1)}$ are better approximations of the solution of the non-linear equations, Eqs. 12.67 through 12.70, than the initial estimated values of $x_1^{(o)}$ to $x_4^{(o)}$. If $|\Delta x_1|$, $|\Delta x_2|$, $|\Delta x_3|$, and $|\Delta x_4|$ are smaller than a specified tolerance, then $x_1^{(1)}$ to $x_4^{(1)}$ are solutions of Eqs. 12.67 through 12.70; otherwise,

assume

$$\left.\begin{aligned} x_1^{(o)} &= x_1^{(1)} \\ x_2^{(o)} &= x_2^{(1)} \\ x_3^{(o)} &= x_3^{(1)} \\ x_4^{(o)} &= x_4^{(1)} \end{aligned}\right\} \tag{12.84}$$

and repeat the foregoing procedure until a solution is obtained. To avoid an unlimited number of iterations in the case of divergence, introduce a counter in the iterative loop so that the computations are stopped if the number of iterations exceed a specified value, e.g., 30. To start the iterations, the first estimated values of $x_1^{(o)}$ to $x_4^{(o)}$ may be taken equal to the known values at the beginning of the time step.

Stability Conditions

The finite-difference scheme presented above is said to be stable[30] if small numerical errors due to truncation and round-off introduced at time t_o are not amplified during successive applications of the difference equations, and the error at subsequent time t are not grown so large as to obscure the valid part of the solution.

Using the technique presented by Courant et al.,[41] it has been shown[7,20,30] that the diffusive scheme is stable if

$$\Delta t \leqslant \frac{\Delta x}{|V| \pm c} \tag{12.85}$$

This is called the *Courant-Friedrichs-Lewy* condition or simply the *Courant condition.*

Computational Procedure

To determine the transient conditions, the channel is divided into n equal reaches such that, if the first section is called 1, then the last section will be $n + 1$ (see Fig. 12.8). Initial steady-state conditions (i.e., V, y, and Q) are computed at these sections. The time step, Δt, is selected so that Eq. 12.85 is satisfied. Equations 12.58 and 12.59 are used to determine y_P and V_P at section numbers 2 to n, and the special boundary conditions are used to compute V_P and y_P at the upstream and at the downstream ends, i.e., at section 1 and $n + 1$. Thus, y_P and V_P, at time $t = 0 + \Delta t$, are known at all the sections, and the value of Q_P is computed by multiplying V_P by the flow area corresponding to y_P.

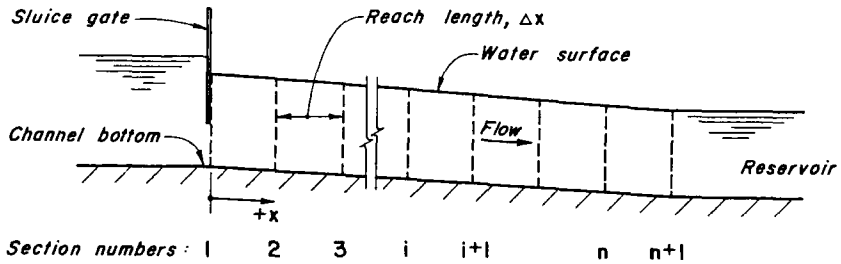

Figure 12.8. Division of channel into n reaches.

Now, assuming these computed values of V_P, y_P, and Q_P as V, y, and Q, the values of y_P and V_P at time $2\Delta t$ are computed. This procedure is continued until the transient conditions for the required time are computed.

If there are two or more channels in the system, then the time step Δt is selected for the shortest channel, and each remaining channel is divided into equal-length reaches such that Eq. 12.85 is satisfied.

It is necessary that the Courant stability condition (Eq. 12.85) is satisfied at each time step. If it is not satisfied, then the time step is reduced (e.g., 0.75 of the previous value), and the conditions at the end of the time step are recomputed *before incrementing the time.* To avoid making Δt too small in this process, its current value is compared at each time step to the value required for stability, and, if permissible, Δt is increased (e.g., by 15 percent) for the next time step.

12.10 INITIAL CONDITIONS

To compute the transient-state conditions, it is necessary that the initial steady-state flow depth and velocity are known at all the sections of the system. If these conditions are not compatible with the St. Venant equations, then small waves will be generated at each section as the transient conditions are computed. These hypothetical disturbances may mask the actual solution of the system. To avoid this, either of the following procedures may be used:

1. Any initial conditions, such as zero velocity and a constant depth, throughout the system are assumed, and the boundary conditions are set equal to the initial steady-state conditions. Using the St. Venant equations, the system conditions are computed for a sufficient length of time until the variation of flow conditions is negligible and the conditions have converged to the steady values corresponding to the initial boundary conditions. The boundary conditions are then set equal to the values for which transient conditions are to be computed.

2. The initial conditions are determined by solving the ordinary differential equation describing the gradually varied flow in open channels.

The former procedure requires a large amount of computer time. In addition, in some finite-difference schemes, the solution may converge to incorrect initial conditions. Therefore, in the author's opinion, the second procedure should be used for determining the initial conditions. Details of this procedure follow.

The steady-state gradually varied flow in open channels is described by the following equation:[1]

$$\frac{dy}{dx} = \frac{S_o - S_f}{1 - \dfrac{Q^2 B}{gA^3}} \tag{12.86}$$

Equation 12.86 is a first-order differential equation. The flow depth along the channel may be computed by integrating this equation. For this purpose, the fourth-order Runge-Kutta method may be used as follows:

Let the depth of flow, y_i at $x = x_i$, be known (Fig. 12.9a); then the depth of flow at $x = x_{i+1}$ is

$$y_{i+1} = y_i + \tfrac{1}{6}(a_1 + 2a_2 + 2a_3 + a_4) \tag{12.87}$$

in which

$$\left.\begin{aligned} a_1 &= \Delta x\, f(x_i, y_i) \\ a_2 &= \Delta x\, f(x_i + \tfrac{1}{2}\Delta x, y_i + \tfrac{1}{2}a_1) \\ a_3 &= \Delta x\, f(x_i + \tfrac{1}{2}\Delta x, y_i + \tfrac{1}{2}a_2) \\ a_4 &= \Delta x\, f(x_i + \Delta x, y_i + a_3) \\ f(x,y) &= \frac{dy}{dx} \end{aligned}\right\} \tag{12.88}$$

By starting from the known depth at a control section, and by repeated application of Eq. 12.87, the flow profile along the whole channel is computed in steps of length, Δx.

The above procedure is used to determine the water profile in a prismatic reach of a channel. However, at the junction of two channels, the depth in one of the channels is initially known, and the depth in the other channel may be calculated from the energy equation as follows:

Let us assume that, at the junction of channels i and $i+1$, $y_{i+1,1}$ is known and $y_{i,n+1}$ has to be determined (Fig. 12.9b). Let the head losses at the junction be given by $k\,V^2_{i+1,1}/2g$. In this expression, the first subscript represents the number of the channel, while the second subscript represents the number of the

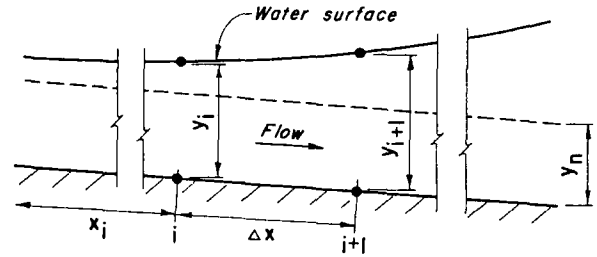

(a) Along channel

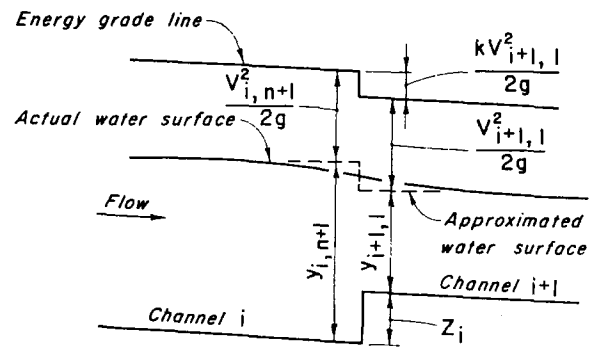

(b) Junction of two channels

Figure 12.9. Notation for computing steady-state conditions.

section on the channel. Unlike the actual water-surface profile, the computed water-surface profile will have a sudden rise or drop at the junction because the losses and the velocity head are assumed to change abruptly at the junction.

Energy equation at the junction may be written as

$$y_{i,n+1} + \frac{V^2_{i,n+1}}{2g} = z_i + y_{i+1,1} + (1+k)\frac{V^2_{i+1,1}}{2g} \tag{12.89}$$

in which z_i = drop in channel bottom at junction i. In this equation, a rise is considered positive, and a drop as negative. Equation 12.89 can be written as

$$y_{i,n+1} = z_i + y_{i+1,1} + (1 + k)\frac{V_{i+1,1}^2}{2g} - \frac{V_{i,n+1}^2}{2g} \qquad (12.90)$$

and then solved by an iterative technique to determine $y_{i,n+1}$.

12.11 VERIFICATION OF EXPLICIT FINITE-DIFFERENCE METHOD–DIFFUSIVE SCHEME

To verify the diffusive scheme of Section 12.9, a mathematical model was developed using this scheme, and its results were compared with the prototype test results. A brief description of the mathematical model, prototype tests, and comparison of the computed and measured results reported earlier[33] by the author are presented in this section.

Mathematical Model

The mathematical model was developed using the equations derived in Section 12.9. The following boundary conditions were included in the model:

1. Flow or stage changes at the upstream or at the downstream end
2. Constant-head reservoir at the upstream or at the downstream end
3. Junction of two channels having different cross sections, friction factors, and/or bottom slopes.

The model was designed to analyze transient conditions in a system having up to 20 prismatic channels in series. As outlined in Computational Procedure (Section 12.9), the value of Δt was checked at each time step and its value was increased by 15 percent or decreased by 25 percent, so that the Courant's stability condition was always satisfied and at the same time Δt did not become too small.

Prototype Tests

Prototype tests were conducted in 1971 on the Seton Canal owned and operated by British Columbia Hydro and Power Authority, Vancouver, Canada. A brief description of the project and the tests is given below:

Project Data

The Seton Canal, concrete-lined throughout its 3820-m length and designed for a flow of 113 m^3/s, conveys water from the Seton Lake to the Seton Generat-

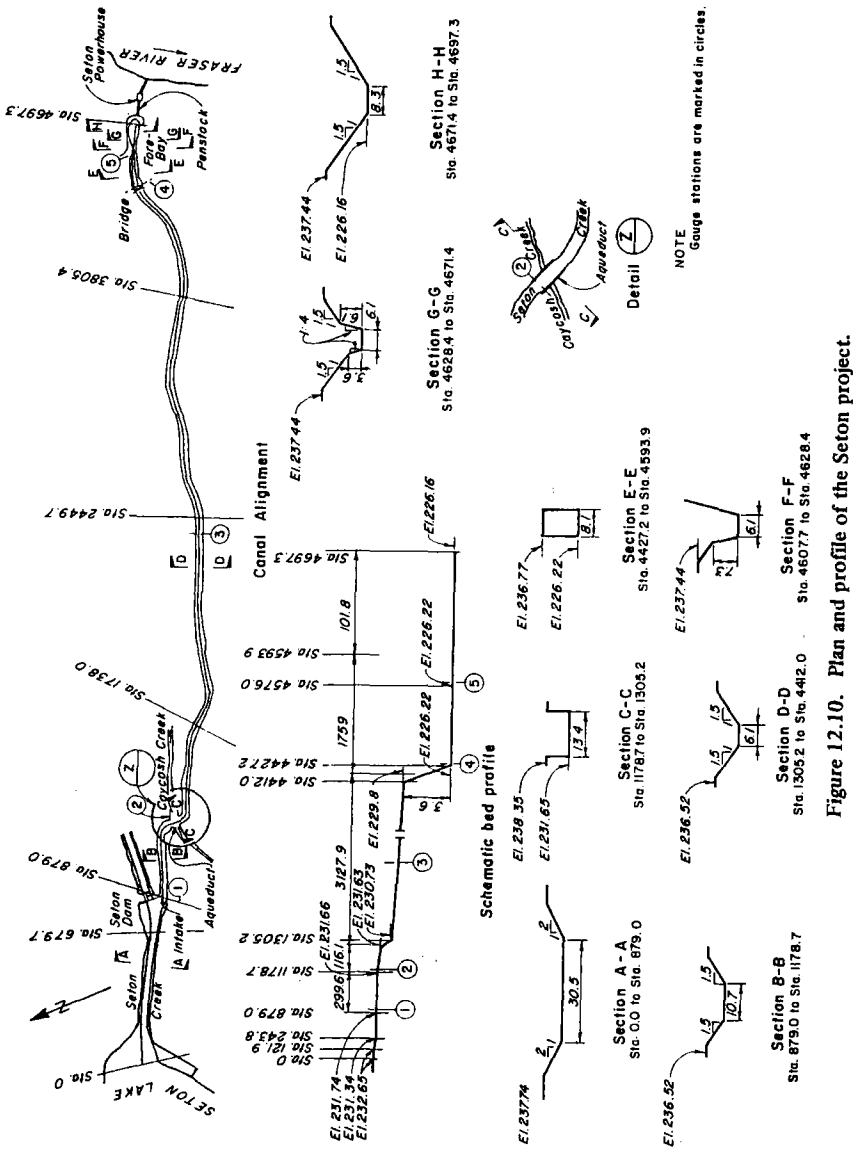

Figure 12.10. Plan and profile of the Seton project.

ing Station. The alignment and typical cross sections of the canal are shown in Fig. 12.10.

The Seton Generating Station has one 44-MW, vertical reaction turbine rated at 44.8-m net head with the centerline of the unit at El. 187.45 m. The effective wicket-gate opening and closing times are 15 and 13 s, respectively.

While starting the turbine from rest, wicket gates are opened to 15 percent (breakaway gate). At this opening, the turbine begins to rotate, and the gates are then closed to speed-no-load gate of 9 percent. The wicket gates are kept at this opening until the unit is synchronized to the system.

Tests

Transient-state conditions in the canal were produced by accepting or rejecting load on the turbine. The following tests were conducted:

1. Acceptance of 44 MW
2. Rejection of 44 MW
3. Acceptance of 44 MW followed by rejection of 44 MW after 42 min and then acceptance of 44 MW after 37 min.

After total-load rejection, turbine gates were kept open at speed-no-load gate (approximately 9 percent).

Instrumentation

To record water-level changes, a special gauge was developed. This gauge consisted of a 12.5-mm-diameter vertical aluminum tube, sealed and weighted at the lower end. The tube was suspended inside a 100-mm-diameter tube from a cantilever. The outer tube was open at both ends and was fastened to the canal bank in a vertical position. Strain gauges were installed on the cantilever to determine its deflection. Water-level fluctuations changed the buoyant force on the bottom of the inner aluminum tube, thus resulting in a change in the deflection of the cantilever, which was picked up by the strain gauges and recorded on a brush-recorder. The gauge was calibrated prior to the tests.

In addition to continuous recording, the transient-state water levels were also read at intervals of 30 s to 1 min from the gauge plates attached to the vertical or inclined side walls. Countdown for the start of the test was given over a VHF/UHF radio. In case there was any disagreement between the recorded and observed water levels, the latter were assumed to be more reliable.

To determine the water levels, five stations were established along the length of the canal. The location of these stations is shown in Fig. 12.10.

Comparison of Computed and Measured Results

The observed and the computed water levels at various stations are shown in Figs. 12.11 and 12.12. In the computations, the canal was represented by six channels, each having a constant cross section along its length. The Manning formula was used to calculate friction losses, and the load acceptance or rejection on the turbine was simulated by assuming a linear discharge variation at the downstream end of the canal. Seton Lake was represented by a constant-head reservoir at the upstream end.

The secondary fluctuations of the water surface (Favre waves) could not be computed by the program because of the inherent limitations of the governing equations (Eqs. 12.31 and 12.44). Therefore, to determine the maximum water levels, the amplitude of the secondary fluctuations were computed using data presented by Benet and Cunge[42] and were superimposed on the maximum-water levels computed by the program. The maximum level of the computed surge fluctuations is marked in Fig. 12.12a–c.

It is clear from these figures that the computed and the measured results agree closely for water levels following the initial surge and for maximum water level of the secondary fluctuations at the upper end of the canal. The computed results for the maximum water level of the fluctuations at Station 3 are, how-

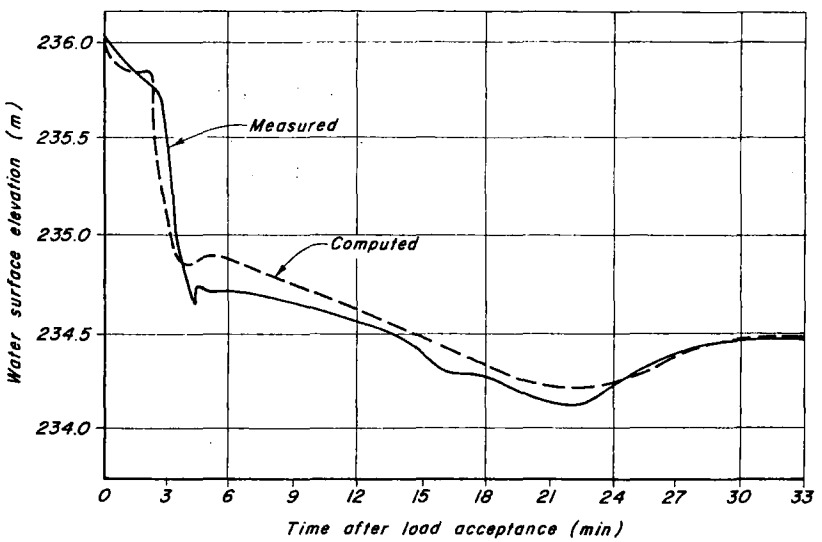

Figure 12.11. Comparison of computed and measured transient-state water levels at Station 5 following 44-MW load acceptance.

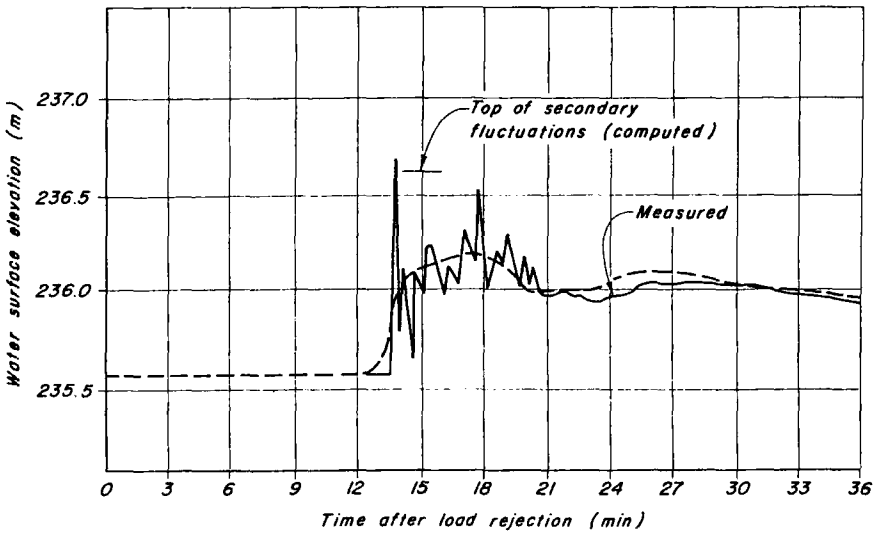

(a) At station 1

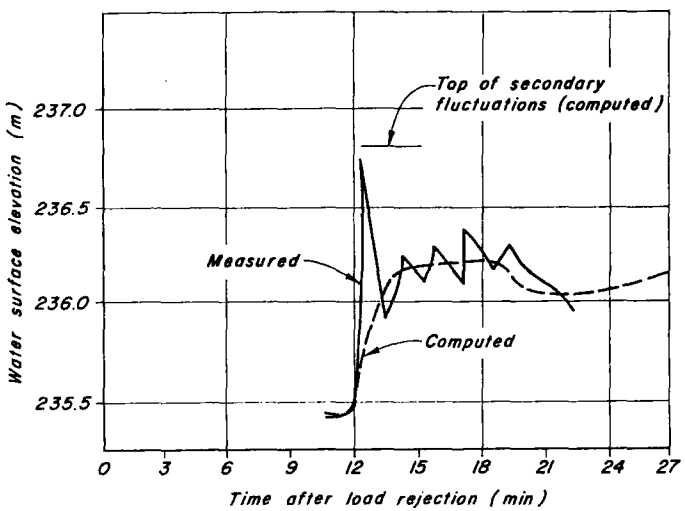

(b) At station 2

Figure 12.12. Comparison of computed and measured transient-state water levels following 44-MW load rejection.

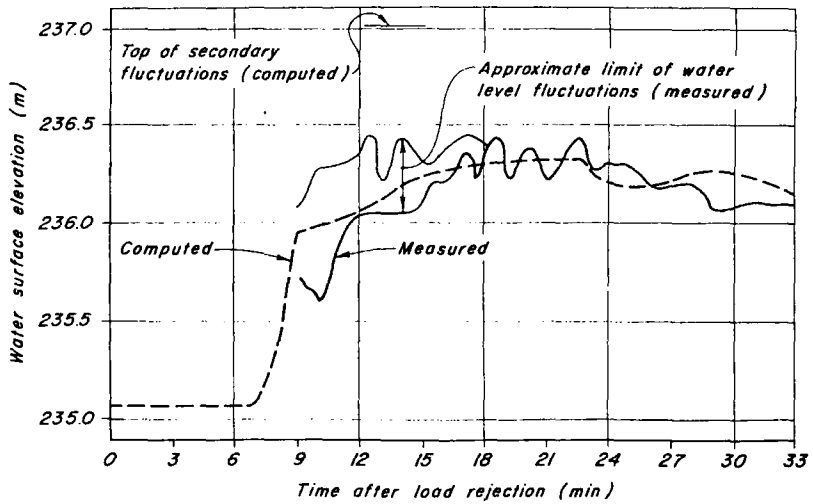

(c) At station 3

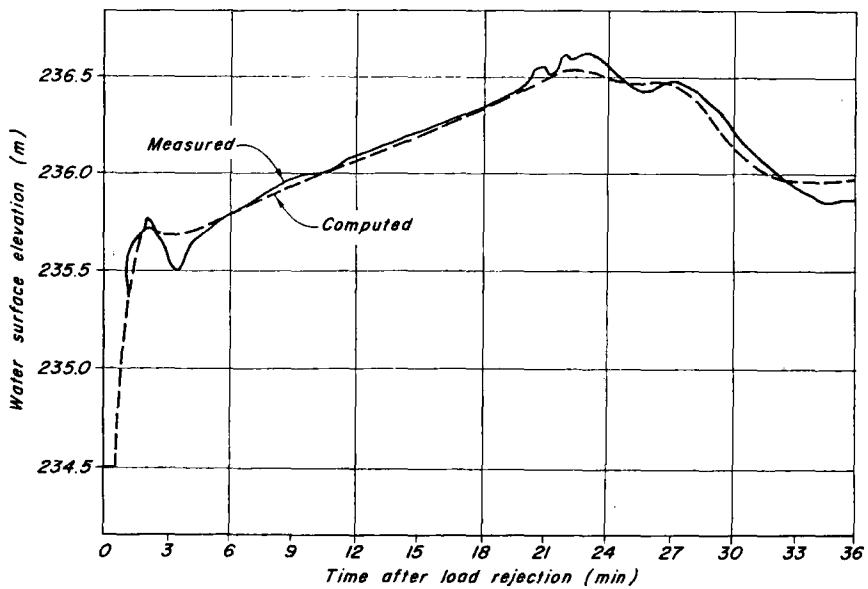

(d) At station 4

Figure 12.12. (*Continued*)

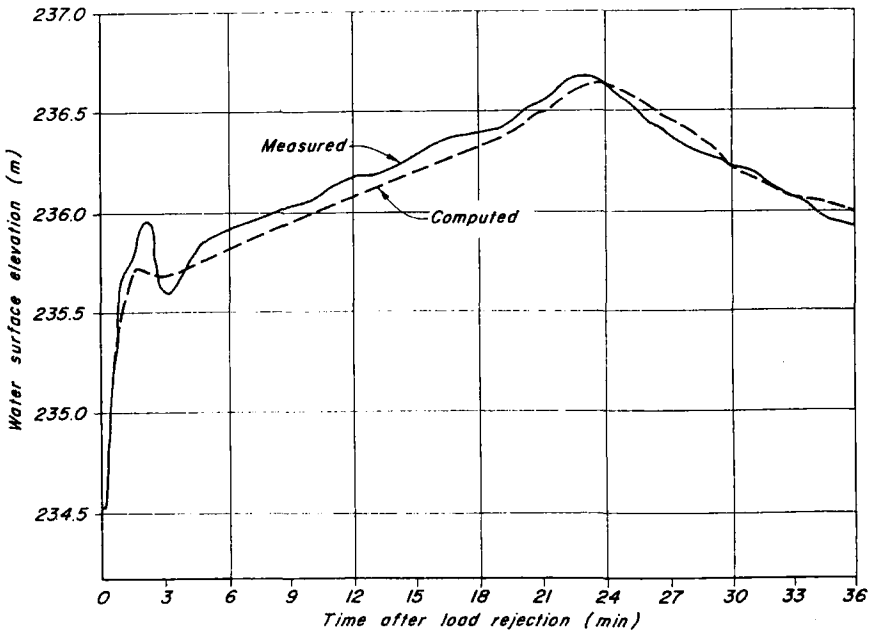

Figure 12.12. (*Continued*)

ever, too high, because the fluctuations were developed in the prototype as the initial wave propagated upstream.

12.12 IMPLICIT FINITE-DIFFERENCE METHODS

Description

In the explicit finite-difference method, we replaced the x-derivatives of the St. Venant equations by finite-difference quotients evaluated at time t_o (Fig. 12.6). The other coefficients, B and S_f, were also evaluated at time t_o. Thus, we had two linear algebraic equations relating the two unknowns, V and y, at point P to the known conditions at points L, M, and R. Because of this explicit relationship, the method was called *explicit finite-difference method*.

In the finite-difference method presented in this section, we will replace the x-derivatives in terms of finite differences evaluated at time $t_o + \Delta t$; thus, the unknowns will appear implicitly (hence, the name, *implicit finite-difference method*) in the resulting algebraic equations, which are usually nonlinear. Solution of these algebraic equations is more complex than that in the explicit method. However, the implicit method has the advantage that it is unconditionally stable. This allows the use of larger values of the computational time step, Δt, thus economizing computer time. We will compare the advantages and disadvantages of the explicit and implicit methods in the next section.

Available Implicit Schemes

Various implicit schemes have been reported in the literature. Of these, the following have been used for studying the open-channel transients: Priessmann's scheme,[7,24,26] Amein's scheme,[9,32] Vasiliev's scheme,[43,44] and Strelkoff's scheme.[30]

While writing the finite-difference quotients for the x-partial derivative, a weighting factor, α, is introduced in the Priessmann's and in the Amein's schemes. The presence of α in the difference schemes introduces artificial damping in addition to the damping due to friction and other losses. To make the scheme stable, the value of α must be greater than 0.5 and less than or equal to 1. Since the value of α is arbitrarily selected, care must be exercised so that an excessive amount of damping is not unintentionally introduced into the system. Vasiliev's scheme has two steps and thus is more complicated and requires more computer time. Compared to the preceding schemes, in the author's opinion, Strelkoff's scheme is the simplest and is easy to program. In addition, the comparison of the results computed by using this scheme with those measured on the prototype and on a hydraulic model has shown good agreement (see Section 12.15). Details of this scheme are presented herein; readers interested in the other schemes should refer to Refs. 7, 9, 24, 26, 30, 32, 43, and 44.

Strelkoff's Implicit Scheme

In Strelkoff's scheme,[30] the partial derivatives of the St. Venant equations are replaced by finite-difference quotients as follows (see Fig. 12.13a):

$$\left.\begin{aligned} \frac{\partial Q}{\partial x} &= \frac{Q_{P_{i+1}} - Q_{P_{i-1}}}{2\Delta x} \\ \frac{\partial y}{\partial t} &= \frac{y_{P_i} - y_i}{\Delta t} \\ \frac{\partial Q}{\partial t} &= \frac{Q_{P_i} - Q_i}{\Delta t} \\ \frac{\partial y}{\partial x} &= \frac{y_{P_{i+1}} - y_{P_{i-1}}}{2\Delta x} \end{aligned}\right\} \tag{12.91}$$

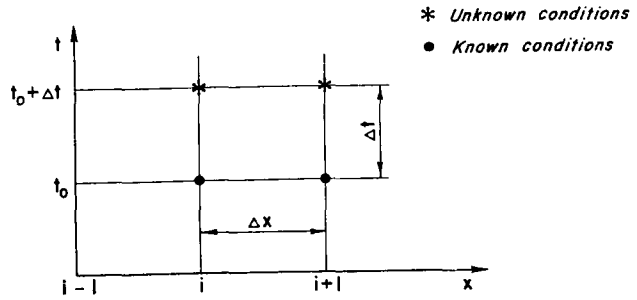

(a) Interior sections

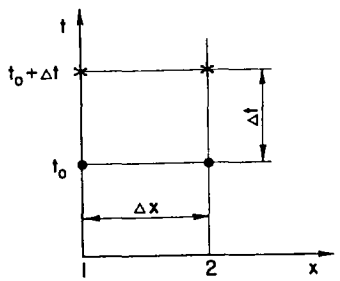

(b) Upstream boundary

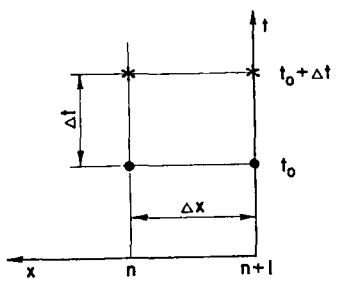

(c) Downstream boundary

Figure 12.13. Notation for implicit finite-difference scheme.

In this equation, the subscript P refers to the variables at time $t_o + \Delta t$. All coefficients of the equations are evaluated at time t_o except the friction slope, S_f, which is evaluated at time $t_o + \Delta t$. However, if we use the value of S_f at time t_o, then the implicit scheme is not unconditionally stable,[30] and the condition, $\Delta t < K_o/(Ag\sqrt{S_o})$, has to be satisfied for stability requirements. In this expression, K_o = conveyance factor at normal depth. If the Manning formula is used to compute S_{fP}, and R = hydraulic radius, then

$$S_{fP} = \frac{Q_P|Q_P|}{K_P^2} \tag{12.92}$$

in which the conveyance factor, K_P, in the SI units* may be written as

$$K_P = \frac{1}{n} AR^{2/3}\bigg|_{y=y_P} \tag{12.93}$$

The resulting algebraic equations will be nonlinear if the expression for S_{fP} given by Eq. 12.92 is used. We can linearize Eq. 12.92 as follows:

$$S_{fP_i} \simeq S_{fi} + \frac{\partial S_f}{\partial Q}\bigg|_i (Q_{P_i} - Q_i) + \frac{\partial S_f}{\partial K}\bigg|_i \frac{\partial K}{\partial y}\bigg|_i (y_{P_i} - y_i) \tag{12.94}$$

Note that $\partial S_f/\partial Q$ and $\partial S_f/\partial K$ in Eq. 12.94 are evaluated at time t_o, and the expressions for these derivatives may be obtained by differentiating Eq. 12.92, i.e.,

$$\frac{\partial S_f}{\partial Q} = \frac{2S_f}{Q} \tag{12.95}$$

$$\frac{\partial S_f}{\partial K} = -2S_f/K \tag{12.96}$$

$$\frac{\partial K}{\partial y} = \frac{dK}{dy} = \frac{K}{A}\left(\frac{5B}{3} - \frac{2}{3}R\frac{dP}{dy}\right) \tag{12.97}$$

In Eq. 12.97, dP/dy is the rate of change of the wetted perimeter, and its value depends upon the side slopes of the channel. As the derivatives are evaluated at time t_o, subscript P is dropped in Eqs. 12.95 through 12.97.

Replacing the partial derivatives of Eqs. 12.31 and 12.45 by the finite differences listed in Eq. 12.91, replacing S_f of Eq. 12.45 by the expression given in Eq. 12.94 and substituting expressions for $\partial S_f/\partial Q$ and $\partial S_f/\partial K$ from Eqs. 12.95 and 12.96, and simplifying the resulting equation, we obtain

$$a_i Q_{P_{i+1}} - a_i Q_{P_{i-1}} + b_i y_{P_i} = C_i \tag{12.98}$$

*In the English units, $K_P = (1.486/n)\, AR^{2/3}|_{y=y_P}$.

$$e_i Q_{P_{i+1}} + f_i Q_{P_i} - e_i Q_{P_{i-1}} + k_i y_{P_{i+1}} + l_i y_{P_i} - k_i y_{P_{i-1}} = D_i \quad (12.99)$$

In these equations, the variables with subscript P are unknowns, and the coefficients a_i, b_i, C_i, e_i, f_i, k_i, l_i, and D_i are evaluated in terms of the known quantities at time t_o. The expressions for these coefficients are

$$a_i = \frac{1}{2\Delta x} \quad (12.100)$$

$$b_i = \frac{B_i}{\Delta t} \quad (12.101)$$

$$C_i = \frac{B_i y_i}{\Delta t} \quad (12.102)$$

$$e_i = \frac{V_i}{\Delta x} \quad (12.103)$$

$$f_i = \frac{1}{\Delta t} + \frac{2gA_i S_{f_i}}{Q_i} \quad (12.104)$$

$$k_i = \frac{gA_i - B_i V_i^2}{2\Delta x} \quad (12.105)$$

$$l_i = -\frac{2g S_{f_i} A_i}{K_i}\left(\frac{dk}{dy}\right)_i \quad (12.106)$$

$$D_i = gA_i\left\{S_o + S_{f_i}\left[1 - \frac{2y_i}{K_i}\left(\frac{dK}{dy}\right)_i\right]\right\} + \frac{Q_i}{\Delta t} \quad (12.107)$$

For the upstream boundary, the negative characteristic equation (Eq. 12.47 written in terms of Q instead of V)* may be written as

$$a_1 Q_{P_1} + b_1 Q_{P_2} + e_1 y_{P_1} + f_1 y_{P_2} = D_1 \quad (12.108)$$

in which

$$a_1 = \frac{1}{\Delta t} + 2g\frac{A_1 S_{f_1}}{Q_1} - \frac{V_1 - c_1}{\Delta x} \quad (12.109)$$

$$b_1 = \frac{V_1 - c_1}{\Delta x} \quad (12.110)$$

*$\left[\frac{\partial Q}{\partial t} + (V - c)\frac{\partial Q}{\partial x}\right] - (V + c)B\left[\frac{\partial y}{\partial t} + (V - c)\frac{\partial y}{\partial x}\right] = gA(S_o - S_f)$

$$e_1 = \frac{-(V_1 + c_1)B_1}{\Delta t} + \frac{(V_1^2 - c_1^2)B_1}{\Delta x} - 2g\left[\frac{A_1 S_{f_1}}{K_1}\left(\frac{dK}{dy}\right)_1\right] \quad (12.111)$$

$$f_1 = \frac{-(V_1^2 - c_1^2)B_1}{\Delta x} \quad (12.112)$$

$$D_1 = gA_1\left\{S_o + S_{f_1}\left[1 - \frac{2y_1}{K_1}\left(\frac{dK}{dy}\right)_1\right]\right\} + \frac{Q_1}{\Delta t} - \frac{(V_1 + c_1)B_1 y_1}{\Delta t} \quad (12.113)$$

In the preceding equations, the variables with subscript P refer to the unknown conditions at time $t_o + \Delta t$, and the coefficients a_1, b_1, e_1, f_1, and D_1 are expressed in terms of the known conditions at time t_o. In addition, the conditions imposed by the upstream boundary may be written in a generalized form as

$$E_1 Q_{P_1} + F_1 y_{P_1} = J_1 \quad (12.114)$$

If the conditions imposed by the boundary are nonlinear, these are linearized and expressed in the above form. Usually, either E_1 is zero and F_1 is unity, or F_1 is zero and E_1 is unity.

Proceeding similarly for the downstream boundary at section $(n + 1)$, the positive characteristic equation (Eq. 12.46 written in terms of Q instead of V)* may be written as

$$a_{n+1} Q_{P_n} + b_{n+1} Q_{P_{n+1}} + e_{n+1} y_{P_n} + f_{n+1} y_{P_{n+1}} = D_{n+1} \quad (12.115)$$

in which

$$a_{n+1} = -\frac{(V_{n+1} + c_{n+1})}{\Delta x} \quad (12.116)$$

$$b_{n+1} = \frac{1}{\Delta t} + 2g\left(\frac{A_{n+1} S_{f_{n+1}}}{Q_{n+1}}\right) + \frac{V_{n+1} + c_{n+1}}{\Delta x} \quad (12.117)$$

$$e_{n+1} = \frac{(V_{n+1}^2 - c_{n+1}^2)B_{n+1}}{\Delta x} \quad (12.118)$$

$$f_{n+1} = \frac{-(V_{n+1} - c_{n+1})B_{n+1}}{\Delta t} - \frac{(V_{n+1}^2 - c_{n+1}^2)B_{n+1}}{\Delta x} - 2g\left[A_{n+1}\frac{S_{f_{n+1}}}{K_{n+1}}\left(\frac{dK}{dy}\right)_{n+1}\right] \quad (12.119)$$

*$\left[\frac{\partial Q}{\partial t} + (V + c)\frac{\partial Q}{\partial x}\right] - (V - c)B\left[\frac{\partial y}{\partial t} + (V + c)\frac{\partial y}{\partial x}\right] = gA(S_o - S_f)$

$$D_{n+1} = gA_{n+1}\left\{S_o + S_{f_{n+1}}\left[1 - \frac{2y_{n+1}}{K_{n+1}}\left(\frac{dK}{dy}\right)_{n+1}\right]\right\}$$

$$+ \frac{Q_{n+1}}{\Delta t} - \frac{(V_{n+1} - c_{n+1})B_{n+1}y_{n+1}}{\Delta t} \qquad (12.120)$$

The conditions imposed by the downstream boundary may be written as

$$E_{n+1}Q_{P_{n+1}} + F_{n+1}y_{P_{n+1}} = J_{n+1} \qquad (12.121)$$

If the channel is divided into n reaches, then there are $(n + 1)$ sections and since there are two unknowns (namely, y_P and Q_P) for each section, the total number of unknowns is $2(n + 1)$. For a unique solution, there must be $2(n + 1)$ equations. As discussed above, two equations (Eqs. 12.108 and 12.114) are provided by the upstream boundary, two equations (Eqs. 12.115 and 12.121) are provided by the downstream boundary, and there are two equations (Eqs. 12.98 and 12.99) for each interior section i, $i = 2, n$. Since there are $(n - 1)$ interior sections, we have $2(n - 1) + 2 + 2 = 2(n + 1)$ equations. Hence, a unique solution can be obtained for each time step. These equations for a system may be expressed in the matrix notation as

$$\mathbf{Ax} = \mathbf{b} \qquad (12.122)$$

in which **A** is a coefficient matrix, **x** is a column vector comprised of the unknown quantities Q_P and y_P, and **b** is a column vector comprised of the constants on the right-hand side of Eqs. 12.98, 12.99, 12.108, 12.114, 12.115, and 12.121. Equation 12.122 may be solved by any standard numerical technique, such as the Gauss elimination technique.[39]

A close examination of matrix **A** shows that the nonzero coefficients lie near the diagonal, and thus **A** is a banded matrix. Special standard computer programs are available for the solution of such a system of linear equations. Such programs not only save computer time and storage requirements, but they also give more accurate results. We used a subroutine called GELB developed by IBM for the case study presented in Section 12.15.

Systems Having Branch and Parallel Channels

The coefficients matrix, **A**, is banded only for a system of channels connected in series. For a branching system (Fig. 12.14), a number of coefficients do not lie on the diagonal, and the procedure for solving a banded matrix cannot be used. In such cases, however, if the channel sections are numbered as shown in Fig. 12.14, the resulting matrix is a banded matrix.[45] Note that the numbering of the channel sections on the branch channel increases in the upstream direction, and the difference between the consecutive section numbers of a channel is 2. These factors have to be properly taken into consideration in the computations.

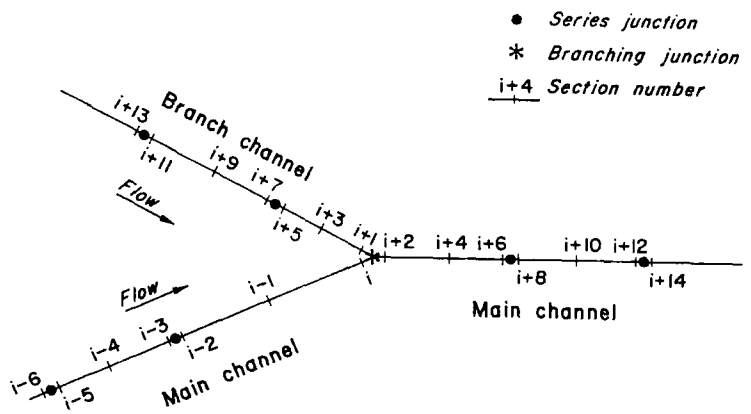

Figure 12.14. Designation of channel sections on a branch system.

Similarly, a matrix for systems having parallel channels (Fig. 12.15) is not banded. For such systems, a procedure[46] may be used in which the matrix **A** is first reduced to the upper triangular form, and then back substitution is done to solve the system of equations; or the sections may be numbered as shown in Fig. 12.15, which results in a banded matrix.[45]

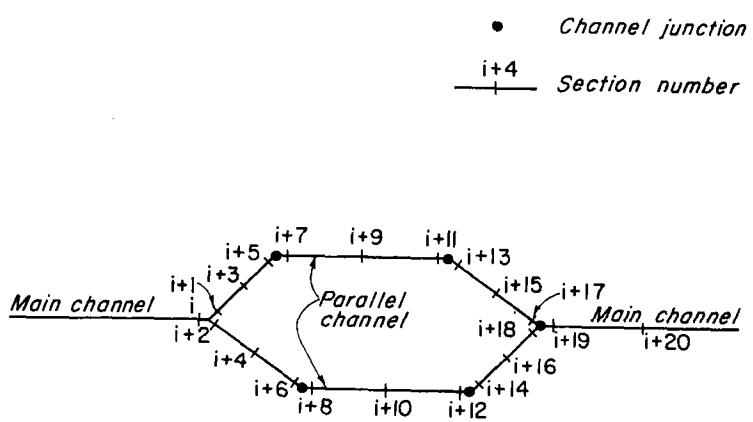

Figure 12.15. Designation of channel sections on a parallel system.

Stability Conditions

Unlike the explicit scheme of Section 12.9, the implicit scheme presented in this section is unconditionally stable, i.e., any arbitrary value of Δt may be used in the computations without making the solution unstable. This fact can be utilized as follows:

1. The channel need not be divided into reaches of equal length. (Note that Eq. 12.91 and hence the coefficients of Eqs. 12.98 and 12.99 will be modified if the value of Δx is not the same for all reaches of a channel.)
2. The size of the time step may be varied during the computations, i.e., when the conditions are varying rapidly, a smaller value of Δt may be used to increase the accuracy of the results, and, when the conditions are varying slowly, the size of the time step may be increased.

Note that the computational time step, Δt, cannot be arbitrarily increased even though the difference scheme is unconditionally stable. Actually, the size of the step is selected taking into consideration both the accuracy of the results and the stability of the scheme. If too large a value of time step is used, then the finite differences no longer approximate the partial derivatives of the original equations. Particularly, if there are sharp peaks, then these are truncated if a large value of Δt is used. Therefore, while investigating a particular case, the accuracy of the results should be checked by reducing the size of Δt and determining the difference between the computed results obtained by using larger and reduced value of Δt. If this difference is negligible, then a larger value of Δt may be used.

12.13 COMPARISON OF EXPLICIT AND IMPLICIT FINITE-DIFFERENCE METHODS

The advantages and disadvantages of the difference methods presented previously are compared in this section.

1. *Stability.* Courant's stability criterion (Eq. 12.85), i.e., $\Delta t \leqslant \Delta x/(|V| \pm c)$, must be satisfied in the explicit method. There is no such restriction on Δt in the implicit method.
2. *Ease of Programming.* The explicit method is easier to program than the implicit method. Therefore, when the time available for developing a program is limited, the explicit method should be used.
3. *Economy.* Because the size of Δt for an implicit scheme is not restricted by any stability criterion, a larger value of Δt is permissible, thus requiring less computer time as compared to the explicit scheme in which Δt is restricted by the Courant's stability condition.

4. *Computer-Memory Requirements.* The computer storage required in an implicit method is usually more than that required in an explicit method. Thus, if the storage capacity of the computer is limited, one may have to use magnetic tapes or discs to increase the effective storage for the implicit method. This may result in more computer time than that required for an explicit scheme because of reading and writing on the tapes during each time step even though a larger value of Δt may be permissible in the implicit method.
5. *Simulation of Special Cases.* Explicit methods are not suitable for conduits having closed tops in which the transient-state water surface either primes or reaches the top of the conduit. In such a situation, the free-water-surface width becomes zero or very small, and the size of Δt has to be reduced to a very small value. Examples of such cases are sewers and tailrace tunnels in hydroelectric power plants. The implicit method should be used for the anlaysis of these cases.
6. *Simulation of Sharp Peaks.* Because of the usually smaller size of Δt, the explicit methods are more suitable for the analysis of transients in which sharp peaks of short duration occur. In the implicit methods, such peaks are usually smoothed out. If, however, time steps of the same size as that in the explicit method are used, the peaks would be reproduced, but the computer time required in the implicit method would be greater than that in the explicit method.
7. *Formation of Bores and Shocks.* The explicit method is more suitable than the implicit method for the analysis of transients in which a bore forms. Lax-Wendroff's two-step explicit scheme[7,31] presented in Chapter 9 may be used to obtain more accurate results.

12.14 SPECIAL TOPICS

A number of special topics are discussed in this section.

Dam-break

The investigation of the dam-break problem is similar to the analysis of open-channel transients in which a bore forms. Stoker[47] studied it for those cases in which there is water in the channel below the dam. He assumed an instant bore formation and a rectangular, horizontal, and frictionless channel. Dronkers[48] used the method of characteristics to determine the gradually varied flow on both sides of the bore and used the conservation equations at the bore. Amein[49] studied this problem both analytically and experimentally, and Shen[50] verified Stoker's theory by conducting experiments on bores created by piston movement or by suddenly opening a gate. Terzidis and Strelkoff[31] showed that the

diffusive scheme presented in Section 12.9 and a two-step Lax-Wendroff-Richtmyer explicit scheme can be used for the analysis of flows in which a bore forms without isolation of the bore. In these schemes, the positive and negative characteristic equations (Eqs. 12.50 and 12.53) are used at the boundaries if the flow there is subcritical, and both the depth and discharge are specified if the flow is supercritical. (If a shock forms, only one of these is specified; the jump conditions yield the other.) Comparison of the computed results using these schemes with the experimental results showed good agreement. It was also shown that the solution of St. Venant equations in their usual form, without inclusion of special dissipation terms, gave erroneous results when applied to flow with bores of height greater than one-half the flow depth. For a bore of smaller height, however, the St. Venant equation yielded satisfactory results. Martin and Zovne[51] showed that the propagation and reflection of bores from a solid wall can be analyzed using the diffusive explicit scheme, and that the isolation of the bore and its treatment as an internal boundary is more of an academic interest than required in real-life practical applications.

In the dam-break investigations, the size of the breach and the time in which it occurs when the dam fails have to be assumed. Instantaneous failure of the total dam has been used by a number of investigators. Such an assumption, however, appears to be rather unrealistic.

When a dam fails, a positive wave propagates downstream, and a negative wave travels upstream in the reservoir. While using a finite-difference method, the boundary conditions at the dam site have to be developed. For this purpose, the relationships (given in Chapter 15 of Ref. 7) for various sizes of the opening in the dam may be used.

Tidal Oscillations

Riverflows influenced by tides can be analyzed by solving the St. Venant equation using the finite-difference methods. The main decision to be made in such investigations is whether a one-dimensional model can be used or not. Two-dimensional models are necessary if the flow conditions cannot be represented by one-dimensional flows.

Various finite-difference schemes have been used successfully for the analysis of tidal flows: the U.S. Geological Survey[16,19] used an explicit method based on the characteristic equations on a rectangular grid and an implicit method. Comparison of the computed results with those measured on the Three-Mile Slough, California, and on the Delaware River showed satisfactory agreement. The National Research Council of Canada used an explicit leapfrog scheme and an implicit scheme[46] to investigate the effects of various channel improvements on navigation in the St. Lawrence River and estuary. The upstream boundary

was a discharge hydrograph, and the downstream boundary was a tidal stage curve. Even though the variation of the channel geometry was rather large (the width varies by a factor of 75, and the cross-sectional area by a factor of 4000), it is claimed that the one-dimensional mathematical models based on the aforementioned finite-difference schemes could be calibrated to yield results close to the observed results.

Unlike the analysis of transients in power canals, rivers, and so on, it is not necessary to determine the initial conditions while studying tidal oscillations. Any initial conditions are assumed, and the system is subjected to tidal cycle a number of times until periodic flows are established. This is similar to the investigation of the steady-oscillatory flows in pipes by the method of characteristics (see Section 8.4).

Secondary Oscillations or Favre's Waves

We discussed in Section 12.4 that the wave front of a positive wave becomes steep as it propagates in a channel. If the energy of the wave is large, then the wave breaks and becomes a moving hydraulic jump or a bore (Fig. 12.16a). However, if the energy of the wave is not large, then the wave front assumes an undular form as shown in Fig. 12.16b. In other words, this is similar to a stationary hydraulic jump in which a strong jump is formed for Froude number $F > 9$ and an undular jump for $F < 1.7$. These secondary water-surface oscillations are called *Favre waves*,[52] as Favre described them first in 1935.

In the case of a bore, the discontinuity in the water surface occurs over a very short distance, and the flow may be assumed to be gradually varied in front of and behind the bore. The length of this discontinuity is usually small compared with the reach length into which the channel is divided. Since the St. Venant equations are valid on both sides of the bore, quite satisfactory results are obtained using these equations, as long as one is not interested in the wave front itself. However, the situation is quite different if the wave front has secondary oscillations. In this case, the water surface has undulations for a long distance, the assumption of hydrostatic-pressure distribution is not valid, and the water levels computed by using the St. Venant equations are the average levels and not the maximum levels. In addition, experience has shown that these oscillations are higher near the banks than in the middle of the channel. Figure 12.17 show the secondary oscillations of the water surface near the wave front. These photographs were taken during the prototype tests conducted on the Seton Canal in British Columbia. (For a description of these tests, see Section 12.11.)

To design power canals or other channels in which the wave fronts have secondary oscillations, the maximum water level near the banks should be known. However, very little data on these waves have been reported in the literature.

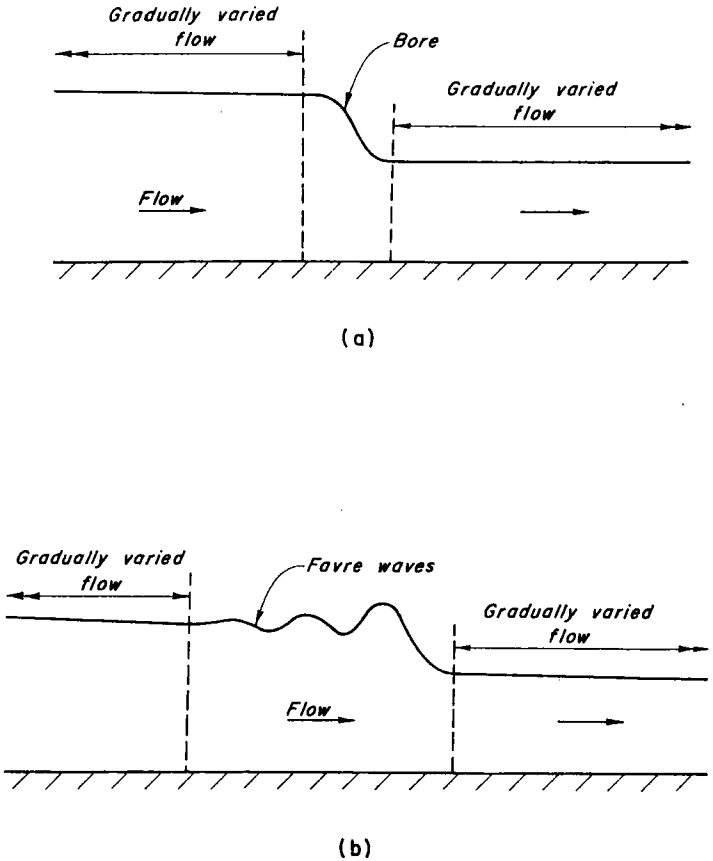

Figure 12.16. Variation of water surface at wave front.

Figure 12.18 taken from Ref. 42 may be used to determine the approximate height of these waves.

Free-Surface-Pressurized Flows

Free-surface flows that may pressurize the conduit during the transient-state conditions are called *free-surface-pressurized flows*. Such flows may occur in sewers or in the tailrace tunnel of a hydroelectric power plant.

Meyer-Peter[53] and Calame[54] studied this type of flow while investigating surges in the tailrace tunnel of the Wettingen Hydroelectric Power Plant. Their computed results were in close agreement with those measured on a hydraulic

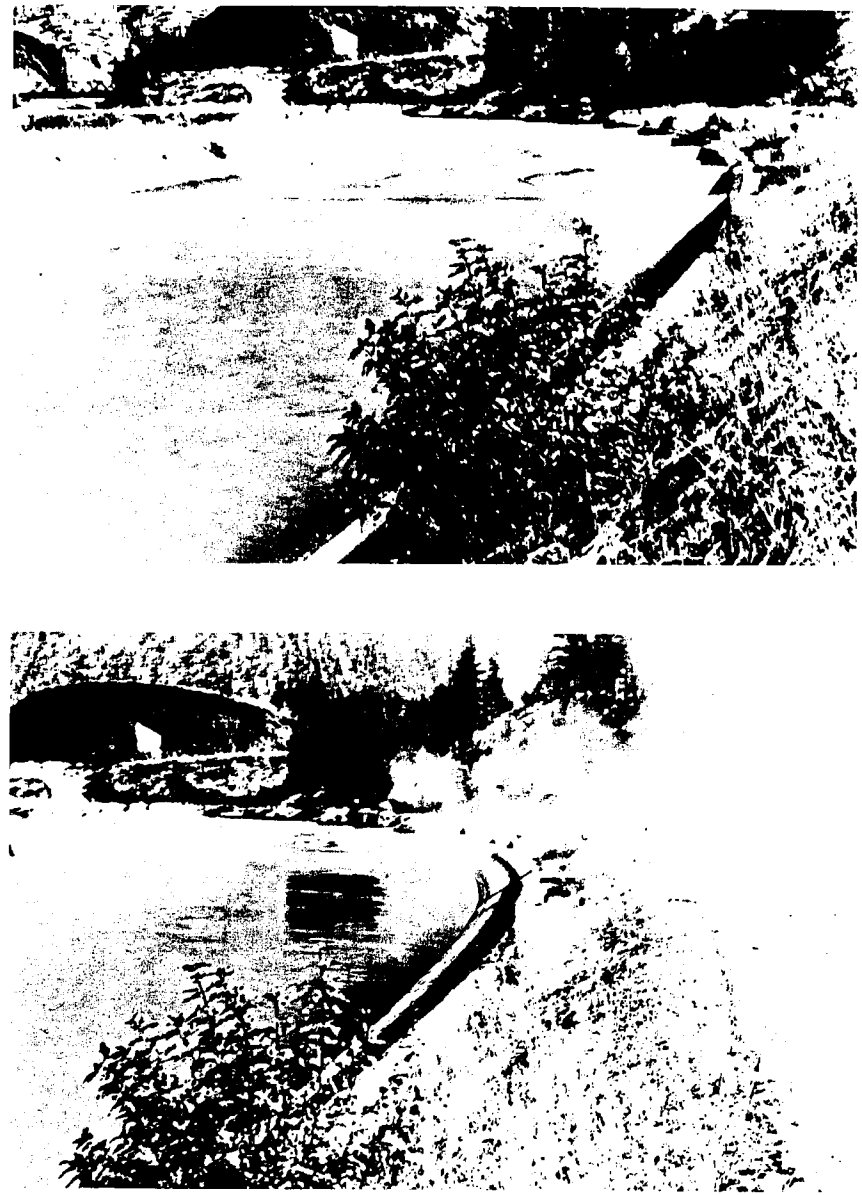

Figure 12.17. Seton Canal, secondary oscillations at wave front. (Courtesy of British Columbia Hydro and Power Authority, Vancouver, Canada).

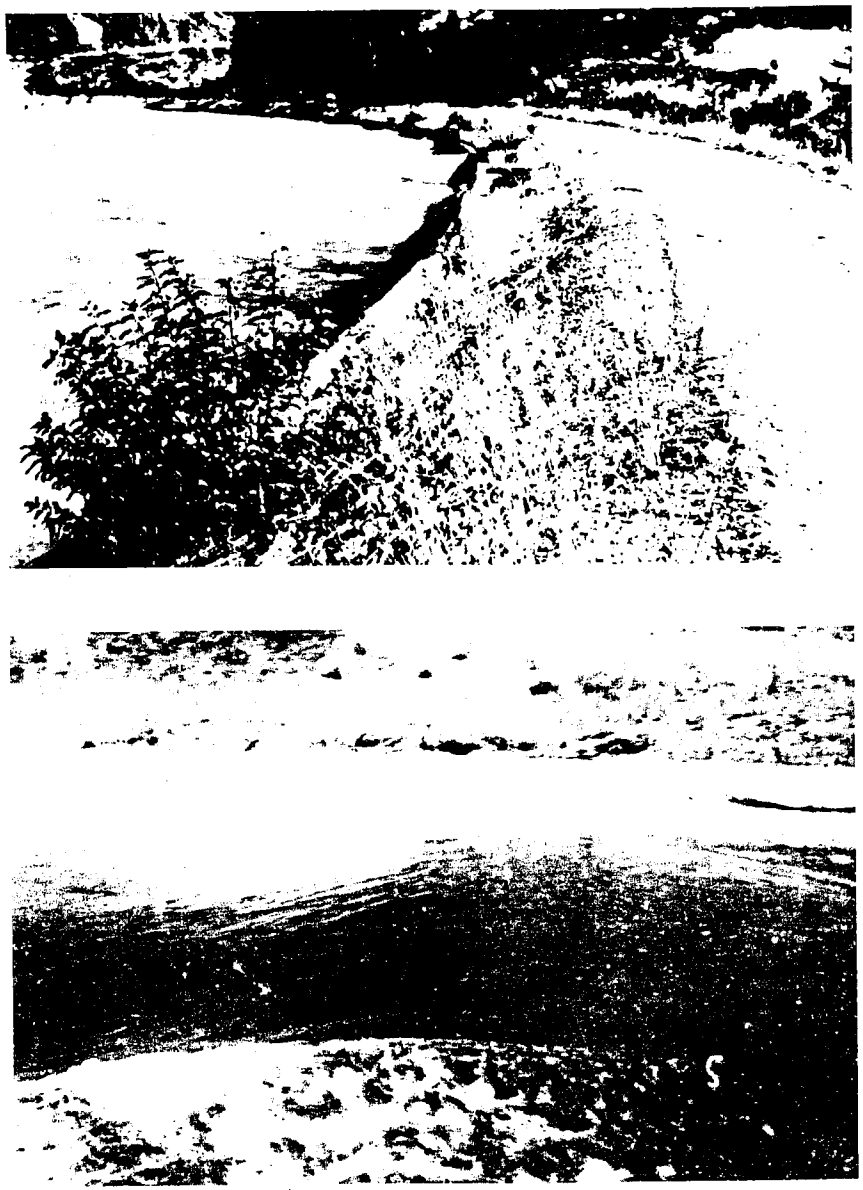

Figure 12.17. (*Continued*)

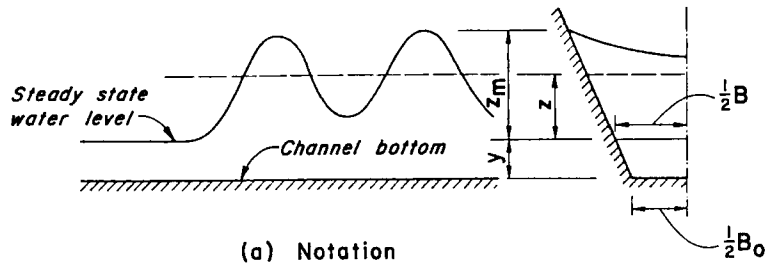

(a) Notation

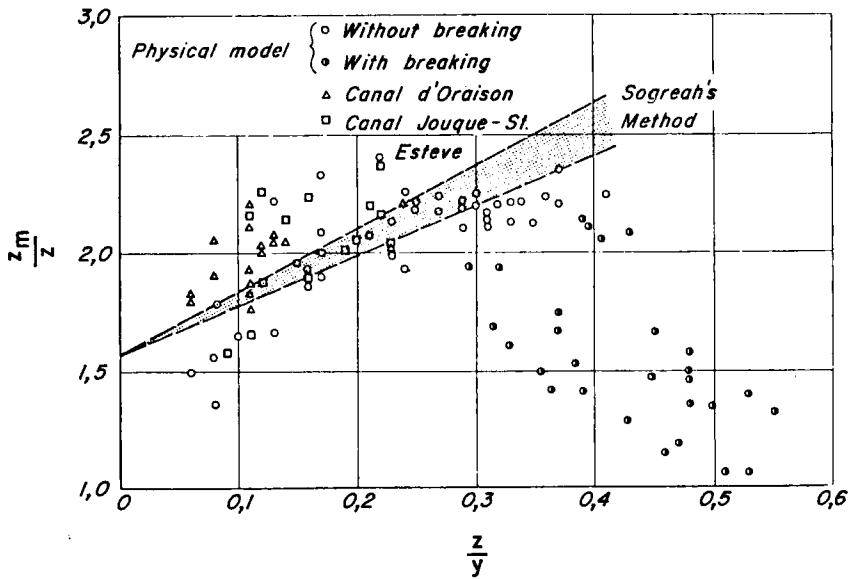

(b)

Figure 12.18. Amplitude of secondary oscillations. (After Benet, F., and Cunge, J. A.[42]).

model. In 1937, Drioli[55] reported his observations on the translation of waves in an industrial canal. Jaeger[56] discussed this problem and presented a number of expressions for various possible cases. Priessmann,[24] Cunge,[57] Cunge and Wegner,[26] Amorocho and Strelkoff,[58] and Wiggert[59,60] studied such flows using digital computers.

To facilitate comparison, let us write the equations describing the transient-state flows in open channels and in closed conduits:

1. Open channels:
   a. Continuity equation

$$\frac{\partial y}{\partial t} + V\frac{\partial y}{\partial x} + \frac{A}{B}\frac{\partial V}{\partial x} = 0 \tag{12.28}$$

   b. Dynamic equation

$$g\frac{\partial y}{\partial x} + \frac{\partial V}{\partial t} + V\frac{\partial V}{\partial x} = g(S_o - S_f) \tag{12.44}$$

2. Closed conduits:
   a. Continuity equation

$$\frac{\partial H}{\partial t} + V\frac{\partial H}{\partial x} + \frac{a^2}{g}\frac{\partial V}{\partial x} = 0 \tag{12.123}$$

   b. Dynamic equation

$$g\frac{\partial H}{\partial x} + \frac{\partial V}{\partial t} + V\frac{\partial V}{\partial x} = g(S_o - S_f) \tag{12.124}$$

in which H = piezometeric head and a = waterhammer wave velocity.

Comparison of Eqs. 12.28 and 12.123, and 12.44 and 12.124 shows that these equations are indentical if the depth of flow, y, is assumed equal to the piezometric head, H, and if $a = \sqrt{gA/B} = c$, in which c = the celerity of surface waves. We can analyze pressurized flow by solving the St. Venant equations by using an interesting technique conceived by Priessmann.[24] In this technique, a very narrow slot is assumed at the top of the conduit (Fig. 12.19) such that this slot does not increase either the cross-sectional area or the hydraulic radius of the pressurized conduit. The width of the slot is selected such that $c = a$. Thus, the free-surface and the pressurized flows do not have to be analyzed separately. Once the conduit primes, then the depth, y, determined by using the St. Venant equation, is the pressure head acting on the conduit walls at that location. This technique has been successfully used for the analysis of storm sewers[7] and for the analysis of surges in the tailrace tunnels of a hydroelectric power plant (see Section 12.15).

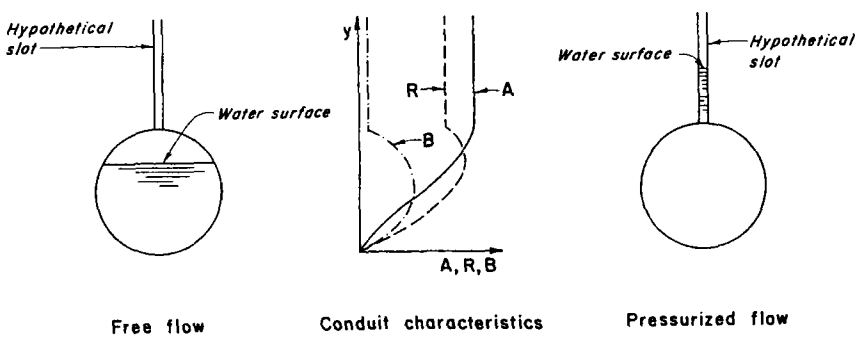

Figure 12.19. Hypothetical slot for analyzing free-surface-pressurized flows.

Landslide-Generated Waves

If a landslide occurs into a body of water, waves are generated due to displacement of water and due to impact of the landslide. These waves, sometimes referred to as *impulse waves*, have caused destruction[61-65] and loss of human life. For example, the waves generated by the Vaiont slide, in Italy, killed about 2300 people.

Landslide-generated waves have been studied on two-dimensional hydraulic models by Wiegel,[66] Prins,[67] Law and Brebner,[68] Kamphuis and Bowering,[69] Noda,[70] Das and Wiegel,[71] and Babcock[72]. Based on the model results. these authors presented empirical relationships or graphs for determining the characteristics of these waves such as initial wave height, wavelength, and type.

Three-dimensional hydraulic model studies were conducted to investigate the waves generated by the movement of slides into reservoirs created by the Mica,[73] Libby,[74] and Revelstoke[75-77] dams. The diffusive scheme of Section 12.9 was used[77,78] for the propagation of slide-generated waves approximately 67 km along the reservoir in both the upstream and downstream directions from the slide site.

The empirical relationships given by Kamphuis and Bowering[69] are presented herein (for similar relationships derived by others, see Refs. 66 through 72). These were derived from data for waves generated by loaded trays sliding down an inclined roller ramp into a 45-m-long, 1-m wide flume. The slides were simulated in the direction of the longitudinal axis of the flume from various heights and various slide angles. The waves were measured at three locations on the flume. It was found that the waves became stable at or upstream of a point located about 17-m from the point of slide impact.

The following equations were presented:

1. *Maximum height of the stable wave:*

$$\frac{H_c}{d} = F^{0.7}(0.31 + 0.2\log q) \tag{12.125}$$

in which

H_c = maximum stable wave height above the still water level
d = water depth

$F = \dfrac{V_s}{\sqrt{gd}}$

V_s = slide velocity upon impact with water

g = acceleration due to gravity

q = slide volume per unit width in dimensionless form, $\dfrac{l}{d} \cdot \dfrac{h}{d}$

l = length of slide up the slope

h = thickness of slide normal to the slope.

2. *Wave-height attenuation:*

$$\frac{H}{d} = \frac{H_c}{d} + 0.35 e^{\frac{-0.08x}{d}} \tag{12.126}$$

in which

H = maximum wave height above still water level at distance x from the slide; and

x = distance downstream from the point of slide impact.

For a given slide, the maximum stable wave height, H_c, can be determined from Eq. 12.125, and height, H, at any point downstream from the slide impact can then be computed by using Eq. 12.126.

3. *Wave period:*

$$\frac{T_1}{\sqrt{gd}} = 11 + 0.225 \frac{x}{d} \tag{12.127}$$

in which

T_1 = period of the first wave (i.e., the time required by the wave to pass any one point).

During the experiments, the waves were produced by small slides falling from above the water level. These waves varied from a pure oscillatory wave train to a wave approaching a solitary wave followed by an oscillatory wave train. No bores were formed. The wave height became stable relatively quickly. Kamphuis and Bowering state that Eq. 12.125 gives a good estimate of the stable wave height for $0.05 \leqslant q \leqslant 1.0$, as long as the slide is thick (i.e., $h/d > 0.5$); the front angle, β, of the slide is 90° or greater; and the angle of the slide plane, θ is about 30°. However, the wave heights determined from Eq. 12.125 are higher for $\beta < 90°$ and $\theta > 30°$ but low for $\theta < 30°$.

Raney and Butler[79] have developed a two-dimensional mathematical model to determine the characteristics of the slide-generated waves. Comparison of the computed results with those measured on a three-dimensional hydraulic model[74] show satisfactory agreement. The finite element method[80] is used to predict landslide-generated waves in a one-dimensional reservoir.

12.15 CASE STUDY

In this section, studies carried out to determine the operating guidelines necessary to keep the surges in the tailrace system of the G. M. Shrum Hydroelectric Generating Station below a critical level[81] are summarized. A brief description is presented of the mathematical model, its verification, and data for surges caused by various loading and unloading operations. Based on the results of this model, the power plant operating guidelines are then summarized.

Project Details

The tailrace system of the G. M. Shrum Generating Station, owned and operated by British Columbia Hydro and Power Authority, Vancouver, Canada, is comprised of two manifolds, two tunnels, a tailrace channel, and a rockfill weir. Units No. 1 to 5 discharge into Manifold No. 1, while Units No. 5 through 9 discharge into Manifold No. 2 (as will Unit No. 10 when it is installed). Water from each manifold is carried to the tailrace channel by a concrete-lined tunnel (see Fig. 12.20). Essential data for the tailrace system are listed in Table 12.1.

Surge levels above the tailrace manifold deck (El. 510.5 m) would cause both a water-pressure loading and an air-pressure differential across the doors, which might lead to their collapse and the subsequent flooding of the powerhouse. Therefore, a mathematical model was developed to determine what, if any, operating restrictions should be applied during periods of high tailwater levels.

Mathematical Model

Description

The dynamic and continuity equations derived in Section 12.5 were solved numerically using Strelkoff's implicit finite-difference scheme (presented in Section 12.12). Because of the branch tunnel, the channels were numbered[45] as shown in Fig. 12.14 so that a banded matrix was obtained. The subroutine GELB, developed by IBM, was used to solve the system of linear equations. Boundary conditions for the manifold, junctions of two or three channels, and the downstream weir were developed and incorporated in the model. As discussed in the last section, the primed tunnel was simulated by the open-channel-flow equations by assuming a very narrow vertical slot at the top of the tunnel. This slot allowed the depth of flow to exceed the tunnel height, thus represent-

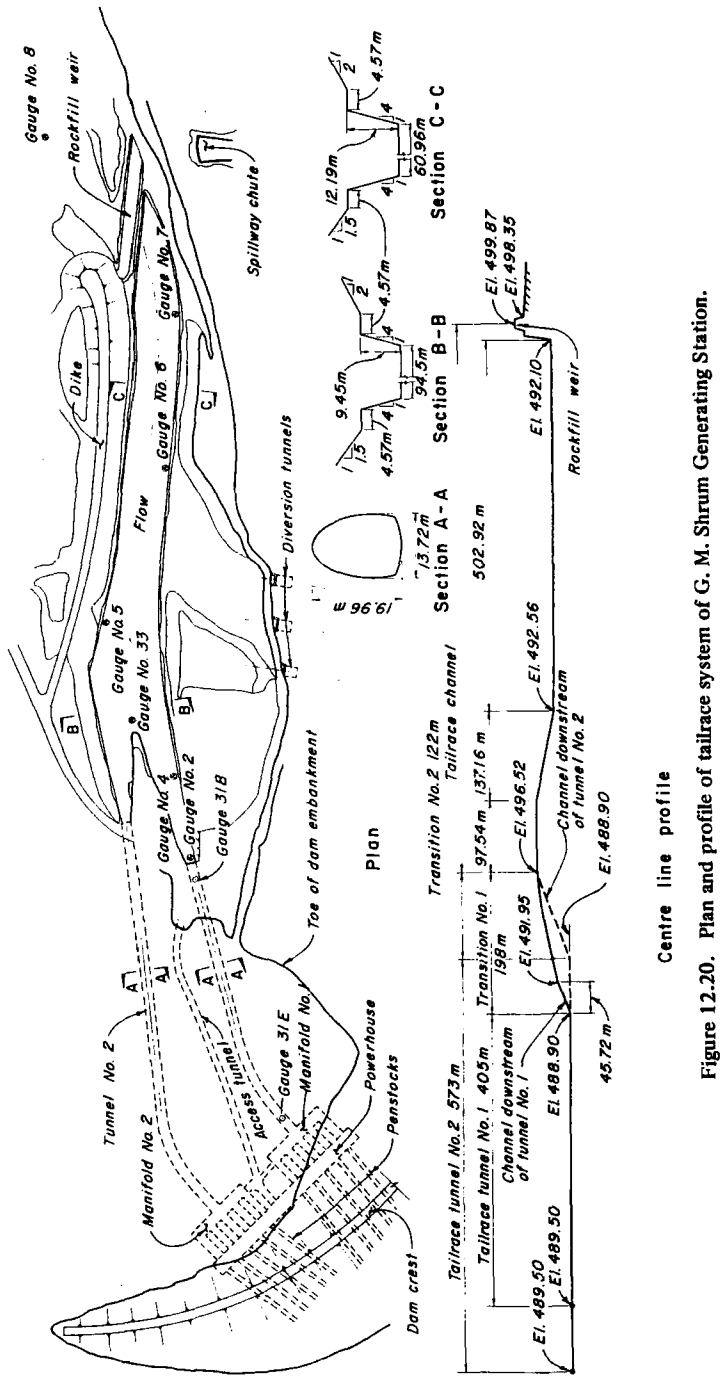

Figure 12.20. Plan and profile of tailrace system of G. M. Shrum Generating Station.

Table 12.1. G. M. Shrum Generating Station, data for tailrace system.

General	
No. of tailrace tunnels	2
No. of manifolds	2
Units on Manifold No. 1	1 to 5
Units on Manifold No. 2	6 to 10
Tailrace Tunnels	
Shape	Modified horseshoe
Size	19.96 m high, 13.72 m wide
Lining	Concrete
Length	Tunnel No. 1, 405 m; No. 2, 573 m
Manifold size	13.71 by 99.67 m
Tailrace Channel	
For the length and cross sections of the channel, see Fig. 12.20.	
Weir length = 192 m.	
Turbines	

Unit No.	Maximum Output[a] (MW)	Discharge[a] per Turbine (m^3/s)
1 to 5	261	178
6 to 8	275	190
9 and 10	300	204

[a]At a net head of 164.6 m.

ing the pressure on the tunnel crown due to priming, but at the same time did not increase either the flow area or the hydraulic radius.

A new dam, called Peace Canyon, is being constructed 22.5 km downstream of the G. M. Shrum Generating Station. The reservoir created by this dam will extend to the rockfill weir. To simulate this reservoir, about 1200 m of its length downstream of the existing rockfill weir was included in the analysis, and the water levels in this reservoir were varied by adjusting the height of a hypothetical weir at its downstream end. Since the return wave-propagation time between the manifolds and this hypothetical weir is more than the time of the transient-state conditions of interest, this weir does not affect the manifold surge levels.

Load acceptance or rejection was simulated by varying the total inflow to each manifold at the rate at which the wicket gates open or close. Since total outflow from all the turbines on each manifold is lumped as inflow to the manifold, load variation on individual units was not simulated.

Verification

The mathematical model was verified prior to the production runs by comparing the computed results with those measured on the prototype or on the hydraulic model.

Comparison with Prototype Results. Load-rejection tests were conducted on the prototype to obtain data to verify the mathematical model. Computed and measured water levels at various gauges for these tests were compared. The results for the largest load rejection (1020 MW) are shown in Fig. 12.21. In this test, the inflow to Manifold No. 1 was reduced from 810 to 133 m^3/s in 8 seconds, and the inflow to Manifold No. 2 remained steady at 240 m^3/s.

As can be seen from this figure, there is good agreement between the computed and measured transient-state water levels, even though there was a slight

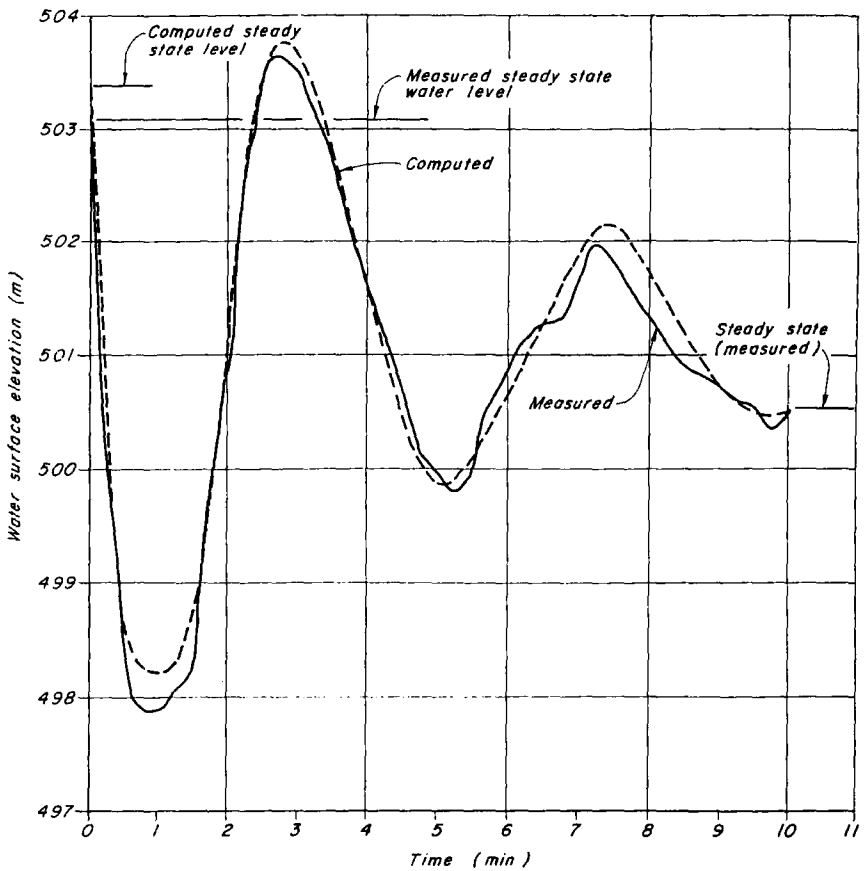

(a) Manifold No. 1

Figure 12.21. Comparison of computed and measured prototype water levels following reduction of inflow to manifold No. 1 from 810 to 133 m^3/s in 8 s. Inflow to manifold No. 2 remained steady at 240 m^3/s.

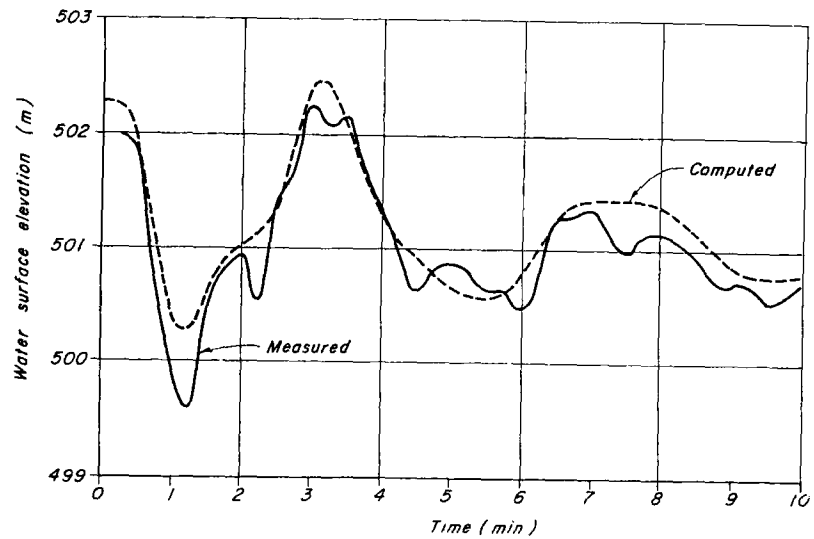

(b) Gauge No. 2

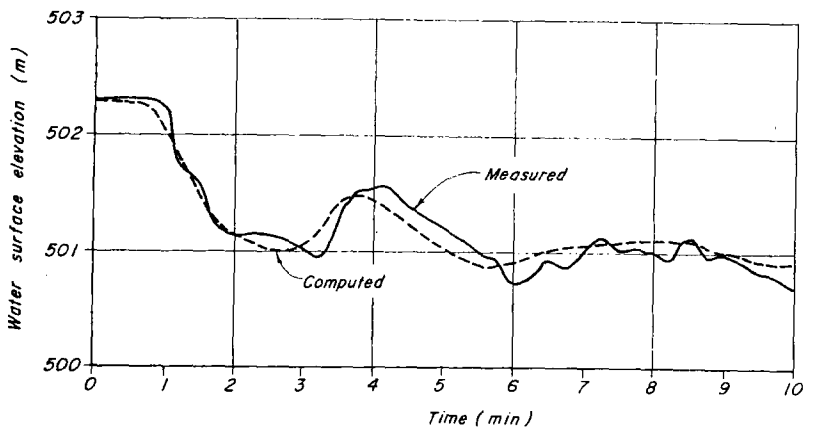

(c) Gauge No. 5

Figure 12.21. *(Continued)*

difference between the computed and measured steady-state water levels. If this difference in the steady-state water levels is taken into consideration, the agreement between the computed and measured water levels would be further improved. The comparisons for the other tests were equally satisfactory.

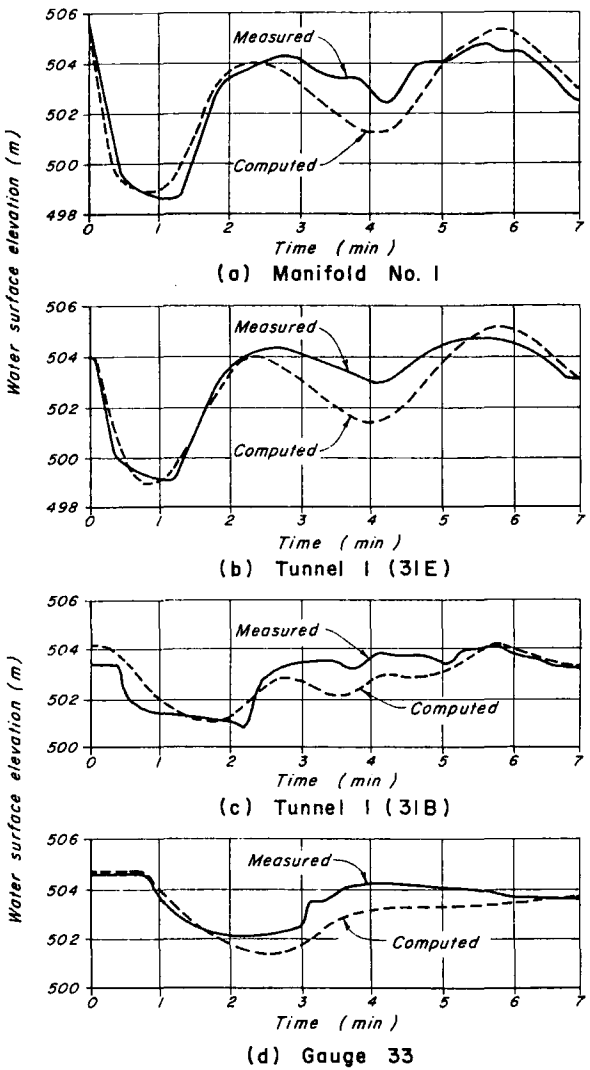

Figure 12.22. Comparison of computed and measured water levels on hydraulic model following simultaneous reduction of inflow to both manifolds from 990 to 0 m^3/s in 8 s. Initial steady-state water level at Gauge No. 8 = El. 507.5 m.

Comparison with Hydraulic Model Results. Limited results were available of the tests conducted on an undistorted, 1:96-scale hydraulic model. Computed and measured water levels are shown in Figs. 12.22 and 12.23.

As can be seen from these comparisons, the agreement between the hydraulic

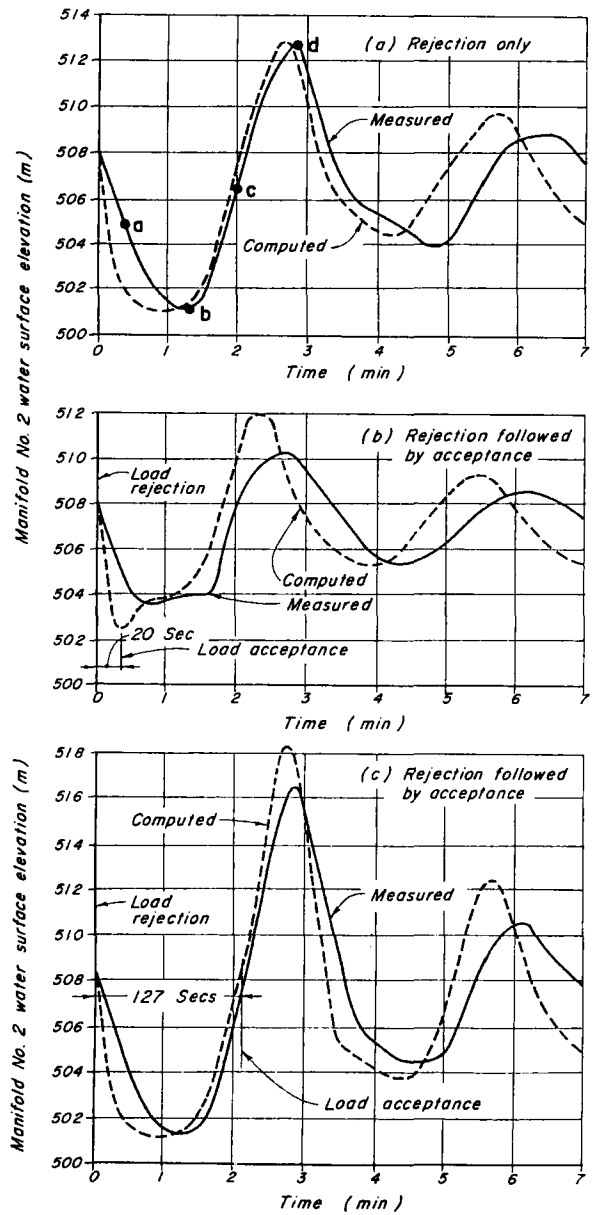

Figure 12.23. Comparison of computed and measured water levels on hydraulic model. Initial steady-state water level at Gauge No. 8 = El. 507.5 m. Inflow to manifold No. 2 varied in 8 s as follows: (a) 990 to 0 m^3/s, (b) 990 on 0 m^3/s and then 0 to 396 m^3/s after 20 s, and (c) 990 to 0 m^3/s and then to 396 m^3/s after 127 s.

model and computed water levels is satisfactory but is not as good as that between the prototype and computed results. The difference may be due to approximation of the channel configuration. This was changed several times during testing, and no records are available of the configuration in use when the surge results shown were obtained.

Results

Prototype transient-state conditions were computed for the following total and partial load changes over a range of steady-state manifold levels:

1. load rejection
2. load acceptance
3. load rejection followed by load acceptance
4. load acceptance followed by load rejection.

Although the load acceptance period is usually much more than 8 s, both the load acceptance and rejection periods were assumed to be 8 s because load acceptance at this rate is possible. Slower operating rates were assumed only while investigating the effects of increasing these periods on the maximum surge levels. Since the units would be synchronized to the system prior to load acceptance, the wicket gates would be at speed-no-load (SNL) gate (about 6 percent). In the analysis, however, it was assumed that the wicket gates are opened from the fully closed position to their final steady-state values. The computed levels are, therefore, slightly higher than would be expected from the actual prototype operation.

For the multiple-turbine operations (i.e., load acceptance followed by load rejection or vice versa), the second operation was started at the most critical time, which is defined as *the time between the start of two operations that produces maximum upsurge*. For example, for a load acceptance following a load rejection, the load was accepted at points *a*, *b*, *c*, and *d* of Fig. 12.23a. It was found that the maximum upsurge was produced when the load was accepted *at point* c *and not when it was accepted at point* d. Tests on the hydraulic model gave the same result.

Operating Guidelines

The operating guidelines were formulated so that the maximum upsurge would not exceed El. 511.5 m, i.e., the top of the manifold parapet wall. A large number of operating conditions were considered in order to identify those that produce the highest upsurges.

The rate of loading, or reloading following a load rejection could be easily restricted. For a load rejection, however, such restrictions could not be imposed without modifying the existing control equipment. The unit goes to runaway speed if the wicket gates are closed slowly following a load rejection, and, as letting the unit operate at runaway speed for long periods was unacceptable, increasing the wicket-gate closing time did not appear to be attractive. A more reasonable alternative was to impose a limit on the initial steady-state load so that, if the load was rejected, the upsurge would remain within the allowable limits.

For reloading following a load rejection, either the rate of reloading could be restricted or reloading could be done at the 8-s rate once the surges in the manifold due to load rejection had subsided. Because of the inherent dangers, no consideration was given to the possibility of reloading on the optimum part of a cycle as a means of allowing more rapid reloading.

High upsurges may be produced even at low tailwater levels depending upon the number, sequence, and size of the loading and unloading operations. Therefore, such multiple loading and unloading operations must be avoided. For example, in case of synchronizing difficulties, or load rejection during a load acceptance, the manifold water level should be allowed to become steady before another attempt is made to load the units.

The operating guidelines showing the allowable amount of load that can be accepted or rejected are presented in Fig. 12.24. This figure also shows, based on the condition of total load rejection, the maximum permissible initial load for various initial manifold levels. Different operating conditions are designated as follows:

Curve No.	Description
1	Total load rejection; maximum allowable initial load
2	Load acceptance from steady state
3	Load rejection following 300-MW acceptance
4	Load rejection following 600-MW acceptance
5	Load rejection following 900-MW acceptance
6	Load rejection following 1200-MW acceptance
7	Load acceptance following 300-MW rejection
8	Load acceptance following 600-MW rejection
9	Load acceptance following 900-MW rejection
10	Load acceptance following 1200-MW rejection
11	Load acceptance following 1500-MW rejection

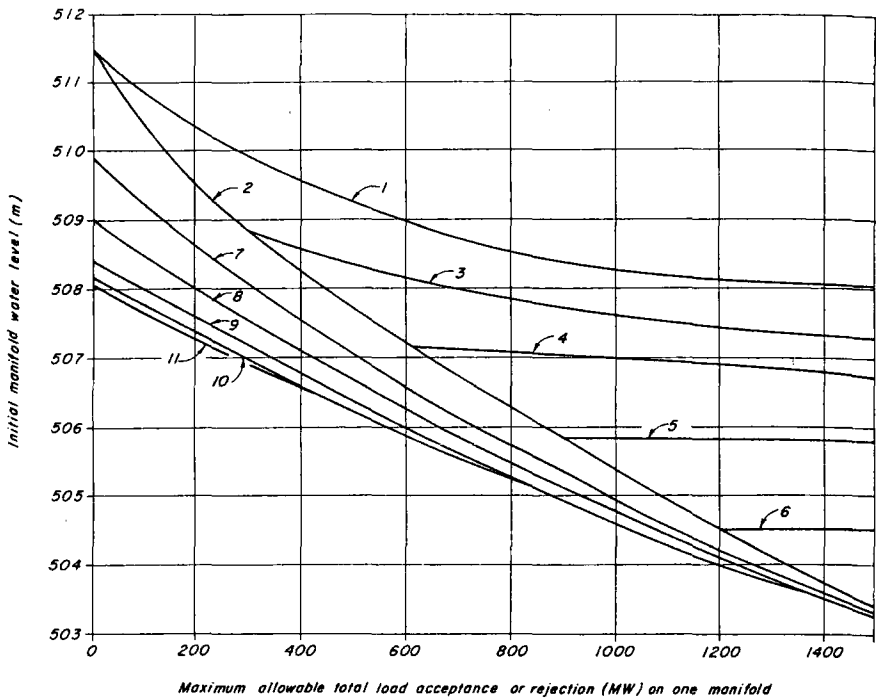

Figure 12.24. Operating guidelines.

12.16 SUMMARY

In this chapter, transient flows in open channels were discussed. A number of terms were first defined, the continuity and dynamic equations were derived, and numerical methods available for their solution were discussed. Details of the explicit and implicit finite-difference methods were presented. The chapter concluded with a case study.

PROBLEMS

12.1. A 6.1-m-wide rectangular canal is carrying 28 m^3/sec at a depth of 3.04 m. The gates at the downstream end are suddenly closed. Determine the initial surge height, z, and the velocity, V_w, of the surge wave.

12.2. An initial steady-state flow of 16.8 m^3/sec in a 3-m-wide rectangular power canal is suddenly reduced to 11.2 m^3/sec at the downstream end. If the initial depth was 1.83 m, determine the height and the velocity of the initial surge wave.

12.3. A trapezoidal canal having a bottom width of 6.1 m and side slopes of 1.5 horizontal to 1 vertical is carrying 126 m^3/sec at a depth of 5.79 m. If the flow is suddenly stopped at the downstream end, what would be the surge height and the wave velocity?

12.4. Prove that if the surge height, z, is small as compared to the initial flow depth, y_o, then

$$c = \sqrt{g\left(\frac{A_o}{y_o} + 1.5\,z\right)}$$

in which A_o = initial steady-state flow area.

12.5. Develop the boundary conditions for the junction of three channels for the diffusive scheme based on the explicit finite differences. Neglect the friction losses at the junction.

12.6. In Eq. 12.121, conditions imposed by the boundary were written in a general form. Determine the values of coefficients for a reservoir, a control gate, and a rating curve. Linearize the relationships if they are nonlinear.

12.7. Plot the variation of water surface at the downstream end of a canal with time following sudden closure of the control gates at the downstream end. Assume the canal is short, horizontal, and frictionless.

12.8. Derive the dynamic and continuity equations for nonprismatic channels having lateral outflow q per unit length of channel. Assume (1) gradual bulk outflow, e.g., over a side spillway; (2) outflow has negligible velocity, e.g., seepage; and (3) gradual inflow, e.g., from tributaries, having velocity component in the positive x-direction as u_1.

Answers

12.1. $z = 0.9$ m; $V_w = -5.13$ m/sec.
12.3. $z = 0.93$ m; $V_w = -5.52$ m/sec.
12.8. 1. Continuity equation:

$$A\frac{\partial V}{\partial x} + BV\frac{\partial y}{\partial x} + B\frac{\partial y}{\partial t} + V\frac{\partial A(x, y)}{\partial x} + q = 0$$

2. Dynamic equation:

$$\frac{\partial V}{\partial t} + V\frac{\partial V}{\partial x} + g\frac{\partial y}{\partial x} = g(S_o - S_f) + D_l$$

in which

$$D_l = 0 \text{ for case 1}$$

$$D_l = \frac{V}{2A} \text{ for case 2}$$

$$D_l = \frac{(V - u_l)q}{A} \text{ for case 3}$$

REFERENCES

1. Chow, V. T., *Open-Channel Hydraulics*, McGraw-Hill Book Co., New York, 1959.
2. Rouse, H. (ed.), *Engineering Hydraulics*, John Wiley & Sons, New York, 1961.
3. Johnson, R. D., "The Correlation of Momentum and Energy Changes in Steady Flow with Varying Velocity and the Application of the Former to Problems of Unsteady Flow or Surges in Open Channels," *Engineers and Engineering*, The Engineers Club of Philadelphia, 1922, p. 233.
4. Rich, G. R., *Hydraulic Transients*, Dover Publications, Inc., New York, 1963.
5. De Saint-Venant, B., "Theorie du movement non-permanent des eaux avec application aux crues des vivieres et a l'introduction des marees dans leur lit," *Acad. Sci. Comptes Rendus*, Paris, vol. 73, 1871, pp. 148-154, 237-240 (translated into English by U.S. Corps of Engineers, No. 49-g, Waterways Experiment Station, Vicksburg, Miss., 1949).
6. Strelkoff, T., "One-Dimensional Equations of Open Channel Flow," *Jour., Hyd. Div., Amer. Soc. of Civil Engrs.*, vol. 95, May 1969, pp. 861-876.
7. Mahmood, K. and Yevjevich, V. (ed.), *Unsteady Flow in Open Channels*, Water Resources Publications, Fort Collins, Colorado, 1975.
8. Yen, B. C., "Open-Channel Flow Equations Revisited," *Jour., Engineering Mech. Div., Amer. Soc. of Civ. Engrs.*, vol. 99, Oct. 1973, pp. 979-1009.
9. Amein, M. and Fang, C. S., "Implicit Flood Routing in Natural Channels," *Jour., Hyd. Div., Amer. Soc. of Civil Engrs.*, vol. 96, Dec. 1970, pp. 2481-2500.
10. Vasiliev, O. F., Temnoeva, T. A., and Shugrin, S. M., "Chislennii Metod Rascheta Neustanoviv-shikhsia Techenni v Otkritikh Ruslakh" ("Numerical Method of Calculating Unsteady Flow in Open Channels"), *Izvestiia Akemii Nauk S.S.S.R., Mekhanika*, No. 2, 1965, pp. 17-25 (in Russian).
11. Stoker, J. J., *Water Waves*, Interscience, New York, 1957.
12. Forsythe, G. E. and Wasow, W. R., *Finite-Difference Methods for Partial Differential Equations*, John Wiley & Sons, New York, 1960.
13. Courant, R. and Hilbert, D., *Methods of Mathematical Physics*, vol. II, Interscience, New York, 1962.
14. Garabedian, P. R., *Partial Differential Equations*, John Wiley & Sons, 1964.
15. Abbot, M. B., *An Introduction to the Method of Characteristics*, American Elsevier, New York, 1966.
16. Lai, C., "Flows of Homogeneous Density in Tidal Reaches: Solution by the Method of Characteristics," *Open File Report*, United States Department of the Interior, Geological Survey, Washington, D.C., 1965.
17. Isaacson, E. J., Stoker, J. J., and Troesch, B. A., "Numerical Solution of Flood Prediction and River Regulation Problems: Report 2, Numerical Solution of Flood Problems in Simplified Models of the Ohio River and the Junction of the Ohio and Mississippi Rivers," New York University, Institute of Mathematical Sciences, Report No. IMM-205, 1954.

18. Isaacson, E. J., Stoker, J. J., and Troesch, B. A., "Numerical Solution of Flood Prediction and River Regulation Problems: Report 3, Results of the Numerical Prediction of the 1945 and 1948 Floods in the Ohio Rivers of the 1947 Flood through the Junction of the Ohio and Mississippi Rivers, and of the Floods of 1950 and 1948 through Kentucky Reservoir," New York University, Institute of Mathematical Sciences, Report No. IMM-NYU-235, 1956.
19. Baltzer, R. A. and Lai, C., "Computer Simulation of Unsteady Flows in Waterways," *Jour., Hyd. Div., Amer. Soc. of Civil Engrs.*, vol. 94, July 1968, pp. 1083-1117.
20. Liggett, J. A. and Woolhiser, D. A., "Difference Solutions of the Shallow-Water Equation," *Jour. Engineering Mech. Div., Amer. Soc. of Civil Engrs.*, vol. 93, April 1967, pp. 39-71.
21. Abbott, M. B. and Verwey, A., "Four-Point Method of Characteristics," *Jour. Hydr. Div., Amer. Soc. of Civil Engrs.*, vol. 96, Dec. 1970, pp. 2549-2564.
22. Lax, P. D., "Weak Solutions of Nonlinear Hyperbolic Partial Differential Equations and Their Numerical Computation," *Communications on Pure and Applied Mathematics*, vol. 7, 1954, pp. 159-163.
23. Lax, P. D. and Wendroff, B., "Systems of Conservation Laws," *Communications on Pure and Applied Mathematics*, vol. 13, 1960, pp. 217-237.
24. Priessmann, A. and Cunge, J. A., "Calcul des intumescences sur machines electroniques," IX Meeting, International Assoc. for Hydraulic Research, Dubrovnik, 1961.
25. Richtmyer, R. D., "A Survey of Difference Methods for Non-Steady Fluid Dynamics," *NCAR Technical Notes* 63-2, National Center for Atmospheric Research, Boulder, Colorado, 1962.
26. Cunge, J. A. and Wegner, M., "Integration Numerique des equations d'ecoulement de Barre de Saint Venant par un schema Implicite de differences finies," *La Houille Blanche*, No. 1, 1964, pp. 33-39.
27. Gelfand, I. M. and Lokutsievski, O. V., "The Double Sweep Method for Solution of Difference Equations," in *Theory of Difference Schemes*, by Godunov, S. K. and Ryabenki, V. S., North Holland Publishing Co., Amsterdam, 1964.
28. Richtmyer, R. D. and Morton, K. W., *Difference Methods for Initial-Value Problems*, 2nd ed., Interscience Publishers, New York, 1967.
29. Martin, C. S. and DeFazio, F. G., "Open Channel Surge Simulation by Digital Computers," *Jour., Hyd. Div., Amer. Soc. of Civil Engrs.*, vol. 95, Nov. 1969, pp. 2049-2070.
30. Strelkoff, T., "Numerical Solution of Saint-Venant Equations," *Jour., Hyd. Div., Amer. Soc. of Civil Engrs.*, vol. 96, January, 1970, pp. 223-252.
31. Terzidis, G. and Strelkoff, T., "Computation of Open Channel Surges and Shocks," *Jour., Hyd. Div., Amer. Soc. of Civil Engrs.*, vol. 96, Dec. 1970, pp. 2581-2610.
32. Amein, M. and Chu, H. L., "Implicit Numerical Modeling of Unsteady Flows," *Jour., Hyd. Div., Amer. Soc. of Civil Engrs.*, vol. 101, June 1975, pp. 717-731.
33. Chaudhry, M. H., "Mathematical Modelling of Transient State Flows in Open Channels," *Proc., International Symposium on Unsteady Flow in Open Channels*, Newcastle-upon-Tyne, 1976, published by British Hydromechanic Research Assoc., Cranfield, Bedford, England, pp. C1-1-C1-18.
34. Cooley, R. L. and Moin, S. A., "Finite Element Solution of Saint-Venant Equations," *Jour., Hyd. Div., Amer. Soc. of Civil Engrs.*, vol. 102, Sept. 1976, pp. 1299-1313.
35. Davis, J. M., "The Finite Element Method: An Alternative Subdomain Method for Modelling Unsteady Flow in Coastal Waters and Lakes," *Ref. 33*, pp. B4-41-B4-53.

36. Patridge, P. W. and Brebbia, C. A., "Quadratic Finite Elements in Shallow Water Problems," *Jour., Hyd. Div., Amer. Soc. of Civil Engrs.*, vol. 102, Sept. 1976, pp. 1299–1313.
37. Houghton, D. D. and Kasahara, A., "Nonlinear Shallow Fluid Flow over an Isolated Ridge," *Comm. on Pure and App. Math.*, vol. XXI, No. 1, Jan. 1968.
38. Dronkers, J. J., "Tidal computations for Rivers, Coastal Areas and Seas," *Jour., Hyd. Div., Amer. Soc. of Civil Engrs.*, vol. 95, Jan. 1965.
39. McCracken, D. D. and Dorn, W. S., *Numerical Methods and FORTRAN Programming*, John Wiley & Sons, New York, 1967.
40. Stark, R. M. and Nicholls, R. L., *Mathematical Foundations for Design*, McGraw-Hill Book Co., 1970, pp. 119–121.
41. Courant, R., Friedrichs, K., and Lewy, H., "Uber die partiellen Differenzengleichungen der Mathematischen Physik," *Math. Ann.*, vol. 100, 1928, pp. 32–74 (in German).
42. Benet, F. and Cunge, J. A., "Analysis of Experiments on Secondary Undulations Caused by Surge Waves in Trapezoidal Channels," *Jour. Hyd. Research*, International Assoc. for Hyd. Research, vol. 9, No. 1, 1971, pp. 11–33.
43. Vasiliev, O. F., et al., "Numerical Method of Computations of Wave Propagation in Open Channels; Application to the Problem of Floods," *Dokl. Akad. Nauk SSSR*, 151, No. 3, 1963 (in Russian).
44. Vasiliev, O. F., et al., "Numerical Methods for the Calculation of Shock Wave Propagation in Open Channels," *Proc. 11th Congress, International Assoc. for Hyd. Research*, Leningrad, vol. III, 1965, 13 pp.
45. Kao, K. H., "Numbering of a Y-Branch System to Obtain a Banded Matrix for Implicit Finite-Difference Scheme," B.C. Hydro interoffice memorandum to W. W. Bell, Hydraulic Section, November 1977.
46. Kamphuis, J. W., "Mathematical Tidal Study of St. Lawrence River," *Jour., Hyd. Div., Amer. Soc. of Civil Engrs.*, vol. 96, No. HY3, March 1970, pp. 643–664.
47. Stoker, J. J., "The Formation of Breakers and Bores," *Communications on Pure and Applied Mathematics*, vol. 1, 1948, pp. 1–87.
48. Dronkers, J. J., *Tidal Computations in Rivers and Coastal Waters*, North Holland Publishing Co., Amsterdam, Netherland, 1964.
49. Amein, M., "Bore Inception and Propagation by the Nonlinear Wave Theory," *Proc., 9th Conference on Coastal Engineering*, Lisbon, Portugal, June 1964, pp. 70–81.
50. Shen, C. C., "Selection and Design of a Bore Generator for the Hilo Harbor Tsunami Model," *Research Report No. 2-5, United States Army Engr. Waterways Experiment Station*, Vicksburg, Miss., June 1965, 94 pp.
51. Martin, C. S. and Zovne, J. J., "Finite-Difference Simulation of Bore Propagation," *Jour., Hyd. Div., Amer. Soc. of Civ. Engrs.*, vol. 97, No. HY7, July 1971, pp. 993–1010.
52. Favre, H., Ondes de translation dans les canaux de'couverts, Dunod, 1935.
53. Meyer-Peter, E. and Favre, H., "Ueber die Eigenschaften von Schwallen und die Berechnung von Unterwasserstollen," *Schweizerische Bauzaitung*, Nos. 4-5, vol. 100, Zurich, Switzerland, July 1932, pp. 43-50, 61-66.
54. Calame, J., "Calcul de l'onde translation dans les canaux d'usines," Editions la Concorde, Lausanne, Switzerland, 1932.
55. Drioli, C., "Esperienze sul moto pertubato nei canali industriali," *L'Energie Elettrica*, no. IV-V, vol. XIV, Milan, Italy, April-May, 1937.
56. Jaeger, C., *Engineering Fluid Mechanics*, Blackie & Son Limited, London, 1956, pp. 381–392.

57. Cunge, J. A., "Comparison of Physical and Mathematical Model Test Results on Translation Waves in the Oraison-Manosque Power Canal," *La Houille Blanche*, no. 1, Grenoble, France, 1966, pp. 55–69, (in French).
58. Amorocho, J. and Strelkoff, T., "Hydraulic Transients in the California Aqueduct," Report No. 2, Department of Water Resources, State of California, June 1965.
59. Wiggert, D. C., "Prediction of Surge Flows in the Batiaz Tunnel," *Research Report, Laboratory for Hydraulics and Soil Mechanics*, Federal Institute of Technology, Zurich, Switzerland, no. 127, June 1970.
60. Wiggert, D. C., "Transient Flow in Free-Surface, Pressurized Systems," *Jour., Hyd. Div., Amer. Soc. of Civ. Engrs.*, Jan. 1972, pp. 11–27.
61. Miller, D. J., "Giant Waves in Lituya Bay, Alaska," Professional Paper 354-L, U.S. Geological Survey, 1960.
62. Kiersch, G. A., "Viaont Reservoir Disaster," *Civ. Engineering, Amer. Soc. of Civ. Engrs.*, vol. 34, no. 3, March 1964, pp. 32–47.
63. McCullock, D. S., Slide-Induced Waves, Seiching, and Ground Fracturing Caused by the Earthquakes of March 27, 1964, at Kenai Lake, Alaska," Professional Paper 543-A, U.S. Geological Survey, 1966.
64. Kachadoorian, R., "Effects of the Earthquake of March 27, 1964, at Whittier, Alaska," Professional Paper, No. 542-B, U.S. Geological Survey, 1965.
65. Forstad, F., "Waves Generated by Landslides in Norwegian Fjords and Lakes," Publication No. 79, Norwegian Geotechnical Institute, Oslo, 1968, pp. 13–32.
66. Wiegel, R. L., "Laboratory Studies of Gravity Waves Generated by the Movement of a Submerged Body," *Trans. Amer. Geophysical Union*, vol. 36, no. 5, Oct. 1955, pp. 759–774.
67. Prins, J. E., "Characteristics of Waves Generated by a Local Disturbance," *Trans. Amer. Geophysical Union*, vol. 39, no. 5, Oct. 1958, pp. 865–874.
68. Law, L. and Brebner, A., "On Water Waves Generated by Landslides," *Third Australasian Conference on Hydraulics and Fluid Mechanics*, Sidney, Australia, Nov. 1968, pp. 155–159.
69. Kamphuis, J. W. and Bowering, R. J., "Impulse Waves Generated by Landslides," *Proc., Twelfth Coastal Engineering Conference, Amer. Soc. of Civ. Engrs.*, Washington, D.C., Sept. 1970, pp. 575–588.
70. Noda, E., "Water Waves Generated by Landslides," *Jour., Waterways, Harbors and Coastal Engineering Div., Amer. Soc. of Civ. Engrs.*, vol. 96, no. WW4, Nov. 1970, pp. 835–855.
71. Das, M. M. and Wiegel, R. L., "Waves Generated by Horizontal Motion of a Wall," *Jour., Waterways, Harbors and Coastal Engineering Div., Amer. Soc. of Civ. Engrs.*, vol. 98, no. WW1, Feb. 1972, pp. 49–65.
72. Babcock, C. I., "Impulse Wave and Hydraulic Bore Inception and Propagation as Resulting from Landslides," a research problem presented to Georgia Inst. of Tech., Atlanta, Georgia, in partial fulfillment of the requirements for the degree of M.Sc. in civil engineering, Oct. 1975.
73. "Wave Action Generated by Slides into Mica Reservoir, Hydraulic Model Studies," *Report, Western Canada Hydraulic Laboratories*, Vancouver, B.C., Canada, Nov. 1970.
74. Davidson, D. D. and McCartney, B. L., "Water Waves Generated by Landslides in Reservoirs," *Jour., Hyd. Div., Amer. Soc. of Civ. Engrs.*, vol. 101, Dec. 1975, pp. 1489–1501.
75. "A Pilot Study of Water Surface Waves in Revelstoke Reservoir in the Event of Downie Slide Movement," *Report, Northwest Hydraulic Consultants*, Vancouver, B.C., Canada, June 1976.

76. "Hydraulic Model Study of Waves from Downie Slide," *Report, Northwest Hydraulic Consultants*, August 1976.
77. Mercer, A. G., Chaudhry, M. H., and Cass, D. E.,"Modelling of Slide-Generated Waves," *Fourth Hydrotechnical Conference*, Vancouver, Canada (under preparation).
78. Chaudhry, M. H. and Cass, D. E., "Propagation of Waves Generated by Rapid Movement of Downie Slide into Revelstoke Reservoir," *Report No. 809, Hydroelectric Design Division, B.C. Hydro and Power Authority*, Vancouver, B.C., Canada, Sept. 1976.
79. Raney, D. C. and Butler, H. L., "A Numerical Model for Predicting the Effects of Landslide-Generated Water Waves," Research Report H-75-1, U.S. Army Engineer Waterways Experiment Station, Vicksburg, Miss., Feb. 1975.
80. Koutitas, C. G., "Finite Element Approach to Waves due to Landslides," *Jour., Hyd. Div., Amer. Soc. of Civ. Engrs.*, vol. 103, Sept. 1977, pp. 1021-1029.
81. Chaudhry, M. H. and Kao, K. H., "G. M. Shrun Generating Station: Tailrace Surges and Operating Guidelines During High Tailwater Levels," *British Columbia Hydro and Power Authority*, Vancouver, B.C., November 1976.

APPENDIX A

FORMULAS AND DESIGN CHARTS FOR PRELIMINARY ANALYSIS

Design charts and approximate formulas are presented in this appendix. These may be used for quick computations during the preliminary design stages when a large number of alternatives are considered to have an economical design or to approximately select the parameters of a system for a detailed analysis.

A-1 EQUIVALENT PIPE

If the diameter, wall thickness, or wall material varies along the length of a pipeline, then the pipeline may be replaced by an "equivalent pipe" for an approximate analysis. By using an equivalent pipe, the partial wave reflections and the spatial variation of the friction losses and of the elastic and inertial effects are not correctly taken into consideration. The approximation is useful, however, and gives satisfactory results provided that the changes in the properties of the original pipeline are minor.

The total friction losses, the wave travel time, and the inertial effects of the equivalent pipe should be equal to those of the pipeline. These characteristics for the equivalent pipe of a pipeline having n pipes in series may be determined from the following equations:

$$A_e = \frac{L_e}{\sum_{i=1}^{n} \frac{L_i}{A_i}} \tag{A-1}$$

$$a_e = \frac{L_e}{\sum_{i=1}^{n} \frac{L_i}{a_i}} \tag{A-2}$$

$$f_e = \frac{D_e A_e^2}{L_e} \sum_{i=1}^{n} \frac{f_i L_i}{D_i A_i^2} \tag{A-3}$$

in which a is the waterhammer wave velocity, and A, L, D, and f are the cross-sectional area, length, diameter, and Darcy-Weisbach friction factor for the pipe, respectively. The subscripts e and i refer to the equivalent pipe and to the ith pipe of the pipeline.

A-2 MAXIMUM PRESSURE DUE TO VALVE CLOSURE

Figures A-1 and A-2 show the maximum pressure rise above the upstream reservoir level at the valve and at the midlength of a pipeline caused by the closure of a downstream valve discharging into atmosphere. The valve closure is assumed to be *uniform*, i.e., valve-opening versus time curve is a straight line.

The following notation is used:

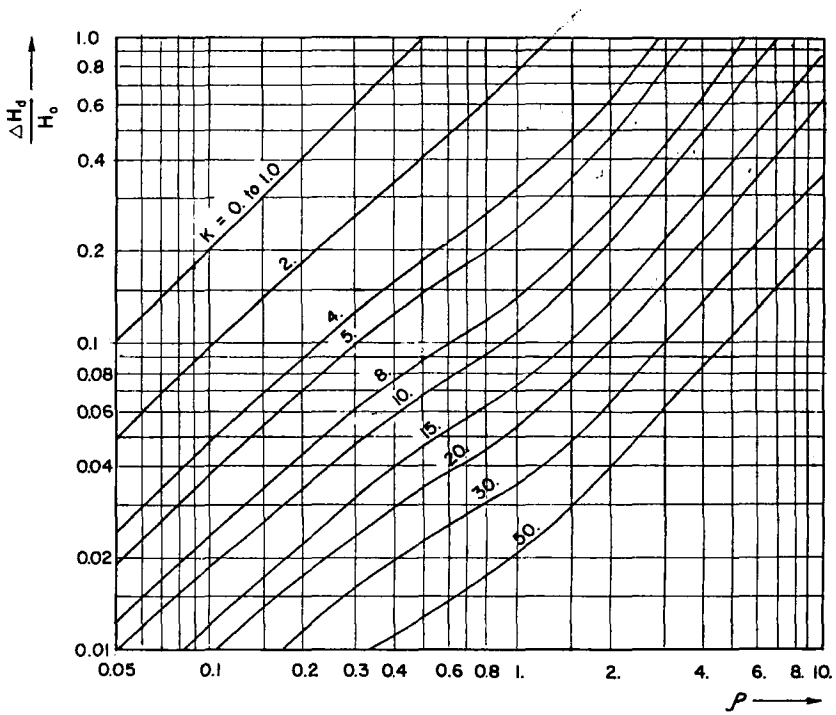

(a) At valve

Figure A-1. Maximum pressure rise due to uniform valve closure; frictionless system ($h = 0$).

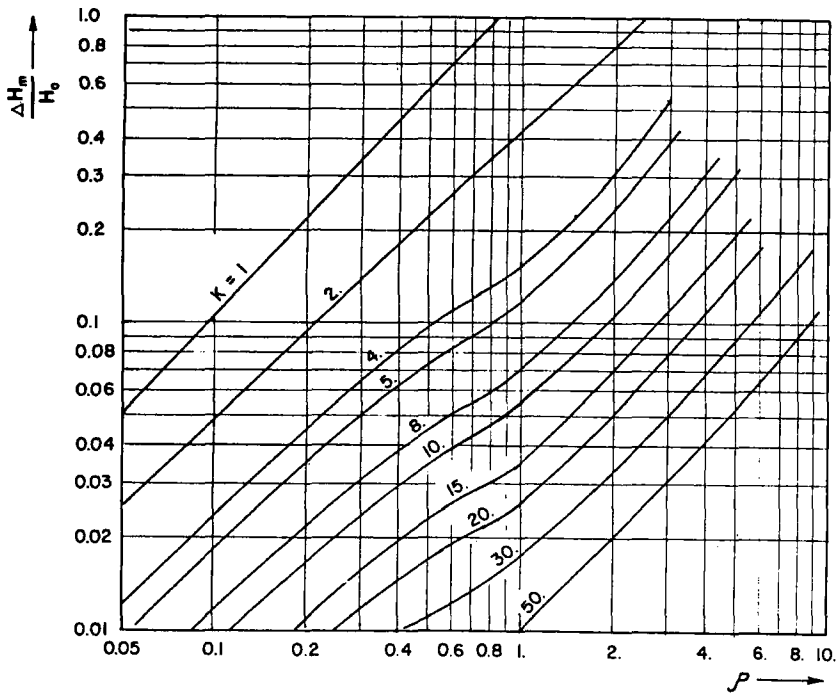

(b) At mid-length

Figure A-1. (*Continued*)

$$\rho = \frac{aV_o}{2gH_o} = \frac{L V_o / g}{2L/a} = \frac{T_w}{T_r}$$ cotiempo agua / tiempo reflexión

$$k = \frac{T_c}{(2L/a)}$$

a = waterhammer wave velocity
g = acceleration due to gravity
H_o = static head (elevation of the reservoir level - elevation of the valve)
L = length of the pipeline
V_o = initial steady-state velocity in the pipeline
T_c = valve closure time
ΔH_m = maximum pressure rise at the midlength *above* the reservoir level
ΔH_d = maximum pressure rise at the valve *above* the reservoir level
h_{f_o} = initial steady-state head loss in the pipeline corresponding to velocity V_o

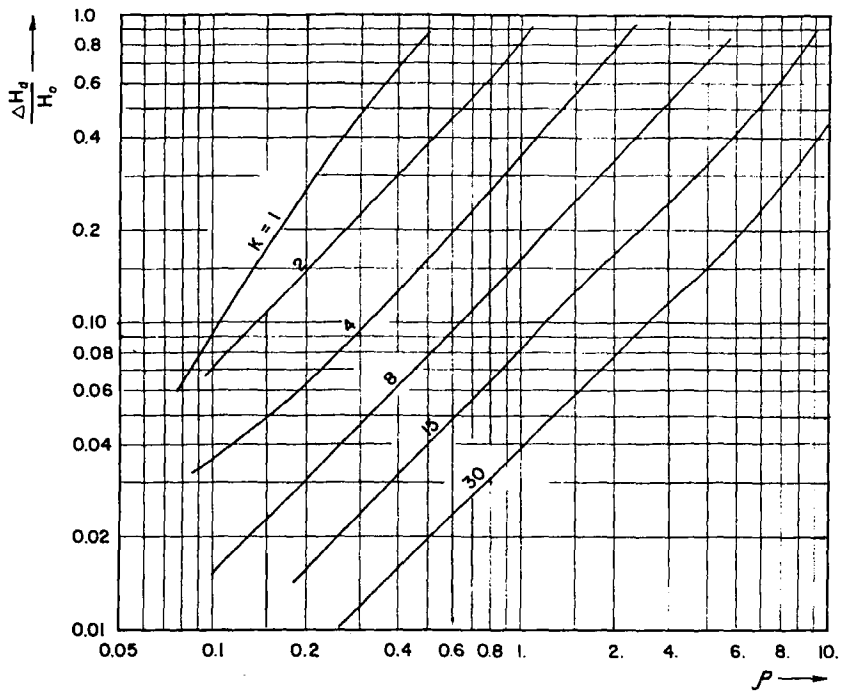

(a) At Valve

Figure A-2. Maximum pressure rise due to uniform valve closure; friction losses taken into consideration ($h = 0.25$).

$h = h_{f_o}/H_o$

H_{max} = maximum pressure head = $H_o + \Delta H_d$ at the valve
$= H_o + \Delta H_m$ at midlength of the pipeline.

A-3 MINIMUM PRESSURE DUE TO VALVE OPENING

Minimum pressure head, H_{min}, at the valve caused by *uniformly* opening the valve from the completely closed position may be determined from the following equation:[1]

$$H_{min} = H_o\,(-k + \sqrt{k^2 + 1})^2 \qquad \text{(A-4)}$$

in which $k = LV_f/(gH_oT_o)$; L = length of the pipeline; V_f = final steady-state velocity in the pipeline; T_o = valve opening time; and H_o = static head. The minimum pressure occurs $2L/a$ seconds after the start of the valve movement.

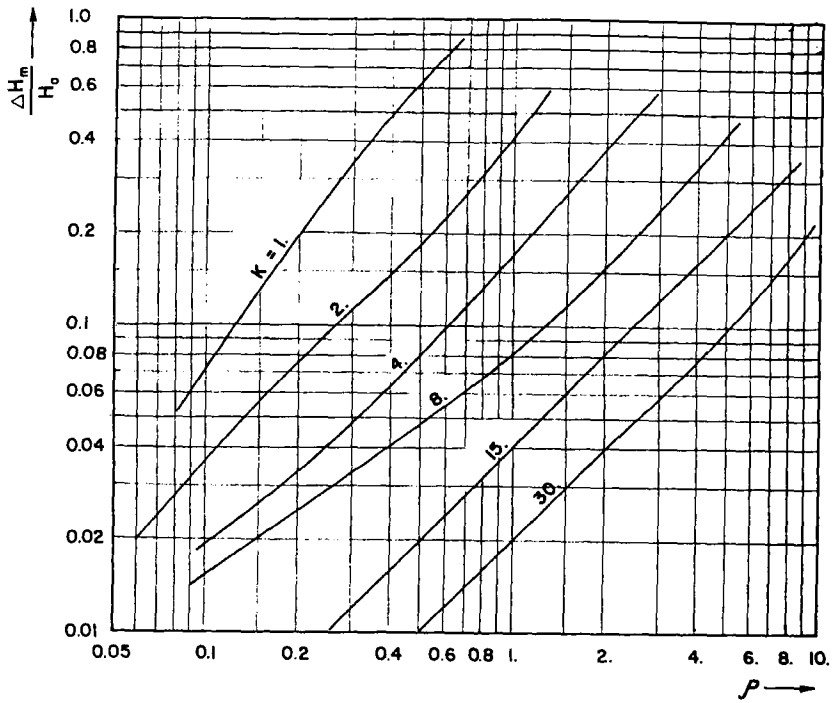

(b) At midlength

Figure A-2. (*Continued*)

Equation A-4 is applicable if $T_o > 2L/a$. For $T_o \leqslant 2L/a$,

$$H_{min} = H_o - \frac{a}{g}\,\Delta V \qquad \text{(A-5)}$$

in which ΔV = change in the flow velocity due to valve opening.

A-4 POWER FAILURE TO CENTRIFUGAL PUMPS

Graphs[2] are presented in Figs. A-3 through A-7 for the minimum and maximum pressure heads at the pump, and at the midlength of a pipeline, and for the time of flow reversal following power failure to the centrifugal pump units. The graphs are applicable to pumps with specific speed of less than 49 (SI units), i.e., 2700 (gpm units); they are not applicable to systems in which there is a valve closure during the transient state or to systems that contain waterhammer control devices other than large surge tanks. In the analysis, the latter are considered as the upstream reservoirs.

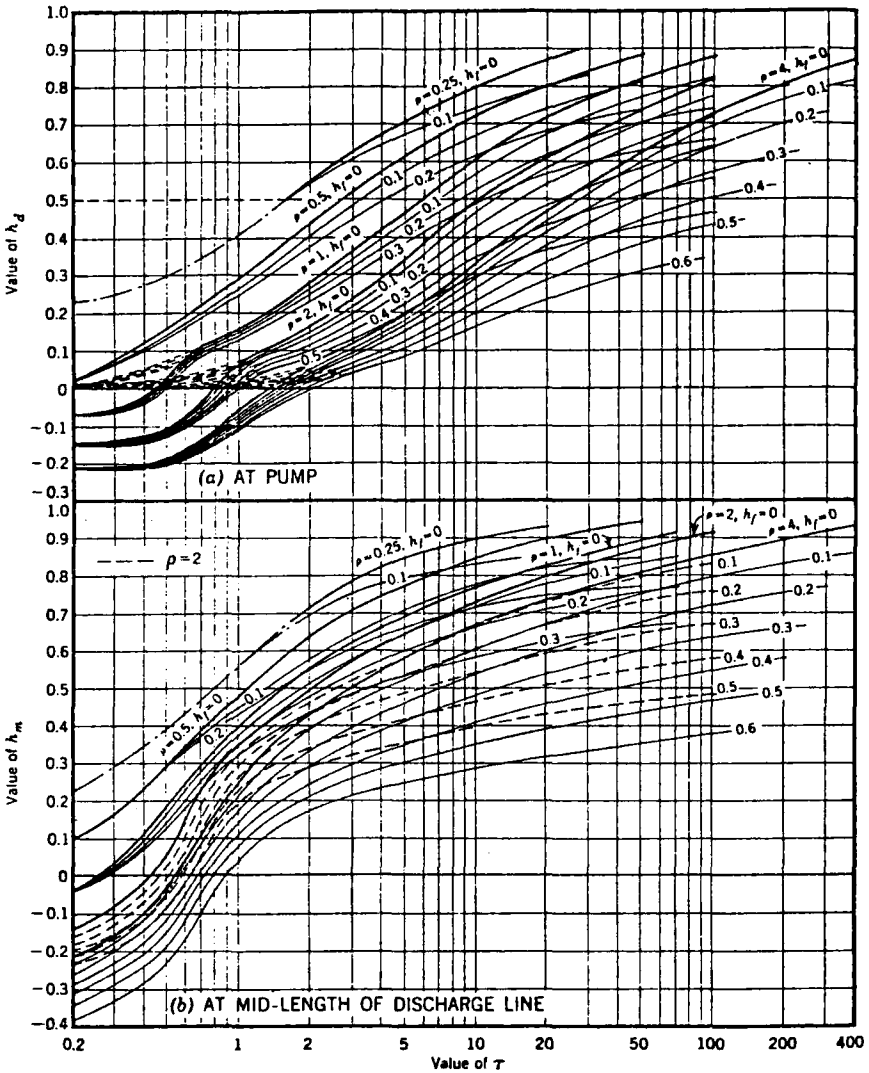

Figure A-3. Minimum head following power failure. (After Kinno and Kennedy[2])

The following notation is used:

a = waterhammer wave velocity
E_R = pump efficiency at rated conditions
g = acceleration due to gravity
H_R = rated head of the pump
H_f = friction losses in the discharge line

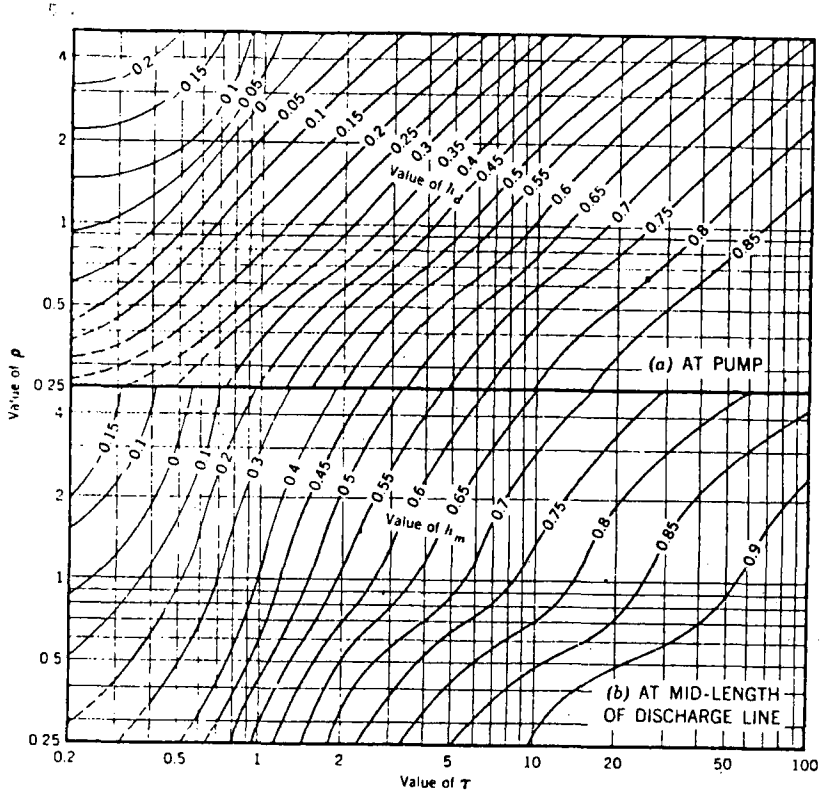

Figure A-4. Minimum head following power failure, no friction losses. (After Kinno and Kennedy[2])

$h_f = H_f/H_R$
H_d = minimum transient-state head at the pump
$h_d = H_d/H_R$
H_m = minimum transient-state head at midlength of the discharge line
$h_m = H_m/H_R$
H_{mr} = maximum transient-state head at midlength of the discharge line
$h_{mr} = H_{mr}/H_R$
H_r = maximum transient-state head at the pump
$h_r = H_r/H_R$

$$k = \frac{892\,770\,H_R Q_R}{E_R\,WR^2\,N_R^2} \text{ (in SI units)*}$$

*Q_R, H_R, WR^2, and N_R are in m^3/s, m, kg m^2, and rpm, respectively; and E_R is in the fractional form, e.g., 0.8.

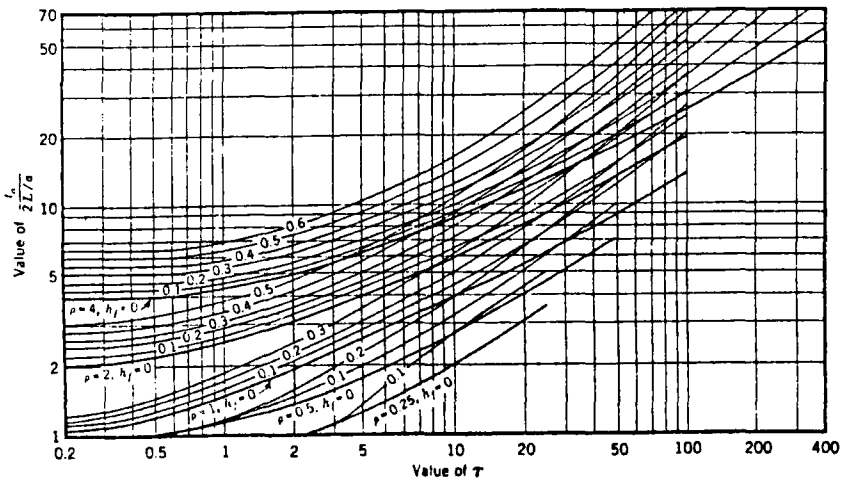

Figure A-5. Time of flow reversal at pump following power failure. (After Kinno and Kennedy[2])

$$= \frac{183\,200\,H_R\,Q_R}{E_R\,WR^2\,N_R^2} \text{ (in English units)*}$$

L = length of the discharge line
N_R = rated pump speed
Q_R = rated pump discharge
t = time
t_o = elapsed time from power failure to flow reversal at the pump
V_R = fluid velocity in the discharge line for rated pump discharge
WR^2 = moment of inertia of rotating components of the pump and motor, and entrained fluid

$$\rho = aV_R/(2gH_R)$$

$$\tau = \frac{1}{\frac{2L}{a}k}$$

A-5 AIR CHAMBERS

Charts[3] are presented in Fig. A-8 for the maximum upsurge and downsurge at the pump end, at the midlength, and at the quarter point on the reservoir side of a discharge line following power failure to the pumps. These charts may be used to determine the required air volume for a discharge line.

*Q_R, H_R, WR^2, and N_R are in ft^3/sec, ft, lb-ft^2, and rpm, respectively; and E_R is in the fractional form, e.g., 0.8.

The charts are based on the following assumptions:

1. Air chamber is located near the pump.
2. Check valve closes simultaneously with the power failure.
3. Darcy-Weisbach formula for computing the steady-state friction losses is valid during the transient state.
4. The absolute pressure head, H^*, and the volume of air, C, inside the air chamber follow the relationship $H^*C^{1.2}$ = constant.

The following notation is used:

a = waterhammer wave velocity
V_o = initial steady-state velocity in the discharge pipe
g = acceleration due to gravity
H_o = static head (Elevation of the reservoir - Elevation of the air chamber)

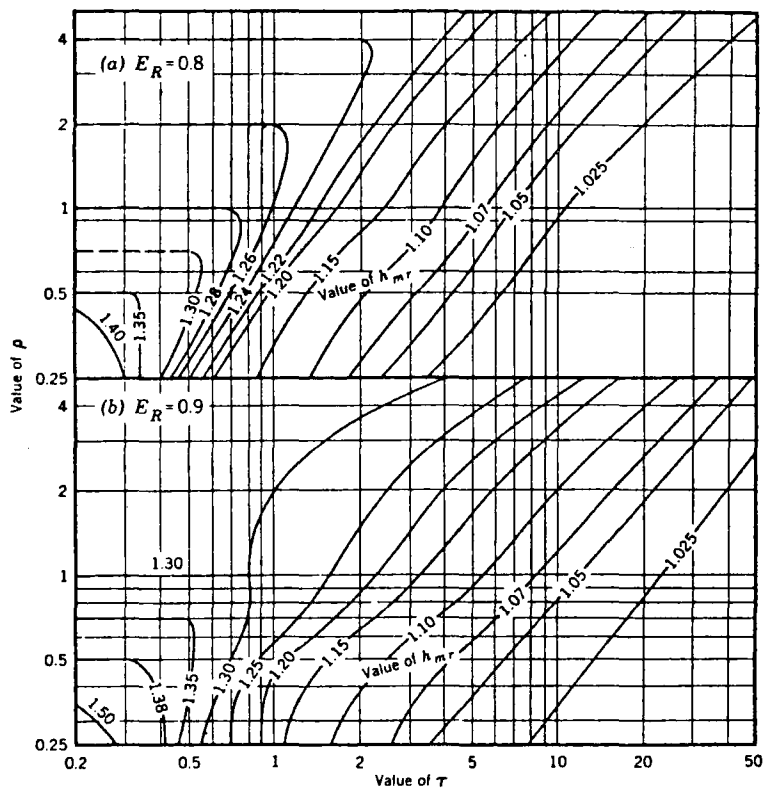

(a) At mid-length of discharge line

Figure A-6. Maximum head following power failure. (After Kinno and Kennedy[2])

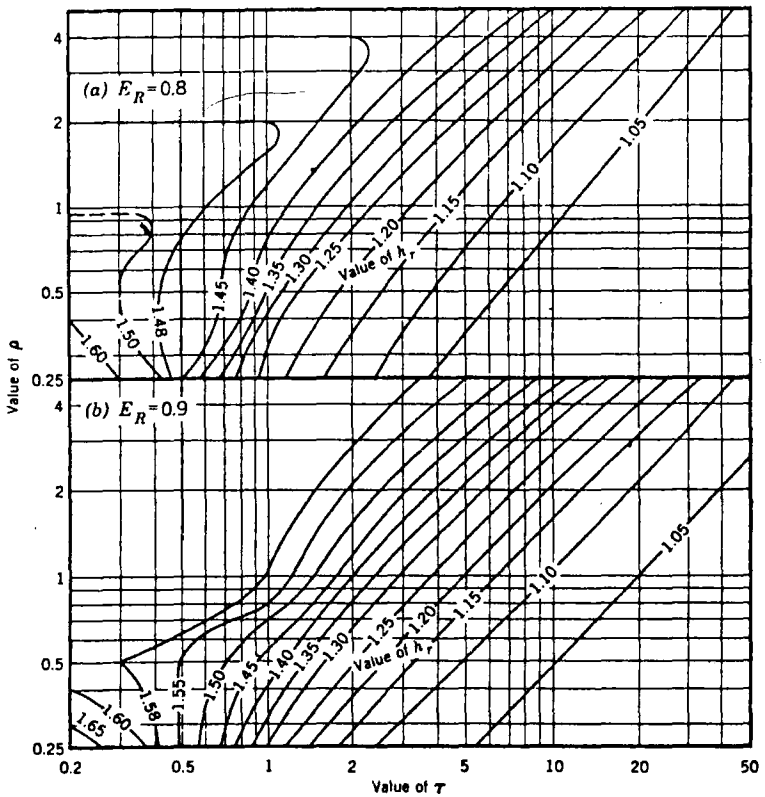

(b) At pump

Figure A-6. (*Continued*)

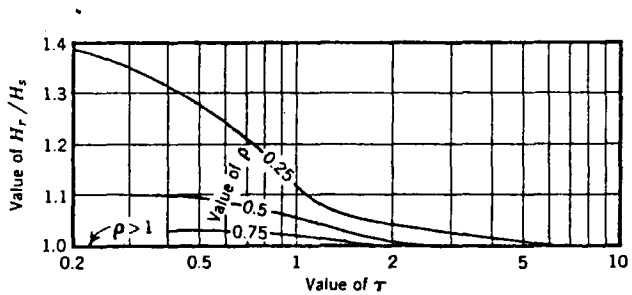

Figure A-7. Maximum head at pump if reverse rotation of pump is prevented. (After Kinno and Kennedy[2])

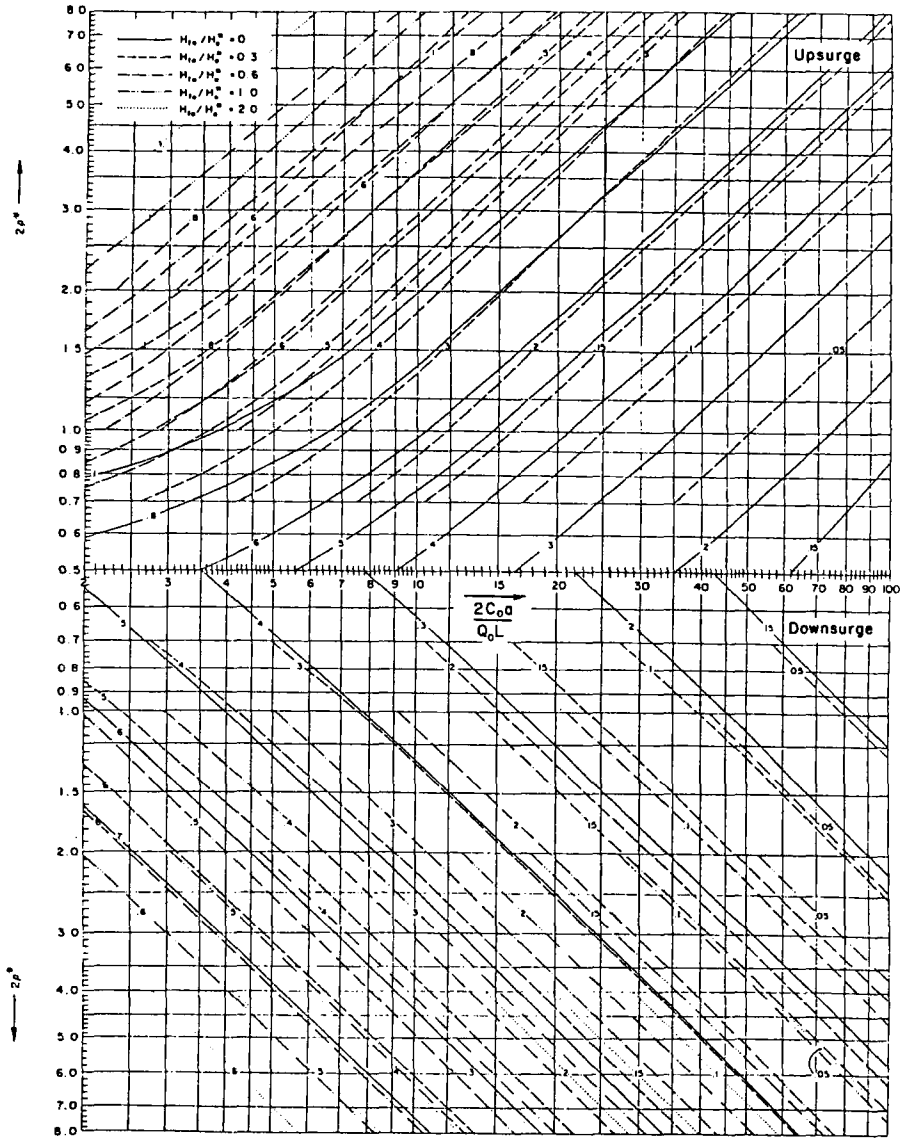

(a) At pump

Figure A-8. Maximum upsurge and downsurge in a discharge line having an air chamber. Numbers on the curves refer to the maximum downsurge or maximum upsurge divided by H_O^*. (After Ruus[3])

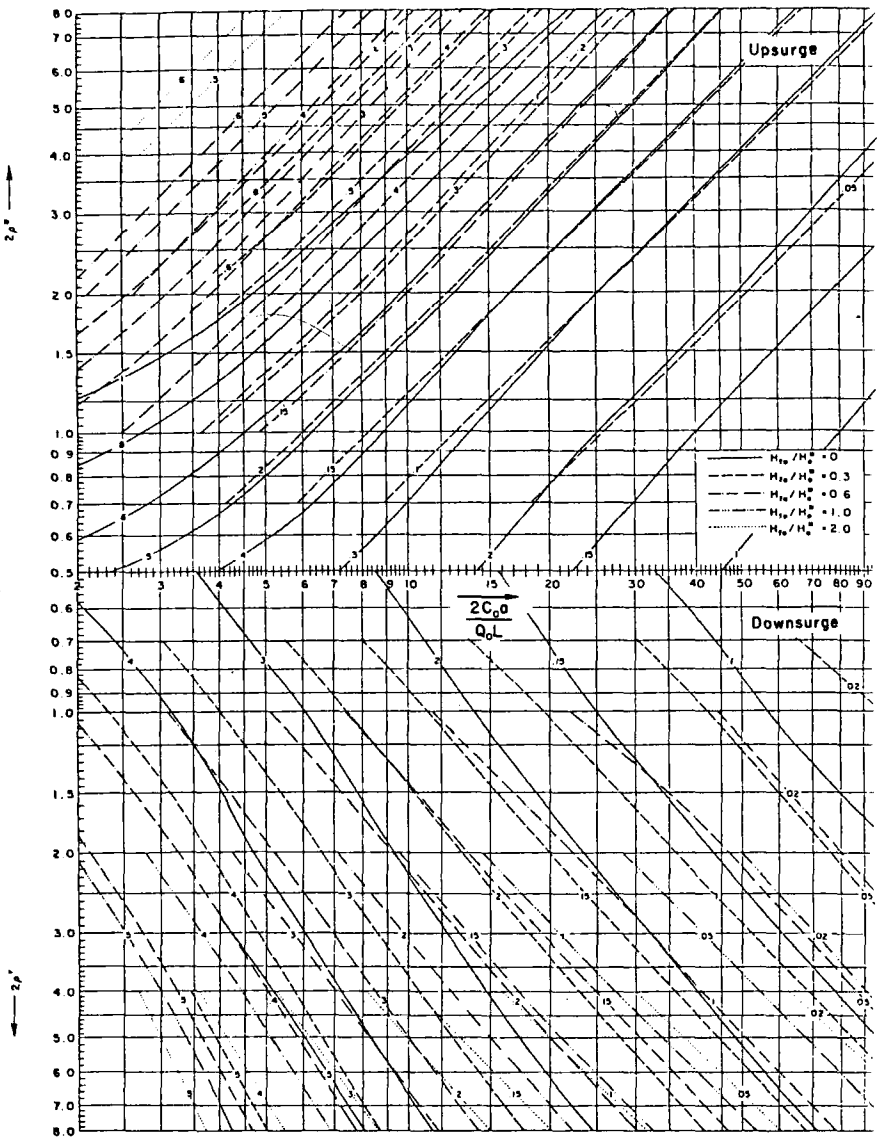

(b) At mid-length of discharge line

Figure A-8. (*Continued*)

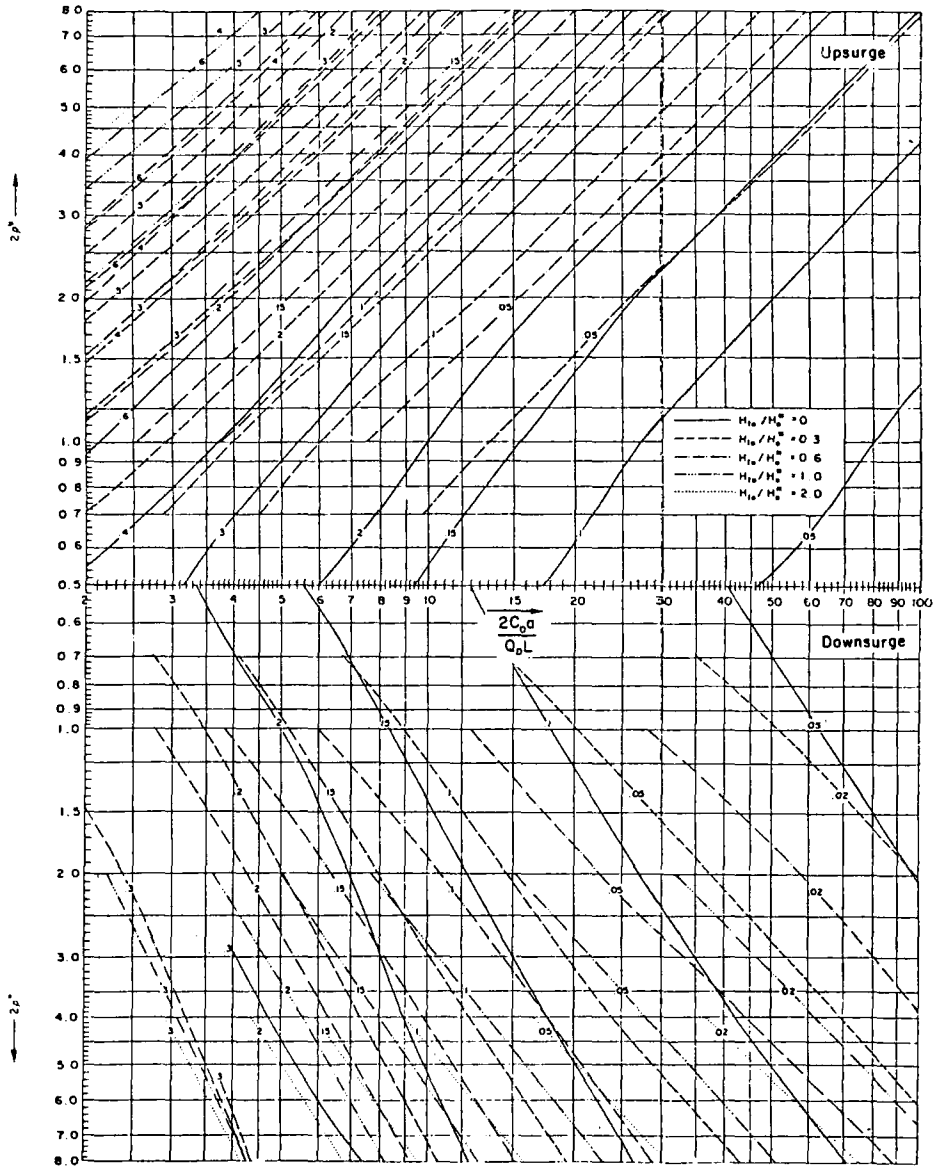

(c) At quarter point of discharge line (reservoir side)

Figure A-8. (*Continued*)

H_o^* = absolute static head = H_o + 10.36 (in the English units, H_o + 34)

$$\rho^* = \frac{aV_o}{2g(H_o^* + H_{fo})}$$

H_{fo} = initial steady-state head losses in the discharge line = $fLV_o^2/(2gD)$
C_o = initial steady-state air volume in the chamber
Q_o = initial steady-state discharge in the pipe
L = length of the discharge line
D = diameter of the discharge line.

The maximum *upsurge* and *downsurge* are *above* and *below* the downstream reservoir level, and the absolute pressure heads are obtained by subtracting or adding the downsurge or upsurge to the reservoir level plus the barometric head.

The air-chamber size for a pipeline may be determined as follows: For the maximum allowable downsurge at any critical point along the pipeline—e.g., a vertical bend—determine $2C_oa/(Q_oL)$ from Fig. A-8. Linear interpolation may be used if the bend is not located either at the midlength or at the quarterpoint. From the expression $2C_oa/(Q_oL)$, compute the minimum initial steady-state air volume, $C_{o\,\min}$. This volume corresponds to the upper emergency level in the air chamber. To this minimum air volume, add the volume of the chamber between the upper and the lower emergency levels—for example, 10 percent of $C_{o\,\min}$ for large size chambers and 20 percent for small chambers. For this new air volume, $C_{o\,\max}$, determine the maximum downsurge at the pump end from Fig. A-8a, and then determine the absolute minimum head, $H_{\min}$, at the pump end by subtracting the maximum downsurge at the pump from the absolute static head, H_o^*. The maximum transient-state air volume, $C_{\max}$, may then be determined from the equation

$$C_{\max} = C_{o\,\max}\left(\frac{H_o^* + H_{fo}}{H_{\min}^*}\right)^{1/1.2} \tag{A-6}$$

in which $H_o^* + H_{fo}$ is the absolute initial steady-state head. To prevent air from entering the pipeline, a suitable amount of submergence should be provided at the chamber bottom. For this purpose, the chamber volume may be selected as about 120 percent of the maximum air volume, $C_{\max}$, for small air chambers and about 110 percent, for large air chambers.

A-6 SIMPLE SURGE TANKS

Figure A-9 shows the maximum upsurge in a simple surge tank following uniform gate closure from 100 percent to 0 percent, and Fig. A-10 shows the maximum downsurge in a tank following uniform gate opening from 0 to 100 percent and from 50 to 100 percent.[4]

In these figures, in region A, only one maximum occurs and that also after the end of the gate movement; in region B, the largest of the maxima is the second one and that occurs after the end of the gate operation; in region C, the largest

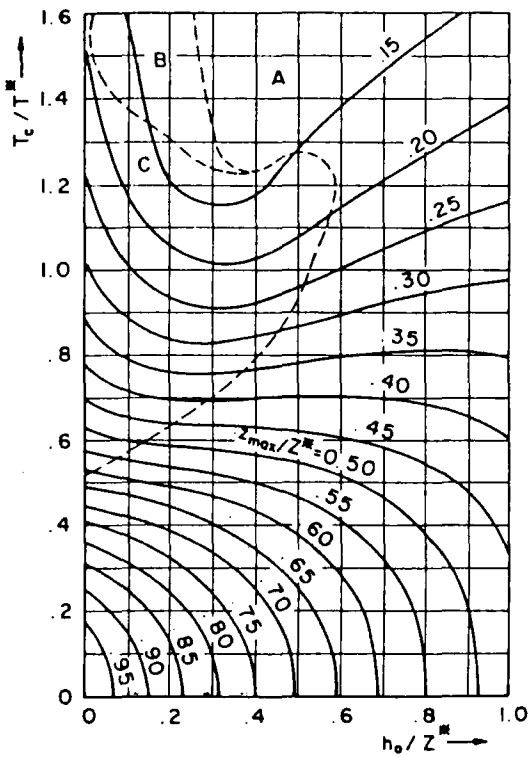

Figure A-9. Maximum upsurge in a simple surge tank for uniform gate closure from 100 to 0 percent. (After Ruus and El-Fitiany[4])

of the two maxima is the first one and that occurs prior to the end of the gate movement.

The following notation is used in these figures:

A_t = cross-sectional area of the tunnel
A_s = cross-sectional area of the surge tank
g = acceleration due to gravity
h_o = head losses plus velocity head in the tunnel corresponding to a steady flow of Q_o
L = length of the tunnel from the upstream reservoir to the surge tank
T_c = gate-closing time
T_o = gate-opening time
$T^* = 2\pi\sqrt{LA_s/(gA_t)}$ = period of surge oscillations following instantaneously stopping a flow of Q_o in a corresponding frictionless system

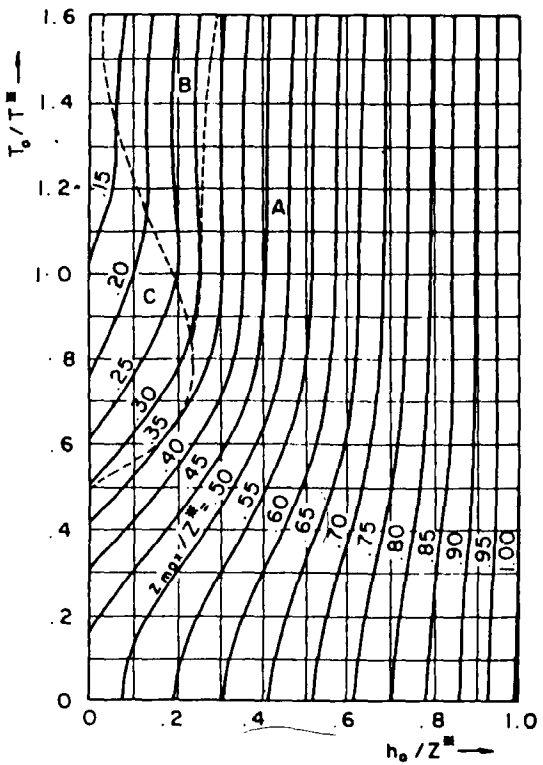

(a) 50 to 100 Percent

Figure A-10. Maximum downsurge in a simple surge tank for uniform gate opening from 0 to 100 percent and from 50 to 100 percent. (After Ruus and El-Fitiany[4])

Z_{max} = maximum upsurge (or *downsurge*) *above* (or *below*) the upstream reservoir level

$Z^* = Q_o\sqrt{L/(gA_tA_s)}$ = maximum surge following instantaneously stopping a flow of Q_o in a corresponding frictionless system.

A-7 SURGES IN OPEN CHANNELS

The height and the celerity of a surge in a trapezoidal or rectangular open channel[5] produced by instantaneously reducing flow at the downstream end of the channel may be computed from Fig. A-11. The height of this wave is reduced as it propagates upstream. Figure A-12 may be used to determine the wave height at any location along the channel.

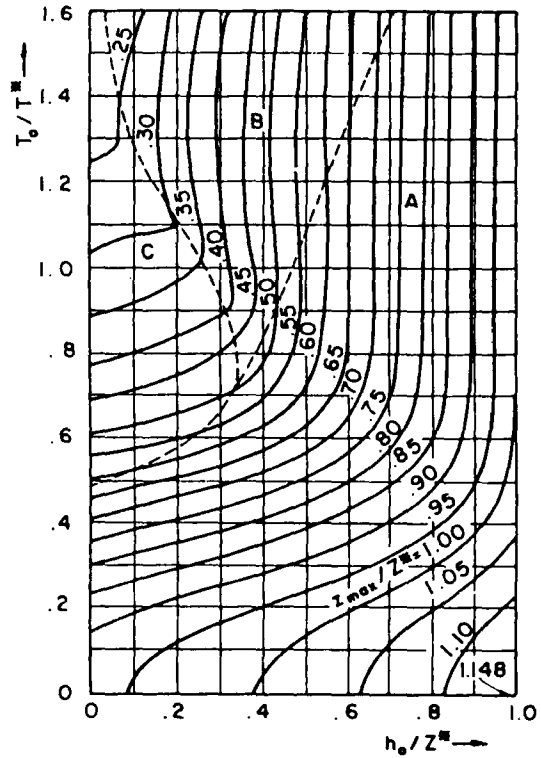

(b) 0 to 100 Percent

Fig. A-10. (Continued)

For the selection of the top elevation of the channel banks, the water surface behind the wave front may be assumed horizontal (see Section 7.2).

The following notation is used in Figs. A-11 and A-12:

b_o = bottom width of channel
c = celerity of surge wave
F_o = Froude number corresponding to initial steady-state conditions, $V_o/\sqrt{gy_o}$
g = acceleration due to gravity
k = dimensionless parameter = $b_o/(my_o)$
K = dimensionless parameter = $1 + 1/(1 + k)$
m = channel side slope, m horizontal to 1 vertical;
Q_o = initial steady-state discharge
Q_f = final steady-state discharge
S_o = channel bottom slope

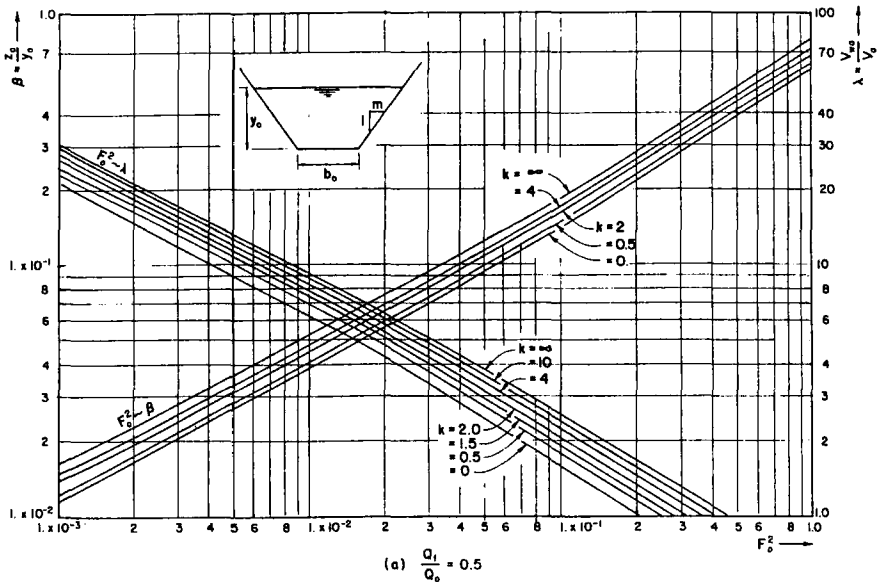

Figure A-11. Height and absolute velocity of a surge in a rectangular or trapezoidal open-channel caused by instantaneous flow reduction at the downstream end. (After Wu[5])

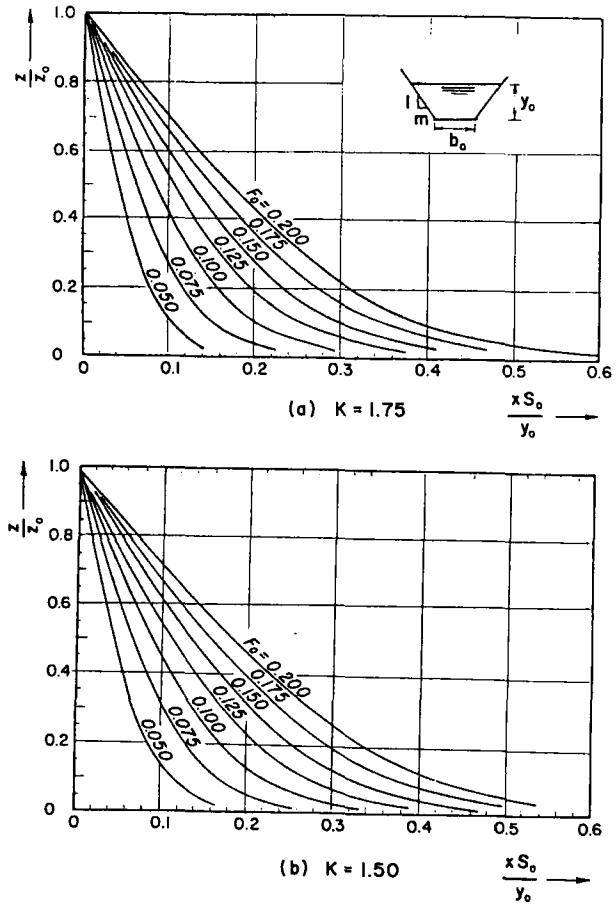

Figure A-12. Variation of wave height of a positive surge propagating in a trapezoidal open channel. (After Wu[5])

V_o = initial steady-state flow velocity
V_w = absolute wave velocity = $V + c$
x = distance along the channel bottom from the control gates
y_o = initial steady-state flow depth
z = surge wave height at distance x
z_o = initial surge wave height at downstream end
β = dimensionless parameter = z_o/y_o
λ = dimensionless parameter = V_{wo}/V_o.

REFERENCES

1. Parmakian, J., *Waterhammer Analysis*, Dover Publications, Inc., New York, 1963, p. 72.
2. Kinno, H. and Kennedy, J. F., "Water-Hammer Charts for Centrifugal Pump Systems," *Jour., Hyd. Div., Amer. Soc. of Civ. Engrs.*, vol. 91, May 1965, pp. 247–270.
3. Ruus, E., "Charts for Waterhammer in Pipelines with Air Chamber," *Canadian Jour. Civil Engineering*, vol. 4, no. 3, September 1977.
4. Ruus, E. and El-Fitiany, F. A., "Maximum Surges in Simple Surge Tanks," *Canadian Jour. Civil Engineering*, vol. 4, no. 1, 1977, pp. 40–46.
5. Wu, H., "Dimensionless Ratios for Surge Waves in Open Canals," thesis presented to the University of British Columbia in partial fulfillment of the requirements for the degree of master of applied science, April 1970.

APPENDIX B*

B-1 PROGRAM LISTING

```
C***  ANALYSIS OF TRANSIENTS IN A PIPELINE CAUSED BY OPENING OR
C        CLOSING OF A VALVE
C
      REAL L
      DIMENSION Q(10,100),H(10,100),QP(10,100),HP(10,100),CA(10),F(10),
     1 CF(10),AR(10),A(10),L(10),N(10),D(10),Y(20),HMAX(10,100),
     2  HMIN(10,100)
      DATA G/9.81/
C
C     READING AND WRITING OF INPUT DATA
C
C     GENERAL DATA
      READ(5,10) NP,NRLP,IPRINT,QO,HRES,TLAST
10    FORMAT(3I3,5F10.2)
      WRITE(6,20) NP,NRLP,QO,HRES,TLAST
20    FORMAT(8X,'NUMBER OF PIPES =',I3/8X,'NUMBER OF REACHES ON LAST PIP
     1E =',I3/8X,'STEADY STATE DISCH. ',F7.3,' M3/SEC' /8X,'RESERVOIR LE
     2VEL =',F7.1, ' M'/8X,'TIME FOR WHICH TRANSIENTS ARE TO BE COMPUTED
     3 =',F7.1, ' SEC'/)
C     DATA FOR VALVE
      READ(5,25) M,TV,DXT,TAUO,TAUF,(Y(I),I=1,M)
25    FORMAT(I2,F8.2,3F10.2/12F6.2)
      WRITE(6,27) M,TV,DXT,(Y(I),I=1,M)
27    FORMAT(8X,'NUMBER OF POINTS ON TAU VS TIME CURVE =',I2/8X,
     1'VALVE OPERATION TIME =',F8.2,' SEC'/8X,'TIME INTERVAL FOR STORING
     2 TAU CURVE =',F6.3,' SEC'/8X,'STORED TAU VALUES'/8X,15F8.3/)
C     DATA FOR PIPES
      READ(5,30) (L(I),D(I),A(I),F(I),I=1,NP)
30    FORMAT(4F10.3)
      WRITE(6,40)
40    FORMAT(/8X,'PIPE NO', 5X, 'LENGTH',5X,'DIA',5X,'WAVE VEL.',5X,'FRI
     2C FACTOR'/21X,'(M)',7X,'(M)',6X,'(M/SEC)'/)
      WRITE(6,50)(I,L(I),D(I),A(I),F(I),I=1,NP)
50    FORMAT(10X,I3,6X,F7.1,3X,F5.2,5X,F7.1,11X,F5.3)
      DT=L(NP)/(NRLP*A(NP))
      WRITE(6,51)
51    FORMAT(/8X,'PIPE NO',5X,'ADJUSTED WAVE VEL'/25X,'(M/SEC)'/)
C     CALCULATION OF PIPE CONSTANTS
      DO 60 I=1,NP
      AR(I)=0.7854*D(I)**2
      AUNADJ=A(I)
      AN=L(I)/(DT*A(I))
      N(I)=AN
      AN1=N(I)
      IF((AN-AN1).GE.0.5) N(I)=N(I)+1
      A(I)=L(I)/(DT*N(I))
      WRITE(6,55) I,A(I)
55    FORMAT(10X,I3,12X,F7.1)
56    CA(I)=G*AR(I)/A(I)
      CF(I)=F(I)*DT/(2.*D(I)*AR(I))
      F(I)=F(I)*L(I)/(2.*G*D(I)*N(I)*AR(I)**2)
```

*The author or publisher shall have no liability, consequential or otherwise, of any kind arising from the use of the computer programs or any parts thereof presented in Appendixes B through D.

```
60    CONTINUE
C
C     CALCULATION OF STEADY STATE CONDITIONS
      H(1,1)=HRES
C
      DO 80 I=1,NP
      NN=N(I)+1
      DO 70 J=1,NN
      H(I,J)=H(I,1)-(J-1)*F(I)*Q0**2
      Q(I,J)=Q0
70    CONTINUE
      H(I+1,1)=H(I,NN)
80    CONTINUE
      NN=N(NP)+1
      HS=H(NP,NN)
      QS=Q0
      DO 85 I=1,NP
      NN=N(I)+1
      DO 85 J=1,NN
      HMAX(I,J)=H(I,J)
      HMIN(I,J)=H(I,J)
85    CONTINUE
      T=0.0
      TAU=TAU0
      WRITE(6,88)
88    FORMAT(/8X,'TIME',2X,'TAU',2X,'PIPE',7X,'HEAD (M)',7X,'DISCH. ',
     1'(M3/S)'/20X,'NO',5X,'(1)',5X,'(N+1)',5X,'(1)',5X,'(N+1)'/)
90    K=0
      I=1
      NN=N(I)+1
      WRITE(6,100) T,TAU,I,H(I,1),H(I,NN),Q(I,1),Q(I,NN)
100   FORMAT(F12.1,F6.3,I4,2F9.2,F9.3,F10.3)
      IF (NP.EQ.1) GO TO 150
      DO 140 I=2,NP
      NN=N(I)+1
      WRITE(6,120) I,H(I,1),H(I,NN),Q(I,1),Q(I,NN)
120   FORMAT(20X,I2,2F9.2,F9.3,F10.3)
140   CONTINUE
150   T=T+DT
      K=K+1
      IF(T.GT.TLAST) GO TO 240
C
C     UPSTREAM RESERVOIR
C
      HP(1,1)=HRES
      CN=Q(1,2)-H(1,2)*CA(1)-CF(1)*Q(1,1)*ABS(Q(1,1))
      QP(1,1)=CN+CA(1)*HRES
C
C     INTERIOR POINTS
C
      DO 170 I=1,NP
      NN=N(I)
      DO 160 J=2,NN
      CN=Q(I,J+1)-CA(I)*H(I,J+1)-CF(I)*Q(I,J+1)*ABS(Q(I,J+1))
      CP=Q(I,J-1)+CA(I)*H(I,J-1)-CF(I)*Q(I,J-1)*ABS(Q(I,J-1))
      QP(I,J)=0.5*(CP+CN)
      HP(I,J)=(CP-QP(I,J))/CA(I)
```



```
160   CONTINUE
170   CONTINUE
C
C     SERIES JUNCTION
C
      NP1=NP-1
      IF(NP.EQ.1) GO TO 178
      DO 175 I=1,NP1
      N1= N(I)
      NN=N(I)+1
      CN=Q(I+1,2)-CA(I+1)*H(I+1,2)-CF(I+1)*Q(I+1,2)*ABS(Q(I+1,2)
     1)
      CP=Q(I,N1)+CA(I)*H(I,N1)-CF(I)*Q(I,N1)*ABS(Q(I,N1))
      HP(I,NN)=(CP-CN)/(CA(I)+CA(I+1))
      HP(I+1,1)=HP(I,NN)
      QP(I,NN)=CP-CA(I)*HP(I,NN)
      QP(I+1,1)=CN+CA(I+1)*HP(I+1,1)
175   CONTINUE
C
C     VALVE AT DOWNSTREAM END
C
178   NN=N(NP)+1
      CP=Q(NP,NN-1)+CA(NP)*H(NP,NN-1)-CF(NP)*Q(NP,NN-1)*ABS(Q(NP,
     1 NN-1))
      IF(T.GE.TV) GO TO 180
      CALL PARAB(T,DXT,Y,TAU)
      GO TO 190
180   TAU=TAUF
      IF (TAU.LE.0.0) GO TO 200
190   CV=(QS*TAU)**2/(HS*CA(NP))
      QP(NP,NN)=0.5*(-CV+SQRT(CV*CV+4.*CP*CV))
      HP(NP,NN)=(CP-QP(NP,NN))/CA(NP)
      GO TO 210
200   QP(NP,NN)=0.0
      HP(NP,NN)=CP/CA(NP)
C
C     STORING VARIABLES FOR NEXT TIME STEP
C
210   DO 230 I=1,NP
      NN=N(NP)+1
      DO 220 J=1,NN
      Q(I,J)=QP(I,J)
      H(I,J)=HP(I,J)
      IF (H(I,J).GT.HMAX(I,J)) HMAX(I,J)=H(I,J)
      IF (H(I,J).LT.HMIN(I,J)) HMIN(I,J)=H(I,J)
220   CONTINUE
230   CONTINUE
      IF(K.EQ.IPRINT) GO TO 90
      GO TO 150
240   WRITE(6,250)
250   FORMAT(/8X,'PIPE NO',3X,'SECTION NO',3X,'MAX PRESS.',3X,
     1 'MIN. PRESS.'/)
      DO 270 I=1,NP
      NN=N(I)+1
      DO 270 J=1,NN
      WRITE(6,260) I,J,HMAX(I,J),HMIN(I,J)
260   FORMAT(9X,I2,13X,I2,2F13.2)
```

```
 270   CONTINUE
       STOP
       END
       SUBROUTINE PARAB(X,DX,Y,Z)
       DIMENSION Y(20)
       I=X/DX
       R=(X-I*DX)/DX
       IF(I.EQ.0) R=R-1.
       I=I+1
       IF(I.LT.2) I=2
       Z=Y(I)+0.5*R*(Y(I+1)-Y(I-1)+R*(Y(I+1)+Y(I-1)-2.*Y(I)))
       RETURN
       END
```

B-2 INPUT DATA

```
002002002   1.        67.7        10.
07  6.       1.         1.         0.
  1.    .9    .7    .5    .3    .1    .0
  550.      .75       1100.      .010
  450.      .60        900.      .012
```

B-3 PROGRAM OUTPUT

```
NUMBER OF PIPES =  2
NUMBER OF REACHES ON LAST PIPE =  2
STEADY STATE DISCH.    1.000 M3/SEC
RESERVOIR LEVEL =    67.7 M
TIME FOR WHICH TRANSIENTS ARE TO BE COMPUTED =    10.0 SEC

NUMBER OF POINTS ON TAU VS TIME CURVE = 7
VALVE OPERATION TIME =     6.00 SEC
TIME INTERVAL FOR STORING TAU CURVE = 1.000 SEC
STORED TAU VALUES
   1.000    0.900    0.700    0.500    0.300    0.100    0.0

PIPE NO      LENGTH      DIA AREA  WAVE VEL.      FRIC FACTOR
              (M)          (M)      (M/SEC)

    1         550.0     0.75 0.442  1100.0            0.010
    2         450.0     0.60 0.283   900.0            0.012

PIPE NO      ADJUSTED WAVE VEL
              (M/SEC)

    1           1100.0
    2            900.0
```


TIME	TAU	PIPE NO	HEAD (M) (I)	HEAD (M) (N+1)	DISCH. (M3/S) (I)	DISCH. (M3/S) (N+1)
0.0	1.000	1	67.70	65.78	1.000	1.000
		2	65.78	60.05	1.000	1.000
0.5	0.963	1	67.70	65.78	1.000	1.000
		2	65.78	63.46	1.000	0.989
1.0	0.900	1	67.70	68.73	1.000	0.988
		2	68.73	69.78	0.988	0.970
1.5	0.813	1	67.70	74.16	0.977	0.967
		2	74.16	79.88	0.967	0.937
2.0	0.700	1	67.70	79.92	0.935	0.922
		2	79.92	95.83	0.922	0.884
2.5	0.600	1	67.70	88.25	0.867	0.847
		2	88.25	110.41	0.847	0.814
3.0	0.500	1	67.70	94.95	0.761	0.755
		2	94.95	125.13	0.755	0.722
3.5	0.400	1	67.70	99.18	0.643	0.633
		2	99.18	139.20	0.633	0.609
4.0	0.300	1	67.70	104.40	0.506	0.496
		2	104.40	149.14	0.496	0.473
4.5	0.200	1	67.70	108.47	0.350	0.344
		2	108.47	158.61	0.344	0.325
5.0	0.100	1	67.70	111.20	0.183	0.177
		2	111.20	165.65	0.177	0.166
5.5	0.038	1	67.70	113.07	0.006	0.004
		2	113.07	149.46	0.004	0.059
6.0	0.0	1	67.70	96.01	-0.175	-0.106
		2	96.01	114.28	-0.106	0.0
6.5	0.0	1	67.70	63.25	-0.217	-0.157
		2	63.25	61.79	-0.157	0.0
7.0	0.0	1	67.70	34.25	-0.139	-0.085
		2	34.25	12.33	-0.085	0.0
7.5	0.0	1	67.70	23.55	0.047	0.035
		2	23.55	6.75	0.035	0.0
8.0	0.0	1	67.70	47.63	0.208	0.126
		2	47.63	34.76	0.126	0.0
8.5	0.0	1	67.70	82.89	0.205	0.148
		2	82.89	88.45	0.148	0.0
9.0	0.0	1	67.70	105.95	0.086	0.054
		2	105.95	130.93	0.054	0.0
9.5	0.0	1	67.70	138.01	-0.097	-0.071
		2	108.01	123.42	-0.071	0.0
10.0	0.0	1	67.70	78.38	-0.229	-0.139
		2	78.38	85.12	-0.139	0.0

PIPE NO	SECTION NO	MAX PRESS.	MIN. PRESS.
1	1	67.70	67.70
1	2	91.18	44.05
1	3	113.07	23.55
2	1	113.07	23.55
2	2	140.26	9.54
2	3	165.65	5.42

APPENDIX C

C-1 PROGRAM LISTING

```
C
C***  ANALYSIS OF TRANSIENTS IN A PIPELINE CAUSED BY PUMPS
C
      REAL L,NR,NO
      DIMENSION Q(10,20),H(10,20),QP(10,20),HP(10,20),CA(10),F(10),
     1 CF(10),AR(10),A(10),L(10),N(10),D(10),FH(60),FB(60),HMAX(10),
     2 HMIN(10)
      COMMON /CP/ALPHA,QR,V,CN,DALPHA,DV,BETA,C5,C6,NPP,T
      COMMON /PAR/FH,FB,DTH
      DATA G/9.81/
C
C     READING AND WRITING OF INPUT DATA
C
C     GENERAL DATA
      READ(5,10) NP,NRLP,IPRINT,NPP,QO,NO,TLAST
10    FORMAT(4I2,5F10.2)
      WRITE(6,20) NP,NRLP,QO,NO,TLAST,NPP
20    FORMAT(8X,'NUMBER OF PIPES =',I3/8X,'NUMBER OF REACHES ON LAST PIP
     1E =',I3/8X,'STEADY STATE DISCH. =' ,F6.3,' M3/S'/8X,'STEADY STATE
     2 PUMP SPEED =', F6.1,' RPM'/8X,'TIME FOR WHICH TRANS. STATE COND.
     3ARE TO BE COMPUTED =',F5.1, ' S'/8X,'NUMBER OF PARALLEL PUMPS ='
     4 ,I3/)
C
C     READING AND WRITING OF PUMP DATA
C
      READ(5,21) NPC,DTH,QR,HR,NR,ER,WR2,(FH(I),I=1,NPC)
21    FORMAT(I2,6F10.2/(7F10.3))
      READ(5,22) (FB(I),I=1,NPC)
22    FORMAT(7F10.3)
      WRITE(6,23)NPC,DTH,QR,HR,NR,ER,WR2,(FH(I),I=1,NPC)
23    FORMAT(8X,'NUMBER OF POINTS ON CHARACTERISTIC CURVE =',I4/
     1 8X,'THETA INTERVAL FOR STORING CHARACTERISTIC CURVE =',F4.0/8X,
     2 'RATED DISCH. =',F5.2,' M3/S'/8X,'RATED HEAD =',F6.1,' M'/8X,
     3 'RATED PUMP SPEED =',F6.1,' RPM' /8X,'PUMP EFFICIENCY =',F6.3/8X,
     4'WR2=',F7.2,' KG-M2'//8X,'POINTS ON HEAD CHARAC'/(8X,10F7.3))
      WRITE(6,25) (FB(I),I=1,NPC)
25    FORMAT(/8X,'POINTS ON TORQUE CHARACTERISTIC'/ (8X,10F7.3))
C     DATA FOR PIPES
      READ(5,30) (L(I),D(I),A(I),F(I),I=1,NP)
30    FORMAT(4F10.3)
      WRITE(6,40)
40    FORMAT(/8X,'PIPE NO', 5X, 'LENGTH',5X,'DIA',5X,'WAVE VEL.',5X,'FRI
     2C FACTOR'/22X,'(M)',6X,'(M)',7X,'(M/S)' )
      WRITE(6,50)(I,L(I),D(I),A(I),F(I),I=1,NP)
50    FORMAT(10X,I3,6X,F7.1,3X,F5.2,5X,F7.1,11X,F5.3)
      DT=L(NP)/(NRLP*A(NP))
      WRITE(6,51)
51    FORMAT(/8X,'PIPE NO',5X,'ADJUSTED WAVE VEL'/26X,'(M/S)')
C     CALCULATION OF PIPE CONSTANTS
      DO 60 I=1,NP
      AR(I)=0.7854*D(I)**2
      AUNADJ=A(I)
      AN=L(I)/(DT*A(I))
      N(I)=AN
```



```
      AN1=N(I)
      IF((AN-AN1).GE.0.5) N(I)=N(I)+1
      A(I)=L(I)/(DT*N(I))
      WRITE(6,55) I,A(I)
55    FORMAT(10X,I3,12X,F7.1)
      CA(I)=G*AR(I)/A(I)
      CF(I)=F(I)*DT/(2.*D(I)*AR(I))
      F(I)=F(I)*L(I)/(2.*G*D(I)*N(I)*AR(I)**2)
60    CONTINUE
C
C     COMPUTATION OF CONSTANTS FOR PUMP
C     THE FOLLOWING CONSTANTS ARE FOR SI UNITS. FOR ENGLISH UNITS,
C     REPLACE  93604.99 BY 595.875 AND 4.775 BY 153.744
      TR=(93604.99*HR*QR)/(NR*ER)
      C5=CA(1)*HR
      C6=-(4.775*TR*DT)/(NR*WR2)
      ALPHA=NO/NR
      V=QO/(NPP*QR)
      DV=0.0
      DALPHA=0.0
C
C     CALCULATION OF STEADY STATE CONDITIONS
C
      IF(V.EQ.0.0) GO TO 65
      TH=ATAN2(ALPHA,V)
      TH=57.296*TH
      GO TO 68
65    TH=0.0
68    CALL PARAB(TH,1,Z)
      HO=Z*HR*(ALPHA**2+V**2)
      H(1,1)=HO
      CALL PARAB(TH,2,Z)
      BETA=Z*(ALPHA**2+V**2)
      DO 80 I=1,NP
      NN=N(I)+1
      DO 70 J=1,NN
      H(I,J)=H(I,1)-(J-1)*F(I)*QO**2
      IF(I.NE.NP.AND.J.EQ.NN) H(I+1,1)=H(I,NN)
      Q(I,J)=QO
70    CONTINUE
      HMAX(I)=H(I,1)
      HMIN(I)=H(I,1)
80    CONTINUE
      NN=N(NP)+1
      HRES=H(NP,NN)
      T=0.0
      WRITE(6,85)
85    FORMAT(/8X,'TIME',2X,'ALPHA',4X,'V',4X,'PIPE',7X,
     1 'HEAD (M)',7X,'DISCH. (M3/S)'/29X,'NO.',5X,'(1)',5X,'(N+1)'
     1,5X,'(1)',5X,'(N+1)'/)
90    K=0
      I=1
      NN=N(1)+1
      WRITE(6,86) T,ALPHA,V,I,H(1,1),H(1,NN),Q(1,1),Q(1,NN)
      DO 89 I=2,NP
      NN=N(I)+1
      WRITE(6,87) I, H(I,1),H(I,NN),Q(I,1),Q(I,NN)
86    FORMAT(F12.1,F7.2,F7.2,I5,F9.1,F9.1,F9.3,F10.3)
87    FORMAT (26X,I5,2F9.1,F9.3,F10.3)
89    CONTINUE
150   T=T+DT
      K=K+1
```

```
      IF(T.GT.TLAST) GO TO 240
C
C     PUMP AT UPSTREAM END
C
      CN=Q(1,2)-H(1,2)*CA(1)-CF(1)*Q(1,1)*ABS(Q(1,1))
      CALL PUMP
      QP(1,1)=NPP*V*QR
      HP(1,1)=(QP(1,1)-CN)/CA(1)
C
C     INTERIOR POINTS
C
      DO 170 I=1,NP
      NN=N(I)
      DO 160 J=2,NN
      CN=Q(I,J+1)-CA(I)*H(I,J+1)-CF(I)*Q(I,J+1)*ABS(Q(I,J+1))
      CP=Q(I,J-1)+CA(I)*H(I,J-1)-CF(I)*Q(I,J-1)*ABS(Q(I,J-1))
      QP(I,J)=0.5*(CP+CN)
      HP(I,J)=(CP-QP(I,J))/CA(I)
160   CONTINUE
170   CONTINUE
C
C     SERIES JUNCTION
C
      NP1=NP-1
      IF(NP.EQ.1) GO TO 178
      DO 175 I=1,NP1
      N1= N(I)
      NN=N(I)+1
      CN=Q(I+1,2)-CA(I+1)*H(I+1,2)-CF(I+1)*Q(I+1,2)*ABS(Q(I+1,2)
     1)
      CP=Q(I,N1)+CA(I)*H(I,N1)-CF(I)*Q(I,N1)*ABS(Q(I,N1))
      HP(I,NN)=(CP-CN)/(CA(I)+CA(I+1))
      HP(I+1,1)=HP(I,NN)
      QP(I,NN)=CP-CA(I)*HP(I,NN)
      QP(I+1,1)=CN+CA(I+1)*HP(I+1,1)
175   CONTINUE
C
C     RESERVOIR AT DOWNSTREAM END
C
178   NN=N(NP)+1
      HP(NP,NN)=HRES
      CP=Q(NP,NN-1)+CA(NP)*H(NP,NN-1)-CF(NP)*Q(NP,NN-1)*ABS(Q(NP,
     1 NN-1))
      QP(NP,NN)=CP-CA(NP)*HP(NP,NN)
C
C     STORING MAX. AND MIN. PRESSURES AND  VARIABLES FOR NEXT TIME STEP
C
210   DO 230 I=1,NP
      NN=N(NP)+1
      DO 220 J=1,NN
      Q(I,J)=QP(I,J)
      H(I,J)=HP(I,J)
220   CONTINUE
      IF (H(I,1).GT.HMAX(I)) HMAX(I)=H(I,1)
      IF (H(I,1).LT.HMIN(I)) HMIN(I)=H(I,1)
230   CONTINUE
      IF(K.EQ.IPRINT) GO TO 90
      GO TO 150
```



```
240   WRITE(6,250)
250   FORMAT(//10X,'PIPE NO.',5X,'MAX. PRESS.',5X,'MIN. PRESS.'/27X
     1 ,'M',16X,'M')
      WRITE(6,260) (I,HMAX(I),HMIN(I),I=1,NP)
260   FORMAT(12X,I3,7X,F7.1,9X,F7.1)
      STOP
      END

      SUBROUTINE PUMP
      DIMENSION FH(60),FB(60)
      COMMON /CP/ALPHA,QR,V,CN,DALPHA,DV,BETA,C5,C6,NPP,T
     1  /PAR/FH,FB,DTH
      KK=0
      JJ=0
C
C     COMPUTATION OF PUMP DISCHARGE
C
      VE=V+DV
5     ALPHAE=ALPHA+DALPHA
8     JJ=JJ+1
10    IF (VE.EQ.0.0.AND.ALPHAE.EQ.0.0) GO TO 20
      TH=ATAN2(ALPHAE,VE)
      TH1=TH
      TH=TH*57.296
      IF (TH.LT.0.0) TH=TH+360.
      IF (TH1.LT.0.0) TH1=TH1+6.28318
      GO TO 30
20    TH= 0.0
      TH1=0.0
30    M=TH/DTH+1.
      A1=FH(M)*M-FH(M+1)*(M-1)
      A2=(FH(M+1)-FH(M))/(DTH*0.017453)
      A3=FB(M)*M-FB(M+1)*(M-1)
      A4=(FB(M+1)-FB(M))/(DTH*0.017453)
      ALPSQ=ALPHAE*ALPHAE
      VESQ=VE*VE
      ALPV=ALPSQ+VESQ
      F1=C5*A1*ALPV+C5*A2*ALPV*TH1-QR*VE*NPP+CN
      F2=ALPHAE-C6*A3*ALPV-C6*A4*ALPV*TH1-ALPHA-C6*BETA
      F1AL=C5*(2.*A1*ALPHAE+A2*VE+2.*A2*ALPHAE*TH1)
      F1V=C5*(2.*A1*VE-A2*ALPHAE+2.*A2*VE*TH1)-QR*NPP
      F2AL=1.-C6*(2.*A3*ALPHAE+A4*VE+2.*A4*ALPHAE*TH1)
      F2V=C6*(-2.*A3*VE+A4*ALPHAE-2.*A4*VE*TH1)
      DENOM=F1AL*F2V-F1V*F2AL
      DALPHA=(F2*F1V-F1*F2V)/DENOM
      DV=(F1*F2AL-F2*F1AL)/DENOM
      ALPHAE=ALPHAE+DALPHA
      VE=VE+DV
      IF (ABS(DV).LE.0.001.AND.ABS(DALPHA).LE.0.001) GO TO 50
      IF (JJ.GT.30) GO TO 70
      GO TO 8
50    TH=ATAN2(ALPHAE,VE)
      TH=57.296*TH
      IF (TH.LT.0.0) TH=TH+360.
      CALL PARAB(TH,2,BETA)
      IF (MB.EQ.M) GO TO 60
```

```
      MB=TH/DTH+1
      IF (MB.EQ.M) GO TO 60
      GO TO 8
60    DALPHA=ALPHAE-ALPHA
      DV=VE-V
      ALPHA=ALPHAE
      V=VE
      BETA= BETA * (ALPHA*ALPHA+V*V)
      RETURN
70    WRITE(6,80) T,ALPHAE,VE
80    FORMAT(8X,'***ITERATIONS IN PUMP SUBROUTINE FAILED' /8X,'T=',F8.2
     2/8X,'ALPHAE =' ,F6.3/8X,'VP =',F6.3)
      STOP
      END

      SUBROUTINE PARAB(X,J,Z)
      COMMON /PAR/FH,FB,DX
      DIMENSION FH(60),FB(60)
      I=X/DX
      R=(X-I*DX)/DX
      IF(I.EQ.0) R=R-1.
      I=I+1
      IF(I.LT.2) I=2
      GO TO (10,20),J
10    Z=FH(I)+0.5*R*(FH(I+1)-FH(I-1)+R*(FH(I+1)+FH(I-1)-2.*FH(I)))
      RETURN
20    Z=FB(I)+0.5*R*(FB(I+1)-FB(I-1)+R*(FB(I+1)+FB(I-1)-2.*FB(I)))
      RETURN
      END
```

C-2 INPUT DATA

```
02020202   .500      1100.     15.
55    5.     .250        60.00       1100.      .84      16.850
  -.53     -.476       -.392      -.291      -.150      -.037      .075
   .200      .345        .500       .655       .777       .900     1.007
  1.115     1.186       1.245      1.278      1.290      1.287     1.269
  1.240     1.201       1.162      1.115      1.069      1.025      .992
   .945      .908        .875       .848       .819       .789      .755
   .723      .690        .656       .619       .583       .555      .531
   .510      .502        .500       .505       .520       .539      .565
   .593      .615        .634       .640       .638       .630
  -.350     -.474       -.180      -.062       .037       .135      .228
   .320      .425        .500       .548       .588       .612      .615
   .600      .569        .530       .479       .440       .402      .373
   .350      .340        .340       .350       .380       .437      .520
   .605      .683        .750       .802       .845       .872      .883
   .878      .860        .823       .780       .725       .660      .580
   .490      .397        .310       .230       .155       .085      .018
  -.052     -.123       -.220      -.348      -.490      -.680
450.0       .750      900.0       .01
550.0       .750     1100.00      .012
```


C-3 PROGRAM OUTPUT

```
NUMBER OF PIPES =  2
NUMBER OF REACHES ON LAST PIPE =  2
STEADY STATE DISCH. = 0.500 M3/S
STEADY STATE PUMP SPEED =1100.0 RPM
TIME FOR WHICH TRANS. STATE COND. ARE TO BE COMPUTED = 15.0 S
NUMBER OF PARALLEL PUMPS =  2

NUMBER OF POINTS ON CHARACTERISTIC CURVE =  55
THETA INTERVAL FOR STORING CHARACTERISTIC CURVE =  5.
RATED DISCH. = 0.25 M3/S
RATED HEAD =  60.0 M
RATED PUMP SPEED =1100.0 RPM
PUMP EFFICIENCY = 0.840
WR2=  16.85 KG-M2

POINTS ON HEAD CHARAC
 -0.530 -0.476 -0.392 -0.291 -0.150 -0.037  0.075  0.200  0.345  0.500
  0.655  0.777  0.900  1.007  1.115  1.188  1.245  1.278  1.290  1.287
  1.269  1.240  1.201  1.162  1.115  1.069  1.025  0.992  0.945  0.908
  0.875  0.848  0.819  0.788  0.755  0.723  0.690  0.656  0.619  0.583
  0.555  0.531  0.510  0.502  0.500  0.505  0.520  0.539  0.565  0.593
  0.615  0.634  0.640  0.638  0.630

POINTS ON TORQUE CHARACTERISTIC
 -0.350 -0.474 -0.180 -0.062  0.037  0.135  0.228  0.320  0.425  0.500
  0.548  0.588  0.612  0.615  0.600  0.569  0.530  0.479  0.440  0.402
  0.373  0.350  0.340  0.340  0.350  0.380  0.437  0.520  0.605  0.683
  0.750  0.802  0.845  0.872  0.883  0.878  0.860  0.823  0.780  0.725
  0.660  0.580  0.490  0.397  0.310  0.230  0.155  0.085  0.018 -0.052
 -0.123 -0.220 -0.348 -0.490 -0.680

PIPE NO      LENGTH      DIA      WAVE VEL.      FRIC FACTOR
               (M)       (M)       (M/S)
    1         450.0     0.75       900.0            0.010
    2         550.0     0.75      1100.0            0.012

PIPE NO      ADJUSTED WAVE VEL
                (M/S)
    1            900.0
    2           1100.0

TIME   ALPHA      V      PIPE      HEAD (M)        DISCH. (M3/S)
                          NO.     (1)    (N+1)     (1)     (N+1)

 0.0    1.00    1.00      1      60.0    59.6     0.500    0.500
                          2      59.6    59.0     0.500    0.500
 0.5    0.72    0.72      1      30.7    59.6     0.359    0.500
                          2      59.6    59.0     0.500    0.500
 1.0    0.56    0.59      1      17.7    27.5     0.297    0.374
                          2      27.5    59.0     0.374    0.500
 1.5    0.46    0.57      1       9.7    13.2     0.287    0.318
                          2      13.2    59.0     0.318    0.248
 2.0    0.39    0.56      1       5.3    36.3     0.279    0.158
                          2      36.3    59.0     0.158    0.137
 2.5    0.34    0.05      1       9.1    45.8     0.027    0.084
                          2      45.8    59.0     0.084    0.068
 3.0    0.32   -0.18      1       9.3    26.9    -0.091   -0.059
                          2      26.9    59.0    -0.059    0.032
```

3.5	0.30	-0.28	1	10.1	17.7	-0.139	-0.131
			2	17.7	59.0	-0.131	-0.185
4.0	0.26	-0.34	1	10.1	37.4	-0.168	-0.270
			2	37.4	59.0	-0.270	-0.294
4.5	0.15	-0.68	1	22.6	46.5	-0.341	-0.342
			2	46.5	59.0	-0.342	-0.355
5.0	-0.05	-0.85	1	29.0	40.6	-0.425	-0.426
			2	40.6	59.0	-0.426	-0.391
5.5	-0.30	-0.93	1	32.4	38.6	-0.464	-0.470
			2	38.6	59.0	-0.470	-0.497
6.0	-0.55	-0.95	1	37.0	48.0	-0.476	-0.538
			2	48.0	59.0	-0.538	-0.548
6.5	-0.79	-1.04	1	51.3	55.1	-0.520	-0.561
			2	55.1	59.0	-0.561	-0.579
7.0	-1.01	-1.04	1	63.4	61.3	-0.519	-0.566
			2	61.3	59.0	-0.566	-0.574
7.5	-1.18	-1.00	1	74.8	67.7	-0.499	-0.537
			2	67.7	59.0	-0.537	-0.554
8.0	-1.30	-0.93	1	82.5	73.9	-0.464	-0.493
			2	73.9	59.0	-0.493	-0.500
8.5	-1.37	-0.86	1	87.1	76.1	-0.428	-0.431
			2	76.1	59.0	-0.431	-0.433
9.0	-1.39	-0.76	1	86.6	74.9	-0.379	-0.368
			2	74.9	59.0	-0.368	-0.363
9.5	-1.37	-0.66	1	82.2	72.2	-0.332	-0.309
			2	72.2	59.0	-0.309	-0.305
10.0	-1.33	-0.59	1	75.4	68.6	-0.293	-0.266
			2	68.6	59.0	-0.266	-0.257
10.5	-1.27	-0.53	1	68.3	63.8	-0.267	-0.237
			2	63.8	59.0	-0.237	-0.228
11.0	-1.21	-0.49	1	61.7	59.7	-0.247	-0.225
			2	59.7	59.0	-0.225	-0.218
11.5	-1.15	-0.48	1	56.3	57.1	-0.241	-0.225
			2	57.1	59.0	-0.225	-0.222
12.0	-1.11	-0.49	1	52.5	55.3	-0.247	-0.236
			2	55.3	59.0	-0.236	-0.232
12.5	-1.08	-0.52	1	50.4	53.8	-0.259	-0.252
			2	53.8	59.0	-0.252	-0.250
13.0	-1.06	-0.55	1	49.4	53.2	-0.273	-0.273
			2	53.2	59.0	-0.273	-0.272
13.5	-1.05	-0.58	1	49.6	53.6	-0.290	-0.293
			2	53.6	59.0	-0.293	-0.295
14.0	-1.06	-0.61	1	50.7	54.4	-0.306	-0.312
			2	54.4	59.0	-0.312	-0.313
14.5	-1.07	-0.64	1	52.6	55.3	-0.320	-0.327
			2	55.3	59.0	-0.327	-0.330
15.0	-1.09	-0.66	1	54.7	56.5	-0.329	-0.338
			2	56.5	59.0	-0.338	-0.341

PIPE NO.	MAX. PRESS. M	MIN. PRESS. M
1	87.4	5.3
2	76.1	13.2

APPENDIX D

D-1 PROGRAM LISTING

```
C
C       FREQUENCY RESPONSE OF A SERIES PIPING SYSTEM HAVING RESERVOIR AT
C        THE UPSTREAM END AND AN OSCILATING VALVE AT THE DOWNSTREAM END
        COMPLEX A,B,C,HV,QV,CC,CMPLX
        REAL L
        DIMENSION L(20),WV(20),L(20),AR(20),P(20),CP(20),A(2,2),B(2,2),
       1 C(2,2),F(20)
        READ(5,10) N,M1,M2,M3,FRAC
10      FORMAT(4I3,F10.2)
        READ (5,20) TAUO,HO,QO,AMP,THPER
20      FORMAT(7F10.3)
        WRITE(6,30) TAUO,HO,QO,AMP,THPER,N
30      FORMAT(8X,'MEAN VALVE OPENING =',F5.3 /8X,'STATIC HEAD =',F7.2,
       1 ' M'/8X,'MEAN DISCHARGE =',F7.2, ' M3/S' /8X,'AMPLITUDE OF VALVE
       2OSCILATIONS =',F5.3 /8X,'THEORETICAL PERIOD OF THE PIPELINE =',
       3 F6.3,' S'/8X,'NUMBER OF PIPES =', I3/)
        READ(5,40) (L(I),D(I),WV(I),I=1,N)
40      FORMAT(3F10.2)
        WRITE(6,50)
50      FORMAT(8X,'LENGTH (M)',5X,'DIA (M)',2X,'WAVE VEL. (M/S)')
        DO 60 I=1,N
        WRITE(6,55) L(I),D(I),WV(I)
55      FORMAT(F16.2,F11.2,F14.2)
        P(I)=L(I)/WV(I)
        CP(I)=7.7047*D(I)**2/WV(I)
C       IN ENGLISH UNITS, REPLACE 7.7047 BY 25.2898
60      CONTINUE
        VC=-(2.*HO*AMP)/TAUO
        TW=6.2832/THPER
        WRITE(6,65)
65      FORMAT(/8X,'WF/WT',5X,'HV/HO',6X,'QV/QO',4X,'PHASE H',3X,'PHASE Q'/)
        DO 80 J=M1,M2,M3
        AJ=J
        W=FRAC*AJ*TW
        A(1,1)=CMPLX(1.,0.)
        A(1,2)=CMPLX(0.0,0.0)
        A(2,1)=CMPLX(0.0,0.0)
        A(2,2)=CMPLX(1.0,0.0)
        DO 70 I=1,N
        G=W*P(I)
        B(1,1)=CMPLX(COS(G),0.0)
        B(1,2)=CMPLX(0.0,-(1./CP(I))*SIN(G))
        B(2,1)=CMPLX(0.0,-CP(I)*SIN(G))
        B(2,2)=CMPLX(COS(G),0.0)
        CALL MULT(B,A,C,2,2)
        CALL COPY(C,A,2,2)
70      CONTINUE
        CC=VC/(C(1,2)-2.*HO*C(2,2)/QO)
        HV=CC*C(1,2)
        QV=CC*C(2,2)
        WR=W/TW
        H=CABS(HV)/HO
```

```
      C=CABS(QV)/QO
      ANGH=57.29578*ATAN2(AIMAG(HV),REAL(HV))
      ANGQ=57.29578*ATAN2(AIMAG(QV),REAL(QV))
      WRITE(6,25) WR,H,C,ANGH,ANGQ
   20 CONTINUE
   25 FORMAT(3X,5F10.3)
      STOP
      END
      SUBROUTINE MULT(A,B,C,N,M)
      COMPLEX A,B,C,CMPLX
      DIMENSION A(N,N),B(N,N),C(N,N)
      DO 6 I=1,N
      DO 6 J=1,N
      C(I,J)=CMPLX(0.0,0.0)
      DO 6 K=1,N
    6 C(I,J)=A(I,K)*B(K,J) + C(I,J)
      RETURN
      END
      SUBROUTINE COPY(C,A,N,M)
      COMPLEX A,C
      DIMENSION A(N,N),C(N,N)
      DO 6 I=1,N
      DO 6 J=1,N
    6 A(I,J)=C(I,J)
      RETURN
      END
```

D-2 INPUT DATA

```
 002001020001   .5
    1.       30.48      .0089      .2          3.
  609.5       .61       1219.
  228.6       .3         914.4
```


D-3 PROGRAM OUTPUT

```
MEAN VALVE OPENING =1.000
STATIC HEAD =  30.48 M
MEAN DISCHARGE =  0.009 M3/S
AMPLITUDE OF VALVE OSCILATIONS =0.200
THEORETICAL PERIOD OF THE PIPELINE = 3.000 S
NUMBER OF PIPES =  2

LENGTH (M)    DIA (M)   WAVE VEL. (M/S)
  609.50        0.61        1219.00
  228.60        0.30         914.40

WF/WT      H/HO      Q/QO      PHASE H    PHASE Q

0.500      0.037     0.199     -95.257     -5.257
1.000      0.123     0.190    -107.887    -17.887
1.500      0.076     0.196     100.897     10.897
2.000      0.046     0.199     -96.552     -6.552
2.500      0.149     0.186    -111.940    -21.940
3.000      0.400     0.000     179.999     89.999
3.500      0.149     0.186     111.940     21.940
4.000      0.046     0.199      96.551      6.551
4.500      0.076     0.196    -100.898    -10.898
5.000      0.123     0.190     107.886     17.886
5.500      0.037     0.199      95.257      5.257
6.000      0.000     0.200     -90.000     -0.000
6.500      0.037     0.199     -95.258     -5.258
7.000      0.123     0.190    -107.888    -17.888
7.500      0.076     0.196     100.896     10.896
8.000      0.046     0.199     -96.552     -6.552
8.500      0.149     0.186    -111.941    -21.941
9.000      0.400     0.000     179.995     89.995
9.500      0.149     0.186     111.939     21.939
10.000     0.046     0.199      96.551      6.551
```

APPENDIX E

PUMP CHARACTERISTIC DATA*

$\theta = \tan^{-1}\frac{\alpha}{\nu}$ (Degrees)	$N_s = 25$		$N_s = 147$		$N_s = 261$	
	$\frac{h}{\alpha^2+\nu^2}$	$\frac{\beta}{\alpha^2+\nu^2}$	$\frac{h}{\alpha^2+\nu^2}$	$\frac{\beta}{\alpha^2+\nu^2}$	$\frac{h}{\alpha^2+\nu^2}$	$\frac{\beta}{\alpha^2+\nu^2}$
0	- 0.530	- 0.350	- 1.560	- 1.560	- 1.000	- 0.560
5	- 0.476	- 0.474	- 1.290	- 1.200	- 0.948	- 0.600
10	- 0.392	- 0.180	- 1.035	- 0.895	- 0.892	- 0.605
15	- 0.291	- 0.062	- 0.795	- 0.600	- 0.820	- 0.580
20	- 0.150	0.037	- 0.540	- 0.355	- 0.665	- 0.503
25	- 0.037	0.135	- 0.308	- 0.135	- 0.475	- 0.355
30	0.075	0.228	- 0.032	0.060	- 0.275	- 0.160
35	0.200	0.320	+ 0.122	0.235	- 0.055	+ 0.070
40	0.345	0.425	0.310	0.380	+ 0.200	0.320
45	0.500	0.500	0.500	0.500	0.500	0.500
50	0.655	0.548	0.635	0.580	0.785	0.620
55	0.777	0.588	0.745	0.645	1.035	0.708
60	0.900	0.612	0.860	0.695	1.280	0.825
65	1.007	0.615	0.992	0.755	1.508	0.955
70	1.115	0.600	1.140	0.850	1.730	1.150
75	1.188	0.569	1.365	0.970	1.970	1.413
80	1.245	0.530	1.595	1.115	2.225	1.608
85	1.278	0.479	1.790	1.300	2.485	1.780
90	1.290	0.440	1.960	1.485	2.740	1.960
95	1.287	0.402	2.048	1.518	2.980	2.150
100	1.269	0.373	2.110	1.540	3.195	2.345
105	1.240	0.350	2.158	1.545	3.380	2.525
110	1.201	0.340	2.203	1.560	3.515	2.710
115	1.162	0.340	2.250	1.592	3.572	2.900
120	1.115	0.350	2.315	1.642	3.570	3.000
125	1.069	0.380	2.390	1.720	3.490	3.010
130	1.025	0.437	2.495	1.900	3.350	2.925
135	0.992	0.520	2.630	2.090	3.140	2.760
140	0.945	0.605	2.785	2.315	2.875	2.500
145	0.908	0.683	2.905	2.530	2.570	2.245
150	0.875	0.750	3.000	2.650	2.300	1.990
155	0.848	0.802	3.020	2.720	2.065	1.750
160	0.819	0.845	2.975	2.740	1.840	1.518
165	0.788	0.872	2.825	2.685	1.633	1.300
170	0.755	0.883	2.652	2.535	1.440	1.085
175	0.723	0.878	2.442	2.310	1.260	0.870
180	0.690	0.860	2.185	2.090	1.080	0.660
185	0.656	0.823	1.890	1.850	0.920	0.500
190	0.619	0.780	1.525	1.570	0.780	0.505
195	0.583	0.725	1.195	1.250	0.710	0.555
200	0.555	0.660	0.935	0.955	0.670	0.615
205	0.531	0.580	0.695	0.730	0.660	0.630
210	0.510	0.490	0.500	0.530	0.555	0.500
215	0.502	0.397	0.374	0.350	0.410	0.315
220	0.500	0.310	0.277	0.175	0.265	0.100
225	0.505	0.230	0.190	0.000	0.065	- 0.075
230	0.520	0.155	0.114	- 0.160	- 0.140	- 0.315
235	0.539	0.085	0.058	- 0.295	- 0.345	- 0.515
240	0.565	0.018	- 0.015	- 0.425	- 0.550	- 0.715
245	0.593	- 0.052	- 0.110	- 0.550	- 0.745	- 0.880
250	0.615	- 0.123	- 0.220	- 0.670	- 0.960	- 1.030
255	0.634	- 0.220	- 0.334	- 0.820	- 1.200	- 1.225
260	0.640	- 0.343	- 0.440	- 0.992	- 1.480	- 1.450
265	0.638	- 0.490	- 0.550	- 1.213	- 1.810	- 1.860
270	0.630	- 0.680	- 0.670	- 1.500	- 2.200	- 2.200

*These pump characteristic data are based on data presented by Thomas[1] and Donsky.[2] For notation, see Section 4.3.

REFERENCES

1. Thomas, G., "Determination of Pump Characteristics for a Computerized Transient Analysis," *Proc., First Inter. Conference on Pressure Surges*, British Hydromech. Research Assoc., England, Sept. 1972, pp. A3-21 to A3-32.
2. Donsky, B., "Complete Pump Characteristics and the Effect of Specific Speeds on Hydraulic Transients," *Jour., Basic Engineering, Trans.*, Amer. Soc. of Mech. Engrs., Dec. 1961, pp. 685-699.

APPENDIX F

SI AND ENGLISH UNITS AND CONVERSION FACTORS

SI (Système Internationale) units for various physical quantities are listed in Section E-1, and the factors for converting them to the English units are presented in Section E-2.

E-1 SI UNITS

Physical Quantity	Name of Unit	Symbol	Definition
Length	Meter	m	-
Mass	Kilogram	kg	-
Force	Newton	N	1 kg m/s^2
Energy	Joule	J	1 N m
Pressure, stress	Pascal	Pa	1 N/m^2
Power	Watt	W	1 J/s
Bulk modulus of elasticity	Pascal	Pa	1 N/m^2

The multiples and fractions of the preceding units are denoted by the following letters:

10^{-3}	milli	m
10^{-1}	deci	d
10^{3}	kilo	k
10^{6}	mega	M
10^{9}	Giga	G

For example, 2.1 GPa = 2.1 X 10^9 Pa; 1.95 Gg m^2 = 1.95 X 10^6 kg m^2.

F-2 CONVERSION FACTORS

Quantity	To Convert: From SI unit	To Convert: To English unit	Multiply by
Acceleration	m/s^2	ft/sec^2	3.28084
Area	m^2	ft^2	10.7639
Density	kg/m^3	lb/ft^3	62.4278 X 10^{-3}
	kg/m^3	slug/ft^3	1.94032 X 10^{-3}
Discharge	m^3/s	ft^3/sec	35.3147
	m^3/s	gal/min (U.S.)	15.8503 X 10^3
	m^3/s	gal/min (Imperial)	13.1981 X 10^3
Force	N	lb$_f$	224.809 X 10^{-3}
Length	m	ft	3.28084
Mass	kg	lb	2.20462
	kg	slug	68.5218 X 10^{-3}
Moment of inertia	kg m^2	lb-ft^2	23.7304
Momentum (Angular)	kg m^2/s	lb-ft^2/sec	23.7304
(Linear)	kg m/s	lb-ft/sec	7.23301
Power	W	ft-lb$_f$/sec	0.737561
	W	hp	1.34102 X 10^{-3}
Torque	Nm	lb$_f$-ft	737.562 X 10^{-3}
Velocity	m/s	ft/sec	3.28084
	m/s	mile/hr	2.23694
Volume	m^3	ft^3	35.3147
	m^3	yd^3	1.30795
	m^3	in.^{3}	61.0237 X 10^3
Specific weight	N/m^3	lbf/ft^3	6.36587 X 10^{-3}
Temperature	°C	°F	1.8; and add 32

1 HP = 550 lb ft/s

AUTHOR INDEX

AUTHOR INDEX

SUBJECT INDEX

SUBJECT INDEX